

Application Handbook  
**Automotive**





---

## Automotive

---

### **Analytical solutions for the complete automotive supply chain**

A driver of jobs and wealth, the automotive industry is also a driver of innovation covering a multitude of technologies and topics such as materials, composites, drivetrain and motors, efficiency in production processes and fuel consumption, comfort and safety. The car industry is cross-linked with various tiers of suppliers providing many different components, modules and systems. To combine consumer and product safety with environmental protection, it is truly global in sourcing, production and distribution as well as in quality control, manufacturing and security standards.

As a leading global supplier of analytical instrumentation, Shimadzu provides solutions in chromatography, spectroscopy, mass spectrometry, TOC and material testing as well as software libraries for all analytical challenges within the complete automotive supply chain. As scientific and analytical know-how grows in parallel, both continuously benefit consumer, product and environmental safety.

From the perspective of automotive quality control, quality assurance, R&D and environmental protection, this application handbook provides a diversity of analytical methods meeting standards, norms, regulations and compliance.

#### **Quality Control**

Quality control covers evaluations and composition analyses of raw materials and their diverse properties, as well as metals and resins. For strength evaluations, tensile, compression, bending and hardness tests are used, while evaluations of

material composition require inorganic element and compound analysis. The strength of polymer material is largely determined by the type and density of the molecules used. Tests of material specifications are complemented by analyses of defects occurring during the manufacturing process with a view towards improvement.

#### **Quality Assurance**

With a variety of tests and analyses, quality assurance secures product performance to meet defined standards or to find and specify causes of defects, damaged parts and malfunctions. In addition, microscopic analyses, surface analyses and morphological observations are performed as well as strength, substantive and endurance evaluations and failure tests.

#### **Research and Development**

In R&D, new candidate materials are tested and analyzed before being applied in the product development. To resolve problems occurring at the prototype stage, trial products are subjected to defect analyses. Furthermore, special cutting-edge tests and analyses are required in addition to proprietary evaluations capable of confirming the performance to be evaluated in developed products.

#### **Environmental Protection**

At plant facilities, analyses of toxic elements and VOCs (volatile organic compounds) in wastewater are performed for environmental protection purposes. In terms of PM2.5 particles, which are increasingly being monitored as air pollutants, measures are applied to reduce the presence of such particles in automobile gas emissions as well as in production plants.

[www.shimadzu.eu/automotive](http://www.shimadzu.eu/automotive)



# Contents

## 1. Chromatography

---

- 1.1 Gas Chromatography (GC)
- 1.2 Liquid Chromatography (LC)

## 2. Mass Spectrometry

---

- 2.1 Gas Chromatography-Mass Spectrometry (GC-MS)
- 2.2 Liquid Chromatography-Mass Spectrometry (LC-MS)

## 3. Spectroscopy

---

- 3.1 Atomic Spectroscopy
  - 3.1.1 Energy Dispersive X-Ray Fluorescence (EDX)
  - 3.1.2 Inductively Coupled Plasma Optical Emission Spectroscopy (ICP-OES)
- 3.2 Molecular Spectroscopy
  - 3.2.1 Ultraviolet Visible Spectroscopy and Near Infrared Analysis (UV-Vis, NIR)
  - 3.2.2 Fourier Transform Infrared Spectroscopy (FTIR)
  - 3.2.3 Fluorescence Spectroscopy

## 4. Life Science Lab Instruments

---

- 4.1 Functional Near-Infrared Spectroscopy (fNIRS)

## 5. Sum Parameter (TOC/TN)

---

- 5.1 Total Organic Carbon Lab Analyzers

## 6. Materials Testing & Inspection

---

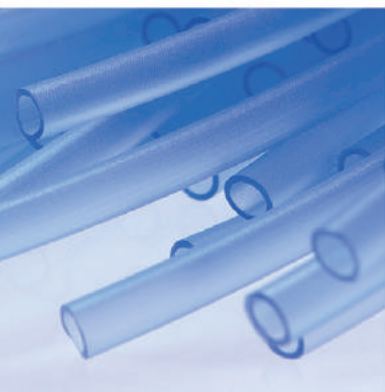
- 6.1 Universal Testing
- 6.2 Fatigue Testing
- 6.3 Hardness Testing
- 6.4 High-Speed Video Camera
- 6.5 Rheometer
- 6.6 Non-destructive Inspection (NDI)

## 7. Particle Size

---

- 7.1 Laser Diffraction Particle Size Measurement

# 1. Chromatography







# 1. Chromatography

---

## 1.1 Gas Chromatography (GC)

---

For applications in automotive industry, chromatographic separation and analysis of volatile and semi-volatile components are used for interior and exterior parts as well as oil, lubrication and others. GC is applied to measure volatile organic compounds (VOCs) inside the automobile cabin, or to detect trace components released from resin samples of parts and materials.

<b>No. 11</b>	Trace analysis of carbon dioxide in high-purity hydrofluorocarbon
<b>SCA-180-020</b>	Robust and sensitive measurement of aldehydes in water via GC-BID
<b>SCA-180-019</b>	VDA 277: Analysis of volatile contaminants from polymers
<b>No. 7</b>	Simultaneous analysis of evolved gas produced by the degradation of a lithium-ion battery
<b>No. 3</b>	Analysis of diesel oil samples in compliance with ASTM D2887 using the Shimadzu simulated distillation gas chromatograph system
<b>No. 5</b>	Analysis of lubricant oil samples in compliance with ASTM D7500 using the Shimadzu simulated distillation gas chromatograph system
<b>eG283</b>	Trace impurity analysis of hydrogen fuel in fuel cell vehicle-related fields

# Application Data Sheet

No. 11

GC  
Gas Chromatograph

## Trace Analysis of Carbon Dioxide in High-Purity Hydrofluorocarbon

Fluorocarbon, a generic term for organic compounds with C-F bonding, is a chemical material used as a refrigerant in refrigerators and freezers, and in air conditioners in cars, buses, other vehicles, and buildings. It is also used as a cleaning agent for electronic components and precision parts. Hydrofluorocarbon (HFC) is classified as a non-ozone-depleting chlorofluorocarbons(CFC) substitute and is used as a gas for semiconductor etching and electronic component cleaning. High-purity HFC is utilized in the semiconductor and electronics industries; confirming its purity requires measuring the concentration of impurities. This data sheet introduces an example of analyzing trace quantities of CO<sub>2</sub> impurities in high-purity HFC using the Shimadzu "Tracera" High-Sensitivity Gas Chromatograph System.

### Instruments Used and Analysis Conditions

#### Instruments Used

Gas chromatograph: Tracera (GC-2010 Plus + BID-2010 Plus)  
Gas sampler: MGS-2010  
Software: LabSolutions

#### Analysis Conditions

Column: PoraPLOT Q (0.32 mm I.D. × 25 m, df = 10 μm)  
Column temp.: \*30 °C (5 min) - 40 °C/min - 100 °C (8.25 min), 15 min in total  
Carrier gas: He: 40 cm/sec, constant linear velocity mode  
Injection mode: Split (1:10)  
Injection port temp.: 150 °C  
Detector temp.: 200 °C  
Discharge gas: He: 50 mL/min  
Injection volume: 1 mL (gas sampler used)

\* The initial column temperature (30 °C) can be set at a room temperature of 25 °C or lower.

Note: It is not possible to separate air components (N<sub>2</sub>, O<sub>2</sub>, Ar) or CO under these analysis conditions.

### Results

Multiple high-purity HFCs were analyzed. Fig.1 shows the resulting chromatograms, and Table 1 shows the quantitative results for CO<sub>2</sub>. The CO<sub>2</sub> concentration in sample #3 was a very low, which was only 0.3 ppm. The S/N ratio was approximately 43. Conventional analysis of trace levels of CO<sub>2</sub> requires using an FID and a methanizer. This example demonstrates how a simply configured Tracera system can analyze trace amounts of CO<sub>2</sub> with high sensitivity.

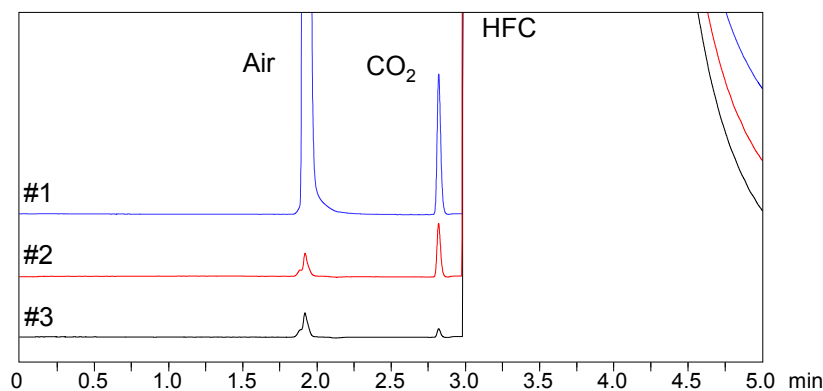


Fig. 1: Chromatograms for High-Purity HFCs

Table 1: CO<sub>2</sub> Quantitative Results

Sample	Quantitative Conc. (ppm)	S/N
#1	5.09	1043.5
#2	1.93	250.7
#3	0.31	43.14

First Edition: August 2013

## Application News

No. SCA-180-020

Gas Chromatography – GC

### Robust and Sensitive Measurement of Aldehydes in Water via GC-BID

Aldehydes and especially their smallest representative formaldehyde are of great importance in chemical industry. Until now, measurement of these compounds via headspace gas chromatography (HS-GC) required prior derivatization. For example, transformation into oximes via PFBHA was carried out in order to improve the stability and detector response for these analytes. Our new barrier ionization discharge (BID) detector (Figure 1) uses helium plasma ionization. It combines high sensitivity and stability with universal detection capabilities. This novel detection option makes preliminary derivatization of aldehydes obsolete and permits their direct measurement via HS-GC. Herein we demonstrate how our HS-20 headspace sampler and our Tracera high-sensitivity GC-BID can be used to measure lower aldehydes from water via HS-GC without prior derivatization.

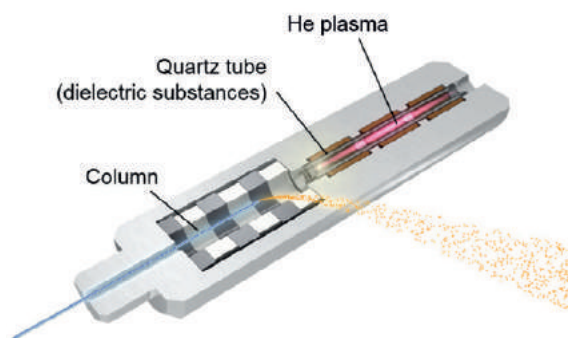


Figure 1: Schematic of the BID detector

#### ■ Experimental work

Instrument calibration was carried out via calibration solutions that contained formaldehyde, acetaldehyde, propionaldehyde and butylaldehyde in water with the following concentration: 0.5, 1, 5, 10 and 50 ppm. Individual 20 mL sample vials were prepared with 10 mL of these solutions and immediately sealed with gas-tight screw caps that are outfitted with silicone/PTFE septa.

First step of the measurement is an incubation of the samples at 80 °C for 20 minutes. During this time, the aldehyde solutions equilibrate with their headspace, which denotes the gas volume that is contained inside the sample flasks alongside the liquid samples. The overlapping routines of the HS-20 automated headspace sampler increase time-efficacy over the course of long measurement series by simultaneous processing of up to 12 samples. Afterwards, 1 mL of the equilibrated sample headspace gas is abstracted from the sample flask by the headspace sampler and introduced into the gas chromatograph. This is carried out via pressurized and heated flow lines and a sample loop, in which the headspace gas is precisely gauged.

Gas chromatographic separation of analytes is realized on a Restek Rt-U-BOND® PLOT-Column (divinylbenzene ethylene glycol/dimethylacrylate) with an internal diameter of 0.53 mm, a coating thickness of 20 µm and a length of 30 m.

An additional particle trap was found to be unnecessary as the bonding technology of the phase was sufficient for preventing contamination of the detector with phase particles. The oven program starts at 95 °C for 5 min, proceeds to 180 °C at 20 K/min and concludes at 180°C for 6 min for cleanup purposes. A sample chromatogram is shown in Figure 3. Since the detector response is inversely correlating to the size of the aldehyde molecules, a close up of the formaldehyde peak is included as well for improved visibility.

The resulting metrological parameters (linear correlation coefficient ( $R^2$ ), relative standard deviation (RSD) and method detection limits (MDL)) of the method are presented in Table 2. MDL were calculated using a detection limit coefficient of 3.3 and the standard deviation at the lowest calibration point (0.5 ppm). The detector noise was approximately 50  $\mu$ V. Assuming a rather clean water matrix, sub-ppm detection limits appear to be effortless possible with the presented method. Similar to the detector response, larger aldehyde molecules could be measured with higher precision (RSD) than their smaller counterpart formaldehyde.

Table 1: Instruments and Analytical Conditions

Instruments	Tracera & HS-20
Incubation temperature	80 °C
Incubation time	20 minutes
Agitation strength	3 (of 5)
Vial pressurization	90 kPa (relative)
Sample line temperature	150 °C
Sample volume	1 mL
Injector temperature	150 °C
Split ratio	1:3
Gas & flow speed	Helium at 60 cm/sec
Oven program time	15.25 min
Detection	Helium ionization (BID)
Detector temperature	180 °C

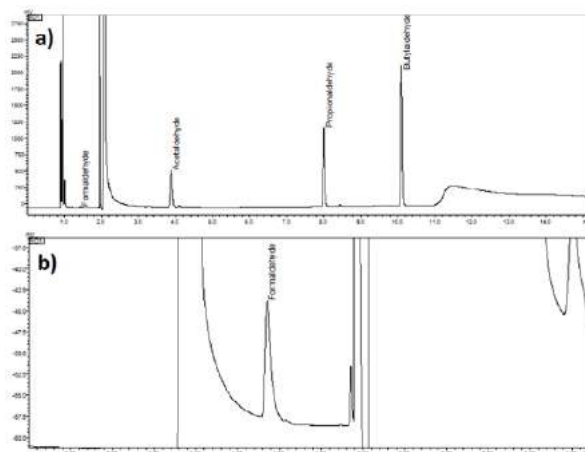


Figure 2: Chromatogram of a 10 ppm aldehyde solution (a) and a close up of the formaldehyde peak (b) from the same measurement

Table 2: Metrological parameters of the method

Compound	$R^2$	RSD (at 0.5 ppm)	MDL (ppm)
Formaldehyde	0.9992	6.6 %	0.17
Acetaldehyde	0.9998	1.5 %	0.02
Propionaldehyde	0.9997	1.3 %	0.03
Butylaldehyde	0.9988	2.3 %	0.05

## ■ Conclusion

The Tracera GC-2010 Plus with BID detection is an excellent option for the measurement of lower aldehydes without prior derivatization. It synergizes perfectly with the HS-20 automated headspace sampler, which combines utmost reproducibility of the sampling with maximum user-friendliness and reliability. The presented method is sensitive, rugged and dependable. Due to the naturally occurring background of e.g. formaldehyde in aqueous matrices, achieved detection limits can be considered top-level.

Further method optimization according to the user demands holds potential for additional improvements in time efficiency e.g. by implementation of fast-GC separation characteristics.



## Application News

No. SCA-180-019

Gas Chromatography – GC

### VDA 277: Analysis of Volatile Contaminants from Polymers

Modern vehicle interiors contain a multitude of different polymers. The car manufacturers' constant strive for an increase in product quality leads to the implementation of softer polymers, e.g. in the dash panel. Such softer materials offer an increased grip feeling and overall quality impression to the customer. Especially these softer formulations and blends containing multiple polymers at various fractions are prone to emit volatile contaminants. The latter can be inhaled by customers, leading to adverse effects on health. Emitted concentrations increase further, when polymers are subjected to higher temperatures. A typical example would be vehicles in summer under the influence of direct sunlight. The evaporated contaminants such as phthalates are frequently misunderstood as “new car smell” by customers, resulting in an underestimation of the associated risks.



Figure 1: Polymer samples in headspace vials

#### ■ Analytical methods: quality assurance

In order to avoid potential health risks for customers, car manufacturers implement various quality control procedures for estimating the contaminant emissions of individual materials. One of these procedures is described in VDA 277 [1]. This procedure uses gas chromatographic analysis with headspace sampling after thermal incubation of polymer samples in gas-tight flasks. The present study uses the GC-2010 Plus gas chromatograph with the HS-20 automated headspace sampler.

#### ■ Experimental work

Instrument calibration is carried out via calibration solutions that contain acetone in - butanol with the following concentrations: 0.1, 0.5, 1, 5, 10, 50 and 100 g/L. Individual 20 mL sample vials are spiked with 4 µL of these solutions and are immediately sealed with gas-tight screw caps that are outfitted with silicone/PTFE septa. Polymer samples are disintegrated into pieces of 10-25 mg. 2 g of these pieces are weighted into each 20 mL sample vial as shown in Figure 1.

First step of the measurement is an incubation of the samples at 120°C, either for 1 hour (calibration samples) or for 5 hours (polymer samples). During this time, the polymer samples equilibrate with their headspace (Figure 2), which denotes the gas volume that is contained inside the sample flasks alongside the solid polymer samples.

The overlapping routines of the HS-20 automated headspace sampler increase time-efficacy over the course of such long incubations by simultaneous processing of up to 12 samples. Afterwards, 1 mL of the equilibrated sample headspace gas is abstracted from the sample flask by the headspace sampler and introduced into the gas chromatograph. This is carried out via pressurized and heated flow lines and a sample loop, in which the headspace gas is precisely gauged.

Gas chromatographic separation of analytes is realized on a Restek Rtx®-Wax column (polyethyleneglycol) with an internal diameter of 0.25 mm, a coating thickness of 0.25 µm and a length of 30 m. The oven program starts at 50 °C for 3 min, proceeds to 200 °C at 12 K/min and concludes at 200°C for 4 min. Two sample chromatograms are shown in Figure 3. Peak separation is of secondary importance, since specific compounds are not analyzed individually but only altogether as a sum parameter. This makes the method very straightforward to use and improves time-efficiency in the laboratory.

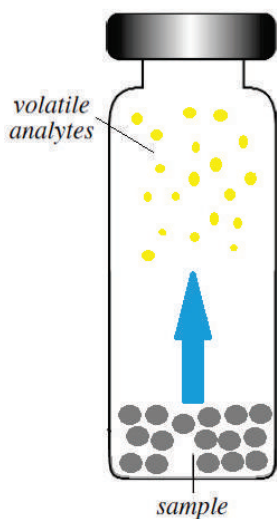


Figure 2: Polymer sample headspace equilibration

Instrument	GC-2010 Plus & HS-20
Incubation temperature	120 °C
Incubation time	5 h for samples
Agitation strength	2 (of 5)
Vial pressurization	90 kPa (relative)
Sample line temperature	200 °C
Sample volume	1 mL
Injector temperature	200 °C
Split ratio	1:20
Gas & flow speed	Helium at 27 cm/sec
Oven program time	19.5 min
Detection	Flame ionization (FID)
Detector temperature	250 °C

Table 1: Instruments and Analytical Conditions

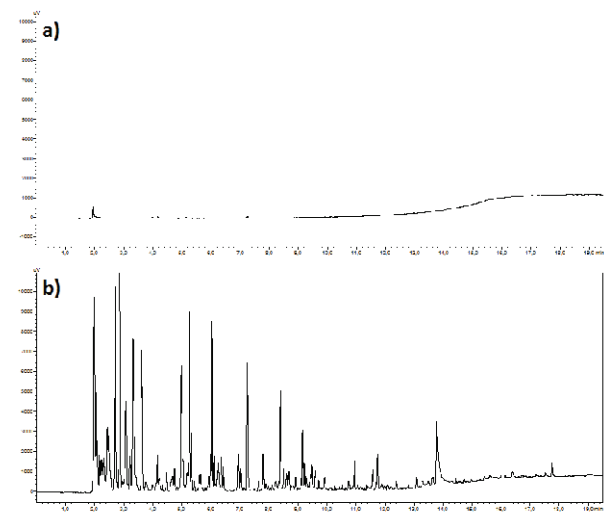


Figure 3: Chromatograms for an inconspicuous (a) (PC/ABS) and a potentially problematic sample (b) (PBT/GF) with clearly visible emissions

Further instrumental details are presented in Table 1. The resulting peak areas of the volatile contaminants are summarized and quantified into µg C per g of initial sample via the preliminary calibration. This permits a straightforward comparison of the outgassing potential of each type of polymer as shown in Figure 4. With the obtained results, potentially problematic polymers can easily be identified.

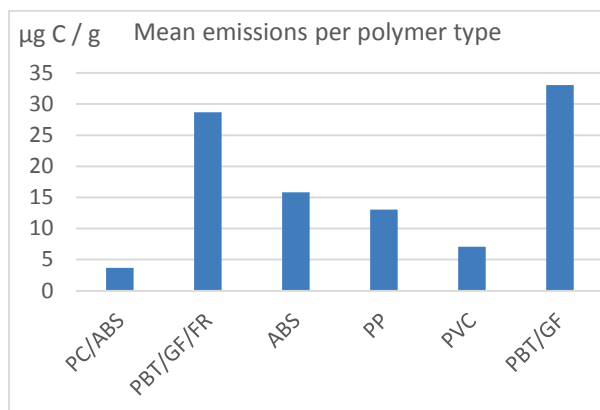


Figure 4: Results for exemplary polymer samples

## ■ Conclusion

GC-2010 Plus equipped with the HS-20 automated headspace sampler is an ideal combination for the assessment of potential outgassing of volatile contaminants from polymer materials in accordance to VDA 277. Sample preparation and analysis process are user-friendly, reliable and reproducible. The quantification of the final results is straightforward and can easily be implemented into quality control mechanisms of the manufacturers. The exemplary measurements showed two potentially problematic PBT/GF polymers blends.

Further method optimization according to the user demands holds potential for additional improvements in time efficiency e.g. by implementation of fast-GC separation columns. Identification of specific, problematic compounds is possible as well and may enable backtracking of contaminations into the production process.

## ■ References

[1] Verband der Automobilindustrie e.V. – VDA 277 (1995)

# Application Data Sheet

No. 7

## GC

Gas Chromatograph

# Simultaneous Analysis of Evolved Gas Produced by the Degradation of a Lithium-Ion Battery

In evaluating the degradation of lithium-ion rechargeable batteries, it is necessary to analyze the gases produced inside the battery. The composition of the sampled internal gases can be investigated by conveying them to a gas chromatograph. The Shimadzu Tracera High-Sensitivity Gas Chromatograph uses a revolutionary plasma technology to detect all compounds except He and Ne. The system is capable of the simultaneous analysis of C1 to C3 hydrocarbons and inorganic gases including hydrogen, so it eliminates the conventional need for carrier gas switching or combined use of multiple systems. In addition, the Tracera's high sensitivity makes it possible to analyze small quantity gas samples.

This Data Sheet introduces the simultaneous analysis of internal gases from a lithium-ion rechargeable battery utilizing the Tracera system.

## Instruments Used and Analysis Conditions

### Instruments Used

Software

GCsolution

Gas chromatograph

Tracera (GC-2010 Plus A + BID-2010 Plus)

### Analysis Conditions

Column

Micropacked ST

Column temperature

35°C(2.5min) - 20°C/min - 250°C(0min) - 15°C/min - 270°C(5.42min) Total.20min

Carrier gas controller

Pressure

Pressure program

250kPa(2.5min) – 15kPa/min – 400kPa(7.5min) (He)

Injection mode

Split (1:10)

Injection port temperature

150°C

Detector temperature

280°C

Discharge gas volume

70mL/min

Injection volume

50μL

## Results

### Analysis of Internal Gases from a Lithium-Ion Rechargeable Battery

Fig. 1 shows the chromatogram for the internal gases from a lithium-ion rechargeable battery. It is evident that the system is capable of the simultaneous analysis of C1 to C3 hydrocarbons and inorganic gases including hydrogen. The concentration ratios (%) for each component excluding oxygen and nitrogen are shown.

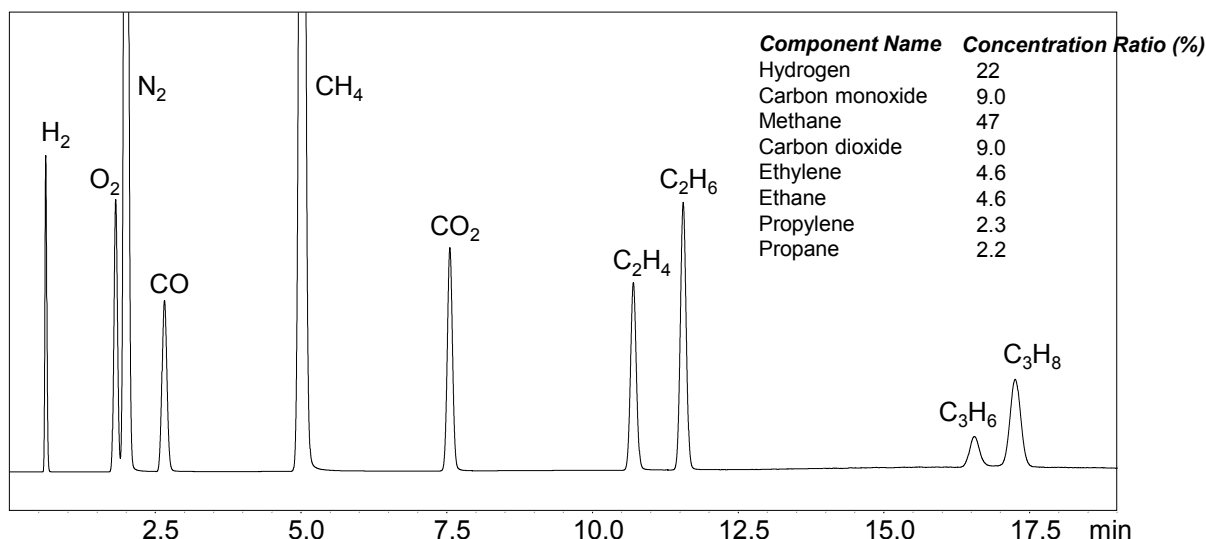


Fig. 1: Chromatogram for the Internal Gases from a Lithium-Ion Rechargeable Battery

Note: With baseline calibration



Linearity for each component of the standard gas was confirmed. The concentration values for each component are shown in Table 1, and the chromatograms and calibration curves for each component are shown in Fig. 2.

Table 1: Concentrations for Each Component

Component name	Concentration (%)			
Hydrogen	0.962	1.92	2.89	4.81
Carbon monoxide	0.404	0.808	1.21	2.02
Methane	2.08	4.16	6.24	10.4
Carbon dioxide	0.412	0.824	1.24	2.06
Ethylene	0.204	0.408	0.612	1.02
Ethane	0.204	0.408	0.612	1.02
Propylene	0.102	0.205	0.307	0.512
Propane	0.101	0.202	0.303	0.505

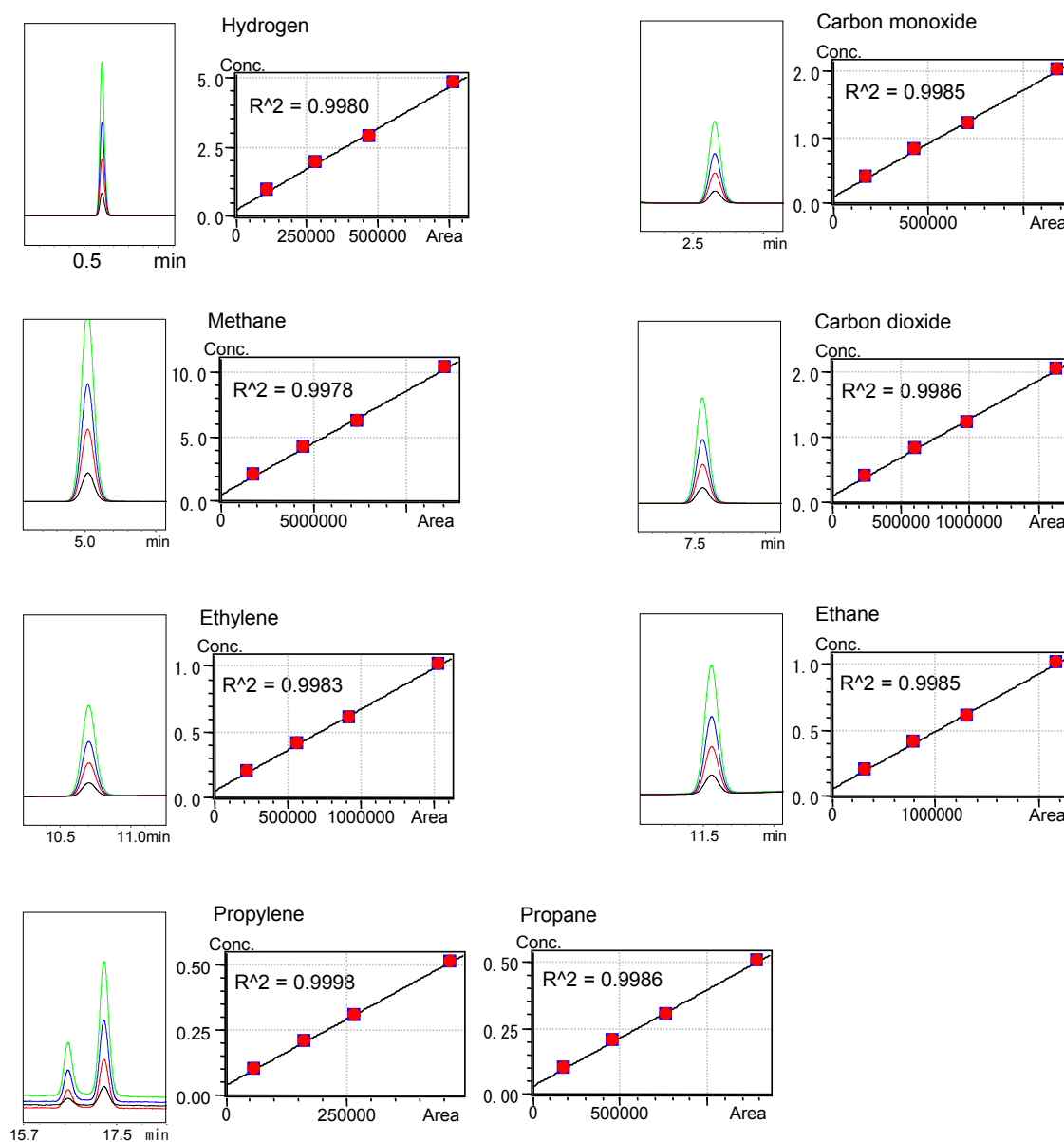


Fig. 2: Linearity for Each Component

First Edition: March, 2013



Shimadzu Corporation

www.shimadzu.com/an/

For Research Use Only. Not for use in diagnostic procedures.

The content of this publication shall not be reproduced, altered or sold for any commercial purpose without the written approval of Shimadzu. The information contained herein is provided to you "as is" without warranty of any kind including without limitation warranties as to its accuracy or completeness. Shimadzu does not assume any responsibility or liability for any damage, whether direct or indirect, relating to the use of this publication. This publication is based upon the information available to Shimadzu on or before the date of publication, and subject to change without notice.

© Shimadzu Corporation, 2013

# Application Data Sheet

No.3

## GC

Gas Chromatography

# Analysis of Diesel Oil Samples in Compliance with ASTM D2887 Using the Shimadzu Simulated Distillation Gas Chromatograph System

In the ASTM D2887 test method, petroleum products with a boiling point range of 538 °C (C44 or equivalent) or lower are analyzed by GC system utilizing the total area method.

The Shimadzu GC-2010 Plus based distillation gas chromatograph system with LabSolutions software is compliant with ASTM D2887, and combines comfortable operability with high-level functionality.

This data sheet introduces an example of the simulated distillation GC analysis of diesel oil in compliance with ASTM D2887, utilizing the Shimadzu simulated distillation gas chromatograph system.

## Instruments Used and Analysis Conditions

### Instruments Used

#### Software

LabSolutions Distillation GC Analysis Software

#### Gas chromatograph

GC-2010 Plus AF

#### Direct injection unit

WBI-2010

#### Auto injector

AOC-20i

### Analysis Conditions

#### Column

BPX 1-Sim Dist 0.53 mm ×10 m, 0.9 μm

#### Column temperature

35 °C - 15 °C /min - 350 °C (5 °C)

#### Carrier gas flow rate

7 mL/min (helium)

#### Injection port temperature

350 °C

#### FID temperature

380 °C

#### Makeup gas flow rate

30 mL/min

#### Hydrogen flow rate

40 mL/min

#### Air flow rate

400 mL/min

#### Injection volume

0.4 μL

## Results

### 1. Analysis of Standard Solutions for Calibration

Two standard solutions were measured, one a mixture of n-C5 to n-C10, and one a mixture of everything from n-C10 to n-C44.

Fig. 1 shows a chromatogram consisting of an overlay of the two data sets.

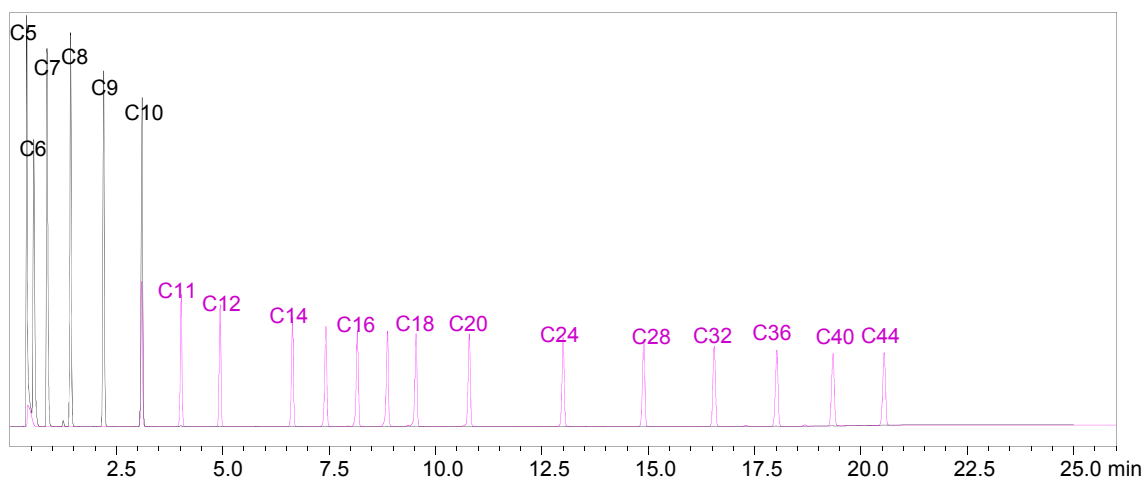


Fig. 1: Chromatogram of the Standard Solutions for Calibration

## 2. Analysis of the Diesel Oil Sample

Fig. 2 shows the chromatogram for the diesel oil.

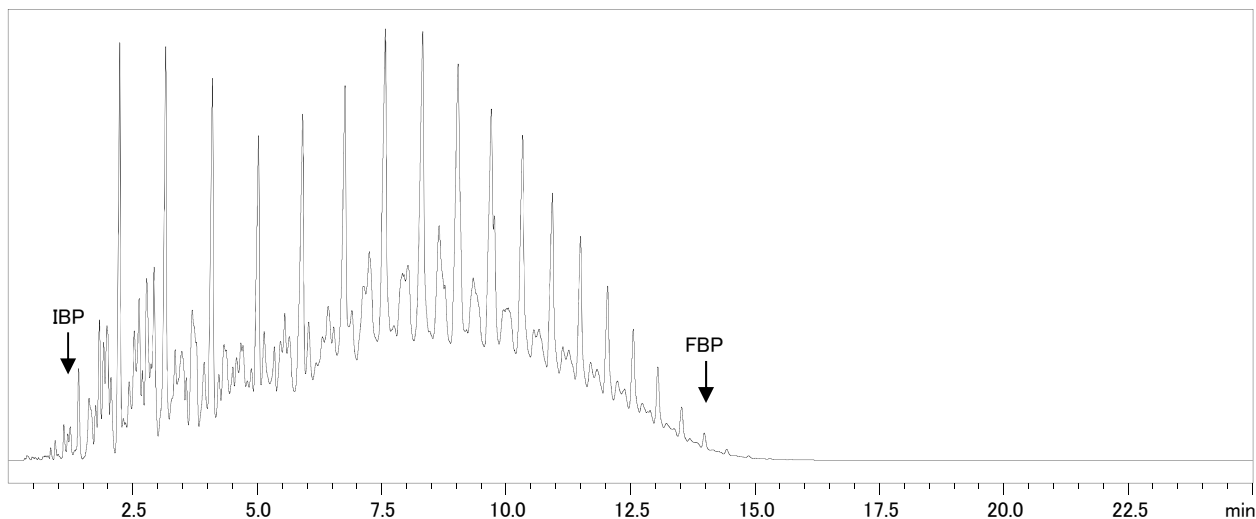


Fig. 2: Diesel Oil Chromatogram

The ASTM reference gas oil (Lot 2) was measured, the distillation characteristics were calculated, and a comparison was made with the standard values provided with the reference gas oil (Table 1). The Shimadzu distillation gas chromatograph system amply met the criterion for inter-laboratory parallel tolerance specified by ASTM D2887, and demonstrated favorable inter-laboratory repeatability.

The respective distillation characteristic curves are shown in Fig. 3. With the LabSolutions distillation GC analysis software, it is possible to display a comparison of distillation characteristic curves for up to 16 samples, simplifying everyday product data management and comparisons with previously accumulated data.

Table 1: Distillation Characteristics for ASTM D2887 Reference Gas Oil (Lot 2)

Distillate volume (mass %)	Standard Diesel Oil Standard Value	Standard Diesel Oil Measured Value	Difference (Measured Value – Standard Value)	Inter-Laboratory Parallel Tolerance
IBP	115	114	-1.3	7.6
5	151	151	0.2	3.8
10	176	175	-0.8	4.1
15	201	201	-0.5	4.5
20	224	224	0.0	4.9
25	243	244	0.5	-
30	259	260	0.7	4.7
35	275	275	0.2	-
40	289	290	0.9	4.3
45	302	304	1.7	-
50	312	313	1.2	4.3
55	321	323	1.5	-
60	332	333	1.4	4.3
65	343	344	1.1	-
70	354	355	0.8	4.3
75	365	367	1.7	-
80	378	379	1.0	4.3
85	391	393	1.5	-
90	407	408	0.7	4.3
95	428	429	1.2	5.0
FBP	475	474	-0.9	11.8

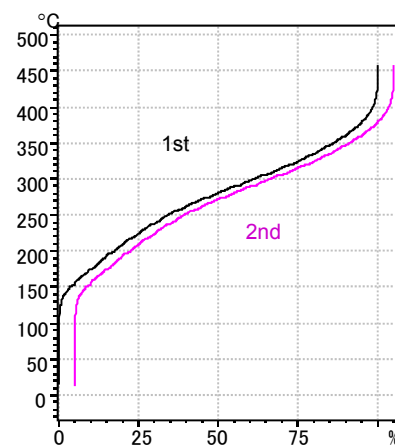


Fig. 3: Distillation Characteristic Curves  
For comparison, the second is shown shifted.

# Application Data Sheet

No.5

## GC

Gas Chromatography

# Analysis of Lubricant Oil Samples in Compliance with ASTM D7500 Using the Shimadzu Simulated Distillation Gas Chromatograph System

The ASTM D7500 test method describes the analysis of base stock oil and lubricant oil with an initial boiling point of 100 °C or higher and a final boiling point of 735 °C or lower (C110 or equivalent) analyzed by a simulated distillation GC system using the total area method. The Shimadzu GC-2010 Plus based simulated distillation gas chromatography system is compliant with ASTM D7500, and combines comfortable operability with high-level functionality.

This data sheet describes the simulated distillation GC analysis of lubricant oil in compliance with ASTM D7500 using the Shimadzu simulated distillation gas chromatograph.

## Instruments Used and Analysis Conditions

### Instruments Used

Software	LabSolutions Distillation GC Analysis Software
Gas chromatograph	GC-2010 Plus AF
On-column injection unit	OCI/PTV-2010
Auto injector	AOC-20i

### Analysis Conditions

Column	UA-SIMDIS (HT) 0.53 mm × 5 m, 0.1 μm
Column temperature	35 °C - 10 °C /min - 440 °C (4.5 min)
Carrier gas flow rate	35 mL/min (helium)
Injection port temperature	100 °C - 50 °C /min - 440 °C (38.2 min)
FID temperature	450 °C
Makeup gas flow rate	30 mL/min
Hydrogen flow rate	40 mL/min
Air flow rate	400 mL/min
Injection volume	1 μL

## Results

### 1. Analysis of Standard Solution for Calibration

Fig. 1 shows the chromatogram for the standard solution, a mixture of n-C12 to n-C-28, C-40 and Polywax655. n-C110, which has a very high boiling point, was eluted as the column temperature was rising.

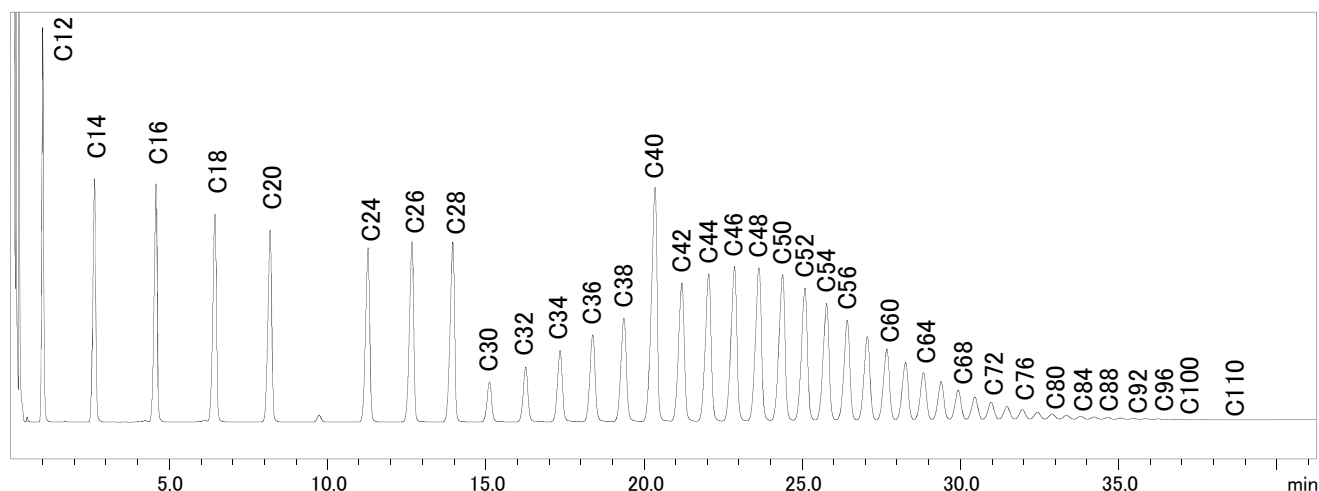


Fig. 1: Chromatogram of the Standard Solution for Calibration



2. Analysis of the Lubricant Oil Sample

Fig. 2 shows the chromatogram for the lubricant oil (used for construction equipment and drivers).

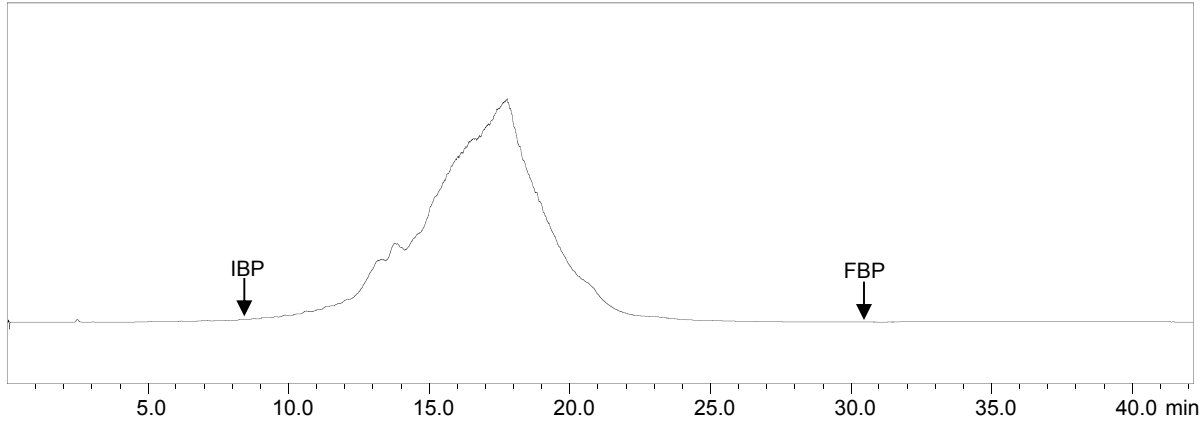


Fig. 2: Lubricant Oil Chromatogram

The reference oil 5010 was repeatedly measured five times, and repeatability was confirmed. Its chromatograms are shown in Fig. 3. The distillation characteristic curves are shown in Fig. 4. The FBP (final boiling point) relative standard deviations (RDS%) are shown in Table 1. Favorable repeatability was obtained even for the high boiling point components.

With the LabSolutions distillation GC analysis software, it is possible to display a comparison of distillation characteristics curves for up to 16 samples, simplifying everyday product data management and comparisons with previously accumulated data.

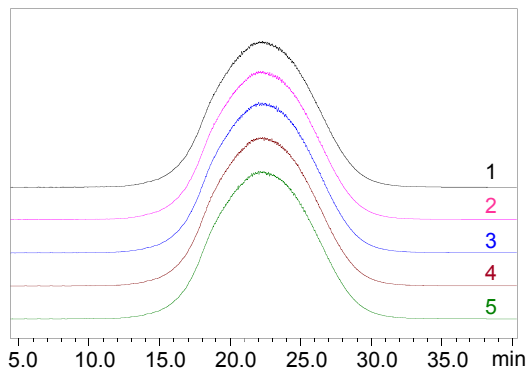


Fig. 3: Reference Oil 5010 Chromatogram

	FBP (°C)
1	643.4
2	644.4
3	642.8
4	643.1
5	643.1
Ave.	643.4
SD	0.619
RSD (%)	0.096

Table 1: FBP (Final Boiling Point) Repeatability (n=5)  
Equivalent to the boiling point of n-paraffin with a carbon number of 73

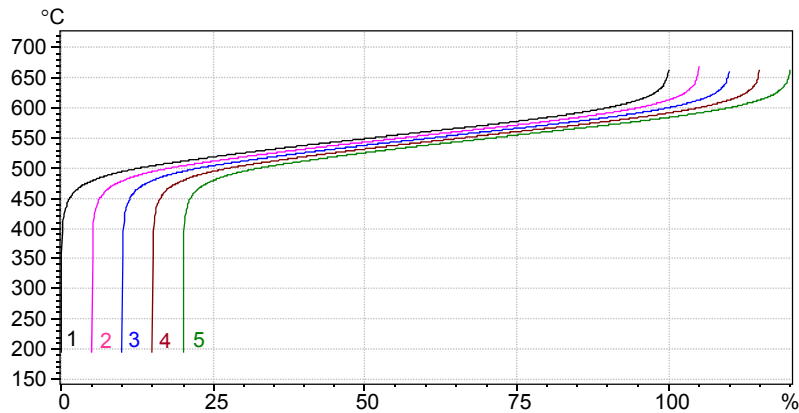


Fig. 4: Distillation Characteristics Curves  
For comparison, the distillation characteristic curves have been shown shifted.

First Edition: December, 2012



## Application News

### No. G283

#### Gas Chromatography

### Trace Impurity Analysis of Hydrogen Fuel in Fuel Cell Vehicle-Related Fields

With the development of fuel cell technology for electricity generation using hydrogen (H) as fuel, attention is turning to household fuel cell systems and fuel cell vehicles. However, one of the problems associated with fuel cells in their current state is the presence of carbon monoxide (CO) in the hydrogen fuel used in the fuel cells. Carbon monoxide adversely affects the performance of the catalyst used in the battery. This phenomenon is referred to as "catalyst poisoning," and therefore necessitates the use of high-purity hydrogen fuel. The international standard (ISO 14687-2) pertaining to hydrogen fuel for fuel cell vehicles, which went into effect in 2012, specifies that, in addition to a maximum concentration of 0.2 ppm carbon monoxide in the hydrogen, maximum concentrations are also specified for oxygen (O) and carbon dioxide (CO<sub>2</sub>) as well as hydrocarbons. In the past, analysis of impurities in hydrogen conventionally required a complex system including multiple detectors and columns, which from the standpoint of cost and maintenance, posed a significant hurdle.

The barrier discharge ionization detector (BID) is a new, universal detector that can detect almost all components, except helium (He, used as the plasma gas) and neon (Ne), with higher sensitivity than that obtained using TCD and FID detectors. This Application News introduces an example of high-sensitivity analysis of carbon monoxide in hydrogen and simultaneous analysis of impurities in hydrogen using the Tracera high-sensitivity gas chromatograph equipped with a BID detector.

#### ■ High-Sensitivity Analysis of Carbon Monoxide Using the Rt-Msieve 5A Column

Molecular sieve 5A columns offer good separation of air components and carbon monoxide, and are a suitable type of column for the analysis of carbon monoxide.

First, a standard gas was diluted with hydrogen to adjust the concentration of each component (excluding air components) to about 0.2 ppm, and measurement of the gas was then conducted using the Rt-Msieve 5A column.

The chromatogram is shown in Fig. 1, and the analytical conditions are shown in Table 1. The lower limit of detection (S/N=3) of carbon monoxide was then calculated as 0.032 ppm.

**Table 1 Analytical Conditions for Trace Impurities in Hydrogen (Rt-Msieve 5A column)**

Model	: Tracera (GC-2010 Plus + BID-2010 Plus)
Column	: RESTEK Rt-Msieve 5A (30 m × 0.53 mm I.D., df = 50 μm) with Particle Trap 2.5 m
Column Temp.	: 35 °C (2.5 min) → 20 °C/min → 250 °C → 15 °C/min → 270 °C (3.42 min)
Inj. Mode	: Split 1:7
Carrier Gas Controller	: Constant linear velocity mode (He)
Linear Velocity	: 45 cm/sec
Det. Temp.	: 280 °C
Discharge Gas	: 50 mL/min (He)
Inj. Volume	: 3 mL

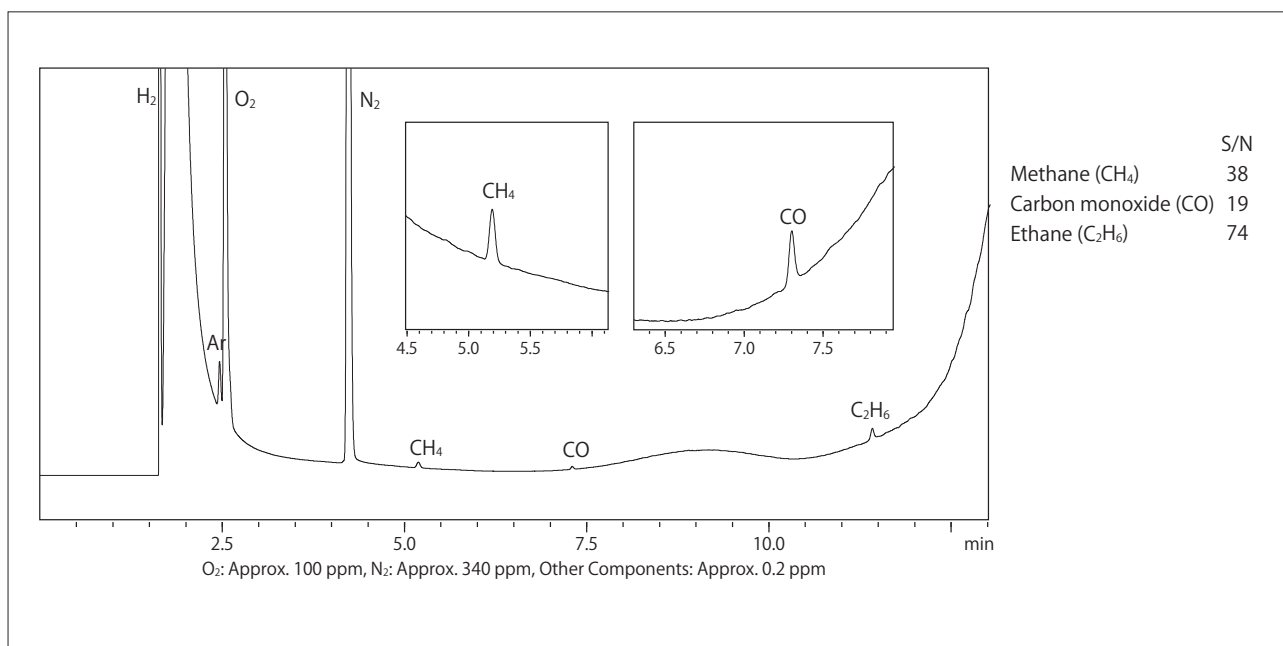


**Fig. 1 Chromatogram of Trace Impurities in Hydrogen (Rt-Msieve 5A Column)**

## ■ Simultaneous Analysis of Impurities in Hydrogen Using the Micropacked ST Column

As carbon dioxide does not elute with the Rt-Msieve 5A column, a different system is required for analysis when carbon dioxide is among the target substances. The Micropacked ST column supports separation of inorganic gasses, including carbon dioxide and lower hydrocarbons, making it suitable for simultaneous analysis of impurities in hydrogen gas.

A standard gas was diluted with hydrogen to adjust the

component concentrations (other than air components) to about 0.2 ppm, and this gas was analyzed using the Micropacked ST column.

The resultant chromatogram is shown in Fig. 2, and the analytical conditions are shown in Table 2. The lower limit of detection of carbon monoxide was calculated as 0.078 ppm (S/N=3). Though not as good as those obtained with the Rt-Msieve 5A column, the results include detection of the maximum concentration stipulated by ISO 14687-2.

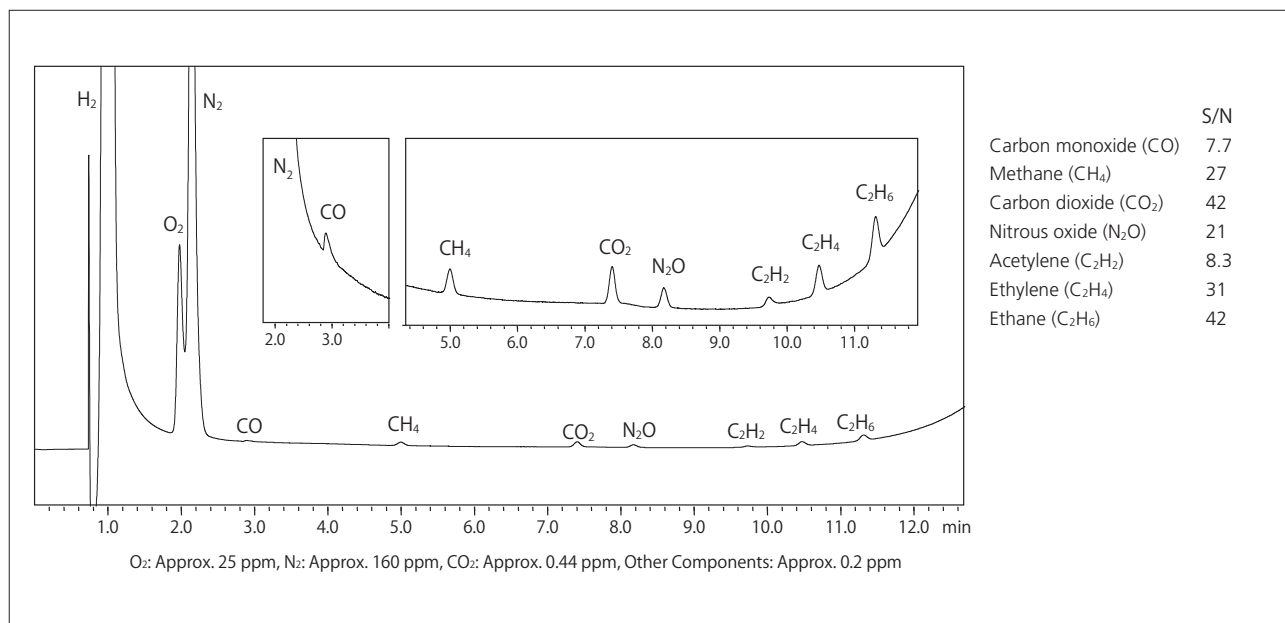


Fig. 2 Chromatogram of Simultaneous Analysis of Impurities in Hydrogen (Micropacked ST Column)

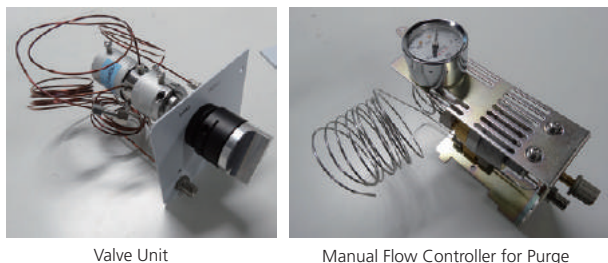
Table 2 Analytical Conditions for Simultaneous Analysis of Impurities in Hydrogen (Micropacked ST Column)

Model	: Tracera (GC-2010 Plus + BID-2010 Plus)
Column	: Micropacked ST (2 m × 1 mm I.D.)
Column Temp.	: 35 °C (2.5 min) → 20 °C/min → 250 °C → 15 °C/min → 265 °C (3 min)
Inj. Mode	: Split 1:4
Carrier Gas Controller	: Pressure mode (He)
Pressure Program	: 226.8 kPa (2.5 min) - 15 kPa/min - 400 kPa (3.2 min)
Det. Temp.	: 280 °C
Discharge Gas	: 50 mL/min (He)
Inj. Volume	: 3 mL

In this analysis, the MGS-2010 gas sampler was used for the introduction of gas into the instrument; the column was connected using the SPLITTER-INJ (P/N: 221-76252-41).

The MGS-2010 is a manual gas sampler for the Tracera (GC-2010 Plus). A purge mechanism is included to reduce the leakage of peripheral air into the system. The SPLITTER-INJ refers to a special injection unit that permits split injection of the sample without requiring that it pass through the standard split/splitless injection unit.

Using the MGS-2010 for sample gas injection together with the SPLITTER-INJ unit, it is possible to quantitatively analyze trace level air components, including Oxygen (O<sub>2</sub>), Nitrogen (N<sub>2</sub>), etc., with high accuracy.



Valve Unit

Manual Flow Controller for Purge

Fig. 3 MGS-2010 Gas Sampler



# 1. Chromatography

---

## 1.2 Liquid Chromatography (LC)

---

By separating and detecting target substances, HPLC and UHPLC systems are able to quantitatively analyze compounds in mixtures containing multiple ingredients. Both methods are also used to purify specific substances once they have been separated. Prominence series HPLC Aldehyde Analysis Systems analyze aldehydes such as formaldehyde that are generated from interior materials, e.g. seats. Aldehydes are analyzed after 2,3-DNPH derivatization.

**L482**

Analysis of polystyrene with antioxidant additive using Prominence-i GPC system



# Application News

## No.L482

### High Performance Liquid Chromatography

## Analysis of Polystyrene with Antioxidant Additive Using Prominence-i GPC System

Gel permeation chromatography (GPC) for the analysis of hydrophobic polymers has traditionally been conducted using a differential refractive index detector. However, when UV-absorbing trace-level additives are present along with the principal synthetic polymer component, these are sometimes analyzed using a UV detector or photodiode array detector (PDA) for high-sensitivity detection. However, a combination of a differential refractive index detector and UV detector makes it possible to conduct simultaneous analysis of the principle component along with any trace-level additives, and further, permits calculation of the molecular weight distribution of the polymer, confirmation of the UV spectra of minor components, and quantitation based on the calibration curve and qualitative analysis results.

The new Prominence-i integrated high-performance liquid chromatograph supports connection with the RID-20A differential refractive index detector. In addition, as the column oven can house up to three 30 cm columns used for GPC analysis, applications that require a long column are also supported.

Here, we introduce an example of GPC analysis of polystyrene using the Prominence-i GPC system.

### ■ GPC Analysis of Polystyrene with Antioxidant

Various types of additives, including plasticizers, antioxidants, lubricants, vulcanization accelerators and flame retardants, are generally added to polymers. This Application News presents an analysis of Irganox 1010, a typical hindered phenolic antioxidant which is added in small amounts to polystyrene (PS). Fig. 1 shows the analytical results obtained using a 5  $\mu$ L injection of the additive-containing PS (5 g/L), Fig. 2 shows the spectrum of Irganox 1010, obtained using the PDA detector incorporated in the Prominence-i, and Table 1 shows the analytical conditions used for the analysis. The KF-804L analytical column, which permits generation of a linear calibration curve, was used with the stabilizer-free tetrahydrofuran (THF) mobile phase.

As shown in Fig. 1, the Irganox 1010 peak was detected directly after PS, which eluted at about 7.5 minutes. The additive peak, which was barely detected by the differential refractive index detector, was detected with high sensitivity by the PDA detector by optimizing the detection wavelength, thereby permitting quantitation. Also, as shown in Fig. 2, qualitative analysis of Irganox 1010 is possible using the UV spectrum obtained using the PDA detector.

**Table 1 Analytical Conditions**

Column	: Shodex KF-804L (300 mm L $\times$ 8 mm I.D.)
Mobile Phase	: THF (without stabilizer)
Flowrate	: 1.0 mL/min
Column Temp.	: 40 $^{\circ}$ C
Injection Volume	: 5 $\mu$ L
Detection (PDA)	: 230 nm
Flow Cell	: Integrated Conventional Cell
Detection (RI)	: RID-20A
Polarity +, Cell temp. 40 $^{\circ}$ C, Response 1.0 sec	

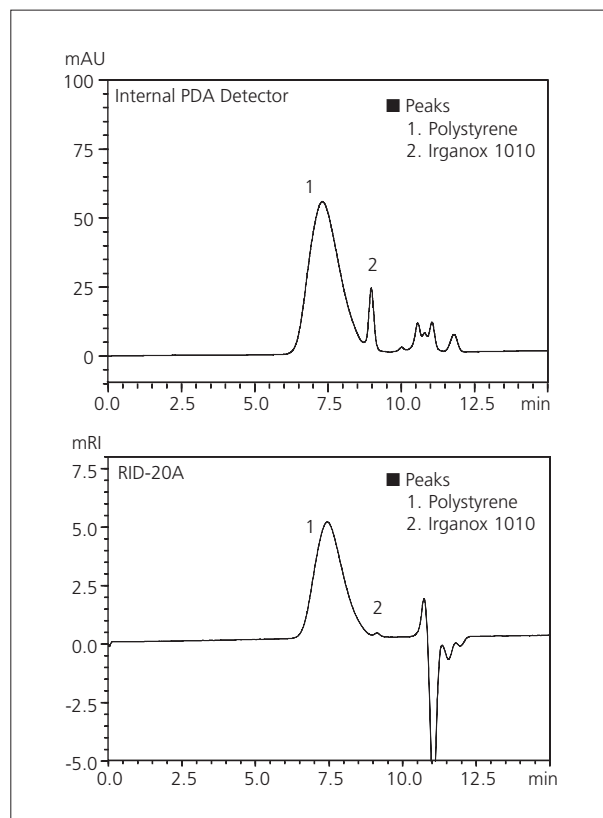


**Fig. 1 Chromatograms of Polystyrene (PS) with Antioxidant (5 g/L, 5  $\mu$ L Injected)**  
Upper: Internal PDA Detector  
Lower: RID-20A Detector

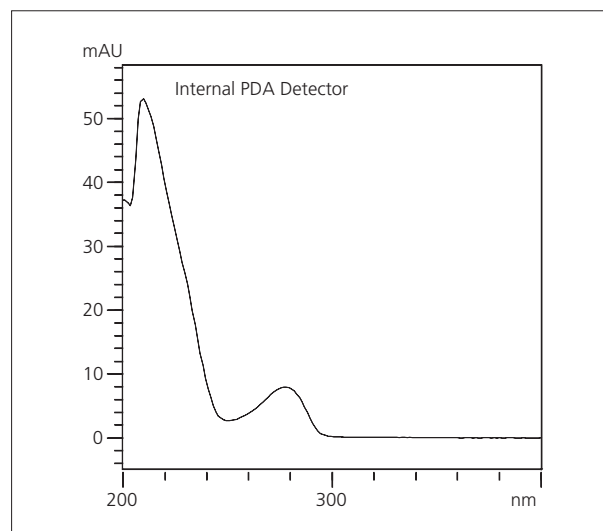


**Fig. 2 Spectrum of Irganox 1010**

### ■ Calibration Curve

Fig. 3 shows the calibration curve of PS that was generated using the analytical conditions of Table 1. Here, a column that would provide a linear calibration curve was selected. The generated calibration curve shows excellent linearity over a molecular weight range of 3,950 to 197,000, with a coefficient of determination greater than  $R^2=0.999$ .

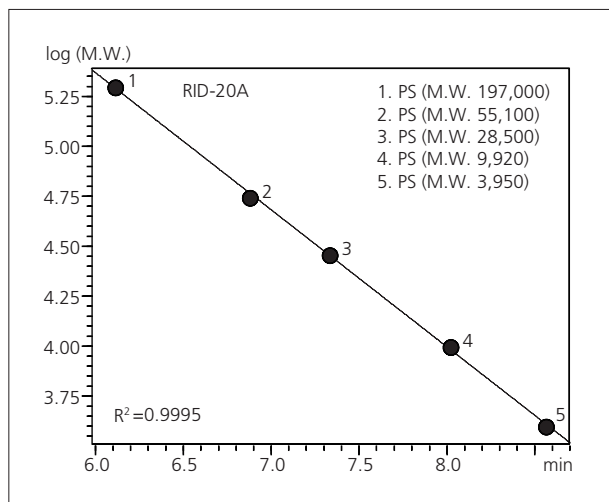


Fig. 3 Calibration Curve for PS (M.W. 3,950 – 197,000, 5  $\mu$ L Injected)

### ■ Linearity and Quantitation

Fig. 5 shows the calibration curve of Irganox 1010 analyzed using the conditions of Table 1. The calibration curve, generated over a concentration range of 10 to 100 mg/L, shows excellent linearity with a coefficient of determination greater than  $R^2=0.999$ .

From this calibration curve, the content of Irganox 1010 of Fig. 1 was calculated to be 10.8 mg/g of polystyrene (PS).

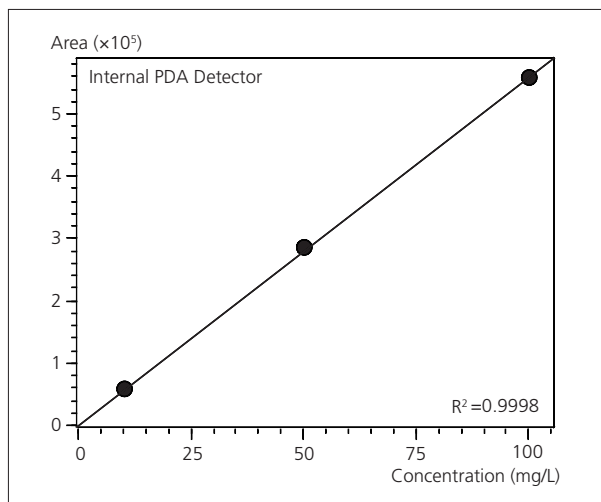


Fig. 5 Calibration Curve for Irganox 1010 (10 – 100 mg/L, 5  $\mu$ L Injected)

### ■ Distribution of Molecular Weight

Fig. 4 shows the molecular weight distribution curve for the additive-containing PS using the analytical conditions of Table 1. The black-colored trace plots the molecular weight data as a differential curve, and the blue-colored trace plots that data as an integral curve. The weight-average molecular weight (Mw) and number-average molecular weight (Mn) were 26078 and 15422, respectively. In this case, the molecular weight distribution (polydispersity: Mw/Mn) was about 1.69.

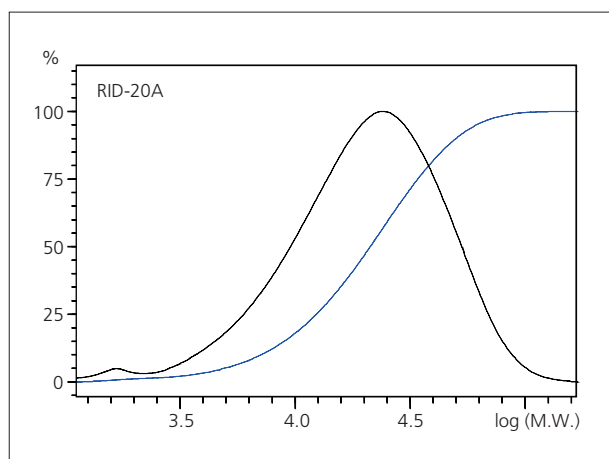
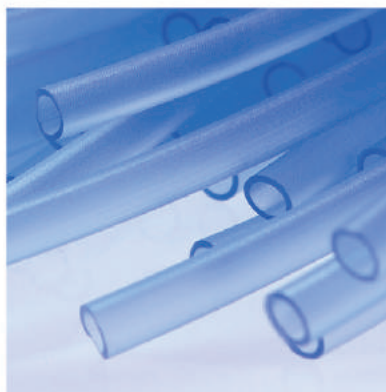


Fig. 4 Molecular Weight Distribution Curve for PS (5 g/L, 5  $\mu$ L Injected)  
Black Line: Differential Curve  
Blue Line: Integral Curve

#### [Precautions]

- 1) Plumbing and fittings from the column out were all changed to SUS (stainless steel).
- 2) The needle seal (at autosampler) was replaced with a Vespel® needle seal.
- 3) The automatic rinse kit is not used.

## 2. Mass Spectrometry





## 2. Mass Spectrometry

---

### 2.1 Gas Chromatography-Mass Spectrometry (GC-MS)

---

GC-MS is a hyphenated technique combining the separating power of gas chromatography (GC) with the detection power of mass spectrometry (MS) to identify different substances within a sample. Mass spectrometry is a wide-ranging analytical method which involves the production, subsequent separation and identification of charged species according to their mass to charge ( $m/z$ ) ratio.

<b>No. 38</b>	Analysis of automobile cabin air by thermal desorption GC-MS using the OPTIC-4 multimode inlet
<b>No. 47</b>	Analysis of brominated flame retardants and phthalate esters in polymers under the same conditions using a pyrolysis GC-MS system (1)
<b>No. 48</b>	Analysis of brominated flame retardants and phthalate esters in polymers under the same conditions using a pyrolysis GC-MS system (2)
<b>No. 67</b>	Analysis of brominated flame retardants and phthalate esters in polymers under the same conditions using a pyrolysis GC-MS system(4)
<b>No. 110</b>	Analysis of phthalate esters using the py-screener (1)
<b>No. 111</b>	Analysis of phthalate esters using the py-screener (2)
<b>C146-E303</b>	Comparison of screening method (Py-GC/MS) and quantitative method (Solvent Extraction–GC/MS) for phthalate esters analysis
<b>ThP 138</b>	Determination of volatile organic compounds (VOCs) present in the interiors of car by using GCMS/MS with static and dynamic headspace
<b>SCA_280_081</b>	Analysis of VOC and FOG emissions from moulded components for automobiles according to VDA 278
<b>MP 283</b>	Development of automated screening and quantitation approach on novel on-line SFE-SFC-MS/MS platform – (I) for 23 restricted perurocompounds in textiles
<b>No. 123</b>	Py-GC/MS analysis of electronic circuit board parts using nitrogen carrier gas
<b>TP 782</b>	Rapid analysis of carbon fiber reinforced plastic using DART-MS

# Application Data Sheet

## No.38

### GCMS

Gas Chromatograph Mass Spectrometer

## Analysis of Automobile Cabin Air by Thermal Desorption GC-MS Using the OPTIC-4 Multimode Inlet

The OPTIC-4 is a multimode injection system with a thermal desorption function that enables performing thermal desorption by placing a Tenax sorbent tube in the injection port liner cup. Direct heating technology enables rapidly heating samples at rates up to 16 °C per second, and introducing samples directly into the analytical column without passing them through a transfer line. This means samples can be analyzed with high sensitivity without loss of high-boiling-point or high-adsorptivity components. This datasheet shows the results where volatile organic compounds in automobile cabin air were adsorbed using Tenax TA (2,6-diphenyl-p-phenylene oxide), a sorbent material commonly used for atmospheric analysis, and analyzed by TD-GC-MS.

### Experiment

#### Air Sampling

A tube filled with Tenax TA 60/80 mesh was placed in the SP208-100Dual II air sampling pump, which was used to sample the air within the automobile cabin for 30 minutes at 100 mL/min (3 L).

#### Analysis

The Tenax tube with collected air sample was placed in the OPTIC-4 inlet, which injected the sample into the GC-MS unit by thermal desorption.



Air Sampling Pump  
SP208-100 Dual II  
(Manufactured by GL Sciences  
Inc.)



Sorbent Tube  
(Tenax TA 60/80 )

Table 1: Analysis Conditions

#### [Sampling condition]

Room temperature : Ave. 27.5 °C  
Humidity : Ave. 33.5 %RH  
Collection amount : 3 L (100 mL/min, 30min)  
Collector : SP208-100Dual II  
Sampling tube : Tenax TA 60/80

#### [Instruments]

Injection(TD) : OPTIC-4 (ATAS GL International BV, Eindhoven, the Netherlands)  
GC-MS : GCMS-QP2010 Ultra (Shimadzu).  
Column : InertCap 1MS 0.25 mm × 60 m, df = 0.25 µm (GL Sciences, Inc , Japan)

#### [TD]

Thermal desorption temperature : 40 °C → (5 °C/ min) → 270 °C  
Thermal desorption time : 10min  
Cryofocus temperature : -130 °C  
Cryoinjection temperature : 270°C  
Carrier gas : He  
Column flow rate : 1 mL/min  
Split ratio : 1:5

#### [MS]

Interface temperature : 280°C  
Ion source temperature : 200°C  
Solvent elution time : 2.5 min  
Data sampling time : 3 – 40min  
Measuring mode : SCAN  
Mass range : 35-450 m/z  
Detector voltage : 0.7 kV  
(absolute value)

#### [GC]

Column oven temperature :  
40°C (5min) → (10 °C /min) → 280 °C(11min)



## Results and Discussion

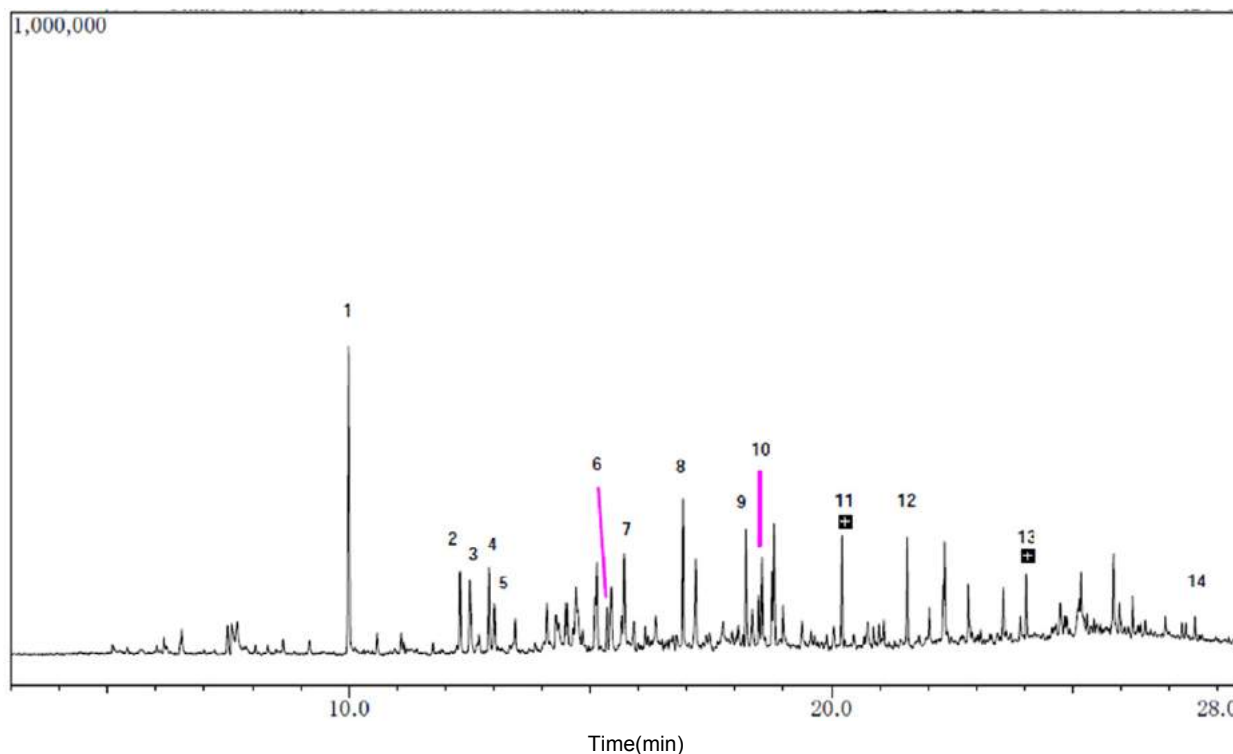


Fig. 1: TD-GC-MS Chromatogram

- |                      |                                |
|----------------------|--------------------------------|
| 1. Toluene           | 8. Nonanal                     |
| 2. Ethylbenzene      | 9. Menthol                     |
| 3. m-,p-Xylene       | 10. Decanal                    |
| 4. Styrene           | 11. Tridecane (C13)            |
| 5. o-Xylene          | 12. Tetradecane (C14)          |
| 6. p-Dichlorobenzene | 13. Hexadecane (C16)           |
| 7. 2-Ethyl-1-hexanol | 14. Di-n-butyl phthalate (DBP) |

## Summary

A measurement of the cabin air in a used car detected toluene, ethylbenzene, xylene, styrene, paradichlorobenzene, nonanal, tetradecane, and other substances for which the Japanese Ministry of Health, Labour and Welfare have issued guideline values. Furthermore, since automobile interiors can become very hot, dibutyl phthalate, which is one of the phthalate esters used as plasticizers in plastics, was also detected.

The OPTIC-4 does not produce a cold point when samples are injected into the column after thermal desorption and, as a multimode inlet with a thermal desorption function, it is capable of handling components with either high or low boiling points. Therefore, in addition to being used for measuring automobile cabin air, as in the above example, it can also be used for a wide range of other applications that involve measuring trace substances in the atmosphere.



# Application Data Sheet

No.47

## GC-MS

Gas Chromatograph - Mass Spectrometer

### Analysis of Brominated Flame Retardants and Phthalate Esters In Polymers Under the Same Conditions Using a Pyrolysis GC-MS System (1) – PBBs and PBDEs –

In recent years, an analysis method is required to determine not only polybrominated biphenyls (PBBs) and polybrominated diphenyl ethers (PBDEs), which are regulated under the RoHS Directive, but also phthalate esters and other brominated flame retardants not governed by the directive (such as tetrabromobisphenol A, hexabromocyclododecane, and bis(pentabromophenyl)ethane). The method was developed to analyze those compounds under the same analytical conditions using EGA/PY-3030D Multi-Shot Pyrolyzer and GCMS-QP2020 Ultra systems. This Application Data Sheet shows the results from analyzing the brominated flame retardants PBB and PBDE using the developed method.

#### Analytical Conditions

Polyethylene and polypropylene samples containing brominated flame retardants (ERM®-EC590 and ERM®-EC591, respectively) were used as evaluating samples. 0.5 mg of shavings from each sample was measured. FASST (Fast Automated Scan/SIM Type), which is capable of simultaneous Scan and SIM measurements, was used as the measurement mode. Table 1 shows the analysis conditions and Fig. 1 shows the SIM measurement program.

Table 1: Analytical Conditions

Pyrolysis Instrument	:EGA/PY-3030D Multi-Shot Pyrolyzer		
GC-MS	:GCMS-QP2010 Ultra		
Column	:Ultra ALLOY-PBDE [15 m length, 0.25 mm I.D., df = 0.05 µm]		
[Pyrolyzer]			
Pyrolysis Furnace Temp.	:200 °C → (20 °C/min) → 300 °C → (5 °C/min) → 340 °C (1 min)		
Interface Temp.	:Manual (300 °C)		
[GC]		[MS]	
Injection Temp.	: 320 °C	Interface Temp.	:320 °C
Column Oven Temp.	:80 °C → (20 °C/min) → 300 °C (5 min)	Ion Source Temp.	:230 °C
Injection Mode	:Split	Solvent Cut Time	:0.5 min
Carrier Gas	:Helium	Tuning Mode	:Normal
Flow Control Mode	:Constant linear velocity (52.1 cm/sec)	Measurement Mode	:FASST (simultaneous Scan/SIM measurements)
Purge Flow Rate	:3.0 mL/min	Scan Mass Range	:m/z 50 - 1000
Split Ratio	:50	Scan Event Time	:0.15 sec
		Scan Speed	:10,000 u/sec
		SIM Monitoring m/z:	See Fig. 2.
		SIM Event Time	:0.3 sec
		SIM Micro-Scan Width	:0.5 u

1 min	Group 1 (No. of m/z channels: 21)	10 min	Group 2 (No. of m/z channels: 11)	16 min
	Tetra-BDE (m/z 325.9, 483.7) Penta-BDE (m/z 403.8, 563.6) Hexa-BDE (m/z 483.7, 641.5) Hepta-BDE (m/z 563.6, 721.4) Tetrabromobisphenol A [TBBPA] (m/z 528.7, 543.7) Hexabromocyclododecane [HBCDD] (m/z 319.1, 560.6) Diisobutyl phthalate [DIBP] (m/z 149.0, 205.1, 223.1) Di-n-butyl phthalate [DIBP] (m/z 149.0, 205.1, 223.1) Benzylbutyl phthalate [BBP] (m/z 91.0, 149.0, 206.1) Bis(2-ethylhexyl) phthalate [DEHP] (m/z 149.0, 167.0, 279.1) Di-n-octyl phthalate [DOP] (m/z 149.0, 261.1, 279.1) Di-isononyl phthalate [DINP] (m/z 149.0, 167.0, 293.1) Di-isodecyl phthalate [DIDP] (m/z 149.0, 167.0, 307.1)		Hexa-BDE (m/z 483.7, 641.5) Hepta-BDE (m/z 563.6, 721.4) Octa-BDE (m/z 641.5, 801.3) Nona-BDE (m/z 719.4, 721.4) Deca-BDE (m/z 799.3, 801.3) Deca-BB (m/z 941.3, 943.3) Bis(pentabromophenyl)ethane (m/z 484.5, 969.2)	

Fig. 1: SIM Measurement Program

**Results**

The total ion current chromatogram and SIM mass chromatogram for the polyethylene containing BDEs (ERM®-EC590) are shown in Fig. 2. The total ion current chromatogram and SIM mass chromatogram for the polypropylene containing BDEs and BB (ERM®-EC591) are shown in Fig. 3.

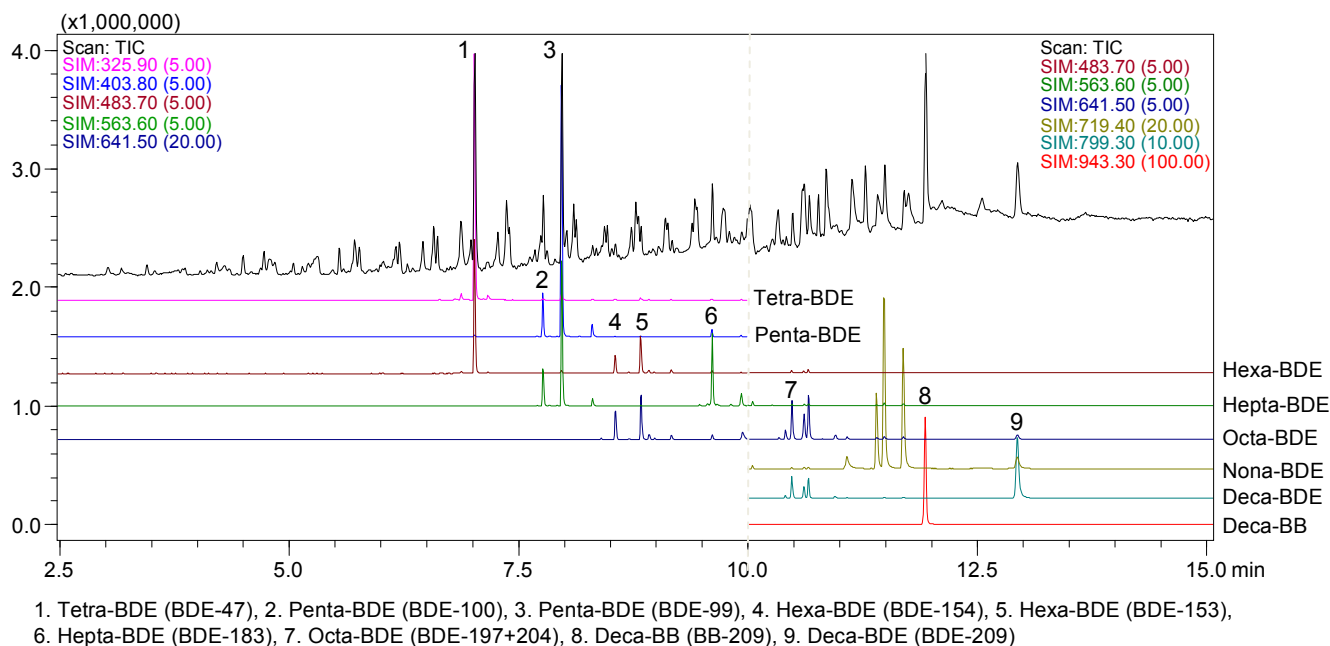


Fig. 2: Total Ion Current Chromatogram of Polyethylene Containing BDEs (ERM®-EC590)

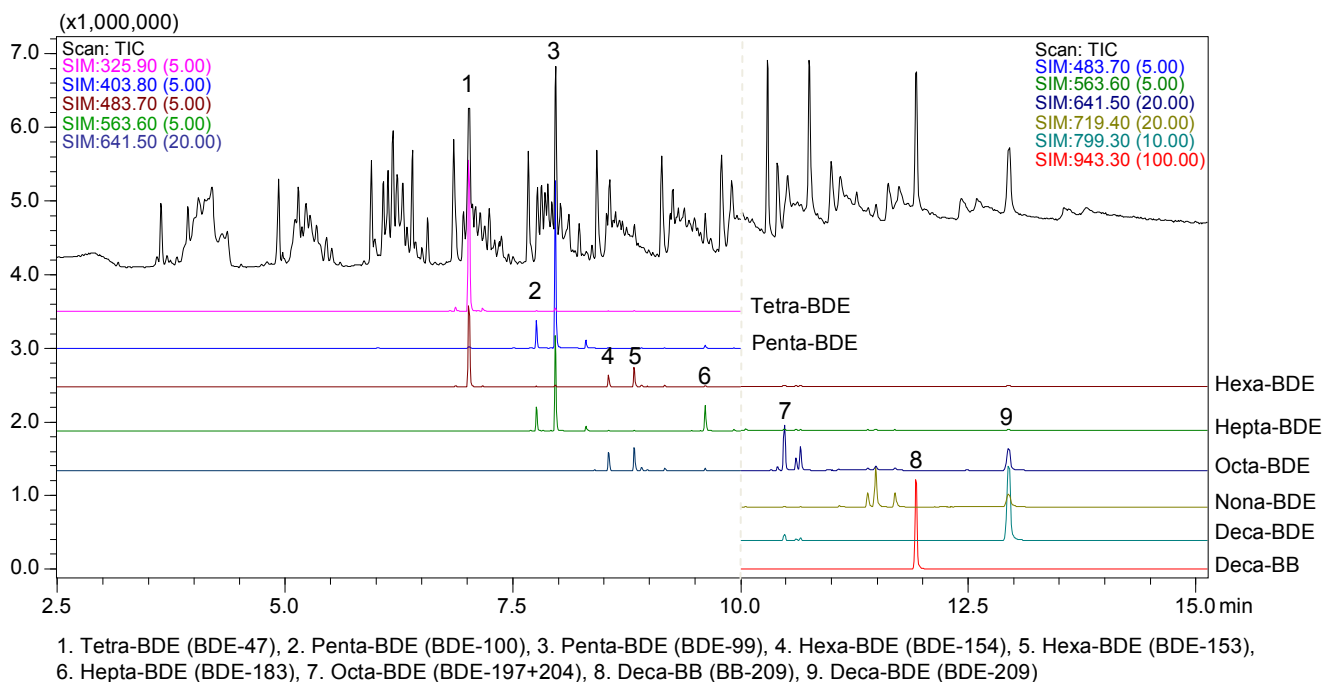


Fig. 3: Total Ion Current Chromatogram of Polypropylene Containing BDEs and BB (ERM®-EC591)

First Edition: June 2012



Shimadzu Corporation

[www.shimadzu.com/an/](http://www.shimadzu.com/an/)

For Research Use Only. Not for use in diagnostic procedures.

The content of this publication shall not be reproduced, altered or sold for any commercial purpose without the written approval of Shimadzu. The information contained herein is provided to you "as is" without warranty of any kind including without limitation warranties as to its accuracy or completeness. Shimadzu does not assume any responsibility or liability for any damage, whether direct or indirect, relating to the use of this publication. This publication is based upon the information available to Shimadzu on or before the date of publication, and subject to change without notice.

© Shimadzu Corporation, 2012

# Application Data Sheet

## No.48

### GC-MS

Gas Chromatograph - Mass Spectrometer

## Analysis of Brominated Flame Retardants and Phthalate Esters In Polymers Under the Same Conditions Using a Pyrolysis GC-MS System (2) - Phthalate Esters -

In recent years, an analysis method is required to determine not only polybrominated biphenyls (PBBs) and polybrominated diphenyl ethers (PBDEs), which are regulated under the RoHS Directive, but also phthalate esters and other brominated flame retardants not governed by the directive (such as tetrabromobisphenol A, hexabromocyclododecane, and bis(pentabromophenyl)ethane). Diisobutyl phthalate (DIBP), di-*n*-butyl phthalate (DBP), benzyl butyl phthalate (BBP), and bis(2-ethylhexyl) phthalate (DEHP) are specified in the REACH SVHC (Substance of Very High Concern) list. This Application Data Sheet shows the results from analyzing seven phthalate esters in polymers under the same analytical conditions as those in Application Data Sheet 47 using EGA/PY-3030D Multi-Shot Pyrolyzer and GCMS-QP2020 Ultra systems.

### Analytical Conditions

Standard mixture solutions were prepared by dissolving and diluting standard samples of the seven phthalate esters with acetone to concentrations of 1, 10, 50, and 100 ng/μL. Solid standard samples were prepared by adding 5 μL of the standard mixtures to an Eco-Cup LF (disposable sample cup) and evaporating the solvent to dryness. Evaluating sample was prepared by shaving cable jacket material (polyvinyl chloride) and weighing 0.5 mg. FASST (Fast Automated Scan/SIM Type), which is capable of simultaneous Scan and SIM measurements, was used as the measurement mode. Table 1 shows the analysis conditions and Fig. 1 shows the SIM measurement program.

Table 1: Analytical Conditions

Pyrolysis Instrument	: EGA/PY-3030D Multi-Shot Pyrolyzer		
GC-MS	: GCMS-QP2010 Ultra		
Column	: Ultra ALLOY-PBDE [15 m length, 0.25 mm I.D. , df = 0.05 μm]		
[Pyrolyzer]			
Pyrolysis Furnace Temp.	: 200 °C → (20 °C/min) → 300 °C → (5 °C /min) → 340 °C ( 1 min)		
Interface Temp.	: Manual (300 °C)	[MS]	
[GC]		Interface Temp.	: 320 °C
Injection Temp.	: 320 °C	Ion Source Temp.	: 230 °C
Column Oven Temp.	: 80 °C → (20 °C/min) → 300 °C (5 min)	Solvent Cut Time	: 0.5 min
Injection Mode	: Split	Tuning Mode	: Normal
Carrier Gas	: Helium	Measurement Mode	: FASST (simultaneous Scan/SIM measurements)
Flow Control Mode	: Constant linear velocity (52.1 cm/sec)	Scan Mass Range	: <i>m/z</i> 50 - 1000
Purge Flow Rate	: 3.0 mL/min	Scan Event Time	: 0.15 sec
Split Ratio	: 50	Scan Speed	: 10,000 <i>u</i> /sec
		SIM Monitoring <i>m/z</i>	: See Fig. 2.
		SIM Event Time	: 0.3 sec
		SIM Micro-Scan Width	: 0.5 <i>u</i>

1 min	Group 1 (No. of <i>m/z</i> channels: 21)	10 min	Group 2 (No. of <i>m/z</i> channels: 11)	16 min
	Tetra-BDE ( <i>m/z</i> 325.9, 483.7) Penta-BDE ( <i>m/z</i> 403.8, 563.6) Hexa-BDE ( <i>m/z</i> 483.7, 641.5) Hepta-BDE ( <i>m/z</i> 563.6, 721.4) Tetrabromobisphenol A [TBBPA] ( <i>m/z</i> 528.7, 543.7) Hexabromocyclododecane [HBCDD] ( <i>m/z</i> 319.1, 560.6) Diisobutyl phthalate [DIBP] ( <i>m/z</i> 149.0, 205.1, 223.1) Di- <i>n</i> -butyl phthalate [DIBP] ( <i>m/z</i> 149.0, 205.1, 223.1) Benzylbutyl phthalate [BBP] ( <i>m/z</i> 91.0, 149.0, 206.1) Bis(2-ethylhexyl) phthalate [DEHP] ( <i>m/z</i> 149.0, 167.0, 279.1) Di- <i>n</i> -octyl phthalate [DOP] ( <i>m/z</i> 149.0, 261.1, 279.1) Di-isononyl phthalate [DINP] ( <i>m/z</i> 149.0, 167.0, 293.1) Di-isodecyl phthalate [DIDP] ( <i>m/z</i> 149.0, 167.0, 307.1)		Hexa-BDE ( <i>m/z</i> 483.7, 641.5) Hepta-BDE ( <i>m/z</i> 563.6, 721.4) Octa-BDE ( <i>m/z</i> 641.5, 801.3) Nona-BDE ( <i>m/z</i> 719.4, 721.4) Deca-BDE ( <i>m/z</i> 799.3, 801.3) Deca-BB ( <i>m/z</i> 941.3, 943.3) Bis(pentabromophenyl)ethane ( <i>m/z</i> 484.5, 969.2)	

Fig. 1: SIM Measurement Program

Results

A total ion current chromatogram (TIC) for 250 ng of the seven phthalate esters is shown in Fig. 2. DOP, DINP, and DIDP could not be separated in the TIC; however, they were successfully separated in the mass chromatogram. The SIM mass chromatogram for 5 ng of DINP is shown in Fig. 3. The calibration curve coefficient of correlation for concentrations from 5 ng to 500 ng is shown in Table 2.

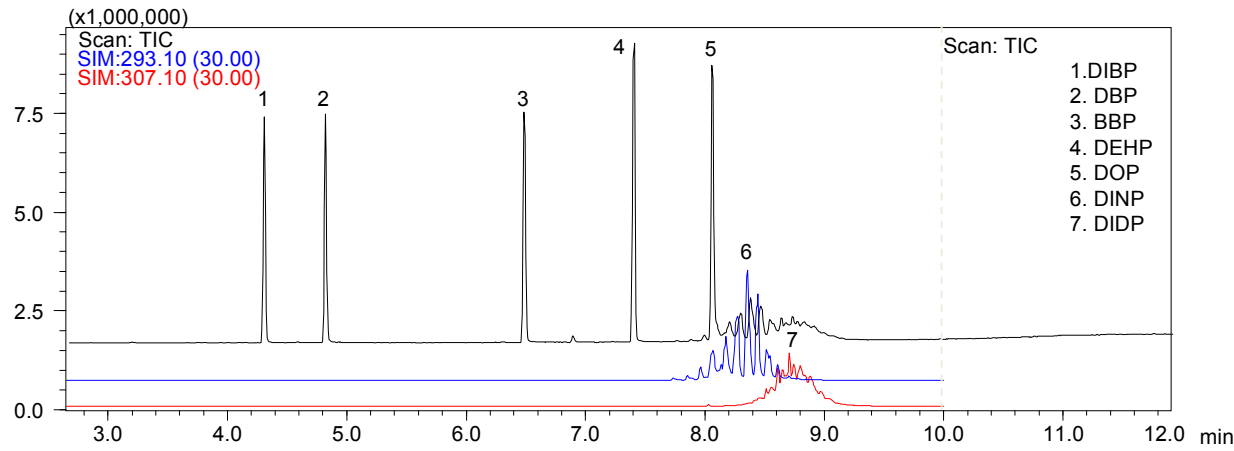


Fig. 2: Total Ion Current Chromatogram and Mass Chromatograms for 7 Phthalate Esters (250 ng)

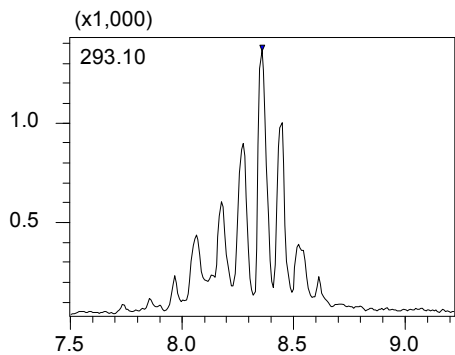


Fig. 3: SIM Mass Chromatogram of DINP (5 ng)

Table 2: Linearity of Calibration Curve for Seven Phthalate Esters (concentration range: 5 to 500 ng)

Compound Name	Correlation Coefficient (R)
DIBP	0.9995
DBP	0.9999
BBP	0.9999
DEHP	0.9999
DOP	0.9999
DINP	0.9999
DIDP	0.9997

The chromatogram from measuring the cable jacket material (polyvinyl chloride) is shown in Fig. 4. The presence of DEHP, DINP, and DIDP was confirmed in the SIM chromatogram. Also, the scan mass spectrum shows that Peak A is bis(2-ethylhexyl)adipate and Peak B is tris(2-ethylhexyl)trimellitate. A FASST measurement enabled quantitating the phthalate esters from the SIM data and identifying unregulated plasticizers from the scan data.

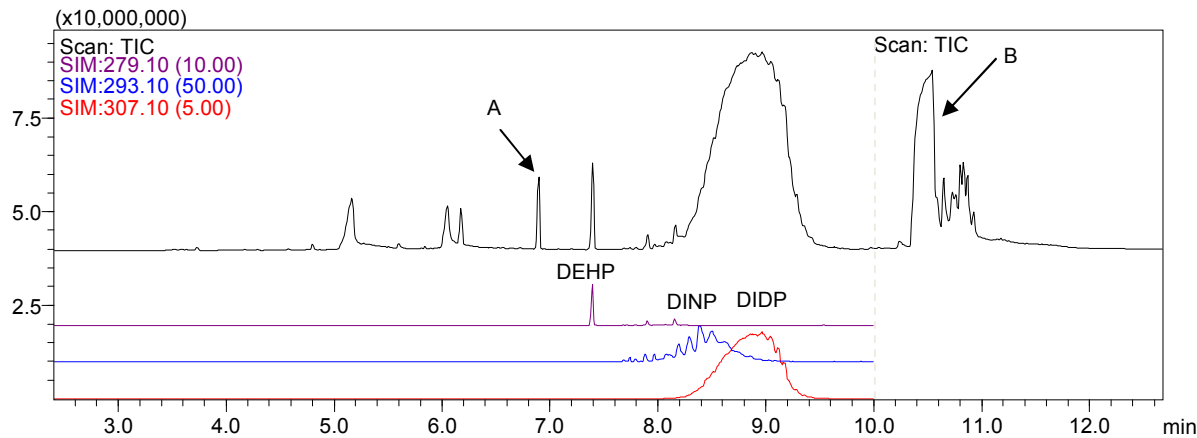


Fig. 4: Chromatogram of Cable Jacket Material

# No. 67

Gas Chromatograph Mass Spectrometer

In recent years, an analysis method has been required to determine not only polybrominated biphenyls (PBBs) and polybrominated diphenyl ethers (PBDEs), which are regulated under the RoHS Directive, but also phthalate esters and other brominated flame retardants not governed by the directive (such as tetrabromobisphenol A (TBBPA), hexabromocyclododecane (HBCDD), and bis(pentabromophenyl)ethane (BPBPE). TBBPA and BPBPE are not regulated by the RoHS Directive; however, they are frequently detected as brominated flame retardant additives by the EDX screening method. This Application Data Sheet shows the results from analyzing TBBPA and BPBPE in polymers under the same analytical conditions as those in Application Data Sheet 47 using the EGA/PY-3030D Multi-Shot Pyrolyzer and GCMS-QP2020 Ultra systems

TBBPA and BPBPE were dissolved with toluene at a concentration of 100 µg/mL, respectively. Polystyrene was dissolved in a mixture of 9:1 (v/v) dichloromethane and xylene at a concentration of 25 mg/mL. 20 µL of polystyrene solution (0.5 mg) and 5 µL of each TBBPA and BPBPE solution (0.5 µg) were added to Eco-Cup LF of the pyrolyzer. The solvent was evaporated to dryness at room temperature. The concentration of TBBPA and BPBPE was 1000 ppm in polystyrene. FASST (Fast Automated Scan/SIM Type), which is capable of simultaneous Scan and SIM measurements, was used as the measurement mode. Table 1 shows the analytical conditions and Fig. 1 shows the SIM measurement program.

Pyrolysis Instrument :EGA/PY-3030D Multi-Shot Pyrolyzer  
GC-MS :GCMS-QP2010 Ultra  
Column :Ultra ALLOY-PBDE [15 m length, 0.25 mm I.D. , df = 0.05  $\mu$ m]

---

Fig. 1: SIM Measurement Program



## Results

The chemical structure and mass spectrum of TBBPA are shown in Fig. 2 and 3. Fig. 4 shows the total ion current chromatogram of TBBPA in polystyrene (1000 ppm). The chemical structure and mass spectrum of BPBPE are shown in Fig. 5 and 6. Fig. 7 shows the total ion current chromatogram of BPBPE in polystyrene (1000 ppm).

These analytical conditions can be applied to analyses of PBBs, PBDEs, and phthalate esters. Moreover, using the scan/ SIM mode (FASST) enable accurate determination of target compounds from the SIM data and identification of unknown compounds from the full-scan data.

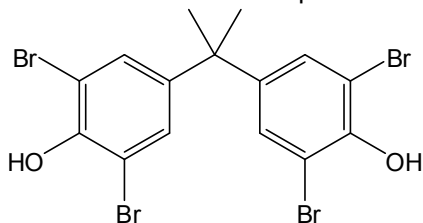


Fig. 2: Compound Structure of TBBPA

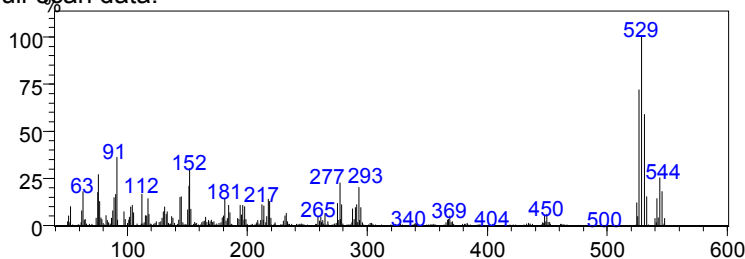


Fig. 3: Mass Spectrum of TBBPA

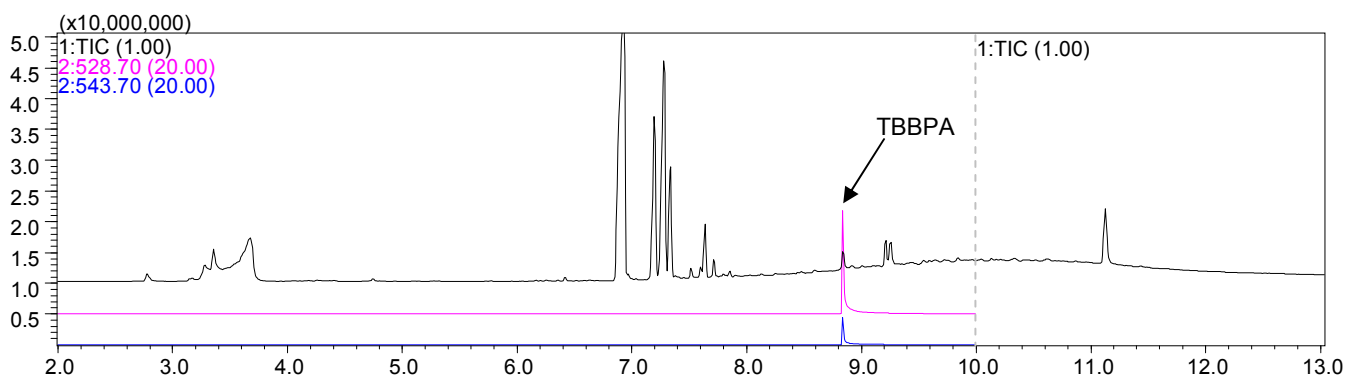


Fig. 4: Total Ion Current Chromatogram of Polystyrene Spiked TBBPA

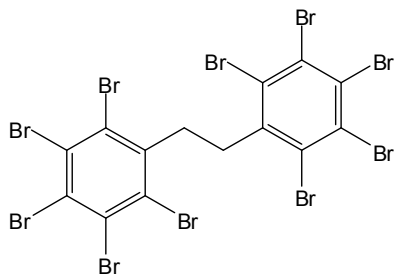


Fig. 5: Compound Structure of BPBPE

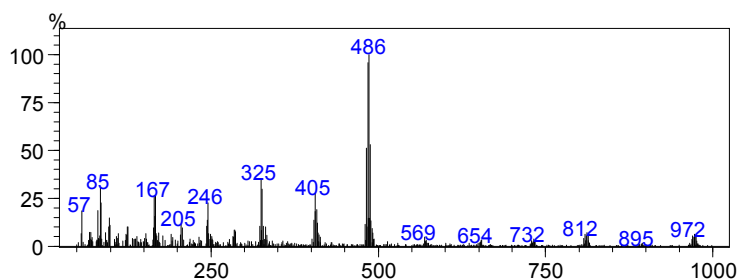


Fig. 6: Mass Spectrum of BPBPE

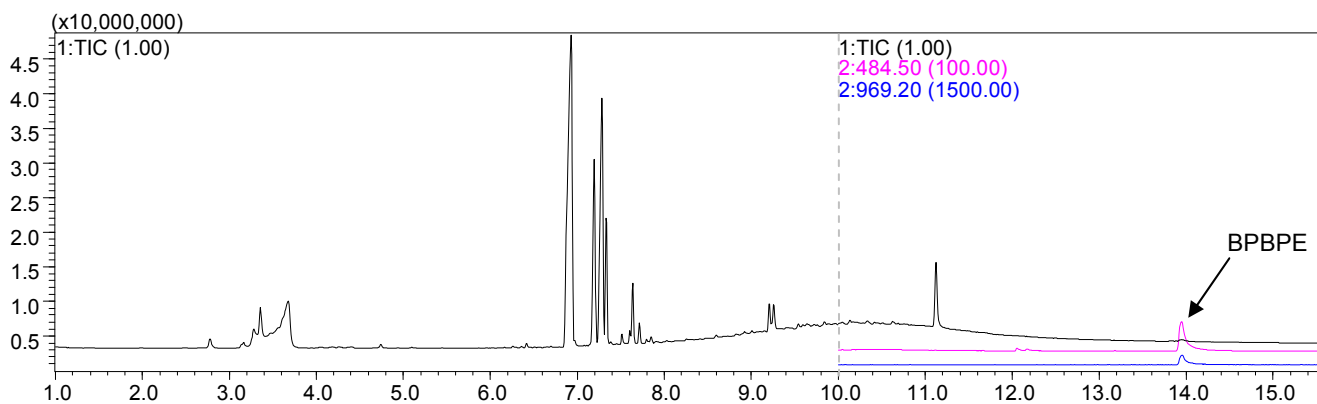


Fig. 7: Total Ion Current Chromatogram of Polystyrene Spiked BPBPE

First Edition: July, 2012

# Application Data Sheet

No. 110

## GC-MS

Gas Chromatograph Mass Spectrometer

### Analysis of Phthalate Esters Using the Py-Screener (1)

In the RoHS directive (directive on the restriction of the use of certain hazardous substances in electrical and electronic equipment), four phthalate esters: diisobutyl phthalate (DIBP), dibutyl phthalate (DBP), benzyl butyl phthalate (BBP), and bis(2-ethylhexyl)phthalate (DEHP), will be added to the six conventionally limited substances starting in 2019.

Of these, the substances that can be measured with GC-MS are the brominated flame retardants, PBBs and PBDEs, and phthalate esters. The Soxhlet extraction-GC/MS method, while an accurate quantitation method, requires time-consuming pretreatment and uses organic solvents. In contrast, the pyrolysis-GC/MS (Py-GC/MS) method does not require complicated pretreatment and is therefore expected to be used as a screening method. The "Py-Screener" is a screening system for phthalate esters using Py-GC/MS. It consists of polymer standard samples containing phthalate esters, a sample preparation sampling kit, and Py-GC/MS analysis files.

This Application Datasheet introduces measurements of phthalate ester standard samples using the Py-Screener.

#### Standard Samples Used in the Py-Screener

The Py-Screener uses the Phthalate Esters Polymer Standards for Py-GC/MS (P/N: S225-31003-91). These polymer standard samples can be prepared easily, without using organic solvents, by using a special sampling toolkit (P/N: PY1-K101 from Frontier Laboratories).

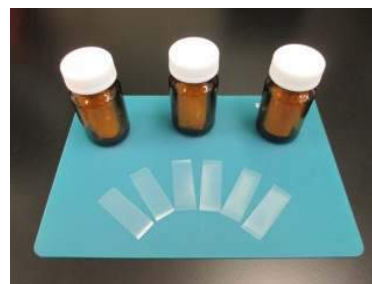


Fig. 1: Phthalate Esters Polymer Standards for Py-GC/MS (S225-31003-91), including seven phthalate esters

(Three types: Blank, 100 mg/kg, and 1000 mg/kg)

#### Preparing the Phthalate Ester Standard Samples

The phthalate ester resin standard samples are ribbon shaped and of uniform thickness. As a result, samples can be prepared just by placing two fragments of the sample (approximately 0.5 mg) in the Py Eco-cup using the 1.25 mm diameter micro puncher included in the special sampling toolkit. Fig. 1 shows the standard samples. Table 1 shows the repeatability for the weight of samples prepared seven times. The RSD is a favorable 2.24 %, and it is evident that the thickness is uniform.

Table 1: Sampling Weight Repeatability for the 100 mg/kg Phthalate Ester Standard

	1st	2nd	3rd	4th	5th	6th	7th	%RSD
Sample Weight (mg)	0.49	0.50	0.52	0.50	0.50	0.51	0.52	2.24

## Analytical Conditions

The conditions registered in the Py-Screener were used as the GC-MS analysis conditions (Table 2).

Table 2: Analytical Conditions

Pyrolyzer	:Multi-Shot Pyrolyzer EGA/PY-3030D		
GC-MS	:GCMS-QP2010 Ultra		
Column	:Ultra ALLOY-PBDE (Length 15 m, 0.25 mm I.D., $\phi$ = 0.05 $\mu$ m)		
[Pyrolyzer]			
Furnace Temp.	:200 °C→(20 °C/min)→300 °C →(5 °C /min)→340 °C(1min)	[MS]	
Interface Temp.	:Manual (300 °C )	Interface Temp.	:320 °C
[GC]		Ion Source Temp.	:230 °C
Injection Temp.	:320 °C	Measurement Mode	:FASST (Scan/SIM mode)
Column Oven Temp.	:80 °C→(20 °C /min)→300 °C (5min)	Scan Mass Range	:m/z 50-1000
Injection Mode	:Split	Scan Event Time	:0.15 sec
Carrier Gas	:He	Scan Speed	:10,000 u/sec
Flow Control Mode	:Linear velocity (52.1cm/sec)	SIM Event Time	:0.3 sec
Purge Flow	:3.0 mL/min	SIM Micro Scan Width	:0.3 u
Split Ratio	:50		

## Results

Fig. 2 shows the mass chromatograms for the phthalate esters obtained by measuring the 100 mg/kg phthalate ester standard sample. They were detected with sufficient sensitivity even at a concentration of 1/10th the prescribed concentration. Table 3 shows the repeatability and MDL calculated after measuring the 100 mg/kg phthalate ester standard sample seven times. The repeatability for the quantitative values obtained (% RSD) ranged from 4.1 % to 5.7 %, and the MDL was 12.3 mg/kg to 16.3 mg/kg, which are favorable results.

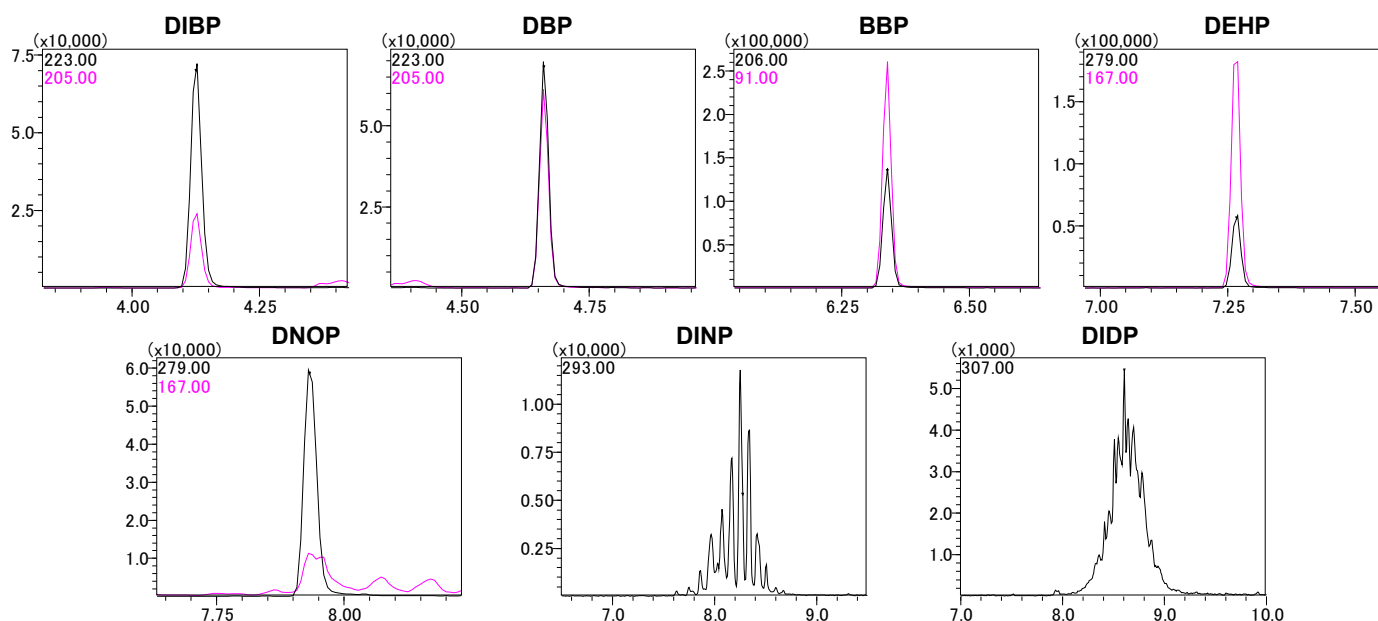


Fig. 2: Mass Chromatograms for the Phthalate Esters Measured in the 100 mg/kg Phthalate Ester Standard Sample

Table 3: Repeatability and MDL for the 100 mg/kg Phthalate Ester Standard Sample (n=7)

	Quantitation Value (mg/kg)							%RSD	MDL (mg/kg)
	1st	2nd	3rd	4th	5th	6th	7th		
DIBP	104.1	102.9	98.6	95.2	103.2	109.3	101.5	4.4	14.0
DBP	107.0	105.2	100.7	98.7	105.9	113.8	106.6	4.6	15.3
BBP	95.5	94.3	91.0	87.9	96.3	100.1	95.1	4.1	12.3
DEHP	110.7	108.5	101.1	101.5	111.2	115.3	108.4	4.8	16.3
DOP	101.2	101.9	93.9	90.3	99.3	103.9	99.1	4.8	15.0
DINP	94.3	95.7	87.4	84.8	92.8	96.8	92.5	4.8	13.7
DIDP	93.3	94.2	83.1	80.9	89.2	91.6	87.3	5.7	15.9

First Edition: Apr, 2015



Shimadzu Corporation

www.shimadzu.com/an/

For Research Use Only, Not for use in diagnostic procedures.

The content of this publication shall not be reproduced, altered or sold for any commercial purpose without the written approval of Shimadzu. The information contained herein is provided to you "as is" without warranty of any kind including without limitation warranties as to its accuracy or completeness. Shimadzu does not assume any responsibility or liability for any damage, whether direct or indirect, relating to the use of this publication. This publication is based upon the information available to Shimadzu on or before the date of publication, and subject to change without notice.

© Shimadzu Corporation, 2015

# Application Data Sheet

No. 111

## GC-MS

Gas Chromatograph Mass Spectrometer

## Analysis of Phthalate Esters Using the Py-Screener (2)

In the RoHS directive (directive on the restriction of the use of certain hazardous substances in electrical and electronic equipment), four phthalate esters: diisobutyl phthalate (DIBP), dibutyl phthalate (DBP), benzyl butyl phthalate (BBP), and bis(2-ethylhexyl)phthalate (DEHP), will be added to the six conventionally limited substances starting in 2019.

Of these, the substances that can be measured with GC-MS are the brominated flame retardants, PBBs and PBDEs, and phthalate esters. The Soxhlet extraction-GC/MS method, while an accurate quantitation method, requires time-consuming pretreatment and uses organic solvents. In contrast, the pyrolysis-GC/MS (Py-GC/MS) method does not require complicated pretreatment and is therefore expected to be used as a screening method. The "Py-Screener" is a screening system for phthalate esters. It consists of resin standard samples containing phthalate esters, a sample preparation sampling kit, and Py-GC/MS analysis files.

This Application Datasheet introduces an example of the analysis of phthalate esters and brominated flame retardants using the Py-Screener.

### Analytical Conditions

The conditions registered in the Py-Screener were used as the GC-MS analysis conditions. For the detailed analysis conditions, refer to GC-MS Application Datasheet No.110, "Analysis of Phthalate Esters Using the Py-Screener (1)."

### Results

A calibration curve was created using the 1000 mg/kg phthalate ester resin standard sample. KRISS CRM113-03-006, which is sold as a phthalate ester certified standard sample, was then measured and quantified based on this calibration curve. Fig. 1 shows the mass chromatograms obtained. Table 1 shows the results of a comparison of the quantified values and the CRM certified values. The yield using the certified values as reference was in the range of 92.9 % to 109.0 %, so the quantitation results obtained were favorable with a view to screening.

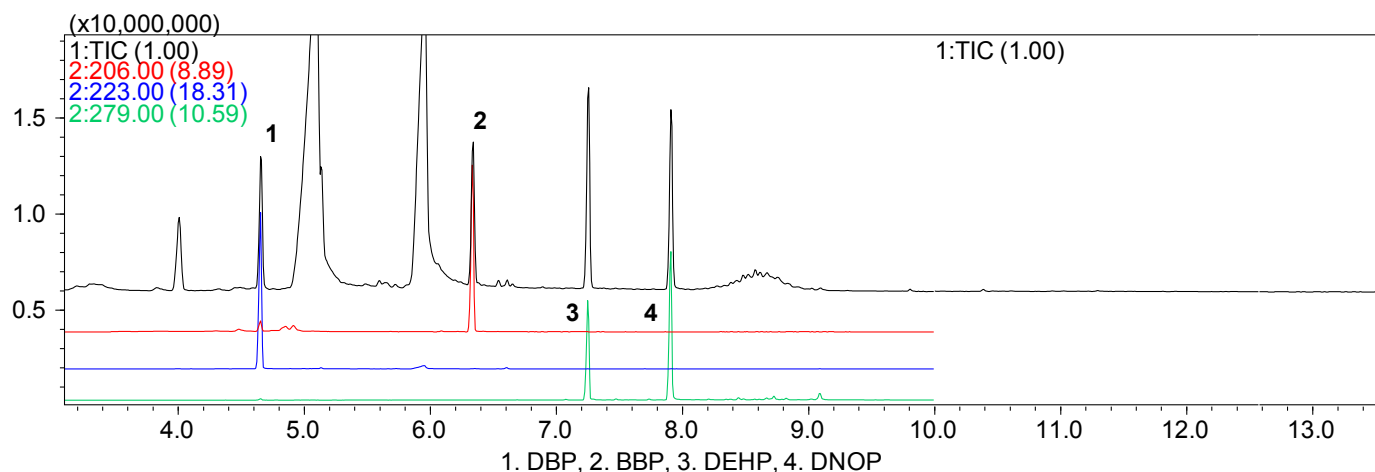


Fig. 1: Mass Chromatograms for the Phthalate Esters Measured in KRISS CRM113-03-006

Table 1: Comparative Results for the Certified Values and the Quantitation Results

	Quantitation Results (mg/kg)	Certified Values (mg/kg)	Yield (%) with the Certified Values as Reference
DBP	1059	972	109.0
BBP	894	962	92.9
DEHP	1015	989	102.6
DNOP	993	967	102.7

Figs. 2 and 3 show the mass chromatograms for a PVC cable and PBT resin measured as testing samples. DBP, DEHP, DINP, and DIDP were detected in the PVC cable, and DEHP and Deca-BDE were detected in the PBT resin. This system can accommodate screening for phthalate esters and brominated flame retardants with a single measurement cycle.

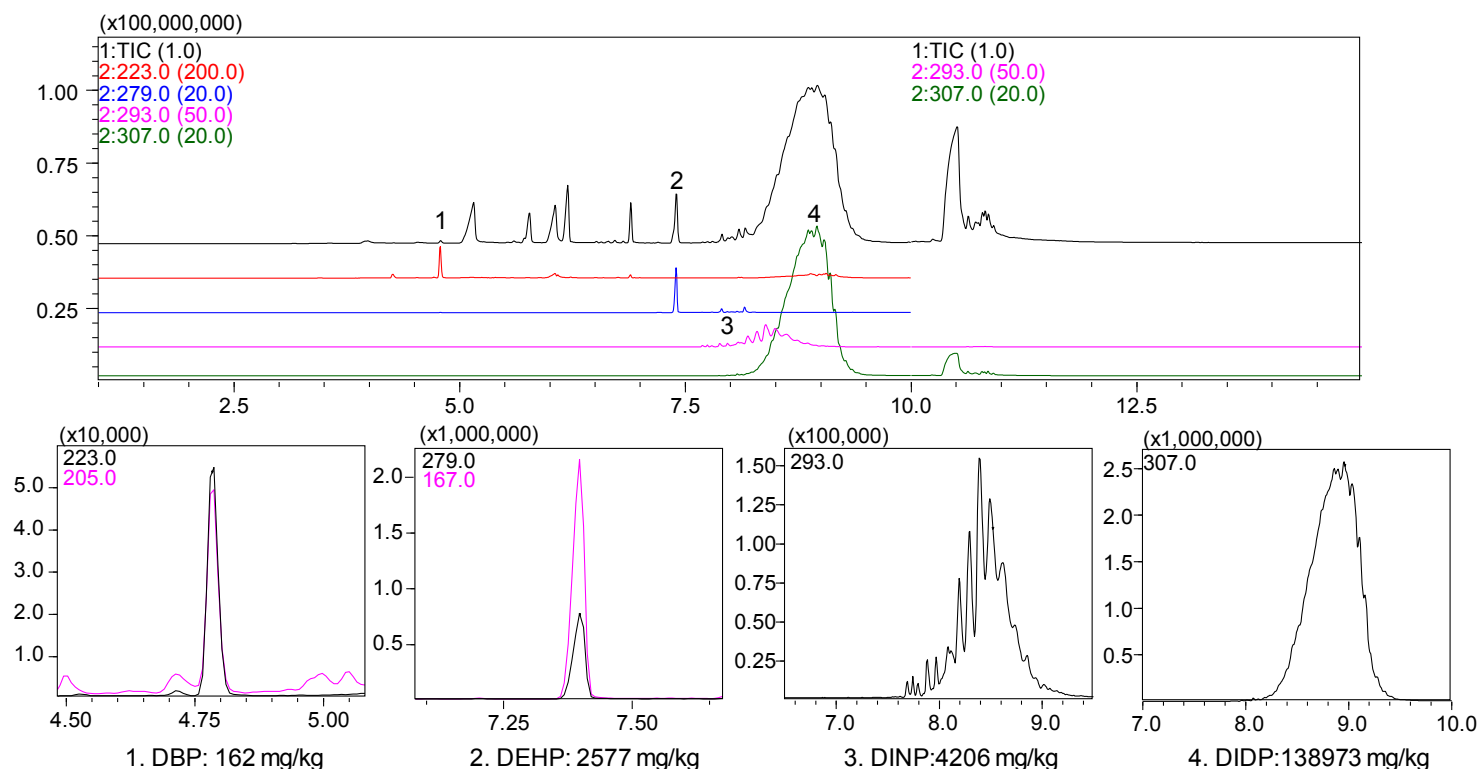


Fig. 2: Mass Chromatograms for Compounds Detected in a PVC Cable

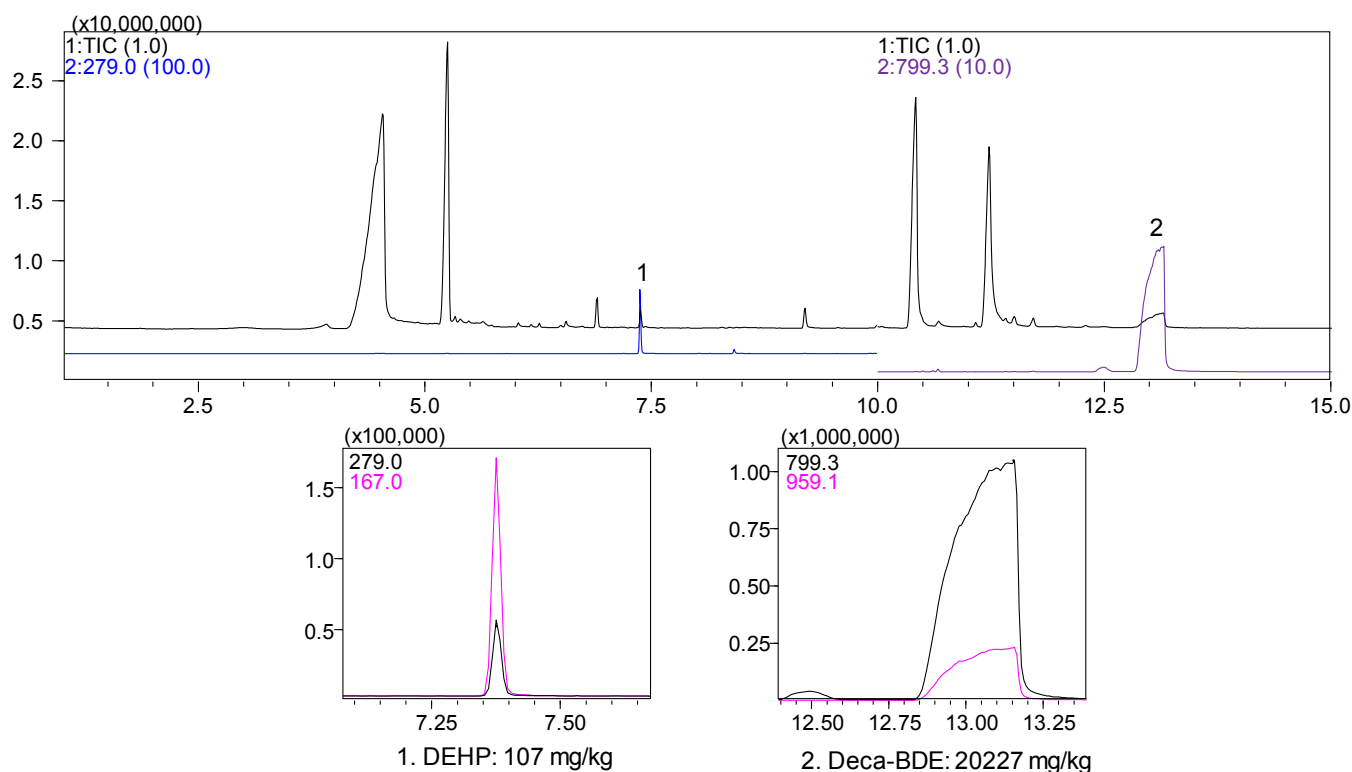


Fig. 3: Mass Chromatograms for Compounds Detected in a PBT Resin

First Edition: Apr, 2015



## Technical Report

# Comparison of Screening Method (Py-GC/MS) and Quantitative Method (Solvent Extraction–GC/MS) for Phthalate Esters Analysis

Jae Woo Kim<sup>1</sup>, Hye Mi Moon<sup>1</sup>, Fumitaka Maruyama<sup>2</sup>, Shigehiro Fujimaki<sup>2</sup>, Yukihiro Kudo<sup>3</sup>, Yuki Sakamoto<sup>3</sup>, Haruhiko Miyagawa<sup>3</sup>, Katsuhiro Nakagawa<sup>3</sup>

### Abstract:

From 2019, four phthalate esters (diisobutyl phthalate (DIBP), *n*-dibutyl phthalate (DBP), benzyl butyl phthalate (BBP) and di(2-ethylhexyl) phthalate (DEHP)) will be added to restricted substances in the amended RoHS Directive (a directive on the restriction of the use of certain hazardous substances in electrical and electronic equipment).

In this technical report, the quantitative results between the solvent extraction-GC/MS method and the Screening System for Phthalate Esters “Py-Screener” (Py-GC/MS method) were compared. The quantitative results using the Py-Screener were equivalent to the results using the solvent extraction-GC/MS method for quantitative measurements in the region of a restricted concentration level of 1000 mg/kg. The Py-Screener was shown to be useful for screening the phthalate esters added to the amended RoHS Directive.

**Keywords:** RoHS, phthalate esters, Py-GC/MS, Py-Screener

## 1. Introduction

Phthalate esters are mainly used as plasticizers in polyvinyl chloride (PVC). However, some phthalate esters are suspected of exhibiting reproductive toxicity, which has led to restriction of their use in toys and food packaging.

Effective 2019, four phthalate esters (diisobutyl phthalate (DIBP), *n*-dibutyl phthalate (DBP), benzyl butyl phthalate (BBP) and di(2-ethylhexyl) phthalate (DEHP)) will be added to the six hazardous substances currently subject to restricted use in the amended RoHS Directive, which restricts the use of certain hazardous substances in electrical and electronic equipment <sup>1)</sup>.

Phthalate esters are commonly analyzed by GC or GC/MS following extraction from a polymer sample. Extraction methods differ depending on the analytical standard (Table 1).

**Table 1 Sample Preparation Procedures According to the Analytical Standard**

Analytical Standard	Sample Preparation Procedures
Japan's Ministry of Health and Welfare Ministerial Notification No. 370 <sup>2)</sup>	Solvent extraction by immersion
EN14372 <sup>3)</sup>	Soxhlet extraction
ASTM D3421-75 <sup>4)</sup>	Soxhlet extraction
CPSC-CH-C1001-09.3 <sup>5)</sup>	Solvent dissolution or precipitation
ISO 8124-6 <sup>6)</sup>	Soxhlet extraction or a solvent extraction
ISO 14389 <sup>7)</sup>	Ultrasonic extraction / dissolution / precipitation
ASTM D7823-14 <sup>8)</sup>	Solvent dissolution and thermal extraction

All of these methods specify the use of organic solvents to extract phthalate esters from the polymer, while only ASTM D7823-14 specifies heating of the polymer to extract the phthalate esters.

However, ASTM D7823-14 is a test method only for determination of low level phthalates in PVC samples, during which the sample must be dissolved in an organic solvent, tetrahydrofuran (THF), prior to thermal extraction. Also, since the standard addition method is used, evaluation must be conducted using the sample and standard solution spiked with multiple concentrations of sample. Furthermore, DIBP, which will be added to the amended RoHS Directive, cannot be analyzed by this analysis standard.

To resolve these issues, Maruyama *et al.* <sup>9)</sup> developed a quantitative method based on thermal extraction alone using a pyrolysis-GC/MS (Py-GC/MS) method, reporting that it is an effective screening method.

Using the method of Maruyama *et al.*, we conducted measurement of certified reference materials, and examined the percentage recovery as compared with the certified levels. We also conducted measurement of a polymer sample using the Py-GC/MS method and a solvent extraction–GC/MS method, and compared the respective quantitative results to evaluate the efficacy of the Py-GC/MS method for screening of phthalate esters, a method that is compliant with the amended RoHS Directive.

<sup>1</sup> KOTITI Testing & Research Institute

<sup>2</sup> SGS Japan Inc.

<sup>3</sup> Shimadzu Corporation



## 2. Experimental

A KRISS CRM 113-03-006 certified reference material and two samples (A and B) of black rubber were used for evaluation.

### 2-1. Py-GC/MS Method

Seven phthalate ester standards (P/N: 225-31003-91) were prepared by kneading together seven standard phthalate ester samples (diisobutyl phthalate (DIBP), *n*-dibutyl phthalate (DBP), benzyl butyl phthalate (BBP), di(2-ethylhexyl) phthalate (DEHP), di-*n*-octyl phthalate (DNOP), di-isononyl phthalate (DNIP), and diisodecyl phthalate (DIDP)) with polyethylene. A blank, 100 mg/kg and 1000 mg/kg standards were used to check for contamination of the instrument due to carryover, to confirm sensitivity, and to create a single-point calibration curve, respectively.

Standard materials were ribbon-like in shape and of uniform thickness, with two 1.25 mm diameter pieces weighing approximately 0.5 mg. Two pieces of each standard material were obtained using a micro-puncher, then placed inside an Eco-Cup (Frontier Laboratories Ltd., Fukushima, Japan) for pyrolysis, and weighed.

The calibration curve was generated using the 1000 mg/kg standard material. About 0.5 mg of the materials cut with a cutter were placed in an Eco-Cup for pyrolysis and weighed for evaluation. The measured weight was used to calculate the quantity of phthalate ester in the polymer.

### 2-2. Solvent Extraction-GC/MS Method

Mixed standard solutions of seven phthalate esters (DIBP, DBP, BBP, DEHP, DNOP, DINP and DIDP) were prepared at concentrations of 0.5, 1.0, 2.5, 5.0 and 10.0 µg/mL, respectively. An anthracene-d10 internal standard was also added to each mixed standard solution to a concentration of 1.0 µg/mL. These mixed standard solutions were used to generate a 5-point calibration curve with internal standards at constant concentration.

Evaluation samples were prepared as described below. First, samples were frozen using liquid nitrogen and then crushed, and approximately 300 mg was weighed out and placed in a 40 mL vial to which 10 mL of THF was added. The vial was stoppered and the sample was subjected to ultrasonic dissolution in solvent for 60 minutes. Once the mixture returned to room temperature, 20 mL of acetonitrile was added dropwise to precipitate the polymer, and the mixture was left for 30 minutes at room temperature while the polymer precipitated. Finally, 1 mL of supernatant was transferred to a GC vial, and 10 µL of an internal standard was added. If a result exceeded the upper limit of the calibration curve, an aliquot of the top layer in the vial was diluted until the result was within the range of the calibration curve. Then, 10 µL of internal standard was added, and the measurement was conducted again using the diluted sample mixture as the GC/MS sample.

## 2-3. Analytical Conditions

Py-GC/MS measurements were conducted using the Py-Screener phthalate ester screening system (Shimadzu). The Py-Screener consists of the EGA/PY-3030D multi-shot pyrolyzer (Frontier Laboratories Ltd.), the GCMS-QP2010 Ultra (Shimadzu) GC-MS system, and dedicated software for instrument control and data Processing. For the separation column, the Ultra ALLOY-PBDE (length 15 m, 0.25 mm I.D., df = 0.05 µm, Frontier Laboratories Ltd.) column was used. The detailed analytical conditions are shown in Table 2.

The GCMS-QP2010 Ultra was used for solvent extraction-GC/MS measurements, along with an HP-5MS (length 30 m, 0.25 mm I.D., df = 0.25 µm, Agilent) column. Detailed analytical conditions are shown in Table 3.

Table 2 Analytical Conditions for the Py-GC/MS Method

Pyrolyzer	
Furnace Temp.	: 200 °C → (20 °C/min) → 300 °C → (5 °C/min) → 340 °C (1 min)
Interface Temp.	: Manual (300 °C)
GC	
Injection Temp.	: 300 °C
Column Oven Temp.	: 80 °C → (20 °C/min) → 300 °C (5 min)
Injection Mode	: Split
Carrier Gas	: He
Flow Control Mode	: Linear velocity (52.1 cm/sec)
Purge Flow	: 3.0 mL/min
Split Ratio	: 50
MS	
Interface Temp.	: 320 °C
Ion Source Temp.	: 230 °C
Measurement Mode	: FASST (Scan/SIM mode)
Scan Mass Range	: <i>m/z</i> 50–1000
Scan Event Time	: 0.15 sec
Scan Speed	: 10000 <i>u</i> /sec
SIM Event Time	: 0.3 sec
SIM Micro Scan Width	: 0.3 <i>u</i>

Table 3 Analytical Conditions for the Solvent Extraction-GC/MS Method

GC	
Injection Temp.	: 300 °C
Column Oven Temp.	: 110 °C (0.5 min) → (20 °C/min) → 280 °C (1 min) → (20 °C/min) → 320 °C (5 min)
Injection Mode	: Splitless
Carrier Gas	: He
Flow Control Mode	: Linear velocity (45.8 cm/sec)
MS	
Interface Temp.	: 320 °C
Ion Source Temp.	: 230 °C
Measurement Mode	: FASST (Scan/SIM mode)
Scan Mass Range	: <i>m/z</i> 50–500
Scan Event Time	: 0.3 sec
Scan Speed	: 1666 <i>u</i> /sec
SIM Event Time	: 0.3 sec

### 3. Results and Discussion

The results obtained from measurement of the KRISS CRM 113-03-006 certified reference material using the Py-Screener are shown in Table 4. Good quantitative results were obtained, with recoveries in

the range of 92.9 – 109.0 % of the certified values, confirming that phthalate esters can be extracted using the Py-GC/MS method with good recovery.

Table 4 Quantitative Results from KRISS CRM113-03-006 using the Py-Screener

	Conc. (mg/kg)	Certified Value (mg/kg)	Recovery* (%)
DBP	1059	972	109.0
BBP	894	962	92.9
DEHP	1015	989	102.6
DNOP	993	967	102.7

\* The recovery of each detected phthalate ester was calculated based on the certified values.

The quantitative results obtained with the Py-Screener, are shown in Fig. 1. All phthalate esters included in the sample were detected automatically. Further, the dedicated software automatically corrects for the weight of the collected sample, and displays the concentration of phthalate esters in the polymer as a quantitative result. The mass chromatogram and quantitative concentrations can be displayed in different colors based on user-specified QC limits. For example, concentrations under 500 mg/kg may be displayed as color-

less, 500 to 1500 mg/kg may be displayed in orange, and samples greater than 1500 mg/kg in red. This permits visual observation of which quantitative results are within which concentration range.

Two evaluation samples were measured using both the Py-GC/MS method and the solvent extraction-GC/MS method, and the quantitative results were compared. Each sample was measured three times and the mean quantitative results were calculated.

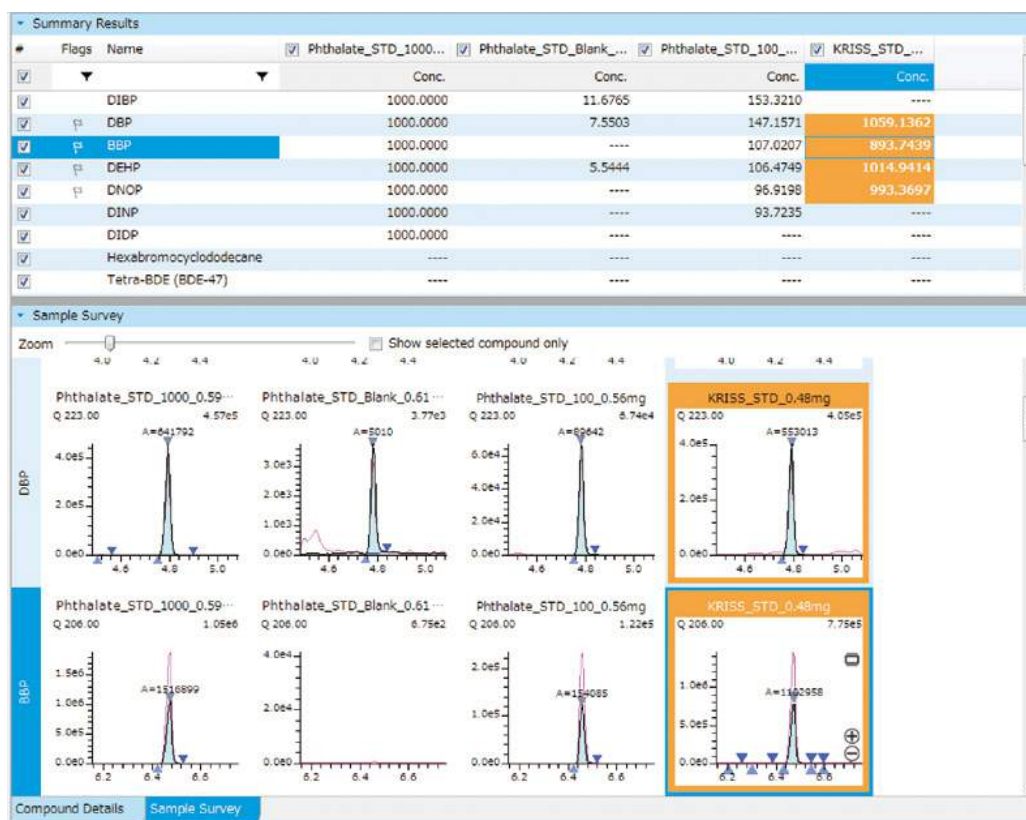


Fig. 1 Summary Screen of Py-Screener with LabSolutions Insight

The results from evaluation sample A are shown in Table 5, with the associated chromatograms shown in Fig. 2. DEHP was detected by both methods. The quantitative results obtained by the Py-GC/MS method were 124 % of those obtained by the solvent extraction-GC/MS method, while the %RSD of the three measurements using the Py-GC/MS method was 5.1 %, which was equivalent to that obtained by the solvent extraction-GC/MS method. Regarding the higher quantitative result obtained with the Py-Screener, the sample used in the measurement by the solvent extraction-GC/MS method was diluted to bring the result below the maximum concentration in the calibration curve. On the other hand, with the Py-Screener, the quantitative value is

calculated using the 1000 mg/kg 1-point calibration method, suggesting that this may be the source of the discrepancy between the detected concentration and the calibration point concentration. However, although the quantitative results substantially exceeded the 1000 mg/kg concentration limit specified in the amended RoHS Directive, from the standpoint of screening, the fact that it exceeded the regulatory value was easily determined.

A large peak detected at a retention time of 8.3 minutes was identified as di(2-ethylhexyl) terephthalate based on a mass spectral library search. Using scan/SIM simultaneous measurements, it is possible to identify an unknown peak based on the mass spectrum of the scan.

Table 5 Comparison of Quantitative Results for Py-GC/MS Method and Solvent Extraction-GC/MS Method for Sample A

	Py-GC/MS method (Py-Screener)			Solvent Extraction-GC/MS method			Relative ratio of conc. (%)
	Average Conc. (mg/kg)	SD	%RSD	Average Conc. (mg/kg)	SD	%RSD	
DEHP	3923	199	5.1	3162	196	6.2	124

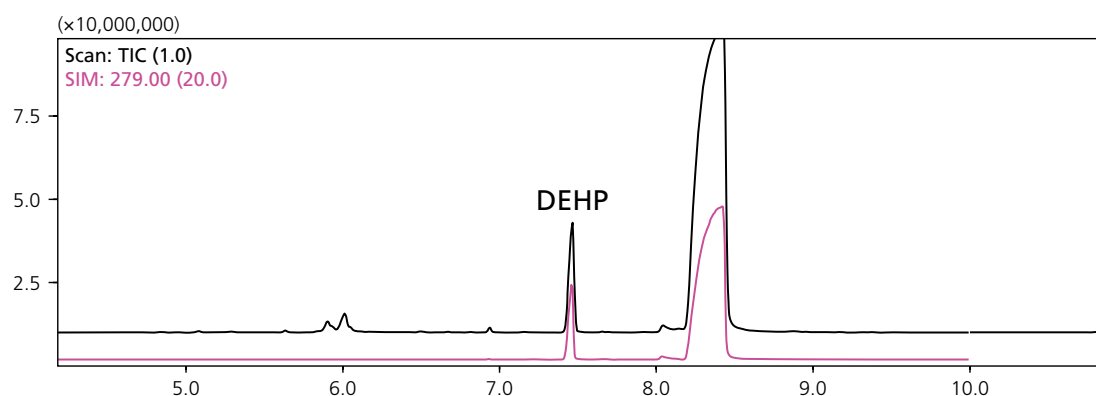


Fig. 2 TIC and Extracted Chromatograms of Sample A Measured using Py-GC/MS Method

The measurement results for sample B are shown in Table 6, with the chromatograms shown in Fig. 3. Five phthalate esters (DBP, BBP, DEHP, DINP and DIDP) were detected by both methods. The quantitative results for each phthalate ester using the Py-Screener were 124, 332, 44041, 2796 and 1516 mg/kg, respectively. The quantitative results were in the range of 68 to 108 % of the quantitative results obtained using the solvent extraction-GC/MS method. Regarding the larger quantitative ratio obtained for DEHP using the solvent extraction-GC/MS method, this was determined to be due to the use of different calibration methods as described above. Regarding the DIDP with its 1500 mg/kg concentration in the vicinity of the 1000 mg/kg Py-Screener calibration point, this quantitative result is considered to be equivalent to that obtained using the solvent extraction-GC/MS method.

This confirmed that when the concentration was in the range of 500 – 2000 mg/kg, such as the 1000 mg/kg obtained here, the calculated concentration was easily compared to the regulatory action level for screening purposes. Analysis precision in terms of repeatability (%RSD) of the Py-Screener was 3.3 to 5.5 %, and analysis precision in terms of repeatability (%RSD) of the solution extraction-GC/MS method was 4.2 to 16.6 %. Analysis precision in terms of repeatability was markedly worse using the solvent ex-

traction- GC/MS method compared to that using the Py-Screener when analyzing phthalate esters of low boiling point: DBP (16.6 %) and BBP (12.7 %). As internal standard correction is used with solvent extraction, this variation is attributed mainly to pretreatment.

Since the amended RoHS Directive sets the regulatory concentration at 1000 mg/kg, tests must be at their most accurate when measuring concentrations in the region of 1000 mg/kg. Therefore, as the Py-Screener demonstrated good recovery at 1000 mg/kg, it is considered effective for the testing described in the amended RoHS Directive, and in particular, for screening when the results are used as the basis for determining the necessity to perform more detailed quantitation. Furthermore, good analytical precision in terms of repeatability is an effective criterion for screening.

A single-point calibration curve is adequate for phthalate ester screening according to the amended RoHS Directive, with a regulatory level of 1000 mg/kg. However, the current 1000 mg/kg single-point calibration method used with the Py-Screener method is not appropriate for performing analysis with respect to a different regulatory concentration level, or when precision across a wide range of concentration measurements is required. In such cases, the Py-Screener must be used in combination with the solvent extraction-GC/MS method for quantitation.

Table 6 Comparison of Quantitative Results Obtained for Sample B using Py-GC/MS Method and Solvent Extraction–GC/MS Method

	Py-GC/MS method (Py-Screener)			Solvent Extraction–GC/MS method			Relative ratio of conc. (%)
	Average Conc. (mg/kg)	SD	%RSD	Average Conc. (mg/kg)	SD	%RSD	
DBP	124	6	5.1	115	19	16.6	108
BBP	332	13	3.8	466	59	12.7	71
DEHP	44041	1456	3.3	64785	2753	4.2	68
DINP	2796	98	3.5	2695	242	9.0	104
DIDP	1516	84	5.5	1511	127	8.4	100

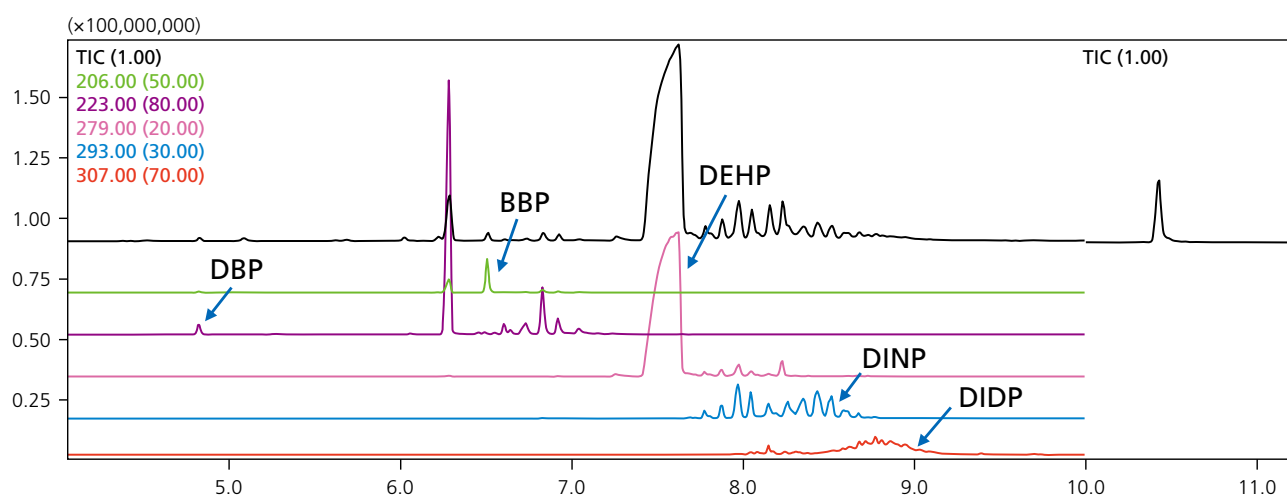


Fig. 3 TIC and Extracted Chromatograms of Sample B Measured using Py-GC/MS Method

## 4. Conclusion

The quantitative results from analysis of phthalate esters in polymer were compared using the solvent extraction–GC/MS method and the Py-Screener, a dedicated system that utilizes the quick and simple Py-GC/MS method, which requires no pretreatment or organic solvents. The results obtained using the Py-Screener and solvent extraction–GC/MS methods were found to be equivalent for quantitative measurements in the region of the regulatory concentration level of 1000 mg/kg. The Py-Screener was shown to be useful for screening of the phthalate esters that were added to the amended RoHS Directive.

## References

- 1) COMMISSION DELEGATED DIRECTIVE (EU) 2015/863 of 31 March 2015 amending Annex II to Directive 2011/65/EU of the European Parliament and of the Council as regards the list of restricted substances.
- 2) *Specifications and Standards for Food and Food Additives, etc.*, Ministry of Health and Welfare Notification No. 370
- 3) EN 14372:2004, *Child use and care articles. Cutlery and feeding utensils. Safety requirements and tests.*
- 4) ASTM D3421-75, *Recommended Practice for Extraction and Determination of Plasticizer Mixtures from Vinyl Chloride Plastics.*
- 5) CPSC-CH-C1001-09.3, *Standard Operating Procedure for Determination of Phthalates.*
- 6) ISO 8124-6:2014, *Safety of toys — Part 6: Certain phthalate esters in toys and children's products.*
- 7) ISO 14389:2014, *Textiles — Determination of the phthalate content — Tetrahydrofuran method.*
- 8) ASTM D7823-14, *Standard Test Method for Determination of Low Level, Regulated Phthalates in Poly (Vinyl Chloride) Plastics by Thermal Desorption—Gas Chromatography/Mass Spectrometry*
- 9) F. Maruyama, S. Fujimaki, Y. Sakamoto, Y. Kudo, and H. Miyagawa, *Anal. Sci.*, **2015**, 31, 3.

## Screening System for Phthalate Esters

# Py-Screener

## Organics Solvents Are Not Required for Sample Preparation

Analytical standards and test samples can be prepared without using organic solvents. Sample preparation videos provide support so that even novices can easily prepare samples.



Sample Preparation Videos

## All Required Items Are Available for Sample Preparation

The analytical standards for this system were developed in cooperation with SGS Japan, the market leader for RoHS tests. Standards for sensitivity confirmation, quantitation, and blank tests can be prepared simply by punching out a portion of a standard material using the micro puncher.



Standards Containing Phthalate Esters for Py-GC/MS



## Tabular Display of Concentrations and Criteria Clarifies the Results

The concentrations of target components detected in continuous measurements are displayed in a table and color-coded using criteria based on concentration ranges. The results for continuously measured test samples can be checked at a glance.



First Edition: January, 2016



Shimadzu Corporation  
www.shimadzu.com/an/

For Research Use Only. Not for use in diagnostic procedures.  
The content of this publication shall not be reproduced, altered or sold for any commercial purpose without the written approval of Shimadzu. The information contained herein is provided to you "as is" without warranty of any kind including without limitation warranties as to its accuracy or completeness. Shimadzu does not assume any responsibility or liability for any damage, whether direct or indirect, relating to the use of this publication. This publication is based upon the information available to Shimadzu on or before the date of publication, and subject to change without notice.

© Shimadzu Corporation, 2016  
Printed in Japan 3655-12507-10ANS

# Determination of Volatile Organic Compounds (VOCs) present in the interiors of car by using GCMS/MS with static and dynamic headspace

**ASMS 2015** ThP 138

Sanket Chiplunkar, Ankush Bhone, Durvesh Sawant,  
Dheeraj Handique, Prashant Hase, Ajit Datar,  
Jitendra Kelkar and Pratap Rasam  
Shimadzu Analytical (India) Pvt. Ltd.,  
1 A/B Rushabh Chambers, Makwana Road, Marol,  
Andheri (E), Mumbai-400059, Maharashtra, India.



## Determination of Volatile Organic Compounds (VOCs) present in the interiors of car by using GCMS/MS with static and dynamic headspace

### Introduction

Volatile Organic Compounds (VOCs) are a large group of carbon-based chemicals that have high vapor pressure at room temperature. They are widely present in both outdoor and indoor air, and are considered to be an important group of air pollutants. They are reported to have a negative impact on human health, and their concentration in indoor air is higher than outdoor air<sup>[1]</sup>. The level of VOCs indoors is generally 3 to 4 times higher than the level of VOCs outdoors. The interior of vehicle (Refer Figure 1) is regarded as a specific microenvironment where the concentration of VOCs may be much higher than in public or private buildings.

Inside the car, sources of VOCs are air fresheners, paints, adhesives, air conditioners, plastic and leather materials etc. Exposure of VOCs may increase risk of cancer, damage to liver, kidney and central nervous system. The extent and nature of the effect on health will depend on many factors including level and duration of exposure. Some of the potential VOCs were measured by Shimadzu GCMS-TQ8040 equipped with HS-20 Loop (Static) and Trap (Dynamic) headspace sampler and by using Multiple Reaction Monitoring (MRM) mode to obtain reliable analytical data.



Figure 1. Interior of car



Figure 2. Headspace vial and monotrapp

### Method of analysis

#### Extraction of VOCs by using static and dynamic headspace

##### 1) Standard stock solution:

Standard solution mixture of VOCs (2000 ppm) were procured from Restek® (P/N:VOC kit #30221). Using this standard solution, 2000 ppb standard stock solution was prepared in methanol containing mixture of 17 VOCs.

##### 2) Calibration curve:

Standard stock solution was further diluted with methanol to make eight linearity levels with different concentration ranging from 5 ppb to 500 ppb. Calibration curve was plotted using above linearity level standard solutions (Refer Figure 5 and 6) in the

concentration range of 5 ppb, 10 ppb, 25 ppb, 50 ppb, 75 ppb, 125 ppb, 250 ppb and 500 ppb. 20 µL of each level standard solution was transferred in separate 20 mL headspace vials and crimped with automated crimper.

## Determination of Volatile Organic Compounds (VOCs) present in the interiors of car by using GCMS/MS with static and dynamic headspace

### 3) Sample preparation:

RSC18 monotraps from GL Sciences P/N:1050-71201 (4 units each) in 20 mL headspace vial was placed inside the car with vial mouth open for 24 hrs <sup>[2]</sup> (Refer Figure 2). 20 µL of methanol was added in the vial and crimped with automated crimper.

Method was partly validated to support the findings by performing precision, linearity, LOD and LOQ determination as summarized in Table 1.

Table 1. Method validation parameters

Parameter	Concentration (ppb)
Linearity (Dynamic)	5, 10, 25, 50, 75, 125, 250 and 500
System precision (Dynamic)	100 (n=6)
Sample precision (Dynamic)	(n=5)
System precision (Static)	100 (n=6)



Figure 3. GCMS-TQ8040 equipped with HS-20 by Shimadzu

### Key Features of GCMS-TQ8040 equipped with HS-20

- Static and dynamic both modes are available in HS-20.
- Advanced Pressure Controller (APC) pressure programming enables removal of carryover.
- Can work on high temp range of Loop (300 °C), trap (350 °C), oven (300 °C) and transferline (350 °C).
- ASSP™ (Advanced Scanning Speed Protocol) enables high-speed scan and data acquisition for accurate quantitation at 20,000 u/sec.
- Ultra Fast UF sweeper® technology efficiently sweeps residual ions from the collision cell for fast, efficient ion transport ensuring no cross-talk.
- Acquisition modes including MRM, Scan/MRM, Precursor Ion, Product Ion, Neutral Loss Scan and SMART MRM Software helps to create method and sequence automatically.

# Determination of Volatile Organic Compounds (VOCs) present in the interiors of car by using GCMS/MS with static and dynamic headspace

## HS-GCMSMS Analytical Conditions

The analysis was carried out using Shimadzu GCMS-TQ8040 equipped with HS-20 (Figure 3) as per conditions given in Table 2.

Table 2. Analytical conditions

Headspace parameters

Sampling Mode

: Static and dynamic

Oven Temp.

: 90.0 °C

Sample Line Temp.

: 100.0 °C

Transfer Line Temp.

: 110.0 °C

Trap Cooling Temp

: -25.0 °C

Trap Desorb. Temp

: 220 °C

Trap Equilib. Temp

: 25.0 °C

Multiple Injection Count

: 3

Equilibrating Time

: 15.00 min

Pressurizing Time

: 2.00 min

Injection Time

: 10.00 min

GC Cycle Time

: 45.00 min

Gas Pressure

: 65.0 kPa

Dry Purge Pressure

: 20 kPa

Chromatographic parameters

Column

: Rxi-VMS (60 m L x 0.45 mm I.D. x 2.55 µm)

Injection Mode

: Split

Split Ratio

: 3.0

Carrier Gas

: Helium

Linear Velocity

: 57.0 cm/sec

Pressure

: 48.6 kPa

Column Flow

: 4.99 mL/min

Total Program Time

: 21.00 min

Column Oven Temp.

:

Rate (°C /min)	Temperature (°C)	Hold time (min)
	40.0	2.00
10.00	230.0	0.00

Mass Spectrometry parameters

Ion Source Temp.

: 200.0 °C

Interface Temp.

: 230.0 °C

Ionization Mode

: EI (Electron ionization)

Mode

: MRM

# Determination of Volatile Organic Compounds (VOCs) present in the interiors of car by using GCMS/MS with static and dynamic headspace

## Results

### MRM method preparation

Mixtures of different VOC standards (four standard solutions - 2000 ppm) were procured from Restek®. For MRM optimization, about 2 ppm of standard stock solution was prepared using above standard solutions. Further above standard stock solution was analyzed using scan mode. For 17 components, retention time and precursor ions were identified and selected. Using selected precursor ions, product ion scan was performed with different Collision Energies (CE). For each

component, MRM transitions with appropriate CEs were determined (Refer Table 3). All the above steps were simplified with the help of Smart MRM optimization tool. These MRM transitions were registered to Smart Database and the final MRM method with optimum segments was generated. Further this optimized MRM method was used to analyze samples (Refer Figure 4) by using both static and dynamic mode of HS-20 headspace sampler.

Table 3. MRM and CE table

Sr. No.	Name of VOCs	Target MRM (m/z)	CE	Reference-1 MRM (m/z)	CE	Reference-2 MRM (m/z)	CE
1	Ethylene, 1,2-dichloro	95.95>61.00	18	97.95>63.00	18	97.95>61.00	18
2	Benzene	78.05>52.10	18	77.05>51.00	18	78.05>39.00	18
3	Ethane, 1,2-dichloro-	62.00>27.00	18	64.00>27.10	18	62.00>60.90	42
4	Trichloroethylene	129.95>95.00	15	131.95>97.00	18	131.95>95.00	15
5	Propane, 1,2-dichloro-	63.00>27.00	15	76.00>41.00	12	76.00>39.00	21
6	Methane, bromodichloro-	82.95>48.00	24	82.95>82.00	33	84.95>47.90	27
7	Toluene	92.10>91.10	18	91.10>65.10	18	91.10>39.00	24
8	Tetrachloroethylene	165.90>130.90	18	163.90>128.90	15	163.90>94.00	27
9	Ethane, 1,1,2-trichloro-	97.00>61.00	18	99.00>61.00	18	99.00>63.00	18
10	Methane, dibromochloro-	128.90>48.00	27	126.90>48.00	27	128.90>127.90	42
11	Ethylbenzene	91.10>65.10	18	106.10>91.10	18	91.10>39.10	27
12	p-Xylene	106.10>91.10	18	91.10>65.10	18	91.10>39.10	27
13	o-Xylene	106.10>91.10	18	91.10>65.10	18	91.10>39.10	27
14	Styrene	104.10>78.10	18	104.10>103.10	18	103.10>77.00	18
15	Benzene, 1,4-dichloro-	146.00>111.00	18	146.00>75.10	27	148.00>75.00	27
16	Benzene, 1,2-dichloro-	146.00>111.00	18	146.00>75.10	27	148.00>75.00	27
17	Benzene, 1,2,4-trichloro-	179.95>145.00	18	179.95>109.00	27	181.95>147.00	15

# Determination of Volatile Organic Compounds (VOCs) present in the interiors of car by using GCMS/MS with static and dynamic headspace

## Summary of validation results

On the basis of statistical data obtained, the method was proved to be highly selective, sensitive and reliable.

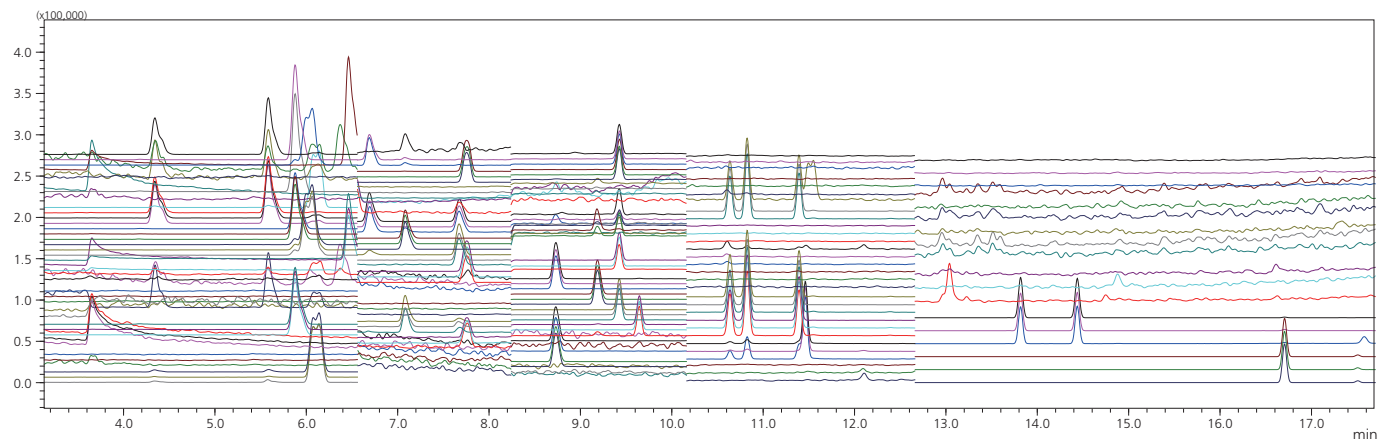


Figure 4. MRM Chromatogram of 100 ppb standard solution

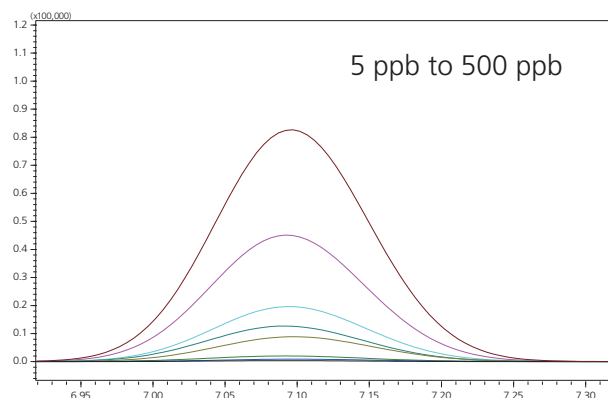


Figure 5. Overlay of linearity levels for Trichloroethylene

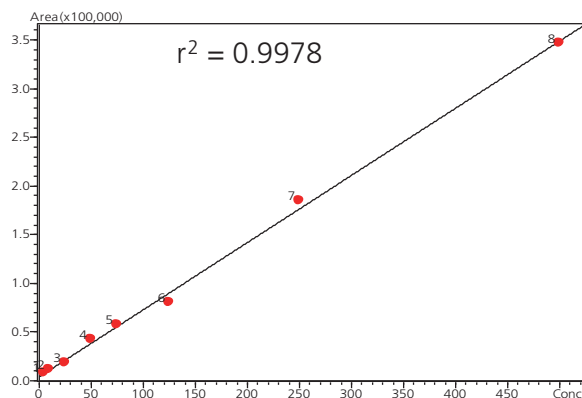


Figure 6. Calibration curve for Trichloroethylene

# Determination of Volatile Organic Compounds (VOCs) present in the interiors of car by using GCMS/MS with static and dynamic headspace

Table 4. Comparative data for static and dynamic headspace mode

Sr. No.	Name of VOCs	In Dynamic mode			System precision (n=6) for 100 ppb			
					Dynamic mode		Static mode	
		Linearity (r <sup>2</sup> )	LOD* (ppb)	LOQ* (ppb)	Avg. Area	% RSD	Avg. Area	% RSD
1	Ethylene, 1,2-dichloro	0.9980	1.7	5.3	113064	2.8	40,714	4.3
2	Benzene	0.9654	0.7	2.1	449,500	2.1	157,837	5.3
3	Ethane, 1,2-dichloro-	0.9978	0.2	0.6	51,176	4.0	16,709	4.9
4	Trichloroethylene	0.9980	1.0	3.2	152,558	2.2	54,970	4.2
5	Propane, 1,2-dichloro-	0.9981	1.4	4.1	53,998	3.3	16,757	7.8
6	Methane, bromodichloro-	0.9967	0.6	1.8	33,745	2.9	9,431	7.5
7	Toluene	0.9956	0.8	2.4	199,811	2.3	66,624	4.3
8	Tetrachloroethylene	0.9978	1.8	5.4	55,502	2.3	17,653	4.2
9	Ethane, 1,1,2-trichloro-	0.9974	2.1	6.2	49,922	1.8	13,145	4.9
10	Methane, dibromochloro-	0.9976	1.1	3.4	9,310	1.7	2,617	6.7
11	Ethylbenzene	0.9981	1.1	3.3	85,477	2.1	26,866	4.2
12	p-Xylene	0.9980	0.6	1.9	222,067	2.7	69,309	4.1
13	o-Xylene	0.9969	1.0	3.1	184,205	1.6	50,763	4.8
14	Styrene	0.9974	0.8	2.5	122,897	3.3	32,467	4.8
15	Benzene, 1,4-dichloro-	0.9968	1.0	3.1	161,920	4.0	45,440	6.8
16	Benzene, 1,2-dichloro-	0.9971	1.0	3.1	163,283	4.5	41,228	4.6
17	Benzene, 1,2,4-trichloro-	0.9971	0.9	2.9	119,406	5.0	30,045	4.8

\*As per software calculations.

Table 4 gives comparison of data obtained on standards using static and dynamic headspace analysis of VOCs.

## Determination of VOCs in interior of car

RSC18 monotraps were kept inside a car for 24 hours to trap VOCs. Then these monotraps with trapped VOCs were analyzed as per instrument parameters given in Table 2. Precision (n=5) for sample analysis was carried out and %RSD for individual VOCs from five replicate injections was found to be less than 15% (Refer Table 5).

Table 5. Summary of sample analysis

Sr. No.	Name of VOCs	System precision (n=5)		
		Dynamic mode		
		Avg. Area	% RSD	Concentration (ppb)
1	Toluene	94,051	14.6	48
2	Ethylbenzene	16,347	14.8	18
3	o-Xylene	63,464	14.6	34
4	Benzene, 1,4-dichloro-	38,930	14.6	22



## Determination of Volatile Organic Compounds (VOCs) present in the interiors of car by using GCMS/MS with static and dynamic headspace

### Conclusion

- HS-GCMSMS method was developed for determination of VOCs from interior of the car by trapping on RSC18 monotraps. Part method validation was performed. Results obtained for reproducibility, linearity and LOQ studies were within acceptable criteria.
- Dynamic mode is almost 4 to 5 times sensitive than static mode and further can be optimized for more sensitivity by optimization of multi injection count.
- Ultra Fast Scan Speed 20,000 u/sec is the characteristic feature of GCMS-TQ8040 mass spectrometer, useful for quantitation of VOCs at very low level (ppb level) with high sensitivity.

### References

- [1] A Study of Indoor air quality certified (IAQ) in Automobile Cabin Interiors GREENGUARD Environmental Institute Released May 31, 2006.
- [2] Easy Enrichment of the VOC in a New Car with MonoTrap® GC Technical Note 33 from GL Science Inc.

First Edition: May, 2015

## Analysis of VOC and FOG emissions from moulded components for automobiles according to VDA 278

### Introduction

In Germany millions of new cars are produced and licensed every year. In the supply chain of a vehicle, control standards have to be followed to ensure a high quality final product. The VDA regulations e.g. address the organic emissions from automotive components. Based on thermodesorption techniques, VDA 278 regulates the test procedure for non-metallic materials used for moulded components in automobiles. With this, two classes of compounds are distinguished: highly and medium volatile substances (VOC) up to C25 and those of low volatility (FOG) in the range of C14 up to C32.

In this application the upper layer material of fairing parts used in automobiles has been analyzed according to VDA 278 regarding its organic emission. The influence of open storage time on the VOC and FOG content has been additionally investigated.

### Workflow and analytical conditions

According to VDA 278 the workflow shown in figure 1 has to be followed. A control standard solution of 18 compounds has to be checked to ensure instrument performance followed by the measurement of 2 standards as calibration substances. In case of VOC toluene, for the FOG calibration hexadecane is used to determine the respective response factor. Each sample has to be measured twice: One sample is used for a VOC analysis only, the second one is measured under VOC conditions subsequently followed by FOG analysis.

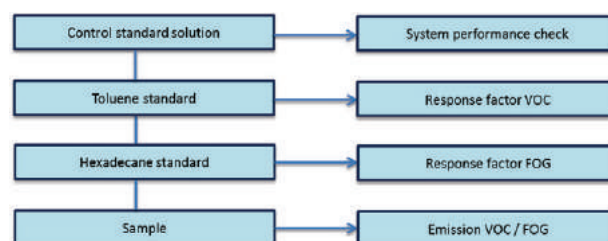


Figure 1: Workflow according to VDA 278

Table 1: Analytical conditions for VOC

TD-20	GCMS
Desorption temperature: 90 / 120 °C	Column: Optima5MS 50 m, 0.32 mm ID, 0.5 µm film thickness
Desorption flow: 80 mL/min	Oven Temp.: 40 °C, 2 min → 3 °C/min to 92 °C → 5 °C/min to 160 °C → 10 °C/min to 280 °C, 10 min
Desorption time: 30 min	Column flow: 1.3 mL/min
Trap cool temperature: -20 °C	Split: 100:1
Line temperature: 280 °C	Ion Source Temp.: 280 °C
Interface temperature: 280 °C	Interface Temp.: 200 °C
	Acquisition Mode: Scan (29 - 450 u)

The measurements were carried out using GCMS-QP2010 SE combined with the TD-20 thermodesorption unit. Following VDA 278, desorption temperatures for the tubes were set to 90 °C (VOC) and 120 °C (FOG) respectively, desorption time was 30 min each. The chromatographic separation was performed by means of an Optima5MS column with 50 m length, 0.32 mm ID, 0.5 µm film thickness. The oven temperature for the FOG run was programmed beginning at 50 °C, held for 2 min, ramped with 25 °C/min to 160 °C followed by a second ramp of 10 °C/min up to 280 °C final temperature, held for 30 min. The settings for the VOC run are summed up in table 1. Compound detection was done by a MS full scan over the expected mass range. Due to the high concentrations both in the standards as well as the samples, a split of 100:1 was used to prevent detector saturation. Additionally, the amount of standards injected into the TD tubes could be decreased by a factor of 4 to 0.5 µg absolute. The sample was cut into small pieces of around 10 mg placed into empty TD tubes as shown in figure 2. For the standard solution, tubes filled with Tenax were used, the solvent was evaporated after injection under a continuous flow of nitrogen gas (5 min at 100 ml/min).

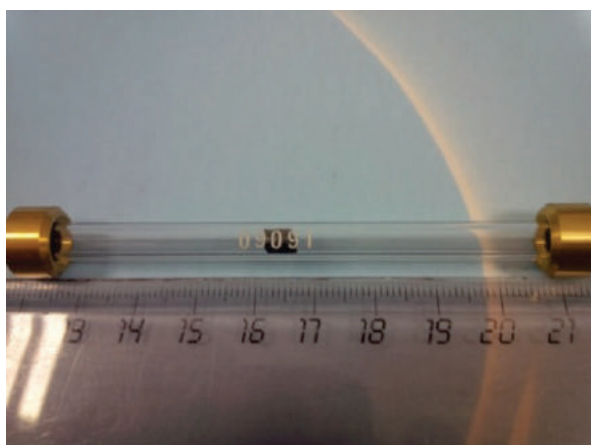


Figure 2: Sample placed into the TD tube

## Results and discussion

The chromatogram of the control standard solution is shown in figure 3. As required by VDA 278, o-xylene and n-nonane are baseline separated. Undecane and 2,5-dimethylphenol coelute (see insert in figure 3) but can both be identified using the library search. Recovery rates for the compounds checked were well within the limits of 60 - 140%. For toluene, the recovery was 98%. Response factors calculated for VOC and FOG were 0.08 and 0.06, respectively. With these, the emissions from the upper layer material of fairing parts were measured directly after opening the package. The chromatograms for the VOC and FOG run are shown in figure 4. For emission calculations all peaks have been summed.

An analogous measurement was repeated after 7 days of open sample storage in a neutral environment as is compulsory for VDA278 analyses. The emission values for all measurements before and after storage are summarized in Table 2. As would be expected, the emission was significantly decreased after longer storage time. The VOC value decreased drastically compared to the FOG content as these compounds have higher volatilities.

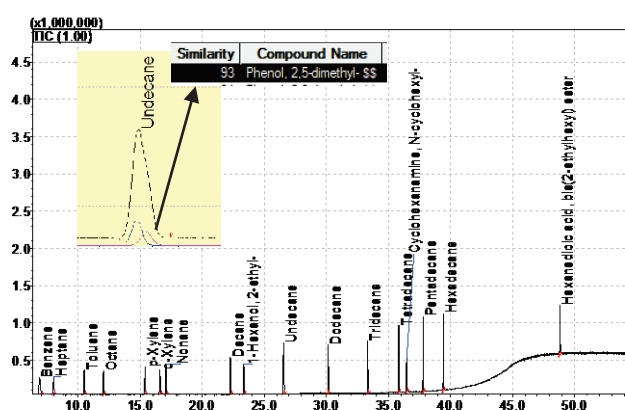


Figure 3: Chromatogram of the control standard

Table 2: VOC and FOG emission from the upper layer material of fairing parts

After unpacking:		After 7 days of open storage:	
Emission VOC 1:	299 µg/g	Emission VOC 1:	160 µg/g
Emission VOC 2:	290 µg/g	Emission VOC 2:	156 µg/g
Emission FOG:	234 µg/g	Emission FOG:	164 µg/g

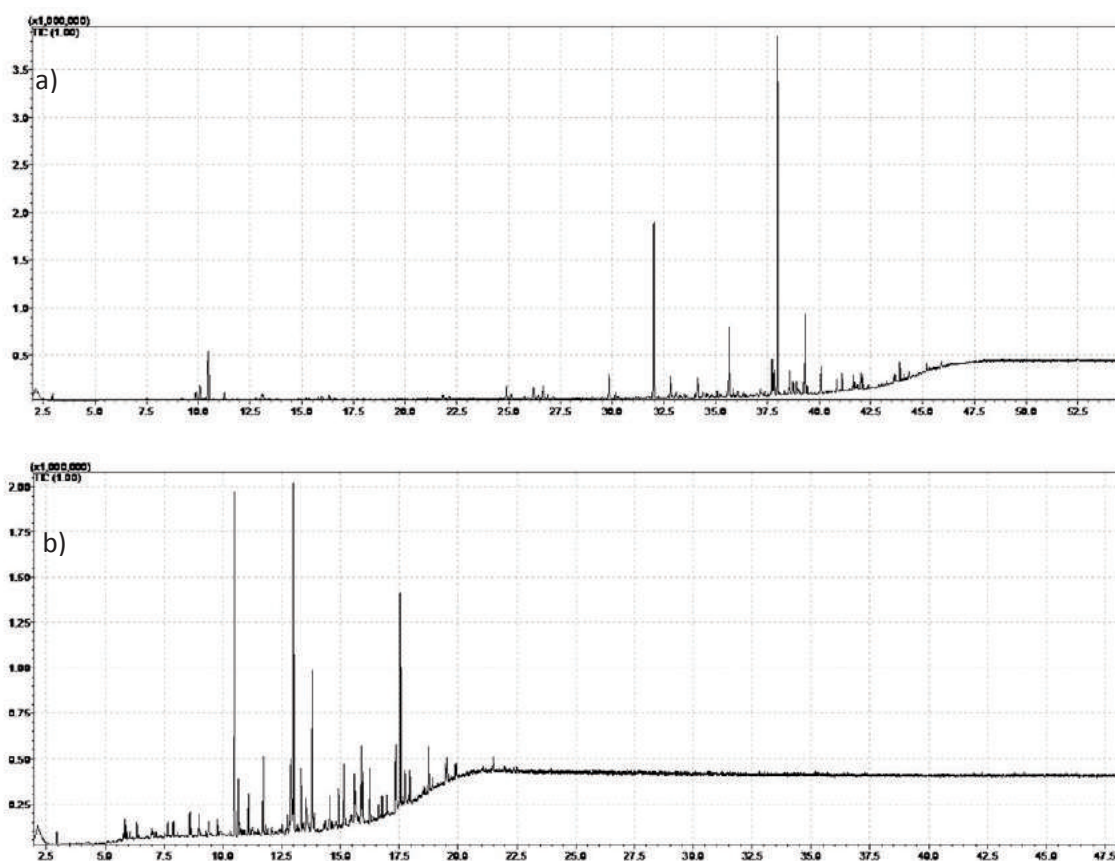


Figure 4: Chromatograms of the upper layer material of fairing parts measured under a) VOC and b) FOG conditions

## Conclusions

In this application the upper layer material of fairing parts used in automobiles was analyzed for VOC and FOG compounds according to VDA 278. The GCMS-QP2010 SE in combination with TD-20 proved to be fully sufficient for such kind of analysis.

Furthermore, a high influence of the storage time on the emission values was determined indicating that following the defined storage time in VDA278 is extremely important for reliable and reproducible detection of the emission values.

# Development of Automated Screening and Quantitation Approach on Novel On-Line SFE-SFC-MS/MS Platform – (I) For 23 Restricted Perfluorocompounds in Textiles

**ASMS 2016** MP 283

Jie Xing, Jun Xiang Lee, Peiting Zeng and Zhaoqi Zhan  
Application Development & Support Centre,  
Shimadzu (Asia Pacific) Pte Ltd, 79 Science Park Drive,  
Singapore

# Development of Automated Screening and Quantitation Approach on Novel On-Line SFE-SFC-MS/MS Platform – (I) For 23 Restricted Perfluorocompounds in Textiles

## Introduction

Supercritical Fluid Chromatography (SFC) with carbon dioxide as eluent has attracted attention recently because of its advantages in low running cost, non-toxicity and wider coverage of analytes in terms of polarity. The combination of SFC with SFE (E=Extraction) has extended the applications to fully-automated sample pre-treatment and analysis as demonstrated by the Nexera UC system introduced by Shimadzu recently. The novel SFE-SFC-MS/MS system has been used successfully for

analysis of 510 residual pesticides in agricultural products [1]. One of the main advantages of the Nexera UC platform allows to set up on-line method to analyse directly different types and forms of un-pretreated samples. We describe the development of an approach on the Nexera UC platform, aiming at screening and quantitation of 23 perfluorocompounds (PFCs) listed under the Restricted Substance List (RSL) in textile, leather and consumer goods industries [2].

## Experimental

A total of 23 PFCs and 2 internal standards (IS), M-PFOS and M-PFOA (refer to Table 2) were obtained from Sigma Aldrich, Wellington Laboratories and Apollo Scientific [3]. Textile samples were cut into smaller pieces and weighed. The sample (60 mg) was loaded into a 0.2 mL stainless steel SFE vessel tightly before proceeding to online-SFE-SFC-MSMS analysis. A schematic diagram of

the Nexera UC system employed in this study is shown in Figure 1. The system can be operated for on-line SFE-SFC-MS/MS experiments or only for SFC-MS/MS analysis. The mobile phase is supercritical fluid CO<sub>2</sub>, with addition of organic modifier like MeOH. Thus, both isocratic and gradient elution modes can be chosen. The details of the analytical conditions are compiled into Table 1.

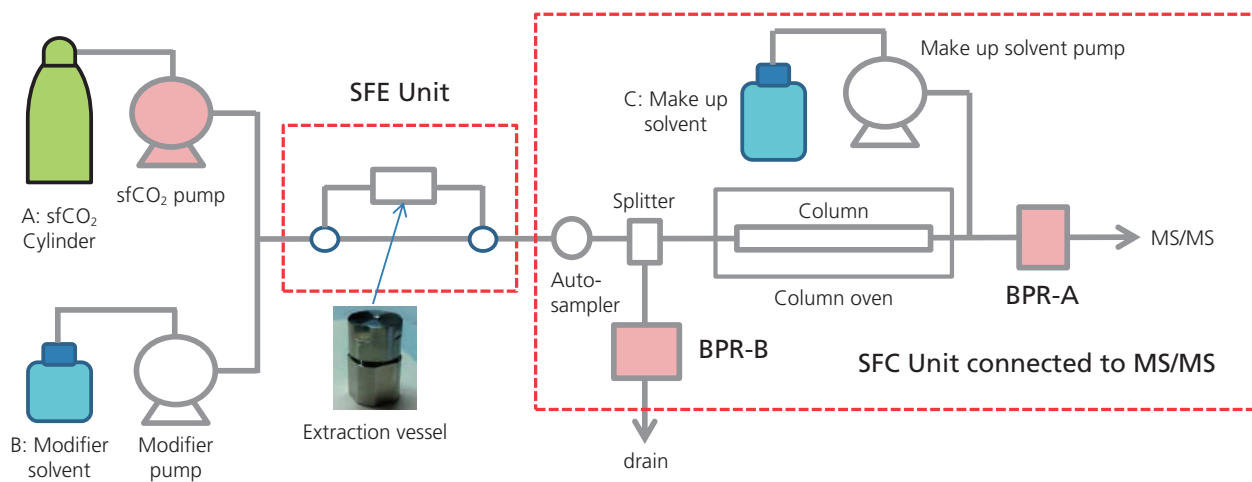


Figure 1: Schematic diagram of Nexera UC system for SFE-SFC-MS/MS analysis of un-pretreated samples



# Development of Automated Screening and Quantitation Approach on Novel On-Line SFE-SFC-MS/MS Platform – (I) For 23 Restricted Perfluorocompounds in Textiles

Table 1: Analytical conditions of 23 PFCs and 2 internal standard on Nexera UC with LCMS-8050

Column	: Shim-pack UC-X Sil (250 mmL x 2.1mm I.D., 3μm)
Flow Rate	: 2.0 mL/min 0.2 mL/min (make up pump of MS)
Mobile Phase	: A : Supercritical Fluid Carbon dioxide (sfCO <sub>2</sub> ) B : Methanol with 5 mM ammonium formate C : Methanol with 5 mM ammonium formate
Temp.	: Column Oven: 40°C; SFE unit: 40°C or RT
Injection vol.	: SFC: 5 μL; SFE-SFC: 200 μL or 3% split ratio
Elution Mode	: Gradient elution, LC program 7 minute 0%B (0.00mins to 0.30mins) → 50%B (4.00mins to 4.50mins) → 0%B (4.70mins to 6.00mins)
Interface	: ESI
MS mode	: Negative
Block Temp.	: 400°C
DL Temp.	: 250°C
Interface Temp.	: 300°C
CID Gas	: Ar (270kPa)
Nebulizing Gas Flow	: N <sub>2</sub> , 3 L/min
Drying Gas Flow	: N <sub>2</sub> , 10 L/min
Heating Gas Flow	: 0 Air, 10 L/min

## Results and Discussion

### Establishment of SFC-MS/MS method

A SFC-MS/MS method was established for the targeted 23 PFCs with 2 IS first. A Shim-pack UC-X Sil column was used and a gradient elution program was adopted. Two MRM transitions (if available) were used for each PFC, one as quantifier ion and the other for confirmation. The SFC-MS/MS chromatograms and calibration curves (only PFOA and PFOS are displayed) are shown in Figure 2. Calibration curves were built based on the two internal

standards with linearity ( $r^2 > 0.97$ ) for all 23 PFCs (Table 2). Instead of using the concentration, absolute amount (pg) was used for the calibration curves. The LOQ ranges from 0.03 ~ 1 ng/mL while the LOD ranges from 0.01 ~ 0.32 ng/mL. The repeatability of the method was evaluated at two concentrations, 5 and 25 pg. The %RSD results of the post-spiked samples are tabulated in Table 2.

# Development of Automated Screening and Quantitation Approach on Novel On-Line SFE-SFC-MS/MS Platform – (I) For 23 Restricted Perfluorocompounds in Textiles

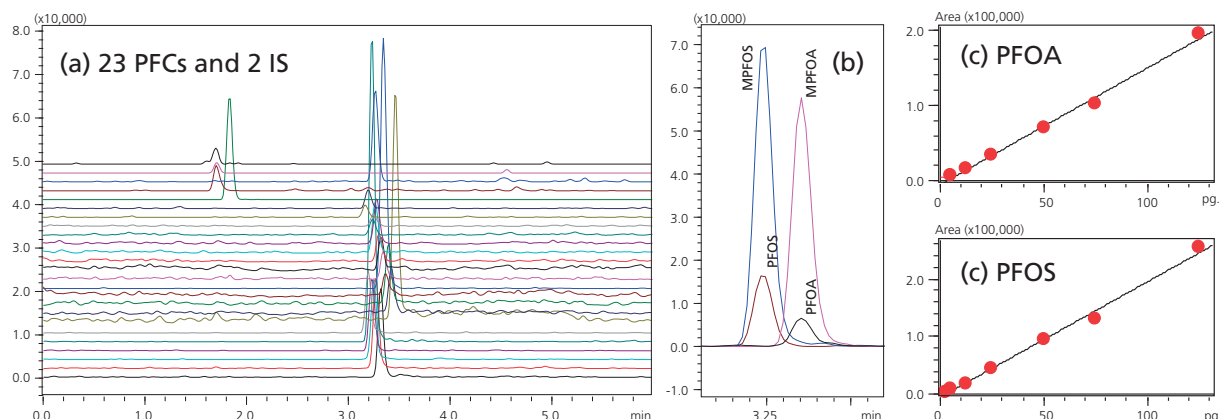


Figure 2: (a) MRM chromatograms of 23 PFC mixed standards with 2 IS, 5 pg for each compound;  
(b) Zoomed MRM peaks of PFOA and PFOS with their IS;  
(c) Calibration curves of PFOA (5~125 pg) and PFOS (2.5~125 pg) based on quantifier ions as shown in table 3.

Table 2: Calibration curves and performance values of the MRM method for quantitative determination of 23 PFCs on SFC-MS/MS.  
Absolute amounts (in pg) of analytes are used for convenience (injection volume: 5  $\mu$ L)

No.	Name	RT (min)	MRM transition	Range (pg)	R <sup>2</sup>	LOD (pg)	LOQ (pg)	RSD (%), n=6	
								(5 pg)	(25 pg)
1	N-EtFOSA-M	1.613	526.10>169.00	5 ~ 125	0.9732	< 2.5	5	34.4	32.3
2	N-MeFOSA-M	1.692	512.00>169.15	2.5 ~ 125	0.9966	< 2.5	5	47.1	18.1
3	H4PFUnA	1.695	491.10>367.00	2.5 ~ 125	0.9877	1.2	3.6	59.9	20.7
4	FOSA	1.831	498.00>77.90	2.5 ~ 125	0.9926	< 2.5	5	23.5	7.9
5	PFODA	3.171	913.00>868.90	2.5 ~ 125	0.9916	0.45	1.3	43.9	12.1
6	PFDHxA	3.2	813.00>768.80	2.5 ~ 125	0.9985	0.25	0.8	16.3	8.3
7	PFDS	3.201	599.00>80.00	2.5 ~ 125	0.9942	0.1	0.3	21.5	8.4
8	PFTeDA	3.23	712.90>668.90	5 ~ 125	0.9947	1.55	4.7	14.4	10.4
9	PFOS	3.233	499.00>79.90	2.5 ~ 125	0.9881	0.1	0.35	21	9.5
10	PFHpS	3.253	449.00>79.85	2.5 ~ 125	0.9924	0.15	0.45	15.6	9.6
11	PFTTrDA	3.257	663.00>619.00	2.5 ~ 125	0.9986	0.75	2.2	23.7	20.7
12	PFDoA	3.265	612.90>569.00	2.5 ~ 125	0.9943	0.5	1.6	13.5	13
13	PF-3,7-DMOA	3.266	469.05>269.00	2.5 ~ 125	0.9918	0.15	0.4	22.3	9.1
14	PFHxS	3.278	399.00>79.90	2.5 ~ 125	0.9923	0.1	0.35	26.9	5.5
15	PFUdA	3.289	563.00>519.00	2.5 ~ 125	0.9975	0.5	1.55	17.7	8.1
16	PFDA	3.307	512.80>468.90	2.5 ~ 125	0.9946	0.75	2.3	25.4	8.3
17	PFBS	3.322	298.80>79.90	2.5 ~ 125	0.9951	0.15	0.45	18.9	8.8
18	PFNA	3.329	462.90>418.90	5 ~ 125	0.9908	1.5	4.55	23.4	12.3
19	PFOA	3.354	413.10>369.10	5 ~ 125	0.9832	1.6	4.8	15	6.1
20	PFHpA	3.38	313.10>269.05	5 ~ 125	0.996	1.25	3.8	14.4	11.8
21	PFHxA	3.399	263.00>219.00	2.5 ~ 125	0.9951	0.3	0.95	18	13.8
22	PFPeA	3.43	212.90>168.95	2.5 ~ 125	0.996	0.35	1.1	18.7	11.4
23	PFBA	3.466	363.10>319.00	2.5 ~ 125	0.9949	0.15	0.5	11.7	8.7
IS1	M-PFOS	3.235	503.00>79.85	10	Not Available				
IS2	M-PFOA	3.349	416.90>372.00	10	Not Available				

## Development of Automated Screening and Quantitation Approach on Novel On-Line SFE-SFC-MS/MS Platform – (I) For 23 Restricted Perfluorocompounds in Textiles

### Development of on-line SFE-SFC-MS/MS approach

Next, an on-line SFE-SFC-MS/MS approach was developed based on the SFC-MS/MS method established. The mixed standard samples for calibration curve construction could be introduced into the system only by pre-loading them onto filter papers. 50  $\mu$ L of mixed standard solution was dropped onto half filter paper (recommended by Shimadzu for Nexara UC use) and left it to dryness under N<sub>2</sub> flow before loading into the SFE vessel (0.2 mL). The results are shown in Figure 3 and Table 3 (columns 1-7). First, with on-line SFE, the elution peaks of the PFCs become broader and RTs delay slightly (about 0.2 min) in comparison with SFC-MS/MS chromatograms. This peak broadening and delay are due to the larger delay volume by the SFE vessel, needles and the tubing from SFE to column, which caused differences in peak areas and intensity. For direct quantitation of PFCs using on-line SFE-SFC-MS/MS,

calibration curves must be established on SFE-SFC-MS/MS too (Figure 3(c) & Table 3 (left)).

If we compare the peak areas obtained on SFE-SFC-MS/MS and SFC-MS/MS, system recovery of the SFE-SFC-MS/MS could be estimated (see Table 3, columns 8-11). Although this system recovery may not be highly accurate, it can be used as a reference to understand the performance of the on-line SFE-SFC-MS/MS for quantitation. The average system recovery measured at the absolute loading amounts of 25 pg and 50 pg are 90 % and 74 %, respectively. The average repeatability (RSD%, n=4) of the system with loading amounts of 25 pg and 50 pg are 12 % and 14 %, respectively. It is worth noting that all of the analysis runs shown above are under the condition without splitting of the flow (sfCO<sub>2</sub> and MeOH) from SFE to SFC-MS/MS (PBR-B was set to zero flow to drain).

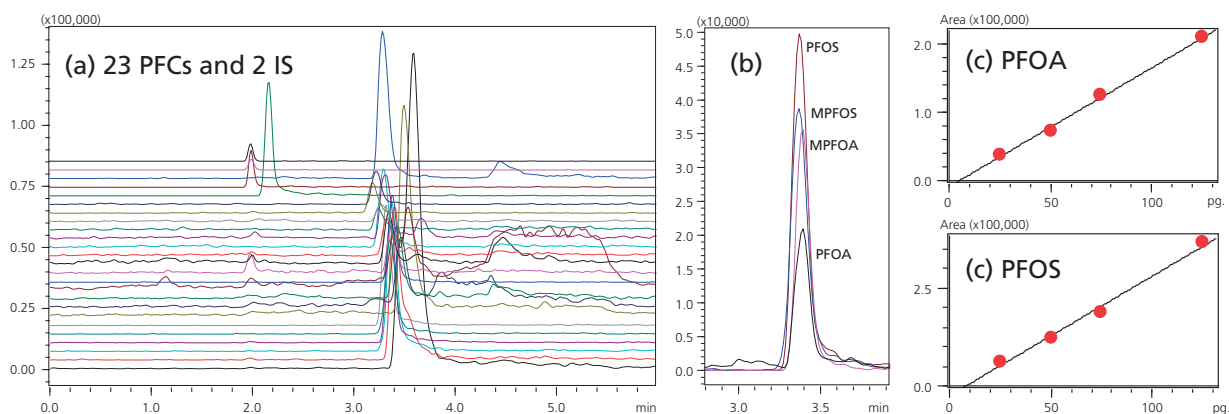


Figure 3: (a) MRM chromatograms of 23 PFC mixed standards with 2 IS on filter paper, 25 pg for each compound.  
(b) Separate display of MRM peaks of PFOA, M-PFOA (IS, 10 pg), PFOS and M-PFOS (IS, 10 pg),  
(c) Calibration curves of PFOA and PFOS on SFE-SPC-MS/MS.

## Development of Automated Screening and Quantitation Approach on Novel On-Line SFE-SFC-MS/MS Platform – (I) For 23 Restricted Perfluorocompounds in Textiles

Table 3: Calibration curves of 23 PFCs (on filter paper in 0.2mL SFE vessel) of on-line SFE-SFC-MS/MS method (left table); System recovery estimated by comparison with SFC-MS/MS method (right Table)

ID#	Name	m/z	Ret. Time	Range (pg)	R <sup>2</sup>	Accuracy (%)	25 pg (spiked)		50 pg (spiked)	
							Recovery %	RSD% (n=4)	Recovery %	RSD% (n=4)
1	N-EtFOSA	526.10>169.00	1.636	25 - 125	0.964	103	137.3	19.4	102.0	12.4
2	N-MeFOSA	512.00>169.15	1.692	25 - 125	0.9668	103.6	89.2	40.1	49.4	33.0
3	H4PFUnA	491.10>367.00	1.694	25 - 125	0.9956	101.2	87.8	24.2	51.6	26.0
4	FOSA	498.00>77.90	1.828	25 - 125	0.9978	100.7	61.0	18.6	40.2	23.8
5	PFODA	913.00>268.95	3.15	25 - 125	0.9946	101.5	91.2	16.9	80.7	20.3
6	PFDHxA	813.00>169.10	3.163	25 - 125	0.988	102.3	83.9	10.7	74.1	14.5
7	PFDS	599.00>98.80	3.3	25 - 125	0.9998	99.7	80.0	11.3	68.9	5.7
8	PFTeDA	712.90>219.20	3.196	25 - 125	0.9968	101.1	104.1	7.7	98.0	13.2
9	PFOS	499.00>98.50	3.344	25 - 125	0.993	101.5	92.6	5.4	75.7	3.5
10	PFHpS	449.00>99.05	3.344	25 - 125	0.9942	101.4	91.9	1.1	77.5	3.6
11	PFTTrDA	663.00>169.10	3.198	25 - 125	0.9956	101.3	72.8	10.0	71.5	19.2
12	PFDoA	612.90>319.00	3.22	25 - 125	0.9947	99.9	101.3	12.0	87.1	10.2
13	PF-3,7-DMOA	469.05>68.80	3.229	25 - 125	0.9949	101.5	98.0	8.4	74.4	5.2
14	PFHxS	399.00>79.90	3.401	25 - 125	0.9958	100.7	87.5	1.1	78.0	4.4
15	PFUdA	563.00>268.90	3.265	25 - 125	0.995	98.7	84.4	1.1	76.6	17.7
16	PFDA	512.80>169.00	3.262	25 - 125	0.9905	101.3	106.1	4.9	89.6	14.6
17	PFBS	298.80>98.80	3.357	25 - 125	0.9912	101.6	89.1	7.9	69.0	8.1
18	PFNA	462.90>168.90	3.31	25 - 125	0.9986	100.6	103.6	8.2	78.8	10.4
19	PFOA	413.10>168.85	3.36	25 - 125	0.9972	100.8	97.8	7.7	87.3	15.0
20	PFHpA	363.10>169.05	3.375	25 - 125	0.9904	101.7	95.9	11.0	83.6	4.0
21	PFHxA	313.10>119.00	3.397	25 - 125	0.9776	100.3	76.6	8.5	74.1	11.4
22	PFPeA	263.00>219.00	3.431	25 - 125	0.9991	100.6	87.0	7.1	62.4	12.4
23	PFBA	212.90>168.95	3.446	25 - 125	0.9997	100	53.0	25.7	41.3	32.5

### Automated SFE-SFC-MS/MS approach for analysis of PFCs in textiles samples

There are two extraction modes in the on-line SFE stage, static extraction and dynamic extraction with sfCO<sub>2</sub> or a mixture of sfCO<sub>2</sub> and MeOH (modifier). For more effective extraction, static extraction is performed first for 4 mins at 40 °C, followed by dynamic extraction for 2 mins. Figure 4 shows an example of the analysis of un-pretreated clothing sample and the same sample spiked with mixed PFCs (25 pg each on 60 mg of sample). The results shows that there are no PFC detected in the textile sample, which is in agreement with the offline LC/MS/MS analysis results [4]. On the other hand, all of the 23 PFCs spiked into the

sample were detected. The amount of PFCs spiked are equal to 0.42 ng/g (ppb), where detection sensitivity meets the requirement for monitoring PFOA and PFOS in consumer products [2]. This preliminary finding reveals the potential possibility of using on-line SFE-SFC-MS/MS as a new automated screening and quantitation system in analysis of un-pretreated samples directly. However, further studies of this novel approach for PFCs and other targeted analytes in various consumer samples are under investigation for optimizing the SFE conditions and improving the recovery for samples with complex matrix.

## Development of Automated Screening and Quantitation Approach on Novel On-Line SFE-SFC-MS/MS Platform – (I) For 23 Restricted Perfluorocompounds in Textiles

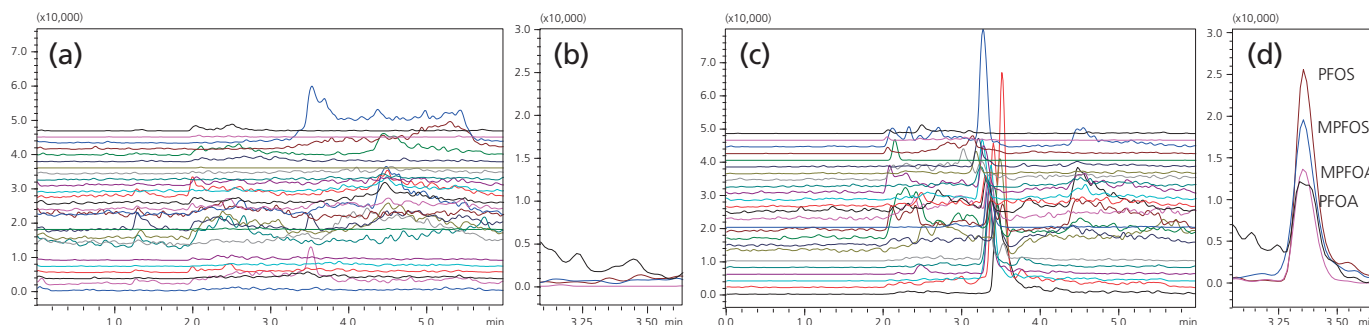


Figure 4: MRM chromatograms for screening of 23 PFCs in a textile sample (a-b) and in the same sample spiked with mixed 23 PFCs standards with 2 IS, 25 pg for each compound (c-d). Only dynamic extraction was used.

## Conclusions

In this study, a new analytical approach on the novel SFE-SFC-MS/MS platform was developed for analysis of 23 PFCs including PFOA and PFOS spiked in textiles. The results indicate that the new approach is potentially possible for screening and quantitation of targeted

analytes in un-pretreated solid samples directly. The detection sensitivity of the 23 PFCs spiked in clothing sample achieved is at the level of 25 pg or 0.42 µg/kg. However, validation of the SFE-SFC-MS/MS approach for actual samples are not carried out yet.

## References

1. Shimadzu Application News No LAAN-A-LC-E273, **Using the Nexera UC Online SFE-SFC-MS System to Analyze Residual Pesticides in Agricultural Products (2015).**
2. I. van der Veen, J. M. Weiss, A. C. Hanning, J. de Boer and P. E. Leonards, *Talanta* **147** (2016), 8-15.
3. Wellington Laboratories, "Quick Reference Guide for Perfluoroalkyl Compounds", <http://www.well-labs.com>
4. J. X. Lee, Z. Sun, J. Xing, J. Y. Tan and Z. Zhan, ASMS 2016, Poster Session TP 485.

Disclaimer: The products and applications in this poster presentation are intended for Research Use only (RUO). Not for use in diagnostic procedures.

First Edition: June, 2016

# Application Data Sheet

No. 123

## GC-MS

Gas Chromatograph Mass Spectrometer

# Py-GC/MS Analysis of Electronic Circuit Board Parts Using Nitrogen Carrier Gas

Helium, which is used as a carrier gas for GC-MS, has in recent years been subject to dramatic price increases and delivery delays. This can, in some cases, make it difficult to obtain Helium. Equipped with a newly developed turbomolecular pump, the GCMS-QP2020 can be operated using replacement carrier gases, such as hydrogen and nitrogen. The measurement range guidelines for each carrier gas is shown in Fig. 1. Although nitrogen provides less sensitivity than helium, its price is ten times lower and it is easily available.

This application data sheet introduces an analysis of the instantaneous pyrolysis of an electronic circuit board using Py-GC/MS, while comparing the usage of nitrogen versus helium as the carrier gas.

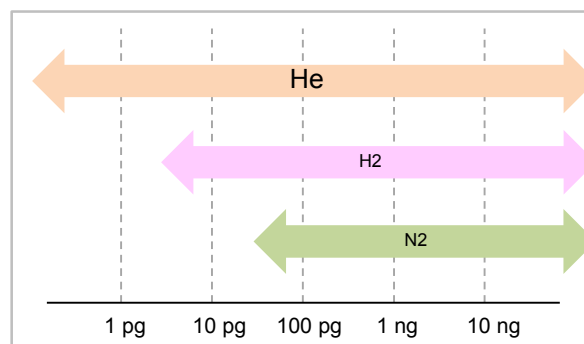


Fig. 1: Measurement Range Guidelines for Each Carrier Gas\* (On-Column Amount)

\* These measurement ranges are at best only guidelines, and may be unsuitable depending on the target compound's sensitivities and characteristics.

## Conversion of Analysis Methods

In changing the carrier gas from helium to nitrogen, the length of the column was changed from 30 m to 20 m and the inner diameter was changed from 0.25 mm to 0.18 mm. The analysis conditions were converted using the web-based "EZGC™ Method Translator\*1" provided by Restek Corporation (<http://www.restek.com/ezgc-mtfc>). For more information regarding the "EZGC™ Method Translator," refer to Application Data Sheet No. 120. The analysis conditions for analyses using helium and nitrogen as the carrier gas are shown in Table 1.

Table 1: Analytical Conditions

Pyrolyzer	: Multi-Shot Pyrolyzer EDA/PY-3030D		
GC-MS	: GCMS-QP2020		
Glass insert	: Deactivated split glass insert with wool (P/N: 225-20803-01)		
[PY]			
Analysis mode	: Single shot		
Furnace temp.	: 600 °C (1 min)		
Interface temp.	: 300 °C		
<b>- Helium carrier gas -</b>			
Purity	: 99.99 %		
Gas purification filter	: Click-ON triple trap (Helium Specific) SGT P/N: SGT-CO1051		
[GC]			
Column	: SH-Rxi™-5Sil MS (length 30 m, 0.25 mm I.D., df=0.25 μm)		
Injection temp.	: 300 °C		
Column oven temp.	: 40 °C (2 min)→(15 °C/min)→320 °C (10 min)		
Injection mode	: Split		
Split ratio	: 50		
Flow control mode	: Linear velocity (39.5 cm/sec)		
Initial column flow	: 1.2 mL/min		
[MS]			
Ionization mode	: EI		
Interface temp.	: 300 °C		
Ion source temp.	: 230 °C		
Acquisition mode	: Scan		
Scan event time	: 0.3 sec		
Scan range	: m/z 60 to 600		
<b>- Nitrogen Carrier Gas -</b>			
Purity	: 99.99 %		
Gas purification filter	: Click-ON triple trap SGT P/N: SGT-CO1005		
[GC]			
Column	: SH-Rxi™-5Sil MS (length 20 m, 0.18 mm I.D., df=0.18 μm)		
Injection temp.	: 300 °C		
Column oven temp.	: 40 °C (2 min)→(14.8 °C/min)→320 °C (10.15 min)		
Injection mode	: Split		
Split ratio	: 50		
Flow control mode	: Linear velocity (26.2 cm/sec)		
Initial column temp.	: 0.32 mL/min		
[MS]			
Ionization mode	: EI		
Interface temp.	: 300 °C		
Ion source temp.	: 230 °C		
Acquisition mode	: Scan		
Scan event time	: 0.3 sec		
Scan range	: m/z 60 to 600		

\*1: EZGC™ Method Translator is a trademark of Restek Corporation.



## Analysis Results

The total ion current chromatograms (TICC) measured for the instantaneous pyrolysis of electronic circuit boards using helium and nitrogen as the carrier gases are shown in Fig. 2. By using the EZGC™ Method Translator, a nearly identical chromatogram pattern could be obtained. Table 2 shows the results of a library search of typical detected peaks using the NIST 14 mass spectral library, and Fig. 3 shows the mass spectrum for the Bisphenol A detected. Even when nitrogen is used as the carrier gas, the mass spectrum is virtually the same as that when helium is used as the carrier gas. This means that existing mass spectral libraries can be used as is. For qualitative applications or quantitative analysis at a  $\mu\text{g/mL}$  (ppm) level, it is possible that a transition to nitrogen carrier gas can be made.

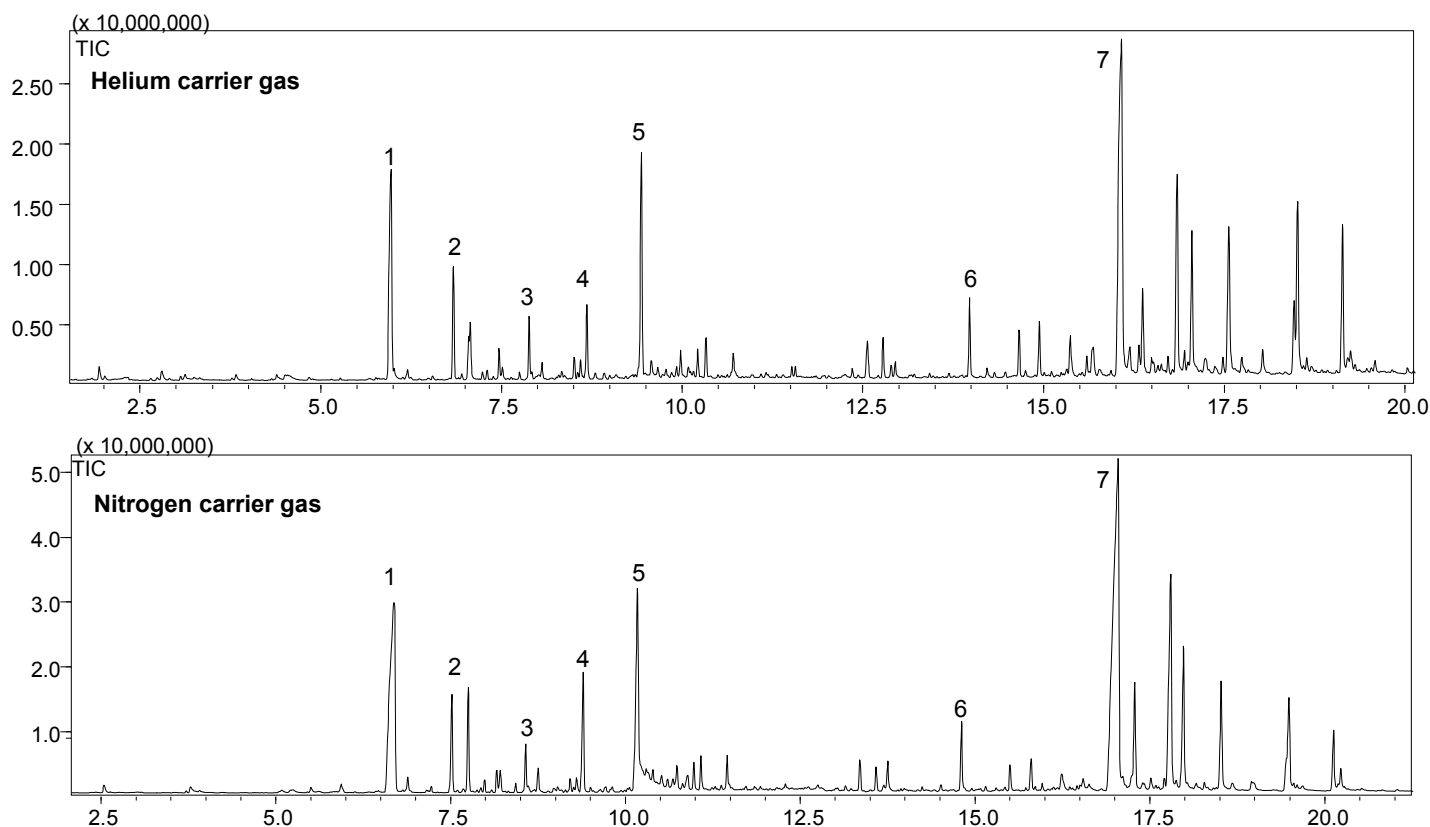


Fig. 2: Total Ion Current Chromatogram (TICC) Measured for the Instantaneous Pyrolysis of Electronic Circuit Board  
Top: Helium Carrier Gas, Bottom: Nitrogen Carrier Gas

Table 2: Results of Library Search for Typical Compounds Detected

No.	Identified Compound	Similarity (SI)	
		He Carrier Gas	N2 Carrier Gas
1	Phenol	99	98
2	Methylphenol	98	98
3	Xylenol	97	98
4	Isopropylphenol	96	97
5	Isopropenylphenol	94	92
6	Cumylphenol	94	93
7	Bisphenol A	95	98

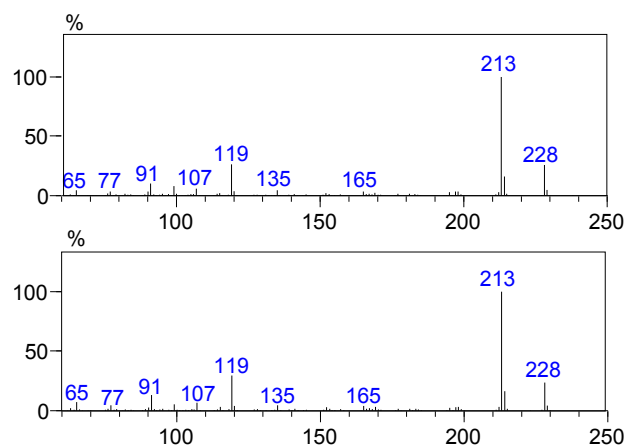


Fig. 3: Mass Spectrum for Bisphenol A Detected  
Top: Helium Carrier Gas, Bottom: Nitrogen Carrier Gas

First Edition: April, 2016

# Rapid analysis of carbon fiber reinforced plastic using DART-MS

**ASMS 2014** TP 782

Hideaki Kusano<sup>1</sup>, Jun Watanabe<sup>1</sup>, Yuki Kudo<sup>2</sup>,  
Teruhisa Shiota<sup>3</sup>

<sup>1</sup> Shimadzu Corporation, Nakagyo-ku, Kyoto, Japan;

<sup>2</sup> Bio Chromato, Inc., Fujisawa, Japan;

<sup>3</sup> AMR Inc., Meguro-ku, Tokyo, Japan

## Rapid analysis of carbon fiber reinforced plastic using DART-MS

### Introduction

DART (Direct Analysis in Real Time) can ionize and analyze samples directly under atmospheric pressure, independent of the sample forms. Then it is also possible to measure in form as it is, without sample preparation. Qualitative analysis of target compounds can be conducted very fast and easily by combining DART with LCMS-2020/8030 which have ultra high-speed scanning and ultra high-speed polarity switching.

Carbon-fiber-reinforced plastics, CFRP is the fiber-reinforced plastic which used carbon fiber for the reinforced material, which is only called carbon resin or

carbon in many cases. An epoxy resin is mainly used for a base material in CFRP. While CFRP is widely used taking advantage of strength and lightness, most approaches which measure CFRP with analytical instruments were not tried, triggered by the difficulty of the preparation. DART (Direct Analysis in Real Time), a direct atmospheric pressure ionization source, is capable of analyzing samples with little or no sample preparation. Here, rapid analysis of carbon fiber reinforced plastic was carried out using DART combined with a mass spectrometer.

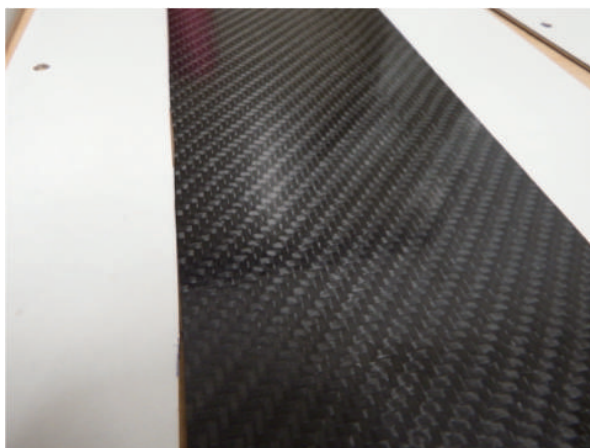


Figure 1 CFRP : carbon-fiber-reinforced plastic

### Methods and Materials

Thermosetting polyimide (carbon-fiber-reinforced plastics) and thermoplastic polyimide (control sample) were privately manufactured. After cutting a sample in a suitable size, it applied DART-MS analysis. They were introduced to the DART gas using tweezers. The DART-OS ion source (IonSense, MA, USA) was interfaced onto the single quadrupole mass spectrometer LCMS-8030 (Shimadzu,

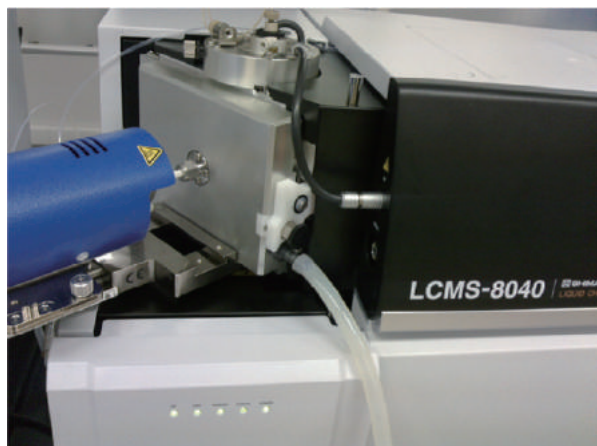
Kyoto Japan). Ultra-fast polarity switching was utilized on the mass spectrometer to collect full scan data.

LCMS-8030 can achieve the polarity switching time of 15msec and the scanning speed of up to 15,000u/sec, therefore the loop time can be set at less than 1 second despite the relatively large scanning range of 50-1,000u.

#### MS condition (LCMS-8030; Shimadzu Corporation)

Ionization	: DART (Direct Analysis in Real Time)
------------	---------------------------------------

## Rapid analysis of carbon fiber reinforced plastic using DART-MS



### High Speed Mass Spectrometer

#### UFswitching

High-Speed Polarity Switching 15msec

#### UFscanning

High-Speed Scanning 15,000u/sec

Figure 2 DART-OS ion source (IonSense) & triple quadrupole LCMS (Shimadzu)

## Result

3 CFRP samples were analyzed by DART-MS. Mass chromatograms of each sample were shown in Figure 3 and mass spectra in Figure 4.

### Sample

- #1 thermoplastic polyimide (control)
- #2 thermosetting polyimide (molded; dried)
- #3 thermosetting polyimide (immediately after molded; wet state with solvent)

### Analytical Condition

Heater Temperature (DART) : 300°C  
Measuring mode (MS) : Positive/Negative scanning simultaneously

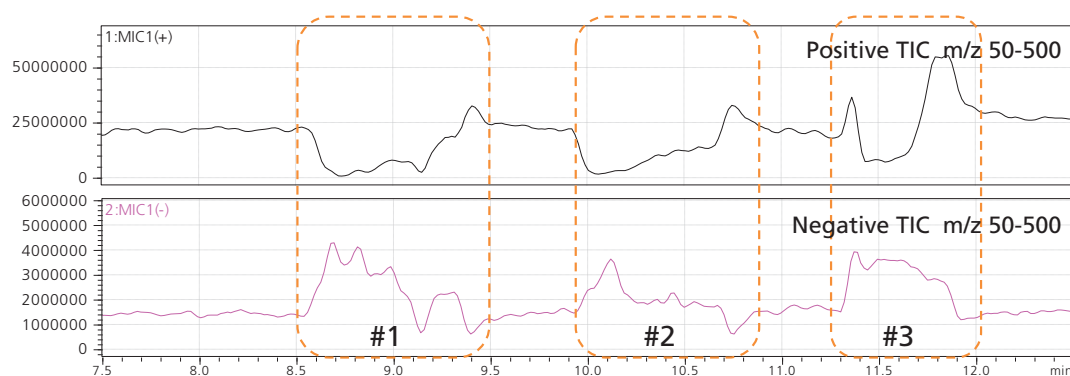


Figure 3 TIC chromatogram of CFRP samples #1, #2, #3

## Rapid analysis of carbon fiber reinforced plastic using DART-MS

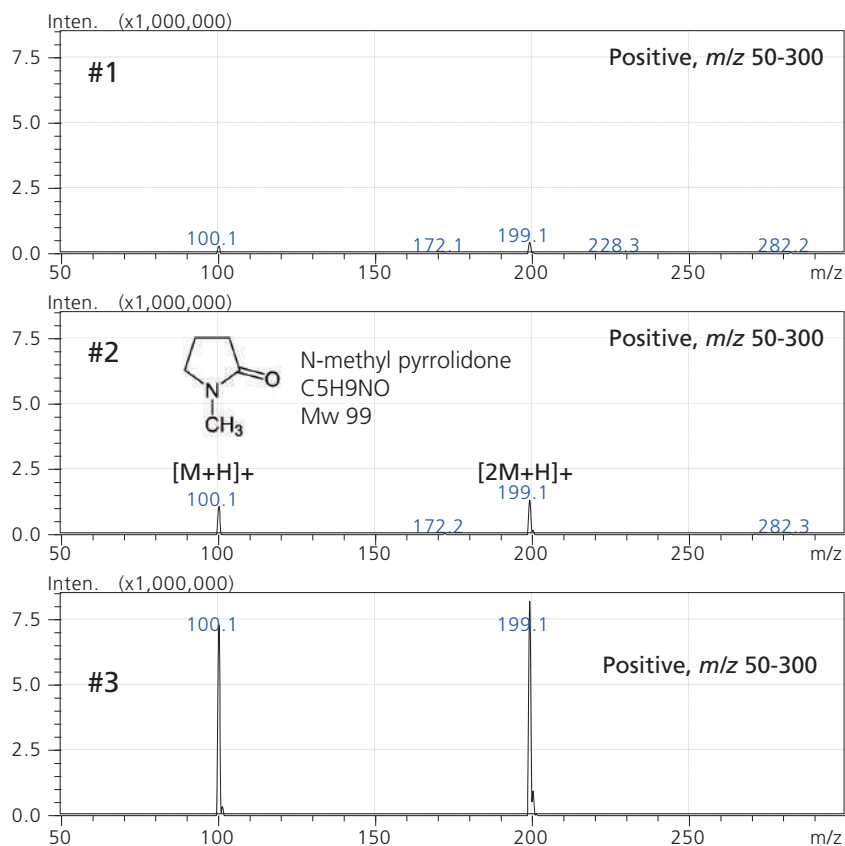


Figure 4 DART-MS spectra of each sample

Since the thermosetting polyimide used for this measurement was molded using the organic solvent (N-methyl pyrrolidone, C<sub>5</sub>H<sub>9</sub>NO, molecular weight 99), molecular related ions of N-methyl pyrrolidone, [M+H]<sup>+</sup> (m/z 100) and [2M+H]<sup>+</sup> (m/z 199), were detected very strongly in the mass spectrum of #1. The mass spectrum of #2 also showed the same ions that intensity was intentionally detected strongly compared with #3 although intensity was weak compared with #1. Even if

it raised the heating gas temperature of DART to high temperature (up to 500°C), MS signal considered to originate in the structural information of CFRP was not able to be obtained.

Then, the optional heating mechanism, ionRocket (Bio Chromato, Inc.; Figure 5), in which a sample could be heated directly was developed to the sample stage of DART, and analysis of CFRP was verified by heating the sample directly up to 600°C.

### Sample

- #4 thermosetting polyimide (molded; dried)
- #5 thermoplastic polyimide (control)

### Analytical Condition

- Heater Temperature (DART) : 400°C
- Temperature control (ionRocket) : 0-1min room temp., 4min 600°C
- Measuring mode (MS) : Positive scanning

## Rapid analysis of carbon fiber reinforced plastic using DART-MS

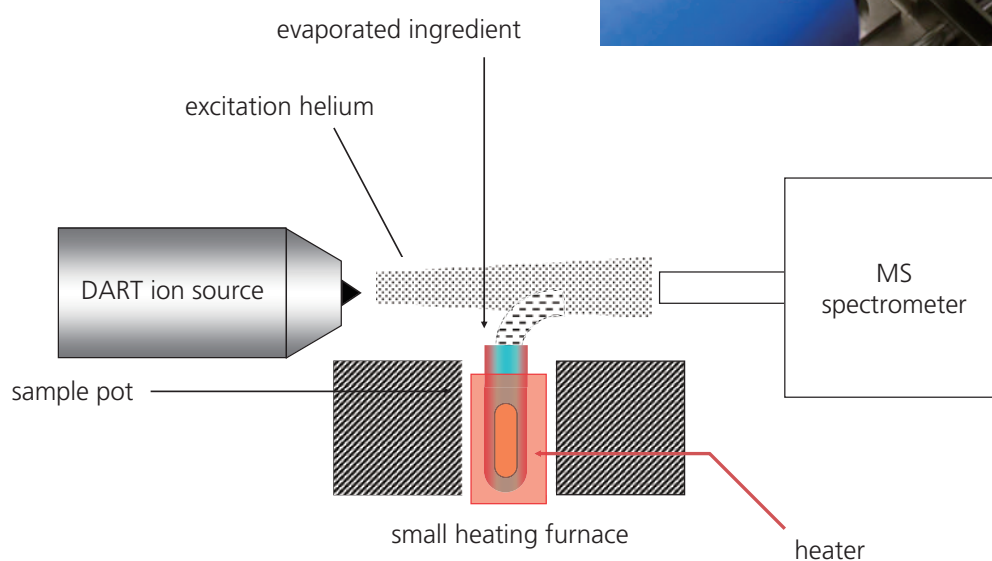
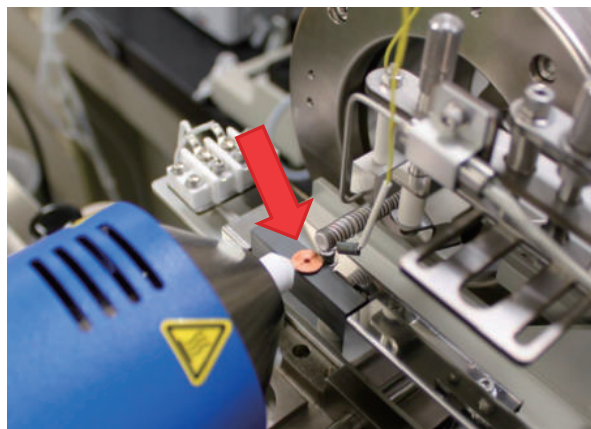
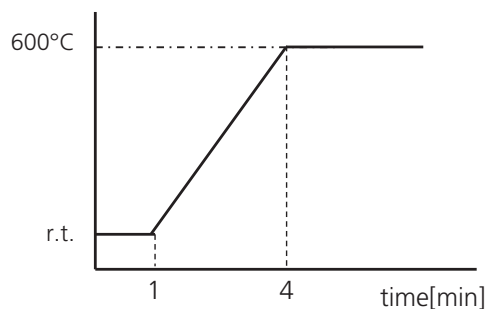


Figure 5 DART-MS system integrated with ionRocket

When heating temperature was set to 600°C, the rudder shape signals of 28u (C<sub>2</sub>H<sub>4</sub>) interval was appeared around m/z 900. This signal was more notably detected with the thermosetting polyimide sample than the thermoplastic sample. Since the sample was heated at

high temperature, it was considered that the thermal decomposition of resin started, the thermal decomposition ingredient of polyimide clustered, and possibly the structures of the rudder signals of equal interval were generated.



## Rapid analysis of carbon fiber reinforced plastic using DART-MS

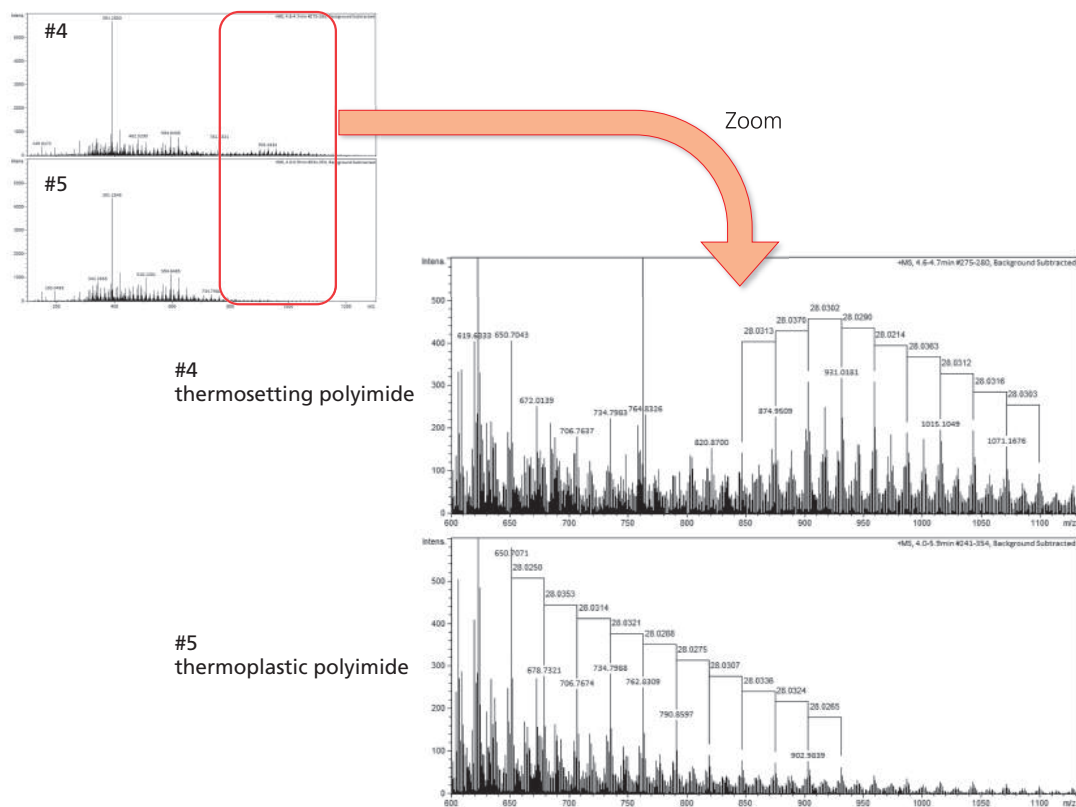


Figure 6 DART-MS with ionRocket spectra of each sample

## Conclusions

The result of having analyzed the carbon fiber plastic CFRP (thermosetting polyimide and thermoplastic polyimide) using DART-MS,

- residue of the solvent used in fabrication was able to be checked by direct analysis of CFRP by DART.
- analyzing CFRP by DART and the heating option ionRocket, the difference between thermosetting polyimide and thermoplastic polyimide was able to be found out.

## Acknowledgment

We are deeply grateful to Mr. Yuichi Ishida, Japan Aerospace Exploration Agency (JAXA), offered the CFRP sample used for this experiment.

First Edition: June, 2014



## 2. Mass Spectrometry

---

### 2.2 Liquid Chromatography-Mass Spectrometry (LC-MS)

---

LC-MS is an analytical chemistry technique that combines the physical separation capabilities of liquid chromatography (LC) with the mass analysis capabilities of mass spectrometry (MS). This powerful method merges very high sensitivity with high selectivity. Its application is aimed at separation, general detection and potential identification of chemicals of particular masses in the presence of other chemicals (e.g. complex mixtures). It is widely used in many application fields such as synthetic dyes in textiles used in automotive segments.

<b>MP122</b>	High speed polarity switching MS/MS applied to polymer additives analysis
<b>TP375</b>	Development of LC/MS/MS method for screening and quantitation of 47 synthetic dyes under restricted substance list in textiles
<b>WP26-541</b>	Analysis of degradation products in electrolyte for rechargeable lithium-ion battery through high mass accuracy MSn and multivariate statistical technique
<b>ThP21 - 455</b>	Differential analysis in vulcanizing accelerators for rubber products by high mass accuracy MSn and multivariate statistical technique

# High speed polarity switching MS/MS applied to polymer additives analysis

ASMS 2011 MP122

Kiyomi Arakawa, Toshikazu Minohata, Natsuyo  
Asano, Jun Watanabe  
SHIMADZU CORPORATION,  
Nishinokyo-kuwabaracho, Nakagyo-ku, Kyoto  
604-8511, Japan

# High speed polarity switching MS/MS applied to polymer additives analysis

## Introduction

Polymer additives include those materials used to make and modify polymers and are used in a highly diverse range of applications such as plastics, synthetic fibers, elastomers, adhesives, polyols, polyurethanes and lubricating oils and greases. As innovation expands polymer types and uses, formulations become increasingly complex and as a result identifying additives in polymer formulations is critical to

product formulation for performance, health, safety and cost of manufacture. It also allows for analysis of competitive products and investigation of alternative technologies.

A fast polarity switching method with high speed data acquisition has been developed for MS/MS analysis to identify unknown additives in polymer formulations.

## Materials and Methods

### A mixture of representative polymer additives (a standard sample):

A sample solution was prepared by mixing the following polymer additives' standard in methanol; Irganox 245, Irganox MD 1024, Irganox 1098, Tinuvin P, Cyanox 2246, Cyanox 425, Irganox 1035, Tinuvin 120, Tinuvin 328, Irganox 1330, Irganox 565, Irganox 1076.

### A sample of plastic laminates preparation:

Polymer additives were extracted from 100mg sample material of plastic laminates using 1mL of tetrahydrofuran (THF) with ultra-sonication for 1 minute. The THF supernatant was then transferred to a clean vial and 5mM ammonium acetate (1mL) was added and resulted supernatant was collected, and filtered with 0.45µm filter. These samples were applied to LC-MS/MS to screen additives by multi-polarity simultaneous scanning (survey scan) and automatic product ion scanning (dependent scan).

### LC-MS/MS:

Samples were analyzed using a Nexera UHPLC system coupled to a LCMS-8030 triple quadrupole mass spectrometer (Shimadzu Corporation, Japan). Polymer additives were separated using a Shim-pack XR-ODS II (2.0 mmI.D. x 75 mm, 2.2µm) using a gradient elution with formic acid and methanol.

### Key features of Nexera UHPLC system

- pressure range up to 130 MPa
- high-speed injection, overlap injection
- highly-efficient gradient mixing
- precise solvent delivery, excellent reproducibility
- near-zero carryover

### Key features of LCMS-8030 triple quadrupole mass spectrometer

- ultra fast polarity switching of 15msec & ultra fast scan speed of up to 15,000 u/sec
- UFSweeper® technology dramatically minimizes cross talk
- excellent linearity with wide dynamic range



Fig. 1 Nexera UHPLC system & LCMS-8030 triple quadrupole mass spectrometer

## Experimental & Results

### LC-MS/MS screening method

Identifying additives in polymer formulations is a critical step for both molecular ion and fragment ion formulation. In this study, sample acquisitions were performed using auto MS/MS Synchronized Survey Scan function on the following condition;

# High speed polarity switching MS/MS applied to polymer additives analysis

## Analytical Conditions

### HPLC (Nexera UHPLC system)

Column: Shim-pack XR-ODS (75 x 2.0 mmI.D., 2.2um)  
 Mobile phase A: 0.1% formic acid  
 Mobile phase B: Methanol  
 Gradient program: 25%B (0 min) - 100%B (2.5-7.5min) - 25%B (7.51-10min)  
 Flow rate: 0.5 mL/min  
 Column temperature: 40 °C

### Mass (LCMS-8030 triple quadrupole mass spectrometry)

Ionization: ESI  
 Polarity: positive & negative  
 Scan mode:

#	type	polarity	range (m/z)	CE
1	Q3 scan	+	200-800	-
2	I- Product ion scan	+	100-800	20 V
3	I- Product ion scan	+	100-800	40 V
4	Q3 scan	-	200-800	-
5	I- Product ion scan	-	100-800	20 V
6	I- Product ion scan	-	100-800	40 V

Synchronized Survey Scanning refers to the execution of MS/MS scanning triggered by survey scan signals (in this case, Q3 scan). Thus, during the elution of a peak in Q3 scan analysis, a full product ion mass spectrum can also be obtained. By applying both fast polarity switching (15msec switching speed) and high speed data acquisition (15,000u/sec) resulted in high information product ion

spectra. This approach generated a sequence of 6 scan modes in less than 400msec. The sequence included 3 positive ion acquisitions scanning, #1 Q3 scan mode; #2 product ion scan mode at a low collision energy (20V) and #3 at a high collision energy (40V); this sequence was then repeated in negative ion mode to complete a cycle of 6 full scan modes in less than 400msecs.

## Analysis of polymer additives samples

At first, a mixture of representative polymer additives (a standard sample) was acquired. All of the 12 polymer additives standard in the sample were clearly detected in

Q3 scan and dependent product ion scan (spectra data of all compounds at two collision energies) at positive and/or negative polarity.

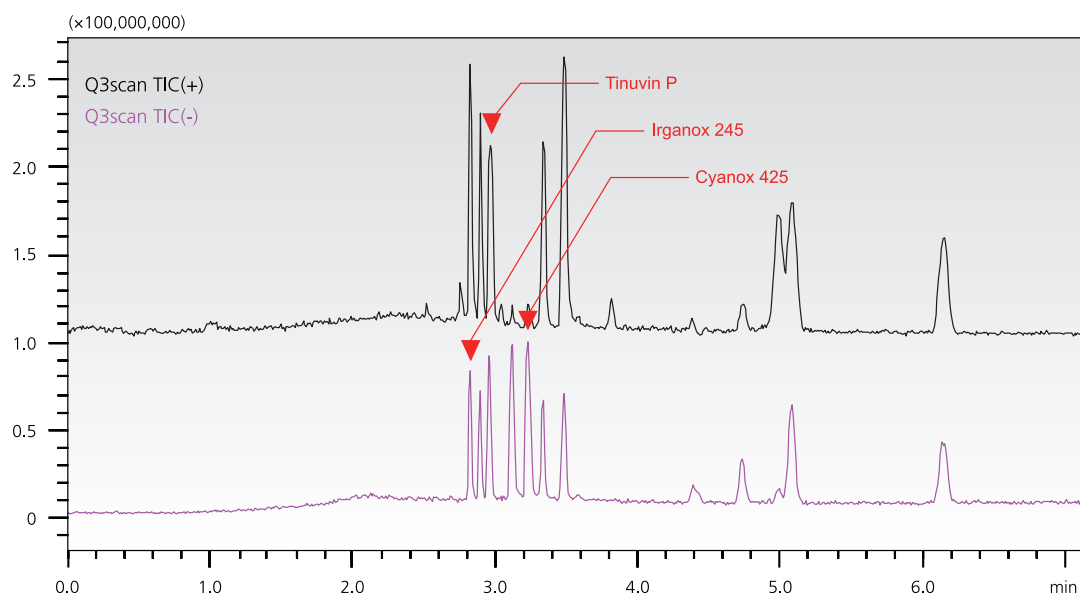


Fig. 2 Q3 scan (positive and negative) TIC of polymer additives standard

# High speed polarity switching MS/MS applied to polymer additives analysis

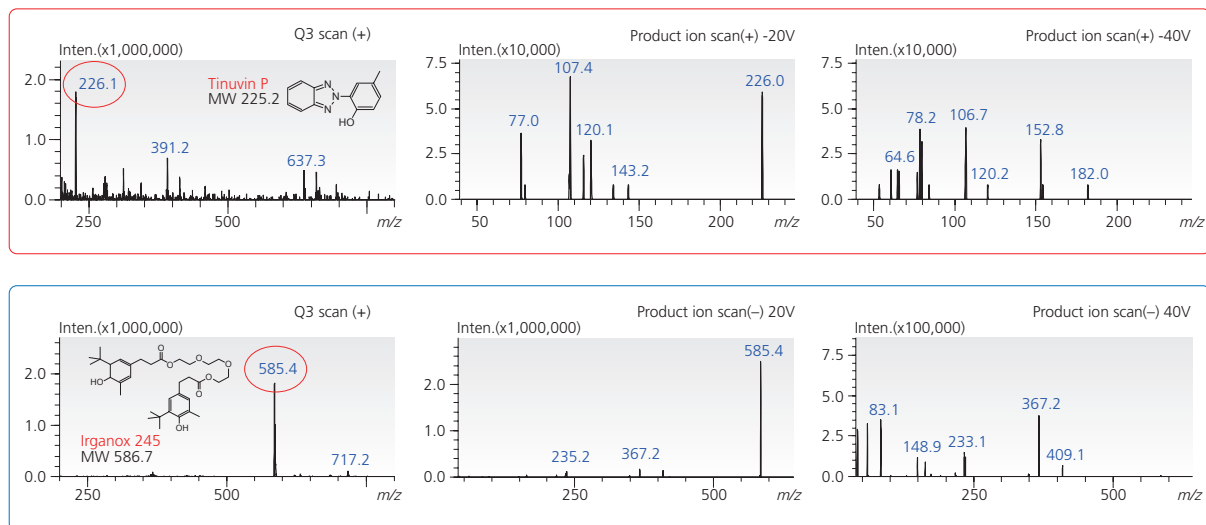


Fig. 3 Q3 scan spectra and Product ion scan spectra of polymers additive standard (a) Tinuvin P and (b) Irganox 245

Next, a sample of plastic laminates was acquired. The polymer additives in the sample were clearly identified using polarity and Q3 scan and product ion spectra data at differing collision energies. Confirming the presence of 12 known additives in a commercial product, three of them were detected, Tinuvin P, Irganox 245, Cyanox 425. Several peaks except for the 12 kinds of additive standard

had been detected, so the existence of other additives was suggested.

As a consequence of the high speed of data acquisition this method can be applied to a diverse range of polymer additive analysis with a high degree of confidence in component identification.

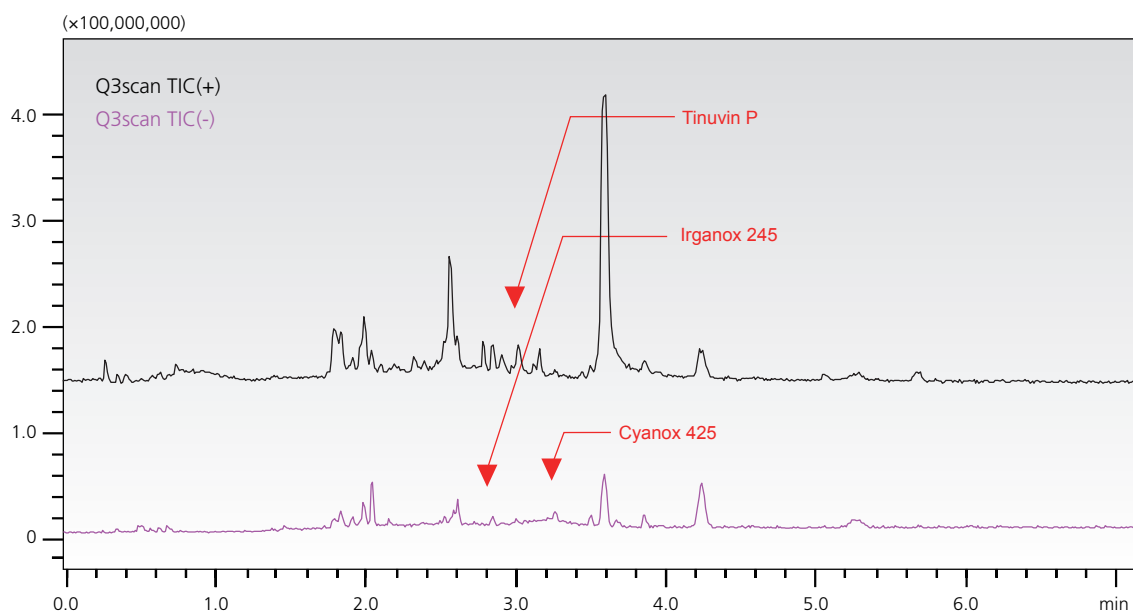


Fig. 4 Q3 scan (positive and negative) TIC of plastic laminate sample



# High speed polarity switching MS/MS applied to polymer additives analysis

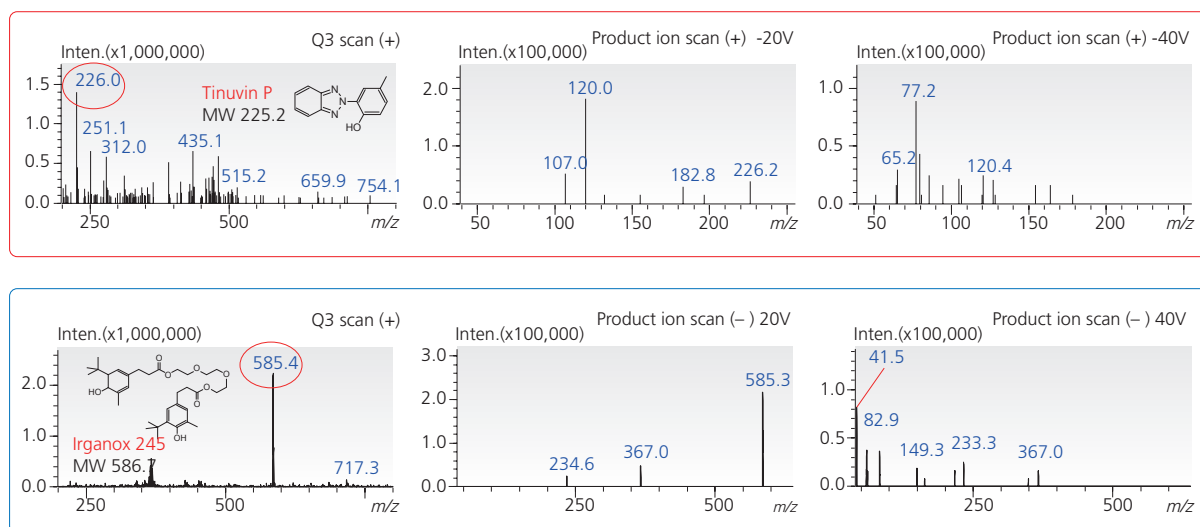


Fig. 5 Q3 scan spectra and Product ion scan spectra of plastic laminate sample (a) Tinuvin P and (b) Irganox 245

Table 1 Screening results of polymer additives

#	Polymer additives	Standard			Plastic laminate	
		R.T.	Detection		R.T.	Detection
1	Irganox 245	2.82	O	-	2.81	O
2	IrganoxMD 1024	2.89	O	-	-	X
3	Irganox1098	2.96	O	+/-	-	X
4	Tinuvin P	2.98	O	+	2.98	O
5	Cyanox 2246	3.12	O	-	-	X
6	Cyanox 425	3.23	O	-	3.25	O
7	Irganox 1035	3.33	O	-	-	X
8	Tinuvin 120	3.48	O	+/-	-	X
9	Tinuvin 328	4.40	O	+	-	X
10	Irganox 1330	4.73	O	-	-	X
11	Irganox 565	5.07	O	+/-	-	X
12	Irganox 1076	6.15	O	-	-	X

## Conclusion

- Data acquisition using Synchronized Survey Scan function with ultra fast polarity switching & ultra fast scan speed enabled to detect all MS and MS/MS spectra of the 12 kinds of polymer additives standard at one run.
- It was confirmed that at least three kinds of polymer additives were contained in plastic laminates by this screening method.
- Lots of qualitative information was obtained from MS spectra and MS/MS spectra in two collision energies at multi polarity acquired by ultra fast polarity switching & ultra high speed scanning function.



JQA-0376

Founded in 1875, Shimadzu Corporation, a leader in the development of advanced technologies, has a distinguished history of innovation built on the foundation of contributing to society through science and technology. We maintain a global network of sales, service, technical support and applications centers on six continents, and have established long-term relationships with a host of highly trained distributors located in over 100 countries. For information about Shimadzu, and to contact your local office, please visit our Web site at **[www.shimadzu.com](http://www.shimadzu.com)**



**SHIMADZU CORPORATION. International Marketing Division**

3. Kanda-Nishikicho 1-chome, Chiyoda-ku, Tokyo 101-8448, Japan

Phone: 81(3)3219-5641 Fax. 81(3)3219-5710

URL <http://www.shimadzu.com>

For Research Use Only. Not for use in diagnostic procedures. Shimadzu Corporation ("Shimadzu") reserves all rights including copyright in this publication. The content of this publication shall not be reproduced, altered or sold for any commercial purpose without the written approval of Shimadzu. The information contained herein is provided to you "as is" without warranty of any kind including without limitation warranties as to its accuracy or completeness. Shimadzu does not assume any responsibility or liability for any damage, whether direct or indirect, relating to, or arising out of the use of this publication. This publication is based upon the information available to Shimadzu on or before the date of publication, and subject to change without notice.

# Development of LC/MS/MS Method for Screening and Quantitation of 47 Synthetic Dyes under Restricted Substance List in Textiles

**ASMS 2016** TP375

Yin Ling Chew<sup>1</sup>; Jie Xing<sup>1</sup>; Leonard Guan Seng Lim<sup>2\*</sup>;  
Zhaoqi Zhan<sup>1</sup>

<sup>1</sup>Application Development & Support Centre,  
Shimadzu (Asia Pacific) Pte Ltd,  
79 Science Park Drive #02-01/08, Singapore;

<sup>2</sup>School of Physical & Mathematical Science,  
Nanyang Technological University, Singapore;

\*Student

# Development of LC/MS/MS Method for Screening and Quantitation of 47 Synthetic Dyes under Restricted Substance List in Textiles

## Introduction

Synthetic dyes such as azodyes and disperse dyes are widely used in the manufacture of various consumer products such as textiles, leather, toys and plastics. Many of these dyes are allergenic that may cause contact dermatitis and others are carcinogenic. Many synthetic dyes using in textiles and apparels are listed in the RSL [1] for protection of the consumers. Legislations such as EU 2002/371/EC and OEKO-TEX Standard 100 were

introduced to ban the use of carcinogenic dyes and restrict the amount of allergenic dyes allowed in textile making and consumer products. Various analysis methods using HPLC, TLC and LC/MS/MS [2] are reported. We describe a fast and high sensitivity LC/MS/MS method for screening and quantitation of 47 synthetic dyes including 23 azodyes, 21 disperse dyes and 3 basic dyes in textile samples.

## Experimental

Forty-seven dye compounds were obtained from Sigma Aldrich, Dr. Ehrenstorfer, Merck Schuchardt, Fischer Scientific, Accustandard, Institute of Leather Industry, Supelco, Fluka and Tokyo Chemical Industry. These compounds were dissolved in MeOH at 100 µg/mL as stock solutions which were used to prepare mixed standards calibrant series and spiked samples. For sample preparation, 1 gram of clothing sample was extracted using 20 mL of MeOH under sonicate at 50 °C for 30 minutes, followed by 10 minutes of centrifugation at

10,000 rpm. The supernatant was filtered with 0.22 µm PTFE filter. It was then evaporated and reconstituted with equal volume of 95:5 water/methanol diluent before analysis. An LCMS-8040 triple quadrupole UFMS system coupled with a Nexera UHPLC was used in this study. A Phenomenex, Kinetex UHPLC column (100 x 2.1 mm, 1.7 µm) was adopted and a gradient elution program was used for separation of the forty-seven compounds. The detailed conditions are compiled into Table 1.

Table 1: Analytical conditions of forty-seven dye compounds on LCMS-8040

Column	: Kinetex C18 100A (100 x 2.1mm, 1.7µm)
Flow Rate	: 0.3 mL/min
Mobile Phase	: A: H <sub>2</sub> O with 0.1% formic acid B: ACN with 0.1% formic acid
Oven Temp.	: 40°C
Injection vol.	: 5 µL
Elution Mode	: Gradient elution, B%: 5% (0.01 to 2 min) → 95% (12min) → 100% (12.01 to 17.50min) → 5% (17.51 to 20min)
Interface	: ESI
MS mode	: Positive & negative
Block Temp.	: 400°C
DL Temp.	: 250°C
CID Gas	: Ar (230kPa)
Nebulizing Gas Flow	: N <sub>2</sub> , 3 L/min
Drying Gas Flow	: N <sub>2</sub> , 15 L/min

## Development of LC/MS/MS Method for Screening and Quantitation of 47 Synthetic Dyes under Restricted Substance List in Textiles

# Results and Discussion

## Establishment of MRM method for detection and quantitation of 47 dye compounds

The MRM auto-optimisation of the 47 dye compounds was carried out using Shimadzu workstation, LabSolutions. Two MRM transitions were produced for each compound used as quantifier and confirmation ions (Table 2). A clothing sample free from the 47 dyes was used as a blank matrix used in preparing post-spiked calibrants for calibration curves construction. Every post-spiked calibrant was injected thrice to obtain the average area for reliable results. Calibration curves with good linearity ( $r^2 > 0.993$ ) were obtained for all 47 dye

compounds. The LOQ ranges from 0.06 – 4.09 ng/mL while the LOD ranges from 0.02 – 1.35 ng/mL. The repeatability of the method was evaluated using post-spiked calibrants at two concentrations, 10 ng/mL and 50 ng/mL. The %RSD (n=6) at concentration 10 ng/mL ranges from 1.2 % to 16.3 % while the %RSD (n=6) at concentration 50 ng/mL ranges from 1.1 % to 12.9 %. The linearity, LOD, LOQ and %RSD results are tabulated in Table 3.

## Matrix effect and recovery of the method

The performance of the method in terms of matrix effect and recovery includes was evaluated for the 47 dyes studied too. The matrix effect and recoveries were performed at two concentrations, 10 ng/mL and 50 ng/mL. Most of the matrix effect ranges from 63.0 – 120.9 %. Four dyes, i.e., disperse red 17, disperse blue 124, disperse blue 35, and disperse yellow 49 exhibit strong matrix effect at both concentrations (ME: 31.0 %~50.9 %). While, disperse orange and disperse orange 37 exhibit strong matrix effect at 10 ng/mL

(ME: 42.1 %~49.5 %) but performed better at 50 ng/mL (ME: 71.3 %~ 87.7 %). On the other hand, another four dyes i.e., disperse blue 7, basic violet 3, disperse yellow 23 and disperse orange 149 exhibit significantly ion enhancement at 50 ng/mL (ME: 141.3 %~257.3 %) but performed better at 10 ng/mL (ME: 74.2 %~120.9 %). The recovery was determined from pre- and post-spiked samples of the 47 dyes, ranging from 81.8 % to 114.1 % at 10 ng/mL and from 84.9 % to 104.1 % at 50 ng/mL.

## Screening and quantitation of the targeted dyes in textile samples

Three light colour clothing samples labelled as OB, OG and OY bought from the local stores were analysed using the method established. In sample OG, disperse red 1 was detected and quantified to be 31 ng/g, which is within the regulatory limits. Samples OG and

OY are free from the 47 dyes. Further studies on sample extraction conditions and validation of the method to various textile samples need to be performed.

# Development of LC/MS/MS Method for Screening and Quantitation of 47 Synthetic Dyes under Restricted Substance List in Textiles

Table 2: Names and information of targeted 47 dyes and MRM transitions on LCMS-8040

No.	Name	CAS	Formula	Quantifier ion				Confirmation ion			
				MRM	Q1 (V)	CE (V)	Q3 (V)	MRM	Q1 (V)	CE (V)	Q3 (V)
1	2,4-toluenediamine	95-80-7	C7H10N2	123.10>106.05	-25.0	-20.0	-21.0	123.10>77.05	-25.0	-29.0	-29.0
2	Benzidine	92-87-5	C12H12N2	185.00>167.10	-30.0	-27.0	-30.0	185.00>168.10	-30.0	-20.0	-19.0
3	4,4'-oxydianiline	101-80-4	C12H12N2O	201.10>80.10	-30.0	-37.0	-16.0	201.10>108.10	-30.0	-20.0	-21.0
4	4,4'-diaminodiphenylmethane	101-77-9	C13H14N2	199.10>106.10	-30.0	-21.0	-21.0	199.10>77.10	-30.0	-50.0	-30.0
5	o-Anisidine	90-04-0	C7H9O1N1	124.00>109.05	-30.0	-25.0	-30.0	124.00>65.05	-30.0	-30.0	-30.0
6	o-toluidine	95-53-4	C7H9N1	108.10>91.10	-20.0	-21.0	-18.0	108.10>65.10	-20.0	-28.0	-26.0
7	p-Cresidine	120-71-8	C8H11O1N1	138.10>123.10	-30.0	-19.0	-24.0	138.10>77.05	-30.0	-34.0	-30.0
8	2,4'-Diaminoanisole	615-05-4	C7H10N2O	139.10>124.05	-14.0	-18.0	-25.0	139.10>107.05	-14.0	-17.0	-21.0
9	2,4-Xylidine	95-68-1	C8H11N	122.10>77.05	-30.0	-29.0	-30.0	122.10>107.05	-30.0	-20.0	-21.0
10	3,3'-dimethoxybenzidine	119-90-4	C14H16N2O2 (2HCl)	245.10>230.05	-17.0	-18.0	-25.0	245.10>187.10	-17.0	-33.0	-21.0
11	4- Chloroaniline	106-47-8	C6H6ClN	128.00>93.10	-30.0	-18.0	-18.0	128.00>75.05	-30.0	-34.0	-28.0
12	o-Tolidine	119-93-7	C14H16N2	213.10>180.05	-23.0	-36.0	-20.0	213.10>198.10	-23.0	-21.0	-23.0
13	4,4'-methylene-bis(2-methylaniline)	838-88-0	C15H18N2	227.10>120.10	-30.0	-26.0	-24.0	227.10>77.10	-30.0	-55.0	-29.0
14	2,6-Xylidine	87-62-7	C8H11N	122.10>77.05	-28.0	-27.0	-30.0	122.10>105.05	-28.0	-20.0	-21.0
15	2,4,5-Trimethylaniline	137-17-7	C9H13N1	136.10>121.10	-13.0	-20.0	-25.0	136.10>91.10	-13.0	-23.0	-19.0
16	2-Naphthylamine	91-59-8	C10H9N	144.10>127.05	-30.0	-24.0	-25.0	144.10>77.05	-30.0	-38.0	-29.0
17	4,4'-thiodianiline	139-65-1	C12H12N2S	217.10>124.05	-15.0	-23.0	-23.0	217.10>80.10	-15.0	-47.0	-30.0
18	4-Chloro-o-toluidine	95-69-2	C7H8ClN	142.10>107.10	-28.0	-18.0	-22.0	142.10>106.05	-28.0	-27.0	-21.0
19	Basic Red 9	569-61-9	C19H17N3.HCl	288.20>195.10	-30.0	-32.0	-20.0	288.20>167.10	-30.0	-54.0	-30.0
20	4-Aminobiphenyl	92-67-1	C12H11N	170.10>152.05	-30.0	-30.0	-30.0	170.10>153.10	-30.0	-23.0	-30.0
21	Basic Violet 14	632-99-5	C20H20ClN3.HCl	302.20>209.10	-30.0	-32.0	-23.0	302.20>195.10	-30.0	-34.0	-22.0
22	5-Nitro-o-toluidine	99-55-8	C7H8N2O2	153.00>107.10	-19.0	-17.0	-25.0	153.00>89.10	-19.0	-40.0	-30.0
23	Disperse Blue 7	3179-90-6	C18H18N2O6	359.10>283.05	-25.0	-34.0	-30.0	359.10>314.05	-25.0	-20.0	-23.0
24	Disperse Yellow 9	6373-73-5	C12H10N4O4	275.10>228.00	-20.0	-22.0	-25.0	275.10>258.10	-20.0	-15.0	-30.0
25	Disperse Blue 3	2475-46-9	C17H16N2O3	297.10>252.05	-21.0	-21.0	-27.0	297.10>251.10	-21.0	-25.0	-29.0
26	Disperse Red 11	2872-48-2	C15H12N2O3	269.10>226.10	-19.0	-30.0	-24.0	269.10>254.10	-19.0	-23.0	-28.0
27	Disperse Blue 102	12222-97-8	C15H19N5O4S	366.10>208.20	-27.0	-18.0	-24.0	366.10>147.15	-27.0	-33.0	-28.0
28	Disperse Red 17	3179-89-3	C17H20N4O4	345.20>164.15	-25.0	-27.0	-18.0	345.20>177.20	-25.0	-32.0	-20.0
29	4-aminoazobenzene	60-09-3	C12H11N3	198.10>93.20	-30.0	-25.0	-19.0	198.10>77.10	-30.0	-21.0	-30.0
30	3,3'-dichlorobenzidine	91-94-1	C12H10Cl2N2	253.00>217.10	-18.0	-19.0	-23.0	253.00>182.05	-18.0	-30.0	-22.0
31	4,4'-methylene-bis-2-chloroaniline	101-14-4	C13H12N2Cl2	267.10>231.05	-19.0	-21.0	-25.0	267.10>140.05	-19.0	-25.0	-27.0
32	Disperse Blue 106	12223-01-7	C14H17N5O3S	336.10>178.15	-24.0	-17.0	-20.0	336.10>147.10	-24.0	-32.0	-29.0
33	Disperse Orange 3	730-40-5	C12H10N4O2	243.10>122.05	-30.0	-17.0	-24.0	243.10>75.05	-30.0	-34.0	-28.0
34	Basic Violet 3	548-62-9	C25H30N3Cl	372.30>356.20	-30.0	-41.0	-24.0	372.30>340.15	-30.0	-55.0	-23.0
35	Disperse Yellow 3	2832-40-8	C15H15N2O2	270.10>107.10	-30.0	-24.0	-21.0	270.10>108.15	-30.0	-31.0	-21.0
36	Disperse Orange 11	82-28-0	C15H11NO2	238.10>165.05	-17.0	-34.0	-30.0	238.10>167.05	-17.0	-37.0	-30.0
37	Disperse Brown 1	23355-64-8	C16H15Cl3N4O4	433.00>153.00	-12.0	-41.0	-29.0	433.00>196.95	-12.0	-32.0	-23.0
38	Disperse Red 1	2872-52-8	C16H18N4O3	315.10>134.10	-30.0	-27.0	-26.0	315.10>122.00	-30.0	-36.0	-24.0
39	Disperse Blue 35	12222-75-2	C20H14N2O5	285.10>270.05	-20.0	-25.0	-29.0	285.10>196.00	-20.0	-46.0	-19.0
40	Disperse Yellow 1	119-15-3	C12H9N3O5	274.20>227.20	19.0	27.0	30.0	274.20>243.05	19.0	20.0	24.0
41	Disperse Yellow 49 (Leather)	54824 - 37-2	C22H22N4O2	375.20>238.20	-27.0	-15.0	-28.0	375.20>208.15	-27.0	-39.0	-24.0
42	Disperse Blue 124	61951-51-7	C16H19N5O4S	378.10>220.15	-14.0	-17.0	-26.0	378.10>87.10	-14.0	-30.0	-17.0
43	Disperse Blue 26	3860-63-7	C16H14N2O4	299.10>284.05	-21.0	-22.0	-20.0	299.10>267.05	-21.0	-30.0	-30.0
44	Disperse Orange 37	13301-61-6	C17H15Cl2N2O5	392.10>133.05	-29.0	-38.0	-25.0	392.10>351.00	-29.0	-22.0	-26.0
45	Disperse Yellow 23	6250-23-3	C18H14N4O	303.10>77.00	-22.0	-35.0	-30.0	303.10>105.05	-22.0	-21.0	-22.0
46	Disperse Orange 1	2581-69-3	C18H14N4O2	319.10>122.05	-30.0	-23.0	-23.0	319.10>169.10	-30.0	-24.0	-19.0
47	Disperse Orange 149	85136-74-9	C25H26N6O3	457.30>121.15	16.0	49.0	19.0	457.30>149.05	16.0	43.0	24.0



# Development of LC/MS/MS Method for Screening and Quantitation of 47 Synthetic Dyes under Restricted Substance List in Textiles

Table 3: Calibration and performance of MRM method for 47 dye compounds on LCMS-8040

No.	Compound	RT (min)	Range (ppb)	Linearity	LOQ	LOD	%RSD (n=6)	
							10 ppb	50 ppb
1	2,4-toluediamine	1.148	1 - 1000	0.9992	0.68	0.22	1.92	3.73
2	Benzidine	1.506	1 - 1000	0.9960	0.52	0.17	4.89	3.88
3	4,4'-oxydianiline	1.268	0.5 - 200	0.9944	0.26	0.09	4.47	4.12
4	4,4'-diaminodiphenylmethane	1.583	0.5 - 1000	0.9992	0.35	0.12	1.28	2.31
5	o-Anisidine	1.733	0.2 - 200	0.9993	0.15	0.05	4.90	2.81
6	o-toluidine	2.049	0.2 - 200	0.9998	0.16	0.05	2.67	1.58
7	p-Cresidine	3.975	0.1 - 200	0.9992	0.06	0.02	3.08	1.36
8	2,4'-Diaminoanisole	3.975	1 - 200	0.9995	0.58	0.19	6.72	2.61
9	2,4-Xylidine	3.933	1 - 200	0.9994	0.73	0.24	1.65	2.33
10	3,3'-dimethoxybenzidine	4.514	0.2 - 200	0.9951	0.20	0.06	2.01	1.12
11	4- Chloroaniline	4.094	1 - 200	0.9997	0.78	0.26	3.75	1.93
12	o-Tolidine	4.395	0.5 - 200	0.9992	0.28	0.10	3.64	1.83
13	4,4'-methylene-bis(2-methylaniline)	4.484	0.5 - 200	0.9993	0.21	0.07	2.62	2.77
14	2,6-Xylidine	4.991	1 - 200	0.9995	0.85	0.28	3.21	3.23
15	2,4,5-Trimethylaniline	5.001	0.5 - 200	0.9995	0.29	0.10	3.22	1.30
16	2-Naphthylamine	5.472	0.2 - 500	0.9994	0.10	0.03	3.54	1.72
17	4,4'-thiodianiline	5.457	0.5 - 1000	0.9993	0.19	0.06	2.91	2.00
18	4-Chloro-o-toluidine	6.282	0.2 - 500	0.9997	0.15	0.05	1.99	2.08
19	Basic Red 9	6.139	0.05 - 100	0.9931	0.02	0.01	1.22	1.93
20	4-Aminobiphenyl	6.612	0.5 - 1000	0.9996	0.45	0.15	1.81	2.45
21	Basic Violet 14	6.479	0.05 - 100	0.9977	0.02	0.01	2.78	1.42
22	5-Nitro-o-toluidine	6.888	5 - 1000	0.9994	1.98	0.65	10.86	8.18
23	Disperse Blue 7	7.459	1 - 200	0.9991	0.71	0.24	3.10	1.33
24	Disperse Yellow 9	7.805	5 - 1000	0.9997	5.00	1.50	15.16	4.16
25	Disperse Blue 3	7.921	0.5 - 200	0.9994	0.28	0.09	5.14	1.91
26	Disperse Red 11	7.936	0.5 - 100	0.9967	0.20	0.06	3.04	2.32
27	Disperse Blue 102	8.294	2 - 200	0.9991	0.97	0.32	16.32	7.61
28	Disperse Red 17	8.489	0.5 - 200	0.9992	0.50	0.15	6.16	3.78
29	4-aminoazobenzene	8.815	2 - 200	0.9995	1.23	0.41	10.43	3.95
30	3,3'-dichlorobenzidine	8.789	2 - 200	0.9994	1.47	0.48	11.04	6.06
31	4,4'-methylene-bis-2-chloroaniline	8.978	2 - 200	0.9993	2.00	0.60	4.77	4.59
32	Disperse Blue 106	8.938	0.1 - 200	0.9994	0.04	0.01	10.34	3.56
33	Disperse Orange 3	9.128	0.1 - 200	0.9994	0.08	0.03	5.81	2.01
34	Basic Violet 3	9.2	0.05 - 200	0.9990	0.02	0.01	4.42	2.45
35	Disperse Yellow 3	9.203	0.5 - 200	0.9991	0.21	0.07	3.97	2.74
36	Disperse Orange 11	9.273	0.5 - 200	0.9992	0.34	0.11	11.59	4.69
37	Disperse Brown 1	9.289	1 - 200	0.9993	1.00	0.33	6.24	8.33
38	Disperse Red 1	9.571	0.2 - 100	0.9942	0.20	0.07	3.16	5.54
39	Disperse Blue 35	9.875	5 - 1000	0.9980	1.98	0.65	10.54	5.99
40	Disperse Yellow 1	8.438	2 - 200	0.9960	2.00	0.63	10.43	8.29
41	Disperse Yellow 49 (Leather)	10.099	0.5 - 200	0.9996	0.26	0.09	3.63	2.40
42	Disperse Blue 124	10.163	1 - 500	0.9981	0.78	0.26	4.70	4.74
43	Disperse Blue 26	10.779	5 - 200	0.9986	4.09	1.35	7.08	12.85
44	Disperse Orange 37	10.864	5 - 200	0.9970	4.05	1.34	4.31	3.35
45	Disperse Yellow 23	11.049	0.2 - 200	0.9969	0.17	0.06	5.19	1.75
46	Disperse Orange 1	11.195	0.2 - 200	0.9979	0.12	0.03	2.57	1.23
47	Disperse Orange 149	12.069	1 - 200	0.9975	0.73	0.24	4.80	7.42

# Development of LC/MS/MS Method for Screening and Quantitation of 47 Synthetic Dyes under Restricted Substance List in Textiles

Table 4: Matrix effects and recoveries of forty-seven dye compounds spiked in MeOH extract of blank textile matrix (white cloth).

No.	Compound	Matrix Effect (%)		Recovery (%)	
		10 ppb	50 ppb	10 ppb	50 ppb
1	2,4-toluenediamine	100.0	99.0	101.5	101.4
2	Benzidine	109.0	101.7	92.4	96.1
3	4,4'-oxydianiline	96.7	100.7	102	94.6
4	4,4'-diaminodiphenylmethane	109.1	105.7	99.3	95.6
5	o-Anisidine	119.0	109.3	107.2	96.8
6	o-toluidine	108.0	102.3	107.9	97.7
7	p-Cresidine	118.6	109.4	107.0	98.9
8	2,4'-Diaminoazole	117.7	106.3	102.6	98.8
9	2,4-Xylidine	116.2	106.4	107.0	97.3
10	3,3'-dimethoxybenzidine	111.1	102.6	102.5	97.8
11	4- Chloroaniline	109.0	108	111.4	98.1
12	o-Tolidine	113.6	108.7	101.6	95.6
13	4,4'-methylene-o- toluidine	97.8	105.5	103.9	98.4
14	2,6-Xylidine	109.5	104	106.6	98.9
15	2,4,5-Trimethylaniline	115.8	109.9	105.5	98.5
16	2-Naphthylamine	108.5	113.3	105.2	100
17	4,4'-thiodianiline	86.7	92.6	95.0	98.9
18	4-Chloro-o-toluidine	106.6	110	108.0	97.7
19	Basic Red 9*	109.6	92.5	81.8	86.3
20	4-Aminobiphenyl	97.2	100.0	102.3	98.0
21	Basic Violet 14*	114.3	93.6	86.5	87.1
22	5-Nitro-o-toluidine	104.0	116.4	110.1	100.3
23	Disperse Blue 7	114.5	141.3	100.5	89.0
24	Disperse Yellow 9	88.9	110.5	106.7	94.2
25	Disperse Blue 3	87.8	101.4	103.5	95.3
26	Disperse Red 11	89.8	86.9	90.4	91.4
27	Disperse Blue 102	76.0	80.9	100.2	88.8
28	Disperse Red 17	31.0	50.9	97.5	95.5
29	4-aminoazobenzene	78.1	90.4	96.5	98.4
30	3,3'-dichlorobenzidine	72.0	90.6	114.1	99.1
31	4,4'-methylene-bis-2-chloroaniline	82.1	89.6	110.4	103.0
32	Disperse Blue 106	82.9	88.7	94.2	95.9
33	Disperse Orange 3	68.2	73.9	100.4	95.3
34	Basic Violet 3	120.9	167.8	104.7	90.2
35	Disperse Yellow 3	72.5	82.5	97.7	94.4
36	Disperse Orange 11	82.9	89	101.3	94.9
37	Disperse Brown 1	63.0	94.1	109.6	98.0
38	Disperse Red 1	71.7	66.1	100.7	104.1
39	Disperse Blue 35	34.7	41.7	104.0	93.1
40	Disperse Yellow 1	113.2	105.5	101.3	100.1
41	Disperse Yellow 49 (Leather)	38.3	45.6	103.5	97.8
42	Disperse Blue 124	31.4	48.5	96.3	93.1
43	Disperse Blue 26	77.1	105.7	99.3	89.2
44	Disperse Orange 37	49.5	71.3	104.6	99.2
45	Disperse Yellow 23	74.2	187	105.7	84.9
46	Disperse Orange 1	42.1	87.7	104.6	85.7
47	Disperse Orange 149	114.1	257.3	107.0	87.6

# Development of LC/MS/MS Method for Screening and Quantitation of 47 Synthetic Dyes under Restricted Substance List in Textiles

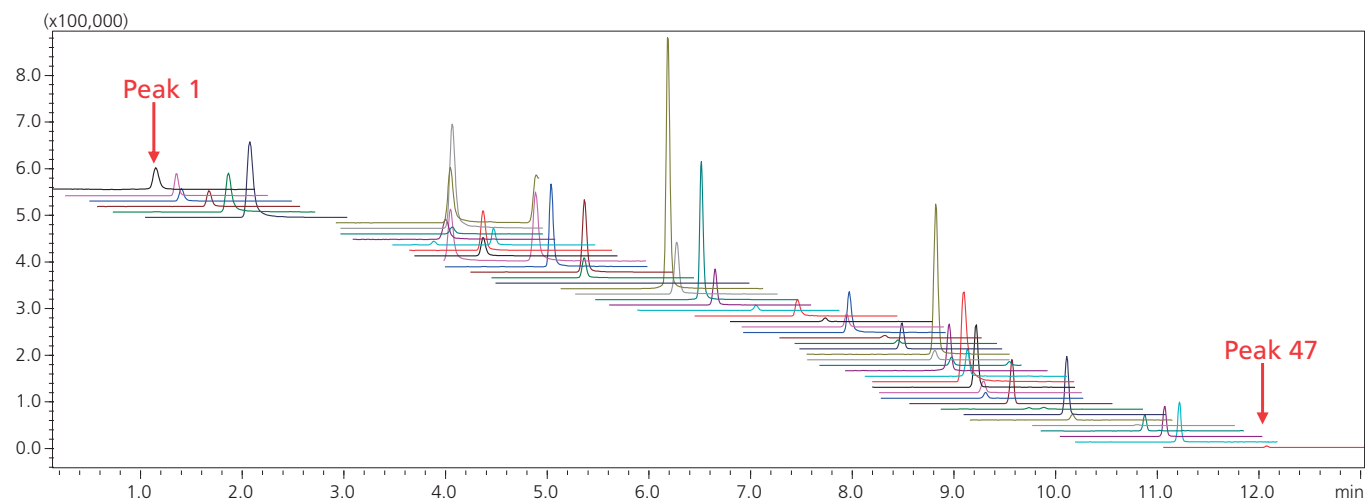


Figure 1: Scheduled MRM chromatograms of 47 dyes spiked in textile blank matrix at 20 ng/mL (ppb) each compound (5  $\mu$ L injection volume). Peak sequence refers to Table 3.

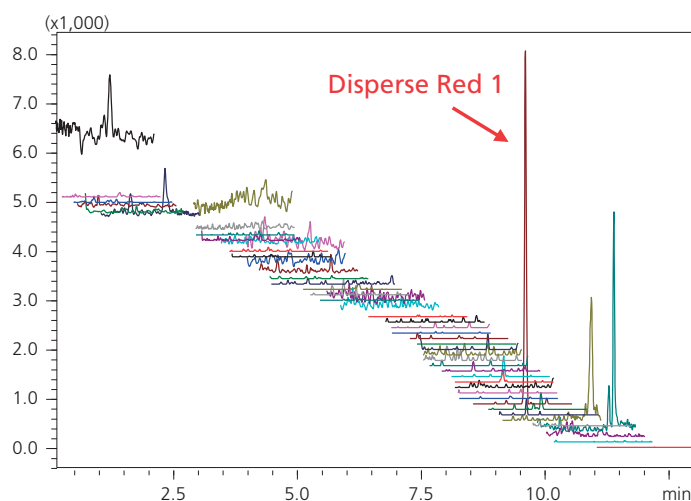


Figure 2: MRM chromatogram of sample 0G.

# Development of LC/MS/MS Method for Screening and Quantitation of 47 Synthetic Dyes under Restricted Substance List in Textiles

## Conclusions

A fast and highly sensitive LC/MS/MS method has been developed on LCMS-8040 for screening and quantitation of 47 restricted or banned synthetic dyes, including 23 azodyes, 21 disperse dyes and 3 basic dyes. The total run

time of the method is less than 20 mins. The LOQs of the method for these dyes are at 0.1~4.1 ng/mL, which are fully complied with the current regulatory requirements.

## References

1. C&A Europe, "C&A - Restricted Substance List (RSL), 2014; American Apparel and footwear Association, "Restricted substances list (RSL), 2013"
2. J. Garcia-Lavandeira, E Blanco, C. Salgado and R. Cela, Talanta, 82 (2010) 261 – 269.

Disclaimer: Shimadzu LCMS-8040, UFLC XR system and Labsolutions Insight are intended for Research Use Only (RUO). Not for use in diagnostic procedures.

First Edition: June, 2016



Shimadzu Corporation  
[www.shimadzu.com/an/](http://www.shimadzu.com/an/)

**For Research Use Only. Not for use in diagnostic procedure.**

This publication may contain references to products that are not available in your country. Please contact us to check the availability of these products in your country.

The content of this publication shall not be reproduced, altered or sold for any commercial purpose without the written approval of Shimadzu. Company names, product/service names and logos used in this publication are trademarks and trade names of Shimadzu Corporation or its affiliates, whether or not they are used with trademark symbol "TM" or "®". Third-party trademarks and trade names may be used in this publication to refer to either the entities or their products/services. Shimadzu disclaims any proprietary interest in trademarks and trade names other than its own.

The information contained herein is provided to you "as is" without warranty of any kind including without limitation warranties as to its accuracy or completeness. Shimadzu does not assume any responsibility or liability for any damage, whether direct or indirect, relating to the use of this publication. This publication is based upon the information available to Shimadzu on or before the date of publication, and subject to change without notice.

© Shimadzu Corporation, 2016

# Analysis of degradation products in electrolyte for rechargeable lithium-ion battery through high mass accuracy $MS^n$ and multivariate statistical technique

**ASMS 2012** WP26-541

Hiroki Nakajima, Satoshi Yamaki, Tsutomu Nishine,  
Masaru Furuta  
SHIMADZU CORPORATION, Kyoto, Japan

# Analysis of degradation products in electrolyte for rechargeable lithium-ion battery through high mass accuracy MS<sup>n</sup> and multivariate statistical technique

## Introduction

Rechargeable lithium-ion batteries (LiB) are one of the major power sources for portable electronic devices and electric vehicles because of their high voltage and high energy density (Fig. 1-(a)). The electrolyte of a LiB is consisting of a lithium salt in an aprotic organic solvent. The typical operational potential of a LiB is between 0 and 5 V. Therefore, solvent can be reduced or oxidized at the

negative and positive electrodes during the battery charging process. As a result, various degradation products are generated in the electrolyte and cause some problems such as a decrease in the capacitance of battery (Fig. 1-(b)). Here, we present the analysis method of degradation products generated in electrolyte using high mass accuracy MS<sup>n</sup> and multivariate statistical technique.

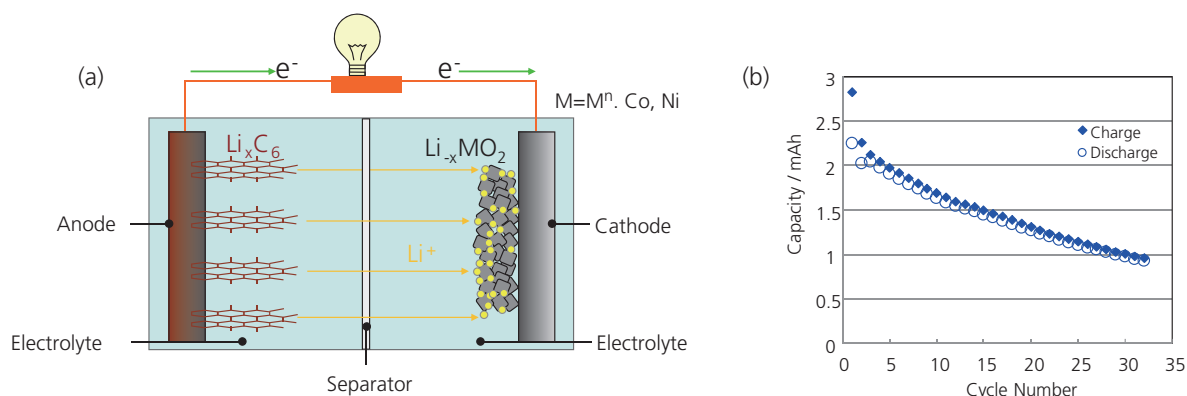


Fig. 1 Rechargeable lithium-ion battery component of lithium-ion battery (a), a decrease in the capacitance of battery (b).

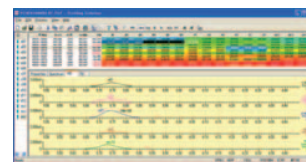
## Experiment

The electrolyte was a mixture of ethylene carbonate (EC) and diethyl carbonate (DEC) (EC : DEC = 1 : 1 vol%) containing 1M lithium hexafluorophosphate (LiPF<sub>6</sub>). The electrolyte A taken from unused lithium-ion battery and the electrolyte B taken from lithium-ion battery repeated charge and discharge cycles (60°C, 30 times) were used as samples. Those samples were prepared 1/10 dilution with methanol for LCMS-IT-TOF (Shimadzu Corporation) measurement. Orthogonal Partial Least Squares

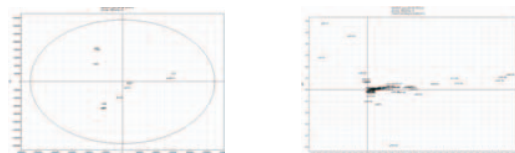
Discriminant Analysis (OPLS-DA) was performed using data acquired by LCMS-IT-TOF measurement of electrolyte A and electrolyte B (n=3) to find the compounds generated in electrolyte B. Then, those compounds were identified chemical formula using software "Formula Predictor" (Shimadzu Corporation). SIMCA-P+ (Umetrics) and Profiling Solution (Shimadzu Corporation) were used for OPLS-DA (Scheme).



1. Acquisition of the high mass accuracy MS<sup>n</sup> data (LCMS-IT-TOF)



2. Peak alignment and generation of peak list (Profiling Solution)



3. Searching of degradation products (SIMCA-P+)



4. Prediction of chemical formula (Formula Predictor)

Structural estimation

Scheme Work flow of the analysis of degradation product in electrolyte for LiB



# Analysis of degradation products in electrolyte for rechargeable lithium-ion battery through high mass accuracy MS<sup>n</sup> and multivariate statistical technique

## Results and discussion

MS data of electrolyte A and electrolyte B were acquired using LCMS-IT-TOF under the analytical conditions shown Table 1. On the score plot of OPLS-DA, the group of electrolyte A and electrolyte B were located at left side and right side, respectively (Figure 2-(a)). 15 unique ions of electrolyte B were observed at right side on S-plot (Figure 2-(b)). And, those ions were not detected on the extracted ion chromatogram (EIC) of electrolyte A (Fig. 3). These results suggested that those ions were degradation products generated in the electrolyte of lithium-ion battery repeated charge and discharge 30 cycles.

Table 1 LCMS analytical conditions

Column	: Shim-pack FC-ODS (2.0 mmI.D.x150 mm, 3 mm)
Flow rate	: water
Column temp.	: 0.2 mL/min
Mobile phaseA	: 40°C
Mobile phaseB	: methanol
Time prog.	: 5%B (0 min) → 55%B (30 min) → 5%B (30.01 min)
Injection volume	: 1 µL
Ionization mode	: ESI(+)
Probe voltage	: 4.5 kV
CDL temperature	: 200°C
BH temperature	: 200°C
Nebulizing gas	: 1.5 L/min
Drying gas	: 0.1 MPa
Scan range	: m/z 80 - 1000

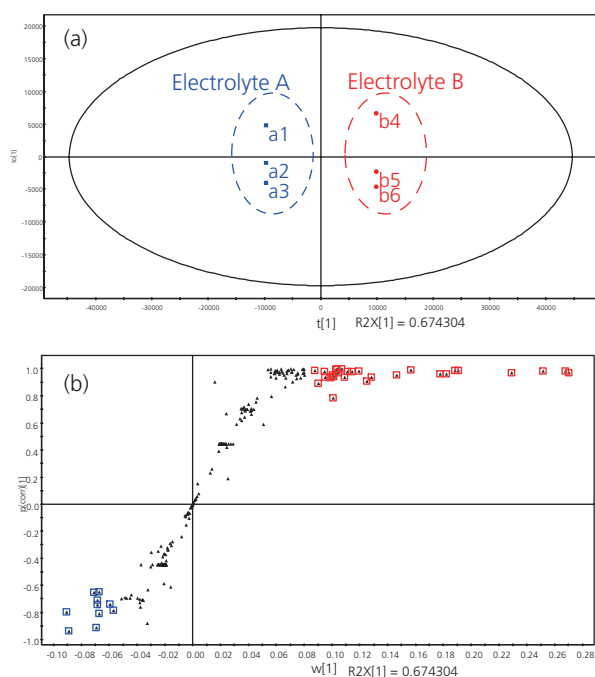


Fig. 2 The result of OPLS-DA, score plot (a), S-plot (b)

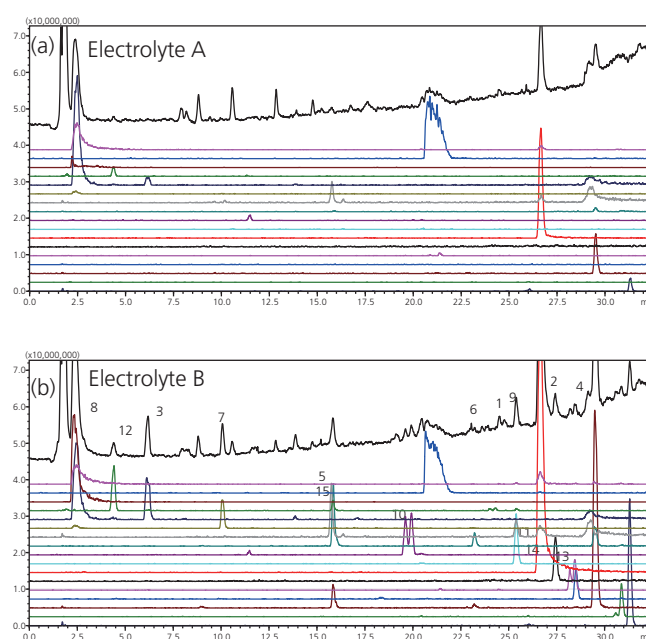


Fig. 3 EICs of ions detected in Electrolyte B (b)  
These ions were not detected on EIC of electrolyte A (a).

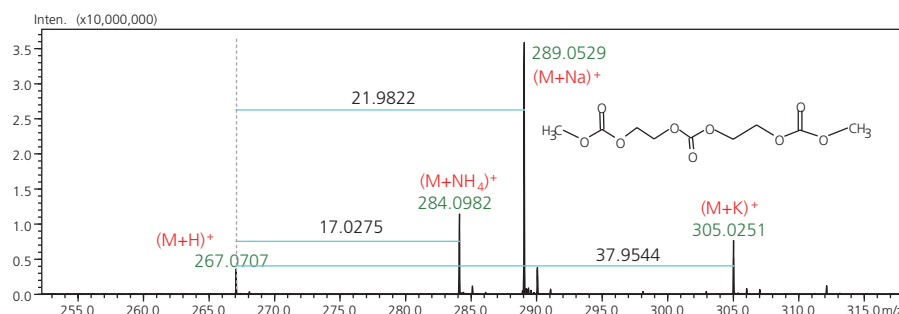


Fig. 4 MS data and predicted structure of peak number 2 (m/z 284.0982) being one of 15 unique ions of electrolyte B

# Analysis of degradation products in electrolyte for rechargeable lithium-ion battery through high mass accuracy MS<sup>n</sup> and multivariate statistical technique

The formula of peak number 2 ( $m/z$  284.0982) being one of 15 unique ions of electrolyte B was predicted as C<sub>9</sub>H<sub>14</sub>O<sub>9</sub> (polycarbonate) using high mass accuracy MS data and formula predictor. Indeed, the structure of C<sub>9</sub>H<sub>14</sub>O<sub>9</sub> was predicted as H<sub>3</sub>C-(OCO<sub>2</sub>-C<sub>2</sub>H<sub>4</sub>)<sub>2</sub>-OCO-CH<sub>3</sub> referring to some articles on degradation products in electrolyte. MS<sup>n</sup>

of the ion ( $m/z$  284.0982) also was measured to determine the validity of the predicted chemical structure. Each product ions and neutral loss in MS<sup>2</sup> and MS<sup>3</sup> data showed that the predicted structure of C<sub>9</sub>H<sub>14</sub>O<sub>9</sub> was correct.

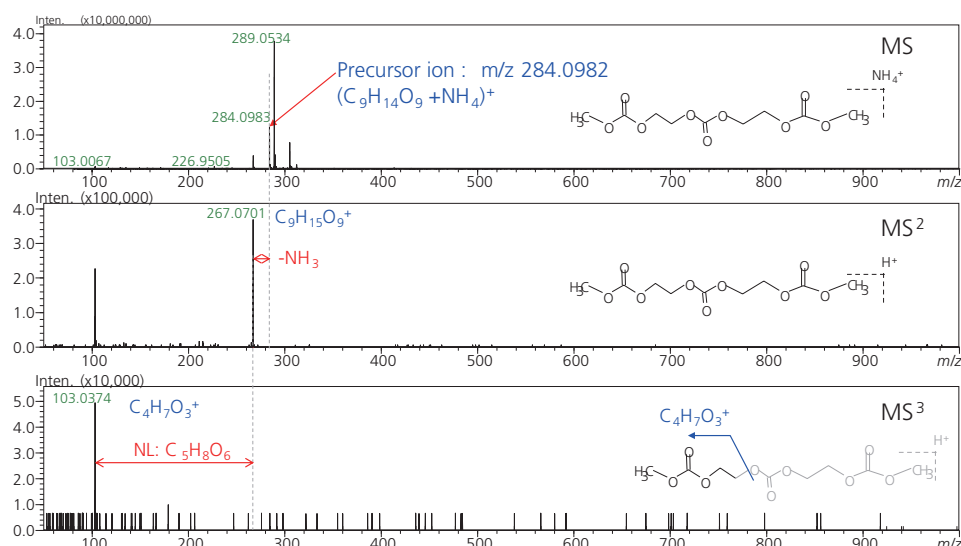


Fig. 5 MS<sup>n</sup> data of peak number 2 ( $m/z$  284.0982) detected in electrolyte B

By the same method, formula of peak number 13 ( $m/z$  283.0336) was identified as C<sub>3</sub>H<sub>7</sub>O<sub>4</sub>P. Structure of it was determined as phosphate shown in Fig. 6.

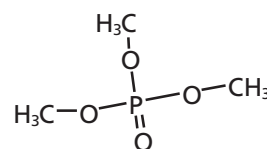


Fig. 6 of Structure peak number 13

## Conclusion

- It was clear that the chemical species of degradation products generated in the electrolyte with increasing charge and discharge cycles were carbonate and phosphate from result of this study.
- The formulae of 15 degradation products detected in Electrolyte B were identified as below.

Peak No.	$m/z$	R.T.(min)	Ion species	M.W	Predicted formula	Mass accuracy (ppm)
1	229.0678	26.645	(M+Na)+	206	C <sub>8</sub> H <sub>14</sub> O <sub>6</sub>	-2.62
2	284.0982	20.401	(M+NH <sub>4</sub> )+	294	C <sub>9</sub> H <sub>18</sub> O <sub>9</sub>	-0.35
3	295.1032	29.482	(M+H)+	170	C <sub>11</sub> H <sub>18</sub> O <sub>9</sub>	+1.69
4	177.0512	6.178	(M+Li)+	382	C <sub>4</sub> H <sub>11</sub> O <sub>5</sub> P	+2.92
5	400.1458	31.294	(M+NH <sub>4</sub> )+	272	C <sub>14</sub> H <sub>22</sub> O <sub>12</sub>	+2.50
6	295.056	15.833	(M+Na)+	244	C <sub>8</sub> H <sub>17</sub> O <sub>8</sub> P	-1.36
7	262.0853	25.374	(M+NH <sub>4</sub> )+	184	C <sub>10</sub> H <sub>13</sub> O <sub>5</sub> P	+1.53
8	185.0577	10.054	(M+H)+	250	C <sub>5</sub> H <sub>13</sub> O <sub>5</sub> P	+4.32
9	251.1111	27.416	(M+H)+	268	C <sub>8</sub> H <sub>17</sub> O <sub>5</sub> F <sub>3</sub>	+2.39
10	269.0162	19.879	(M+H)+	332	C <sub>7</sub> H <sub>7</sub> O <sub>2</sub> F <sub>6</sub> P	-2.60
11	350.1003	28.426	(M+NH <sub>4</sub> )+	138	C <sub>8</sub> H <sub>17</sub> O <sub>7</sub> F <sub>4</sub> P	+1.14
12	283.0336	4.385	(2M+Li)+	358	C <sub>3</sub> H <sub>7</sub> O <sub>4</sub> P	+4.32
13	381.0938	30.857	(M+Na)+	270	C <sub>12</sub> H <sub>23</sub> O <sub>10</sub> P	-1.57
14	293.0777	28.487	(M+Na)+	222	C <sub>9</sub> H <sub>19</sub> O <sub>7</sub> P	+1.36
15	245.0641	15.713	(M+Na)+	266	C <sub>8</sub> H <sub>14</sub> O <sub>7</sub>	-0.41



Shimadzu Corporation

[www.shimadzu.com/an/](http://www.shimadzu.com/an/)

For Research Use Only. Not for use in diagnostic procedures.

The content of this publication shall not be reproduced, altered or sold for any commercial purpose without the written approval of Shimadzu. The information contained herein is provided to you "as is" without warranty of any kind including without limitation warranties as to its accuracy or completeness. Shimadzu does not assume any responsibility or liability for any damage, whether direct or indirect, relating to the use of this publication. This publication is based upon the information available to Shimadzu on or before the date of publication, and subject to change without notice.

© Shimadzu Corporation, 2012

# Differential Analysis in vulcanizing accelerators for rubber products by High mass Accuracy MS<sup>n</sup> and Multivariate Statistical Technique

**ASMS 2012** ThP21 - 455

Takahiro Goda, Hiroki Nakajima, Satoshi Yamaki,  
Tsutomu Nishine, Masaru Furuta, Naoki Hamada  
Shimadzu Corporation, Kyoto, JAPAN

# Differential Analysis in vulcanizing accelerators for rubber products by High mass Accuracy MS<sup>n</sup> and Multivariate Statistical Technique

## Introduction

Vulcanization is a cross-linking reaction for forming bridges between individual polymer chains via addition of sulfur (Fig. 1). The purpose of vulcanization is to convert the rubber into a more durable material. In general, a reaction rate of vulcanization is increased by adding vulcanizing accelerator to mixture of rubber and sulfur. Each tire manufacturer employs one particular accelerator from among many commercially available reagents in order to meet set standards. Therefore, analyzing vulcanizing

accelerator compounds is a key stage in the tire manufacturing process, however, it is difficult to detect differences in similar structures when produced by different manufacturers.

In this study we show differential analysis of similar structured sulfenamide-based vulcanizing accelerators (Fig. 2) produced by different manufacturers using high mass accuracy MS<sup>n</sup> and multivariate statistical technique.

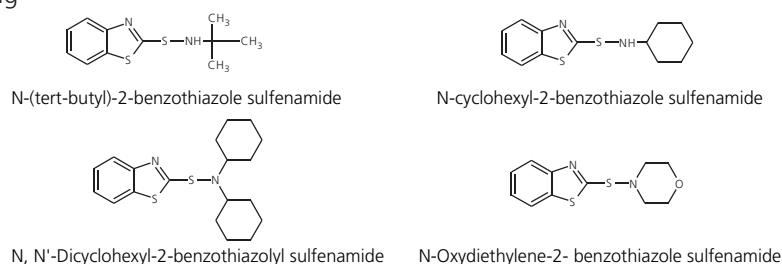
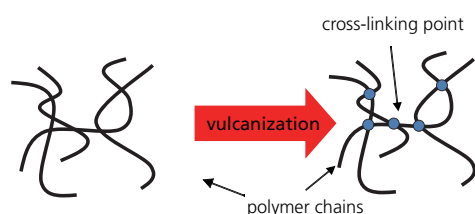


Fig. 2 Typical sulfenamide-based vulcanizing accelerators.

## Methods

Five N-(tert-butyl)-2-benzothiazole sulfenamide (NS; NS-1, NS-2, NS-3, NS-4, NS-5) and five N-cyclohexyl-2-benzothiazole sulfenamide (CZ; CZ-1, CZ-2, CZ-3, CZ-4, CZ-5) were used in this study. Each NS and each CZ were produced by different manufacturers. Sample solutions were prepared at 100 mg/L dissolved in tetrahydrofuran and acetonitrile. Equal amount of NS solutions were mixed and used as a quality control (QC) sample for NS analysis to identify robust and reproducible ion signals. The QC sample for CZ analysis also was

prepared by the same method. LCMS measurement was performed by LCMS-IT-TOF (Shimadzu Corporation, Kyoto, Japan). SIMCA-P+ (Umetrics) and MetID Solution (Shimadzu Corporation) were used for multivariate statistical analysis and for searching structural analogues using MS<sup>n</sup> data acquired by LCMS-IT-TOF measurement, respectively. Formula Predictor (Shimadzu Corporation) was used for predicting the formulae of characteristic compounds (Fig. 3).

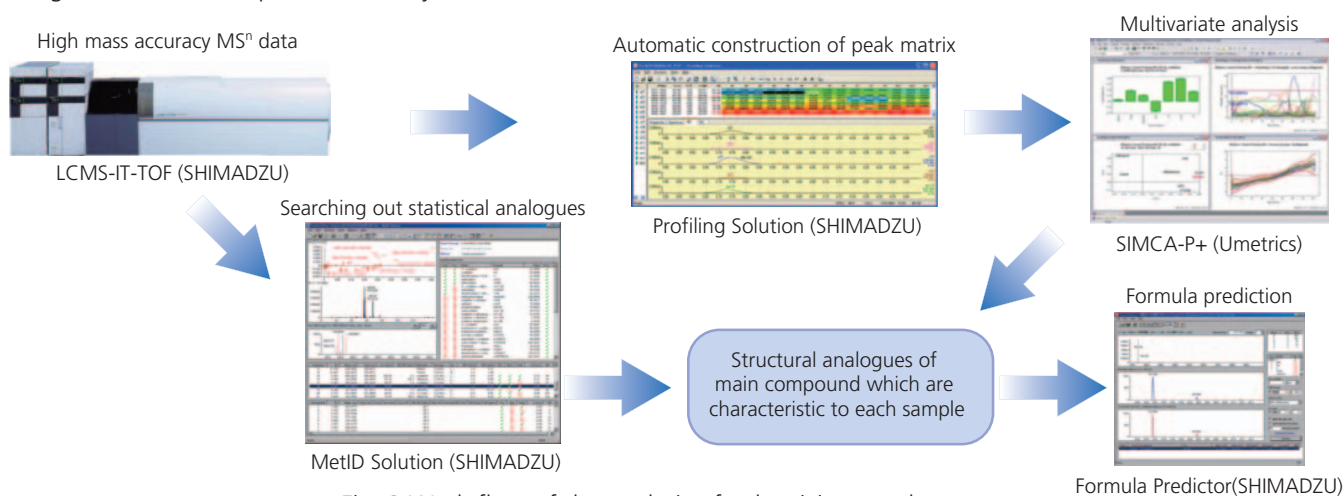


Fig. 3 Work flow of the analysis of vulcanizing accelerators.

# Differential Analysis in vulcanizing accelerators for rubber products by High mass Accuracy MS<sup>n</sup> and Multivariate Statistical Technique

Table 1 LCMS analytical conditions.

Column	: Shim-pack XR-ODS (2.0 mmID.x75 mmL, 2.2 mm)
Flow rate	: 0.45 mL/min
Column temperature	: 40°C
Mobile phaseA	: water containing 5 mmol ammonium acetate
Mobile phaseB	: acetonitrile
Time program	: 0%B(0 min) – 100%B(9 – 12 min) – 0%B(12.01 – 15 min)
Injection volume	: 1 mL
Ionization mode	: ESI(+)
Probe voltage	: 4.5kV
CDL temperature	: 200°C
BH temperature	: 200°C
Nebulizing gas flow	: 1.5 L/min
Drying gas pressure	: 0.1 MPa
Scan range	: <i>m/z</i> 100 - 1000

## Results and discussion

As a result of principal component analysis (PCA) for NS, the groups of each sample type were located at the different sites on the score plot (Fig. 4a) showing that they were comprised of different components. The unique peaks of each sample were observed on the loading plot (Fig. 4b). Candidates of the structural analogues of NS were

identified using unique peaks based on fragment ions and neutral losses (Fig. 5).

The extracted ion chromatograms (EICs) suggested that these were characteristic components of each sample (Fig. 6). By the same method, each sample of CZ was identified as containing characteristic components.

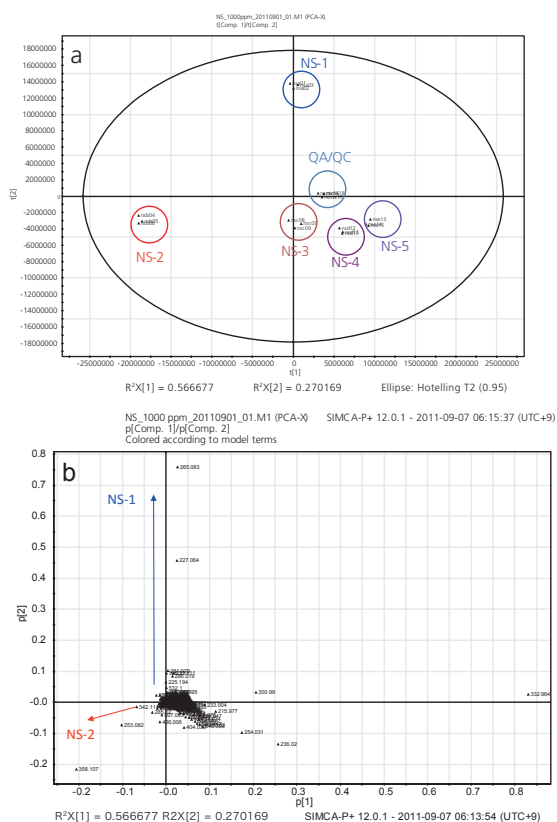


Fig. 4 Result of PCA for NS (a: score plot, b: loading plot).

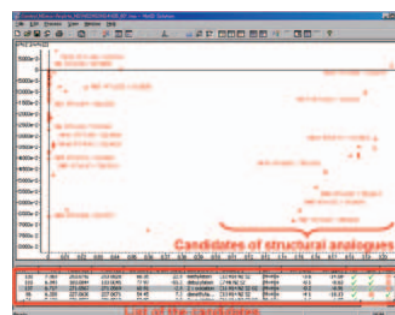


Fig. 5 Analysis window of MetID Solution.

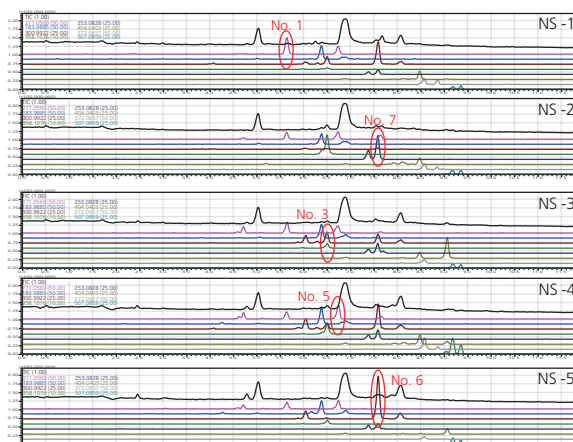


Fig. 6 EICs of characteristic peaks of each samples.



# Differential Analysis in vulcanizing accelerators for rubber products by High mass Accuracy MS<sup>n</sup> and Multivariate Statistical Technique

The formula of peak No. 7 (Fig.6) of NS-2 was predicted as C<sub>12</sub>H<sub>16</sub>N<sub>2</sub>S<sub>2</sub>. Considering MS<sup>n</sup> spectra and neutral loss ions, it was determined that peak No. 7 has the structure of NS with addition of -CH<sub>2</sub> to the phenyl group (Fig. 7). We also

determined the structures of other characteristic compounds and thought to be either impurities or by-products in the process of synthesis.

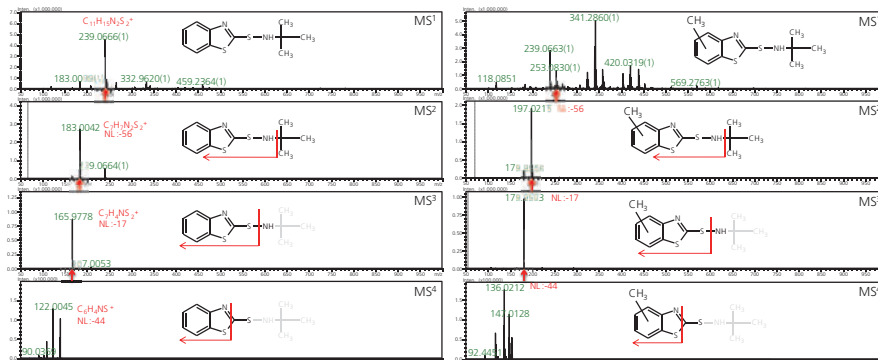


Fig. 7 MS<sup>n</sup> spectra of NS (left) and peak No. 7 (right) detected from NS-2 sample (see Fig. 6).

Table 2 Predicted formulae and structures of characteristic components of NS (left) and CZ (right).

No.	R.T. (min)	Predicted formula and structure	Ions			Sample
			Measured value (m/z)	Theoretical value (m/z)	Error (ppm)	
1	5.62	<chem>C11H11N2O2S2</chem>	271.0567	271.0569	-0.74	1
2	6.35	<chem>C11H11N2O2S2</chem>	183.9887	183.9885	1.09	4
3	6.48	<chem>C11H11N2S2</chem>	300.9923	300.9922	0.33	3
4	6.50	<chem>C11H11N2O2S2</chem>	358.1062	358.1076	-3.91	2
5	6.72	<chem>C11H11N2O2S2</chem>	271.0582	271.0569	4.80	4
6	7.52	<chem>C11H11N2S2</chem>	300.9921	300.9922	-0.33	5
7	7.58	<chem>C12H16N2S2</chem>	253.0831	253.0828	1.24	2
8	8.48	<chem>C12H17N2O2S2</chem>	404.0399	404.0403	-0.99	4
9	8.85	<chem>C11H11N2S2</chem>	372.0647	372.0657	-2.69	4
10	9.17	<chem>C11H11N2O2S2</chem>	507.0850	507.0859	-1.77	4

No.	R.T. (min)	Predicted formula and structure	Ions			Sample
			Measured value (m/z)	Theoretical value (m/z)	Error (ppm)	
1	3.62	<chem>C10H11NO3</chem>	200.1280	200.1281	-0.50	4
2	4.78	<chem>C11H11NO2S2</chem>	254.0308	254.0304	1.57	4
3	5.07	<chem>C11H11NO2S2</chem>	286.0207	286.0202	1.75	4
4	6.25	<chem>C11H11N2S2</chem>	227.0628	227.0637	-3.96	4
5	6.83	<chem>C11H11N2S2(NS)</chem>	239.0671	239.0671	0.00	1
6	7.30	<chem>C11H11N2S2</chem>	332.9648	332.9643	1.50	4
7	8.25	<chem>C10H11NO</chem>	468.3956	468.3948	1.71	1
8	8.31	<chem>C11H11NO2S2</chem>	297.0533	297.0540	-2.36	4
9	8.36	<chem>C11H11N2S2</chem>	279.0985	279.0984	0.36	1
10	8.90	<chem>C11H11NO2S2</chem>	500.0950	500.0953	-0.3	4

## Conclusion

- Differences in similar structured sulfenamide-based vulcanizing accelerators were identified from different manufacturers with characteristic components of each sample detected using high mass accuracy MS<sup>n</sup> and multivariate statistical techniques.
- The structural analogues of main compounds were

- detected using MS<sup>n</sup> data analysis software (MetID Solution).
- Formulae and structures of the analogues were assigned using Formula Predictor software.
- The impurities detected from each sulfenamide-based vulcanizing accelerator differed from manufacture to manufacture.

## Acknowledgement

We wish to thank Dr. Fumito Yatsuyanagi and Ms. Yuko Sekine of THE YOKOHAMA RUBBER CO.,LTD. for supplying the samples and their constructive comments.

First Edition: May, 2012



Shimadzu Corporation

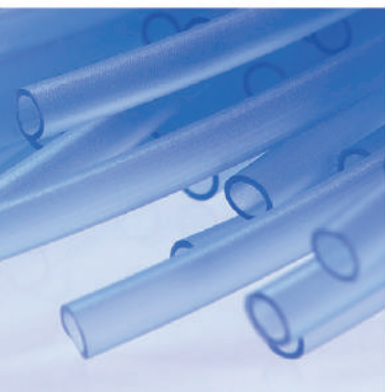
[www.shimadzu.com/an/](http://www.shimadzu.com/an/)

For Research Use Only. Not for use in diagnostic procedures.

The content of this publication shall not be reproduced, altered or sold for any commercial purpose without the written approval of Shimadzu. The information contained herein is provided to you "as is" without warranty of any kind including without limitation warranties as to its accuracy or completeness. Shimadzu does not assume any responsibility or liability for any damage, whether direct or indirect, relating to the use of this publication. This publication is based upon the information available to Shimadzu on or before the date of publication, and subject to change without notice.

© Shimadzu Corporation, 2012

# 3. Spectroscopy





## 3. Spectroscopy

---

### 3.1 Atomic Spectroscopy

---

#### 3.1.1 Energy Dispersive X-Ray Fluorescence (EDX)

XRF allows the analysis of element composition of samples in a wide variety of applications. This technique provides non-destructive and fast measurements of liquid and solid samples and is best suited to analysis of the elemental range from sodium/ carbon to uranium, covering the majority of metallic elements.

<b>A499</b>	Confirmation of raw material quality – dealing with “silent change” counterfeiting
<b>A527</b>	Quantifying “silent change” using EDXIR-analysis software: EDX-FTIR contaminant finder/material inspector
<b>A530</b>	Observing and measuring contaminants – advantages of the wide-field camera
<b>X253</b>	Quantitative analysis of waste oil by EDX-7000
<b>A488</b>	Analysis of inorganic additives in resin by FTIR and EDX

#### 3.1.2 Inductively Coupled Plasma Optical Emission Spectroscopy (ICP-OES)

ICP-OES measures light emitted by all elements present in a sample introduced into an ICP source. The emission intensities measured are then compared with the intensities of standard samples of known concentration to obtain the elemental concentrations in the unknown samples. The argon plasma is generated by an RF field and ionized argon gas. The advantage of the plasma in comparison to other energy sources is the high temperature of 10,000 °K, enabling complete atomization of the elements in a sample while minimizing interferences.

<b>J113</b>	Simultaneous analysis of major and trace elements in plating solution by ICPE-9820
<b>J95</b>	Analysis of additive elements in lubricating oil using ICPE-9000
<b>J111A</b>	Analysis of additive elements in lubricating oil according to ASTM D4951: ICPE-9820
<b>J114A</b>	Analysis of additive elements, wear metals, and contaminants in used lubricating oil according to ASTM D5185: ICPE-9820

# Application News

## No.A499

### Spectrophotometric Analysis

## Confirmation of Raw Material Quality -Dealing with "Silent Change" Counterfeiting-

### ■ Introduction

Safe and good quality raw materials are essential to the consistent production of high-quality products. However, materials may be changed by suppliers without the knowledge of the manufacturer, either in order to reduce costs or because they are unable to accommodate changes in materials that have been dictated by regulations. This kind of change is known as a "silent change" in Japan. Use of a non-standard raw material in a product means not only quality can no longer be assured, but has been known to cause accidents and is becoming a problem for society. Manufacturers can avoid these situations by checking at receipt whether the raw materials delivered are according to standard.

In this article, we use samples that may have been subject to a "silent change" (hereafter called "silent change" product) and introduce case analyses that confirm such changes using energy dispersive X-ray fluorescence spectrometry (EDX) (Fig. 1) and FTIR infrared spectrophotometry (Fig. 2).

### ■ Case of Replacement with a Cheaper Metal Material

Stainless steels are a special type of steel that are resistant to rust, that are created by adding various materials including chrome and nickel to iron. The stainless steel known as SUS316 has the composition 18Cr-12Ni-2.5Mo. It is created by adding molybdenum to SUS304 stainless steel, thereby improving its resistance to corrosion by sea water and other materials. We used EDX to analyze the stainless steel in a "silent change" product and in a genuine product. Analytical conditions are shown in Table 1, and EDX profiles are shown in Fig. 3.

Fig. 3 shows that the molybdenum peak present in the genuine SUS316 is missing from the "silent change" product, which exhibits a profile identical to SUS304. This result shows the steel material in the "silent change" product has been replaced with a cheaper type.

Though it is impossible to tell by visual examination whether steel material has been changed, taking measurements by EDX provides confirmation of a "silent change."



Fig. 1 EDX-7000 Energy Dispersive X-Ray Fluorescence Spectrometer

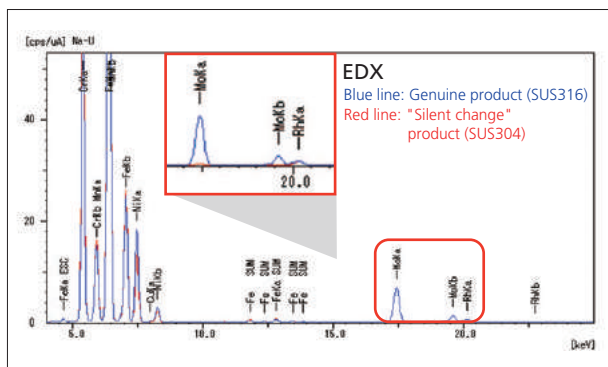


Fig. 2 IRAffinity-1S with MIRacle 10 Single-Reflection ATR Accessory

Table 1 EDX Analytical Conditions

Instrument	: EDX-7000
X-Ray Tube	: Rh target
Voltage/Current	: 50 kV (Na-U) /Auto
Atmosphere	: Air
Measurement Diameter	: 10 mmφ
Integration Time	: 30 sec.





**Fig. 3 Results of EDX Analysis of SUS316 Genuine Product and "Silent Change" Product (SUS304)**

### ■ Case of Replacement of a Plastic Material

We used FTIR to analyze a genuine polypropylene (PP) product and a "silent change" product. Analytical conditions are shown in Table 2, and the spectra obtained are shown in Fig. 4. Fig. 4 shows a peak was detected in the "silent change" product originating from  $\text{CH}_2$  rocking vibrations in the region of  $718\text{ cm}^{-1}$  (marked with a star). Spectral search confirmed that the "silent change" product contains polyethylene (PE) mixed in with PP.

This result indicates that recycled plastic may have been mixed into the raw material.

**Table 2 FTIR Analytical Conditions**

Instrument	: IRAffinity-1S MIRacle 10 (Diamond/ZnSe)
Resolution	: $4.0\text{ cm}^{-1}$
Accumulation	: 20
Apodization	: Happ-Genzel
Detector	: DLATGS

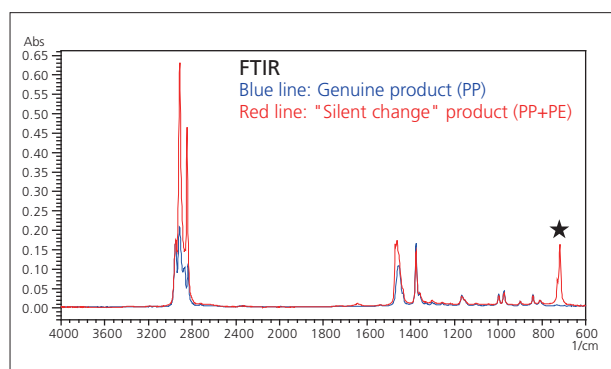


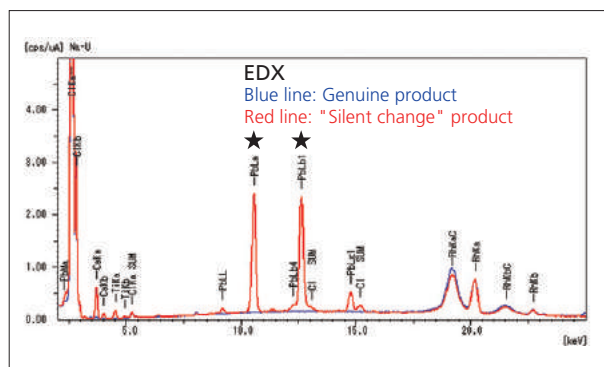
**Fig. 4 Results of FTIR Analysis of Genuine PP Product and "Silent Change" Product (PP+PE)**

### ■ Case of Toxic Element and Different Material Mixed into a Plastic Material

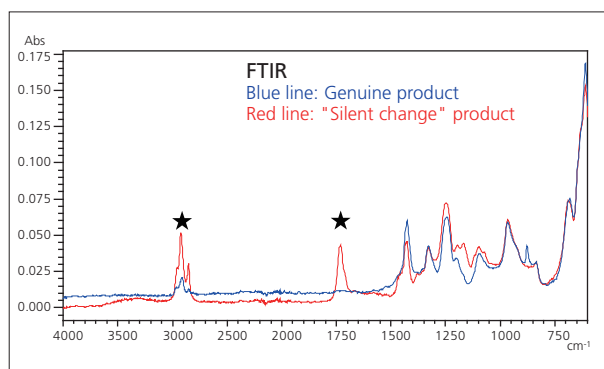
We used EDX and FTIR to analyze a genuine polyvinyl chloride (PVC) product, and a "silent change" plastic product. The EDX analytical conditions are shown in Table 1 with corresponding profiles shown in Fig. 5, while FTIR analytical conditions are shown in Table 2 with corresponding spectra shown in Fig. 6.

Fig. 5 shows that lead (marked with a star) was detected in the "silent change" product that was not detected in the genuine product. The plastic material analyzed in this experiment is subject to regulation under the Restriction on Hazardous Substances Directive (RoHS) and must not contain any lead. The results show that the "silent change" product does not meet the RoHS regulations.

Fig. 6 also shows that apart from peaks originating from PVC, peaks originating from acrylic were detected in the region of  $2900\text{ cm}^{-1}$  and  $1700\text{ cm}^{-1}$  (marked with a star). This result shows the presence of a different material mixed in with the material in the "silent change" product.



**Fig. 5 Results of EDX Analysis of Genuine Plastic Product and "Silent Change" Plastic Product**



**Fig. 6 Results of FTIR Analysis of Genuine Plastic Product and "Silent Change" Plastic Product**

### ■ Conclusion

Using EDX and FTIR to check inorganic materials and organic materials allows for a more robust response to the problem of "silent change" counterfeiting.

# Application News

## No. A527

### Spectrophotometric Analysis

## Quantifying "Silent Change" Using EDXIR-Analysis Software: EDX-FTIR Contaminant Finder/Material Inspector

The act of changing raw materials without notifying business partners for the purpose of reducing costs is known as "silent change."

Since products manufactured with non-standard raw materials cannot be guaranteed in terms of quality and usage of such materials can lead to incidents, this has become a social issue. The management of safe and good quality raw materials is indispensable in the manufacture of high quality products.

The EDXIR-Analysis software features a data comparison function. EDX data or FTIR data, or both, can be used to quantify the differences between genuine products and test products in terms of similarity. This function facilitates verification of raw materials as standard materials and proves effective in acceptance inspections, sampling inspections, and primary screening.

In this article, we introduce an example analysis that utilizes the data comparison function.

S. Iwasaki

### ■ Analysis of Plastic Contaminated with Toxic Elements

In order to use the data comparison function, genuine product data is registered into the library first. Next, after a comparison is performed between the genuine product data and test product data, the similarity and comparisons of the respective element contents, profiles, and EDX images of the EDX analysis data and the similarity of FTIR spectra of the FTIR analysis data are displayed.

The following data comparison was performed for a genuine product and test product of polyvinyl chloride (PVC) plastic. The results are indicated in Fig. 1 and 2.

The similarities determined using the data comparison function were 0.8332 with EDX data and 0.8680 with FTIR data, which resulted in a composite similarity of 0.8506. Similarity is displayed in a 0 to 1 range and higher values indicate greater similarity between data. In other words, a value close to 1 is obtained when the components in the samples for comparison are equivalent. However, we can conclude that the sample tested here may include different raw materials due to the resulting composite similarity of 0.8506.

The EDX profile and FTIR spectrum of the test product also indicate that it contains lead (Pb) and components derived from acrylic (indicated with stars), which are not detected in the genuine product.

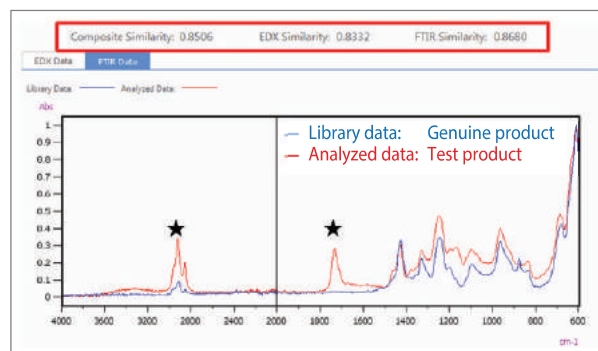


Fig. 2 Comparison of FTIR Spectra

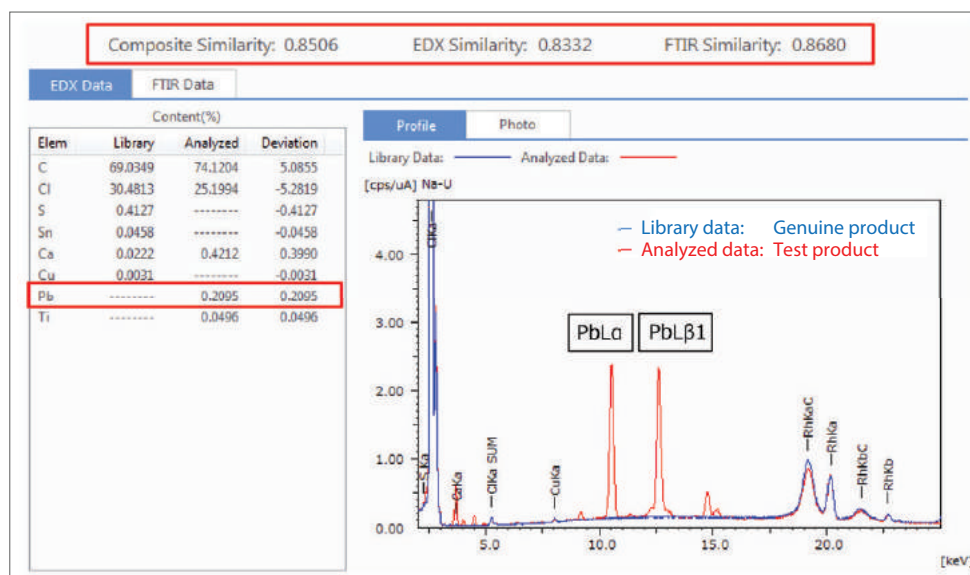


Fig. 1 Data Comparison Result and EDX Profiles



■ Analysis of Elemental Content Differences in Plastic Materials

RoHS compliant ERM-EC680 and ERM-EC681 polyethylene reference materials were selected for data comparison as a genuine product and test product respectively. Qualitative and quantitative analysis was performed with EDX and a single reflection ATR attachment was used to measure their infrared spectra. The results are indicated in Fig. 3 and 4 and the instruments and analysis conditions are listed in Table 1.

By overlapping the EDX profiles and FTIR spectra respectively of the genuine product and test product, we can see that while there are content differences for S, Cl, Cr, Zn, Br, Cd, Sn, and Sb, there is no difference with respect to plastic (main component).

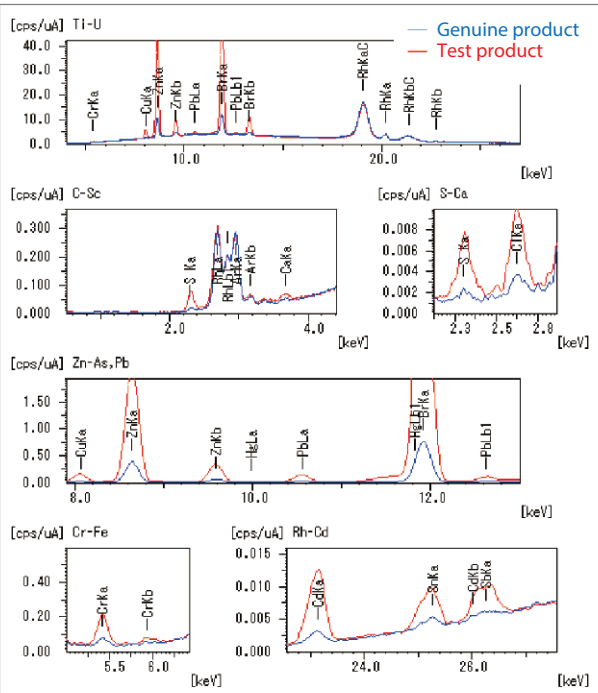


Fig. 3 Comparison of EDX Qualitative Profiles

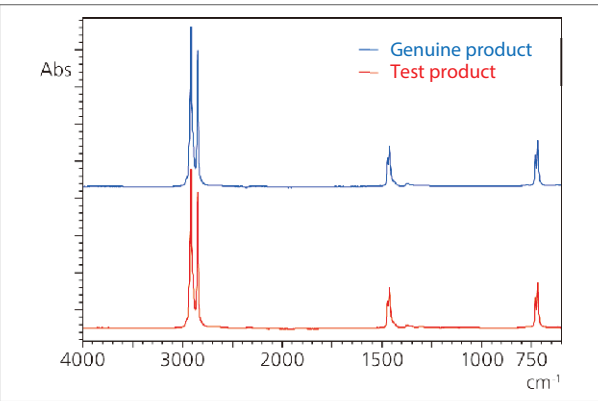


Fig. 4 Comparison of FTIR Spectra

The similarities determined using the data comparison function were 0.9616 with EDX data and 0.9830 with FTIR data, which resulted in a composite similarity of 0.9723 that suggests a difference in materials.

Table 2 indicates the result of determining whether there is a significant difference in similarity between genuine products and between a genuine product and test product, based on the repeatability accuracy observed through multiple comparisons. The EDX data results show a significant difference whereas the FTIR data results do not, which supports the assumption that the elemental content of the test product differs from the genuine product.

Table 1 Instruments and Analysis Conditions  
[EDX]

Instrument	: EDX-8000
X-ray Tube	: Rh target
Voltage/Current	: 15 kV (C-Sc), 50 kV (Ti-U)/Auto
Atmosphere	: Air
Measurement Diameter	: 10 mm φ
Primary Filter	: Without (Ti-U, C-Sc), #1 (Rh-Cd), #2 (S-Ca), #3 (Cr-Fe), #4 (Zn-As, Pb)
Integration Time	: 30 sec (without Primary Filter) 60 sec (with Primary Filter)

Instruments	: IRAffinity-1S, MIRacle10 (Diamond prism)
Resolution	: 4 cm <sup>-1</sup>
Accumulation	: 40
Apodization	: Happ-Genzel
Detector	: DLATGS

Table 2 Similarity Calculation Result

n	EDX		FTIR	
	Genuine product	Test product	Genuine product	Test product
1	0.9969	0.9616	0.9790	0.9830
2	0.9948	0.9613	0.9800	0.9800
3	0.9962	0.9613	0.9830	0.9810
4	0.9966	0.9612	0.9820	0.9830
5	0.9960	0.9613	0.9860	0.9790
Average	0.9961	0.9613	0.9820	0.9812
Standard deviation	0.0008	0.0002	0.0027	0.0018
Significant difference *	Yes		No	

\* According to t-test (significant level: 5%)  
Using commercially-available spreadsheet software

■ Summary

This time we introduced an example in which genuine products and test products were analyzed by utilizing the data comparison function of the EDXIR-Analysis software. By not only checking data visually but also quantifying them, differences between samples were easily distinguished.

Use of both EDX and FTIR instruments allows a multifaceted approach by enabling analysis of both organic and inorganic substances and assists in the risk management of raw materials in relation to safety. This software enables linkage and storage of various data as electronic files and provides powerful support in developing measures against silent change.



Shimadzu Corporation  
www.shimadzu.com/an/

For Research Use Only. Not for use in diagnostic procedure.

This publication may contain references to products that are not available in your country. Please contact us to check the availability of these products in your country.

The content of this publication shall not be reproduced, altered or sold for any commercial purpose without the written approval of Shimadzu. Company names, product/service names and logos used in this publication are trademarks and trade names of Shimadzu Corporation or its affiliates, whether or not they are used with trademark symbol "TM" or "®". Third-party trademarks and trade names may be used in this publication to refer to either the entities or their products/services. Shimadzu disclaims any proprietary interest in trademarks and trade names other than its own.

The information contained herein is provided to you "as is" without warranty of any kind including without limitation warranties as to its accuracy or completeness. Shimadzu does not assume any responsibility or liability for any damage, whether direct or indirect, relating to the use of this publication. This publication is based upon the information available to Shimadzu on or before the date of publication, and subject to change without notice.

## Application News

# No. A530

### Spectrophotometric Analysis

## Observing and Measuring Contaminants - Advantages of the Wide-Field Camera -

In contaminant analysis, it is important to check for significant differences between the contaminant and normal areas by measuring the contaminant together with an area that is assumed to be normal in the vicinity of the contaminant. If the border between the contaminant and normal area is unclear, the measurement area of the contaminant can be determined by extending the observation area of which is assumed to be normal and sequentially comparing measurements.

The AIM-9000 infrared microscope is equipped with a wide-field camera (option) capable of observing a maximum field of view (FOV) of 10 × 13 mm. This enables efficient observation and checking over an extended range of a measurement area that includes contaminants. In this article, we introduce an example of using the wide-field camera in contaminant analysis.

Y. Suzuki, H. Taniguchi

### Wide-Field Camera

The microscope camera installed on general infrared microscopes performs image observation via a reflection objective mirror used in infrared spectrum measurement and the FOV is limited to a very narrow range of about a few hundred square  $\mu\text{m}$ .

In addition to the conventional microscope camera, the AIM-9000 is equipped with a wide-field camera that enables wide-field observation which facilitates observation and checking of measurement targets with good efficiency over an extended range. The wide-field camera is capable of observing at a size visible to the human eye (FOV of 10 × 13 mm) and also features a variable digital zoom function with maximum 5x magnification (2.0 × 2.6 mm).

### Observation of a Contaminant Adhered to an Electronic Component

(1), (2), and (3) in Fig. 1 show observation images of an electronic component captured using the wide-field camera. Observation using the wide-field camera revealed what looked like a contaminant on the right of the letter "J." Switching to the high-magnification microscope camera, (4) and (5) in Fig. 1 show observation images of a contaminant in the area right of the letter "J." A contaminant about 30 × 40  $\mu\text{m}$  in size is clearly visible. Since position information is shared by the microscope camera and wide-field camera, switching cameras does not shift the FOV, thereby allowing observation to proceed smoothly. Furthermore, the microscope camera features a 10x digital zoom (0.03 × 0.04 mm) function, which provides a total magnification range of 330x from the FOV of the wide-field camera. Using the wide-field camera enables smooth, sequential operation from observation at a wide FOV through to confirming the positions of minute contaminants.

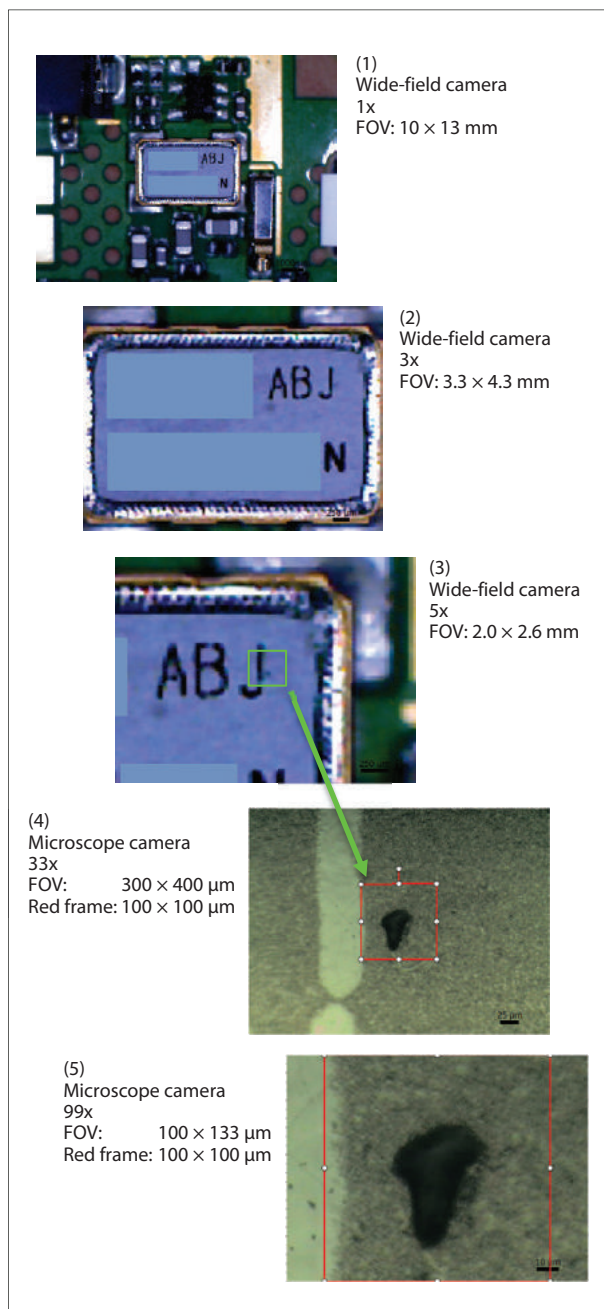


**Fig. 1 Electronic Component Observation with Wide-Field Camera and Microscope Camera**

■ Observation and Measurement of Contaminants Adhered to a Coin

Contaminants adhered to a coin were observed and measured. Fig. 2 shows observation images of the coin surface captured using the wide-field camera. Green and white contaminants can be observed to the right of center on the coin.

The wide-field camera features independent illumination from four directions that can be adjusted by selecting which lights to turn on and off in order to obtain optimal illumination. This is useful when, for example, observation is difficult due to bright reflected light. The right image in Fig. 2 shows illumination weakened, enabling a clear view of contaminants compared to the left image.

Next, the background (BKG) was set to a clean area near the contaminants and the contaminants were measured using the reflection spectroscopy. Fig. 3 shows tiling images of the coin surface captured using the microscope camera and the measurement positions. The yellow flag indicates the BKG measurement position and the blue flags indicate the sample measurement positions.

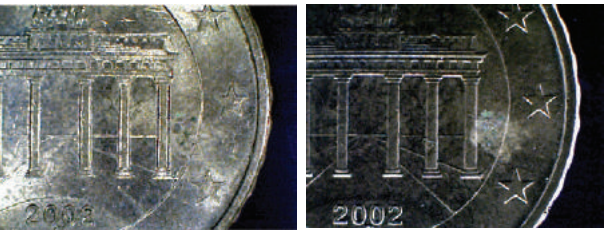


Fig. 2 Observation Images of Coin Surface Captured Using the Wide-Field Camera  
Left: Bright State, Right: Dark State

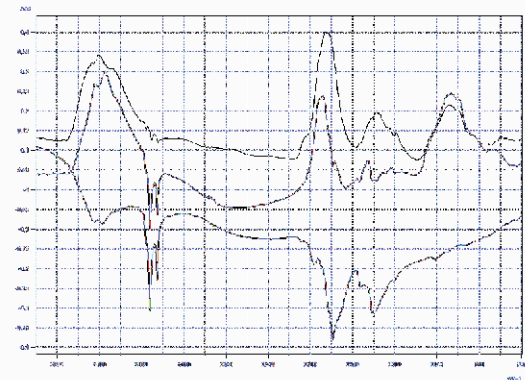


Fig. 4 Measurement Results for BKG Measurement Position Set Above Contaminants  
Sample Measurement Positions: 1: Black, 2: Red, 3: Green

Table 1 Measurement Conditions	
Instrument	: IRTracer-100, AIM-9000
Resolution	: 8 cm <sup>-1</sup>
Accumulation	: 100
Apodization	: Happ-Genzel
Detector	: MCT

The left image in Fig.3 shows the BKG measurement position set above the contaminants and Fig. 4 shows the spectra measured in this state.

Table 1 lists the measurement conditions. Depending on the measurement position, some peaks of the absorbance spectra are inverted downward. This likely occurred because contaminants that could not be verified in the image exist at the BKG measurement position and the amount of these contaminants is less at the sample measurement position compared to the BKG measurement position, thus causing corresponding peaks to invert downward.

Next, the right image in Fig.3 shows the BKG measurement position set below the contaminants and Fig. 5 shows the spectra measured in this state. This time the peaks of all the spectra are facing upward meaning that the set BKG measurement position was appropriate.

The spectra of the contaminants resemble the spectra of a carboxylate, such as alginate, and fat/oil (library spectra are not shown), which points to a mixture derived from food and food additives. From this result, we could conclude that these contaminants adhered to the coin during the course of circulation.

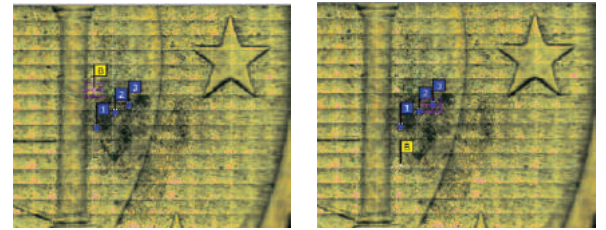


Fig. 3 Tiling Images of Coin Surface Captured Using the Microscope Camera and Measurement Positions  
Left: BKG Measurement Position Set Above Contaminants  
Right: BKG Measurement Position Set Below Contaminants

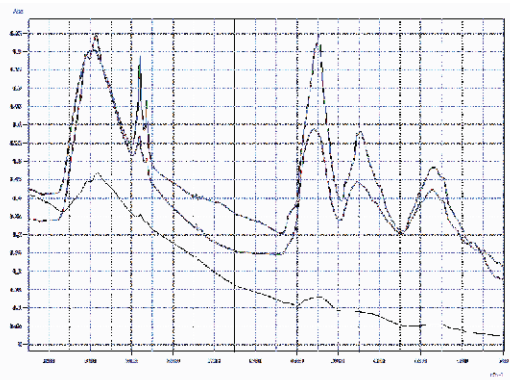


Fig. 5 Measurement Results for BKG Measurement Position Set Below Contaminants  
Sample Measurement Positions: 1: Green, 2: Red, 3: Black

■ Summary

We introduced an example of using the wide-field camera in contaminant analysis. The wide-field camera enables efficient observation and checking over an extended range of a measurement area that includes contaminants. It also reduces the workload of setting and changing BKG measurement positions and sample measurement positions, thereby facilitating rapid acquisition and evaluation of contaminant spectra.



Shimadzu Corporation  
www.shimadzu.com/an/

For Research Use Only. Not for use in diagnostic procedure.  
This publication may contain references to products that are not available in your country. Please contact us to check the availability of these products in your country.  
The content of this publication shall not be reproduced, altered or sold for any commercial purpose without the written approval of Shimadzu. Company names, product/service names and logos used in this publication are trademarks and trade names of Shimadzu Corporation or its affiliates, whether or not they are used with trademark symbol "TM" or "®". Third-party trademarks and trade names may be used in this publication to refer to either the entities or their products/services. Shimadzu disclaims any proprietary interest in trademarks and trade names other than its own.  
The information contained herein is provided to you "as is" without warranty of any kind including without limitation warranties as to its accuracy or completeness. Shimadzu does not assume any responsibility or liability for any damage, whether direct or indirect, relating to the use of this publication. This publication is based upon the information available to Shimadzu on or before the date of publication, and subject to change without notice.

# Application News

## No.X253

### X-ray Analysis

## Quantitative Analysis of Waste Oil by EDX-7000

In recent years, elemental analysis by EDX has been increasing due to the heightened concern for the environment. Even waste oil can quickly and easily be analyzed by EDX by merely pouring it as is into a container.

We evaluated the repeatability and limit of detection in analysis using new, unused commercially available general oil that is similar waste oil using the EDX-7000. The results demonstrated an improvement in sensitivity that was 1.5 to 4 times that obtained with the conventional model\*1, while achieving a shorter measurement time for each sample.

\*1: Shimadzu Application News No.X242

### Sample

Wear Metals in 75 cSt Hydrocarbon Oil  
A23-10, 30, 50, 100, 300, 500  
(each 10, 30, 50, 100, 300, 500 ppm)  
Conostan Base Oil (0 ppm)

### Elements

<sup>22</sup>Ti, <sup>23</sup>V, <sup>24</sup>Cr, <sup>28</sup>Ni, <sup>29</sup>Cu, <sup>30</sup>Zn, <sup>47</sup>Ag, <sup>48</sup>Cd, <sup>50</sup>Sn, <sup>51</sup>Sb,  
<sup>56</sup>Ba, <sup>82</sup>Pb

### Sample Preparation

Approximately 8 mL of sample was placed as is in a container covered with 5-μm thick polypropylene film. Analysis was then conducted.

A photograph of the sample is shown in Fig. 1.



Fig. 1 Sample Preparation

### Qualitative Analysis, Lower Limits of Detection (L.L.D.)

The spectral profiles for the elements of interest are shown in Fig. 2. The following expression was used to calculate the theoretical lower limits of detection from the spectral intensities (NET, BG) of A23 – 50. The results are shown in Table 1.

In addition, intensity overlap correction was applied when there was overlapping with coexisting elements such as Ti, V, Cr, etc.

$$L.L.D. = 3 \cdot \frac{C}{NET} \sqrt{\frac{BG}{T \cdot A}}$$

Intensity [cps/μA]  
C : Concentration in oil [ppm]  
T : Integration time [sec]  
A : Current value [μA]

Table 1 Theoretical Lower Limits of Detection

Element	<sup>22</sup> Ti	<sup>23</sup> V	<sup>24</sup> Cr	<sup>28</sup> Ni	<sup>29</sup> Cu	<sup>30</sup> Zn	<sup>47</sup> Ag	<sup>48</sup> Cd	<sup>50</sup> Sn	<sup>51</sup> Sb	<sup>56</sup> Ba	<sup>82</sup> Pb
L.L.D. (300 sec)	1.2	1.3	1.2	0.4	0.3	0.3	0.7	0.9	1.9	2.8	9.9	0.3
L.L.D. (100 sec)	2.2	2.2	2.1	0.7	0.6	0.5	1.3	1.5	3.2	4.9	17.2	0.5

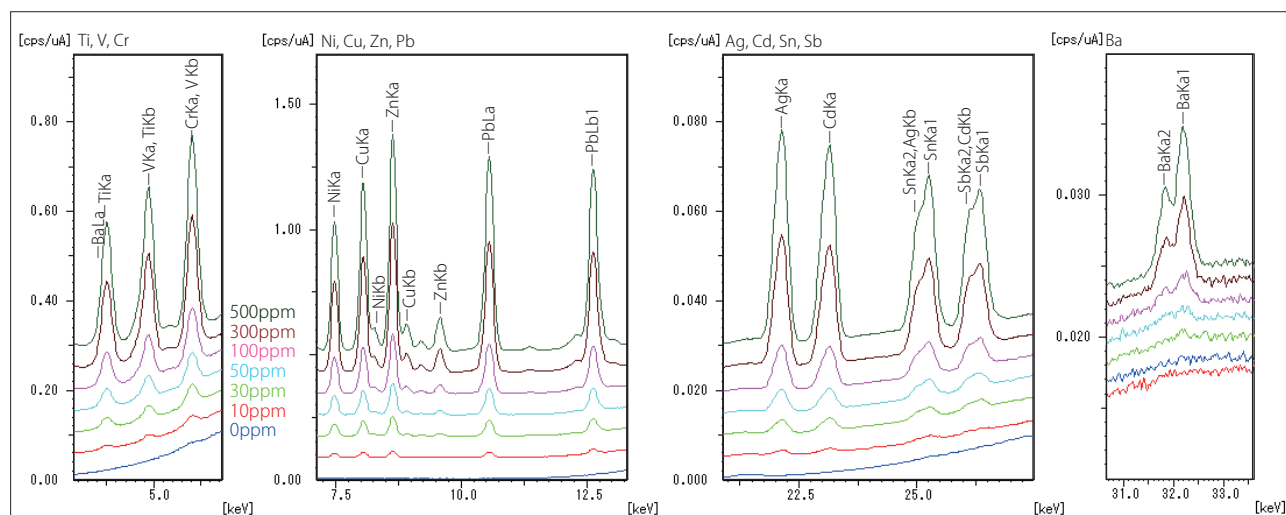


Fig. 2 X-Ray Fluorescence Spectra of Measured Elements



## ■ Calibration Curves

The calibration curves for Cr, Ni, Ag, Cd, Sb and Pb are shown in Fig. 3, and the accuracy ( $1\sigma$ ) of the respective calibration curves are shown in Table 2. To obtain linearity of the calibration curves, internal standard scattered radiation correction was conducted for Ti, V, Cr, Ni, Cu, Zn and Pb.

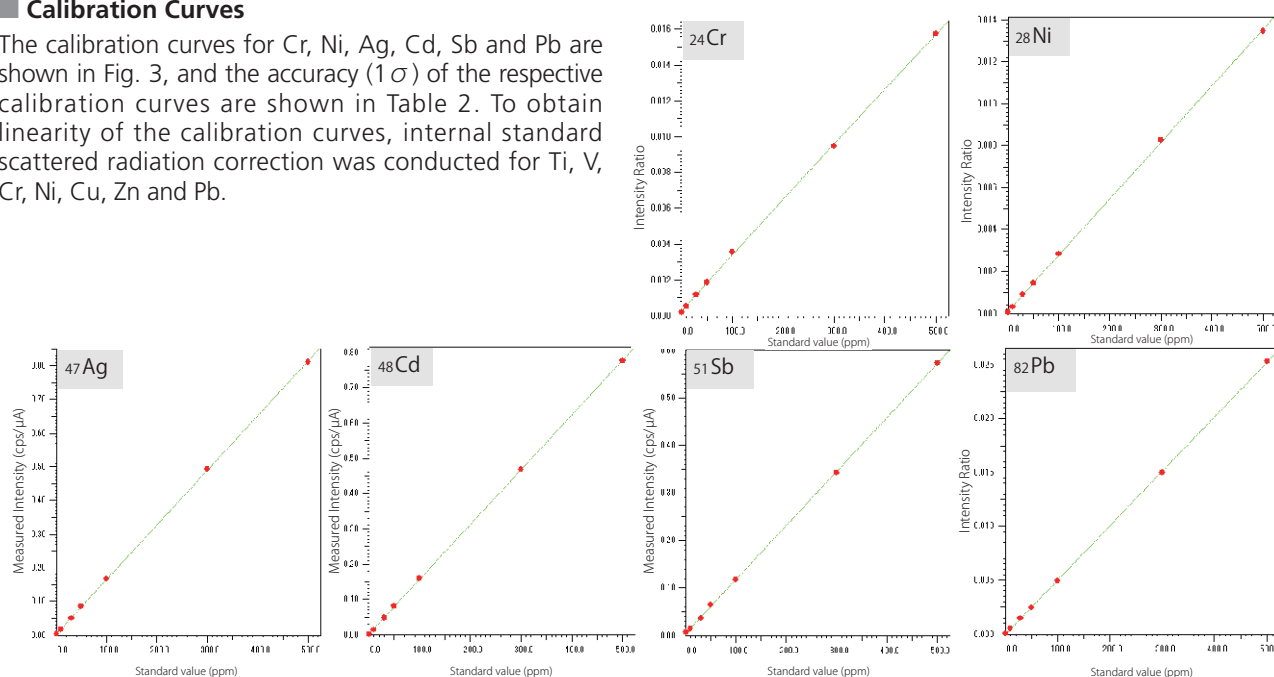


Fig. 3 Calibration Curves for Cr, Ni, Ag, Cd, Sb, Pb

Table 2 Accuracy of Calibration Curves

Element	22Ti	23V	24Cr	28Ni	29Cu	30Zn	47Ag	48Cd	50Sn	51Sb	56Ba	82Pb
Accuracy ( $1\sigma$ )	1.5	1.0	3.3	2.2	1.7	1.6	1.3	1.4	1.3	2.1	3.9	1.6

## ■ Repeatability

Using the above calibration curve method, the repeatability test results for A23 – 300 shown Table 3 were obtained by simply conducting 10 repeat measurements. An integration time of 100 seconds was used for each element.

Table 3 Repeatability for A23 – 300

Element	22Ti	23V	24Cr	28Ni	29Cu	30Zn	47Ag	48Cd	50Sn	51Sb	56Ba	82Pb
Concentration	300	300	300	300	300	300	300	300	300	300	300	300
1	300	298	295	305	300	299	301	304	303	304	312	295
2	297	295	297	300	299	295	302	304	296	299	303	298
3	303	298	301	300	298	302	303	302	306	298	301	298
4	299	294	297	306	298	303	302	303	304	299	310	299
5	302	299	297	303	302	298	306	303	300	301	303	300
6	305	299	296	302	303	299	302	303	306	297	316	295
7	300	298	295	306	305	298	304	304	301	297	321	299
8	306	298	297	302	302	299	300	301	301	302	298	299
9	299	298	300	303	297	304	304	305	306	298	295	297
10	306	299	298	301	301	300	305	300	303	299	320	299
Average	302	298	297	303	300	300	303	303	303	299	308	298
Standard Deviation	3.0	1.7	2.0	2.2	2.4	2.4	2.0	1.6	3.3	2.3	9.3	1.6
Coefficient of Variation [%]	1.0	0.6	0.7	0.7	0.8	0.8	0.7	0.5	1.1	0.8	3.0	0.6

### Analytical Conditions

Instrument	:EDX-7000	Collimator[mmφ]	:10
Elements	:Ti, V, Cr, Ni, Cu, Zn, Ag, Cd, Sn, Sb, Ba, Pb	Primary Filter	:#1, #2, #4
Analytical Group	:Working Curve	Atmosphere	:Air
X-ray Tube	:Rh target	Detector	:SDD
Tube Voltage [kV]	:15, 50	Integration Time[sec]	:100, 300
Current [μA]	:Auto	Dead time [%]	:Max. 30

First Edition: Nov. 2013



Shimadzu Corporation

www.shimadzu.com/an/

For Research Use Only. Not for use in diagnostic procedures.

The content of this publication shall not be reproduced, altered or sold for any commercial purpose without the written approval of Shimadzu. The information contained herein is provided to you "as is" without warranty of any kind including without limitation warranties as to its accuracy or completeness. Shimadzu does not assume any responsibility or liability for any damage, whether direct or indirect, relating to the use of this publication. This publication is based upon the information available to Shimadzu on or before the date of publication, and subject to change without notice.

© Shimadzu Corporation, 2013

# Application News

## No. A488

### Spectrophotometric Analysis

## Analysis of Inorganic Additives in Resin by FTIR and EDX

Additives enhance the quality of products by improving the functionality, workability, and stability of the materials used in the product. They are utilized in a wide range of products, including electronics, foods, pharmaceuticals, cosmetics, plastics, etc., and play an important role by adding value to products.

The approach taken in the analysis of additives is dependent on whether the additive is organic or inorganic. Organic additives are typically identified by first extracting the additives using a suitable pretreatment procedure, and after chromatographic separation of the extracted components, a suitable analytical instrument is used for qualitative analysis. On the other hand, comprehensive identification of inorganic additive components is typically based on the results obtained using elemental analysis, infrared spectroscopy or morphologic observation, etc<sup>1)</sup>.

Here, we introduce examples of FTIR analysis to obtain useful information regarding some typical inorganic additives, in addition to an example of analysis of a resin containing an inorganic additive using FTIR and EDX.

### ■ Analysis of Inorganic Additives by FTIR

FTIR is used mainly for organic analysis, but useful information can also be obtained by applying FTIR to the analysis of some inorganic additives.

Here, we conducted single-reflection ATR measurement using a diamond prism. Table 1 shows the analytical conditions using FTIR, and the infrared spectra and peak positions of the four substances used as additives (aluminum silicate, aluminum hydroxide, magnesium silicate, and calcium carbonate) are shown in Fig. 1 to 4. A spectral characteristic of inorganic additives is the appearance of a relatively wide peak in the lower wavenumber region. In addition, as is clearly evident in Fig. 1 to 3, a characteristic peak is sometimes present in the higher wavenumber region. In such cases, qualitative identification is possible by FTIR alone.

**Table 1 Analytical Conditions**

Instruments	: IR Tracer-100, Quest, Diamond
Resolution	: 4.0 cm <sup>-1</sup>
Accumulation	: 40
Apodization	: Happ-Genzel
Detector	: DLATGS

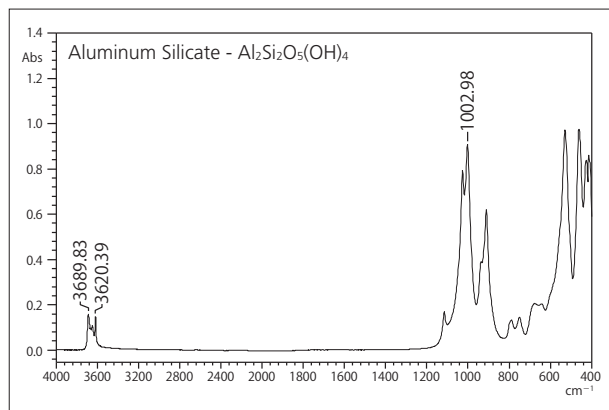


**Fig. 1 IR Spectrum and Peak Position of  $\text{Al}_2\text{Si}_2\text{O}_5(\text{OH})_4$**

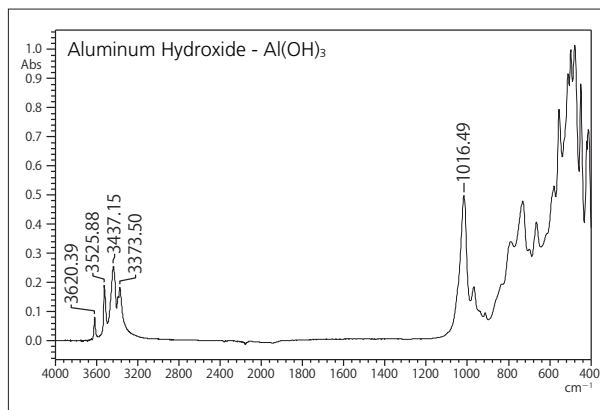


**Fig. 2 IR Spectrum and Peak Position of  $\text{Al}(\text{OH})_3$**

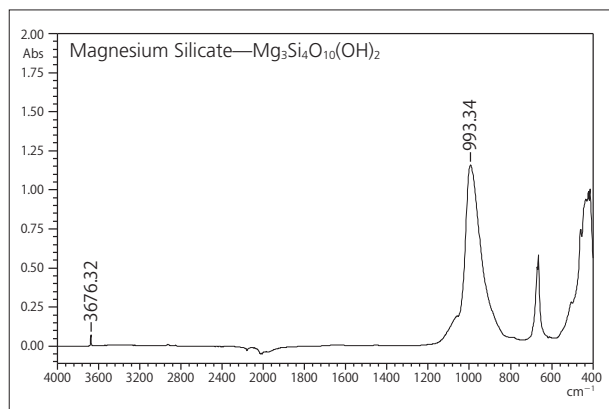


**Fig. 3 IR Spectrum and Peak Position of  $\text{Mg}_3\text{Si}_4\text{O}_{10}(\text{OH})_2$**

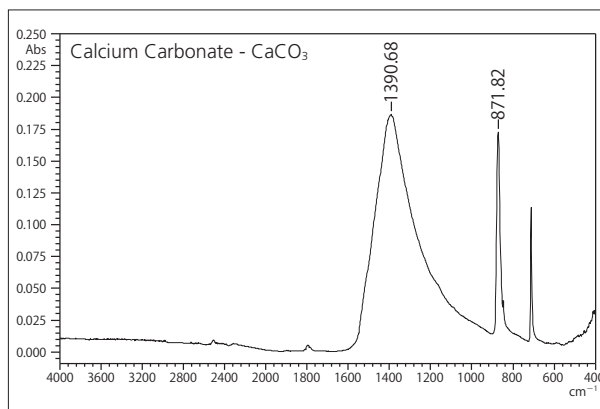


**Fig. 4 IR Spectrum and Peak Position of  $\text{CaCO}_3$**

## ■ Analysis of Inorganic Additives in Resin

FTIR was used for the analysis of a connector cover as a sample that contains an inorganic additive. Fig. 5 shows a photograph of the sample, and Fig. 6 shows the results of analysis.



Fig. 5 Connector Cover

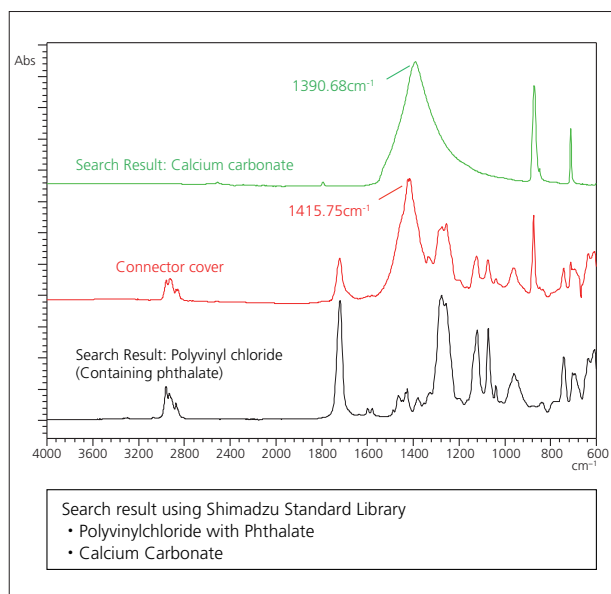


Fig. 6 IR Spectra and FTIR Search Results

From the infrared spectra and search results of Fig. 6, the principal component of the connector cover was determined to be polyvinylchloride (PVC). Also, the peak in the vicinity of  $1415\text{ cm}^{-1}$  in the infrared spectrum suggests the presence of calcium carbonate ( $\text{CaCO}_3$ ).

However, a comparison of the connector cover peak at  $1415\text{ cm}^{-1}$  with the peak at  $1390\text{ cm}^{-1}$  of calcium carbonate alone indicates a peak position shift of  $25\text{ cm}^{-1}$ . Therefore, there is clearly insufficient basis to irrefutably conclude that calcium carbonate is included as an additive from the infrared spectrum alone.

Thus, we followed up this result by conducting EDX analysis to reconcile this discrepancy. The analytical conditions used are shown in Table 2, and the qualitative analytical results are shown in Fig. 7. Table 3-1 and Table 3-2 show the quantitative analytical results by the FP method<sup>2)</sup>.

Table 2 EDX Analytical Conditions

Instrument	: EDX-7000
X-ray Tube	: Rh target
Voltage / Current	: 15 kV(Na-Sc), 50 kV(Ti-U) / Auto
Atmosphere	: Vacuum
Measurement Diameter	: 10 mmφ
Integration Time	: 100 sec

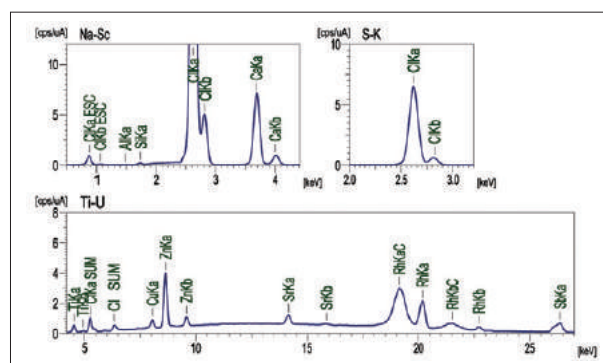


Fig. 7 Results of Qualitative Analysis of Connector Cover by EDX

Table 3-1 Results A of Quantitative Analysis of Connector Cover by EDX

Element	Cl	Ca	Sb	Zn	Ti	Si	Al	Cu	Sr
Quantitation Value	72.56	26.11	0.40	0.31	0.23	0.21	0.096	0.054	0.030

Table 3-2 Results B of Quantitative Analysis of Connector Cover by EDX

Element	$\text{C}_2\text{H}_3\text{Cl}$	$\text{CaCO}_3$	$\text{SiO}_2$	$\text{Sb}_2\text{O}_3$	$\text{TiO}_2$	$\text{ZnO}$	$\text{Al}_2\text{O}_3$	$\text{CuO}$	$\text{SrO}$
Quantitation Value	73.14	25.55	0.31	0.30	0.25	0.25	0.13	0.046	0.024

As clearly indicated in Table 3-1, chlorine (Cl) and calcium (Ca) are the principal constituent elements. This is consistent with the polyvinyl chloride results obtained by FTIR, supporting the presence of calcium carbonate. Table 3-2 shows the quantitative analytical results for specific compounds identified from the results of both FTIR and EDX. It should be noted that other detected elements are assumed to be oxides<sup>3)</sup>. Thus, the combination of FTIR and EDX has provided sufficient evidence that calcium carbonate is present as an additive.

## ■ Conclusion

By applying a combination of FTIR and EDX, we were able to more accurately identify the additives included in an actual sample. Such an analysis is applicable to contaminant analysis and confirmation testing, and should be considered an effective means for conducting such confirmation testing in a wide range of fields, including electrical and electronic, chemical, pharmaceutical, and foods, etc.

- 1) Toshikatsu Nishioka, Tatsuya Housaki: (2011) "A Guide on Plastic Analysis," Maruzen Publishing Co., Ltd.
- 2) Hiroto Ochi, Hideo Okashita: Shimadzu Review, 45 (1-2), 51 (1988)
- 3) Sachio Murakami, et.al: Shimadzu Review, 69 (1-2), 133 (2012)



# Application News

## No.J113

### Inductively Coupled Plasma Atomic Emission Spectrometry

## Simultaneous Analysis of Major and Trace Elements in Plating Solution by ICPE-9820

### ■ Introduction

Plating is a technique in which a thin film of metal is coated on the surface of a material to enhance the performance of a product. Management of the components in the plating solution is very important from the standpoint of maintaining the quality of the plating. Aside from the main components in the plating solution, management of the trace components and additives, typically present at different concentrations, is also important.

Efficient analysis of these metallic components requires an analytical instrument capable of both high-sensitivity measurement and measurement over a wide concentration range. ICP atomic emission spectrometry is a method of analysis that is suitable for such analyses due to its wide dynamic range, permitting analysis over a wide range of concentrations, from  $\mu\text{g/L}$  to the percentage level.

We performed simultaneous elemental analysis of the zinc plating solution, from the principle to trace level elements, using the Shimadzu ICPE-9820 multi-type ICP atomic emission spectrometer. Typically, when analyzing metals in plating solution, the principle elements are measured after diluting the sample between 1,000 and 10,000 times, whereas the trace level elements are measured in a low-dilution sample. As a result, many samples must be prepared at different dilutions, significantly lengthening the analysis time. With the ICPE-9820, however, the vertically-oriented torch – which prevents salt precipitation – coupled with automatic dual-view (axial and radial) observation, makes it possible to conduct simultaneous analysis of both high- and low-concentration elements.

### ■ Samples

Zinc plating solution (2 types: Sample 1, Sample 2)

### ■ Sample Preparation

The measurement samples were prepared by diluting each sample 10-fold using 1 mol/L hydrochloric acid. The calibration curve samples were prepared by appropriately diluting each of the single-element standard solutions (1000 mg/L) with 1 mol/L hydrochloric acid. The Zn high-concentration solution was prepared by appropriately diluting the Zn 210 g/L zinc plating solution with 1 mol/L hydrochloric acid. Yttrium (Y) was added to all of the measurement solutions for use as an internal standard (concentration in solution: 0.5 mg/L).

To validate the measurements of the high-concentration elements, Sample 1 was diluted 100-fold and 1,000-fold, respectively, to prepare diluted test samples. For the trace elements, Sample 1 was diluted 10-fold with hydrochloric acid, and then spiked with a standard solution of the measurement elements to prepare a spike-and-recovery test solution.

### ■ Instrument and Analytical Conditions

The Shimadzu ICPE-9820 multi-type ICP atomic emission spectrometer was used for measurement, and the measurement conditions are shown in Table 1. With the ICPE-9820, the principle components, consisting of high-concentration elements, can be measured using the radial view for low-sensitivity wavelengths, while the trace elements can be measured using the axial view for high sensitivity. As a result, simultaneous analysis of the principle zinc plating elements, in addition to the trace-level elements, can be performed using a single dilution procedure (10-fold dilution solution).

**Table 1 Analytical Conditions**

Instrument	: ICPE-9820
Radio frequency power	: 1.2 kW
Plasma gas Flowrate	: 14 L/min
Auxiliary gas Flowrate	: 1.2 L/min
Carrier gas Flowrate	: 0.8 L/min
Sample introduction	: Nebulizer 10
Misting chamber	: Cyclone chamber
Plasma torch	: Torch for high salt content
Observation	: Axial (AX) / Radial (RD)

### ■ Analysis

The calibration curve-internal standard method was used to measure zinc (Zn), calcium (Ca), iron (Fe), manganese (Mn), titanium (Ti), aluminum (Al), cadmium (Cd) and copper (Cu) elements in the plating solution, with an internal standard used to correct for interferences.

The dilution test was conducted for the high-concentration elements, Zn, Ca, Fe, Mn and Ti, and the spike-and-recovery test was conducted for the low-concentration elements, Al, Cd and Cu.

### ■ Analytical Results

Table 2 shows both the dilution and the spike-and-recovery test results. Table 3 shows the analysis results. Both the dilution test and spike-and-recovery test showed excellent results, with nearly 100 % recovery. Good results were obtained for the main constituent Zn using the low-sensitivity wavelength, radial-view measurement, and a 21 g/L upper limit calibration curve, and high-accuracy results were obtained for the trace elements using the axial-view measurement.

Fig. 1 shows the spectral profiles of Mn, Fe and Ti. Fig. 2 shows the calibration curve for Zn, and Fig. 3 shows the spectral profiles of Zn.

### ■ Conclusion

Using the ICPE-9820, it is possible to conduct simultaneous analysis of all the elements in a zinc plating solution, from the principle components to the trace-level elements, using just a single dilution operation. These results demonstrate that reduced pretreatment time, shortened analysis time and lower running costs can be achieved with the ICPE-9820 instrument.

Table 2 Results of Dilution Test and Spike-and-Recovery Test for Zinc Plating Solution

Concentration in Measurement Solution	Zn	Ca	Fe	Mn	Ti	Al	Cd	Cu
	mg/L	mg/L	mg/L	mg/L	mg/L	mg/L	mg/L	mg/L
Sample 1 (10-fold dilution)	21400	3.95	45.6	0.760	3.51	0.220	0.013	0.022
Dilution Test – Sample 1 (100-fold dilution)	-	0.404	4.70	0.077	0.345	-	-	-
Dilution Test – Sample 1 (1,000-fold dilution)	211	-	-	-	-	-	-	-
Dilution Test Results (%)	101	98	97	99	102	-	-	-
Spike-and-Recovery Test								
Sample 1 (10-fold dilution + spiked element)	-	-	-	-	-	0.422	0.063	0.125
Spike Concentration	-	-	-	-	-	0.2	0.05	0.1
Spike-and-Recovery Rate (%)	-	-	-	-	-	101	99	103

Dilution test result (%) = {10-fold diluted sample analysis result / (100-fold or 1,000-fold diluted sample quantitation value × dilution factor / 10)} × 100

Spike-and-recovery rate (%) = {(sample analysis results for spike-and-recovery test – 10-fold dilution sample analysis results) / spike concentration} × 100

Table 3 Analytical Results for Zinc Plating Solution

Concentration in Original Sample	Zn	Ca	Fe	Mn	Ti	Al	Cd	Cu
	g/L	mg/L	mg/L	mg/L	mg/L	mg/L	mg/L	mg/L
Sample 1	214	39.5	456	7.60	35.1	2.20	0.13	0.22
Sample 2	189	113	23.8	2.10	3.47	0.30	0.24	0.22

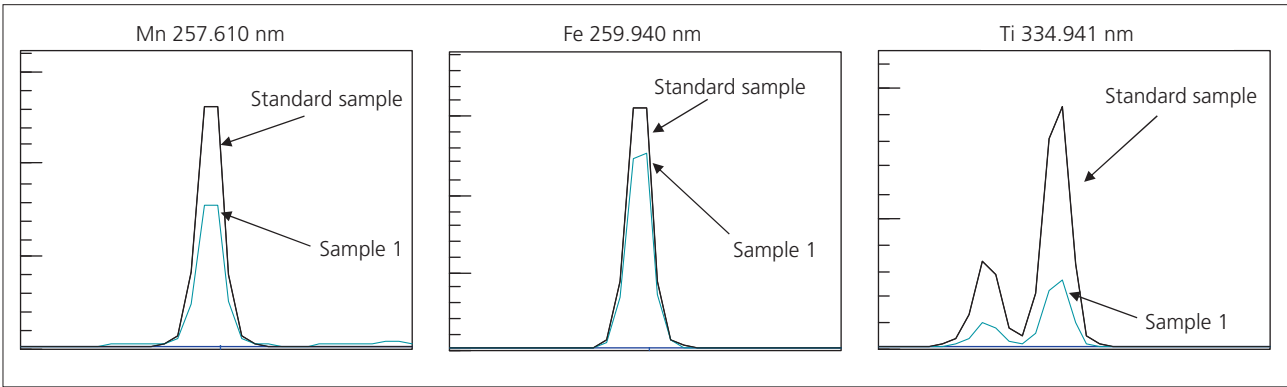


Fig. 1 Spectral Profiles of Mn, Fe and Ti

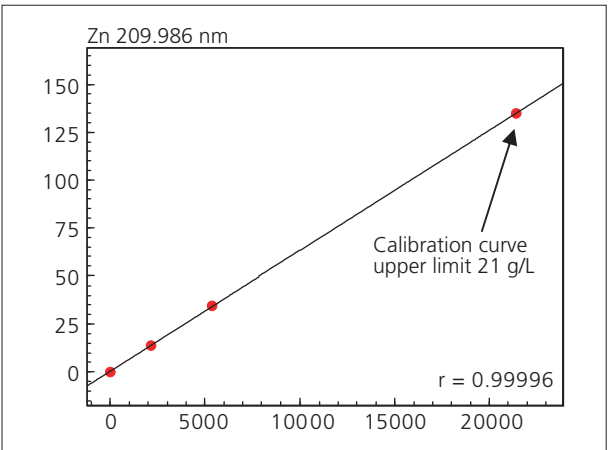


Fig. 2 Calibration Curve for Zn

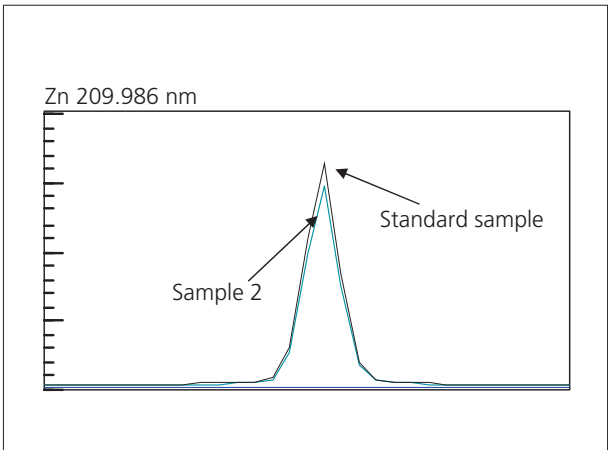


Fig. 3 Spectral Profiles of Zn

# Application News

## No. J95

### Inductively Coupled Plasma Atomic Emission Spectrometry

## Analysis of Additive Elements in Lubricating Oil Using ICPE-9000

Additives consisting of various types of organic metal substances are added to lubricating oils to enhance performance. They include detergents (to prevent and inhibit the deposition of degradation products formed during high-temperature operation of engines, etc.), antioxidants (which react with free radicals and peroxides to suppress the formation of varnish and sludge that originate during oxidation of oil), corrosion inhibitors (to neutralize the corrosive oxidation products formed due to degradation of the lubricant), solid lubricants (used as powder or thin film to reduce

friction and wear), etc. Analysis of these additive elements is important for quality management of lubricating oils, and ICP emission spectrometry is one of the effective methods available for this analysis. Here, using the ICPE-9000 multitype inductively coupled plasma emission spectrometer, we conducted analysis of additive elements in commercially available engine oil, ATF oil and gear oil. The ICPE-9000 can simultaneously measure multiple elements, and quickly analyze many additive elements.

#### ■ Samples

- Engine oil (3 types)
- ATF oil (1 type)
- Gear oil (2 types)

#### ■ Sample Preparation

Each sample was weighed out to 1 g, diluted with 100 mL of xylene (100-to-1 dilution), and then measured. In the case of sample 6 (gear oil), a 10 mL aliquot of the 100-to-1 dilution was further diluted with 50 mL of xylene (500 to 1 dilution) to serve as the measurement sample. When diluting the samples, Y (yttrium) was added to the sample solutions at the rate of 1 mg/L to be used as an internal standard element. Furthermore, the 100-to-1 dilution of sample 1 (engine oil) was again diluted by 5 to 1 to prepare a very concentration solution (500-to-1 dilution). The standard samples were prepared by appropriately diluting the SPEX oil base multi-element mixture of 21 elements (900 ppm, 500 ppm) and the CONOSTAN oil base single element standard solutions (5000 ppm), respectively, with xylene. As with the measurement samples, Y (yttrium) was added at 1 mg/L.

#### ■ Analysis

Quantitative analysis of the lubricant samples was conducted by the calibration curve-internal standard method using the ICPE-9000.

Regarding sample 1 (engine oil), the dilution test was conducted using the 100-to-1 and 500-to-1 diluted samples. The following expression was used for the dilution test.

$$\text{Dilution test value (\%)} = I/S \times 100$$

(I: 100-to-1 dilution sample quantitation value,

S: 500-to-1 dilution sample quantitation value × 5)

#### ■ Analytical Conditions

Instrument	: ICPE-9000
Radio Frequency Power	: 1.4 kW
Plasma Gas Flowrate	: 16 L/min
Auxiliary Gas Flowrate	: 1.4 L/min
Carrier Gas Flowrate	: 0.70 L/min
Sample Introduction	: Nebulizer 10
Spray Chamber	: Co-axial chamber
Plasma Torch	: Torch
Observation	: Radial

#### ■ Analytical Results

Table 1 shows the quantitative analysis results. The dilution test value using sample 1 (engine oil) was excellent, achieving nearly 100 %.

In addition, highly stable test results over 3 hours were obtained using sample 1 (engine oil), as shown in Fig. 1. Excellent repeatability was obtained for all elements in the measurements, repeated over a period of 3 hours. An RSD (relative standard deviation) of 1 % or less was obtained for each element. The plasma torch utilized in Shimadzu's ICP emission spectrometer provides measurement with extremely low precipitation of carbon, eliminating the necessity to introduce oxygen as a means of suppressing carbon precipitation even when measuring organic solvent samples. The stable results obtained in the analyses presented here also were achieved over a long period of time without introducing oxygen.

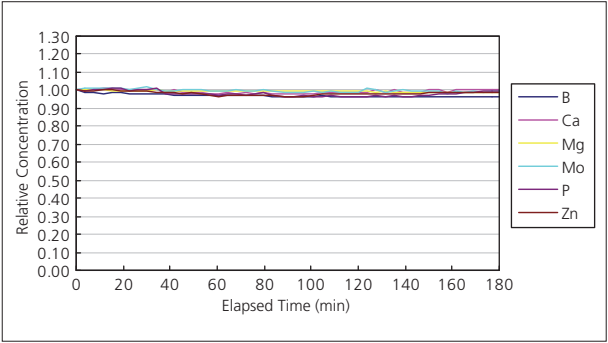
Fig. 2 shows spectral profiles of Ca and Mo.

Fig. 3 shows the calibration curves for Ca, Mo, and Zn.

**Table 1 Quantitative Analysis Results for Lubricating Oils (µg/g)**

	Engine Oil			ATF Oil	Gear Oil	
	Sample 1	Sample 2	Sample 3	Sample 4	Sample 5	Sample 6
B	113 (101)	83	9.1	68	18	2040
Ca	1070 (96)	2920	1720	165	67	73
Mg	737 (99)	19	5.2	1.0	1.7	5.9
Mo	84 (103)	96	60	—	—	—
P	604 (100)	696	682	278	984	3320
Zn	699 (104)	841	770	19	8.6	2640

The values in parentheses for sample 1: Dilution test value (%) =  $I / S \times 100$   
(I: quantitation value prior to sample dilution, S: Quantitation value  $\times$  5 of 5-to-1 diluted sample)



**Fig. 1 Variation with Time Over 3 Hours (Sample1: Engine Oil)**

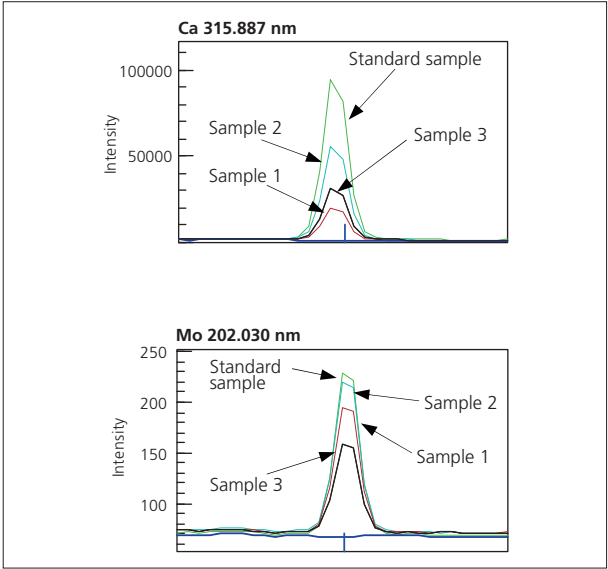


**Fig. 2 Spectral Profiles of Ca and Mo**

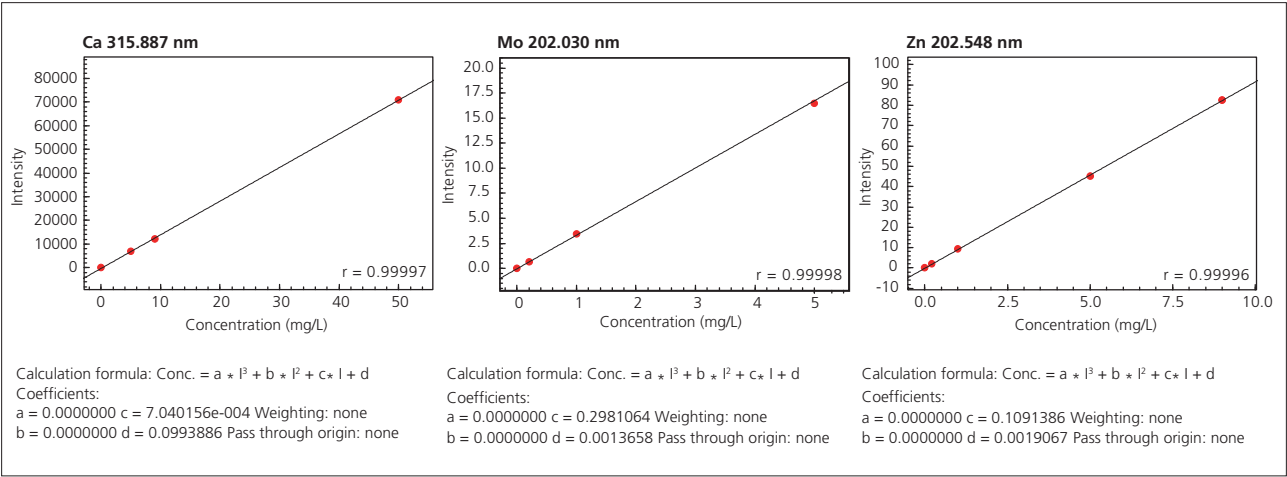


**Fig. 3 Calibration Curves for Ca, Mo and Zn**

# Application News

## No.J111A

### Inductively Coupled Plasma Atomic Emission Spectrometry

## Analysis of Additive Elements in Lubricating Oil According to ASTM D4951: ICPE-9820

### ■ Introduction

Numerous additives consisting of various types of organometallic substances are added to lubricating oils to enhance performance. It is important to manage the concentrations of these additives for the quality control of lubricating oils. Table 1 shows the main types of additives that contain organometallic compounds, and their functions.

Both ASTM D4951 of the ASTM International standards and JPI-5S-38-2003 of the Japan Petroleum Institute standards (Lubricating Oils - Determination of Additive Elements) specify the use of ICP atomic emission spectrometry with organic solvent dilution as the test measurement method for elements in additives.

We performed elemental analysis of the additives in commercially available engine oil, automatic transmission fluid (ATF), and gear oil, using the Shimadzu ICPE-9820 multi-type ICP atomic emission spectrometer, after diluting the samples with an organic solvent. The adoption of a vertically-oriented plasma torch in the ICPE-9820 reduces the possibility of carbon precipitation, while providing stable analytical results without requiring the flow of oxygen through the system.

**Table 1 Function of Main Additive Agent That Contains Organometallic Compounds**

Type	Function	Additive Elements
Cleaner	Prevents and suppresses deposition of degradation byproducts generated due to high temperature operation of machines such as engines.	Ba, Ca, Mg, etc.
Antioxidant	Reacts with radicals and peroxide to suppress formation of varnish and sludge, which form due to oxidation of oil.	Zn, etc.
Anti-corrosion additive	Neutralizes corrosive oxidation products resulting from the breakdown of lubricating oil.	P, Zn, etc.
Solid lubricant	Used as thin film or powder to reduce friction and wear.	Mo, B, etc.

### ■ Samples

- Engine oil (2 types)
- ATF (1 type)
- Gear oil (1 type)

### ■ Sample Preparation

Approximately 1 g of each sample was weighed, diluted with 100 mL of xylene, and then measured. For the dilution test sample, a 5-fold dilution of the engine oil (Sample 1) described above was used.

Additionally, a 5000 µg/g Y-in-oil standard (Conostan®) was diluted with xylene and added to each sample at a concentration of 1 mg/L, for use as an internal standard.

The standard samples were prepared by diluting the SPEX® multi-element oil standard (21 elements; 900 µg/g / 500 µg/g) and the Conostan® single element

oil standards (5000 µg/g) with xylene. As with the measurement samples, each was spiked with Y at a concentration of 1 mg/L, for use as an internal standard.

### ■ Instrument and Analytical Conditions

The Shimadzu ICPE-9820 multi-type ICP atomic emission spectrometer was used to measure the samples. The measurement conditions are shown in Table 2.

When conducting analysis of organic solvent samples with conventional ICP instruments, it is typically required to introduce oxygen into the plasma to suppress the deposition of carbon at the tip of the torch. With the Shimadzu ICPE-9820, however, the vertical orientation of the plasma torch greatly reduces the likelihood that carbon from the sample will precipitate at the tip of the torch. Therefore, even for the analysis of samples in organic solvents such as xylene, kerosene, and MIBK, the ICPE-9820 eliminates the need to introduce oxygen to suppress the precipitation of carbon.

**Table 2 Analytical Conditions**

Instrument	: ICPE-9820
Radio Frequency Power	: 1.40 kW
Plasma Gas Flowrate	: 16.0 L/min
Auxiliary Gas Flowrate	: 1.40 L/min
Carrier Gas Flowrate	: 0.70 L/min
Sample Introduction	: Nebulizer UES10
Misting Chamber	: Chamber drain straight
Plasma Torch	: Torch
Observation	: Radial (RD)

### ■ Analysis

The calibration curve-internal standard method was used to conduct analysis for six types of additive elements used in lubricating oil (B, Ca, Mg, Mo, P, Zn).

### [References]

- 1) ASTM International ASTM D4951  
Standard Test Method for Determination of Additive Elements in Lubricating Oils by Inductively Coupled Plasma Atomic Emission Spectrometry
- 2) Japan Petroleum Institute Standard JPI-5S-38-2003  
Lubricating Oils - Determination of Additive Elements - Inductively Coupled Plasma Atomic Emission Spectrometry

## Analytical Results

Table 3 shows the quantitative analysis results. The dilution test values using engine oil (Sample 1) showed excellent results at nearly 100 % recovery. Fig. 1 shows the spectral profiles of Ca and Mo, and Fig. 2 shows calibration curves for Ca, Mo, and Zn.

## Conclusion

Use of the ICPE-9820 to perform elemental analysis of additives in lubricating oil permits stable analysis without the need to introduce oxygen.

**Table 3 Analytical Results of Lubricating Oil (µg/g)**

Element	Engine Oil			ATF Oil	Gear Oil
	Sample 1	Sample 1 Dilution test (%)	Sample 2	Sample 3	Sample 4
B	113	103	80	68	---
Ca	1100	100	2940	156	64
Mg	754	101	21	1.0	0.7
Mo	87	100	96	---	---
P	637	100	733	262	1010
Zn	736	103	848	20	7.6

Dilution test value (%) =  $I / S \times 100$

(I: quantitation value prior to sample dilution, S: Quantitation value of 5-fold diluted sample × 5)

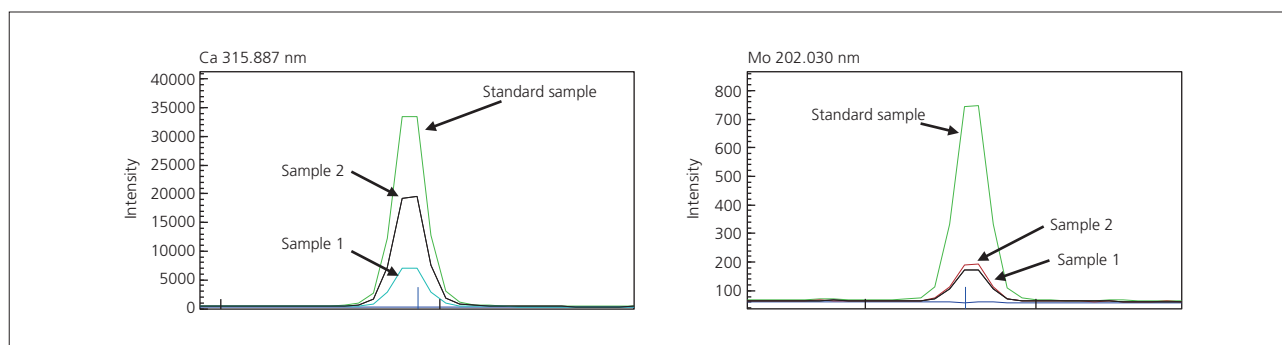


**Fig. 1 Spectral Profiles of Ca and Mo**

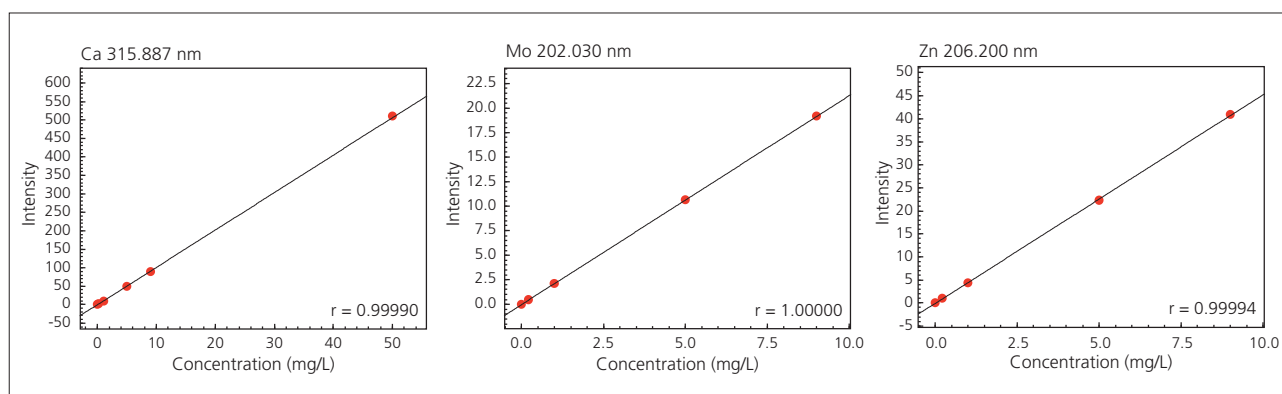


**Fig. 2 Calibration Curves for Ca, Mo and Zn**



# Application News

## No. J114A

### Inductively Coupled Plasma Atomic Emission Spectrometry

## Analysis of Additive Elements, Wear Metals, and Contaminants in Used Lubricating Oil According to ASTM D5185: ICPE-9820

### ■ Introduction

Analysis of lubricants added to engine oils such as those used in automobiles and ships is an effective as well as important way to diagnose the state of the engine and other equipment.

According to ASTM International Standard D5185 <sup>1)</sup>, inductively coupled plasma (ICP) atomic emission spectrometry with organic solvent dilution is specified for measurement of additive elements, wear metals and contaminants present in used lubricants. Also, the Japan Petroleum Institute standard JPI-5S-44-2011 stipulates the use of ICP atomic emission spectrometry in Japan for analysis of Fe, Cu, Al, Pb, Cr and Sn in used lubricating oil. <sup>2)</sup> Here, using the Shimadzu ICPE-9820 multi-type ICP atomic emission spectrometer, we conducted analysis of 22 elements specified according to ASTM D5185 in samples consisting of a used lubricant (commercially available automotive lubricating oil) and, as a reference, the same, but unused lubricating oil, both of which were diluted with organic solvent. The ICPE-9820, which adopts a vertically-oriented plasma torch which reduces the possibility of carbon precipitation, provides stable analytical results for organic solvent samples without requiring the flow of oxygen through the system.

### ■ Samples

- Used lubricating oil (commercially available automotive lubricant, used for approximately 4000 km)
- Same lubricating oil as above, but in unused state

### ■ Sample Preparation

Approximately 10 g of each sample was weighed and then diluted with 100 mL of kerosene. The standard solutions were prepared by appropriately diluting with kerosene the SPEX oil-based 21-element mixed standard solution (500 µg/g), the Conostan® and SPEX oil-based single-element standard solution (5000 µg/g), and the Tokyo Kasei Kogyo Co., Ltd. heavy oil sulfur content standard sample (1.05 % by weight).

For validation of the measurement values, the above standard solution was added to the used lubricating oil to prepare a 5 mg/L solution to serve as a low-concentration element spike-and-recovery test sample. In addition, for high-concentration elements, the used lubricant was diluted 50-fold with kerosene to prepare a diluted test sample.

Finally, the Conostan® oil-based Y (yttrium) single-element standard solution (5000 µg/g) was diluted with kerosene and added to all the samples as the internal standard element so as to occupy a fixed concentration in all the samples.

### ■ Instrument and Analytical Condition

Measurement was conducted using the Shimadzu ICPE-9820 multi-type ICP atomic emission spectrometer. The measurement conditions are shown in Table 1.

When conducting analysis of organic solvent samples with most conventional ICP instruments, oxygen must typically be introduced into the plasma torch to suppress

carbon deposition at the tip of the torch. With the Shimadzu ICPE-9820, however, the vertical orientation of the plasma torch and adoption of a plasma torch that suppresses carbon deposition has nearly completely eliminated the deposition of carbon originating from the sample. Therefore, even in analysis of organic solvent samples such as kerosene, xylene and MIBK, the ICPE-9820 eliminates the need to introduce oxygen to suppress the precipitation of carbon.

Also, since the Shimadzu ICPE-9820 adopts a vacuum spectrometer, elements such as S with a wavelength in the vacuum ultraviolet region can be analyzed at a low running cost without the need for costly high-purity gas, typically required with a purge-type spectrometer.

**Table 1 Analytical Conditions**

Instrument	: ICPE-9820
Radio Frequency Power	: 1.40 kW
Plasma Gas Flowrate	: 16.0 L/min
Auxiliary Gas Flowrate	: 1.40 L/min
Carrier Gas Flowrate	: 0.70 L/min
Sample Introduction	: Nebulizer, 10UES
Misting Chamber	: Organic solvent chamber
Plasma Torch	: Torch
Observation	: Radial (RD)

### ■ Analysis

The calibration curve method – internal standard method was used to conduct analysis of 22 elements (Al, Ba, B, Ca, Cr, Cu, Fe, Pb, Mg, Mn, Mo, Ni, P, K, Si, Ag, Na, S, Sn, Ti, V, Zn) specified according to the ASTM standard.

### ■ Analytical Results

Table 2 shows the analytical results. Excellent results near 100 % were obtained in the dilution test for the high-concentration elements and the spike-and-recovery test for the low-concentration elements, both with respect to the used lubricating oil. In addition, the analytical results obtained in analysis of the unused lubricating oil are also listed for reference.

The spectral line profiles for Fe and P are shown in Fig. 1. The calibration curves for Fe, Mg and S are shown in Fig. 2.

### ■ Conclusion

Using the ICPE-9820, dissolved elements in used lubricating oil can be analyzed stably without the introduction of oxygen.

### ■ References

- 1) ASTM International Standard D5185  
Standard Test Method for Determination of Additive Elements, Wear Metals, and Contaminants in Used Lubricating Oils and Determination of Selected Elements in Base Oils by Inductively Coupled Plasma Atomic Emission Spectrometry (ICP-AES)
- 2) The Japan Petroleum Institute Standard JPI-5S-44-2011  
Method for Analyzing Fe, Cu, Al, Pb, Cr and Sn Contents in Used Lubricating Oil Using Solvent Dilution - Inductively Coupled Plasma Atomic Emission Spectrometry



**Table 2 Analytical Results of Lubricating Oil**

Element	Used lubricant (μg/g)	Used lubricant spike recovery rate (%)	Used lubricant dilution test (%)	Unused lubricant (μg/g)	Detection limit (μg/g)
Ag	<	100	-	<	0.02
Al	10	101	-	6.51	0.3
B	65.9	-	98	121	-
Ba	0.123	101	-	<	0.02
Ca	3970	-	98	2250	-
Cr	1.03	101	-	<	0.01
Cu	0.65	100	-	<	0.02
Fe	10.8	101	-	0.43	0.01
K	22.1	99	-	<	0.6
Mg	10.4	100	-	5.48	0.02
Mn	0.618	101	-	0.139	0.002
Mo	184	-	98	183	-
Na	2.5	100	-	<	0.4
Ni	<	102	-	<	0.05
P	756	-	99	731	-
Pb	<	100	-	<	0.5
S	3980	-	100	3810	-
Si	8.96	103	-	5.07	0.03
Sn	<	100	-	<	0.5
Ti	<	100	-	<	0.01
V	<	103	-	<	0.02
Zn	872	-	97	882	-

Spike recovery rate (%) =  $(C1-C2)/B \times 100$  (C1: Spiked sample quantitative value; C2: Non-spiked sample quantitative value; B: Spike concentration)

Dilution test (%) =  $I/S \times 100$  (I: Quantitative value of sample before dilution; S: Quantitative value of 5-fold diluted sample  $\times 5$ )

Detection limit:  $DL = 3 \times \sigma_{BL} \times \kappa$  ( $\sigma_{BL}$ : Standard deviation of background intensity;  $\kappa$ : Concentration/intensity)

<: Less than the detection limit

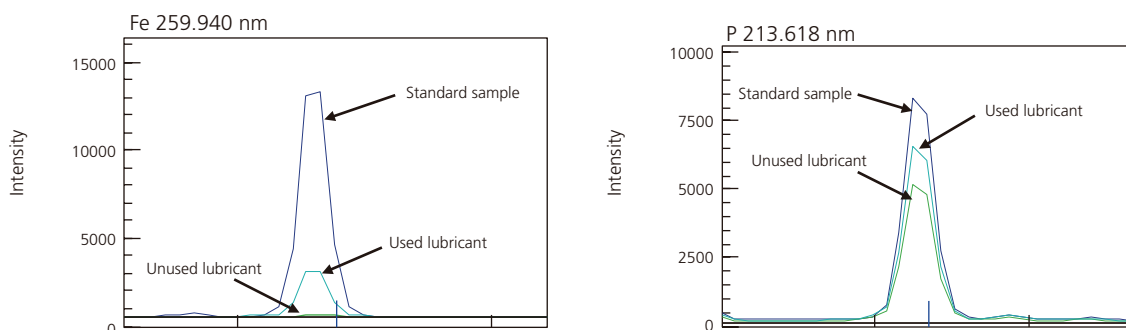


**Fig. 1 Spectral Profiles of Fe and P**

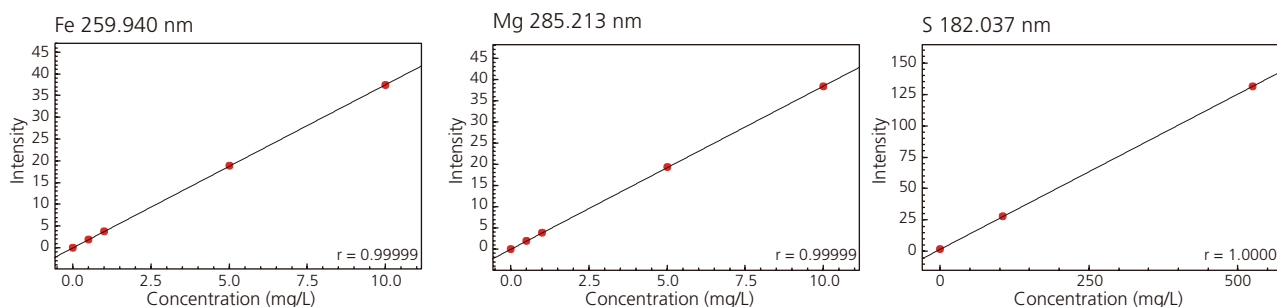


**Fig. 2 Calibration Curves of Fe, Mg and S**

Second Edition: Jul. 2015  
First Edition: Apr. 2015



Shimadzu Corporation

[www.shimadzu.com/an/](http://www.shimadzu.com/an/)

For Research Use Only. Not for use in diagnostic procedures.

The content of this publication shall not be reproduced, altered or sold for any commercial purpose without the written approval of Shimadzu. The information contained herein is provided to you "as is" without warranty of any kind including without limitation warranties as to its accuracy or completeness. Shimadzu does not assume any responsibility or liability for any damage, whether direct or indirect, relating to the use of this publication. This publication is based upon the information available to Shimadzu on or before the date of publication, and subject to change without notice.

© Shimadzu Corporation, 2015



## 3. Spectroscopy

---

### 3.2 Molecular Spectroscopy

---

#### 3.2.1 Ultraviolet Visible Spectroscopy and Near Infrared Analysis (UV-Vis, NIR)

UV-Vis spectrophotometers are applied to analysis of metals, ions, colors and molecules. The instruments were developed originally for measurement of the absorption of liquid samples. In recent years, however, high-precision, high-energy spectrophotometers have hit the market due to the rapid increase in reflection and absorption measurements of solid samples including semiconductors, films, glass and absorbing materials. Shimadzu develops hardware and software to meet all market requirements.

**A442** Transmittance measurement of IR-cut glass using a UV-2600 UV-VIS spectrophotometer with ISR-2600Plus Integrating Sphere

#### 3.2.2 Fourier Transform Infrared Spectroscopy (FTIR)

FTIR spectroscopy focusses on the quantification and identification of substances. FTIR can analyze all materials which react with heat. The physical vibration correlated to this heat is an identification tool for each material.

**A499** Confirmation of raw material quality – dealing with “silent change” counterfeiting  
**A513** Measuring micro-contaminants on optical parts: measurement and identification by AIM-9000 infrared microscope  
**A488** Analysis of inorganic additives in resin by FTIR and EDX  
**A467** Investigation of additives in plastics by FTIR-ATR spectroscopy

#### 3.2.3 Fluorescence Spectroscopy

Spectrophotometers are instruments that measure the optical absorbance (absorption spectrophotometers) and the emission intensity of chemical substances. To determine the wavelength dependency, light from the light source is normally separated into wavelengths by a diffraction grating.

**AD-0133** Excitation-emission matrix (EEM) fluorescence spectroscopy for analysis of dissolved organic matter (DOM) in natural water and wastewaters  
**A494** Simplified measurement of coumarin in diesel oil  
**A529** Fluorescence measurement of glass and plastic

# Application News

## No. A442

### Spectrophotometric Analysis

## Transmittance Measurement of IR-Cut Glass Using a UV-2600 UV-VIS Spectrophotometer with ISR-2600Plus Integrating Sphere

With the evolution of mankind and the accompanying development of technology, energy consumption has steadily increased. However, because energy sources such as oil and natural gas are limited, a variety of innovations have been introduced with the aim of reducing energy consumption. One of these is IR-cut glass, which effectively limits the rise of indoor temperature by filtering out near-infrared rays. On the

other hand, while cutting near-infrared radiation is an effective means of conserving energy, it is also important to ensure that visible light is effectively transmitted to the interior to permit outside light to help illuminate the interior of a room. Here we introduce use of the auto point pick feature newly added to the standard software to verify the effectiveness of IR-cut processing in window glass.

### Analytical Conditions and Results

Shimadzu's UV-2600 ultraviolet-visible spectrophotometer together with the ISR-2600Plus integrating sphere allows measurement over the entire wavelength range from 220-1400 nm. Here we conducted measurement of 3 types of glass, one type of transparent glass and two types (A, B) of IR-cut glass. Fig. 1 shows an external view of the UV-2600 with the ISR-2600Plus mounted inside. Transmittance measurement was conducted with the sample mounted in the position indicated by the arrow in Fig. 1. The measurement conditions are shown in Table 1, and the transmittance spectra of the glass samples are shown in Fig. 2. In addition, the transmittance was checked by selecting wavelengths in the ultraviolet region (300 nm), the visible region (550 nm), and near-infrared region (1350 nm), respectively. Table 2 shows the transmittance at each of the wavelengths.

From Fig. 2, it is clear that in contrast to the high transmittance exhibited by the transparent glass in the visible to near-infrared region, the IR-cut glass A and B samples exhibited transmittance that was reduced to less than 50 % in the near-infrared region. Moreover, compared to the IR-cut glass A, the IR-cut glass B exhibited lower transmittance in the near-infrared region but higher transmittance in the visible region, indicating that while acting to suppress the rise in temperature inside the room, IR-cut glass B simultaneously permitted external light to enter the room.

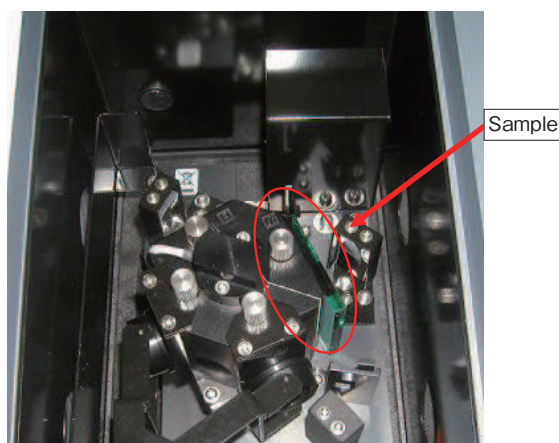


Fig. 1 UV-2600 with the ISR-2600Plus Mounted

Table 1 Analytical Conditions

Instrument	: Shimadzu UV-2600 ultraviolet-visible spectrophotometer ISR-2600Plus integrating sphere
Measurement Wavelength Range	: 220-1400 nm
Scan Speed	: Medium
Sampling Pitch	: 1.0 nm
Photometric Value	: Transmittance
Slit	: 5 nm
Detector Switching Wavelength	: 830 nm
Lamp Switching Wavelength	: 323 nm

Table 2 Analytical Results

	300 nm	550 nm	1350 nm
Transparent glass	0.02 %	89.22 %	76.68 %
IR-cut glass A	0.01 %	46.97 %	41.90 %
IR-cut glass B	0.02 %	77.64 %	27.74 %

### ■ Auto Point Pick Feature

When the auto point pick feature is used, the photometric value at the specified wavelength is automatically displayed simultaneously with the completion of measurement. This feature is convenient for verification of the photometric value when the same wavelength is to be used for each measurement, eliminating the need to repeatedly set and verify the value.

The auto point pick setting is easily conducted while setting the other analytical conditions. Just select the [Data Process] checkbox, and select [Point Pick], as shown in Fig. 3. By registering the point in a template file beforehand using the [Template] setting, and then loading that file prior to measurement, the photometric value at the specified wavelength is automatically displayed simultaneously with the completion of measurement.

An example of the settings for automatic implementation of point picking is shown in Fig. 4.

### ■ Other Convenient Auto Data Processing Functions

In addition to the point pick feature introduced here, there are various other convenient functions provided in the data processing part of the UVProbe software. Some of these include peak detection in which peaks are detected automatically, smoothing and data arithmetic operations included in data operations (smoothing, integration, arithmetic operations, etc.), in addition to area calculation for a specified range in area calculation, etc. Utilizing these features permits the data processing results to be obtained simultaneously with the completion of measurement.

### ■ Conclusion

Measurement results over a wide spectral range from the ultraviolet to near-infrared region can be obtained using the Shimadzu UV-2600 ultraviolet-visible spectrophotometer together with the ISR-2600Plus integrating sphere. In addition, utilizing the wide variety of data processing functions that are included in the UVProbe software makes it extremely convenient to check the processed data as soon as the measurement is completed.

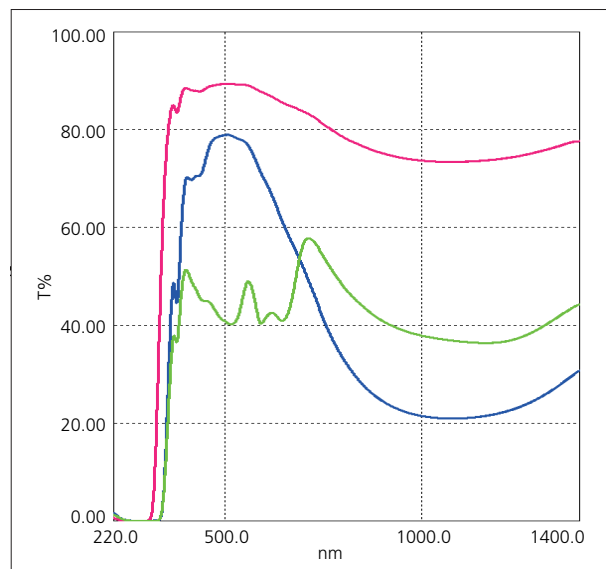


Fig. 2 Transmittance Spectra  
(Red: Transparent glass, Green: IR-cut glass A, Blue: IR-cut glass B)

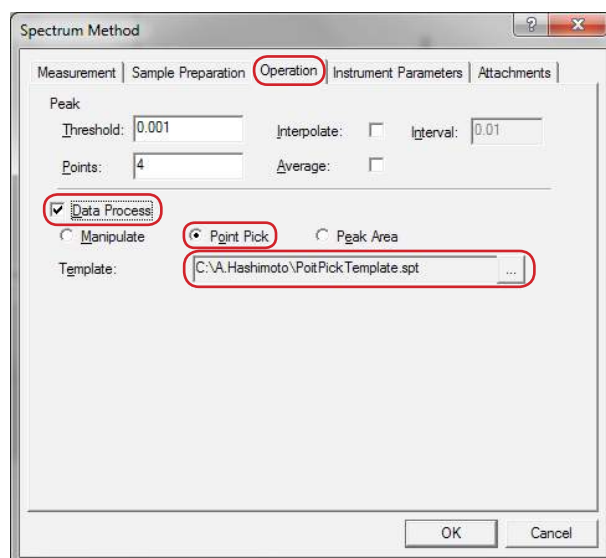


Fig. 3 Method Window for Auto Point Pick Settings

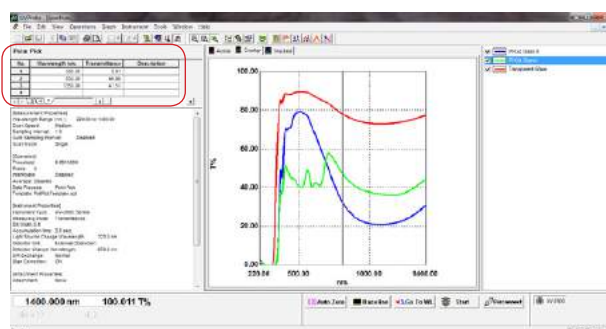


Fig. 4 Auto Point Pick Window

# Application News

## No.A499

### Spectrophotometric Analysis

## Confirmation of Raw Material Quality -Dealing with "Silent Change" Counterfeiting-

### ■ Introduction

Safe and good quality raw materials are essential to the consistent production of high-quality products. However, materials may be changed by suppliers without the knowledge of the manufacturer, either in order to reduce costs or because they are unable to accommodate changes in materials that have been dictated by regulations. This kind of change is known as a "silent change" in Japan. Use of a non-standard raw material in a product means not only quality can no longer be assured, but has been known to cause accidents and is becoming a problem for society. Manufacturers can avoid these situations by checking at receipt whether the raw materials delivered are according to standard.

In this article, we use samples that may have been subject to a "silent change" (hereafter called "silent change" product) and introduce case analyses that confirm such changes using energy dispersive X-ray fluorescence spectrometry (EDX) (Fig. 1) and FTIR infrared spectrophotometry (Fig. 2).

### ■ Case of Replacement with a Cheaper Metal Material

Stainless steels are a special type of steel that are resistant to rust, that are created by adding various materials including chrome and nickel to iron. The stainless steel known as SUS316 has the composition 18Cr-12Ni-2.5Mo. It is created by adding molybdenum to SUS304 stainless steel, thereby improving its resistance to corrosion by sea water and other materials. We used EDX to analyze the stainless steel in a "silent change" product and in a genuine product. Analytical conditions are shown in Table 1, and EDX profiles are shown in Fig. 3.

Fig. 3 shows that the molybdenum peak present in the genuine SUS316 is missing from the "silent change" product, which exhibits a profile identical to SUS304. This result shows the steel material in the "silent change" product has been replaced with a cheaper type.

Though it is impossible to tell by visual examination whether steel material has been changed, taking measurements by EDX provides confirmation of a "silent change."



Fig. 1 EDX-7000 Energy Dispersive X-Ray Fluorescence Spectrometer

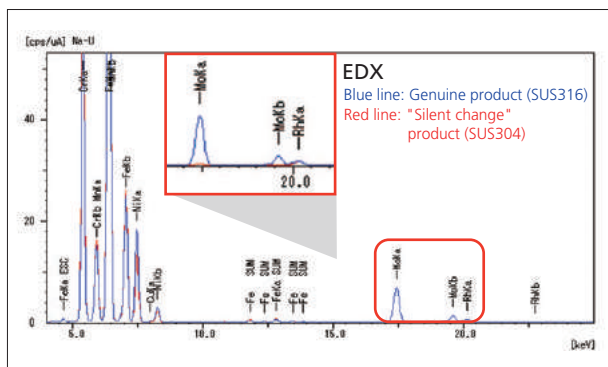


Fig. 2 IRAffinity-1S with MIRacle 10 Single-Reflection ATR Accessory

Table 1 EDX Analytical Conditions

Instrument	: EDX-7000
X-Ray Tube	: Rh target
Voltage/Current	: 50 kV (Na-U) /Auto
Atmosphere	: Air
Measurement Diameter	: 10 mmφ
Integration Time	: 30 sec.





**Fig. 3 Results of EDX Analysis of SUS316 Genuine Product and "Silent Change" Product (SUS304)**

### ■ Case of Replacement of a Plastic Material

We used FTIR to analyze a genuine polypropylene (PP) product and a "silent change" product. Analytical conditions are shown in Table 2, and the spectra obtained are shown in Fig. 4. Fig. 4 shows a peak was detected in the "silent change" product originating from  $\text{CH}_2$  rocking vibrations in the region of  $718\text{ cm}^{-1}$  (marked with a star). Spectral search confirmed that the "silent change" product contains polyethylene (PE) mixed in with PP.

This result indicates that recycled plastic may have been mixed into the raw material.

**Table 2 FTIR Analytical Conditions**

Instrument	: IRAffinity-1S MIRacle 10 (Diamond/ZnSe)
Resolution	: $4.0\text{ cm}^{-1}$
Accumulation	: 20
Apodization	: Happ-Genzel
Detector	: DLATGS

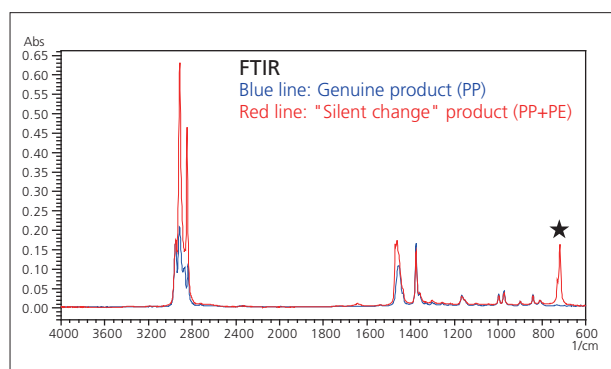


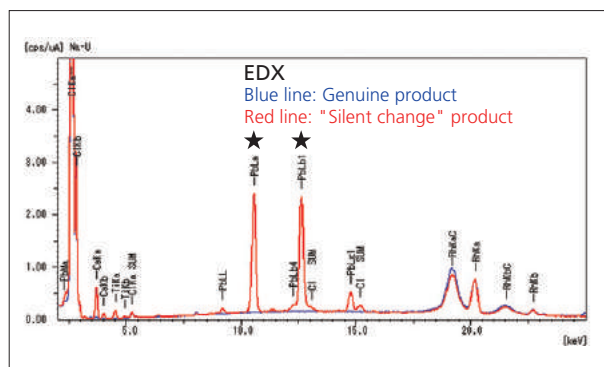
**Fig. 4 Results of FTIR Analysis of Genuine PP Product and "Silent Change" Product (PP+PE)**

### ■ Case of Toxic Element and Different Material Mixed into a Plastic Material

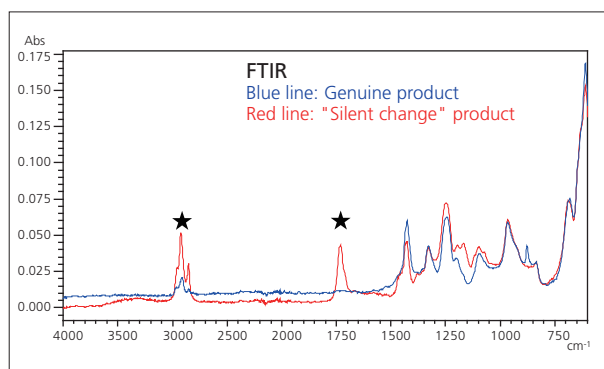
We used EDX and FTIR to analyze a genuine polyvinyl chloride (PVC) product, and a "silent change" plastic product. The EDX analytical conditions are shown in Table 1 with corresponding profiles shown in Fig. 5, while FTIR analytical conditions are shown in Table 2 with corresponding spectra shown in Fig. 6.

Fig. 5 shows that lead (marked with a star) was detected in the "silent change" product that was not detected in the genuine product. The plastic material analyzed in this experiment is subject to regulation under the Restriction on Hazardous Substances Directive (RoHS) and must not contain any lead. The results show that the "silent change" product does not meet the RoHS regulations.

Fig. 6 also shows that apart from peaks originating from PVC, peaks originating from acrylic were detected in the region of  $2900\text{ cm}^{-1}$  and  $1700\text{ cm}^{-1}$  (marked with a star). This result shows the presence of a different material mixed in with the material in the "silent change" product.



**Fig. 5 Results of EDX Analysis of Genuine Plastic Product and "Silent Change" Plastic Product**



**Fig. 6 Results of FTIR Analysis of Genuine Plastic Product and "Silent Change" Plastic Product**

### ■ Conclusion

Using EDX and FTIR to check inorganic materials and organic materials allows for a more robust response to the problem of "silent change" counterfeiting.

# Application News

## No.A513

### Spectrophotometric Analysis

## Measuring Micro-Contaminants on Optical Parts: Measurement and Identification by AIM-9000 Infrared Microscope

Due to the miniaturization and increasingly sophisticated functionality of electrical and electronic devices, an increasing number of optical devices are being used today, such as ultra-small and high-performance semiconductor devices and sensors. However, in such miniaturized devices, micron-sized tiny contaminants can cause the devices to malfunction. Therefore, manufacturers need to determine what caused such contaminants to enter the devices, so their recurrence can be prevented.

Shimadzu AIM-9000 infrared microscope features optics that are designed especially for measuring microscopic areas, and allows users to obtain good spectra in short time even for micron-sized tiny contaminants. The following describes an example of using this system to measure micro-contaminants about 10  $\mu\text{m}$  in diameter on the surface of an optical part.

### ■ Micro-Contaminants on an Optical Part

Fig. 1 shows a microscope photograph of the contaminants on the surface of an optical part installed in an electronic device. The contaminants, which are between about 3 and 10  $\mu\text{m}$  in diameter, are lying scattered on a part surface.



**Fig. 1 Microscope Image of Micro-Contaminants (shown with a 10  $\mu\text{m}$  blue box)**

### ■ Measurement

These contaminants were discovered on a shiny, flat, and smooth metal part surface. Therefore, a measurement using specular reflection spectroscopy is appropriate due to no necessity of sampling the part and the low risk of part damage or loss. An infrared spectrum measured from the contaminant using an infrared microscope by specular reflection spectroscopy and corresponding search results are shown in Fig. 2. Measurement conditions are indicated in Table 1. Even for tiny contaminants only about 10  $\mu\text{m}$  across, a spectrum with minimal noise can be obtained using a short measurement time of only about 20 seconds. Results from analyzing the data using the spectrum library included standard with the system determined that the contaminant is probably a lactate.

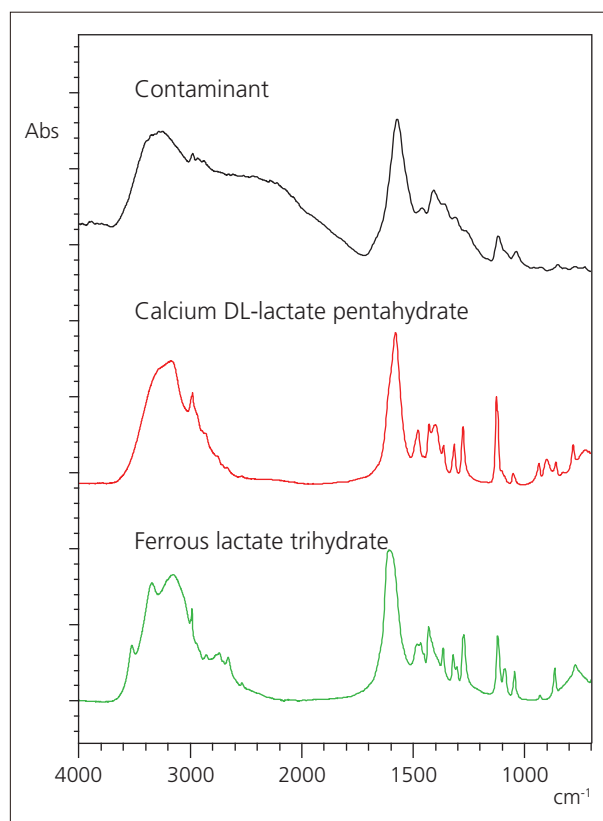


**Fig. 2 Infrared Spectrum and Search Results for the Contaminant**

**Table 1 Measurement Conditions**

Instrument	: IRTracer-100, AIM-9000
Resolution	: 8 $\text{cm}^{-1}$
Accumulation	: 40
Apodization	: Happ-Genzel
Detector	: MCT



■ AIM-9000 Infrared Microscope

Due to the optics that are designed specifically for measuring extremely small areas, the AIM-9000 infrared microscope achieves the highest signal-to-noise ratios (30,000:1) in its class. That means it can obtain excellent spectra very quickly, even from extremely small contaminants. As an example, results from measuring 10  $\mu\text{m}$  polystyrene beads scattered on a BaF<sub>2</sub> window plate are shown. A microscope photograph of the polystyrene beads is shown in Fig. 3. A comparison of measurements obtained by transmission spectroscopy using both the AIM-9000 and the Shimadzu's previous model is shown in Fig. 4. Measurement conditions are listed in Table 2 and a photograph of the AIM-9000 system connected to an IRTracer-100 infrared spectrophotometer is shown in Fig. 5.

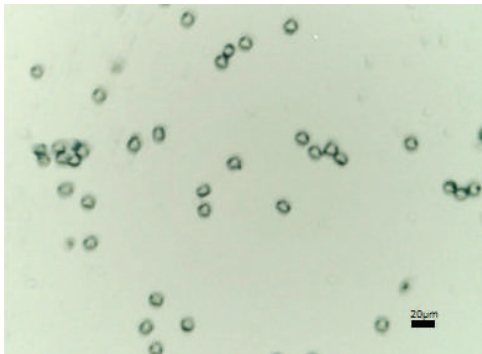


Fig. 3 Microscope Image of Polystyrene Beads of 10  $\mu\text{m}$  in Diameter

Table 2 Measurement Conditions

Instrument	: IRTracer-100, AIM-9000, and previous model (AIM-8800)
Resolution	: 8 $\text{cm}^{-1}$
Accumulation	: 40
Apodization	: Happ-Genzel
Detector	: MCT

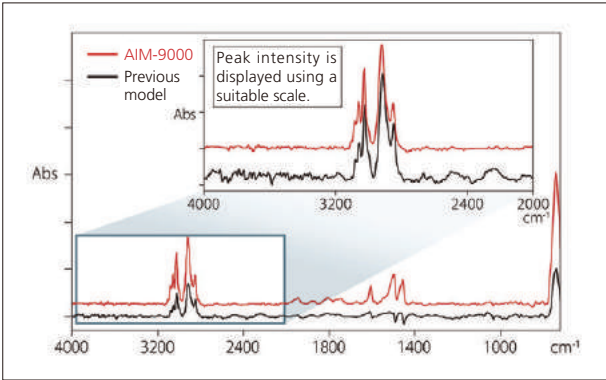


Fig. 4 Infrared Spectra of Polystyrene Beads of 10  $\mu\text{m}$  in Diameter (with Baseline Correction)

These results show that the AIM-9000 detects the polystyrene absorption peaks more clearly and with higher intensity. The inset enlargement shows the results from displaying the spectra with peak intensity matched near 2,920  $\text{cm}^{-1}$ . It demonstrates how the AIM-9000 can provide superior spectra with less noise than the previous model.

■ Conclusion

This article describes measuring micro-contaminants about 10  $\mu\text{m}$  in diameter on the surface of an optical part. The AIM-9000 infrared microscope is ideal for identifying contaminants and analyzing defects in extremely small areas.



Fig. 5 AIM-9000 Infrared Microscope Connected to IRTracer-100 Fourier Transform Infrared Spectrophotometer

First Edition: Nov. 2016



Shimadzu Corporation  
[www.shimadzu.com/an/](http://www.shimadzu.com/an/)

**For Research Use Only. Not for use in diagnostic procedure.**  
This publication may contain references to products that are not available in your country. Please contact us to check the availability of these products in your country.

The content of this publication shall not be reproduced, altered or sold for any commercial purpose without the written approval of Shimadzu. Company names, product/service names and logos used in this publication are trademarks and trade names of Shimadzu Corporation or its affiliates, whether or not they are used with trademark symbol "TM" or "®". Third-party trademarks and trade names may be used in this publication to refer to the entities or their products/services. Shimadzu disclaims any proprietary interest in trademarks and trade names other than its own.

The information contained herein is provided to you "as is" without warranty of any kind including without limitation warranties as to its accuracy or completeness. Shimadzu does not assume any responsibility or liability for any damage, whether direct or indirect, relating to the use of this publication. This publication is based upon the information available to Shimadzu on or before the date of publication, and subject to change without notice.

# Application News

## No. A488

### Spectrophotometric Analysis

## Analysis of Inorganic Additives in Resin by FTIR and EDX

Additives enhance the quality of products by improving the functionality, workability, and stability of the materials used in the product. They are utilized in a wide range of products, including electronics, foods, pharmaceuticals, cosmetics, plastics, etc., and play an important role by adding value to products.

The approach taken in the analysis of additives is dependent on whether the additive is organic or inorganic. Organic additives are typically identified by first extracting the additives using a suitable pretreatment procedure, and after chromatographic separation of the extracted components, a suitable analytical instrument is used for qualitative analysis. On the other hand, comprehensive identification of inorganic additive components is typically based on the results obtained using elemental analysis, infrared spectroscopy or morphologic observation, etc<sup>1)</sup>.

Here, we introduce examples of FTIR analysis to obtain useful information regarding some typical inorganic additives, in addition to an example of analysis of a resin containing an inorganic additive using FTIR and EDX.

### ■ Analysis of Inorganic Additives by FTIR

FTIR is used mainly for organic analysis, but useful information can also be obtained by applying FTIR to the analysis of some inorganic additives.

Here, we conducted single-reflection ATR measurement using a diamond prism. Table 1 shows the analytical conditions using FTIR, and the infrared spectra and peak positions of the four substances used as additives (aluminum silicate, aluminum hydroxide, magnesium silicate, and calcium carbonate) are shown in Fig. 1 to 4. A spectral characteristic of inorganic additives is the appearance of a relatively wide peak in the lower wavenumber region. In addition, as is clearly evident in Fig. 1 to 3, a characteristic peak is sometimes present in the higher wavenumber region. In such cases, qualitative identification is possible by FTIR alone.

**Table 1 Analytical Conditions**

Instruments	: IR Tracer-100, Quest, Diamond
Resolution	: 4.0 cm <sup>-1</sup>
Accumulation	: 40
Apodization	: Happ-Genzel
Detector	: DLATGS

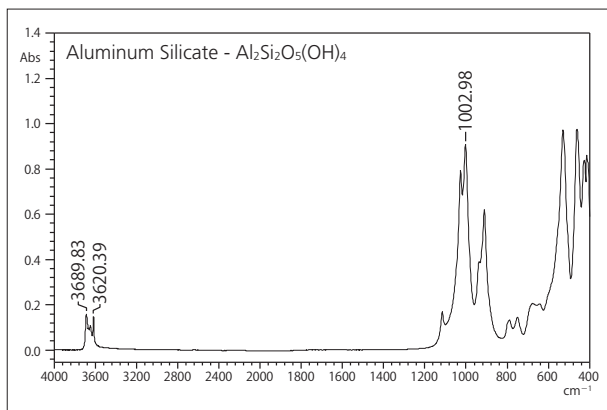


**Fig. 1 IR Spectrum and Peak Position of  $\text{Al}_2\text{Si}_2\text{O}_5(\text{OH})_4$**

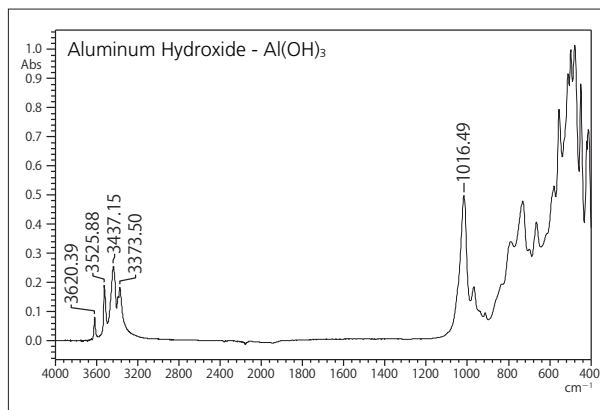


**Fig. 2 IR Spectrum and Peak Position of  $\text{Al}(\text{OH})_3$**

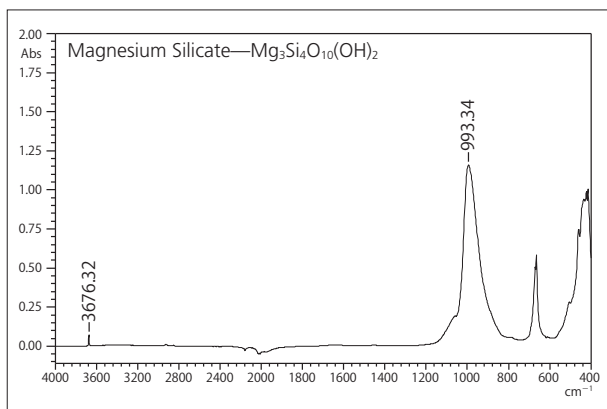


**Fig. 3 IR Spectrum and Peak Position of  $\text{Mg}_3\text{Si}_4\text{O}_{10}(\text{OH})_2$**

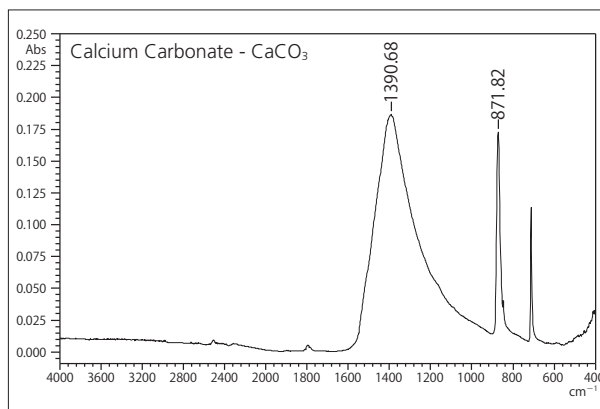


**Fig. 4 IR Spectrum and Peak Position of  $\text{CaCO}_3$**

## ■ Analysis of Inorganic Additives in Resin

FTIR was used for the analysis of a connector cover as a sample that contains an inorganic additive. Fig. 5 shows a photograph of the sample, and Fig. 6 shows the results of analysis.



Fig. 5 Connector Cover

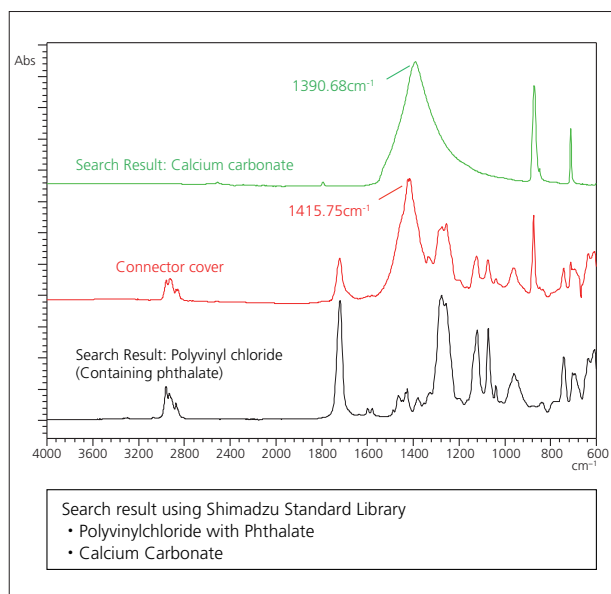


Fig. 6 IR Spectra and FTIR Search Results

From the infrared spectra and search results of Fig. 6, the principal component of the connector cover was determined to be polyvinylchloride (PVC). Also, the peak in the vicinity of  $1415\text{ cm}^{-1}$  in the infrared spectrum suggests the presence of calcium carbonate ( $\text{CaCO}_3$ ).

However, a comparison of the connector cover peak at  $1415\text{ cm}^{-1}$  with the peak at  $1390\text{ cm}^{-1}$  of calcium carbonate alone indicates a peak position shift of  $25\text{ cm}^{-1}$ . Therefore, there is clearly insufficient basis to irrefutably conclude that calcium carbonate is included as an additive from the infrared spectrum alone.

Thus, we followed up this result by conducting EDX analysis to reconcile this discrepancy. The analytical conditions used are shown in Table 2, and the qualitative analytical results are shown in Fig. 7. Table 3-1 and Table 3-2 show the quantitative analytical results by the FP method<sup>2)</sup>.

Table 2 EDX Analytical Conditions

Instrument	: EDX-7000
X-ray Tube	: Rh target
Voltage / Current	: 15 kV(Na-Sc), 50 kV(Ti-U) / Auto
Atmosphere	: Vacuum
Measurement Diameter	: 10 mmφ
Integration Time	: 100 sec

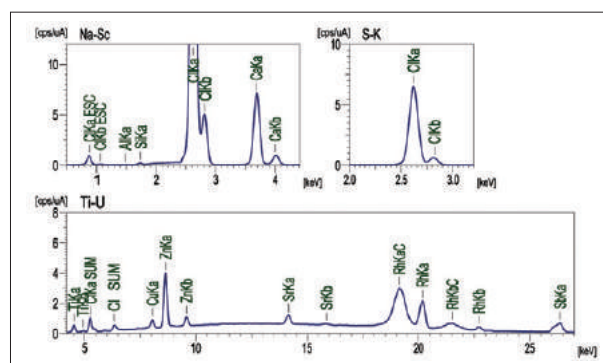


Fig. 7 Results of Qualitative Analysis of Connector Cover by EDX

Table 3-1 Results A of Quantitative Analysis of Connector Cover by EDX

Element	Cl	Ca	Sb	Zn	Ti	Si	Al	Cu	Sr
Quantitation Value	72.56	26.11	0.40	0.31	0.23	0.21	0.096	0.054	0.030

Table 3-2 Results B of Quantitative Analysis of Connector Cover by EDX

Element	$\text{C}_2\text{H}_3\text{Cl}$	$\text{CaCO}_3$	$\text{SiO}_2$	$\text{Sb}_2\text{O}_3$	$\text{TiO}_2$	$\text{ZnO}$	$\text{Al}_2\text{O}_3$	$\text{CuO}$	$\text{SrO}$
Quantitation Value	73.14	25.55	0.31	0.30	0.25	0.25	0.13	0.046	0.024

As clearly indicated in Table 3-1, chlorine (Cl) and calcium (Ca) are the principal constituent elements. This is consistent with the polyvinyl chloride results obtained by FTIR, supporting the presence of calcium carbonate. Table 3-2 shows the quantitative analytical results for specific compounds identified from the results of both FTIR and EDX. It should be noted that other detected elements are assumed to be oxides<sup>3)</sup>. Thus, the combination of FTIR and EDX has provided sufficient evidence that calcium carbonate is present as an additive.

## ■ Conclusion

By applying a combination of FTIR and EDX, we were able to more accurately identify the additives included in an actual sample. Such an analysis is applicable to contaminant analysis and confirmation testing, and should be considered an effective means for conducting such confirmation testing in a wide range of fields, including electrical and electronic, chemical, pharmaceutical, and foods, etc.

- 1) Toshikatsu Nishioka, Tatsuya Housaki: (2011) "A Guide on Plastic Analysis," Maruzen Publishing Co., Ltd.
- 2) Hiroto Ochi, Hideo Okashita: Shimadzu Review, 45 (1-2), 51 (1988)
- 3) Sachio Murakami, et.al: Shimadzu Review, 69 (1-2), 133 (2012)

# Application News

## No. A467

### Spectrophotometric Analysis

## Investigation of Additives in Plastics by FTIR-ATR Spectroscopy

Commercially available plastic products contain polymers, such as polyethylene (PE) and polypropylene (PP), as their main components, in addition to various trace components that are added to enhance performance and maintain quality. Here we introduce an evaluation of additives used in plastic bags taking advantage of the high S/N ratio of the Shimadzu FTIR IRTracer-100 spectrophotometer.

### ■ Shimadzu IRTracer-100 FTIR Spectrophotometer and ATR Attachment MIRacle A

Single reflection ATR is commonly used as an infrared spectroscopy method for easy, non-destructive evaluation of additives in plastic products. Because measurement can be conducted without the need for pretreatment of the sample, the single reflection ATR method is widely used in various applications, including contaminant identification. As the depth of penetration of the infrared light into the sample surface using the ATR method is on the order of a few microns, this method can be used effectively, especially for additives that are localized on the sample surface.

As the content ratio of the target component becomes smaller, its peak intensity in the measured infrared spectrum will decrease accordingly, so an instrument with a high S/N ratio is required to obtain good evaluation results. The high 60000:1 S/N ratio of the Shimadzu FTIR IRTracer-100 ensures that clear and stable peak information is obtained from additives present even at trace levels. Fig. 1 shows an image of the Shimadzu FTIR IRTracer-100, and Fig. 2 shows an image of the MIRacle A Single Reflection ATR Accessory.



Fig. 1 Shimadzu IRTracer-100 FTIR Spectrophotometer



Fig. 2 MIRacle A Single Reflection ATR Accessory

### ■ Measurement

Using the single reflection ATR method, we measured the surface of commercially available plastic bags. A photograph of the plastic bags is shown in Fig. 3. The measurement conditions used are shown in Table 1, and the measurement results and spectrum search results are shown in Fig. 4.



Fig. 3 Plastic Bags

Table 1 FTIR Measurement Conditions

Instruments	: IRTracer-100, MIRacle A (Diamond prizm – ZnSe support element)
Resolution	: 4 cm <sup>-1</sup>
Accumulation	: 20
Apodization	: Happ-Genzel
Detector	: DLATGS

The results obtained from analysis of the plastic bag are consistent with the library spectrum of polyethylene, indicating that the principal component is polyethylene. Fig. 5 shows an expanded view in the vicinity of the baseline of Fig. 4. It is believed that the arrow-indicated peaks in the figure are derived from additives present in the plastic bags, and these are consistent with the spectra of aliphatic amides such as oleamide. Aliphatic amides are one type of substance added to resins to serve as a lubricant.

Also, after completing the measurement shown in Fig. 4, the plastic bag sample was removed from the ATR prism, and without washing the prism, another measurement was taken. The results are shown in Fig. 6. Here, the results resemble the spectrum of the aliphatic amide shown in Fig. 5, indicating the possible transfer of the additive in the plastic bag to the ATR prism.

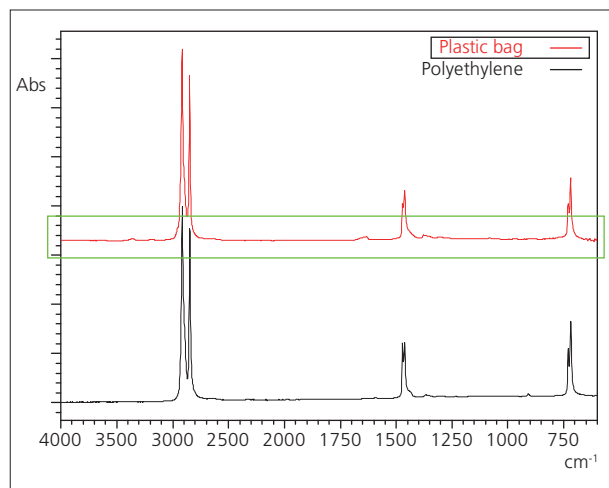


Fig. 4 Infrared Spectrum and Search Result for Plastic Bag

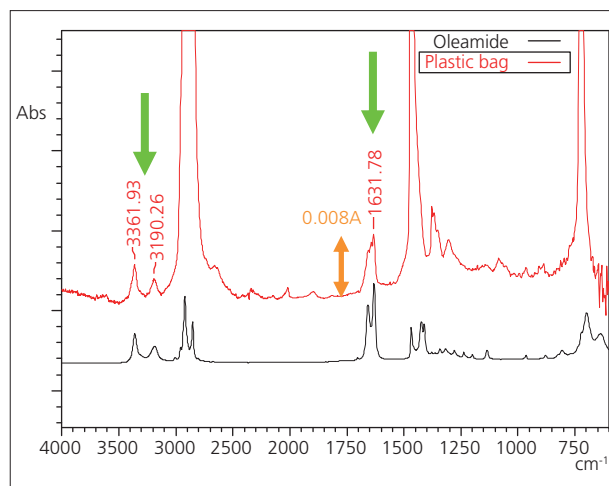


Fig. 5 Expanded Infrared Spectrum of Figure 4 and Spectrum of Oleamide

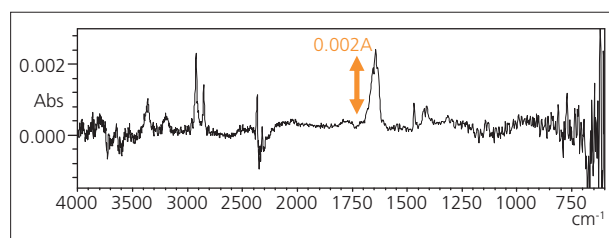


Fig. 6 Infrared Spectrum of Substance Transferred to ATR Prism

The peaks associated with the aliphatic amide that appeared in the measurement results of Figs. 5 and 6, respectively, show very weak intensity with absorbance values less than 0.010 A. Also, there is a peak in the vicinity of 1631 cm<sup>-1</sup>, a region that easily reflects the presence of water vapor in the air. Deeming that purging the measurement system with dry air or nitrogen gas was unnecessary led to the clear detection of these minute peaks.

### ■ Investigation of Repeatability of Small Peaks

It is generally possible to gain an understanding of content level using the height and area value of the peak originating from the target component, but for small peaks derived from additives, it is important to grasp the measurement repeatability. Ten continuous repeat measurements were taken with a plastic bag sample in close contact with the ATR prism. The peak area values of the peak in the vicinity of 1631 cm<sup>-1</sup> and the calculated CV values are shown in Table 2. The integration was repeated twenty times and one time, and these values were compared, respectively, with those obtained with the Shimadzu IRPrestige-21. The better stability of measurement values obtained with the IRTracer-100 is attributed to its higher S/N ratio.

Table 2 Peak Area and CV Values

	IRPrestige-21		IRTracer-100	
	No. of Integrations 20 times	No. of Integrations 1 times	No. of Integrations 20 times	No. of Integrations 1 times
Area value	1.034	0.956	1.039	1.034
	1.049	1.006	1.025	1.021
	1.034	1.138	1.015	0.957
	1.008	1.052	1.006	0.952
	1.029	0.888	0.991	1.055
	0.967	0.974	0.996	1.055
	0.983	0.965	1.001	0.940
	0.967	0.970	0.972	0.995
	0.972	1.038	0.972	0.995
	0.957	1.011	0.982	0.995
CV value %	3.46	6.72	2.19	4.16

\*The displayed area values represent normalized values based on the average of 10 repeat measurements.

### ■ Conclusion

Here we introduced an evaluation of trace additives in plastic resin. The high S/N ratio of the Shimadzu FTIR IRTracer-100 enabled stable and clear acquisition of minute peaks originating from additives present at minute levels.



# Application News

No. AD-0133

*Water Quality / RF-6000 with EEM Spectroscopy*

## Excitation-Emission Matrix (EEM) Fluorescence Spectroscopy for Analysis of Dissolved Organic Matter (DOM) in Natural Water and Wastewaters

### □ Introduction

Dissolved organic matter (DOM) are soluble organic materials in water from various sources such as soils, decomposed plant materials, living organisms and discharges from human activities. DOM is an important natural water quality indicator as it reflects the microbial activities, human activities and geological conditions around the area where the water sample has been collected. Excitation-emission matrix (EEM) fluorescence spectroscopy has been used to characterize the DOM and identify fluorescence emitting organic substances in natural water [1-2]. Here, we describe analysis examples of DOM in natural water and wastewater samples using the 3-dimensional (3D) EEM measurement on the RF-6000 Spectrofluorophotometer.

### □ Experimental

A few organic compounds standards are used for EEM measurement. The compounds, including tryptophan, tyrosine and humic acid, were purchased from Sigma Aldrich, USA. Type E-1 ultra pure water with resistivity of 18 MΩ was used.

The tryptophan and tyrosine were dissolved with ultra pure water to a concentration of 1 mg/L. The humic acid was dissolved with ultra pure water to a concentration of 20 mg/L and adjusted to a pH of 8 to 9 using sodium hydroxide solution. The samples used in this study were surface water from a local pond and wastewater samples from two different industrial sources. The samples were filtered through a 0.2 μm nylon filter prior to measurement.

EEM spectra of the samples were measured using the 3D spectrum mode in LabSolutions RF workstation on RF-6000. The measurement conditions are shown in Table 1.

Table 1. Instrument and Analytical Conditions

Instruments	: RF-6000 Spectrofluorophotometer
Spectrum Type	: 3D spectrum
Wavelength Range	: Excitation (Ex) 250 nm to 400 nm, Emission (Em) 250 nm to 600 nm
Wavelength Interval	: Ex 2.0 nm, Em 1.0 nm
Scan Speed	: 2000 nm/min
Bandwidth	: Ex 3 nm, Em 3 nm

### □ Results and Discussion

#### EEM spectra of standards:

Organic acids such as humic and fulvic acids, along with amino acids of proteins are the indicative components of DOM which can be characterized by the EEM of aquatic fluorophores. For example, tryptophan, tyrosine and phenylalanine have fluorescence due to the presence of an indole group, and can be used to indicate the presence of protein and peptides.

Table 2 lists the common aquatic fluorophores and their Ex and Em wavelength ranges [1]. Figure 1 shows the measured EEM spectra of tryptophan, tyrosine and humic acid in this study. The Em of tryptophan is in the range of 300~400 nm at Ex of 250~300 nm. The peak ( $\lambda_{Max}$ ) at Em 350 nm / Ex 275 nm are in accordance with the literature data shown in Table 2 [1]. Likewise, the Em and Ex of tyrosine is in the range of 280~340 nm and 250~290 nm respectively. The peaks ( $\lambda_{Max}$ ) are at Em 310 nm / Ex 275 nm. Both tryptophan and tyrosine EEM spectra indicate the presence of protein-like DOM in the aquatic sample.

The EEM spectrum of humic acid in water is less define. It has a broad range with Em of 400~600 nm at Ex of 250~370 nm, which is the similar as reported in literature [1]. The humic acid EEM is used to characterize the presence of humic-like or marine humic-like DOM in aquatic samples.



It is worth to note that humic acid has multi-chromophoric groups and its fluorescence behavior differs from a single chromophore molecule. The fluorescence of humic acid differs with source since there is a difference in the molecular components of humic acid from one source to another.

EEM analysis of natural water and wastewaters:

The EEM spectrum of the pond surface water (Figure. 2a) shows tyrosine-like fluorescence as well as a broad Em 350~500 nm with Ex 250~370 nm which could be attributed to humic-like fluorescence.

Table 2. Characteristic aquatic fluorophores published in literature [1]

	Fluorophore	Excitation (nm)	Emission (nm)
A	Tryptophan-like, protein-like	225-237	340-381
		275	340
B	Tyrosine-like, protein-like	225-237	309-321
		275	310
C	Humic-like	237-260	400-500
		300-370	400-500
	Marine humic-like	312	380-420

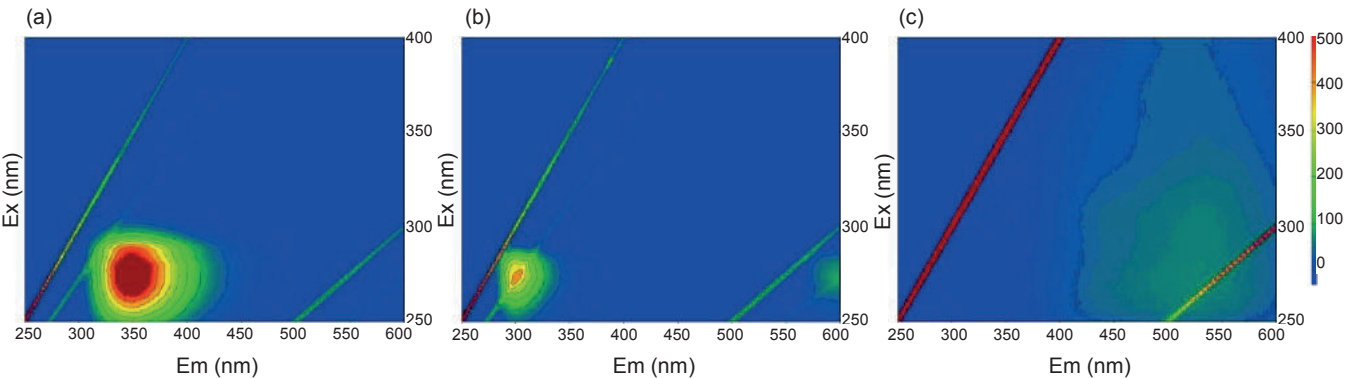


Figure 1. EEM 3D spectra of (a) tryptophan, (b) tyrosine, (c) humic acid in pure water

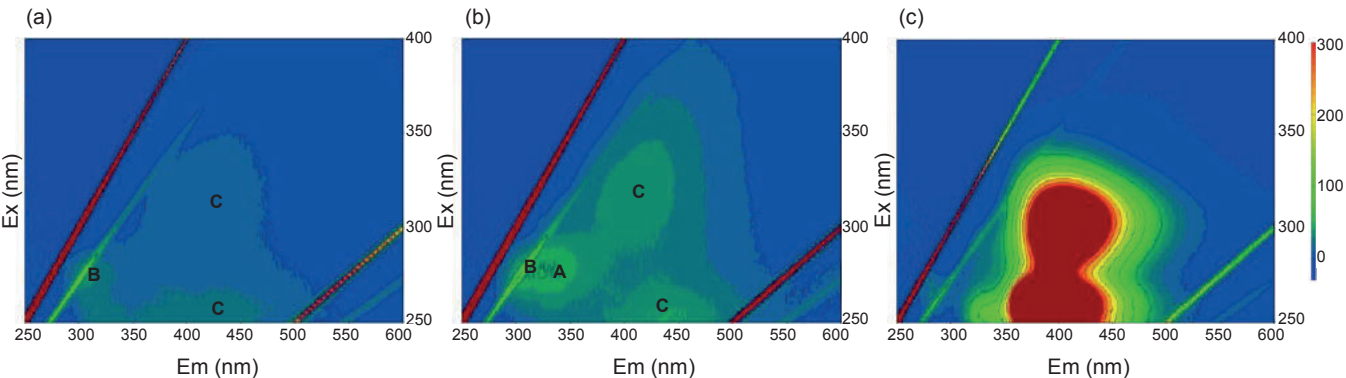


Figure 2. EEM spectra of (a) pond surface water, (b) wastewater from source X, (c) wastewater from source Y

The two wastewater samples have different EEM spectra. The wastewater from source X show tryptophan-like (A), tyrosine-like (B) and humic-like fluorescence (C) (Figure 2b). The wastewater from source Y shows the presence of unknown strong fluorophore of Em 350~480 nm at Ex 250~280 nm and 280~350 nm (Figure. 2c), which could not be identified directly to the above DOM (Table 2).

**Conclusions**

The excitation-emission matrix (EEM) fluorescence spectroscopy can be used as a rapid analytical tool in

the characterization of DOM in natural water and wastewater. Hence, it could be potentially used to assess water quality, wastewater treatment process and monitor pollution of natural water.

**References**

1. Hudson, N., Baker, A. and Reynolds, D. (2007). *Fluorescence analysis of dissolved organic matter in natural, waste and polluted waters - a review*. River Research and Applications 23: 631-649.
2. Yan, Y., Li, H. and Myrick, M. L. (2000). *Fluorescence fingerprint of waters: excitation-emission matrix spectroscopy as a tracking tool*. Applied Spectroscopy 54(10): 1539-1542.
3. Matthews, B.J.H., Jones, A.C., Theodorou, N.K. and Tudhope, A.W. (1996). *Excitation-emission-matrix fluorescence spectroscopy applied to humic acid bands in coral reefs*. Marine Chemistry 55: 317-332.

# Application News

## No. A494

### Spectrophotometric Analysis

## Simplified Measurement of Coumarin in Diesel Oil

### ■ Introduction

In Japan, diesel oil is subject to a consumption tax (national tax) and a diesel oil delivery tax (regional tax). However, kerosene and low-sulfur / high-sulfur A fuel oil are not subject to the delivery tax. Therefore, to avoid the tax, some vendors have been known to sell fraudulent diesel oil that has been mixed with kerosene or fuel oil. As a countermeasure, starting in March 1991, the then Ministry of Trade and Industry required addition of a 1 ppm concentration of coumarin to commercial kerosene and low-sulfur / high-sulfur A fuel oil products, so that they can be easily identified. Consequently, local tax bureaus have been using this marker for inspecting diesel oil by random sampling. If coumarin is detected, it means kerosene or low-sulfur / high-sulfur A fuel oil was mixed in with the diesel oil and legal measures or other actions are taken against the violator.

Therefore, on December 10, 2010, the Japan Petroleum Institute (Testing and Analysis sub-committee of the Product committee) established standard JPI-55-71-2010 as the official method for analyzing coumarin. In this example, we used Method A of the standard to measure the fluorescence spectrum of coumarin.

### ■ Analytical Procedure

The procedure for analyzing coumarin is summarized below and a photograph of the RF-6000 spectrofluorophotometer used to identify the coumarin diesel oil marker substance is shown in Fig. 1. Equipment and reagents required for the analysis are listed in Table 1.

#### Analytical Procedure

- (1) Prepare various solutions.
- (2) Prepare a standard sample for creating a calibration curve.
- (3) Prepare sample for quantitative analysis.
- (4) Shake and isomerize (UV irradiation).
- (5) Prepare calibration curve.
- (6) Measure unknown sample.



**Fig. 1 RF-6000 Spectrofluorophotometer Coumarin (Diesel Oil Marker) Identification System**

**Table 1 Equipment and Reagents Required for Coumarin Analysis**

(1)	RF-6000 spectrofluorophotometer system
(2)	Coumarin analysis kit (test tube holder with stirrer)
(3)	Dedicated coumarin measurement test tube (with stirrer)
(4)	Volumetric flasks (100 mL, 200 mL, and 500 mL)
(5)	Volumetric pipettes (1 mL, 2 mL, 5 mL, 6 mL, 8 mL, and 10 mL)
(6)	Measuring pipettes (0.5 mL, 1 mL, 2 mL, and 10 mL)
(7)	Test tube stand for 23 mm diameter tubes
(8)	Disposable gloves
(9)	Coumarin
(10)	Toluene
(11)	n-Dodecane
(12)	Sodium hydroxide and sodium nitrate for preparing alkaline aqueous solutions
(13)	1-Butanol and ethanol reagents for preparing alcohol solutions

Note: Items (9), (12), and (13) can be substituted with the Shimadzu RF Quantitation Reagent Kit.  
A test tube shaker would also be helpful.

■ Preparing Solutions

Prepare each solution according to steps (a) to (e) below.

- (a) Coumarin standard stock solution (10,000 mg/L)  
(Can be stored for 3 months in a sealed container in a cool dark location)  
Accurately weigh 1.0 ±0.005 g of coumarin into a 100 mL volumetric flask and fill to volume with toluene.
- (b) Coumarin standard solution (100 mg/L)  
Measure 5 mL of the coumarin standard stock solution (a) with a volmetric pipette and place it in a 500 mL volumetric flask. Then fill to volume with n-dodecane.
- (c) Coumarin standard solution (1 mg/L)  
Measure 5 mL of coumarin standard solution (b) with a volmetric pipette and place it in a 500 mL volumetric flask. Then fill to volume with n-dodecane.
- (d) Alkaline aqueous solution (can be stored sealed for 1 month in a cool dark location)  
Weigh 10 ±0.1 g sodium hydroxide and 20 ±0.1 g sodium nitrate and place them in a 100 mL volumetric flask. Then fill to volume with water.
- (e) Alcohol solution (can be stored sealed for 1 month in a cool dark location)  
Mix 80 mL 1-butanol and 60 mL ethanol.

■ Preparing Measurement Samples and Standard Samples for Creating a Calibration Curve

Insert stirrers in five test tubes used for creating the calibration curve. Then dispense the solutions indicated in Table 2. Prepare the measurement sample by inserting the stirrer in the test tube and then dispensing 1 mL of the measurement sample, 6 mL n-dodecane, 5 mL alkaline aqueous solution, and 8 mL alcohol solution.

■ Shaking and Isomerization

Install each test tube in the shaker and shake for three minutes at 240 rpm or faster. If a shaker is not available, shake by hand. Let stand for five minutes after shaking. Then confirm that the contents have separated into three layers, as shown in Fig. 2. From the top, these layers are the dodecane, alcohol solution, and alkaline aqueous solution layers.

Next, place the test tubes in the cell holder of the RF-6000 spectrofluorophotometer coumarin diesel oil marker identification system. Isomerize the coumarin by irradiating with 360 nm UV excitation wavelength (10 nm bandwidth) for three minutes while stirring with the stirrer. The isomerization progress can be checked by setting the fluorescence wavelength to 500 nm (10 nm bandwidth) and confirming the change in fluorescence intensity over time. Analytical conditions are indicated in Table 3. A time-course graph is shown in Fig. 3, with elapsed time on the horizontal axis and fluorescence intensity on the vertical axis. Irradiating samples with UV light causes the fluorescence intensity to increase with elapsed time. When the fluorescence intensity becomes constant isomerization is considered stabilized.

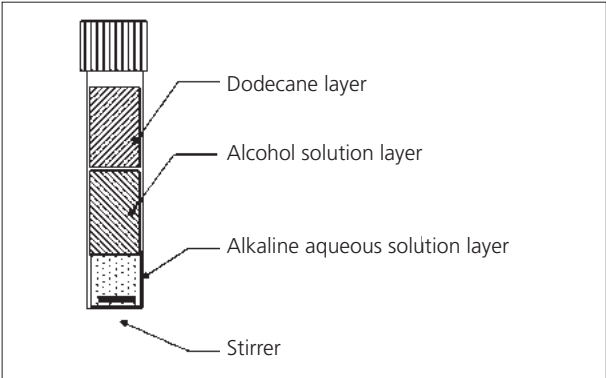


Fig. 2 Diagram of Test Tube Contents Separated into Three layers

Table 3 Analytical Conditions

Measurement mode	: Time course
Excitation wavelength	: 360 nm
Emission wavelength	: 500 nm
Bandwidth	: Ex: 10 nm, Em: 10 nm

Table 2 Preparing Standard Samples for Creating Calibration Curve

Types of Calibration Curves	Mixture Ratio (%)	0.0	10.0	40.0	80.0	120.0
	Coumarin Content (mg/L)	0.00	0.10	0.40	0.80	1.20
Reagent Acquisition Quantity (mL)	Coumarin Standard Solution (1.0 mg/L)	0	0.10	0.40	0.80	1.20
	n-Dodecane	7.0	6.9	6.6	6.2	5.8
	Alkaline Aqueous Solution	5.0	5.0	5.0	5.0	5.0
	Alcohol Solution	8.0	8.0	8.0	8.0	8.0

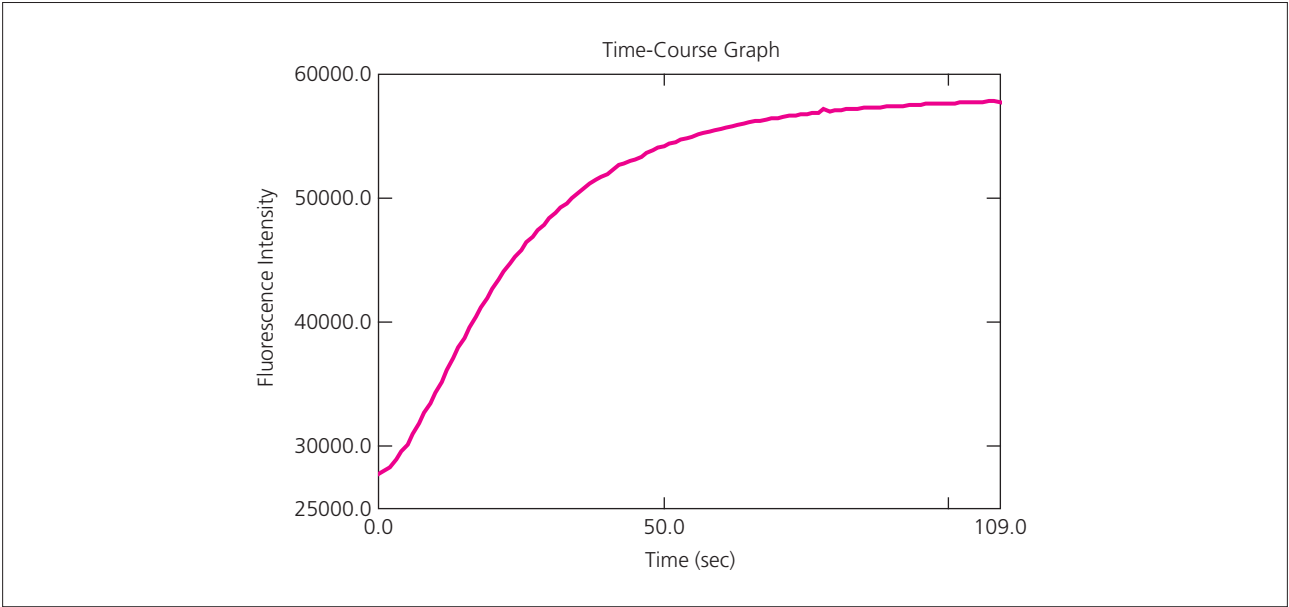


Fig. 3 Change in Fluorescence Intensity Due to Coumarin Isomerization

■ Isomerization Reaction of Coumarin

In an alkaline solution, coumarin breaks down by hydrolysis to form *cis*-*o*-hydroxycinnamic acid. If additionally irradiated with UV rays, it is isomerized to form *trans*-*o*-hydroxycinnamic acid. The structure of these isomers are shown in Fig. 4. When coumarin changes to *trans*-*o*-hydroxycinnamic acid, it emits fluorescent light. Coumarin can be quantitated by measuring the associated fluorescence intensity.

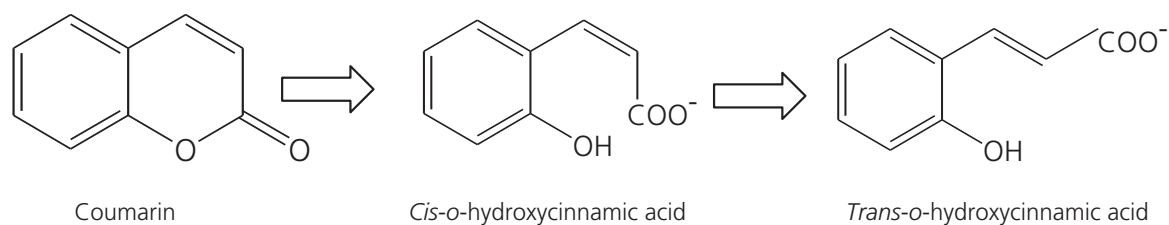


Fig. 4 Isomerization Reaction of Coumarin

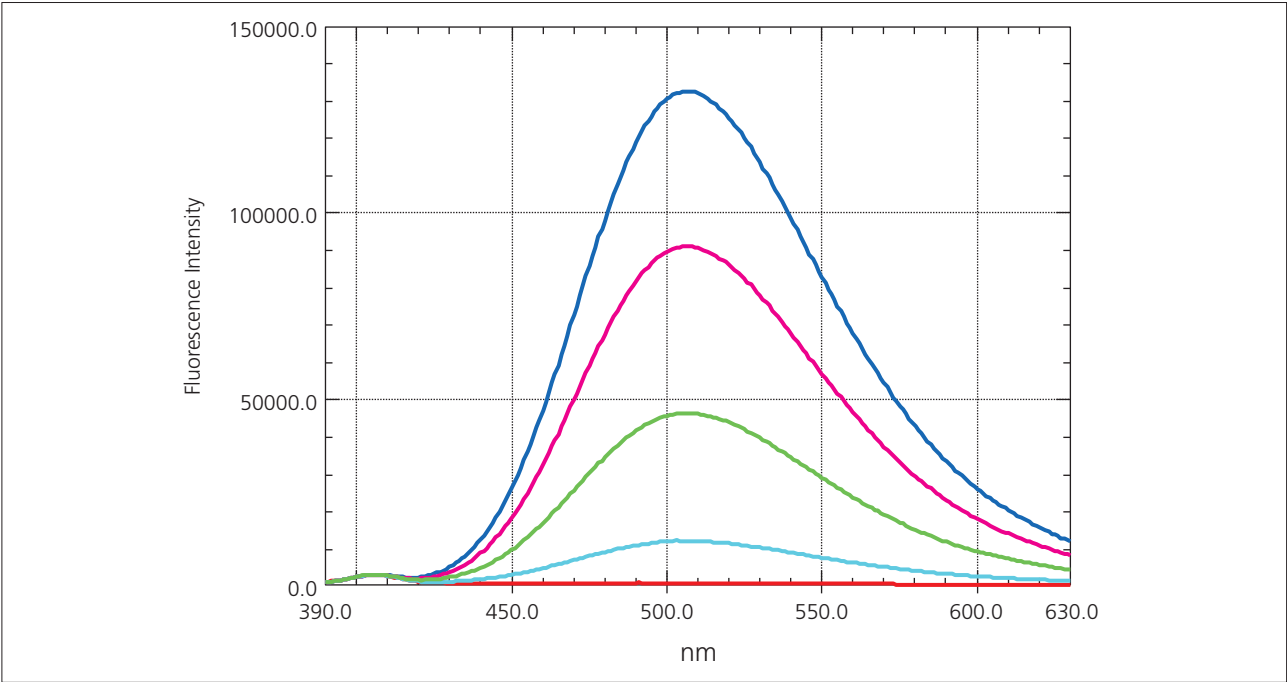
■ Preparing a Calibration Curve and Measuring Coumarin Added to Diesel Oil

After irradiation with UV light, samples are measured using the analytical conditions indicated in Table 4. The fluorescence spectrum measured from the standard sample is shown in Fig. 5. The calibration curve is shown in Fig. 6. The squared correlation coefficient of the calibration curve,  $r^2$ , was 0.99965.

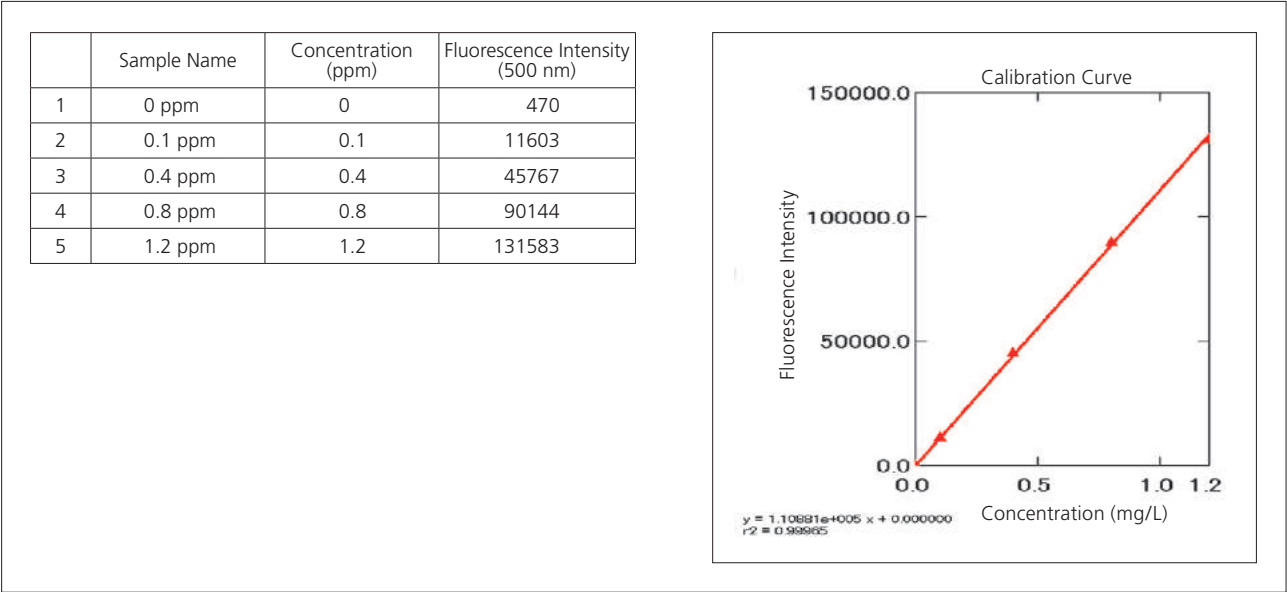
Results from measuring the measurement sample prepared by adding 0.5 ppm coumarin to commercial diesel oil are shown in Table 5. The quantitative results were approximately equivalent to the added quantity.

Table 4 Analytical Conditions

Excitation wavelength	: 360 nm
Emission wavelength	: 500 nm (390 to 630 nm when scanning spectra)
Bandwidth	: EX: 10 nm, EM: 10 nm



**Fig. 5 Fluorescence Spectra of Standard Samples**  
In order of fluorescence intensity, with the highest intensity first, the corresponding concentrations are 1.2 ppm, 0.8 ppm, 0.4 ppm, 0.1 ppm, and 0 ppm.



**Fig. 6 Calibration Curve**

**Table 5 Measurement Results for Coumarin Added to Diesel Oil**

Quantity Added (ppm)	Fluorescence Intensity	Measurement Result (ppm)
0.50	57440	0.514

**Conclusion**

This example showed that the Shimadzu RF-6000 spectrofluorophotometer can be used to easily and accurately measure coumarin according to Method A of the standard specified by the Japan Petroleum Institute.



## Application News

# No. A529

### Spectrophotometric Analysis

## Fluorescence Measurement of Glass and Plastic

### ■ Introduction

In observations and analyses with a fluorescence microscope or Raman spectroscopy instrument, the objects used to contain or fix samples in place are often made with common items such as glass and plastic. While glass and plastic are convenient from the perspective of workability and durability, these materials can affect measurement data if they have fluorescent properties themselves.

This article introduces the results of examining the presence and absence of fluorescence in glass and plastic objects using the RF-6000 spectrofluorophotometer.

K. Sobue

### ■ 3D Fluorescence Spectra Measurement of Glass and Plastic Objects

Fig. 1 and Fig. 2 show the types of samples we measured. The glass samples consist of a glass marble, uranium-glass marble, glass cell, and quartz cell. The plastic samples consist of films of polyethylene (PE) and polypropylene (PP), sheets of polyvinylchloride (PVC), polyethylene terephthalate (PET), and polymethyl methacrylate (PMMA), and a PMMA sheet treated with fluorescent coloring. Each sample was set on a solid sample holder and measured according to the conditions listed in Table 1.

**Table 1 Measurement Conditions**

Instrument used	: RF-6000
Options	: Solid sample holder, IHU310
Spectrum type	: 3D spectrum
Measurement wavelength range	: Ex 280 nm to 600 nm Em 310 nm to 600 nm
Scanning speed	: 6,000 nm/min
Wavelength interval	: Ex 5.0 nm, Em 1.0 nm
Bandwidth	: Ex 5.0 nm, Em 5.0 nm
Sensitivity	: Low

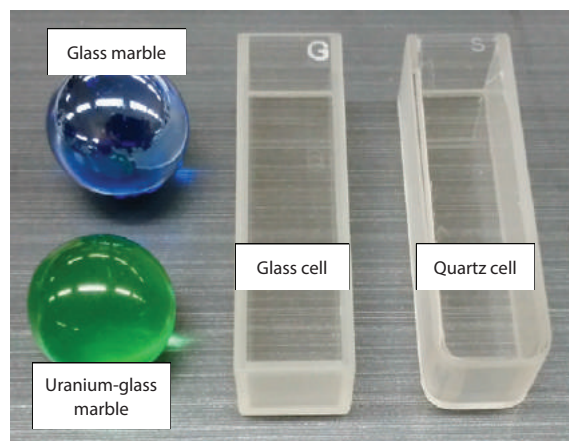


**Fig. 1 Glass Samples**

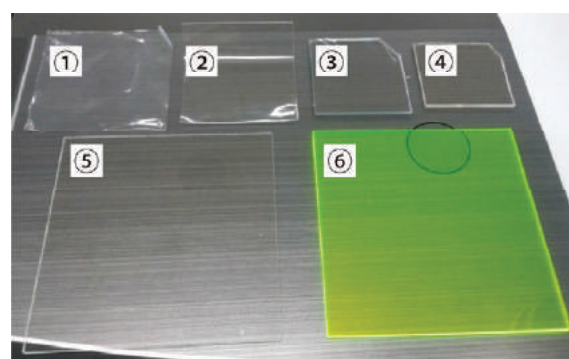


**Fig. 2 Plastic Samples**  
1: PE, 2: PP, 3: PVC, 4: PET, 5: PMMA,  
6: PMMA (Fluorescent Coloring)

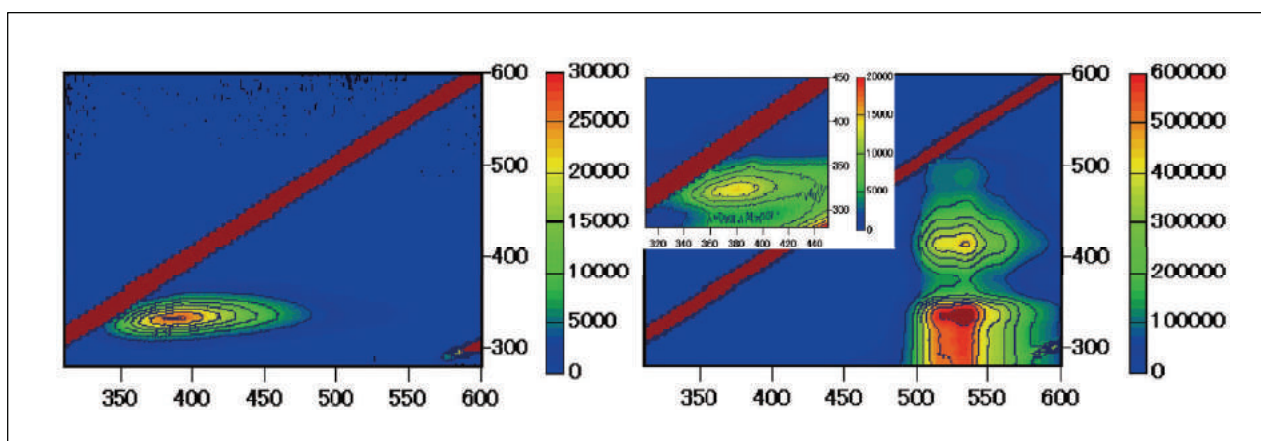


**Fig. 3 3D Fluorescence Spectra** Left: Glass Marble, Right: Uranium-Glass Marble



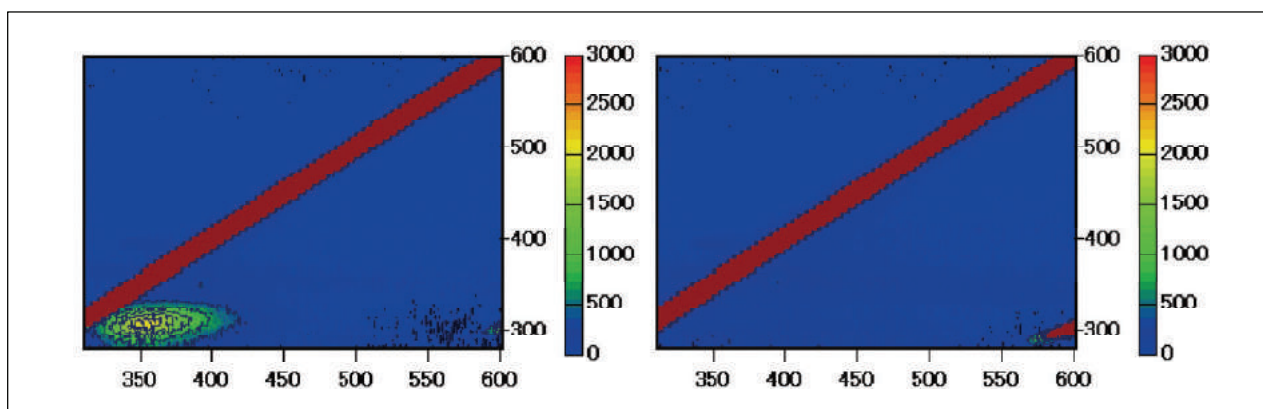


Fig. 4 3D Fluorescence Spectra Left: Glass Cell, Right: Quartz Cell

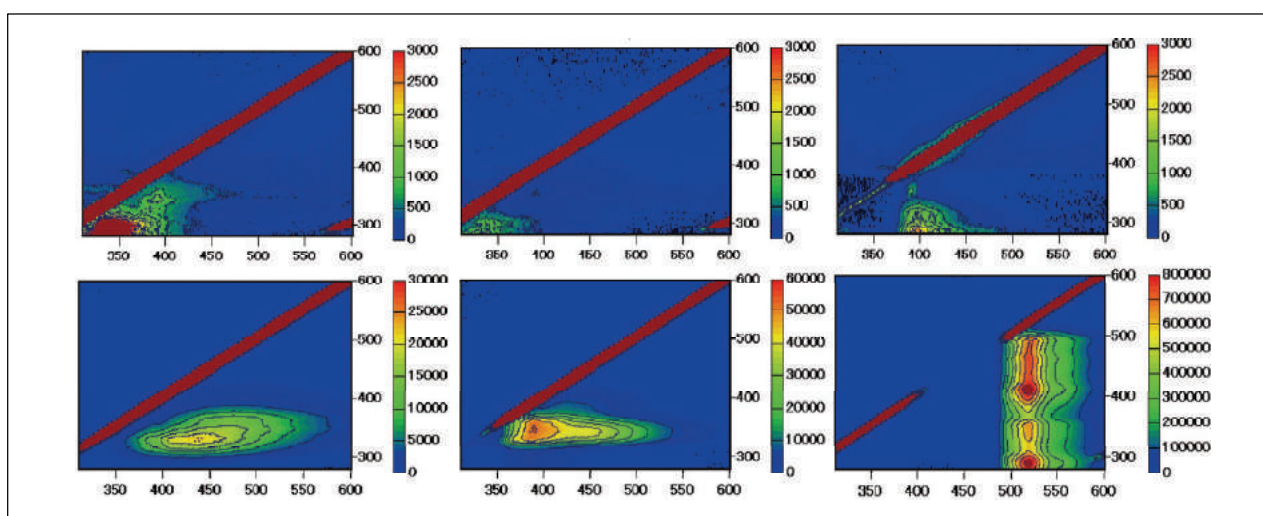


Fig. 5 3D Fluorescence Spectra

Upper Left: PE, Lower Left: PVC, Upper Center: PP, Lower Center: PET, Upper Right: PMMA, Lower Right: PMMA (Fluorescent Coloring)

Fig 3. to Fig 5 show the results of 3D fluorescence spectrum measurement. For the excitation wavelength range of 310 nm to 340 nm, the glass marble showed fluorescence in the 350 nm to 450 nm region and the uranium-glass marble showed fluorescence from uranium in the 500 nm to 600 nm region in addition to fluorescence from glass. However, while the glass cell showed faint fluorescence in the 330 nm to 400 nm region for the excitation wavelength range of 290 nm to 320 nm, the quartz cell did not exhibit fluorescence.

For the plastics, PE and PP showed faint fluorescence around 340 nm for the excitation wavelength of 300 nm. PVC showed fluorescence centered around 440 nm for the excitation wavelength of 330 nm and PET showed a different fluorescence centered around 390 nm for the excitation wavelength of 350 nm. Even without fluorescent coloring treatment, PMMA showed faint fluorescence in the 380 nm to 450 nm region for the excitation wavelength of 300 nm. On the contrary, the yellow PMMA treated with fluorescent coloring showed intense fluorescence in the 500 nm to 550 nm region <sup>\*1</sup>.

## Summary

In this research, we examined the presence and absence of fluorescence in various glass and plastic objects using the RF-6000 spectrofluorophotometer. We were able to confirm the presence and absence of fluorescence and differences in excitation and fluorescence wavelengths between samples. The ability to ascertain the presence of fluorescence in glass and plastic objects helps to determine its effect on measurement data in advance when using a fluorescence microscope or Raman spectroscopy instrument.

\*1 The observed fluorescence is not guaranteed since the measured samples are commercially available items.

First Edition: Mar. 2017



For Research Use Only. Not for use in diagnostic procedure.

This publication may contain references to products that are not available in your country. Please contact us to check the availability of these products in your country.

The content of this publication shall not be reproduced, altered or sold for any commercial purpose without the written approval of Shimadzu. Company names, product/service names and logos used in this publication are trademarks and trade names of Shimadzu Corporation or its affiliates, whether or not they are used with trademark symbol "TM" or "®". Third-party trademarks and trade names may be used in this publication to refer to either the entities or their products/services. Shimadzu disclaims any proprietary interest in trademarks and trade names other than its own.

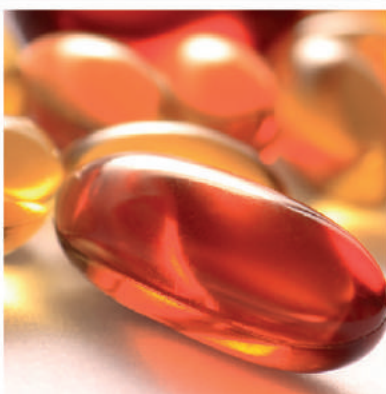
The information contained herein is provided to you "as is" without warranty of any kind including without limitation warranties as to its accuracy or completeness. Shimadzu does not assume any responsibility or liability for any damage, whether direct or indirect, relating to the use of this publication. This publication is based upon the information available to Shimadzu on or before the date of publication, and subject to change without notice.

© Shimadzu Corporation, 2017

Shimadzu Corporation

[www.shimadzu.com/an/](http://www.shimadzu.com/an/)

# 4. Life Science Lab Instruments





## 4. Life Science Lab Instruments

---

### 4.1 Functional Near-Infrared Spectroscopy (fNIRS)

---

fNIRS is a versatile functional neuroimaging technology with a non-invasive method monitoring the brain activity. Recently, a hot topic is to explore the wide area network in the brain such as functional connectivity or spontaneous brain activity functions.

**C297-E119**

functional Near-Infrared Spectroscopy System for Research

# functional Near-Infrared Spectroscopy System for Research

## — Examples in the Automotive and Transportation Equipment Fields —

Functional near-infrared spectroscopy (fNIRS), which uses light to visualize the activity of living organisms, measures brain activity safely and in a more natural state. Consequently, it is being used in a wide range of applications, including healthcare, psychology, education, cognitive science, and engineering.

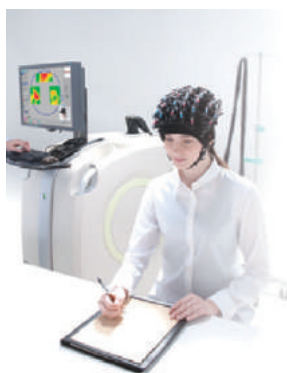
### Features

Brain functions can be measured in a posture and environment that closely approximates everyday life. Two models, applicable to different research applications/environments, are available.

functional Near-Infrared Spectroscopy System for Research

## LABNIRS

labnirs



- This is a laboratory model designed for a wide variety of basic research fields.
- A broad range of measurement regions can be customized depending on experimental conditions.

Portable functional Near-Infrared Spectroscopy System for Research

## LIGHTNIRS

lightnirs



- The portable model is ideal for field research.
- Expands the possibilities for measuring brain function in a diverse range of applications and research fields.

### Expansion Holder

The expansion holder provides even more freedom for selecting measurement areas.

#### Type A

For mainly measuring frontal brain areas



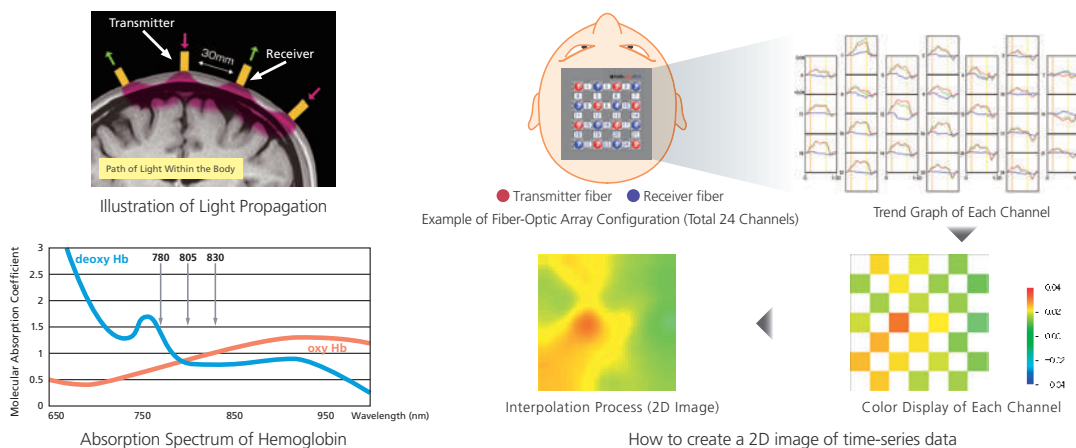
#### Type B

For measuring the frontal, temporal, parietal, and occipital areas



### Measurement Principle

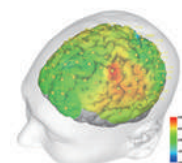
Brain activity at the surface of the brain is visualized in real time by shining near infrared light, which readily penetrates biological tissue, onto the head and then detecting a portion of that light that is reflected, as it is scattered and absorbed within the body.



### Main Applications

- **Drug discovery and medical research:**  
Mental illness, neuroscience, drug discovery research, etc.
- **Rehabilitation research:**  
Exercise therapy, occupational therapy, speech/hearing, etc.
- **Industrial applications:**  
Neuromarketing, etc.

- **Basic research:**  
Brain functional network research, multimodality research, etc.
- **Information engineering:**  
Robotics, ergonomics, kansei engineering, etc.
- **Education and psychology:**  
Cognitive psychology, social psychology, developmental psychology, etc.



Example of Overlay on MRI Image



### Measuring Brain Function During Driving

#### Evaluating Task Loads During Driving

K. Yanagisawa et al. (2012). "Measurement of driver's brain function by using NIRS (Evaluation of reduction in driver's workload by driving assistance system)." The Transactions of Human Interface Society 14(1-4): 209-217. (In Japanese with English abstract)

#### Brain Function for Left and Right Curves

N. Oka et al. (2015). "Greater Activity in the Frontal Cortex on Left Curves: A Vector-Based fNIRS Study of Left and Right Curve Driving." PLoS One 10(5): e0127594.

#### Relationship Between Driving Speed and Brain Activity

K. Yoshino et al. (2013). "Correlation of prefrontal cortical activation with changing vehicle speeds in actual driving: a vector-based functional near-infrared spectroscopy study." Frontiers in Human Neuroscience 7(895): 1-9.

### Evaluating Occupant Space and Comfort

#### Scents

H. Kanai et al. (2008). "Influence on Heart Rate Variability and Neuronal Activity by Inhalation of Fragrance with Different Preference." Kansei Engineering International Journal 7(3), 469-476. In Japanese with English abstract

#### Lighting

K. Mori (2012). "Light/Sound/Brain: Toward the Fusion of Neuroscience and Media Art." Bulletin of the Institute for Interdisciplinary Studies of Culture, Doshisha Women's College of Liberal Arts. 29: 1-15. In Japanese with English Abstract

#### Music

M. Shimo et al. (2008). "Evaluation of the level of "music relaxation" utilizing hemo-dynamics by near-infra-red-spectroscopy." Bulletin of the faculty of education, Chiba University, 56 343-348. In Japanese with English abstract

#### Sensation of Hot and Cold

Lei Hou et al. (2015). "Analysis of brain activity during local hot-cold stimulus using near-infrared spectroscopy (Analysis of brain activity during pain stimulus by cold stimulus)." Transactions of the JSME (in Japanese) 81(830). In Japanese with English abstract

#### Sense of Happiness

S. Oonishi et al. (2014). "Influence of subjective happiness on the prefrontal brain activity: an fNIRS study." Adv Exp Med Biol 812: 287-293.

#### Pleasant and Unpleasant Stimuli

Y. Hoshi et al. (2011). "Recognition of Human Emotions from Cerebral Blood Flow Changes in the Frontal Region: A Study with Event-Related Near-Infrared Spectroscopy." Neuroimage, 21(2), e04-101.

### Operability and Driver Attention

#### Evaluation of Driver Interruptibility

T. Tanaka and K. Fujita (2009). "Discussion on Duration of Uninterruptibility Reduction at Focused Application-Switching." CHINOUI TO JOUHO (intelligence and information) 21, 827-836. In Japanese

#### Switching Attention

N. Yamaguchi et al. (2011). "The Activation in a Prefrontal Area at the Time of Alternating Tasks Enforcement Related to the Age, Performance and Task -A Study in the Use of Near-Infrared Spectroscopy-" Annual Reports of Human Health Sciences, Graduate School of Medicine, Kyoto University: health science 7: 9-16. In Japanese with English abstract

### Safety and Proficiency

#### Study of Probability of Driving Again After Brain Injury

S. Watanabe et al. (2011). "Cerebral Activation Patterns of Patients Operating a Driving Simulator after Brain Injury: A Functional Near-infrared Spectroscopy Study." Japanese Journal of Occupational Medicine and Traumatology 59(5), 238-244. In Japanese with English abstract

#### Task Proficiency in Virtual Space

Lei HOU, K. Watanuki. (2012). "Measurement of Brain Activity under Virtual Reality Skills Training Using Near-Infrared Spectroscopy." Journal of Advanced Mechanical Design, Systems, and Manufacturing 6(1): 168-178.

#### Text-Entry Proficiency

S. Kotani et al. (2011). "Proficiency evaluation of three Japanese Input Methods using an eye-controlled communication device for users with disabilities." 2011 IEEE International Conference on Systems, Man, and Cybernetics (SMC), 3230 - 3235.

### Related Research

#### Trains

T. Kojima et al. (2007). "Measurement of Brain Function of Train Driver Using Functional Near-infrared Spectroscopy (fNIRS)." The Japanese Journal of Ergonomics 43(4): 193-200. In Japanese with English abstract

#### Development of Smart Glasses

O. Amft et al. (2015). "Making regular eyeglasses smart." Pervasive Computing, IEEE 14(3): 32-43.



Shimadzu Corporation

[www.shimadzu.com/an/](http://www.shimadzu.com/an/)

#### For Research Use Only. Not for use in diagnostic procedures.

This publication may contain references to products that are not available in your country. Please contact us to check the availability of these products in your country.

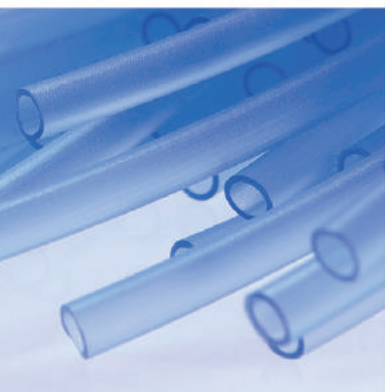
Company names, products/service names and logos used in this publication are trademarks and trade names of Shimadzu Corporation, its subsidiaries or its affiliates, whether or not they are used with trademark symbol "TM" or "®".

Third-party trademarks and trade names may be used in this publication to refer to either the entities or their products/services, whether or not they are used with trademark symbol "TM" or "®".

Shimadzu disclaims any proprietary interest in trademarks and trade names other than its own.

The contents of this publication are provided to you "as is" without warranty of any kind, and are subject to change without notice. Shimadzu does not assume any responsibility or liability for any damage, whether direct or indirect, relating to the use of this publication.

## 5. Sum Parameter (TOC/TN)







## 5. Sum Parameter (TOC/TN)

---

### 5.1 Total Organic Carbon Lab Analyzers

---

In the automotive industry, high-quality TOC analyzers are used for wastewater treatment plant influents (upstream monitoring) and effluents. Detections at a short measuring cycle (4 minutes minimum) rapidly capture dramatic changes in organic matter or abnormal effluent. The powerful oxidation capacity of a combustion-type analyzer can detect organic matter that cannot be captured using a UV meter. Combined with switching between up to six flow lines, the short measuring cycle and powerful oxidation offer detailed monitoring of treatment plants.

<b>SCA-130-102</b>	TOC – Determination in wastewater
<b>SCA-130-201</b>	TOC determination in ultrapure water – Comparison of the various oxidation techniques
<b>SCA-130-301</b>	TOC – Determination in hydrochloric acid
<b>SCA-130-302</b>	TOC – Determination in nitric acid
<b>SCA-130-303</b>	TOC – Determination in sulfuric acid
<b>SCA-130-304</b>	TOC – Determination in brines
<b>SCA-130-305</b>	TOC – Determination in sodium hydroxide solution
<b>SCA-130-306</b>	TOC – Determination in soda solution
<b>SCA-130-307</b>	TOC – Determination in ammonia or ammonium salt solutions
<b>SCA-130-308</b>	TOC – Determination in sodium nitrate and sodium nitrite
<b>SCA-130-309</b>	TOC determination in phosphoric acid
<b>SCA-130-310</b>	TOC – Determination in diluted hydrofluoric acid
<b>SCA-130-501</b>	TOC – Determination methods according to EN 1484
<b>SCA-130-502</b>	Determination of the purgeable organic carbon (POC)
<b>SCA-130-503</b>	TN <sub>b</sub> – total bound nitrogen
<b>SCA-130-504</b>	Kit for high-salt samples
<b>SCA-130-507</b>	Calibration with automatic dilution function
<b>SCA-130-514</b>	Comparison of different sum parameters – COD, BOD and TOC
<b>SCA-130-515</b>	COD and TOC correlation factor – Conversion examples
<b>SCA-130-601</b>	Continuous TOC/TN determination in wastewater treatment plants
<b>SCA-130-603</b>	Continuous TOC determination in the chemical industry
<b>SCA-130-604</b>	Continuous condensate monitoring using the TOC-4200
<b>SCA-130-605</b>	TOC-4200 – High sensitivity measurement option
<b>SCA-130-609</b>	TOC-4200 – Carryover free TOC determination
<b>056</b>	Measurement of a cement admixture by a TOC solid sample measurement system

## Application News

**No.** SCA-130-102

Sum parameter Total Organic Carbon

### TOC – Determination in wastewater

Wastewater is water that has been contaminated by use. In terms of its composition, wastewater is not homogeneous but as diverse as its possible sources.



According to the German Water Resources Act (Wasserhaushaltsgesetz, WHG) wastewater is defined as follows:

“Wastewater is

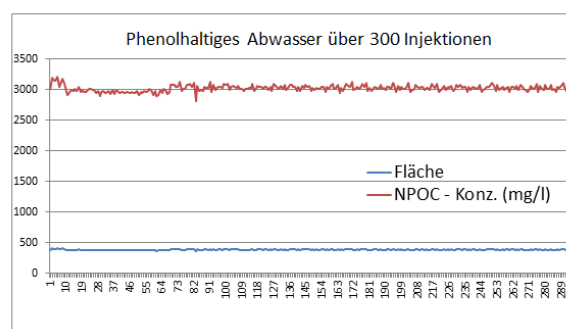
- 1) water whose properties have been changed by domestic, commercial, agricultural or other use and the water (sewage) discharged with it during dry weather conditions as well as
- 2) the run-off and collected water (rainwater) from built-up or paved areas following precipitation.

Sewage also includes the liquids that are discharged and collected from waste treatment and storage plants”.

This diversity of wastewaters should also be taken into account during the analysis. Wastewater can thus contain small amounts of organic pollutants with little matrix, as well as highly saline products with high amounts of organic components.

#### ■ Example of wastewater measurement

Below, a strongly saline wastewater from the chemical industry was analyzed. In addition to various substances present in low amounts, the wastewater mainly contained high amounts of phenolic substances originating from production processes.



	Fläche	NPOC (mg/l)
Mittelwert	381,1	3024
Standardabweichung abs.	6,6	51,8
Standardabweichung in %	1,7	1,7

Fig. Result of the wastewater

A TOC-L<sub>CPN</sub> was used for the analysis. To ensure efficient use of the instrument for large sample quantities, the fully automated dilution function and the additional high-salt sample kit were applied. With a dedicated function, samples could be diluted up to a factor of 1:50. For the phenol-containing wastewater, the sample was diluted by a factor of 1:10. The high-salt sample kit increases the lifetime of the catalyst for high salt loads.



Fig. Combustion tube (of salt kit)  
after the long term test

To test long-term stability, more than 300 injections of the saline wastewater were compared.

The graph shows the stability of measurement of over 300 injections with a standard deviation of 1.7%. Mean value was 3042 mg/L.

In many cases, wastewater contains particles. Where the wastewaters are not filtered, the particles need to be held in suspension by stirring. In order to prevent inhomogeneity of the particles by sedimentation within the syringe body, multiple injections from the same syringe may not be carried out in this case.



#### ■ Recommended Analyzer / Configuration

TOC-L<sub>CPN</sub> with normal sensitive Catalyst or kit for high salt samples (B-Type-Scrubber)  
ASI-L (40ml) with stirrer option (for samples with particles) and External Sparge-Kit

#### ■ Useful instrument parameters::

- Use of integrated dilution function for automated sample dilution
- In the presence of particles: deactivation of multiple injection via the syringe.

## Application News

**No.** SCA-130-201

Sum parameter – Total Organic Carbon

### TOC determination in ultrapure water – Comparison of the various oxidation techniques

Ultrapure water is one of the most widely used excipients in the production of pharmaceuticals. It is also used for cleaning purposes. Different application areas require different grades of ultrapure water quality. These grades are defined in the European Pharmacopoeia, which distinguishes between 'Purified Water', 'Highly Purified Water' and 'Water for Injection' ('The United States Pharmacopoeia, however, does not use the same classification as the European Pharmacopoeia').



**Water for injection** is used for the preparation of injection solutions and is produced by distillation. The TOC content may not exceed 0.5 mg/L (water for injection in bulk).

**Water Highly Purified** is a sterile ultrapure water for the manufacture of pharmaceuticals that do not require a 'Water for Injection' standard. It is also often used for the final rinse during cleaning and is usually produced by reversed osmosis. The TOC content may not exceed 0.5 mg/L.

**Water Purified** is used in the manufacture of pharmaceuticals that do not require any other standard. The organic content is determined either via the TOC value (0.5 mg/L) or via the permanganate test (purified water in bulk).

#### ■ TOC determination in ultrapure water

Two oxidation techniques are now commonly used in TOC analysis:

1. Catalytic combustion, where carbon compounds are converted into CO<sub>2</sub> using a catalyst under high temperatures with subsequent detection of the resulting CO<sub>2</sub> using an NDIR detector.
2. Wet chemical oxidation, which uses a combination of UV irradiation and persulfate for oxidation. Both methods can be applied for the determination of ultrapure water.



#### ■ TOC-L<sub>CPH</sub>: Oxidation via catalytic combustion

The TOC-L<sub>CPH</sub> uses the proven catalytic oxidation at 680 °C.



The integrated ISP sample preparation unit (an 8-position switching valve with syringe and sparging gas connection) considerably reduces the users' workload, as the instrument carries out dilution, acidification and sparging fully automatically.

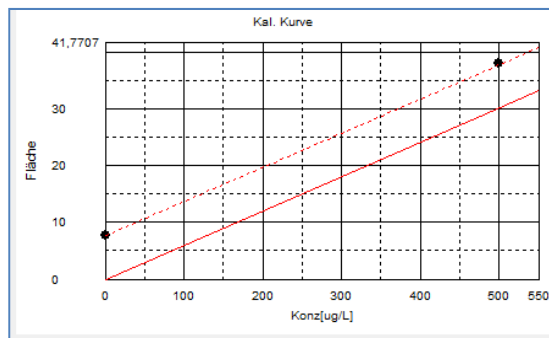


Fig. NPOC- Calibration (Blank and 500µg/L)

When using the high sensitivity catalyst, the detection limit is approximately 4µg/L. In addition, the combustion technique can be used in combination with the TNM-L module, whereby a single injection is sufficient for simultaneous determination of the total bound nitrogen. Simultaneous TOC/TN<sub>b</sub> determination is highly suitable for cleaning validation, as this enables differential determination between cleaning agent and product.

#### ■ TOC-V<sub>WP/WS</sub>: Wet chemical oxidation

The key technique of the TOC-V<sub>WP/WS</sub> analyzer is the powerful oxidation via the combination of sodium persulfate and UV oxidation at 80 °C. The TOC-V<sub>WP/WS</sub> features an automatic reagent preparation function that eliminates possible contamination of the persulfate solution. This ensures that the TOC value truly originates from the sample – and not from the reagent solution used. The large injection volume (up to 20.4 mL) in combination with the highly sensitive NDIR detector, leads to an extremely low

detection limit (0.5µg/L) and excellent reproducibility in the lower ppb range. The TOC-V<sub>WP/WS</sub> is therefore highly suitable for TOC determination in the ultra-trace range.

#### TOC-V WP Sample measurement

Method: NPOC (3% Acid, 3 min sparge)

Persulfatsol.: 1,5mL

Injection vol.: 20,4 mL

Result: 2,44 ± 0,42 µg/L TOC (NPOC)

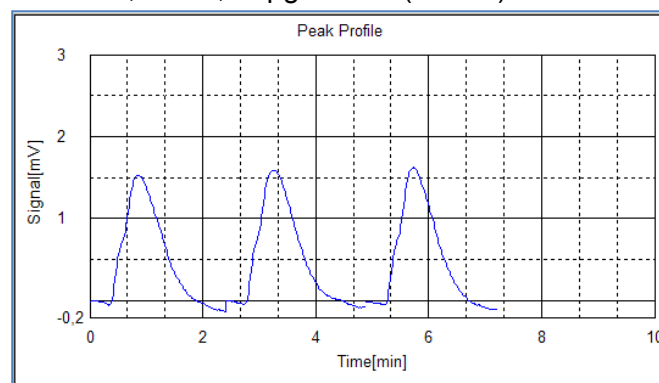


Abb. Peak graphik of TOC-V<sub>WP</sub> measurement

#### ■ Conclusions

Both types of instruments with their different oxidation methods can be used for TOC determination according to the European Pharmacopoeia. The advantage of the combustion method is its high oxidation potential, particularly for samples containing particulate matter. Moreover, simultaneous TOC/TN<sub>b</sub> measurements can be carried out, leading to a higher information content of the analysis. The advantage of wet-chemical oxidation is its high injection volume, which leads to higher sensitivity and therefore enables high precision measurements in the lower ppb range.

#### ■ Recommended analyzer / Configuration

TOC-L<sub>CPH</sub> with high sensitivity catalyst  
ASI-L (40ml), External Sparge-Kit.

TOC-V<sub>WP</sub> with ASI-V (40ml)

## Application News

**No.** SCA-130-301

Sum parameter – Total Organic Carbon

### TOC – Determination in hydrochloric acid

Acids, in particular concentrated hydrochloric acid, represent a large group of inorganic chemicals frequently used in the chemical industry. TOC determination in concentrated hydrochloric acid poses an enormous challenge to the analyzers that are used for this purpose.

In general, it is possible to greatly dilute the substance to be analyzed in order to eliminate matrix interferences. But sometimes it is necessary to achieve very low limits of detection (with reference to 37% hydrochloric acid) of 1 mg/L.



TOC-L CPH with OCT-L

#### ■ Acid challenge

The great challenge is to develop protective mechanisms to help protect instruments and their components, as well as to prevent damage by acidic fumes. For this purpose, the TOC-L series offers several gas washers that bind and eliminate the chlorine gas formed in the flow line of the system in various ways.

Another challenge is to attain a stable and reproducible oxidation process to ensure that no fluctuating or tailing peaks are being recorded. In addition, the measuring values should remain stable over a longer measuring interval.

#### ■ TOC Measuring Method

The 37% hydrochloric acid solution was manually diluted to a ratio of 1:2 with water in order to obtain an 18.5% hydrochloric acid solution.

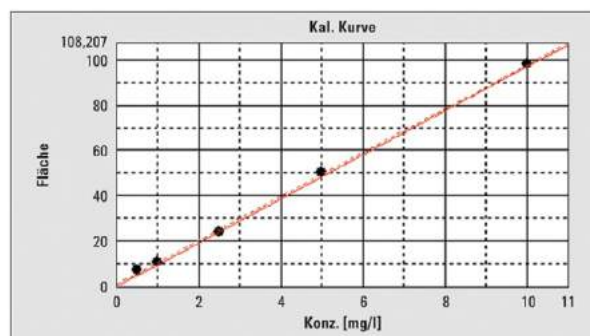


Abb. 2 Mehrpunktkalibration mit Verdünnungsfunktion

Calibration was carried out in the range of 0.5 to 10 ppm. The automatic dilution function of the analyzer automatically executes this calibration from a single stock solution. The injection volume was 150 µL. In case the TOC contamination of the hydrochloric acid exceeds the measuring range of the calibration, the automatic dilution function of the analyzer will readjust the hydrochloric acid solution to fit the measuring range.

#### ■ Verification the measuring method

After calibration, the TOC content of the concentrated hydrochloric acid solution was determined.



To investigate matrix influences, a potassium hydrogen phthalate solution was subsequently added to the 18.5% hydrochloric acid solution to increase the TOC by 5 ppm (Figure 3 and Table 1).

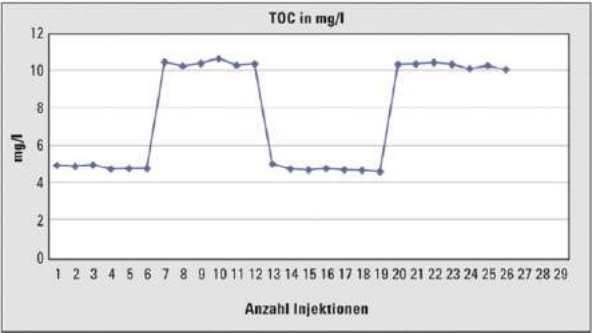


Fig.3: Results of original and spiked hydrochloric solution

Figure 3 and Table 1 show the results of the individual measurements of the hydrochloric acid as well as the measurements of the spiked hydrochloric acid.

TOC result of 18,5% hydrochloric acid in mg/l		
Injection	Original	Spiked with 5ppm TOC
1	4,901	10,46
2	4,858	10,24
3	4,91	10,39
4	4,716	10,64
5	4,728	10,28
6	4,739	10,35
7	4,966	10,34
8	4,71	10,36
9	4,662	10,42
10	4,733	10,33
11	4,659	10,11
12	4,625	10,27
13	4,552	10,06
Mean value	4,75	10,33
SD	0,12	0,15
RSD in %	2,6	1,4

Tab. 1: Values of each injection

#### ■ Long-term stability

To investigate the long-term stability of the method, the 37% hydrochloric acid solution was again diluted to a ratio of 1:2 with water and injected 76 times (150 µL).

The relative standard deviation over all measurements was 3.4%. The following graph shows the progression of the TOC values of the hydrochloric acid injections.

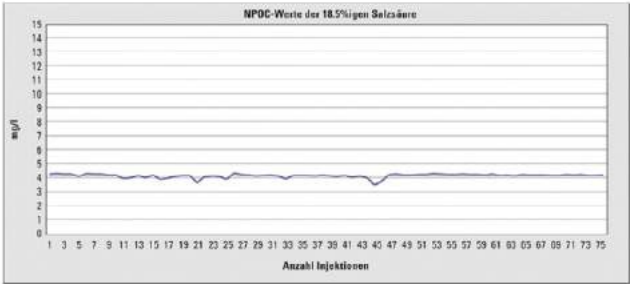


Fig.4: Result of longterm stability

Blank values and standards (10 ppm) were alternately measured between the individual measurements.

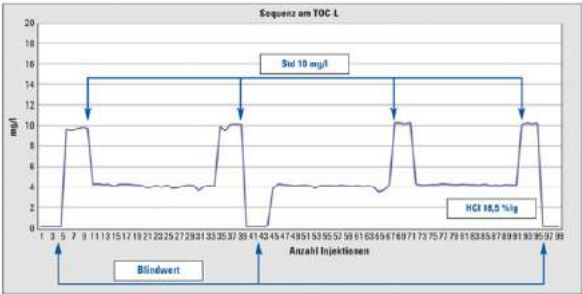


Fig. 5: Sequence of hydrochloric acid, blank (pure water) and Standards (10 mg/l)

#### ■ Recommended analyzer / configuration

- TOC-L<sub>CPH</sub> with a normal sensitive catalyst (without glass wool at the bottom of the catalyst tube)
- B-Type scrubber with SnCl<sub>2</sub> solution
- Copper bead scrubber with pH paper
- Bypassing the blank check vessel
- Substituting water for phosphoric acid (IC vessel)
- OCT-L 8-port sampler

## Application News

Sum parameter – Total Organic Carbon

### TOC – Determination in nitric acid

**No.** SCA-130-302

Organic contaminants present in basic chemicals may constitute the impurities in products. This is why quality control of the reactants is indispensable.



The determination of organic contaminations in concentrated nitric acid (69%) becomes a challenge when the required detection limit does not allow large dilution steps.

An example is the TOC determination in a 69%  $\text{HNO}_3$  solution with a detection limit of < 10 mg/L.

#### ■ Sample preparation

For sample preparation, the 69%  $\text{HNO}_3$  solution was diluted to a ratio of 1:10 with ultrapure water.

Compound (concentration)	Dilution	Conz. [%]
Nitric Acid (69%)	1 : 10 diluted with water (5ml / 50ml)	Ca. 7%

Calibration of the TOC-L system was carried out using the automatic dilution function in the range of 0.5 mg/L to 10 mg/L.

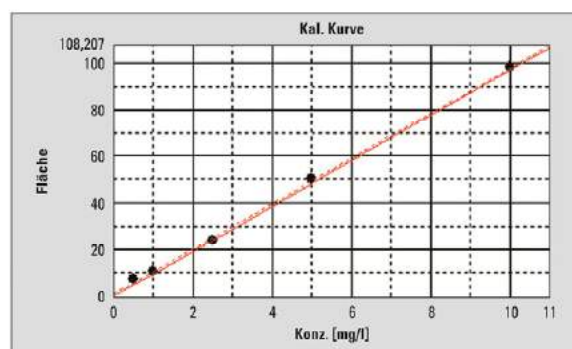


Fig. Multi-point calibration with dilution function

To protect the NDIR detector, the B-type scrubber was used together with the halogen scrubber.

#### ■ Matrix interferences

In addition to  $\text{CO}_2$ , various nitrogen oxides are formed from the organic components during the combustion of nitric acid. Excessively high levels of  $\text{NO}_3$  can lead to significant amounts of  $\text{N}_2\text{O}$  (nitrous oxide). Nitrous oxide exhibits absorption bands in the same IR detection range as  $\text{CO}_2$  and can, therefore, be misinterpreted for  $\text{CO}_2$ . In addition, nitrous oxide can cause tailing and can affect the peak symmetry.

Due to the high solubility of  $\text{N}_2\text{O}$  in water, the gas is dissolved in the B-type scrubber and will not reach the detector.

## ■ Result

The duplicate NPOC determination of a nitric acid produced the following results:

Sample	NPOC [mg/l]	RSD [%]
Nitric Acid (69%)	36,9	1,4
Nitric Acid (69%)	33,4	3,0

To investigate this matrix influence, an additional dilution (1:10) of a 69% nitric acid solution was carried out and a potassium hydrogen phthalate stock solution was subsequently added to increase the NPOC content by 5 ppm. (Note: This corresponds to an increase to 50 ppm for the 1:10 dilution).

Sample	NPOC [mg/l]	RSD [%]
Nitric Acid (69%)	25,1	1,3
Nitric Acid (69%) Spiked with 50 ppm KHP	76,2	1,8

The use of suitable gas washers (scrubbers) enables reproducible TOC measurements in concentrated nitric acid.



## ■ Recommended Analyzer / Configuration

TOC-L<sub>CPH</sub> with normal sensitive Catalyst

B-Type-Scrubber

OCT-L (8-port Sampler)

## Application News

**No. SCA-130-303**

Sum parameter – Total Organic Carbon

### TOC – Determination in sulfuric acid

Acids are a group of frequently used inorganic chemicals used in the chemical industry. In particular, sulfuric acid is used in a wide range of applications.



Sulfuric acid in a concentration range to 1% can be directly measured using a TOC-L analyzer. Higher sulfuric acid concentrations can lead to tailing and, consequently to increased measurement values because high sulfate concentrations (> 5000 mg/L) can lead to the formation of large amounts of SO<sub>2</sub> vapors. SO<sub>2</sub> exhibits absorption bands in the same IR detection range as CO<sub>2</sub> and can, therefore, be misinterpreted for CO<sub>2</sub>.

To determine organic contaminations in highly concentrated sulfuric acid, additional SO<sub>2</sub> scrubbers are used.

The following SO<sub>2</sub> scrubbers are available:

- Sulfix (WAKO Chemicals, Fuggerstr. 12, 41468 Neuss, Germany). The Sulfix scrubber is installed underneath the normal sensitive catalyst and enables selective filtration of the formed SO<sub>2</sub>.
- Mist scrubber (cartridge)  
Just like the halogen scrubber, the 'Mist scrubber' is used in the flow line for SO<sub>2</sub> absorption.

In the experiment described below, the NPOC content of a 98% sulfuric acid solution is determined.

The required purity criterion and the required limit of detection was < 10 mg/L.

#### ■ Sample preparation

The concentrated sulfuric acid was diluted with ultrapure water to a ratio of 1:10 to decrease the concentration as well as the viscosity of the sulfuric acid.

Compound (Concentration)	Dilution	Conc.
Sulfuric acid (98%)	1 : 10 diluted with water (5m/50ml)	Ca. 10%

The dilution has to be carried out with the utmost care and caution, as the sulfuric acid reacts violently upon the addition of water (heat generation).

The system is calibrated using the automatic dilution function in the range of 0.5 mg/L to 10 mg/L.

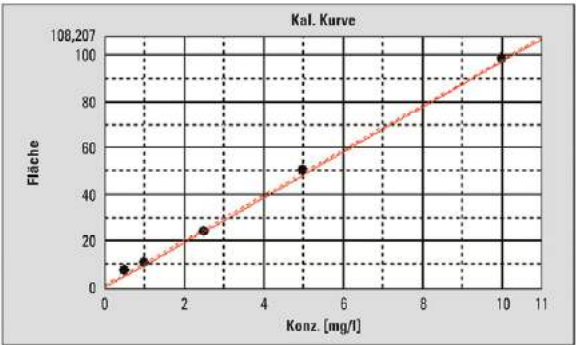


Fig. Multi-point calibration with dilution function

■ **Kit for high-salt samples**

For the determination, a TOC-L<sub>CPH</sub> equipped with a kit for high salt loads was used. The kit consists of a special catalyst tube, a special mixture of various catalyst beads and a ceramics grid, which replaces the platinum net.

Sample acidification when using the high-salt kit, is carried out with sulfuric acid. Sulfuric acid is used to modify the sample matrix. While NaCl has a melting point of 801 °C, the melting point of NaSO<sub>4</sub> is higher (881 °C). This has a positive effect on the lifetime of the combustion tube.

For this reason, sulfuric acid is measured directly using the high-salt kit.

■ **Result**

The duplicate determination of sulfuric acid yielded the following results:

Sample	NPOC [mg/l]	RSD [%]
Sulfuric acid (98%)	<10 (4,6)	-
Sulfuric acid (98%)	<10 (5,4)	-

The sulfuric acid fulfilled the required purity criteria of TOC < 10 mg/L.

The use of suitable gas washers (scrubbers) enables reproducible TOC measurements in concentrated sulfuric acid.



■ **Recommended analyzer / Configuration**

- TOC-L<sub>CPH</sub>
- OCT-L
- High-Salt-Kit
- B-Type-Scrubber with diluted hydrochloric acid with wire net.
- Mist-Scrubber



## Application News

Sum parameter – Total Organic Carbon

### TOC – Determination in brines

**No.** SCA-130-304

The determination in difficult matrices, such as brines or heavily contaminated wastewaters, presents a special challenge for TOC analyzers. In the chemical industry, brines with a salt load (NaCl) of up to 28% are used for chlor-alkali electrolysis. For this process it is important to know the TOC content.

The unique feature of this application does not inherently lie in the conversion of the carbon components to carbon dioxide, but in the salt load associated with the matrix. This leads to higher maintenance needs, as the salt can crystallize in the combustion system.

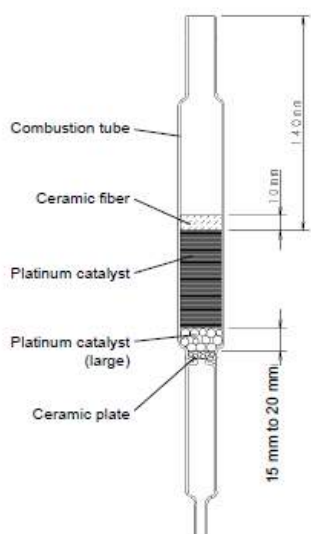
#### ■ Kit or high-salt samples

The TOC-L series features a kit for high-salt samples, which significantly increases the instrument's availability. The kit consists of a combustion tube of a special geometry and a unique catalyst mixture.

In this application, sample acidification is carried out with sulfuric acid. Sulfuric acid modifies the sample matrix. Whereas the melting point of NaCl is 801 °C, NaSO<sub>4</sub> has a higher melting point is (888 °C). The potassium salts of sulfuric acid also have a significantly higher melting point than those of hydrochloric acid. This extends the lifetime of the combustion tube.

Compound	Melting point
NaCl	801°C
KCl	773°C
Na <sub>2</sub> SO <sub>4</sub>	888°C
MgCl <sub>2</sub>	708°C
CaCl <sub>2</sub>	782°C
K <sub>2</sub> SO <sub>4</sub>	1.069°C

Tab. Melting point of different salts



#### ■ Sample preparation

The determination of organic contaminations in a pure brine (30% sodium chloride solution) is described below. For such highly concentrated salt solutions, the principle of diluting the sample as much as possible applies. As the required detection limit was at < 1 mg/L, the samples were diluted with ultrapure water to a ratio of 1:1. Dilution was carried out manually in a 50 mL volumetric flask under the addition of several drops of concentrated sulfuric acid (25%).



Compound (Concentration)	Dilution	Conc.
Brine solution (30%)	1 : 2 diluted with water (25ml/50ml) add. 1-2 drops Sulfuric acid until pH<7	ca. 15%ig

For the analysis a TOC-L<sub>CPH</sub> equipped with a kit for high salt loads was used. The system is calibrated using the automated dilution function in the range of 0.5 mg/L to 10 mg/L.

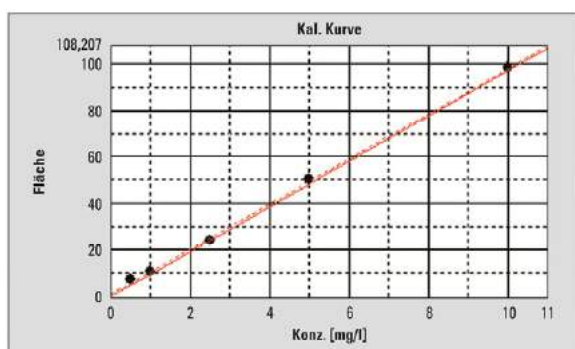


Fig. Multi-point calibration with dilution function

## Result

The duplicate determination of the TOC analysis yielded the following results:

Sample	NPOC [mg/l]	RSD [%]
Brine solution (30%)	3,6	1,8
Brine solution (30%)	3,6	1,8

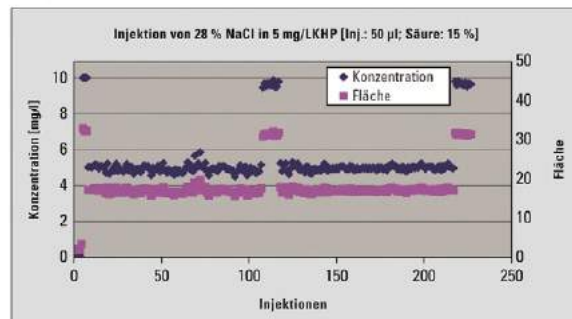
## Stability test

In this test, the long-term stability of the combustion system was tested. The system was calibrated to 10 mg/L with an injection volume of 50 µL.

A 28% NaCl solution was prepared and spiked with a KHP solution to obtain a 5 mg/L TOC solution and a 15% sulfuric acid solution was added.

Initially, a blank value and a control standard (10 mg/L) were measured, and the NaCl solution was subsequently injected.

The control standards were tested after 110 and 220 injections of the brine solution, respectively.



Maintenance of the combustion tube and the catalyst was not necessary after the measurements were completed. Only the TC-slider needed to be cleaned. The figure above shows the excellent reproducibility's and the stability of the measurement.



## Recommended Analyzer / Configuration

TOC-L<sub>CPH</sub>  
High-Salt-Kit  
B-Type-Scrubber

## Application News

**No.** SCA-130-305

Sum parameter – Total Organic Carbon

### TOC – Determination in sodium hydroxide solution

Organic contaminants in basic chemicals may lead to impurities in the products. Therefore, quality control of the reactants is necessary.



The TOC determination in sodium hydroxide can lead to various problems. The catalyst and the combustion tube wear out very rapidly. This, in turn, will lower the sensitivity at an equally fast rate and leads to very poor reproducibilities.

NaOH can also absorb CO<sub>2</sub> from the environment. As air contains approximately 400 ppm CO<sub>2</sub>, direct TC determination in sodium hydroxide can lead to much higher values. The NPOC method is, therefore, recommended for the determination of organic contaminations in sodium hydroxide. The sample should also be diluted as much as possible.

In the present case, a 50% sodium hydroxide solution was analyzed. The purity criterion and the required limit of detection was < 10 mg/L.

#### ■ Sample Preparation

The sample was first manually diluted to a ratio of 1:10 with ultrapure water and a suitable amount of acid.

Several mL of ultrapure water were placed in a 50 mL volumetric flask. Subsequently, 5 mL of the concentrated sodium hydroxide was pipetted into the flask. Finally, concentrated sulfuric acid was added until the solution has reached a pH < 2. The flask was then filled with ultrapure water up to the mark. The addition of sodium hydroxide, as well as the addition of sulfuric acid to the water must be done with the utmost care and caution, as a violent chemical reaction occurs.

Compound (Concentration)	Dilution	Conz. [%]
Sodium hydroxide solution (50%)	1 : 10 diluted (5 ml / 50 ml) add. 1-2 drops Sulfuric acid until pH<7 (Note: generation of heat)	approx. 5% + Sulfuric acid

Calibration of the TOC-L system was carried out using the automatic dilution function within the range of 0.5 mg/L to 10 mg/L.

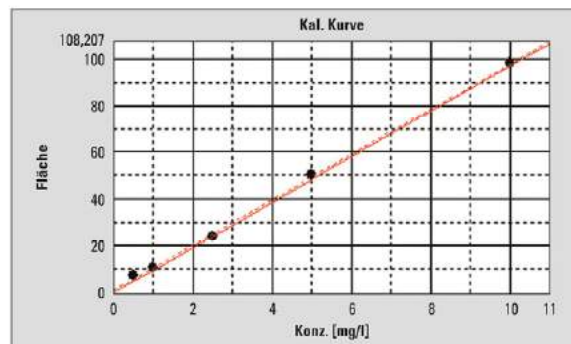
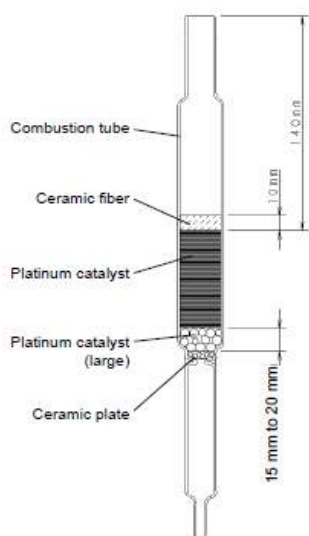


Fig. Multi-point calibration with dilution function

### ■ Kit for high salt samples

For the determination, a TOC-L<sub>CPH</sub> was equipped with a kit for high salt loads. The kit consists of a special catalyst tube, a special mixture of various catalyst beads and a ceramics grid, which replaces the platinum net.



When using the high-salt kit, sample acidification is carried out with sulfuric acid, which is used here to modify the sample matrix. Compared to NaCl with a melting point of 801 °C, the melting point of NaSO<sub>4</sub> is higher (881 °C) which extends the lifetime of the combustion tube.

### ■ Results

The 5% sodium hydroxide can now be measured using the NPOC method. The duplicate determination of the sodium hydroxide yielded the following results.

Sample	NPOC [mg/l]	RSD [%]
Sodium hydroxide (50%)	<10 (8,2)	-
Sodium hydroxide (50%)	<10 (8,3)	-

The sodium hydroxide met the required purity criteria of < 10 mg/L TOC.

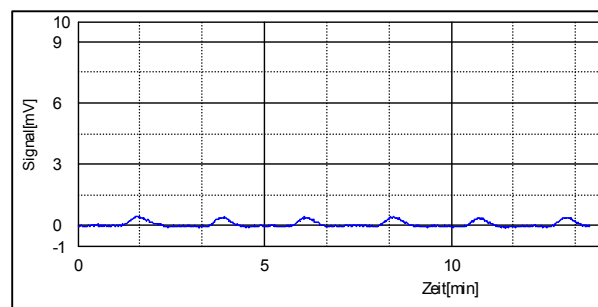


Fig. Example peaks of 50% sodium hydroxide solution



### ■ Recommended Analyzer / Configuration

TOC-L<sub>CPH</sub>  
OCT-L (8-port samples)  
High-Salt-Kit  
B-Type-Scrubber

## Application News

Sum parameter – Total Organic Carbon

### TOC – Determination in soda solution

**No.** SCA-130-306

Impurities in products can be caused by organic contaminants present in basic chemicals to. That is a reason why quality control of the reactants is indispensable.



In the determination of organic contaminations in concentrated soda solutions, various issues must be considered. In comparison to organic carbon, the soda solution to be investigated has a very high inorganic carbon content in the form of carbonates. In addition, the solution has a high pH value and tends to absorb carbon dioxide from the air.

A soda solution must, therefore, be analyzed using the NPOC method.

In the case described here, a 50% soda solution was investigated. The required detection limit was 10 mg/L.

#### ■ Sample preparation

The sample was first manually diluted to a ratio of 1:10 with ultrapure water and a corresponding amount of acid. Several mL of ultrapure water were placed in a 50 mL volumetric flask. Subsequently, 5 mL of the concentrated soda solution was pipetted into the flask. Finally, concentrated sulfuric acid was added until the solution has reached a pH < 2.

The flask was then filled with ultrapure water up to the mark.

Compound (Concentration)	Dilution	Conc.
Soda hydroxide solution  (50%)	1 : 10 diluted with water (5ml/50ml)  add. 1-2 drops Sulfuric acid until pH<7	Approx. 5%

**Caution:** During the addition of the sulfuric acid, the carbonates decompose under a violent reaction (heat dissipation / gas formation).



Calibration of the TOC-L system was carried out using the automatic dilution function in the range of 0.5 mg/L to 10 mg/L.

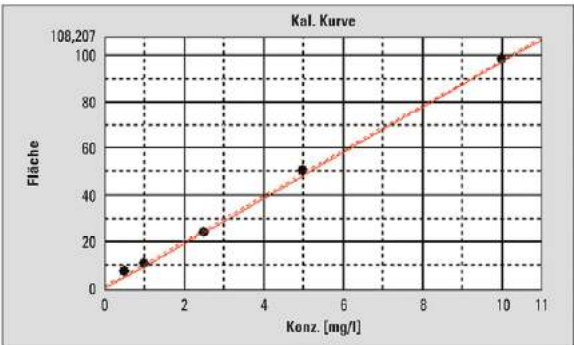
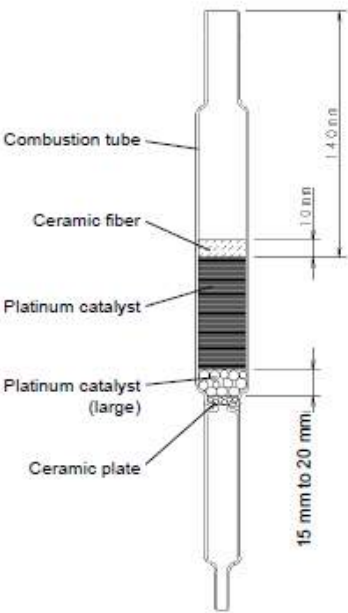


Fig. Multi-point calibration with dilution function

For the determination, a TOC-L<sub>CPH</sub> was equipped with a kit for high salt loads. A special catalyst tube, a special mixture of various catalyst beads and a ceramics grid, which replaces the platinum net are part of the kit.



Sample acidification when using the high-salt kit, is carried out with sulfuric acid in order to modify the sample matrix.

The higher melting point point of NaSO<sub>4</sub> (881 °C) compared to NaCl (801 °C) has a positive influence on the lifetime of the combustion tube.

■ Results

The duplicate determination of the soda solution yielded the following results:

Sample	NPOC [mg/l]	RSD [%]
Soda solution (50%)	56,4	7,1
Soda solution (50%)	54,8	4,9

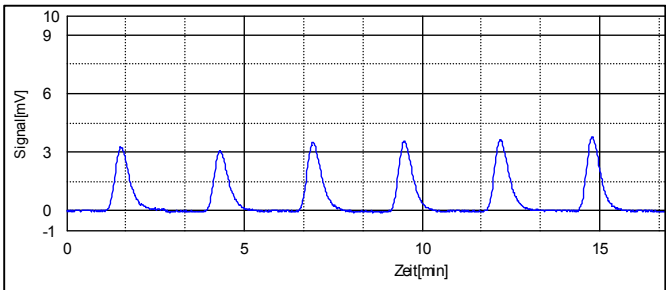


Fig. Peak graphs of a diluted soda solution (ca.5%)



■ Recommended Analyzer / Configuration

- TOC-L<sub>CPH</sub>
- ASI-L
- High-Salt-Kit
- B-Type- Scrubber

## Application News

**No.** SCA-130-307

Sum parameter – Total Organic Carbon

### TOC – Determination in ammonia or ammonium salt solutions

Basic chemicals may contain organic contaminants polluting end products. This is why quality control of the reactants is a must.

In the TOC determination of ammonia water or concentrated ammonium salt solutions, various issues must be considered. Ammonia and some ammonium salts are alkaline. The catalyst and combustion tube are sensitive to alkaline media and are subjected to increased wear.



The solutions should, therefore, be acidified and possibly be diluted.

The decomposition during oxidation of the ammonium or ammonia proceeds to completion without the formation of residues on the catalyst. Therefore, it is not necessary to use a high-salt kit.

In the case described below, the NPOC content of a 40% ammonium nitrate solution was determined. The required detection limit was < 10 mg/L.

#### ■ Sample preparation

The ammonium nitrate solution was diluted with ultrapure water to a ratio of 1:10. Dilution was carried out manually in a 50 mL volumetric flask under addition of several drops of concentrated sulfuric acid (25%).

Compound (Concentration)	Dilution	Conc.
Ammonium nitrate solution (40%)	1 : 10 diluted (5 ml / 50 ml) add. 1-2 drops Sulfuric acid until pH<7 (Note: generation of heat)	Approx. 4%

Calibration of the TOC-L system was executed using the automatic dilution function in the range of 0.5 mg/L to 10 mg/L.

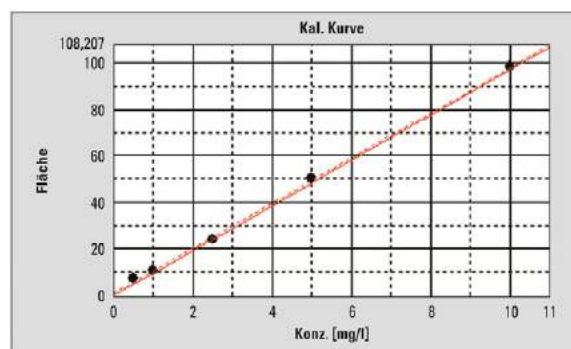


Fig. Multi-point calibration with dilution function



### ■ Interferences

In addition to CO<sub>2</sub> formed from the organic components, various nitrogen oxides are formed during the combustion of ammonium salts or ammonia water. Excessively high nitrogen levels can lead to the formation of significant amounts of N<sub>2</sub>O (nitrous oxide). Nitrous oxide exhibits absorption bands in the same IR detection range as CO<sub>2</sub> and can, therefore, be misinterpreted for CO<sub>2</sub>. In addition, nitrous oxide can cause tailing and can affect the peak symmetry.

A B-type scrubber is used to eliminate possible interference by nitrous oxide. Due to the high solubility of N<sub>2</sub>O in water, the gas is dissolved in the B-type scrubber and will not reach the detector.

### ■ Results

The duplicate determination of the ammonium nitrate solution yielded the following results:

Probe	NPOC [mg/l]	RSD [%]
Ammonium nitrate solution (40%)	56,5	0,8
Ammonium nitrate solution (40%)	56,7	1,2

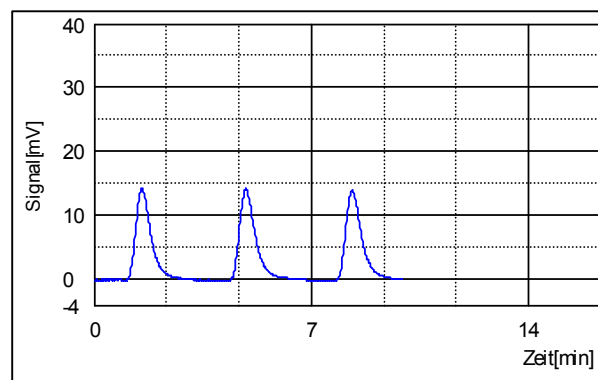


Fig. Example peaks of 40% ammonium nitrate solution



### ■ Recommended analyzer / Configuration

TOC-L CPH

OCT-L (8-port sampler)

B-Type- Scrubber

## Application News

**No.** SCA-130-308

Sum parameter – Total Organic Carbon

### TOC – Determination in sodium nitrate and sodium nitrite

Basic chemicals may contain organic contaminants influencing the quality of products. Quality control procedures of the reactants are, therefore, necessary in order to detect impurities.

For the determination of organic contaminations in salts, solutions of these salts can be prepared and subsequently measured using a TOC-L analyzer.



High salt concentrations generally present a problem for TOC analysis. These salts can crystallize in the combustion system and lead to higher maintenance needs.

In the case described below, the NPOC content of two salts was determined. The difficulty was the required detection limit of 10 mg/kg.

#### ■ Sample preparation

For sample preparation, 5 g of both salts (sodium nitrite and sodium nitrate) were weighed into a 50 mL volumetric flask and diluted with ultrapure water. During dilution, the solutions were acidified with concentrated sulfuric acid (25%).

Compound (Concentration)	Dilution	Conz.
Sodium nitrate (>99,9%)	Weighted Sample 5 g / 50 ml add. 1-2 drops Sulfuric acid until pH<7	approx. 10%
Sodium nitrite (>99,9%)	Weighted Sample 5 g / 50 ml add. 1-2 drops Sulfuric acid until pH<7 Caution: Nitrogen oxide gas is released	approx. 10%

Caution: Nitrite salts react to form of toxic nitrous gases. Sample preparation should, therefore, always be carried out under a hood. The samples should only be removed from the hood, when no more nitrous gases escape.

Calibration of the TOC-L system was done applying the automatic dilution function in the range of 0.5 mg/L to 10 mg/L.

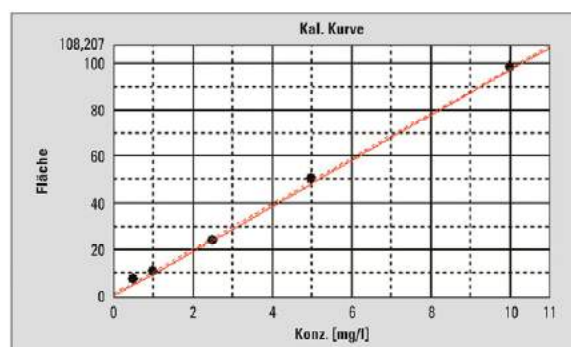
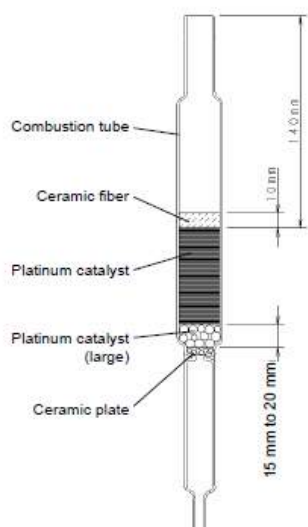


Fig. Multi-point calibration with dilution function

### ■ Kit for high-salt samples

The TOC-L series features a kit for high-salt samples, which significantly increases the instrument's availability. The kit consists of a combustion tube of a special geometry and a unique catalyst mixture.



In this application, sample acidification is carried out with sulfuric acid which is used to modify the sample matrix. Due to the higher melting point of  $\text{NaSO}_4$  (888 °C) compared to 801 °C of  $\text{NaCl}$  the lifetime of the combustion tube is longer.

### ■ Interferences

The combustion of nitrogen compounds can lead to the formation of nitrous oxide gas. Nitrous oxide exhibits absorption bands in the same IR detection range as  $\text{CO}_2$  and can, therefore, be misinterpreted for  $\text{CO}_2$ . In addition, nitrous oxide can cause tailing and can affect the peak symmetry.

A B-type scrubber is used to eliminate possible interference by nitrous oxide. Due to the high solubility of  $\text{N}_2\text{O}$  in water, the gas is dissolved in the B-type scrubber and will not reach the detector.

### ■ Results

The duplicate determination of the salt solutions yielded the following results:

Sample	NPOC [mg/kg]	RSD [%]
Sodium nitrate (>99,9%)	22,8	4,7
Sodium nitrate (>99,9%)	24,0	6,8
Sodium nitrate (>99,9%)	<10 (9,0)	-
Sodium nitrate (>99,9%)	10,2	5,4

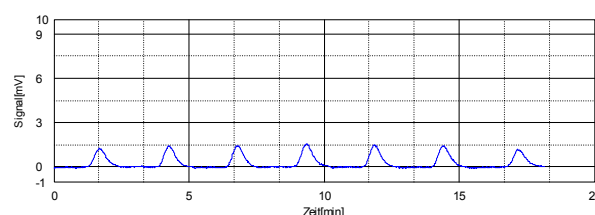


Fig. Example peaks: Sodium nitrate



### ■ Recommended Analyzer / Configuration

TOC-L<sub>CPH</sub>  
ASI-L  
High-Salt-Kit  
B-Type-Scrubber

## Application News

No. SCA-130-309

Sum parameter – Total Organic Carbon

### TOC determination in phosphoric acid

Phosphoric acid is one of the most frequently used inorganic acids in industrial applications. It is applied as starting material for the manufacture of phosphate-containing fertilizers as well as for the production of water-softening agents such as detergent additives.

Phosphoric acid is also used in the food industry – as acidification agent and preservative in beverages or as antioxidant in meats and meat products.



Particularly for these types of applications, it is important to apply acids that are pure and free from foreign substances. Manufacturers and processors of phosphoric acids are increasingly using the TOC (Total Organic Carbon) sum parameter for quality control. This parameter is a measure of the contamination of phosphoric acids by organic components.

The TOC method by using the catalytic combustion is not suitable for the determination of phosphoric acid,

because the phosphoric acid damages the combustion tube and the catalyst.

Due to this, the wet chemical TOC method is used to measure TOC in phosphoric acid.

#### ■ Wet-chemical UV oxidation at 80 °C

The determination of the TOC content in phosphoric acid is carried out via wet-chemical UV oxidation using Shimadzu's TOC-V<sub>WP</sub>.



Its core technology is the powerful oxidation applying a combination of sodium persulfate and UV oxidation at 80 °C. This ensures that all dissolved carbon compounds are converted to CO<sub>2</sub>.

In the presence of persulfate ions and UV illumination, OH-radicals are formed which have a strong oxidative effect and convert organic compounds to carbon dioxide. A carrier gas transports the carbon dioxide formed to the NDIR detector where they are detected.



Automated reagent preparation eliminates any contamination of the reagent solutions and minimizes the blank value of the instrument.

#### ■ TOC determination

Due to lower TOC concentration, the instrument is calibrated in a range of 0,1 – 1 mg/L.

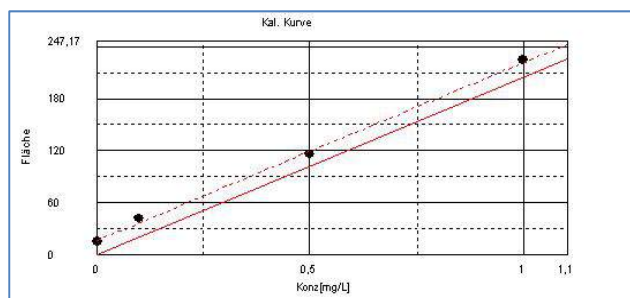


Figure: Calibration of NPOC between 0,1 – 1 mg/l.

Concentration of the phosphoric acid does not play a significant role in the determination; it is only necessary to ensure that the acid is not too viscous. The 85% phosphoric acid solution was therefore diluted 1:5 with water.

The resulting 17% acid solution was transferred into the instrument using an OCT-1 autosampler.



The autosampler OCT-1 has a big advantage for the measurement of aggressive matrices, because its parts are done of Teflon.

#### ■ Method of phosphoric acid measurement

The concentrated phosphoric acid (85%) is diluted by 1:5.

TOC determination in phosphoric acid was carried out using the NPOC (Non-Purgeable Organic Carbon) method. Prior to TOC determination, neutral or alkaline samples are acidified in order to decompose all inorganic carbonates and bicarbonates. This step could be omitted for phosphoric acid.

Acidification: 0%  
Spurge-time: 2 minutes  
Injection volume: 3000µl

#### ■ Results

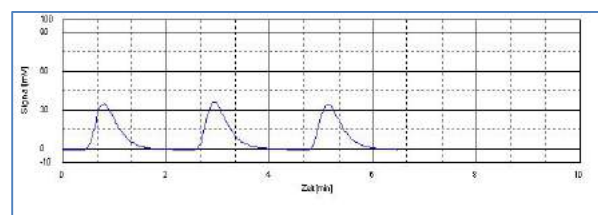


Abb.: Peak graph of diluted phosphoric acid(17%)

The 17% phosphoric acid solution measured in this way resulted in a TOC concentration of 0.61 mg/L. The relative standard deviation over three injections was 1.8%.

#### ■ Recommended Analyser / Configuration

- TOC-V<sub>WP/WS</sub>
- OCT-1

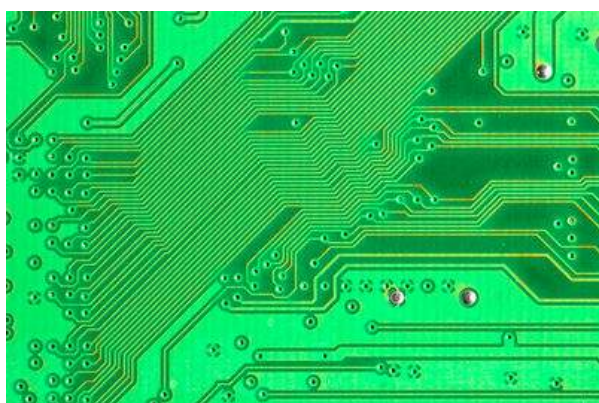
## Application News

**No.** SCA-130-310

Sum parameter – Total Organic Carbon

### TOC – Determination in diluted hydrofluoric acid

Hydrofluoric acid is the only acid that attacks glass (glass etching). Because of this chemical property, it plays a distinct role in several industrial processes, for instance in the manufacturing of solar cells and wafers as well as in microchip production. Hydrofluoric acid is the most widely used etching agent in the semiconductor industry.



When carrying out etching processes, it is important to ensure that the etching agent used will etch the respective layers and not leave any contaminants.

This raises questions on the impurities of etching agents, where both the purity of the starting acid and that of the etching solutions after the etching process are of interest.

To determine the degree of contamination, the TOC parameter is particularly suitable, as it is a sum parameter that detects all organic carbon compounds.

#### ■ TOC determination

In the following measurement, a 4% hydrofluoric acid was manually diluted to 1:10 with water and measured using the TOC-L<sub>CPH</sub>. Given the acidity of the hydrofluoric acid, the IC content can be neglected. With regard to the dilution, the solution was slightly acidified and sparged for 3 minutes. The NPOC was subsequently determined by means of combustion oxidation.

An aliquot of the sample is injected onto a hot (680 °C) platinum catalyst. The organic substances are converted to CO<sub>2</sub> and detected via an NDIR detector.

#### ■ Calibration

Due to mostly working in a small measuring range, calibration was carried out in a range of 0.25 mg/L – 5.0 mg/L. For dilutions, the automatic dilution function of the TOC-L system was applied. The injection volume was 150 µL respectively.

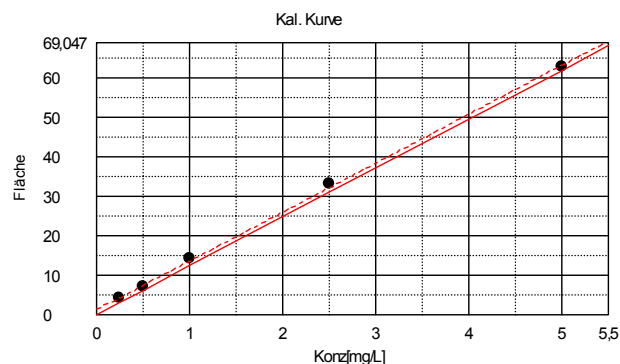


Figure: Calibration curve, TC 5 mg/L.



### ■ Measurement example

A total of 3 different hydrofluoric acids (0,4%) were measured:

- Hydrofluoric acid prior to etching (HF1)
- Hydrofluoric acid after etching (a seemingly clean wafer (HF2))
- Hydrofluoric acid after etching (a seemingly dirty wafer (HF3))



### ■ NPOC method

Acidification: 1.5%  
Purging time: 3 minutes  
Injection volume: 150 µL  
Number of injections: 3

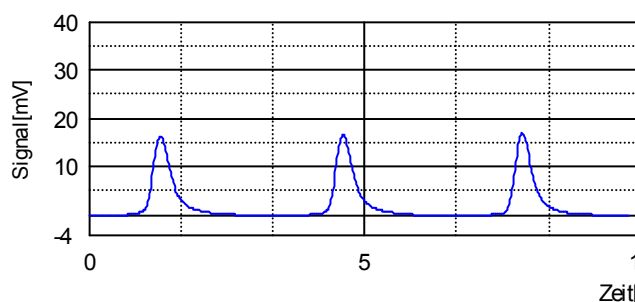


Figure: Peaks of the diluted HF solution.

The measurements were already stable after two or three injections. It is advantageous to carry out several HF injections prior to the actual sample measurement.

### ■ Results

Sample	NPOC [mg/L]	RSD [%]
HF 1	2.42	4.8
HF 2	3.09	3.2
HF 3	4.38	2.1

### ■ Protection and safety

For such measurements, comprehensive protective measures for dealing with hydrofluoric acid must be urgently observed. This also includes wearing protective clothing, gloves and safety goggles.

After measurement, the instrument must be rinsed several times with water. In addition, 20 injections with ultrapure water must be carried out.

Nevertheless the lifetime of syringe, combustion tube and catalyst will be shortening, due to HF solution.

### ■ Recommended instrument/ equipment

TOC-L<sub>CPH</sub> / CPN  
OCT-L

## Application News

**No.** SCA-130-501

Sum parameter – Total Organic Carbon

### TOC – Determination methods according to EN 1484

The EN 1484 standard “Guidelines for the determination of total organic carbon (TOC) and dissolved organic carbon (DOC)” defines various terms and parameters.

#### ■ Definitions according to EN 1484

**TC:** Total carbon – the sum of organically bound and inorganically bound carbon present in water, including elemental carbon.

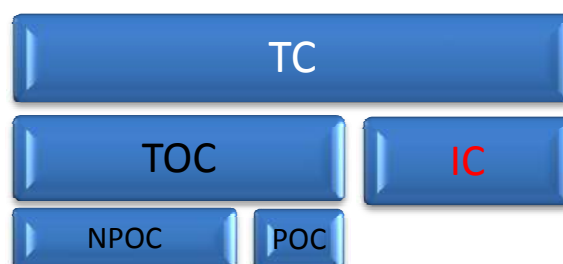
**TIC:** Total inorganic carbon – the sum of carbon present in water, consisting of elemental carbon, carbon monoxide, carbon dioxide (also carbonates and hydrogen carbonates), cyanide, cyanate, and thiocyanate. TOC instruments mainly detect CO<sub>2</sub>, originating from hydrogen carbonates and carbonates, just like TIC.

**TOC:** Total Organic Carbon – organically bound carbon present in water, bonded to dissolved or suspended matter. Cyanate, thiocyanate and elemental carbon are also determined.

**POC:** Purgeable Organic Carbon – the TOC content that is purgeable under the conditions of this method.

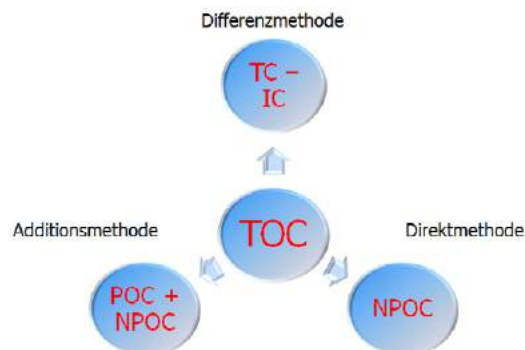
**NPOC:** Non Purgeable Organic Carbon – the TOC content that is not purgeable under the conditions of this method.

The following graph shows how the parameters are linked:



#### ■ Determination methods

The TOC can be determined according to three different methods:



#### ■ Difference method

For the difference method, the parameters TC and IC are measured. The TOC is then determined by way of calculation.

**TC:** The analysis of the total organic carbon is carried out via oxidation (thermal or wet-chemical) and subsequent determination of the resulting carbon dioxide using NDIR detection.

**TIC:** Through acidification of the sample using a mineral acid at room temperature and subsequent NDIR detection of the expelled carbon dioxide the inorganic carbon is detected.

The TOC is calculated from the difference between TC and TIC:  $TOC = TC - TIC$

#### ■ Limitations of the difference method

The inorganic carbon content may not be too high in comparison to the TOC.

Error propagation can result in a high level of uncertainty for the calculated TOC value. The EN 1484 standard recommends that the TOC value, when using the differential method, should be higher or equal to the TIC value ( $TOC \geq TIC$ ).

#### Example:

TC – Value = 100 mg/l (RSD = 2%)  $\pm$  2 mg/l  
(98 – 102 mg/l)

IC – Value = 98 mg/l (RSD= 2%)  $\pm$  1,96 mg/l  
(96,04 – 99,96mg/l)

$TOC = 2 \text{ mg/l} \pm 3,96\text{mg/l}$  (- 1,96 - 5,96 mg/l)

Due to error propagation, the total error is  $\pm$  3.96 mg/L.

According to the difference method, the error of the total result is larger than the calculated TOC content! In the worst case, this can result in a negative TOC value.

#### ■ Addition method

For the addition method, the parameters POC and NPOC are measured. The TOC is then calculated.

**POC:** Degassing of the volatile compounds with subsequent catalytic combustion at 680°C and determination of the resulting carbon dioxide using NDIR detection.

**NPOC:** Measurement of the non-purgeable organic compounds, after POC analysis using catalytic combustion at 680°C and subsequent determination of the resulting carbon dioxide using NDIR detection.

The TOC is calculated via addition:

$$TOC = POC + NPOC$$

#### ■ Direct method

For the direct or NPOC method, it is assumed that the sample does not contain any significant amounts of volatile or purgeable organic compounds. According to this assumption, the TOC is directly determined as NPOC.

**NPOC:** Acidification of the sample using a mineral acid (for instance HCL) to a pH < 2, whereby carbonates and hydrogen carbonates are completely converted to carbon dioxide. The carbon dioxide is removed from the sample solution via a sparge gas. Direct NPOC measurement (similar to TC measurement) via oxidation to CO<sub>2</sub>. Subsequent NDIR detection.

The TOC corresponds to the NPOC:

$$TOC = NPOC$$



## Application News

**No.** SCA-130-502

Sum parameter – Total Organic Carbon

### Determination of the purgeable organic carbon (POC)

According to EN 1484, which contains the instructions for TOC determination, the POC (purgeable organic carbon) is the TOC content that can be expelled under the conditions of this method. This information is very unspecific and should be described here in more detail.

The instruments in the TOC-L series can be extended with an option to include measurement of the POC parameter. The core feature of this option is the LiOH trap, which is placed in the flow line of the analyzer.



For POC determination, the sample is aspirated using the TOC-L injection syringe, acidified with HCL and subsequently purged using carrier gas. In this step, CO<sub>2</sub> originating from carbonates and hydrogen carbonates as well as all volatile organic compounds (POC) are purged from the solution. The LiOH trap binds the CO<sub>2</sub> from the gas mixture (originating from the TIC). The volatile compounds pass the trap and reach the catalyst.

Here, the volatile organic compounds are converted to CO<sub>2</sub> and detected via NDIR detector.



Fig. The addition method (NPOC + POC)

During the course of the addition method, the remainder is used for NPOC determination. However, in the drinking water application or ultrapure water application, the POC content is completely negligible. Here, TOC = NPOC

The POC can, nevertheless, play an important role in wastewaters, particularly in industrial effluents.

#### ■ Calibration

Particular attention should be paid to calibration of the POC. Standards that are prepared with volatile, purgeable organic substances are inherently very unstable. This is why IC standard solutions (prepared from carbonates and/or hydrogen carbonates) are used for POC calibration. Sampling of the IC solutions for POC determination is carried out using the TOC-L injection syringe. The IC solution is acidified in the syringe. The inorganic substances of the standard solution are converted to CO<sub>2</sub> and transferred to the NDIR detector using a carrier gas.

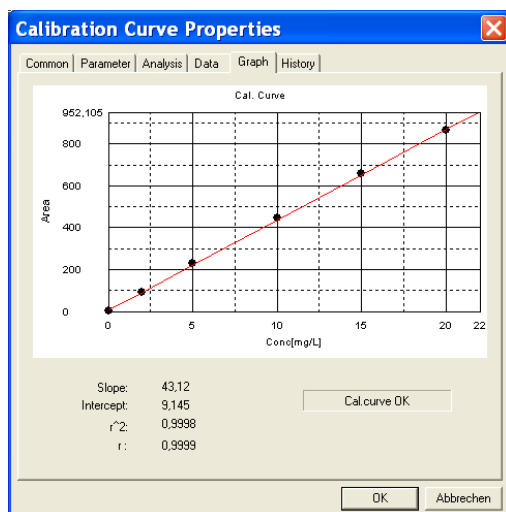


Fig. POC-Calibration with IC-standard

### ■ System testing

In POC analysis, it is of great importance that the LiOH trap functions perfectly. A test should, therefore, be carried out to confirm the efficiency of the CO<sub>2</sub> trap. This test should be carried out each working day:

An IC control solution (TIC = 1000 mg/L) is prepared and analyzed as a POC sample. For efficient functioning of the LiOH trap, the POC measuring result must be < 0.1 mg/L.

### ■ Example of a POC measurement

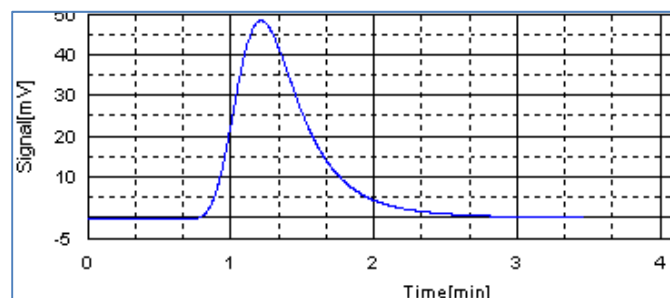
Sample: Toluene in ultrapure water

Toluene is a compound that is fully purgeable. In the addition method, the toluene sample is completely determined as POC.

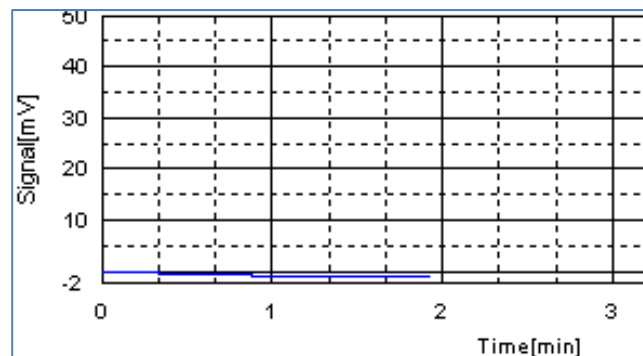
### POC measuring method:

Injection volume: 800  $\mu$ L  
Purging time: 3 min

### POC-Peak:



### NPOC-Peak:



### Result:

TOC=4,05mg/l

POC=4,05mg/l => 100%

NPOC=0mg/l

### ■ Recommended Analyzer / Configuration

TOC-L<sub>CXX</sub>  
ASI-L  
POC-Option

## Application News

Sum parameter – Total Organic Carbon

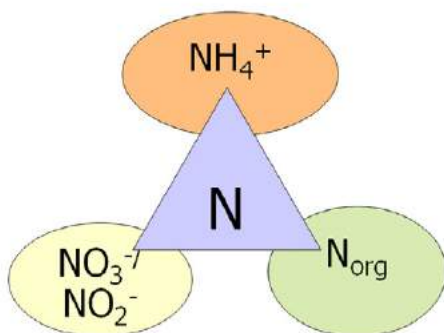
TN<sub>b</sub> – total bound nitrogen

**No.** SCA-130-503

Although nitrogen compounds are essential for nature and the environment, high nitrogen depositions can lead to problems. Nitrogen compounds enter the environment primarily through agricultural processes. Nitrogen-containing fertilizers constitute the largest proportion. But nitrogen compounds can also enter the environment via chemical industrial processes.

Excessively high concentrations of nitrogen compounds in the environment can cause eutrophication of water bodies. Eutrophication is the process of uninhibited growth of algae and other organisms due to an excess supply of nutrients. This overgrowth results in a lack of oxygen in the water, which can lead to fish mortality and to the formation of aquatic dead zones.

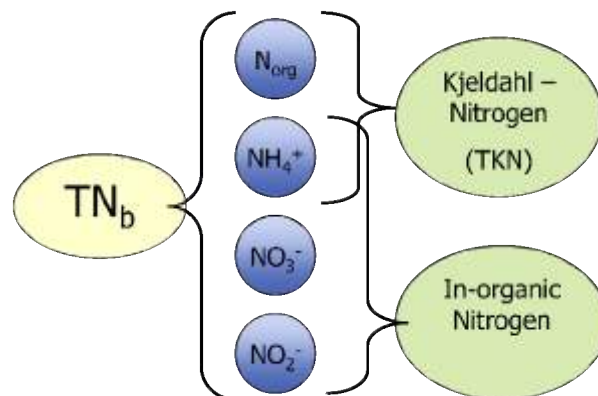
Bound nitrogen occurs in nearly all waters, mostly in the form of ammonia, nitrate, nitrite or organic compounds.



### ■ Total nitrogen TN<sub>b</sub>

The variety of possible nitrogen compounds necessitated the definition of a sum parameter that represents the total nitrogen compounds. For this purpose, the so-called TN<sub>b</sub> (total bound nitrogen) was defined and standardized.

The TN<sub>b</sub> is the total nitrogen content of a sample in the form of ammonium, nitrite, nitrate, as well as organic compounds. The TN<sub>b</sub> does not include dissolved or gaseous nitrogen (N<sub>2</sub>). A differentiation between inorganic and organic nitrogen compounds is, by definition, not possible.



### ■ Determination according EN 12260

EN 12260 describes the determination of nitrogen in the form of free ammonia, ammonium, nitrite, nitrate and organic compounds that can be converted under the described oxidative conditions.



The conversion of the nitrogen containing compounds takes place via combustion in an oxygen atmosphere higher than 700 °C to nitrogen oxide, which reacts with ozone to activated nitrogen dioxide (NO<sub>2</sub>\*). In the subsequent reaction to NO<sub>2</sub>, light quanta are emitted (chemiluminescence) that are measured by the detector.

#### ■ Simultaneous TN determination using the TNM-L

Based on the similar oxidation process, the TN<sub>b</sub> determination can be carried out simultaneously with the TOC measurement. For this application, the TNM-L option is installed on the top of the main TOC-L system.



Fig. TOC-L CSH with TNM-L Modul

The benefit is that no additional laboratory space is required.

For the simultaneous determination, the sample is injected onto the catalyst at 720 °C. All carbon atoms present in the sample are converted to CO<sub>2</sub> and, in parallel, the nitrogen atoms to NO. The gas mixture is then transported by the carrier gas stream through the NDIR detector, where the carbon dioxide content is measured.

Subsequently, the gas mixture enters the chemiluminescence detector, connected in series, where the nitrogen content is determined (See Figure below).

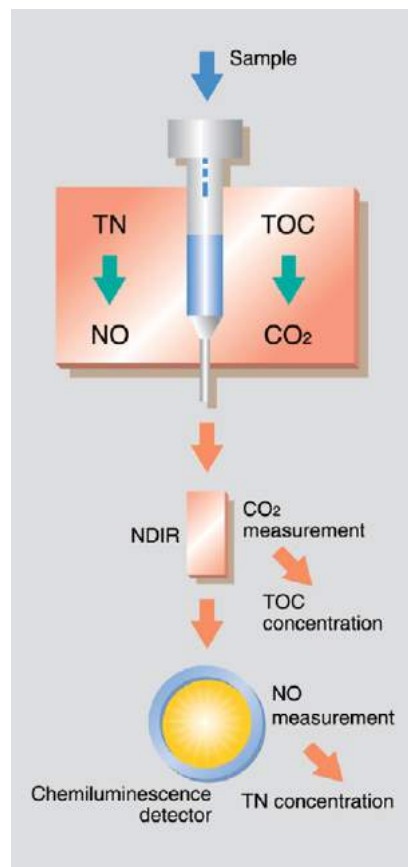


Fig. Simultaneous TOC/TN-Determination

It should be noted that an optimal injection volume must be selected for both parameters.

#### ■ Recommended Analyzer / Configuration

TOC-L <sub>CXX</sub> with TNM-L  
ASI-L

## Application News

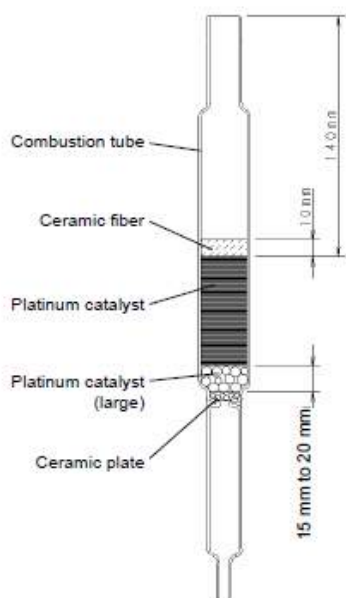
Sum parameter – Total Organic Carbon

### Kit for high-salt samples

#### No. SCA-130-504

Samples with high-salt loads generally are a problem for TOC analysis. The problem is less the conversion of organic compounds to CO<sub>2</sub> than the effects of the salt on the catalyst. This leads to higher maintenance needs, as the salt can crystallize in the combustion system.

In many applications for the instruments in the TOC-L and the TOC-4110/4200 series, the kit for salt-containing samples is an important component. It consists of a combustion tube of a special geometry and a unique mixture of catalyst beads.



#### ■ Sample preparation

In this application, sample acidification is carried out with sulfuric acid which is used to modify the sample matrix.

While NaCl has a melting point of 801 °C, the melting point of Na<sub>2</sub>SO<sub>4</sub> is higher (888 °C). The potassium salts of sulfuric acid also have a significantly higher melting point than those of hydrochloric acid. This has a positive effect on the lifetime of the combustion tube.

Compound	Melting point
NaCl	801°C
KCl	773°C
Na <sub>2</sub> SO <sub>4</sub>	888°C
MgCl <sub>2</sub>	708°C
CaCl <sub>2</sub>	782°C
K <sub>2</sub> SO <sub>4</sub>	1.069°C

Tab. Melting point of different salts

Results indicate that the stability of the catalyst is increased, and that up to 12 times the number of samples can be measured before the catalyst must be exchanged and the instrument needs servicing.



Fig. Catalyst filling

## ■ Endurance test

To determine the performance of this option, a brine solution was measured in a long-term test. For this purpose, a 28 % NaCl solution (matrix adapted with a 15 % sulfuric acid solution and spiked to a 5 ppm TOC solution using a KPH solution) was injected 220 times. Initially, a blank value and a control standard with 10 ppm TOC were measured. The control standards were tested after 110 and 220 injections, respectively. The injection volume was 50 µL.

The following figure shows the excellent reproducibilities and the stability of the measurement.

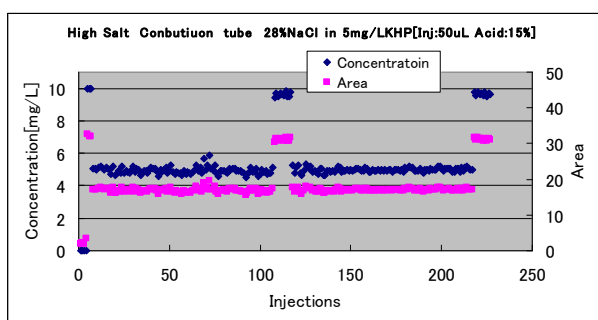


Fig. Results of endurance test

## ■ Related application

The high-salt kit is used for many different applications in order to keep the maintenance need for difficult matrices as low as possible.

Examples:

- 104 TOC-Determination in seawater
- 304 TOC-Determination in brine solution
- 306 TOC-Determination in soda solution
- 308 TOC-Determination in sodium nitrate
- 603 TOC-Determination in chemical industry



## ■ Recommended Analyzer / Configuration

TOC-L CXX

ASI-L

Kit for high-salt samples

B-Type Scrubber

(At very high halogen concentrations in the matrix, the B-type scrubber is recommended. This scrubber protects the detector cell of the NDIR detector.)

## Application News

**No.** SCA-130-507

Sum parameter – Total Organic Carbon

### Calibration with automatic dilution function



The core feature of the TOC-L series is the ISP module (Integrated Sample Pretreatment). The ISP module consists of an 8-port valve and a syringe with sparging gas connector. In addition to acidification and sparging in the syringe, the system enables automated dilution. This allows for the wide measuring range, dilutes highly polluted samples and enables the creation of dilution series from a stock solution. The various possibilities offered by the ISP module thus reduce the time expenditure by the user.

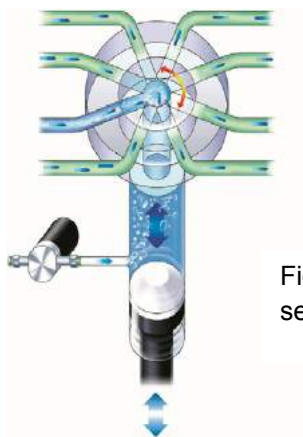
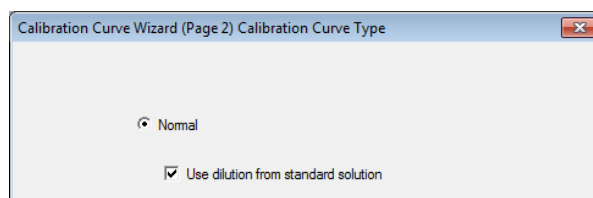


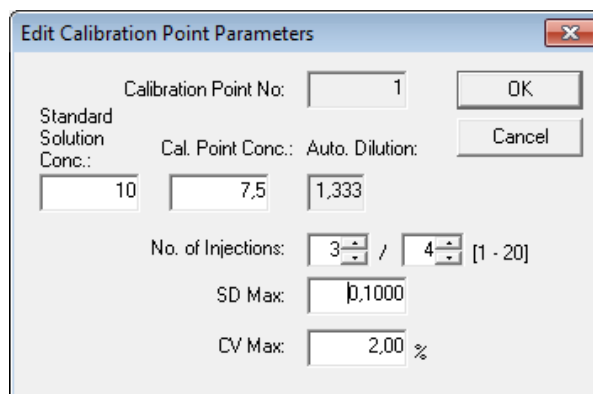
Fig. ISP-Module of TOC-L series

#### ■ Calibration with automatic dilution function

To create calibration curves, the dilution function is activated via the wizard:



When filling the data of the calibration points, the concentration of the standard solution (stock) is entered first, followed by the desired calibration curve point. The software calculates the required dilution factor:



Since fractional factors are allowed, it is possible to create a 10-point calibration curve with equidistant concentration intervals from one standard solution.

The following figure shows the list of calibration points of a 10-point calibration curve in the range of 1 to 10 mg/L:

Calibration Curve Properties

Common | Parameter | Analysis | Data | Graph | History

Inj. Volume: 50  $\mu$ l

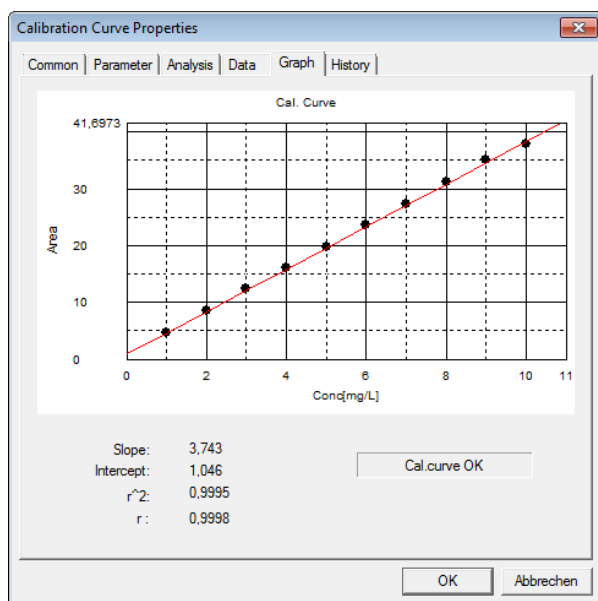
Calibration Points:

No.	Conc.	Auto...	Std. Sol. Co...	Mean Area	No. of Inj.	Excluded
1	1,000 mg/L	10,00	10,00 mg/L	4,679	3/4	
2	2,000 mg/L	5,000	10,00 mg/L	8,464	3/4	
3	3,000 mg/L	3,333	10,00 mg/L	12,34	3/4	
4	4,000 mg/L	2,500	10,00 mg/L	16,00	3/4	
5	5,000 mg/L	2,000	10,00 mg/L	19,68	3/4	
6	6,000 mg/L	1,667	10,00 mg/L	23,60	3/4	
7	7,000 mg/L	1,429	10,00 mg/L	27,34	3/4	
8	8,000 mg/L	1,250	10,00 mg/L	31,28	3/4	
9	9,000 mg/L	1,111	10,00 mg/L	35,01	3/4	
10	10,00 mg/L	1,000	10,00 mg/L	37,91	3/4	

Edit Add Delete Delete All Exclude

OK Abbrechen

The measured calibration curve exhibits a linear range with a very good correlation coefficient ( $r = 0.9995$ ).



## ■ Calibration with automatic dilution function over two decades

In addition, there is the possibility to use different standard solutions for the dilution. Calibration was carried out from 1 to 100 mg/L using two standard solutions (10 and 100 mg/L).

Kal. Kurveneigenschaften

Allgemein | Parameter | Analyse | Daten | Graphik | Ereignis

Inj. Vol.: 90  $\mu$ l

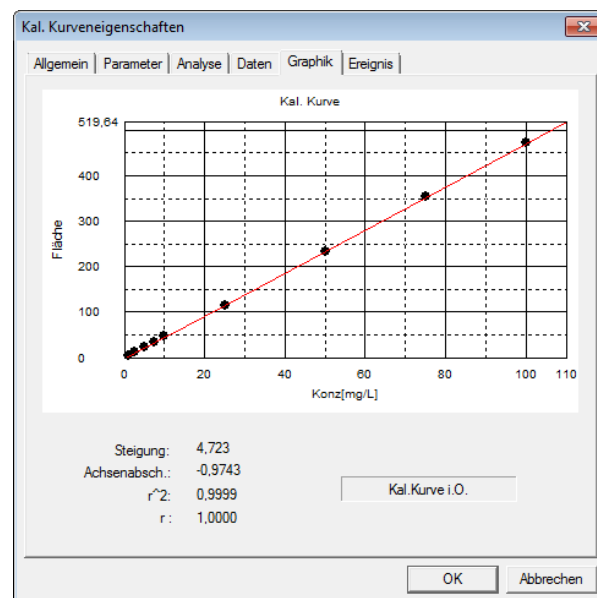
Kalibrierpunkte:

Nr.	Konz.	Aut. Ve...	Std. Lsgl. Ko...	MW Fläche	Anz. Inj.	Ausgeschl.
1	1,000 mg/L	10,00	10,00 mg/L	4,944	3/4	
2	2,500 mg/L	4,000	10,00 mg/L	11,73	3/4	
3	5,000 mg/L	2,000	10,00 mg/L	22,92	3/4	
4	7,500 mg/L	1,333	10,00 mg/L	34,86	3/4	
5	10,00 mg/L	1,000	10,00 mg/L	46,26	3/4	
6	25,00 mg/L	4,000	100,0 mg/L	114,8	3/4	
7	50,00 mg/L	2,000	100,0 mg/L	232,8	3/4	
8	75,00 mg/L	1,333	100,0 mg/L	354,1	3/4	
9	100,0 mg/L	1,000	100,0 mg/L	472,4	3/4	

Bearbeiten Hinzufuegen Löschen Alles Löschen Ausschließen

OK Abbrechen

Also here, the measured calibration curve exhibits a linear range with a very good correlation coefficient ( $r = 0.9995$ ).





## Application News

**No.** SCA-130-514

Sum parameter – Total Organic Carbon

### Comparison of different sum parameters – COD, BOD and TOC

Identification of organic pollutants in wastewater is essential for performance evaluation, construction and operation of a wastewater treatment plant. Several parameters are currently used in wastewater analysis applications. Some of these are based on oxygen demand, for instance BOD (biochemical oxygen demand), COD (chemical oxygen demand) and TOD (total oxygen demand). Using TOC analysis, however, the total organic carbon content is determined directly so the method is relatively free from matrix effects. The advantages of TOC analyses are apparent especially during continuous monitoring.



#### ■ BOD (Biochemical Oxygen Demand)

The BOD value indicates the amount of oxygen in water needed for biological decomposition of organic compounds dissolved in wastewater. For BOD determination, microorganisms are added to the water sample. After a predefined time interval, usually five days, the oxygen consumed by bacteria during decomposition of organic compounds in the water sample is determined. The BOD<sub>5</sub> test is much too slow to provide suitable information and the results

obtained are therefore not useful for monitoring and controlling of wastewater treatment procedures. For continuously operated BOD analyzers, determination within 5 -15 minutes has been attempted.

#### ■ COD (Chemical Oxygen Demand)

The COD value indicates the amount of oxygen needed to chemically oxidize organic compounds present in wastewater. A chemical oxidizing agent is added to the sample and its consumption is subsequently measured. In addition to the organic compounds, other compounds (nitrites, bromides, iodides, metal ions and sulfur compounds) present in the water sample can also be oxidized and have an influence on the measuring value.

The COD determination is a subject of critical discussion due to the use of environmentally hazardous substances such as mercury and chromium compounds.

#### ■ TOD (Total Oxygen Demand)

This rather seldom parameter evolved from the idea that chemical oxidation via COD could be replaced by thermal oxidation, whereby the amount of oxygen required for high-temperature combustion of all contaminants is determined. This reduces the measuring time when compared with COD determination. However, during TOD measurements, non-carbon containing compounds, for example sulfur and nitrogen compounds, are also oxidized. This is probably the reason why this parameter is not used by most well-known regulatory agencies.



### ■ TOC, total organic carbon

The TOC content is a measure of the concentration of organically bound carbon and is therefore a direct indication of the pollution levels by organic compounds in wastewater. For TOC determination, the sample is typically first acidified in order to convert the inorganic carbonate and hydrogen carbonate compounds into carbon dioxide. The dissolved  $\text{CO}_2$  is subsequently removed from the sample via sparging with a stream of carrier gas. The remaining organic carbon compounds are then converted to  $\text{CO}_2$  via high temperature (catalyst) or wet-chemical oxidation. The amount of  $\text{CO}_2$  obtained is subsequently determined via NDIR detection. NDIR is a specific detection mode that renders TOC determination free from the effects described above when using other parameters. Based on this, the TOC parameter is used in many environmental regulations. Another advantage is the relatively simple conversion of TOC measurements into a continuous monitoring procedure.

### ■ Correlation between COD and TOC

In recent years, COD measurements are increasingly being replaced by TOC analysis. However, as the threshold values for organic pollution levels in wastewater are usually described and determined as COD values, efforts are underway to find a correlation between the two parameters.

For single compounds the factor can be calculated.

1. Example Glucose ( $\text{C}_6\text{H}_{12}\text{O}_6$ ) 1000mg/L  
COD= 1067mg/L  
TOC= 400mg/L  
Correlation COD/TOC= 2,66

2. Example Acetone ( $\text{C}_3\text{H}_6\text{O}$ ) 1000mg/L  
COD=2207mg/L  
TOC= 621mg/L  
Correlation COD/TOC= 3,55

3. Example Ethanol ( $\text{C}_2\text{H}_6\text{O}$ ) 1000mg/L  
COD=2087mg/L  
TOC= 522mg/L  
Correlation COD/TOC= 4,00

The examples show the diversity of correlation factors. In addition to the organic compounds, other compounds like nitrites, bromides, iodides, metal ions or sulfur compounds may be oxidized and influenced the factor.

Due to this, the correlation factor can be vary between 2,5 and 4 depending of the wastewater.

In order to simplify the determination of the correlation factor, paragraph 6 of the German wastewater law (AbwV) of June 17, 2004 includes the following: "One of the values for the chemical oxygen demand (COD) as defined in the wastewater regulatory law is, under compliance with paragraph 1, also valid when the four-fold value of the total organically bound carbon (TOC) in mg/L, does not exceed this value".

In the European Union, the factor „3“ is used for conversion of TOC in COD.

The instrument software of Shimadzu TOC systems (TOC-L standalone, TOC-Control L, TOC-4200 standalone) enables the automatic conversion of measured TOC values into COD value (if the correlation is known).

# Application News

No. SCA-130-515

Sum parameter – Total Organic Carbon

## COD and TOC correlation factor – Conversion examples

The determination of the chemical oxygen demand (COD) is time-consuming and complex. After the sample has been mixed with various reagents, it is left to boil at 120°C (according to DIN regulation) under reflux (air cooler), subsequently an aliquot of the mixture is back-titrated or photometrically measured (rapid test).

In addition, environmentally hazardous substances, such as a mercury-containing sulfuric acid and a potassium-dichromate solution are used.

The determination of TOC (Total Organic Carbon), on the other hand, is fast and easy to perform. In addition, less than 1 mL of a diluted hydrochloric acid solution is used for each analysis.

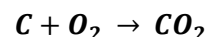
### ■ COD and TOC in the German Waste Water Ordinance (AbwV)

For decades, there have been efforts to replace the COD by the TOC parameter. However, to date the COD is laid down in the German Waste Water Ordinance. In order to still use the TOC parameter, Article 6 “Compliance with the requirements” of the German Waste Water Ordinance states the following:

(3) “With due regard for paragraph (1) above, a chemical oxygen demand (COD) level specified in the water discharge permit shall also be deemed to have been met provided the quadruple amount of total organically bonded carbon (TOC), specified in milligrams per liter, does not exceed this level.”

### ■ Theoretical COD/ TOC factor

If the TOC is used as an analytical parameter to calculate the COD, a conversion factor is required. The AbwV specifies the factor 4. A theoretical factor is derived from the reaction ratios between C and O<sub>2</sub>:



As the COD corresponds to the required oxygen amount, the O<sub>2</sub> consumption corresponds to the COD value – C represents to the TOC value.

Since the COD or the TOC concentrations must be expressed in terms of mass concentration, the molar masses of the two reactants are used here for the conversion. The ratio of carbon concentration to oxygen concentration corresponds to the TOC/COD correlation. Based on the reaction equation above, this means

$$\text{for C: } 1000 \frac{mg}{L} : 12 \frac{g}{mol} = 83.33 \frac{mmol}{L}$$

$$\text{for O}_2: 1000 \frac{mg}{L} : 32 \frac{g}{mol} = 31.25 \frac{mmol}{L}$$

The COD factor is derived from the molar ratio of C to O<sub>2</sub>:

$$83.33 \frac{mmol}{L} : 31.25 \frac{mmol}{L} = 2.667$$

In this case, the conversion from TOC to COD is as follows:

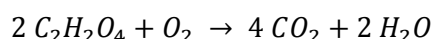
$$COD (O_2) \left[ \frac{mg}{L} \right] = TOC \left[ \frac{mg}{L} \right] * 2.667$$

The example above describes the oxidation of carbon with oxygen. For organic substances the ratio between carbon atoms and oxygen atoms is different, which is of direct influence on the conversion factors from TOC to COD.

Here are a few examples.

#### ■ Oxalic acid

Oxidation of oxalic acid proceeds as follows:



4 carbons react with an oxygen molecule.  
This is the calculation:

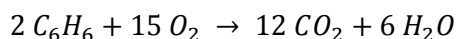
$$\text{for C: } 1000 \frac{\text{mg}}{\text{L}} : (4 * 12 \frac{\text{g}}{\text{mol}}) = 20.83 \frac{\text{mmol}}{\text{L}}$$

$$\text{for O}_2: 1000 \frac{\text{mg}}{\text{L}} : (1 * 32 \frac{\text{g}}{\text{mol}}) = 31.25 \frac{\text{mmol}}{\text{L}}$$

$$20.83 \frac{\text{mmol}}{\text{L}} : 31.25 \frac{\text{mmol}}{\text{L}} = 0.667$$

#### ■ Benzene

The way oxidation of benzene proceeds:



12 Carbons react with 15 oxygen molecules.  
The calculation is as follows:

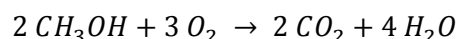
$$\text{for C: } 1000 \frac{\text{mg}}{\text{L}} : (12 * 12 \frac{\text{g}}{\text{mol}}) = 6.94 \frac{\text{mmol}}{\text{L}}$$

$$\text{for O}_2: 1000 \frac{\text{mg}}{\text{L}} : (15 * 32 \frac{\text{g}}{\text{mol}}) = 2.08 \frac{\text{mmol}}{\text{L}}$$

$$6.94 \frac{\text{mmol}}{\text{L}} : 2.08 \frac{\text{mmol}}{\text{L}} = 3.34$$

#### ■ Methanol

Oxidation of methanol:



2 Carbons react with 3 oxygen molecules.  
The calculation is as follows:

$$\text{for C: } 1000 \frac{\text{mg}}{\text{L}} : (2 * 12 \frac{\text{g}}{\text{mol}}) = 41.67 \frac{\text{mmol}}{\text{L}}$$

$$\text{for O}_2: 1000 \frac{\text{mg}}{\text{L}} : (3 * 32 \frac{\text{g}}{\text{mol}}) = 10.42 \frac{\text{mmol}}{\text{L}}$$

$$41.67 \frac{\text{mmol}}{\text{L}} : 10.42 \frac{\text{mmol}}{\text{L}} = 4.000$$

#### ■ Real water samples

These examples show how the COD factor can be calculated. They also illustrate why, due to the composition of a sample, the COD factor may vary so much.

In addition, real water samples usually contain a large number of different organic substances. This is why the bandwidth of the conversion factors ranges from < 1 to > 5, depending on the amount of oxygen that is already bound in the organic compounds.

Furthermore, COD determination also measures oxidizable inorganic compounds, such as nitrites, bromides, iodides, metal ions and sulfur compounds and this may influence the conversion factor.

The instrument software of Shimadzu TOC systems (TOC-L standalone, TOC-Control L, TOC-4200 standalone) enables the automatic conversion of measured TOC values into COD value (if the correlation is known).

## Application News

**No.** SCA-130-601

Sum parameter – Total Organic Carbon

### Continuous TOC/TN determination in wastewater treatment plants

A uniform definition of wastewater does not yet exist. Wastewater is often used as a generic term for sludge, industrial wastewater and infiltration water. The contents of wastewater can vary widely depending on their origin, and a distinction is made between oxygen consuming compounds, nutrients, harmful substances and contaminants [1].

Wastewater treatment is carried out to eliminate wastewater contents and to restore the natural water quality.



In municipal wastewater treatment plants, biological processes are used in aerobic and anaerobic wastewater treatment for the degradation of organically highly polluted wastewater. These plants use microbiological degradation processes. A stable nutrient ratio (carbon : nitrogen : phosphorus) is a precondition for an optimal degradation capacity of the microorganisms. Therefore, it is important to continuously monitor the inflow to the sewage plant. The treated effluent leaving the sewage plant must also be monitored continuously. Only when the limit levels of the German Wastewater Ordinance are reached, the water may flow back.

#### ■ TOC determination in wastewater

Two oxidation techniques are now commonly used in TOC analysis:

- catalytic combustion, where carbon compounds are converted into CO<sub>2</sub> using a catalyst under high temperatures with subsequent detection of the resulting CO<sub>2</sub> using an NDIR detector
- wet chemical oxidation, which applies a combination of UV irradiation and persulfate for oxidation. The resulting CO<sub>2</sub> is either detected via an NDIR detector or using a conductivity detector.

For TOC determination in wastewater, catalytic combustion has become the method of choice based on its higher oxidation potential, especially for particles. Regarding TOC methods, the German Wastewater Ordinance states the following: "A TOC system with thermal-catalytic combustion (minimum temperature of 670 °C) must be used."

#### ■ TOC-4200

The TOC-4200 is a high-performance analyzer with catalytic combustion at 680 °C. Depending on the sample characteristics, three TOC analysis methods can be selected (direct method, difference method, addition method). The automatic dilution function enables TOC analyses up to 20,000 mg/L. In addition, the TOC-4200 can be extended with a module for measuring the total bound nitrogen (TN). An automatic dilution function and the self-calibration option allow a virtually independent operation of the measuring system.

### ■ Sampling

An analysis system is only as good as the sample preparation preceding it. Various sample preparation systems are available for the 4200 series, which can be optimally tuned to the individual application area. When sewage plant inlet and outlet are to be measured using the same instrument, the sample stream switcher is used.

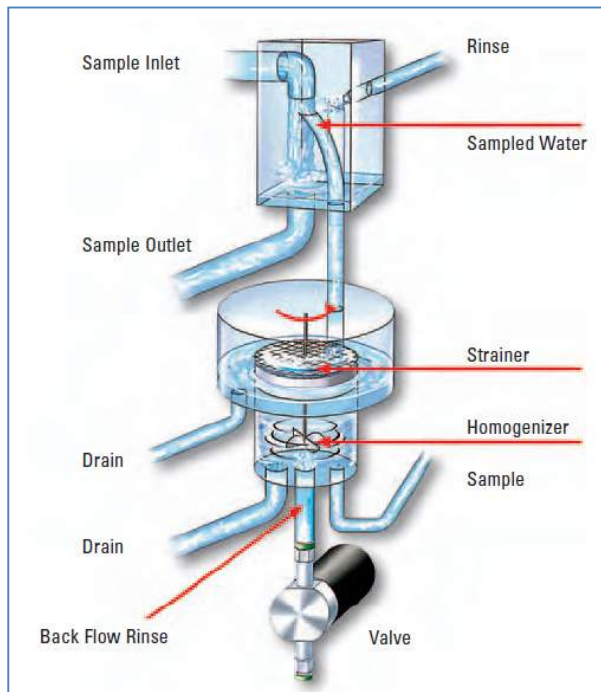


Fig. Multi-Stream switcher

The sample enters the sample chamber via a strainer, where it is homogenized through a rotating knife before it is transferred to the instrument for analysis. This way, even samples containing large amounts of particulate matter can be measured without any problems. After sampling, the chamber and the strainer are cleaned with rinsing water. Depending on the application, the rinsing water can be acidified in order to prevent the growth of algae. The rinsing function prevents any carry-over effects when changing sample streams. The measuring program can be individually selected for each sample stream. In addition, the user can freely choose the measuring sequence of the sample streams.

### ■ Remote control

The measuring instruments can be started and calibrated from a control station, and a selection between the different measuring streams is possible. Numerous alarm and status signals simplify detection of exceeded limit levels and indicate the need for maintenance. In addition to the conventional communication modes, a Modbus communication channel is available. An optional web browser enables a 'view' of the instrument from any networked computer. The software counts consumables such as acids and pure water for dilution, and emits a signal to the measuring station for refilling the consumables.

### ■ Recommended analyzer / Configuration

TOC-4200

Multi-Stream suspended solids sampling unit  
Acid Rinse option



[1] Source: Wikipedia



## Application News

**No.** SCA-130-603

Sum parameter – Total Organic Carbon

### Continuous TOC determination in the chemical industry

The high demand for many different products from the chemical industry and the required efficiency of the manufacturing processes often requires around-the-clock production. This results in huge amounts of wastewater. This water mostly originates from flowing water bodies.



Industrial wastewaters must be pretreated before being discharged into public sewage treatment plants. Direct discharge into water bodies requires an extensive cleaning process. This is why many large companies or industrial parks operate their own wastewater treatment plants.

#### ■ TOC determination in industrial wastewater

The TOC content (Total Organic Carbon) is a measure of the concentration of organically bound carbon and is an indication of the pollution level by organic compounds in wastewater. This is why the TOC is often used in sewage treatment plants as measuring parameter to monitor and optimize the treatment process and to calculate pollution levels. The matrix in industrial effluents can vary greatly and can – prior to sewage treatment –

be polluted with high salt loads. For TOC determination in wastewater, catalytic combustion has become the method of choice based on its higher oxidation potential, especially for particles.

#### ■ Are high salt loads a problem?

During thermal catalytic combustion of the test sample, the dissolved salts crystallize. High salt loads can lead to pollution of the catalyst, or even clogging of the system. Maintenance measures (for instance exchanging the catalyst) would then be required in order to render the instrument operational again. Of course, it is desirable to keep the maintenance intervals as long as possible.

#### ■ TOC-4200

The TOC-4200 offers various possibilities to keep the maintenance needs for highly polluted samples at a minimum. The TOC-4200 with catalytic combustion at 680 °C is a high-performance analyzer. This temperature is lower than the melting point of sodium chloride and will, therefore, prevent deactivation of the active centers of the catalyst by a melt. The use of a platinum catalyst ensures the complete conversion of the organic compounds to CO<sub>2</sub>. The highly sensitive NDIR detector allows small injection volumes (typically 20 - 50 µL) that reduce the absolute sample input onto the catalyst. A further reduction can be achieved using the integrated dilution function.



This can take place when measurement values are exceeded or can be applied permanently. In this case, the user specifies the desired dilution factor in the selected method.

#### ■ Kit for high-salt samples

For the continuous TOC determination of samples with high salt loads ( $> 10 \text{ g/L}$ ), Shimadzu has developed a salt kit. The combustion tube has a special shape and uses two different catalyst beads. This combination prevents crystallization that can lead to clogging of the system.

#### ■ TOC-4200 in daily practice

To verify the robustness and the reliability of the TOC-4200 during practical operation, the analyzer has been subjected to an endurance test in a German chemical park. For three months, the TOC-4200 had to stand the test under the most difficult conditions at one measuring station. The wastewater under investigation was alkaline ( $\text{pH} \geq 12$ ) and highly saline (conductivity  $4 \geq \text{mS/cm}$ ).



Fig. TOC-4200 on site

This is why the instrument was equipped with a kit for salt-containing samples. In addition, the automatic dilution function was used to dilute the samples (including the matrix).

The software enables planning of various automatic maintenance and calibration tasks. This way, automatic calibration of the measuring method was programmed to take place every 48 hours and automatic regeneration of the catalyst twice a week. Sampling took place in the counterflow mode with backflushing in order to prevent clogging.

#### ■ Results of the practice test

As described in the test, a sample was collected every 4 minutes over a period of three months, and subsequently diluted, acidified and analyzed. After three months a total of approximately 27,000 measurements was achieved. Within this period, the instrument was automatically calibrated 45 times and the catalyst was regenerated nearly 25 times. These functions can be easily programmed via a calendar on the touch screen. The calibration function gradients remained stable over the entire time period.

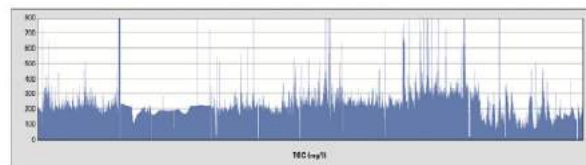


Fig. Diagram of 27.000 Measurement results (three months)

The test did not require any catalyst exchange or a single maintenance operation. There was also no instrument or software failure or any other component failure. In short: the TOC-4200 has successfully passed the endurance test.

#### ■ Recommended analyzer / Configuration TOC-4200

Kit for high-salt samples

## Application News

**No.** SCA-130-604

Sum parameter – Total Organic Carbon

### Continuous condensate monitoring using the TOC-4200



The chemical and petrochemical industry uses superheated steam as energy carrier for the supply of energy needed in various thermal processing steps. Superheated steam is usually generated from ultrapure water, which prevents damage to the boilers. In order to use as little water as possible, the reflux condensate is redirected to the boiler. It is, therefore, important to ensure that the condensate is free from organic pollutants.

#### ■ TOC determination in condensate

The TOC parameter provides information on organic pollution. The TOC can be easily determined and is easy to implement in process analysis. Two oxidation techniques are now commonly used in TOC analysis:

- Catalytic combustion, where carbon compounds are converted into CO<sub>2</sub> using a catalyst under high temperatures with subsequent detection of the resulting CO<sub>2</sub> using an NDIR detector
- Wet chemical oxidation, which uses a combination of UV irradiation and persulfate for oxidation. The resulting CO<sub>2</sub> is either detected via an NDIR detector or a via conductivity detector.

When applying TOC determination to condensates, few particles are usually expected, but here as well, it is better to be on the safe side with the higher oxidation potential offered by catalytic combustion. It is important to be able to quickly and reliably detect every possible organic contamination. Due to the low pollution level of the sample, the catalyst remains stable over a long time span, whereby the need for maintenance is relatively low.

#### ■ TOC-4200

The high-performance TOC-4200 analyzer applies catalytic combustion at 680 °C. Three TOC analysis methods can be selected depending on the sample characteristics: differential method, addition method, direct method. Due to the automatic dilution function TOC analyses up to 20,000 mg/L are possible. In order to measure the total bound nitrogen (TN), the TOC-4200 can be extended with a specific module.



The self-calibration option and an automatic dilution function enable a virtually independent operation of the measuring system which can be started and calibrated from one measuring station. The different measuring streams can be selected.

Numerous status and alarm signals simplify detection of exceeded limit levels and indicate the need for maintenance. A Modbus communication channel complements the conventional communication modes. An optional web browser gives access to the instrument from any networked computer.

### ■ Sampling

For the 4200 series, various sample preparation systems are available, which can be optimally tuned to the individual application area. As condensates are homogeneous samples (in contrast to wastewater), an extra sample preparation step is not necessary. Two sampling systems are, therefore, suitable:

- an overflow tube, from which the sample is automatically drawn.
- filling the sampling chamber through a strainer (50 Mesh), in case the sample does contain particles that need to be removed prior to measurement. Compressed air empties the chamber and cleans the strainer.

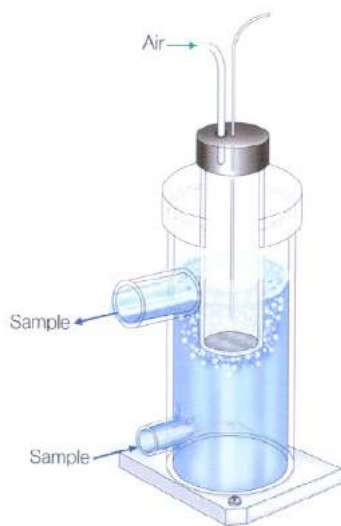


Fig. Sampling

### ■ TOC measuring method

TOC determination is often carried out via the NPOC method,

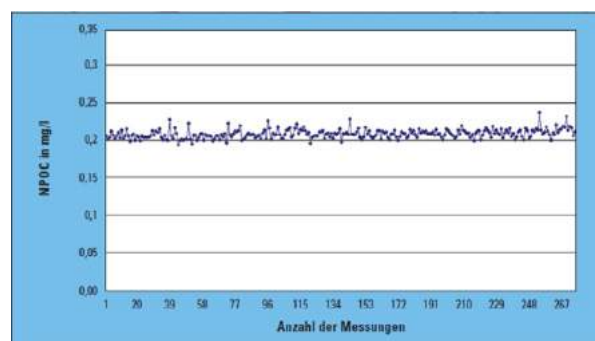
whereby the inorganic carbon content (carbonates and hydrogen carbonates) is removed prior to the actual analysis. For this purpose, the sample is drawn from the continuous sample stream into a syringe and automatically acidified via the 8-port valve (pH 2).

Using the sparging gas connection, the CO<sub>2</sub> formed (from the carbonates and hydrogen carbonates) is purged from the sample. The remaining solution containing the organic components is subsequently injected (septum-free) into the oxidation unit using the sliding valve technique. The syringe and 8-port valve allows automatic dilution and creation of calibration curves.

### ■ TOC measurement in the condensate

The system is calibrated using a 2-point calibration curve, blank water and 2 mg/L. This is realized using a standard catalyst and an injection volume of 200 µL. Typical measuring values are around 0.2 mg/L.

The measuring values of 275 consecutive measurements of a condensate monitoring are presented in the Figure below:



The mean value is 0.208 mg/L with a standard deviation of 0.006 mg/L. The results show that the required detection limit of 0.05 mg/L presents no problem.

### ■ Recommended analyzer / Configuration

TOC-4200

Backwash Strainer Sampling unit

## Application News

**No.** SCA-130-605

Sum parameter – Total Organic Carbon

### TOC-4200 - High Sensitivity Measurement Option

Ultra pure water is one of the most widely used reagents in industry and its quality is therefore of utmost importance in all industrial processes. Quality control has, for many years, been carried out and documented via conductivity measurements, which provide an assessment of the concentration of all inorganic species present in water. This detection method does not take organic pollutants into account, as they typically do not contribute to conductivity. Organic pollutants can, however, greatly influence further industrial processes and it has become increasingly more important to include quantitative determination of all organic species in quality control of water samples.



#### ■ TOC (Total Organic Carbon)

The TOC value (Total Organic Carbon) can be used as a sum parameter for organic compounds. Similar to conductivity signals composed of various ionic compounds, the TOC value is a measure of the contribution of the numerous organic compounds present in a water sample.

When industrial processes require large volumes of ultra pure water, it is recommended to monitor its TOC content continuously.

#### ■ TOC-4200



The high-performance TOC-4200 analyzer applies catalytic combustion at 680 °C. Three TOC analysis methods can be selected depending on the sample characteristics: difference method, addition method, direct method. Due to the automatic dilution function TOC analyses up to 20,000 mg/L are possible. In order to measure the total bound nitrogen (TN<sub>b</sub>), the TOC-4200 can be extended with a specific module.

The self-calibration option and an automatic dilution function enable a virtually independent operation of the measuring system which can be started and calibrated from one measuring station. The different measuring streams can be selected.

Numerous status and alarm signals simplify detection of exceeded limit levels and indicate the need for maintenance. A Modbus communication channel complements the conventional communication modes. An optional web browser gives access to the instrument from any networked computer.

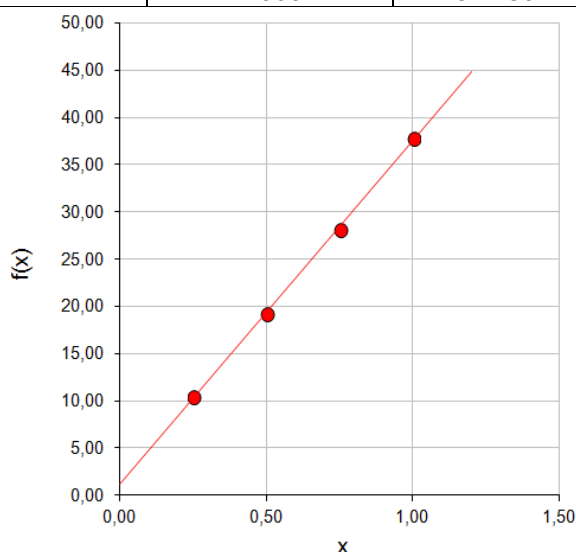


### ■ High Sensitivity Measurement Option

Adding the high-sensitivity measurement option enables high-sensitivity measurements in the 0 to 1 mgC/L range FS. This option achieves high sensitivity by using a highly sensitive catalyst and increasing the maximum sample injection volume to 500 µL (standard specification is 150 µL).

### ■ Calibration Curve

Calibration Point	Concentration [mg/L]	Area counts
1	0.250	10.420
2	0.500	19.210
3	0.750	28.100
4	1.000	37.780



### ■ Calibration Curve Characteristics

Slope a: 36.88  
Intercept b: 1.135  
Correlation coeff r: 0.9997  
Result uncertainty: 33.33%  
Probability of error: 5%

Number of measurements n

Standard error of estimate Sy

Standard error of procedure Sx

Sum of squared deviations

Quantile (one-sided)

Quantile (two-sided)

3
0,333
0,009
0,313
2,920
4,303

### Analytical limits according to DIN 32645

Limit of detection	0,036	mg/L	
Limit of quantitation	0,142	mg/L	(approximation)
	0,137	mg/L	(exact)

### ■ Recommended analyzer / Configuration

TOC-4200

High Sensitivity Measurement Option

Carrier Gas: High-purity air or  
High-purity nitrogen,  
(N<sub>2</sub> Carrier Gas High  
Sensitivity Measurement  
Option required)

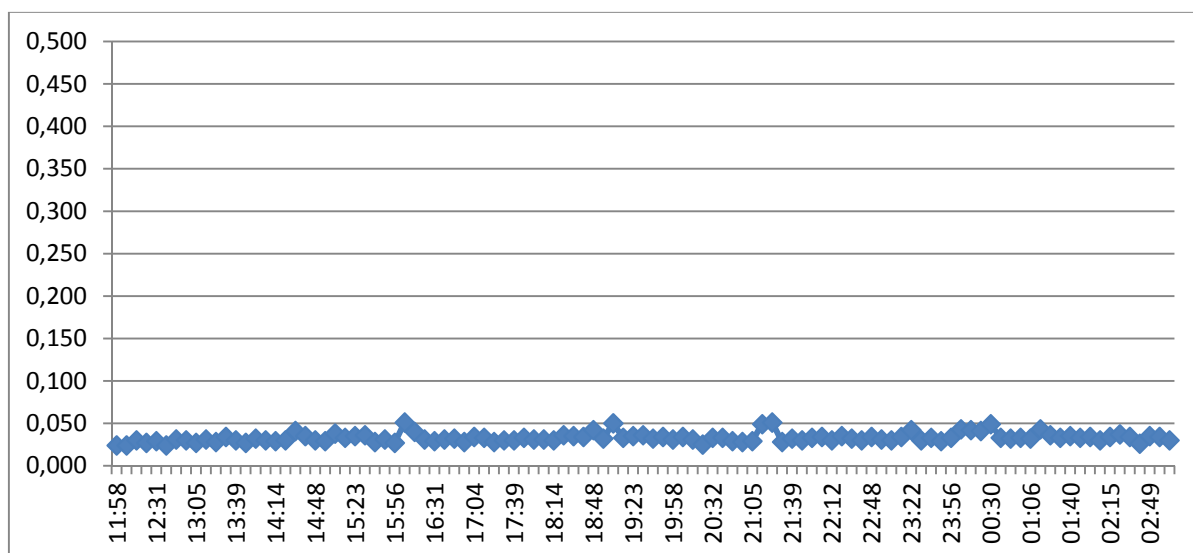


Fig. TOC-4200 Measurement results in mg/l of ultra pure water

## Application News

No. SCA-130-609

Sum Parameter – Total Organic Carbon

### TOC-4200 – Carryover free TOC determination

The TOC (Total Organic Carbon) parameter for organic pollution of wastewater can serve as an indicator for accurate and efficient control of industrial processes. Using Shimadzu's TOC-4200 and switching between measuring points, up to six sample streams can be monitored – even in sample streams of different concentration levels.

#### ■ Example: wastewater treatment plant

In industrial water purification and wastewater treatment plants, a variety of processes are used to purify wastewaters in different subprocesses (for instance, biological or filtration processes). The TOC sum parameter provides important information on the remaining organic contamination and thus on the efficiency of the treatment plant.



*Fig.: Example from paper industry:  
Four very diverse sample streams*

At the inlet of such plants, TOC concentrations of well over 1,000 mg/L as well as high salt loads can be expected. Dissolved organic substances are decomposed in biological intermediate stages. Flocculation or precipitation agents added at this stage modify the sample composition (matrix).

At the outlet of such purification or wastewater treatment plants, the TOC content of the effluent water is usually less than 50 mg/L. The sample matrices and measuring ranges of these sample streams thus vary widely. Monitoring these sample streams using a single analyzer will place high demands on the instrument and the sampling method used.

#### ■ ISP-Module in the TOC-4200

The ISP module (Integrated Sample Pretreatment) is the heart of the TOC-4200 series. It consists of an 8-port valve and a syringe pump. The consistent use of inert materials reduces the risk of cross-contamination. In addition to automated sample pretreatment (acidification and sparging), the module enables dilution of the sample. It is also possible to determine self-cleaning sequences for the module as well as the sample inlets.

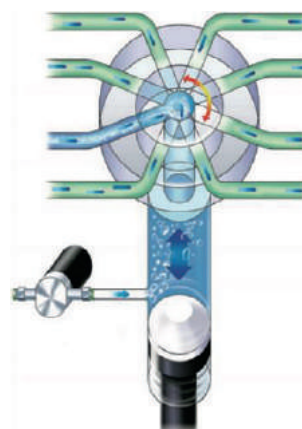


*Fig.: ISP-Module TOC-4200 Series*

The automated dilution function serves not only for measurement range extension, but also for matrix reduction. This reduces maintenance and lowers operating costs.



### ■ Sampling method

Incorrect measurement values often already occur due to carryover effects in the sample inlet line or in the sampler. Biological growth and deposits in the inlet line constitute a further risk of contamination. To minimize this, the sample should be directed to the sampler at a flow rate of higher than 1 m/s. Inspection openings and valves for manual or even automated flushing of the tubing should be provided for. The sampler should be constructed of inert materials. Automated rinsing steps between individual samplings further reduce time expenditure by the operator. To reduce problems during operation, it is important to pay particular attention to sampling during the project development phase.



### ■ Practical test

In a practical test, two sample streams with different matrices and TOC contents were analyzed. To demonstrate sample carry-over between these sample streams, they were alternately sampled and analyzed 90 times respectively.

Stream	S#1	S#2
Matrix	Pure water	3% NaCl-solution
Target conc.	1 mg/l	1000 mg/l
Parameter	NPOC	NPOC
Acid added	100µl	100µl
Inj. Volume	150µl	50µl
Dilution	None	Factor 10

### ■ Conclusions

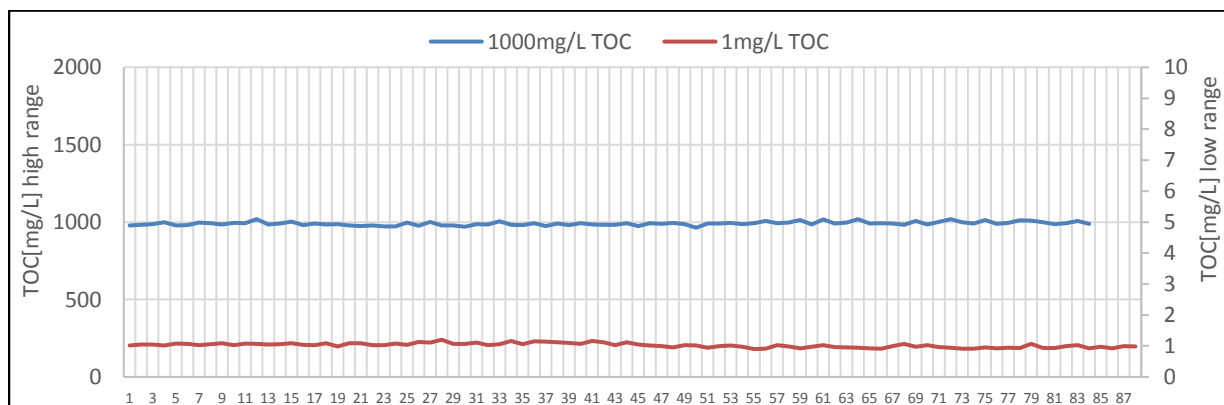
	S#1	S#2
Mean Value TOC (mg/l)	1,02	992,67
Standard deviation (mg/l)	0,07	13,32

Even with significant concentration and matrix differences between both sample streams, the TOC-4200 operated free from carry-over thanks to its inert construction and automated rinsing function.

### ■ Recommended analyzer / Configuration

TOC-4200

Individual sampling system



# Application News

## No.056

### Total Organic Carbon Analysis

## Measurement of a Cement Admixture by a TOC Solid Sample Measurement System

Cement is used for concrete and other construction materials, which have been used for a variety of applications since ancient times. Many varieties are used, with different qualities and properties, depending on their function.

To modify and improve the performance of concrete, water reducing agents, water proofing agents and other admixtures are added to cement. Accordingly, to confirm the strength and properties of existing building structures, it is important to assess the amount of cement admixtures included in the concrete.

As an analysis method for organic admixtures, concrete is pulverized and extracted by boiling, and the filtrate is measured for COD and TOC. However, depending on the type of admixture, the extraction efficiency may be biased, and the concentration may be low, resulting in poor measurement accuracy.

Using the Shimadzu TOC solid sample measurement system, the pulverized concrete can be directly loaded into the instrument to measure the amount of organic carbon. As a result, measurement process and time are reduced, and the impact of variance in the measurement values due to extraction can be reduced. This document introduces an example of the measurement of a cement admixture in pulverized concrete using the TOC solid sample combustion system, which combines the TOC-L total organic carbon analyzer with the SSM-5000A solid sample combustion unit.

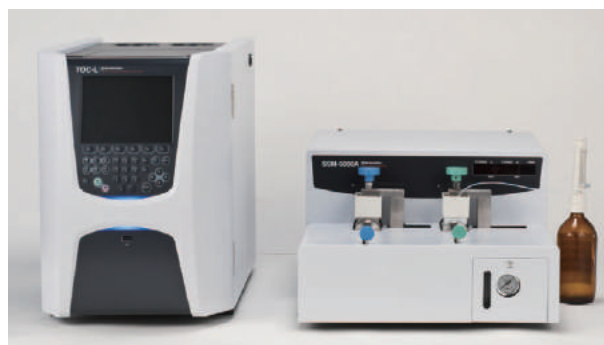


Fig. 1 TOC Solid Sample Measurement System

### ■ Analysis Method

The coarsely pulverized concrete sample was finely pulverized using a vibrating mill to create a powder. This was weighed into a special ceramic sample boat, and then analyzed using the TOC solid sample measurement system (Fig. 1).

To measure the TC, a sample boat containing approximately 100 mg of the sample was loaded into the TC combustion furnace, where it was oxidized by combustion. To measure the IC, phosphoric acid was added to a sample boat containing approximately 70 mg of the sample. The sample boat was then loaded into the IC furnace, where it was measured. The TOC value was then found by subtracting the IC value from the TC value obtained.

The following method was used to calibrate the analyzer. The calibration curve for the TC measurement was created by weighing glucose powdered reagent (carbon concentration = 40 %C) into a sample boat, and then measuring the TC.

The calibration curve for the IC measurement was created by weighing sodium carbonate (carbon concentration = 11.3 %C) into a sample boat, adding phosphoric acid, and then measuring the IC.

### Measurement Conditions

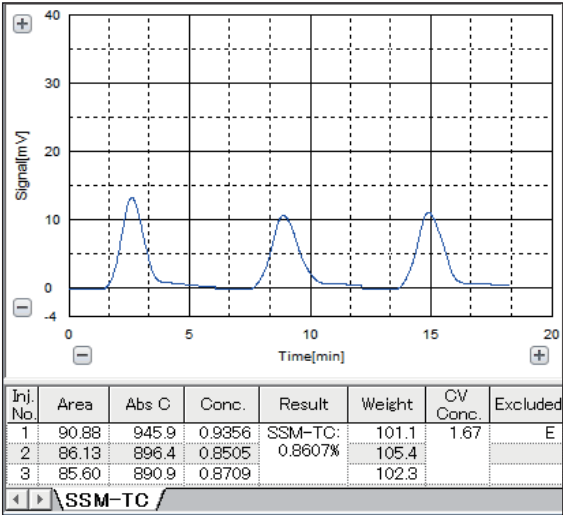
Analyzer	: TOC Solid Sample Measurement System (TOC-L <sub>CPH</sub> Total Organic Carbon Analyzer + SSM-5000A Solid Sample Combustion Unit)
Measurement item	: TOC (=TC-IC)
TC oxidation method	: Combustion catalyst oxidation (TC furnace at 980 °C)
IC reaction method	: Extraction of carbon dioxide via acidification with phosphoric acid (IC furnace at 200 °C)
Calibration curve	: TC: 1-point calibration curve from glucose powdered reagent IC : 1-point calibration curve from sodium carbonate powdered reagent
Sample	: Coarsely pulverized concrete A, B

Analysis Results

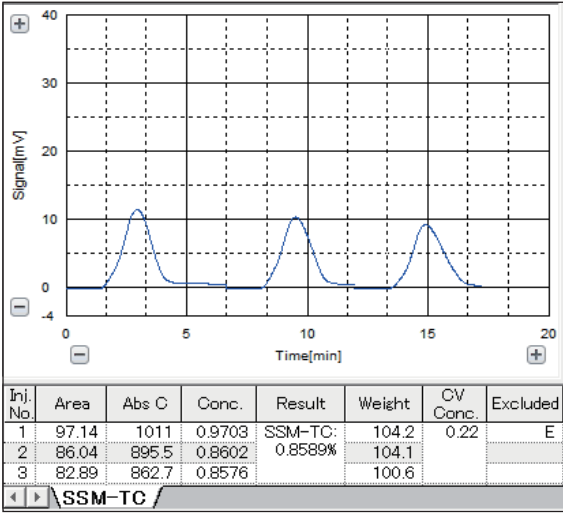
Samples A and B of coarsely pulverized concrete were measured with the TOC solid sample system. The results are shown in Table 1, and the measurement charts are shown in Fig. 2. Samples A and B were treated under different conditions, so it is evident that the TOC values depend on the treatment conditions.

Table 1 TOC Measurement Results

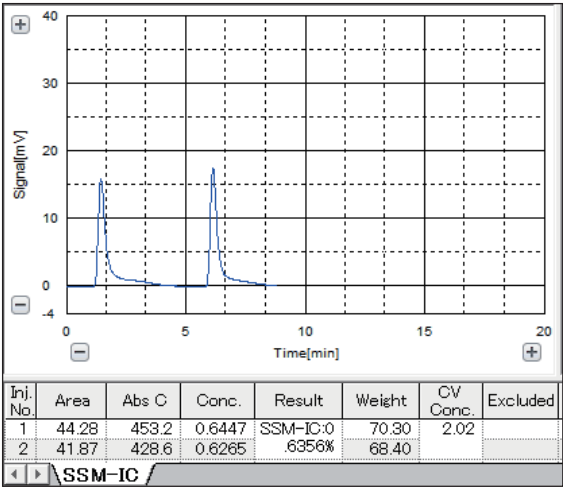
Sample Name	TC Value (%C)	IC Value (%C)	TOC Value (%C)
Sample A	0.861	0.636	0.225
Sample B	0.859	0.756	0.103



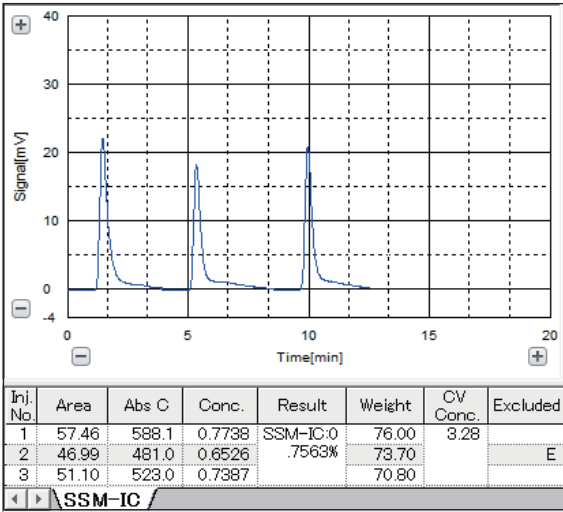
Sample A: TC measurement



Sample B: TC measurement



Sample A: IC measurement

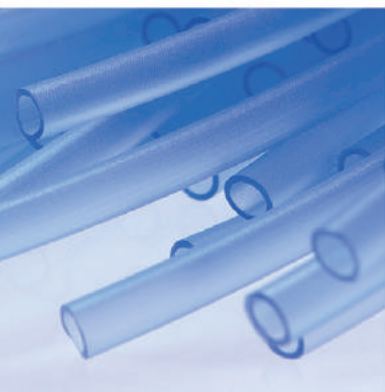


Sample B: IC measurement

Fig. 2 TOC Measurement Data



# 6. Materials Testing & Inspection







## 6. Materials Testing & Inspection

---

### 6.1 Universal Testing

---

In automotive applications, tests of static characteristics of springs are required as well as failure testing of parts and strength evaluations of the various materials used in automobile parts including metals, plastics, rubbers and films. These include acceptance inspections, the evaluation of materials selected, and tests to confirm changes in characteristics due to machining. Tests can be performed in accordance with ISO, ASTM and other standards.

<b>SCA_300_049</b>	Seat belt test tensile test according to manufacturer's specification
<b>i245</b>	Evaluation of temperature-dependent strength properties of lithium-ion battery separator by piercing and tensile testing
<b>i244</b>	Tensile test for metallic materials using strain rate control and stress rate control
<b>No. 14</b>	Tensile testing of metallic materials with stress rate control
<b>No. 15</b>	Tensile testing of metallic materials with strain rate control
<b>SCA_300_045</b>	Jigs for measuring baushinger effect
<b>i250</b>	Shear test of composite material (v-notched beam)
<b>i251</b>	Shear test of composite material (v-notched rail shear)
<b>i254</b>	Compression after impact testing of composite material
<b>i255</b>	Compression test of composite material
<b>i256</b>	Open-hole compression test of composite material
<b>No. 8</b>	Flexural testing of CFRP boards
<b>No. 16</b>	Tensile testing of carbon fiber
<b>No. 30</b>	Evaluating the strength of carbon fiber reinforced plastics (CFRP)
<b>No. 31</b>	Materials testing using digital image correlation
<b>No. 39</b>	Evaluation of open-hole CFRP
<b>No. 1</b>	Tensile test of various plastic materials
<b>No. 2</b>	Flexural testing of plastics
<b>No. 3</b>	Tensile tests of plastic materials at low temperatures
<b>No. 5</b>	Tear tests of crescent-shaped rubber specimens
<b>No. 6</b>	Tear tests of angle-shaped rubber specimens
<b>No. 7</b>	Tensile tests of films
<b>No. 9</b>	Measurements of modulus of elasticity and poisson's ratio for films
<b>No. 17</b>	Measurement of friction coefficient of film
<b>No. 18</b>	90-degree peel resistance test of adhesive tape
<b>No. 19</b>	180-degree peel resistance test of adhesive tape
<b>No. 20</b>	Measurement of friction coefficient of film
<b>i253</b>	Tensile test of plastic materials
<b>No. 5</b>	Fluidity evaluation of unvulcanized rubber
<b>No. 6</b>	Evaluation of the temperature characteristics of general plastics
<b>No. 4</b>	Tensile tests of rubber dumb-bell specimens
<b>SCA_300_038</b>	Tension – Compression major deformation test of rubber vibration isolator by Shimadzu Autograph Series



## Application News

Material Testing System AG-X plus

No. SCA\_300\_049

### Seat Belt test Tensile test according to manufacturer's specification

#### ■ Purpose and Definition:

The three point seat belt design, created by VOLVO in 1959, has saved approximately 1 000 000 lives worldwide since then. Tensile tests are a fundamental test within material science and is performed on more or less all materials. For seat belt manufacturers it's of great importance to perform continuous quality control on the products they produce to ensure that the final product is according to specification and will withstand the forces, which occurs during an accident and again saving a life...

#### ■ Equipment used:

**Testing machine:** AG-100kNX with protective doors for camera.  
**Load cell:** 100kN, 1/1000 Class 0,5  
**Jig:** 100kN belt grips.  
**Extensometer:** TRViewX single camera for protective doors, FOV 500 mm  
**Software:** Trapezium-X Single / Tensile.  
**Environment:** Room temp 21°+/-2°C, humidity ca. 50 +/-5% RHT  
**Test execution:** 5 samples was prepared.

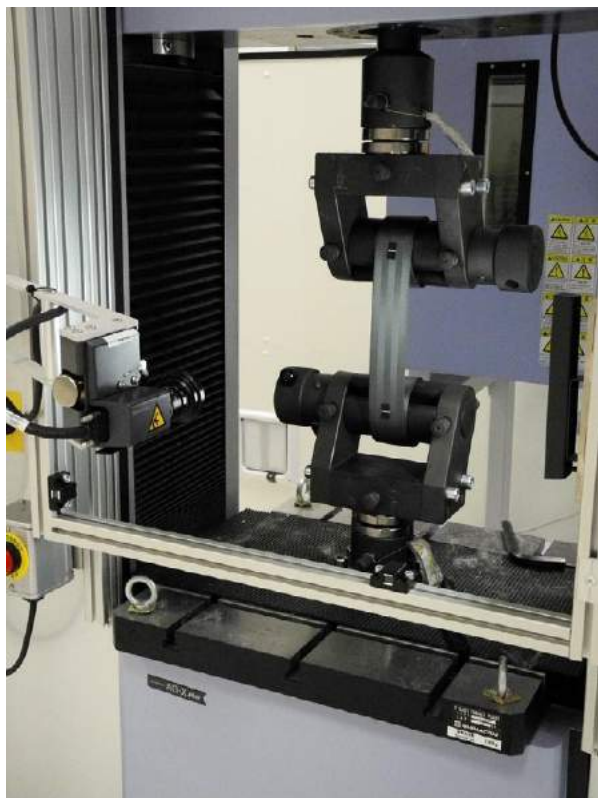
Sample length has to be long enough to be rolled on the grips and ensure a secure gripping.

In this case the total sample length was approximately 1200 mm.

There must still be enough grip separation to set the gauge length...

A method is prepared according to customer request. Test type is single and tensile. Test speed is set to 20 mm/min Gauge length is 200 mm and the TRViewX was selected as extensometer because of the sample dimensions and the violent break properties. Some data points that are requested in this test are: Elongation at 980 daN, 1000 daN, 1110 daN and 1130 daN. Break elongation in %. Maximum force in daN. With the help of TrapeziumX all requested parameters are set quickly with a few clicks exactly according to the specification.





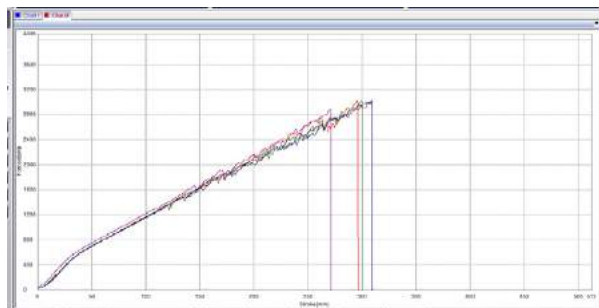
## ■ Test Results:

Tensile properties are always important in most materials and is the most common test made in universal testing machines. Generally, a customer is looking for elastic, maximum and break properties.

The fact that seat belts are tested we all understand very well and like in the measurements, purpose is to find out material strength and tensile properties at different loads.

Examples of applicable standards:

ASTM D6775 Test Method for Breaking Strength and Elongation of Textile Webbing, Tape and Braided Material



Result (Batch)						
Name	Max. Force	980 Ext1(Strain)	1000 Ext1(Strain)	1110 Ext1(Strain)	1130 Ext1(Strain)	Break Ext 1(Strain)
Parameter	Calc. at Entire Areas	Force 980 daN	Force 1000 daN	Force 1110 daN	Force 1130 daN	Sensitivity: 10
Pass/Fail						
Unit	daN	%	%	%	%	%
P1st						
Peak 1	✓ 3011.01	9.61522	9.64517	11.1213	11.2647	21.4502
Peak 3	✓ 3027.53	9.75866	10.0505	11.2209	11.3641	22.4308
Peak 5	✓ 2883.12	9.73363	9.97919	11.2152	11.4356	21.3222
Peak 7	✓ 3004.81	9.69150	9.93167	11.1725	11.3387	22.0457
Peak 9	✓ 2987.14	9.77825	10.0117	11.2215	11.4175	22.4387
Average	2982.73	9.71546	9.96555	11.1909	11.3581	21.3375
Standard Deviation	57.5262	0.06473	0.07722	0.04243	0.06088	0.52570
Maximum	3027.53	9.77825	10.0505	11.2215	11.4356	22.4387
Minimum	2883.12	9.61522	9.64517	11.1943	11.2647	21.3922
Range	144.410	0.16303	0.20133	0.09720	0.15090	1.10650
Median	3004.81	9.73363	9.97919	11.2152	11.3641	22.0457
Variation	0.01929	0.00666	0.00775	0.00379	0.00536	0.02415

# Application News

## No.i245

### Material Testing System

## Evaluation of Temperature-Dependent Strength Properties of Lithium-Ion Battery Separator by Piercing and Tensile Testing

### ■ Introduction

Lithium-ion secondary cells, also called rechargeable batteries, (referred to here as "lithium-ion batteries") are widely used as energy sources for information terminals and consumer electronics, etc. because of their high energy density and cell voltage. Recently, their growing rate of dissemination into areas of general household applications, including hybrid and electric vehicles, is quite evident, and it appears obvious that the demand will further increase in the future.

Because lithium-ion batteries can sometimes become unstable due to short-circuit, over charging and discharging, impact, etc., a variety of protection mechanisms are incorporated at the battery component level to ensure safety.

Of these component parts, the lithium-ion battery separator prevents contact between the positive and negative electrodes, while at the same time playing a role as a spacer which permits the passage of lithium ions. However, it also performs the function of

preventing a rise in battery temperature due to excessive current in the event of a short circuit.

Because the lithium-ion battery separator is set in place so that it comes into contact with the rough surfaces of the positive and negative terminals, high mechanical strength is required. This mechanical strength must be maintained even if there is some rise in temperature, which is common to some degree, for example, during battery charging. Therefore, we conducted piercing and tensile testing measurements of the separator to evaluate changes in strength with respect to changes in temperature. This document introduces actual examples of these tests.

Supplement) Regarding the lithium-ion battery separator, previous evaluation examples were also introduced in Application News T146 "Measurement of Separator in Lithium-Ion Battery" and i229 "Multi-Faceted Approach for Evaluating Lithium-Ion Battery Separators."

### ■ Piercing Test

The samples consisted of separators removed from two lithium-ion batteries (cylindrical) used in small electrical devices, and we measured the changes in piercing characteristics due to changes in environmental

temperature. Fig. 1 shows an overview of the test conditions, and Table 1 presents details of the test conditions.

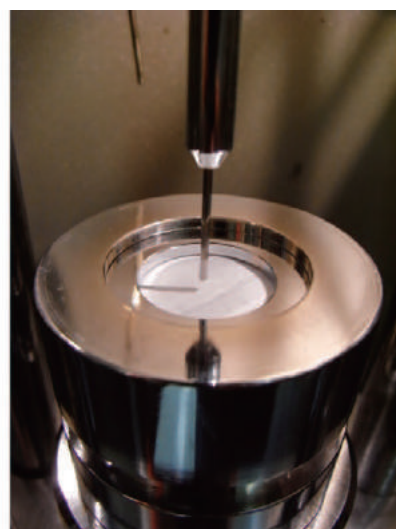
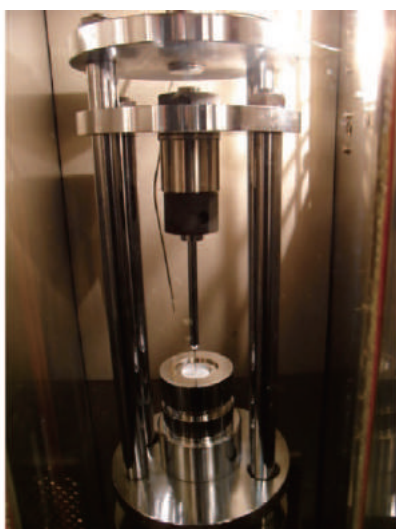
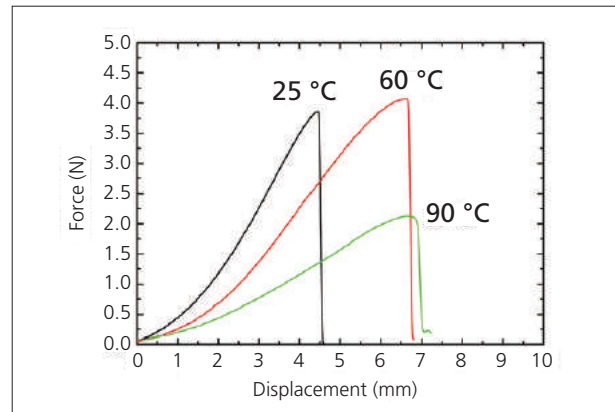


Fig. 1 Overview of Piercing Test

**Table 1 Test Conditions (Piercing Test)**

1) Instrument	Shimadzu AG-X Precision Universal Tester
2) Load cell capacity	1 kN
3) Jigs	Boil-in-bag piercing jig
4) Thermostatic chamber	TCR-1W
5) Load rate	50 mm/min
6) Temperature	25 °C, 60 °C, 90 °C
7) Software	TRAPEZIUMX (Single)

Fig. 2 shows the force – displacement curve, and Table 2 shows the maximum force and maximum displacement with respect to temperature. Comparing the test results at 25 °C and 60 °C, it is evident that there is not much difference in the maximum force, but the maximum displacement is greater at 60 °C. Comparing characteristic values at 60 °C and 90 °C, the decrease in maximum force is obvious at 90 °C, but the maximum displacement value is about the same. From the above, it can be assumed that at 60 °C, there is no decrease in strength of the lithium-ion battery separator, despite the apparent increase in its elongation property.

**Fig. 2 Test Result (Piercing Test)****Table 2 Summary of Results (Piercing Test)**

Temperature (°C)	Maximum Force (N)	Maximum Displacement (mm)
25	3.85	4.45
60	4.07	6.63
90	2.13	6.68

### ■ Tensile Test

The separators used for the tensile testing were removed from commercially available lithium-ion batteries (square-shaped), so 2 types of samples (below, referred to as samples (1) and (2)) which contained PE (polyethylene) as the principle constituent were used. When conducting the tensile tests, each separator

sample (as shown in Fig. 3(a)) was fashioned into dumbbell-shaped specimens oriented in the lengthwise and widthwise directions of each separator, as shown in Fig. 3(b). The total length of all specimen was 35 mm, with the parallel section measuring 10 (L) × 2 (W) mm.

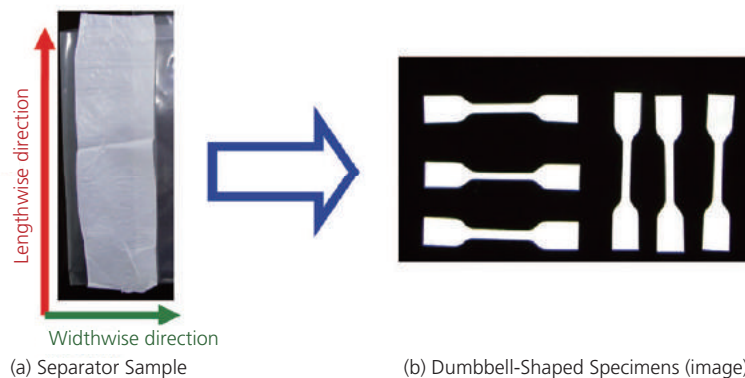
**Fig. 3 Test Samples**

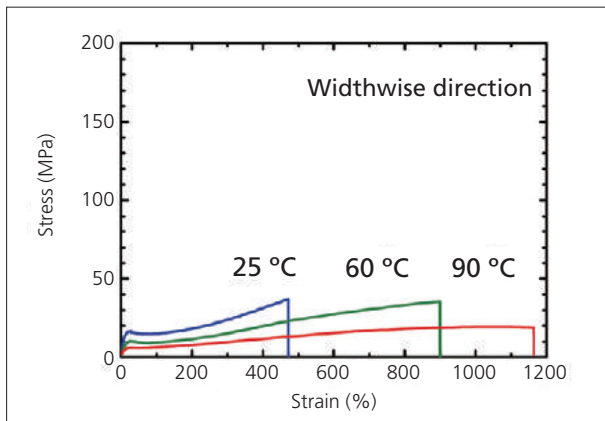


Table 3 shows the tensile test conditions that were used.

**Table 3 Test Conditions (Tensile Test)**

1) Instrument	Shimadzu AG-X Precision Universal Tester
2) Load cell capacity	100 N
3) Jig	50 N capacity pneumatic flat grips (flat surface teeth, pneumatic pressure 0.4 MPa)
4) Thermostatic chamber	TCR-1W
5) Load rate	50 mm/min
6) Temperature	25 °C, 60 °C, 90 °C
7) Software	TRAPEZIUMX (Single)

Fig. 4 and Fig. 5 show the stress – strain curves for the widthwise and lengthwise directions, respectively of sample (1). Fig. 6 and Fig. 7 show the stress – strain curves for the widthwise and lengthwise directions, respectively of sample (2). Table 4 shows the test values of the mechanical properties obtained at each temperature.



**Fig. 4 Test Results (Sample (1), widthwise direction)**

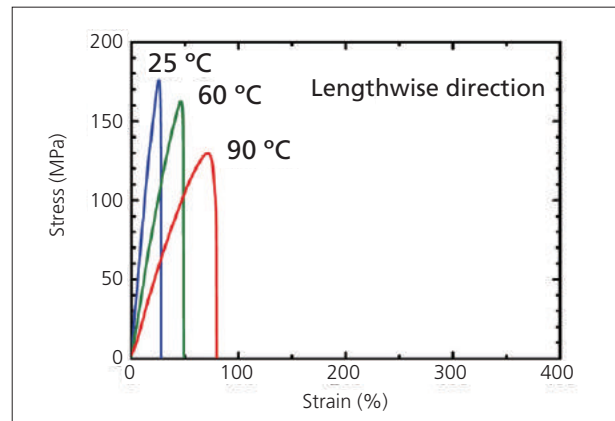


**Fig. 5 Test Results (Sample (1), lengthwise direction)**

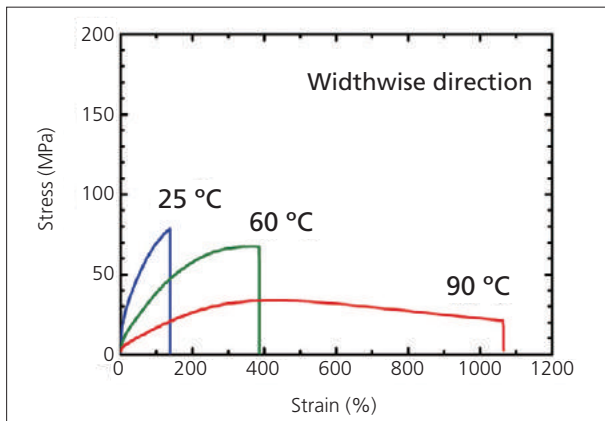


**Fig. 6 Test Results (Sample (2), widthwise direction)**

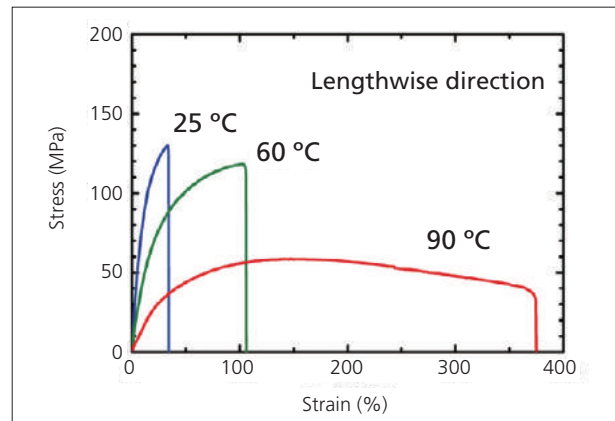


**Fig. 7 Test Results (Sample (2), lengthwise direction)**



**Table 4 Summary of Results of Tensile Test**

Sample	25 °C		60 °C		90 °C	
	Tensile Strength (MPa)	Strain at Break (%)	Tensile Strength (MPa)	Strain at Break (%)	Tensile Strength (MPa)	Strain at Break (%)
(1) Widthwise direction	36.9	471.4	35.4	898.8	19.3	1044.0
(1) Lengthwise direction	175.6	26.8	162.5	57.0	129.9	76.7
(2) Widthwise direction	78.2	138.5	68.8	347.6	33.8	427.9
(2) Lengthwise direction	129.5	34.1	118.3	105.3	58.7	367.2

In each of the samples, a lower tensile strength and greater elongation was seen in the widthwise direction than in the lengthwise direction. When comparing the numbers in Table 4, the lengthwise tensile strength for sample (1) is about 5 times greater than the widthwise tensile strength of sample (1). Also, the strain at break, for sample (1) in the lengthwise direction is lower by about a factor of 15 than that of sample (1) in the widthwise direction. From the above results, it is supposed that this separator (sample (1)) was manufactured using uniaxial drawing in the lengthwise direction. The widthwise tensile strength for sample (2) is about twice that of sample (1), and the strain at break is much lower. The tendency similar to that of sample (2) in the widthwise direction is seen with respect to sample (2) in the lengthwise direction. Therefore, due to the tendency of greater tensile strength and lower strain at break with sample (2) in the lengthwise direction, it is presumed that sample (2) was manufactured with a low biaxial drawing ratio, and that the drawing ratio in the lengthwise direction was greater than that in the widthwise direction. The data obtained regarding the mechanical properties with respect to the sample temperature are also

interesting. When comparing the sample strain at break and tensile strength at 25 °C and 60 °C, even though the strain at break value increased by a factor of 2 due to the test temperature increase to 60 °C, there was just a slight decrease in tensile strength. Similarly, when comparing the physical property measurement values at 60 °C and 90 °C, the strain at break showed the same tendency to greatly increase as when the values were compared at 25 °C and 60 °C. However, in this case, the tensile strength value shows a significant decrease. From the above, it is evident that the lithium-ion battery separators used in this test maintain excellent mechanical strength at 60 °C, notwithstanding its elevated elongation characteristics.

High-mechanical strength specifications are required for separators in order to withstand changing temperature in the cell. Here, as is clear from the results of piercing and tensile testing of lithium-ion battery separators under atmospheric temperature control, the mechanical properties of lithium-ion battery separators can be reliably evaluated using the Shimadzu Precision Universal Tester AG-X with its abundant array of accessories.

# Application News

## No.i244

### Material Testing System

## Tensile Test for Metallic Materials Using Strain Rate Control and Stress Rate Control

### ■ Introduction

International standards for tensile testing of metallic materials have been revised as specified in ISO 6892 and JIS Z2241, such that strain rate control, where strain is measured with an extensometer, has recently been added as a test item to the current stress rate control method, in which a load is applied to a material until its yield point is reached. As a result, it can be assumed that there will be situations where both stress rate control and strain rate control tensile testing of

metallic materials will be required.

Here, we introduce examples of strain rate control and stress rate control tensile testing of metallic samples, including cold-rolled steel, austenitic stainless steel, aluminium alloy and brass, according to ISO 6892, using the Shimadzu Autograph AG-50kNX Precision Universal Tester, and the SSG50-10H strain gauge type one-touch extensometer (Fig. 1, Fig. 2).



Fig. 1 Overview of Universal Testing System

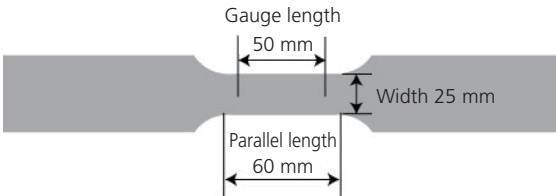


Fig. 2 Specimen and Jigs for Tensile Testing

### ■ Specimens and Test Conditions

Information on the sample specimens are shown in Table 1, and the test conditions are shown in Table 2.

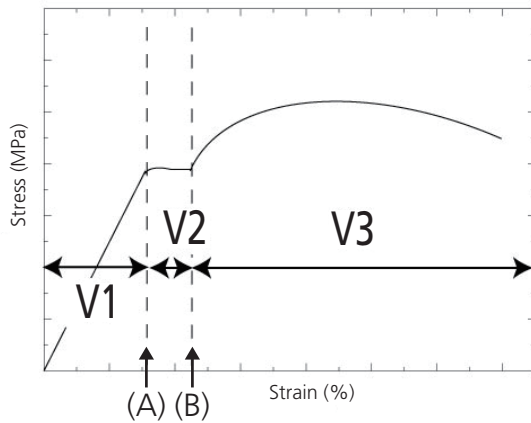
Table 1 Test Specimens

Sample Name	A	B	C	D
Material	Cold-rolled steel	Stainless steel (austenitic)	Aluminium alloy	Brass
Sample size	 <p>Width 25 mm, thickness 1 mm, gauge length 50 mm, parallel length 60 mm (JIS Z 2241 No. 5 test specimen)</p>			

**Table 2 Test Conditions**

1) Load cell capacity	50 kN
2) Jig	50 kN Non-shift wedge type grips (file teeth for flat specimen)
3) Test speed	See Table 3
4) Test temperature	Ambient temperature
5) Software	TRAPEZIUMX (single)

Fig. 3 shows an image diagram of the test speed, and Table 3 and Table 4 show the applicable test speeds for the strain control and stress control tests, respectively.



(A): Upper yield point (or its corresponding point)  
(B): Upper limit of strain measurement (point after proof strength point)

**Fig. 3 Image of Test Strain Rate****Table 3 Test Strain Rate (based on strain rate control)**

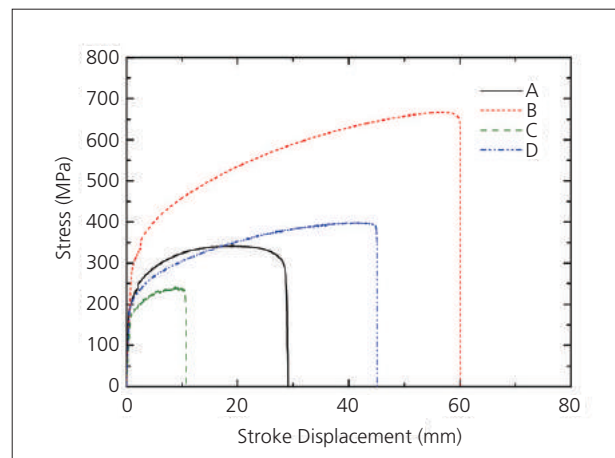
V1: Strain rate	0.00025/s (1.5 %/min)
V2: Strain rate	0.00025/s (1.5 %/min)
V3: Predicted strain rate	0.0067/s (40 %/min)

**Table 4 Test Stress Rate (based on stress rate control)**

V1: Stress rate	10 MPa/s
V2: Strain rate	0.00083/s (5 %/min)
V3: Predicted strain rate	0.0067/s (40 %/min)

## Test Results

Fig. 4 shows a diagram of the stress – stroke displacement for each sample using strain-rate control, and Table 5 shows their characteristic values. In Fig. 4, the point at which the stress becomes discontinuous, as indicated by the jump in the stress-stroke displacement curve, corresponds to the point at which the strain rate is switched.

**Fig. 4 Test Results for Each Metallic Material (stress-stroke curve based on strain rate control)****Table 5 Test results (Average n = 3)**

Sample Name	Elastic Modulus (GPa)	0.2 % Proof Strength (MPa)	Tensile Strength (MPa)	Elongation at Break (%)
A (cold-rolled steel)	194	185.5	341.5	43.3
B (stainless steel)	200	278.5	660.8	55.0
C (aluminum)	71	170.1	236.3	13.0
D (brass)	109	193.1	398.1	49.1

Note 1) Strain rate refers to the amount of increase in strain, obtained using an extensometer to measure the gauge length of a test specimen, per unit time.

Note 2) Predicted strain rate was obtained using the displacement of the testing machine crosshead at each point in time and the test specimen's parallel length. Thus, it is defined as the increase in strain of the specimen's parallel length per unit time.

Fig. 5 (a) – (d) shows the strain rate and predicted strain rate obtained from tensile testing of the respective metallic materials using strain rate control. The red solid lines show the strain rate, the blue solid lines the predicted strain rate, and the black broken lines show the stress. In addition, the green dotted lines represent the permissible value  $\pm 20\%$  relative tolerance in the strain rate control (as specified in ISO 6892). As for the actual load rate, it is clear that the values are well

within the permissible strain rate control range, indicating excellent strain rate control. Regarding samples A and B, displacement is measured up to 2 % of the gauge length using an extensometer. In the case of samples C and D, the strain measured using an extensometer was only up to 0.8 %, because of the appearance of serration when strain corresponding to about 1 % was applied.

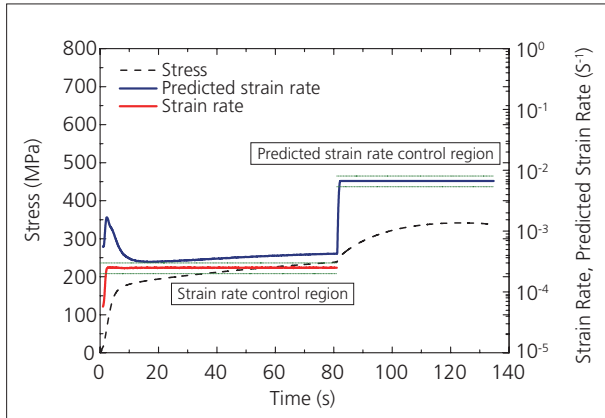


Fig. 5 (a) Test Results (Sample A)

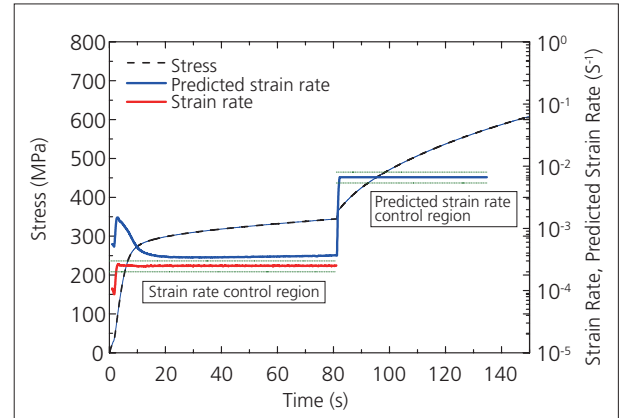


Fig. 5 (b) Test Results (Sample B)

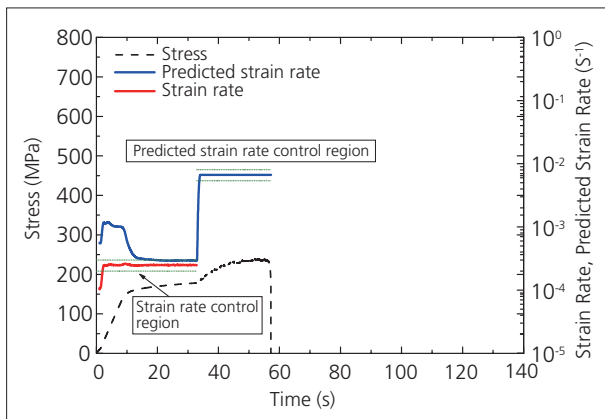


Fig. 5 (c) Test Results (Sample C)

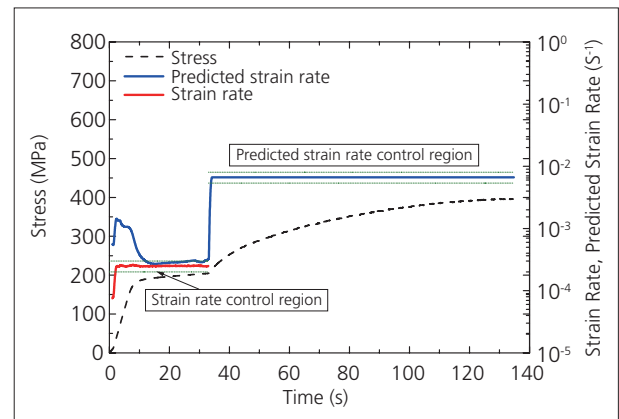


Fig. 5 (d) Test Results (Sample D)

Fig. 6 shows the stress-stroke displacement curve diagram obtained from tensile testing of each of the metallic materials using stress rate control, and the characteristic values are shown in Table 6.

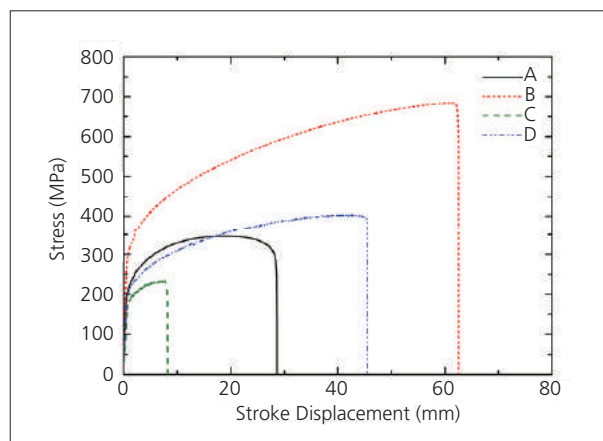


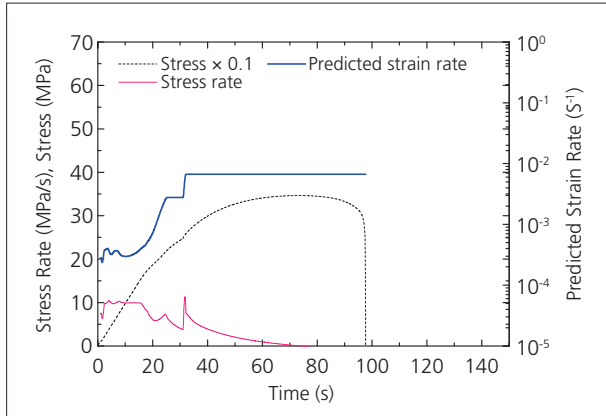
Fig. 6 Test Results (stress-stroke curve based on stress rate control)

**Table 6 Test Results (Average n = 3)**

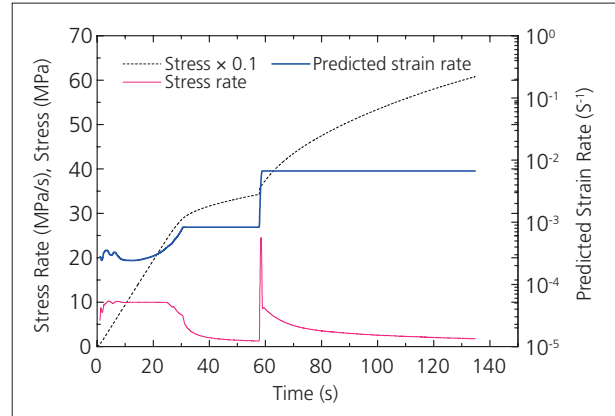
Sample Name	Elastic Modulus (GPa)	0.2 % Proof Strength (MPa)	Tensile Strength (MPa)	Elongation at Break (%)
A (cold-rolled steel)	194	193.3	349.3	42.0
B (stainless steel)	205	290.7	687.0	54.8
C (aluminum)	69	177.0	233.5	12.6
D (brass)	112	196.7	405.5	48.8

Fig. 7 (a) – (d) shows the strain rate and predicted strain rate obtained from tensile testing of the respective metallic materials using stress rate control. The pink

solid lines show the stress rate, the blue solid lines the predicted strain rate, and the black broken lines show the stress.



**Fig. 7 (a) Test Results (Sample A)**



**Fig. 7 (b) Test Results (Sample B)**

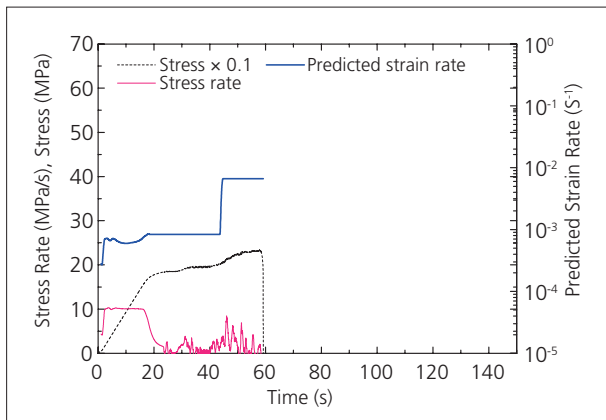


**Fig. 7 (c) Test Results (Sample C)**

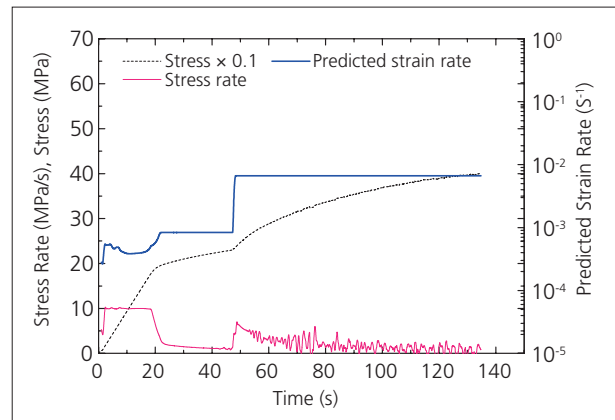


**Fig. 7 (d) Test Results (Sample D)**

It is clear that at the set rates, suitably stable data could be acquired for both stress rate and predicted strain rate.

The above results demonstrate that in the tensile testing of the various types of metallic materials using the Shimadzu Autograph AG-50kNX Precision Universal Tester, the strain rate control values were well within the range of the permissible values ( $\pm 20\%$ ) specified in ISO 6892. Similarly, stable testing using stress rate control was also achieved. When using typical universal

testing machines, testing control methods other than the crosshead rate control, e.g. strain rate control and stress rate control, normally require burdensome adjustment of the control gain depending on the material being tested. However, with this instrument, strain rate control and stress rate control in tensile testing of any metallic material are easily conducted because the gain is adjusted automatically (auto-tuning feature).



# Application Data Sheet

No. 14

## Autograph Precision Universal Tester

Material Testing & Inspection

## Tensile Testing of Metallic Materials with Stress Rate Control

Standard No. ISO6892:2009 (JIS Z 2241: 2011)

### Introduction

Metallic materials have excellent extensibility and ductility and are comparatively easy to mechanically process. Consequently, they are widely used in industrial components, building materials, and everyday goods. Tensile tests using stress rate control have long been used for quality control and new material development as a means of evaluating the mechanical properties of metallic materials. This Application Data Sheet introduces examples of static tensile testing using stress rate control performed on dumbbell-shaped test specimens of 4 types of metallic materials (cold-rolled steel, austenitic stainless steel, aluminium alloy, brass), in which basic mechanical properties such as tensile strength and elongation are evaluated.

T. Murakami

### Measurement and Jigs

Most metallic materials have tensile strengths higher than those of resin and rubber materials, so it is necessary to select grips that are capable of reliably and stably holding the material during testing up to fracture. For tensile testing of metallic materials, non-shift wedge-type or hydraulic grips are used for samples with a large test force. For samples with a small maximum test force, pneumatic flat and screw-type flat grips are also used.

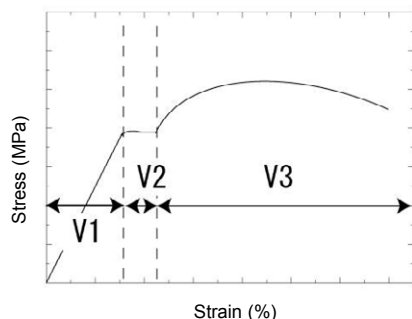
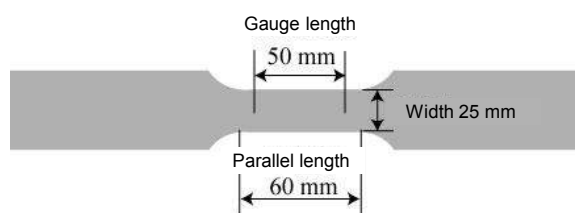


Fig. 1: Image of Controlling Rates

Table 1: Sample Information

Sample	A	B	C	D
Material	Cold-rolled steel	Stainless steel	Aluminum alloy	Brass



Width: 25 mm, thickness: 1 mm, gauge length: 50 mm, parallel length: 60 mm

Fig. 2: Sample Shape

V1: Rate of increase of stress: 10 MPa/s

V2: Estimated strain rate: 0.00084/s (5 %/min)

V3: Estimated strain rate: 0.0067/s (40 %/min)

Point of switching rate from V1 to V2: Point at which V1 exceeds V2 value

Point of switching rate from V2 to V3: Point at which measurement of displacement by extensometer is terminated

Note: The estimated strain rate is obtained based on the displacement per unit time of the crosshead of the testing machine and the parallel length of the test specimen. It is the increment of strain in the parallel length of the test specimen per unit time.

### Measurement Results

Table 2: Test Results

Sample	Elastic modulus (GPa)	Proof strength (offset method) (MPa)	Tensile strength (MPa)	Percentage elongation after fracture (%)
A (Cold-rolled steel)	194	193.3	349.3	42.0
B (Stainless steel)	205	290.7	687.0	54.8
C (Aluminum alloy)	69	177.0	233.5	12.6
D (Brass)	112	196.7	405.5	48.8

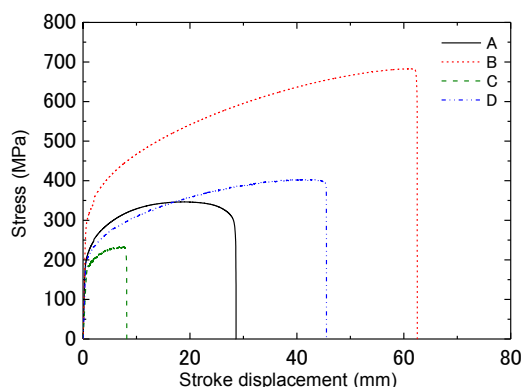


Fig. 3: Stress-Stroke Displacement Curves for Each Metal Material

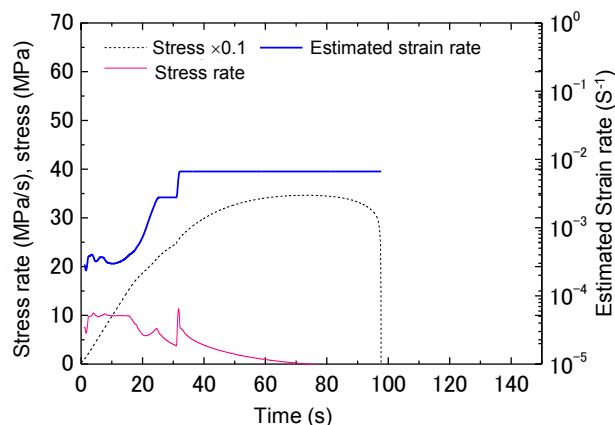


Fig. 4: Example of Stress Rate Results (Sample A: Cold-rolled steel plate)

Fig. 4 shows the stress rate and the estimated strain rate obtained from tensile testing the cold-rolled steel plate using stress rate control. It can be seen that stable data has been acquired in accordance with the set speed, for both the stress rate and estimated strain rate.

### Metal Stress Rate Control Tensile Testing System

Tester: AG-Xplus  
Load Cell: 50 kN  
Test Jig: 50 kN non-shift wedge type grips  
Extensometer: Strain gauge type one-touch extensometer: SSG50-10H  
Software: TRAPEZIUM X (Single)



AG-Xplus Floor-Type Precision Universal Tester

### Features

- A high-precision load cell is adopted. (The high-precision type is class 0.5; the standard-precision type is class 1.) Accuracy is guaranteed over a wide range, from 1/1000 to 1/1 of the load cell capacity. This supports highly reliable test evaluations.
- Crosshead speed range  
Tests can be performed over a wide range from 0.0005 mm/min to 1,000 mm/min.
- High-speed sampling  
Ultrafast sampling, as fast as 0.2 msec, allows assessment of sudden changes in test force, such as when brittle materials fracture.
- TRAPEZIUMX X operational software  
Designed for intuitive operation, it offers a variety of convenient and user-friendly features.
- Smart controller  
Real-time test force and position data are readily confirmed, and the manual dial enables fine adjustments to jig positioning.
- Optional Test Devices  
A variety of tests can be performed by switching between an abundance of jigs in the lineup.

First Edition: February 2013



Shimadzu Corporation

www.shimadzu.com/an/

For Research Use Only. Not for use in diagnostic procedures.  
The content of this publication shall not be reproduced, altered or sold for any commercial purpose without the written approval of Shimadzu. The information contained herein is provided to you "as is" without warranty of any kind including without limitation warranties as to its accuracy or completeness. Shimadzu does not assume any responsibility or liability for any damage, whether direct or indirect, relating to the use of this publication. This publication is based upon the information available to Shimadzu on or before the date of publication, and subject to change without notice.

© Shimadzu Corporation, 2013

# Application Data Sheet

No. 15

## Autograph Precision Universal Tester

Material Testing & Inspection

### Tensile Testing of Metallic Materials with Strain Rate Control

Standard No. ISO6892:2009 (JIS Z 2241: 2011)

#### Introduction

The international standard for tensile testing of metallic materials, ISO 6892, includes a strain rate control test method (strain measurement with an extensometer). This is in addition to the conventional stress rate control method as the loading method up to the yield point of the material. It is expected that tensile testing of metallic materials using both stress rate control and strain rate control will increase in the future. As a result, many existing testing machine users are interested in whether or not it is possible to obtain stable data from both test methods using existing and/or new testing machines. This Application Data Sheet introduces examples of static tensile tests using strain rate control carried out on dumbbell-shaped test specimens of 4 types of metallic material (cold-rolled steel, austenitic stainless steel, aluminium alloy, brass), in which basic mechanical properties such as tensile strength and elongation are evaluated.

T. Murakami

#### Measurement and Jigs

Most metallic materials have tensile strengths higher than those of resin and rubber materials, so it is necessary to select grips that are capable of reliably and stably holding the material during testing up to fracture. For tensile tests of metallic materials, non-shift wedge-type or hydraulic grips are used for samples with a large test force. For samples with a small maximum test force, pneumatic flat and screw-type flat grips are also used.

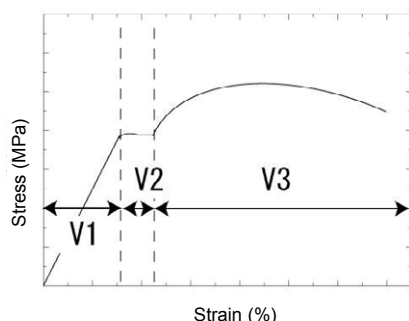
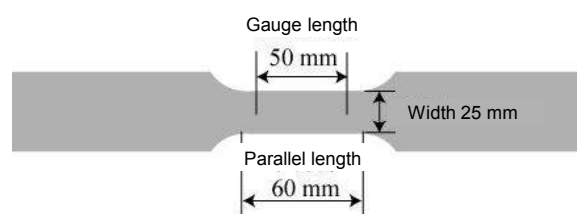


Fig. 1: Image of Controlling Rates

Table 1: Sample Information

Sample	A	B	C	D
Material	Cold-rolled steel	Stainless steel	Aluminum alloy	Brass



Width: 25 mm, thickness: 1 mm, gauge length: 50 mm, parallel length: 60 mm

Fig. 2: Sample Shape

V1, V2: Strain rate: 0.00025/s  $\pm 20$  % (feedback of strain from extensometer to testing machine)

V3: Estimated strain rate: 0.0067/s (40 %/min)  $\pm 20$  %

Point of switching rate from V2 to V3: Point at which measurement of displacement by extensometer is terminated (For samples A and B, displacement was measured using an extensometer up to 2 % of the gauge length. For samples C and D, serrations occurred when a strain equivalent to 1 % was applied, so measurement with the extensometer was used up to 0.8 %.)

Note: The estimated strain rate is obtained based on the displacement per unit time of the crosshead of the testing machine and the parallel length of the test specimen. It is the increment of strain in the parallel length of the test specimen per unit time.

#### Measurement Results

Table 2: Test Results

Sample	Elastic modulus (GPa)	Proof strength (offset method) (MPa)	Tensile strength (MPa)	Percentage elongation after fracture (%)
A (Cold-rolled steel)	194	185.5	341.5	43.3
B (Stainless steel)	200	278.5	660.8	55.0
C (Aluminum alloy)	71	170.1	236.3	13.0
D (Brass)	109	193.1	398.1	49.1

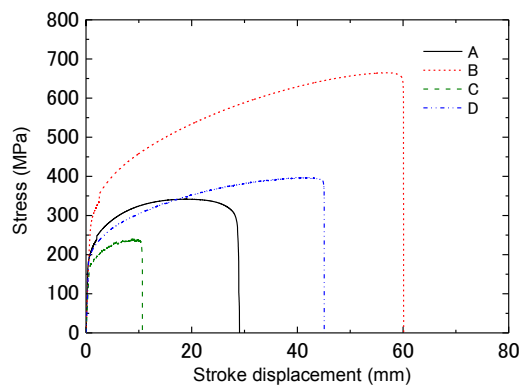


Fig. 3: Stress-Stroke Curves

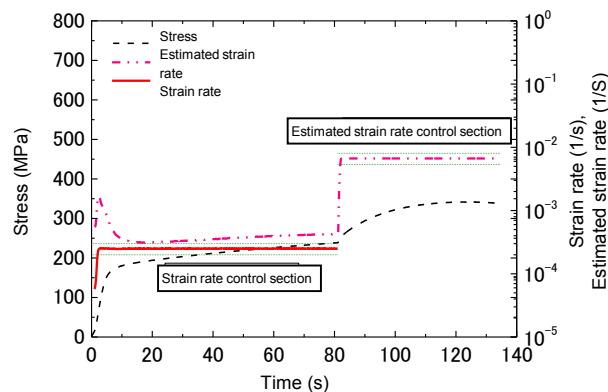


Fig. 4: Example of Strain Rate Results  
(Sample A: Cold-rolled steel plate)

Fig. 3 shows an example of the strain rate and estimated strain rate obtained from tensile testing the cold-rolled steel plate using strain rate control. The red solid line indicates strain rate, the pink double dotted broken line indicates the estimated strain rate, and the blue broken line indicates the stress. The green dotted line indicates the tolerance of the strain increase rate ( $\pm 20\%$  specified by ISO 6892). The actual load rate is sufficiently within the tolerance of the strain rate control range, which indicates that good strain rate control has been performed.

### Metal Strain Rate Control Tensile Testing System

Tester: AG-Xplus  
Load Cell: 50 kN  
Test Jig: 50 kN non-shift wedge type grips  
Extensometer: Strain gauge type one-touch extensometer SSG50-10H  
Software: TRAPEZIUM X (Single)

TRAPEZIUM X



AG-Xplus Floor-Type Precision Universal Tester

### Features

- A high-precision load cell is adopted. (The high-precision type is class 0.5; the standard-precision type is class 1.) Accuracy is guaranteed over a wide range, from 1/1000 to 1/1 of the load cell capacity. This supports highly reliable test evaluations.
- Crosshead speed range  
Test can be performed over a wide range from 0.0005 mm/min to 1,000 mm/min.
- High-speed sampling  
Ultrafast sampling, as fast as 0.2 msec, allows the assessment of sudden changes in test force, such as when brittle materials fracture.
- TRAPEZIUMX X operational software  
Designed for intuitive operation, it offers a variety of convenient and user-friendly features.
- Smart controller  
Real-time test force and position data are readily confirmed, and the manual dial enables fine adjustments to jig positioning.
- Optional Test Devices  
A variety of tests can be performed by switching between an abundance of jigs in the lineup.

First Edition: February 2013



Shimadzu Corporation

www.shimadzu.com/an/

For Research Use Only. Not for use in diagnostic procedures.  
The content of this publication shall not be reproduced, altered or sold for any commercial purpose without the written approval of Shimadzu. The information contained herein is provided to you "as is" without warranty of any kind including without limitation warranties as to its accuracy or completeness. Shimadzu does not assume any responsibility or liability for any damage, whether direct or indirect, relating to the use of this publication. This publication is based upon the information available to Shimadzu on or before the date of publication, and subject to change without notice.

© Shimadzu Corporation, 2013

## Application News

Material Testing System AG-X

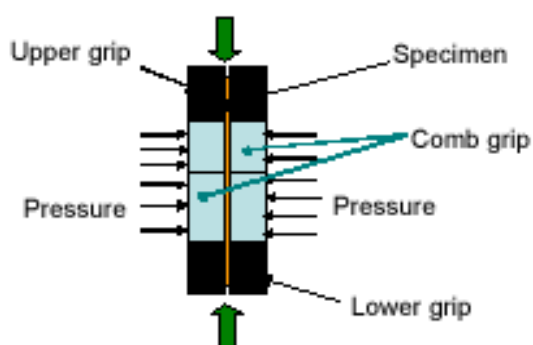
No. SCA\_300\_045

### Jigs for Measuring Bauschinger Effect

Use Autograph to simply perform in-plane reverse loading tests on sheet metal.

#### ■ In-Plane Reverse Loading Test

It is a testing method, where a sheet metal is subjected to tensile → compression → tensile reverse loading and continuously measuring the stress-strain curve. It can be used to make highly accurate measurements of the Bauschinger effect or the strain dependence of the elastic modulus required for forming simulation. In-plane reverse loading is possible by gripping the specimen with a die (comb grips) movable in the testing axis direction to prevent a specimen from buckling.



#### ■ Features

##### Space-saving:

Perform tests by attaching the jigs to Autograph. No specialized equipment required.

##### Good operability:

The jigs can be used sideways, making specimen setting easy. All operations from attachment of the jigs to testing can be performed by one person.

##### Simple displacement measurement:

Extension of the specimen can be measured using the strain gauge type extensometer. No need to attach a strain gauge to the specimen, making it possible to perform tests more efficiently.

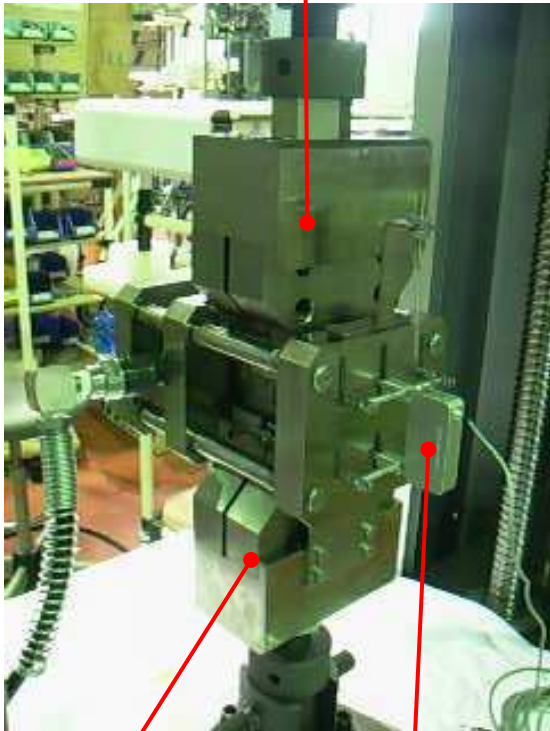
##### Simple operation:

Any straightening pressure can be set easily using the hydraulic jack and hydraulic hand pump.



■ External View of Jigs

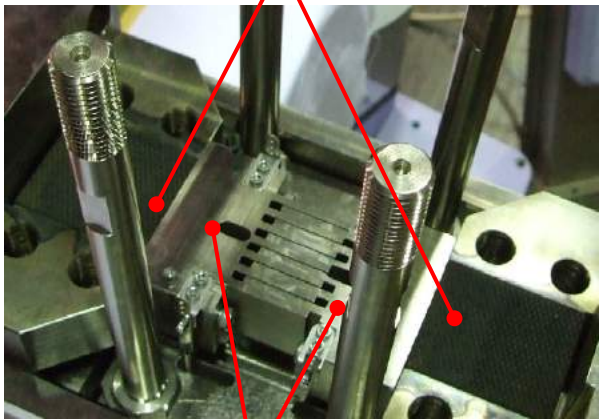
Upper Grip



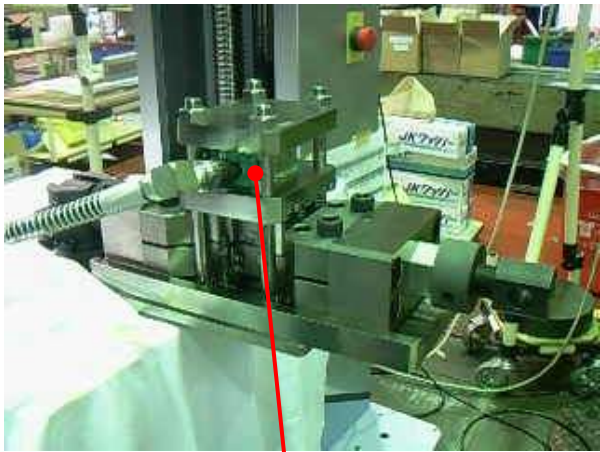
Lower Grip

SG Extensometer

Grip faces



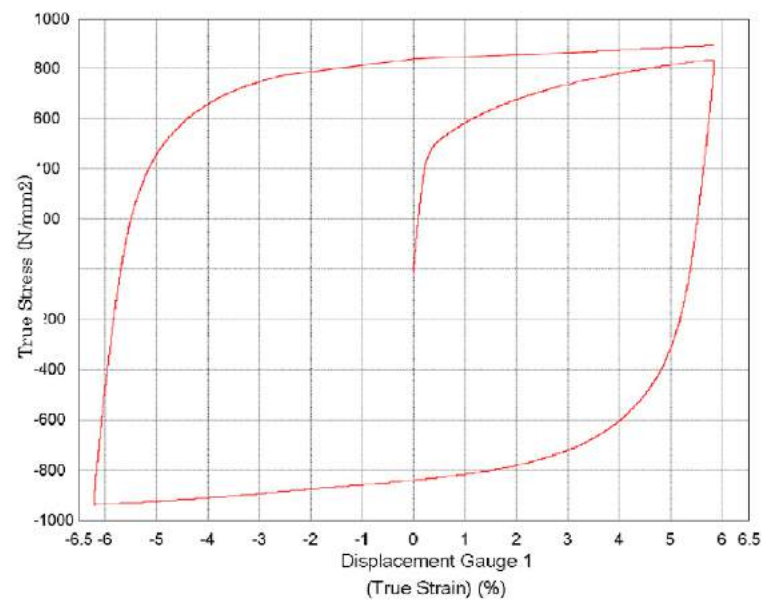
Comb Grip



Hydraulic Jack

■ Example of Test Results True Stress-True Strain Curve

Specimen: DP780 high strength steel, sheet thickness 1.4 mm



Specifications		
Applicable Testing Machine		AG-100kN
Loading Capacity		Tensile: 100 kN / Compression: 100 kN
Buckling Prevention Unit	Hydraulic Unit	Hydraulic hand pump
	Straightening Pressure	Max. 40 kN
Extensometer	Type	Strain gauge type
	Gauge Length	50 mm
	Measurement Range	+50 %/-10 %
	Measurement Precision	JIS B 7741 Class 1
Applicable Specimen	JIS 5	L200 mm x W40 mm
		Parallel section L60 mm x W40 mm
		1–3 mm thick
	JIS 5 Special Size (Wide specimen)	L200 mm x W45 mm
		Parallel section L60 mm x W35 mm
		1–3 mm thick
Operational Temp. Range		Room temperature

The test data is used with kind permission from G-TEKT Corporation

# Application News

## No.i250

### Material Testing System

## Shear Test of Composite Material (V-Notched Beam)

### ■ Introduction

Carbon fiber reinforced plastic (CFRP) do not oxidize or rust and have a higher specific strength and stiffness than existing materials. Applications of CFRP are being investigated, with a focus on applications as industrial products that require strength and durability. Compared to existing homogeneous materials, composite materials like CFRP are anisotropic, and display complex failure behaviors as a result of tension, compression, bending, in-plane shear, out-of-plane shear, or a combination of these stresses arising from loading in the principal-axis direction. In recent years, use of CAE analysis in industry has become widespread since it can reduce numbers of prototypes and reduce the cost of new product development. Because values for each of the stress properties stated above are needed to increase precision when predicting product characteristics during product design, there is a strong demand for test methods able to evaluate pure failure behaviors in CFRP.

This article describes an example of V-notched beam method (Iosipescu method, ASTM D5379) that is widely used as an in-plane shear test method for composite material specimens. The test method can apply load as a pure in-plane shear stress on the evaluation area (see Fig. 1) by using a specimen cut with V-notches and supported at four asymmetrical points. Setting up the specimen and jig for this test method is relatively easy, and the test method can be used with a variety of CFRP laminate materials, including unidirectional materials, orthogonally laminated materials, and discontinuous fiber materials.

### ■ Measurement System

The equipment configuration is shown in Table 1. Information on the specimen prescribed by ASTM D5379 is shown in Fig. 1. The specimen is a  $[0/90]_{10s}$  orthogonally laminated material made from Toray T800S prepreg that was molded in an autoclave. A two-axis strain gauge was attached at the mid-point between the upper and lower V-notches machined into the specimen (evaluation area), and oriented to measure strain in  $-45^\circ$  and  $+45^\circ$  directions. Shear strain can be calculated by inserting the strain values obtained from these two strain gauges into equation (1). Shear strain is a property needed to evaluate the shear modulus. In this test, strain gauges were attached on both the front and rear of the specimen. Calculating the mean of outputs obtained from strain gauges on both sides allows for more accurate measurement of the shear strain in the specimen, and confirms whether shear strain is being applied symmetrically on the front and rear of the specimen.

$$\gamma = |\epsilon_{+45}| + |\epsilon_{-45}| \quad \text{Equation (1)}$$

$\gamma$  : Shear strain

$\epsilon_{+45}$  : Strain at  $+45^\circ$

$\epsilon_{-45}$  : Strain at  $-45^\circ$

**Table 1 Test Conditions**

Testing Machine	: AG-50kNX plus
Load Cell	: 50 kN
Test Jig	: ASTM D 5379 jig
Software	: TRAPEZIUM X (Single)
Test Speed	: 2 mm/min

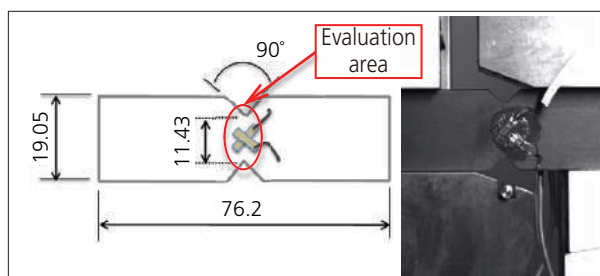


**Fig. 1 Shape of Specimen**



**Fig. 2 Testing Apparatus**



**Fig. 3 Imaging Apparatus**

The testing and imaging apparatus are shown in Fig. 2 and 3. Images captured using a TRViewX (Shimadzu Digital Video Extensometer) were gathered simultaneous to values obtained from the strain gauge outputs and specimen stress obtained by the testing apparatus. This made it easy to compare and evaluate images of the CFRP failure process against each specimen property values, something that was difficult to perform only with previous testing systems. Strain distribution can also be evaluated using digital image correlation (DIC, ARAMIS, GOMmbH) analysis of the images captured by TRViewX. To perform DIC analysis, paint must be sprayed on the specimen surface to create a random pattern on the front surface of the specimen.

■ Analytical Results

Each specimen property value obtained from this test is shown in Table 2. A photograph of the specimen after testing is shown in Fig. 4, a shear stress-normal strain curve is shown in Fig. 5 (strain values obtained from strain gauges), a shear stress-shear strain curve is shown in Fig. 6 (shear strain calculated from Equation (1)), and a shear stress-stroke curve is shown in Fig. 7. Table 2 shows that the results obtained for each shear property were highly reproducible. Fig. 5 and Fig. 6 show that the same strain values were obtained from the front and rear strain gauges, and highly symmetrical shear strain was applied to the specimen.

Table 2 Test Results

Specimen	Shear Modulus [GPa]	Shear Strength [MPa]
Test 1	4.62	136.0
Test 2	4.63	133.0
Test 3	4.50	131.0
Mean	4.58	133.0

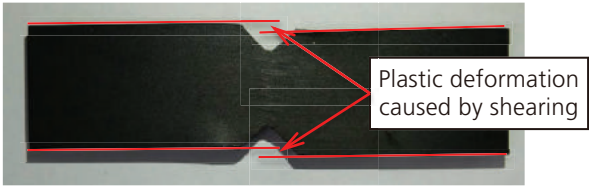


Fig. 4 Specimen After Testing

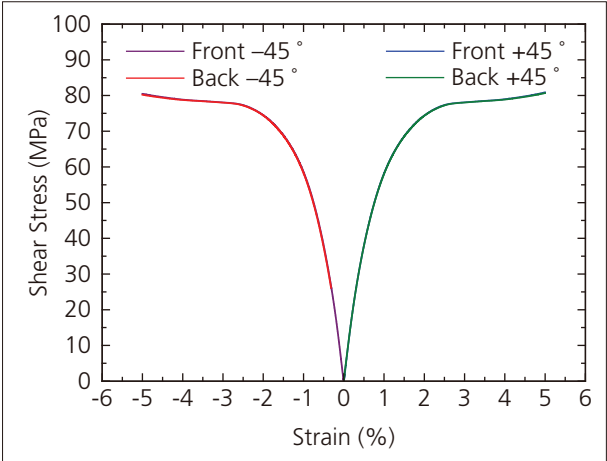


Fig. 5 Shear Stress-Normal Strain Curve

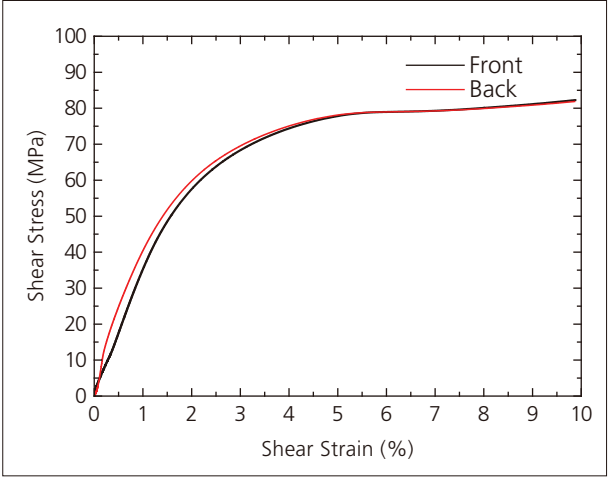


Fig. 6 Shear Stress-Shear Strain Curve

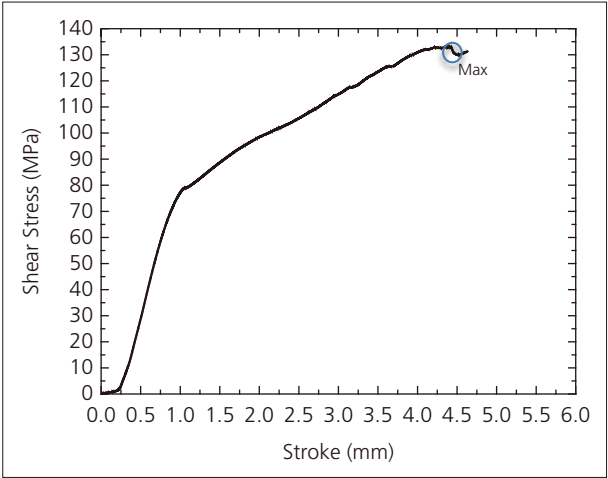


Fig. 7 Shear Stress-Stroke Curve

Failure of the specimen is shown in Fig. 8. Images of the shear strain distribution obtained by DIC analysis are shown in Fig. 9. The amount of strain occurring in the specimen is shown in terms of color, with low strain areas in cooler colors (black and blue) and high strain areas in warmer colors (orange and red). The images show that as the test progresses strain accumulates and is localized between the V-notches.



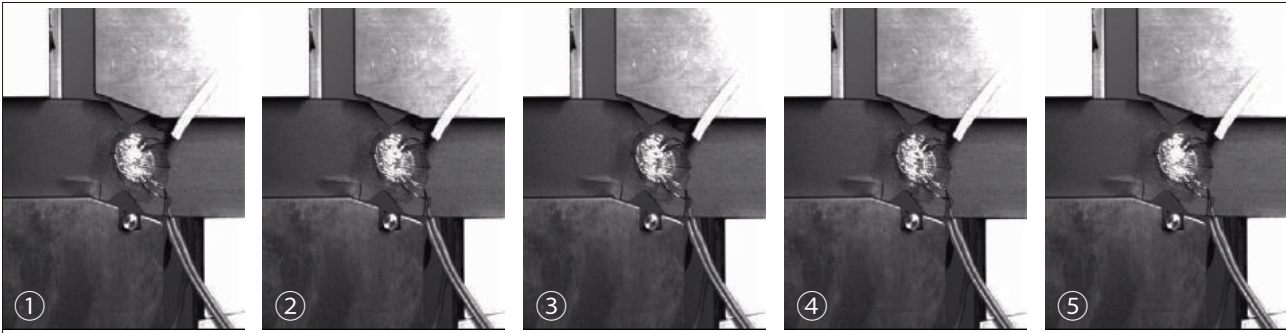


Fig. 8 Specimen e Failure Process (images show the point at which the specimen fails)

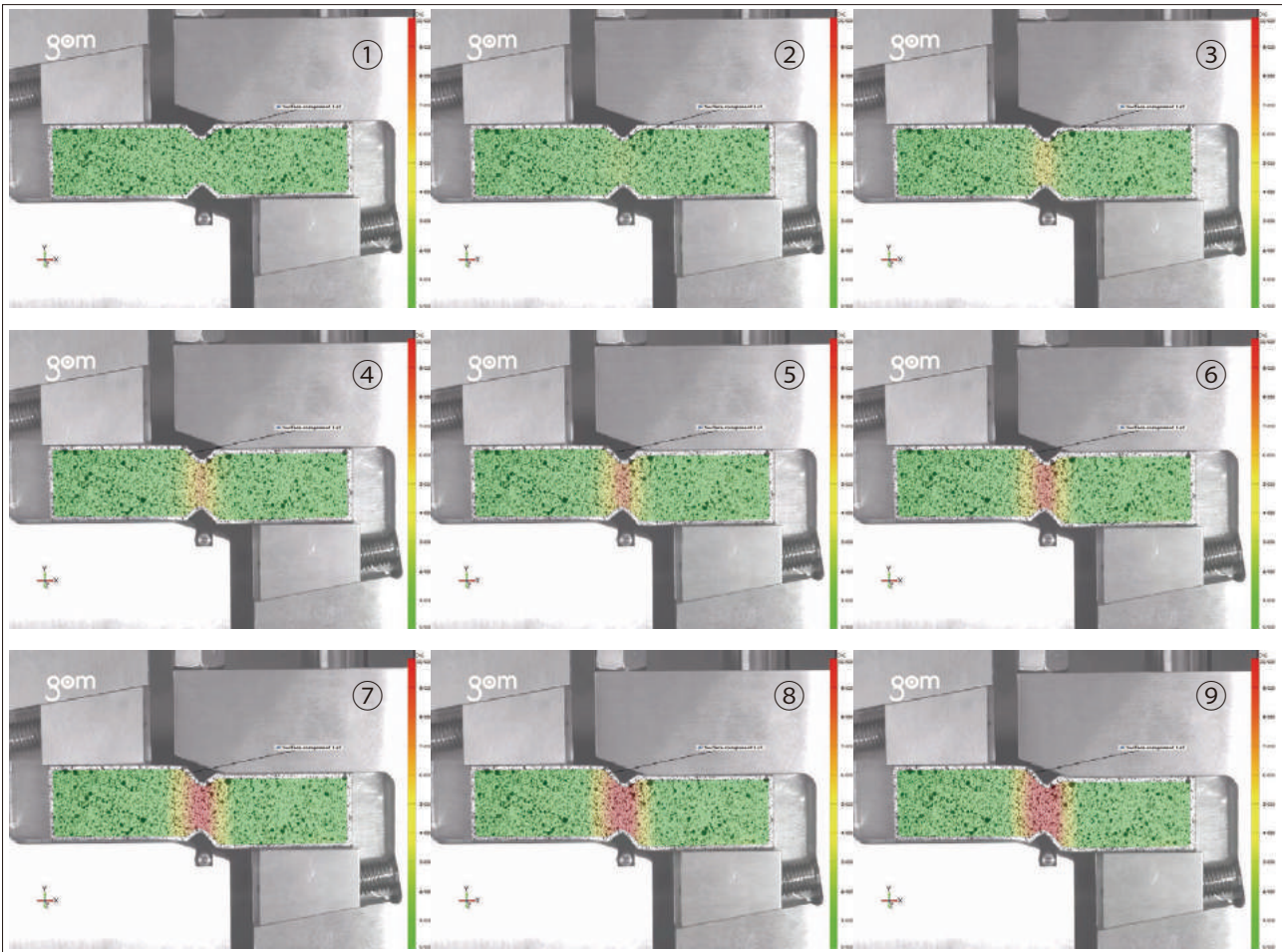


Fig. 9 Shear Strain Distribution (DIC analysis images)



## ■ Conclusion

We used this test system to successfully implement the V-notched beam method (ASTM D5379). In addition to evaluating the basic properties of shear modulus and shear strength, integrating a Digital Video Extensometer into the test system enabled us to capture reference data that can be used to elucidate the mechanism of failure of CFRP, allowing strain analysis to be performed in terms of specimen failure mode and DIC analysis.

First Edition: Aug. 2016



Shimadzu Corporation  
[www.shimadzu.com/an/](http://www.shimadzu.com/an/)

**For Research Use Only. Not for use in diagnostic procedure.**

This publication may contain references to products that are not available in your country. Please contact us to check the availability of these products in your country.

The content of this publication shall not be reproduced, altered or sold for any commercial purpose without the written approval of Shimadzu. Company names, product/service names and logos used in this publication are trademarks and trade names of Shimadzu Corporation or its affiliates, whether or not they are used with trademark symbol "TM" or "®". Third-party trademarks and trade names may be used in this publication to refer to either the entities or their products/services. Shimadzu disclaims any proprietary interest in trademarks and trade names other than its own.

The information contained herein is provided to you "as is" without warranty of any kind including without limitation warranties as to its accuracy or completeness. Shimadzu does not assume any responsibility or liability for any damage, whether direct or indirect, relating to the use of this publication. This publication is based upon the information available to Shimadzu on or before the date of publication, and subject to change without notice.

© Shimadzu Corporation, 2016

# Application News

## No.i251

### Material Testing System

## Shear Test of Composite Material (V-Notched Rail Shear)

### ■ Introduction

Carbon fiber reinforced plastic (CFRP) do not oxidize or rust and have a higher specific strength and stiffness than existing materials. Applications of CFRP are being investigated, with a focus on applications as industrial products that require strength and durability. Compared to existing homogeneous materials, composite materials like CFRP are anisotropic, and display complex failure behaviors as a result of tension, compression, bending, in-plane shear, out-of-plane shear, or a combination of these stresses arising from loading in the principal-axis direction. In recent years, use of CAE analysis in industry has become widespread since it can reduce numbers of prototypes and reduce the cost of new product development. Because values for each of the stress properties stated above are needed to increase precision when predicting product characteristics during product design, there is a strong demand for test methods able to evaluate pure failure behaviors in CFRP.

There are various tests methods for evaluating composite materials. Of these methods, two commonly used in-plane shear test methods to test in the direction of fibers in fiber reinforced composite materials and to test textile laminated materials are the Iosipescu method (ASTM D5379) that applies an asymmetrical four-point bending load to a specimen cut with notches, and method (ISO 14129) that applies a  $\pm 45^\circ$  tensile load on laminated materials. We used the V-notched rail shear method (ASTM D7078) that can be used to test in-plane shear. Because this method uses a large gauge area on the specimen, it can accommodate specimens without holes and CFRP laminate materials that have discontinuous fibers.

### ■ Measurement System

The equipment configuration is shown in Table 1. Information on the specimen prescribed by ASTM D7078 is shown in Fig. 1. The specimen is a  $[0/90]_{10S}$  orthogonally laminated material made from Toray T800S prepreg that was molded in an autoclave. The specimen has a 31-mm evaluation area (see Fig. 1), and two-axis strain gauges attached at the mid-point between the V-notches (center of evaluation area) that are able to measure strain in  $-45^\circ$  and  $+45^\circ$  directions. Shear strain can be calculated by inserting the strain values obtained from these two strain gauges into equation (1). Shear strain is a property needed to evaluate the shear modulus.

$$\gamma = |\epsilon_{+45}| + |\epsilon_{-45}| \quad \text{Equation (1)}$$

$\gamma$  : Shear strain

$\epsilon_{+45}$  : Strain at  $+45^\circ$

$\epsilon_{-45}$  : Strain at  $-45^\circ$

In this test, strain gauges were attached on both the front and rear of the specimen. Calculating the mean of outputs obtained from strain gauges on both sides allows for more accurate measurement of the shear strain in the specimen, and confirms whether shear

strain is being applied symmetrically on the front and rear of the specimen.

**Table 1 Test Conditions**

Testing Machine	: AG-50kNX plus
Load Cell	: 50 kN
Test Jig	: ASTM D7078 jig
Software	: TRAPEZIUM X (Single)
Test Speed	: 2 mm/min

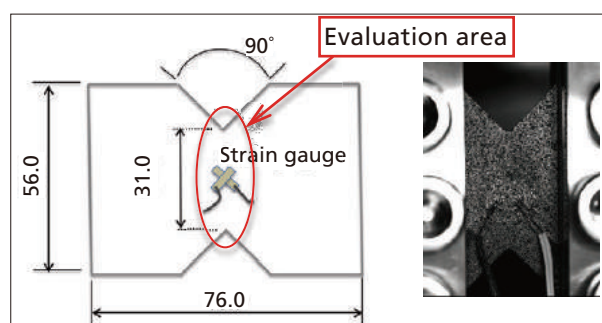


**Fig. 1 Shape of Specimen**

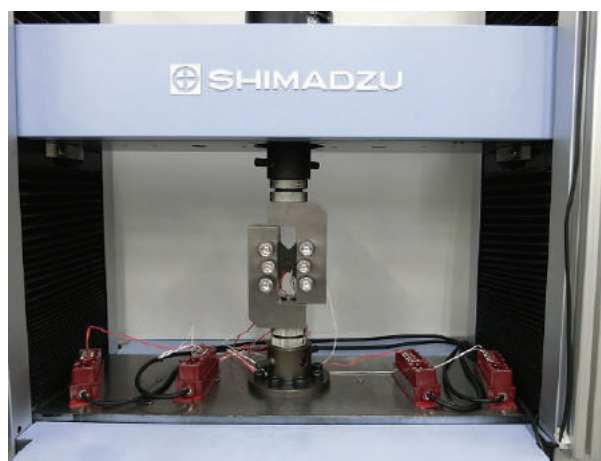


**Fig. 2 Testing Apparatus**

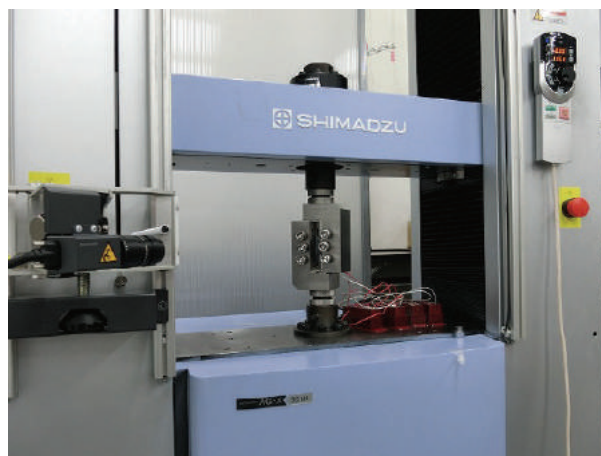


**Fig. 3 Imaging Apparatus**

The testing and imaging apparatus are shown in Fig. 2 and Fig. 3. Images captured using a TRViewX (Shimadzu Digital Video Extensometer) were gathered simultaneous to values obtained from the strain gauge outputs and specimen stress obtained by the testing apparatus. This made it easy to compare and evaluate images of the CFRP failure process against each specimen property values, something that was difficult to perform only with previous testing systems. Strain distribution can also be evaluated using digital image correlation (DIC, ARAMIS, GOMmbH) analysis of the images captured by TRViewX. To perform DIC analysis, paint must be sprayed on the specimen surface to create a random pattern on the front surface of the specimen.

■ Analytical Results

Each specimen property value obtained from this test is shown in Table 2. A photograph of the specimen after testing is shown in Fig. 4, a shear stress-normal strain curve is shown in Fig. 5 (strain values obtained from strain gauges), a shear stress-shear strain curve is shown in Fig. 6 (shear strain calculated from Equation (1)), and a shear stress-stroke curve is shown in Fig. 7. Table 2 shows that the results obtained for each shear property were highly reproducible. Fig. 5 and Fig. 6 show that the same strain values were obtained from the front and rear strain gauges, and highly symmetrical shear strain was applied to the specimen.

Table 2 Test Results

Specimen	Shear Modulus [GPa]	Shear Strength [MPa]
Test 1	4.63	121.72
Test 2	4.55	120.00
Test 3	4.58	120.05
Mean	4.59	120.60

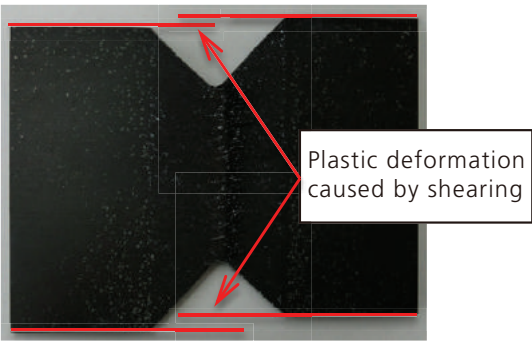


Fig. 4 Specimen After Testing

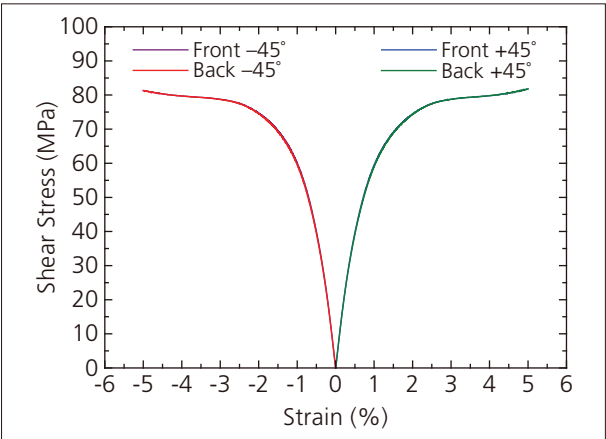


Fig. 5 Shear Stress-Normal Strain Curve

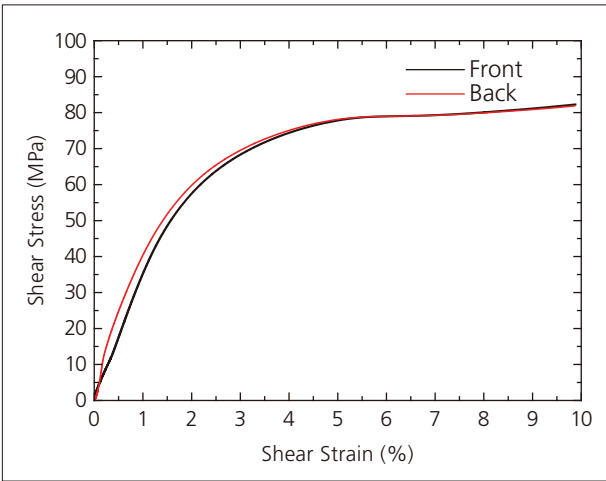


Fig. 6 Shear Stress-Shear Strain Curve

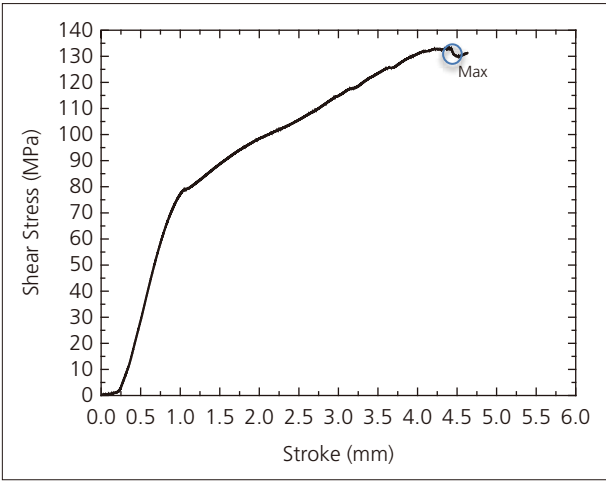


Fig. 7 Shear Stress-Stroke Curve

Failure of the specimen is shown in Fig. 8. A crack that appears close to the upper notch quickly propagates down toward the bottom notch during a simultaneous decrease in test force. Images of the shear strain distribution obtained by DIC analysis are shown in Fig. 9. The amount of strain occurring in the specimen is shown in terms of color, with low strain areas in cooler colors (black and blue) and high strain areas in warmer colors (orange and red). The images show that as the test progresses strain accumulates and is localized between the V-notches.



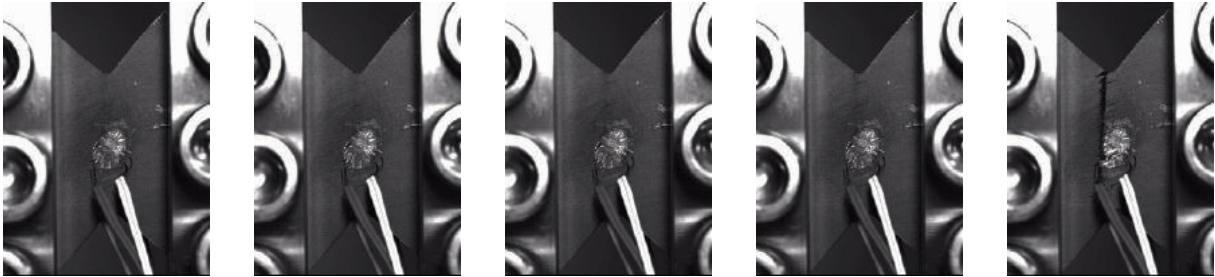


Fig. 8 Specimen Failure Process (images show the point at which the specimen fails)

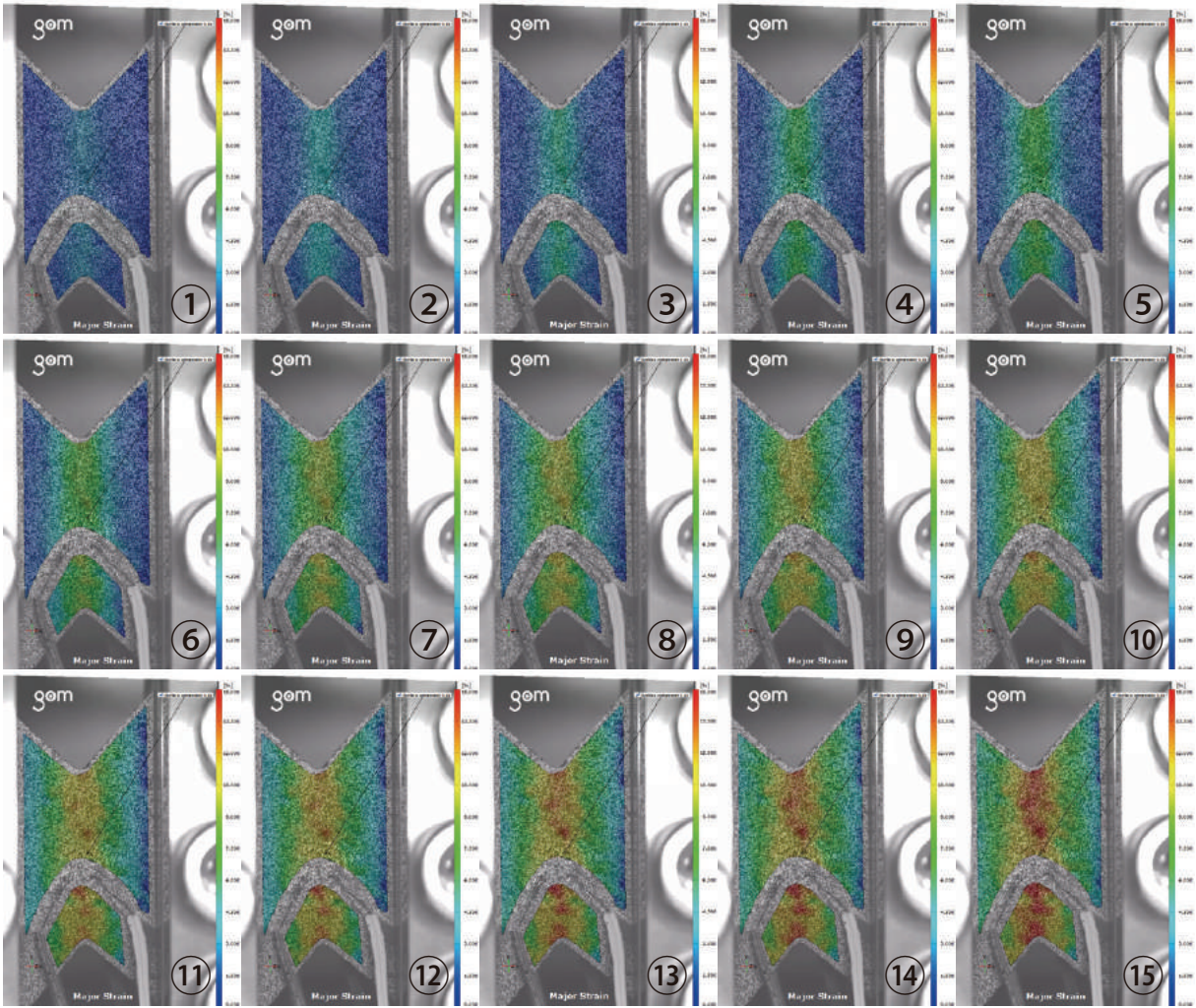


Fig. 9 Shear Strain Distribution (DIC analysis images)

### ■ Conclusion

We used this test system to successfully implement the V-notched rail shear method (ASTM D7078). In addition to evaluating the basic properties of shear modulus and shear strength, integrating a Digital Video Extensometer into the test system enabled us to capture reference data that can be used to elucidate the mechanism of failure of CFRP, allowing strain analysis to be performed in terms of specimen failure mode and DIC analysis.

First Edition: Aug. 2016



Shimadzu Corporation  
[www.shimadzu.com/an/](http://www.shimadzu.com/an/)

**For Research Use Only. Not for use in diagnostic procedure.**

This publication may contain references to products that are not available in your country. Please contact us to check the availability of these products in your country.

The content of this publication shall not be reproduced, altered or sold for any commercial purpose without the written approval of Shimadzu. Company names, product/service names and logos used in this publication are trademarks and trade names of Shimadzu Corporation or its affiliates, whether or not they are used with trademark symbol "TM" or "®". Third-party trademarks and trade names may be used in this publication to refer to either the entities or their products/services. Shimadzu disclaims any proprietary interest in trademarks and trade names other than its own.

The information contained herein is provided to you "as is" without warranty of any kind including without limitation warranties as to its accuracy or completeness. Shimadzu does not assume any responsibility or liability for any damage, whether direct or indirect, relating to the use of this publication. This publication is based upon the information available to Shimadzu on or before the date of publication, and subject to change without notice.

© Shimadzu Corporation, 2016



# Application News

## No.i254

### Material Testing System

## Compression After Impact Testing of Composite Material

### ■ Introduction

Carbon fiber reinforced plastic (CFRP) has a higher specific strength and rigidity than metals, and is used in aeronautics and astronautics to improve fuel consumption by reducing weight. However, CFRP only exhibits these superior properties in the direction of its fibers, and is not as strong perpendicular to its fibers or between its laminate layers. When force is applied to a CFRP laminate board, there is a possibility that delamination and matrix cracking will occur parallel to its fibers. Furthermore, CFRP is not particularly ductile, and is known to be susceptible to impacts. When a CFRP laminate board receives an impact load, it can result in internal matrix cracking and delamination that is not apparent on the material surface. There are many situations in which CFRP materials may sustain an impact load, such as if a tool being dropped onto a CFRP aircraft wing, or small stones hitting the a CFRP wing during landing. Consequently, tests are required for these scenarios. One of these tests is compression after impact (CAI) testing. CAI testing involves subjecting a specimen to a prescribed impact load, checking the state of damage to the specimen by a nondestructive method, and then performing compression testing of that specimen. This article describes CAI testing performed according to the ASTM D7137 (JIS K 7089) standard test method.

### ■ Measurements Taken Before Compression After Impact Testing

#### (1) Impact Test

The impact test involved dropping a 5 kg steel ball striker formed with a 16 mm diameter hemispherical point in the middle of the specimen. The specimen is fixed in place with four toggle clamps. The standard test method states that avoiding a second impact is preferred, so impact testing was performed with a mechanism that prevented second impacts. The impact energy recommended in the standard test method is 6.67 J per 1 mm of specimen thickness. For the purpose of comparison, the test was performed at four impact energies of 6.7, 5.0, 3.3, and 1.7 J per 1 mm thickness. Information on the specimen used is shown in Table 1. The test setup is shown in Fig. 1, and test conditions are shown in Table 2.

**Table 1 Specimen Information**

Dimensions [mm]	: 100 × 150 × 4.56
Lamination Method	: [45/0/-45/90] <sub>ns</sub>
Material	: T800, 2252S-21

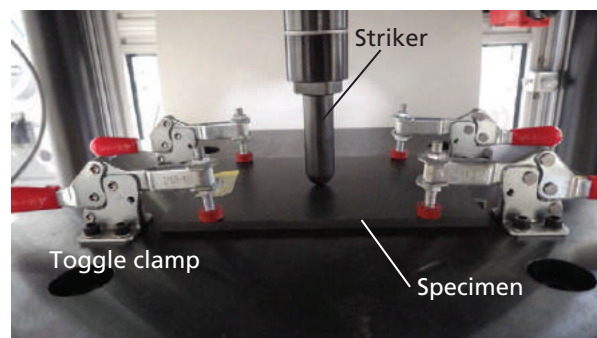


**Fig. 1 Impact Test Setup**

**Table 2 Impact Test Conditions**

Impact Energy	: 30.5, 22.9, 15.2, 7.6 [J]
No. of Tests	: n = 4

#### (2) Non-Destructive Inspection

After the impact test, the delamination area and maximum delamination length that resulted inside the laminate board were measured by nondestructive analysis. An ultrasonic flaw detection device is normally used for the non-destructive inspection step of CAI testing. The standard test method states that if ultrasonic flaw detection shows damage is present across more than half the width of the specimen, edge effects cannot be ignored and lowering the impact energy should be considered. Fig. 2 shows the setup for ultrasonic flaw detection.

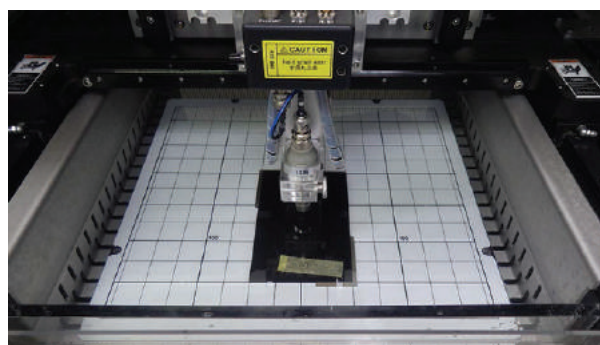


**Fig. 2 Ultrasonic Flaw Detection**

Fig. 3 shows the specimen after an impact test with an impact energy of 30.5 J. Fig. 3 shows an indentation in the middle of the specimen, but does not show the area of damage caused by delamination. Fig. 4 shows the results of ultrasonic flaw detection at each impact energy. The white areas in Fig. 4 are regions of delamination. Brighter areas show greater delamination. Comparison with Fig. 3 shows that delamination also occurs in areas other than the indentation in the center of the specimen, and the extent of internal damage cannot be determined based on external damage. The results also show that the damage area increases as the impact energy increases.

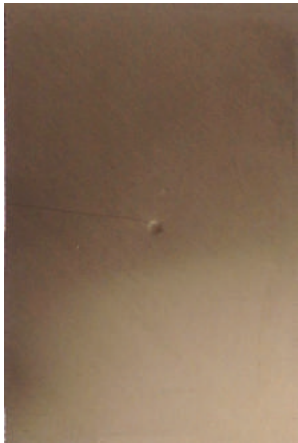


Fig. 3 Specimen After Impact Test (30.5 J Impact Energy)

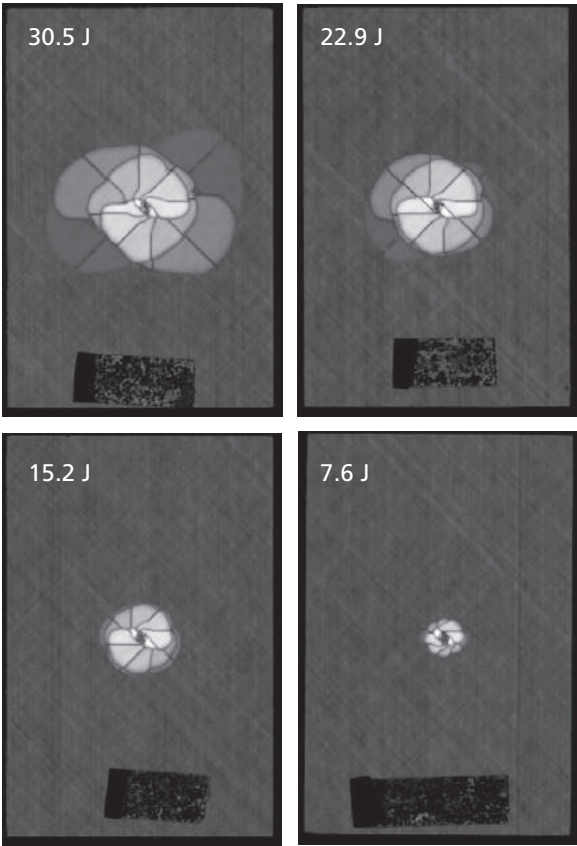
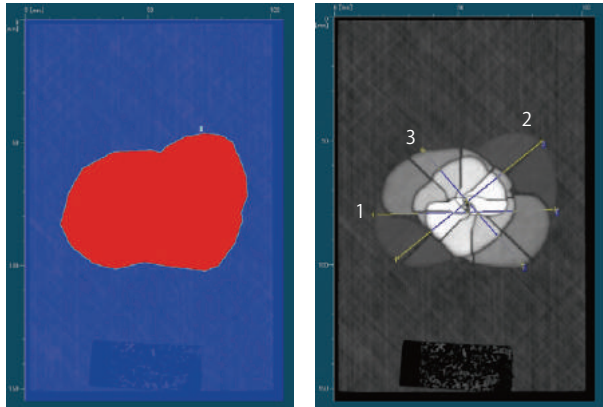


Fig. 4 Results of Ultrasonic Flaw Detection at Each Impact Energy

The damage area and maximum damage length are calculated from the images obtained by ultrasonic flaw detection. As an example, images used to calculate the damage area and maximum damage length after an impact energy of 30.5 J are shown in Fig. 5. Fig. 6 shows the relationship between damage area and impact energy, and Fig. 7 shows the relationship between maximum damage length and impact energy.



Region No.	Percentage Area (%)	Absolute Area (mm <sup>2</sup> )	No.	Length (mm)
1	99.9988	3326.2400	1	73.03
			2	75.50
			3	61.37

Fig. 5 Images of Damaged Area and Maximum Damage Length

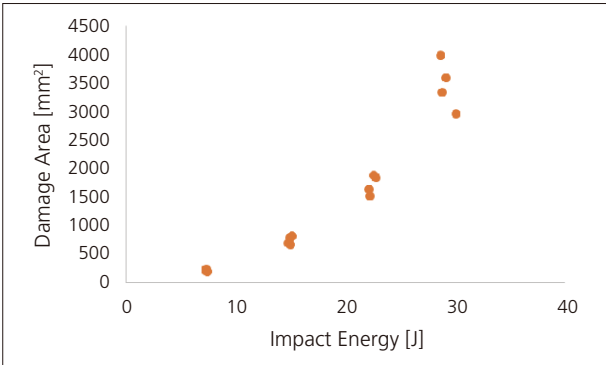


Fig. 6 Relationship between Damage Area and Impact Energy

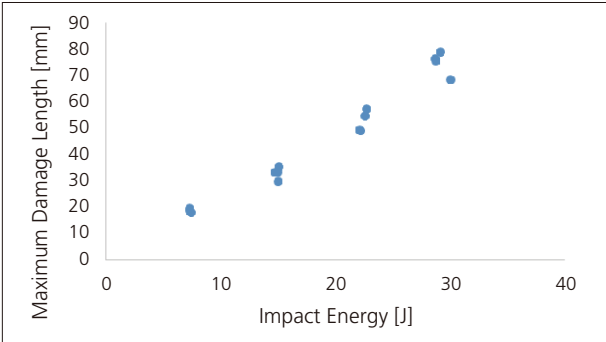


Fig. 7 Relationship between Maximum Damage Length and Impact Energy

■ Measurement System for Compression After Impact Testing

Two strain gauges must be attached to the front and back of the specimen. A specimen with strain gauges attached is shown in Fig. 8. The specimen shown in Fig. 8 is compressed at up to 10 % its expected compressive strength following impact in a longitudinal direction, and the CAI testing is performed after confirming the difference between front and rear strain gauges is within 10 %. Test conditions are shown in Table 3. The test setup is shown in Fig. 9, and test equipment used is shown in Table 4.

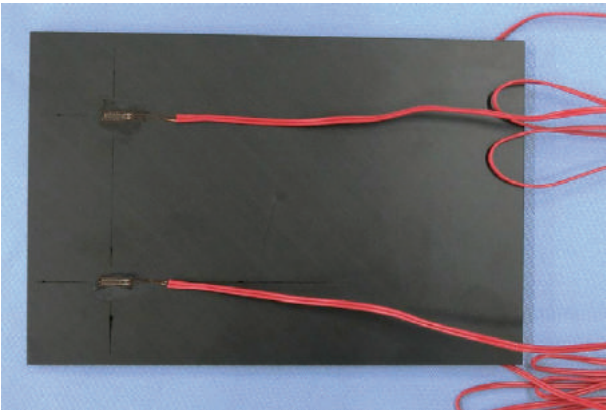


Fig. 8 Specimen

Table 3 Test Conditions

Test Speed	: 1.25 mm/min
No. of Tests	: n = 4

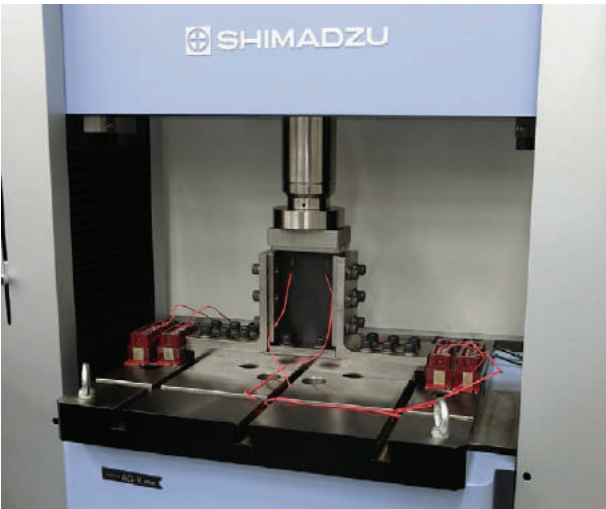


Fig. 9 Test Setup

Table 4 Experimental Equipment

Testing Machine	: AG-Xplus
Load Cell	: 250 kN
Test Jig	: Compression after impact test jig

■ Test Results

Examples of stress-strain curves at each impact energy are shown in Fig. 10. The compression-after-impact strength and mean compressive elastic modulus after impact are shown for each impact energy in Table 5. The standard test method states the compressive elastic modulus after impact should be calculated in the range of 0.1 % to 0.3 % strain. However, the breaking strain of one or more specimens was  $\leq 0.3$  % after the 30.5 J impact energy, and so for these specimens the elastic modulus was calculated from a linear region. Fig. 10 and Table 5 show the smaller the impact energy the larger the compression-after-impact strength. They also show the compressive elastic modulus after impact is almost constant regardless of impact energy.

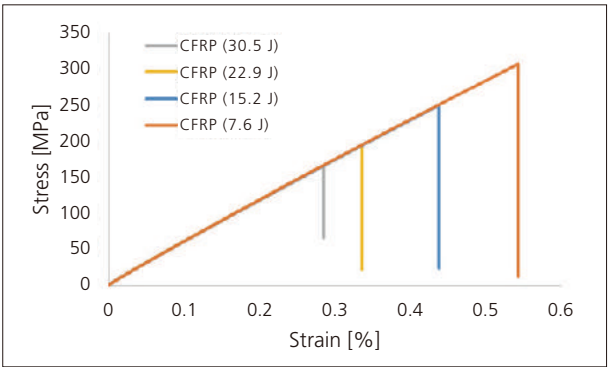


Fig. 10 Stress-Strain Curve

Table 5 Test Results (Mean)

Impact Energy [J]	Compression-After-Impact Strength [MPa]	Compressive Elastic Modulus After Impact [GPa]
30.5	162.9	57.2
22.9	203.3	56.4
15.2	246.4	56.0
7.6	308.6	56.3

The relationship between damage area and compression-after-impact strength is shown in Fig. 11, and the relationship between maximum damage length and compressive elastic modulus after impact is shown in Fig. 12. Fig. 11 and Fig. 12 show the smaller the damage area or maximum damage length, the larger the compression-after-impact strength. As a reference, the compressive strength of a specimen tested without applying any impact energy was 388 MPa.

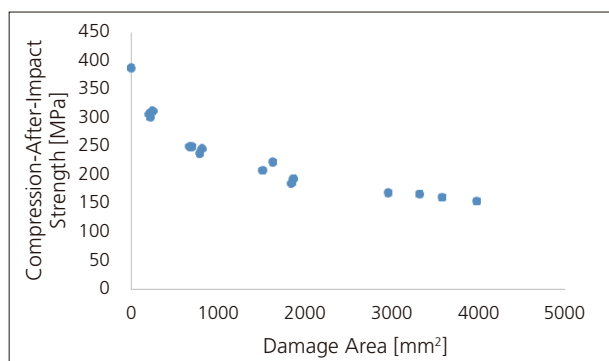


Fig. 11 Relationship between Damage Area and Compression-After-Impact Strength

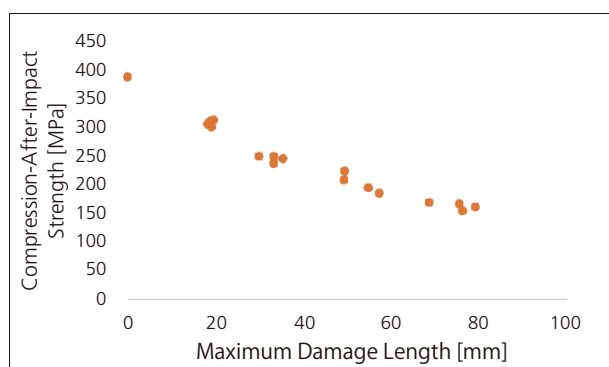


Fig. 12 Relationship between Maximum Damage Length and Compression-After-Impact Strength

## Conclusion

CAI testing was performed on specimens at four different impact energies. As shown by the results, the larger the impact energy the smaller the compression-after-impact strength. Also, even a small amount of impact energy (in this experiment, an impact energy of 7.6 J amounted to 5 kg dropped from 0.15 m) reduced the compression-after-impact strength compared to the undamaged compressive strength, showing the importance of testing scenarios for impact loading. Shimadzu's testing system was used successfully to perform CAI testing according to ASTM D7137 (JIS K 7089), and can be used for evaluation of CFRP materials.

First Edition: Aug. 2016



Shimadzu Corporation  
[www.shimadzu.com/an/](http://www.shimadzu.com/an/)

### For Research Use Only. Not for use in diagnostic procedure.

This publication may contain references to products that are not available in your country. Please contact us to check the availability of these products in your country.

The content of this publication shall not be reproduced, altered or sold for any commercial purpose without the written approval of Shimadzu. Company names, product/service names and logos used in this publication are trademarks and trade names of Shimadzu Corporation or its affiliates, whether or not they are used with trademark symbol "TM" or "®". Third-party trademarks and trade names may be used in this publication to refer to either the entities or their products/services. Shimadzu disclaims any proprietary interest in trademarks and trade names other than its own.

The information contained herein is provided to you "as is" without warranty of any kind including without limitation warranties as to its accuracy or completeness. Shimadzu does not assume any responsibility or liability for any damage, whether direct or indirect, relating to the use of this publication. This publication is based upon the information available to Shimadzu on or before the date of publication, and subject to change without notice.

© Shimadzu Corporation, 2016



# Application News

## No.i255

### Material Testing System

## Compression Test of Composite Material

### ■ Introduction

Even among composite materials, carbon fiber reinforced plastic (CFRP) has a particularly high specific strength, and is used in aeroplanes and some transport aircraft to improve fuel consumption by reducing weight. Compressive strength is an extremely important parameter in the design of composite materials that is always tested. However, due to the difficulty of testing compressive strength there is a variety of test methods. A major compression test method is the combined loading compression (CLC) method found in ASTM D6641. The CLC method can be performed with a simple jig structure, untabbed strip specimens, and can be used to simultaneously evaluate strength and measure elastic modulus. We performed compression testing of CFRP according to ASTM D6641.

### ■ Measurement System

A CFRP specimen of T800S/3900 was used. Other information on the specimen is shown in Table 1. The test equipment used is shown in Table 2. Based on the CLC method in ASTM D6641, the specimen was attached to the jig shown in Fig. 1 and compressed using compression plate. Fig. 2 shows a photograph of the specimen. As shown in Fig. 2, a strain gauge was attached on the front and rear in the middle of the specimen. Outputs from the front and rear strain gauges confirmed that the specimen was aligned straight in the jig during specimen attachment. The specimen was attached using a torque wrench to fasten it in place uniformly. The test was performed with the test speed set to 1.3 mm/min.

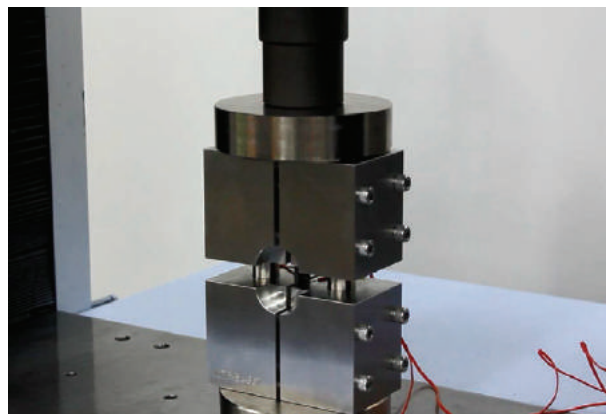


Fig. 1 Test Fixture



Fig. 2 Specimen

Table 1 Specimen Information

Length	: 140 mm
Width	: 13 mm
Thickness	: 3 mm
Lamination Method	: [90/0] <sub>45</sub>

Table 2 Experimental Equipment

Testing Machine	: AG-Xplus
Load Cell	: 50 kN
Test Jig	: CLC test fixture



■ Test Results

Measurements were performed twice, and stress-strain curves are shown in Fig. 3. The strain used is the mean strain taken from the front and rear sides of the specimen. The relationship between the first strain measurement and time is shown in Fig. 4 to show the outputs obtained from the strain gauges. Fig. 4 shows the outputs from both strain gauges were almost the same up to around 40 seconds, which is evidence that the test was successful. A small amount of deviation between the strain gauges arises after around 0.5 % strain, which is caused by a small amount of specimen flexure. Table 3 shows the test results. The mean compressive strength was 640.7 MPa, and the mean elastic modulus was 72.9 GPa. Elastic modulus was calculated using the mean of the strain gauge outputs.

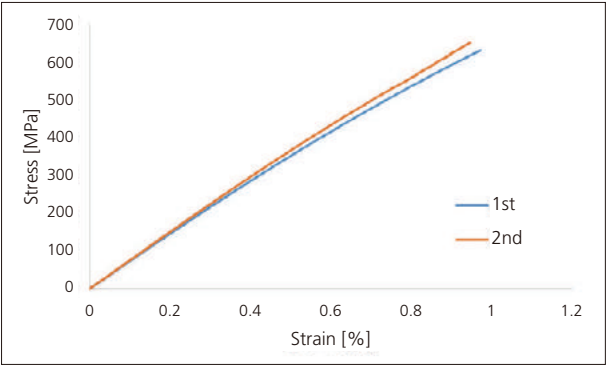


Fig. 3 Stress-Strain Curves (n = 2)

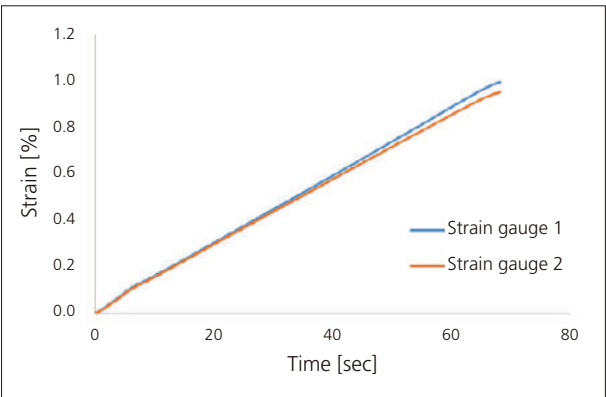


Fig. 4 Displacement-Time Curves (1st)

Table 3 Test Results

	Compressive Strength [MPa]	Elastic Modulus [GPa]
1st	629.9	71.4
2nd	651.4	74.3
Mean	640.7	72.9

■ Conclusion

Using this test system, compression testing of a CFRP was successfully performed according to ASTM D6641. Because this standard test method allows the testing of untabbed strip specimens, compressive strength and elastic modulus can be determined relatively easily for CFRPs.



# Application News

## No.i256

### Material Testing System

## Open-Hole Compression Test of Composite Material

### ■ Introduction

Carbon fiber reinforced plastic (CFRP) has gained attention due to their strength and low weight, and have quickly been adopted for use in aeronautics and astronautics. CFRP has excellent strength characteristics in terms of specific strength and high rigidity, but lose much of their strength when a cutout is made. Consequently, composite materials used in aeroplanes must be evaluated by tests that use specimens with a hole cut out of their center. We performed open-hole compression testing of a CFRP according to ASTM D6484.

### ■ Measurement System

The CFRP specimen used was T800S/3900. As shown in Fig. 1, a hole was created in the middle of the specimen. ASTM D6484 describes test methods in both SI and Imperial units, where the dimensions of the jigs and specimens differ in each. We performed testing with Imperial units. Specimen information is shown in Table 1. ASTM D6484 includes two loading methods, which are described as Method A and Method B. In Method A, the specimen and test fixture are clamped in a gripping device, and the specimen is compressed by shear force applied by the fixture and gripping device. In Method B, compression plate is present at the ends of the specimen and fixture, and are used to compress the specimen. Method B was used, as shown in Fig. 2. Table 2 shows a list of the equipment used and Table 3 shows the test conditions used.

**Table 1 Specimen Information**

Length	: 300 mm
Width	: 38.1 mm
Thickness	: 3.1 mm
Lamination Method	: [45/0/-45/92] <sub>25</sub>



**Fig. 1 Specimen**

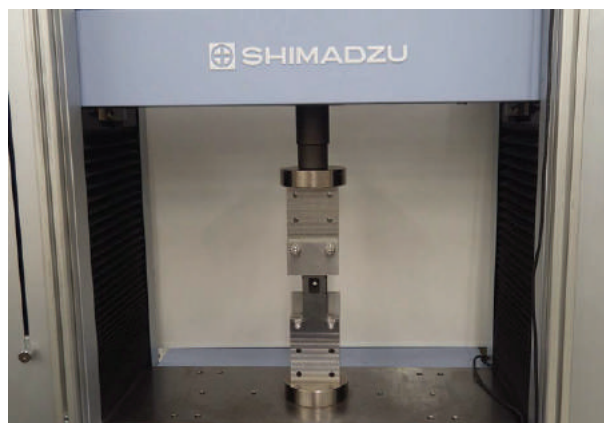


**Fig. 2 Test Setup**

**Table 2 Experimental Equipment**

Testing Machine	: AG-Xplus
Load Cell	: 50 kN
Test Fixture	: Open-Hole Compression Test Fixture

**Table 3 Test Conditions**

Test Speed	: 2 mm/min
------------	------------

### ■ Results

Measurements were performed twice. Test results are shown in Table 4 and stress-displacement curves are shown in Fig. 3. As shown in Table 4, the mean open-hole compressive strength was 275.6 MPa.

**Table 4 Test Results**

Specimen Name	Open-Hole Compressive Strength
1st	278.2 MPa
2nd	273.0 MPa
Mean	275.6 MPa

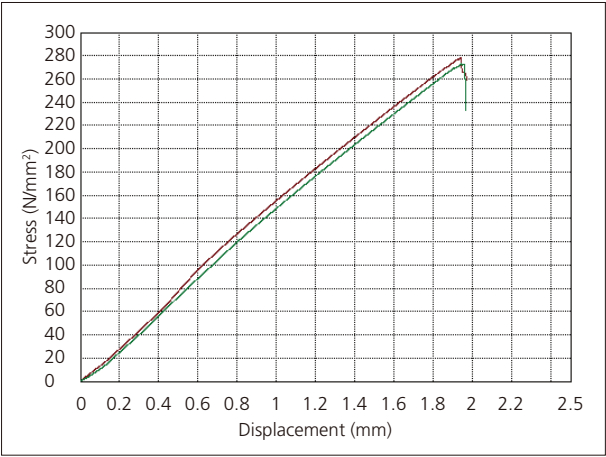


Fig. 3 Stress-Displacement Curves

■ Results (DIC Analysis)

Using the TRViewX non-contact extensometer allows for images and video of the specimen to be collected synchronized with test result collection. Also, applying a random pattern of paint to the observed specimen surface allows the images or video to be used to determine the strain distribution on the observed specimen surface during the test by DIC analysis<sup>1)</sup>. Open-hole compression testing and DIC analysis were performed using the specimen described in Table 5. Fig. 4 shows a photograph of the open-hole compression test system with a non-contact extensometer. Fig. 5 shows strain distributions around the open hole in the specimen that were obtained by DIC analysis. Fig. 5 shows that strain accumulates at the vertical sides of the open hole (regions (1) and (3)), strain appears along the axis of compression from those points, and the final break occurs at the vertical sides of the hole. Meanwhile, almost no strain appears in the central part of the hole (region (2)) throughout the test. This strain distribution probably occurred due to a 0° fiber orientation on the surface of the specimen.

Table 5 Specimen Information (DIC)

Length	: 300 mm
Width	: 38 mm
Thickness	: 1.6 mm
Lamination Method	: [0/90] <sub>25</sub>

1) DIC analysis is an analysis method that measures strain and shows the strain distribution in a specimen based on movement of a random pattern of paint applied to the observed specimen surface before and during testing.

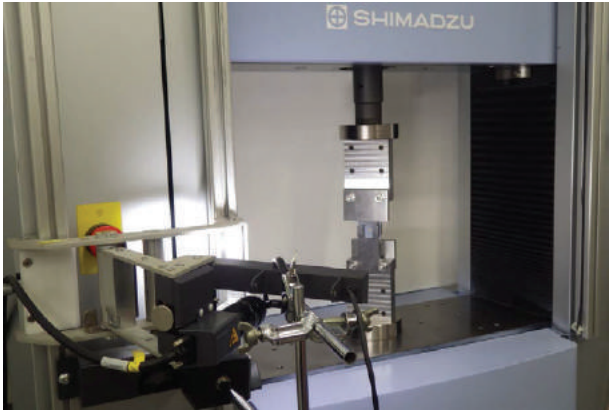


Fig. 4 Experimental Setup (DIC)

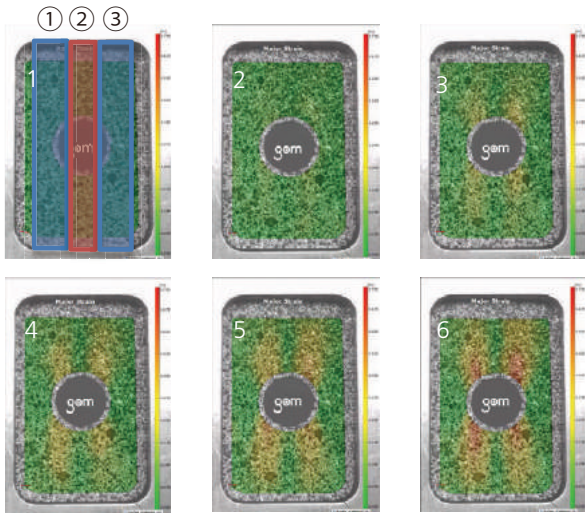


Fig. 5 DIC Analysis Results

■ Conclusion

Using this test system, open-hole compression testing of a CFRP was successfully performed according to ASTM D6484. Using a non-contact extensometer, we were also able to capture video (images) synchronized with the test force and crosshead displacement data obtained from the testing machine. Performing DIC analysis based on this video allowed an evaluation of the strain distribution on the observed specimen surface. This testing system will be extremely useful for the development of CFRPs and products that use CFRPs.



Shimadzu Corporation  
[www.shimadzu.com/an/](http://www.shimadzu.com/an/)

**For Research Use Only. Not for use in diagnostic procedure.**  
This publication may contain references to products that are not available in your country. Please contact us to check the availability of these products in your country.  
  
The content of this publication shall not be reproduced, altered or sold for any commercial purpose without the written approval of Shimadzu. Company names, product/service names and logos used in this publication are trademarks and trade names of Shimadzu Corporation or its affiliates, whether or not they are used with trademark symbol "TM" or "®". Third-party trademarks and trade names may be used in this publication to refer to either the entities or their products/services. Shimadzu disclaims any proprietary interest in trademarks and trade names other than its own.  
  
The information contained herein is provided to you "as is" without warranty of any kind including without limitation warranties as to its accuracy or completeness. Shimadzu does not assume any responsibility or liability for any damage, whether direct or indirect, relating to the use of this publication. This publication is based upon the information available to Shimadzu on or before the date of publication, and subject to change without notice.

# Application Data Sheet

No. 8

## Autograph Precision Universal Tester

Material Testing & Inspection

### Flexural Testing of CFRP Boards

Standard No. JIS K 7074: 1988

#### Introduction

Carbon fiber reinforced plastic (CFRP) is a composite material with excellent relative strength. This plastic was quickly adopted in the aviation and space sectors, and has contributed significantly to reducing fuselage weight. Initially, this plastic was only used for partial replacement of metal materials. In the latest aircraft, however, composite materials, primarily CFRP, represent 50 % of the fuselage weight. Improved productivity and reduced costs are expected due to subsequent technical developments, and it can be expected that this plastic will also become popular as a main material in automobile frames. In this Data Sheet, a CFRP cloth was subjected to a flexural testing using a precision universal tester in order to evaluate the strength of the material.

F. Yano

#### Measurements and Jigs

In flexural testing specified in JIS K7074, a loading edge radius of 5 mm, and a support radius of 2 mm are specified. The specimen standard dimensions are specified as follows:

Length = 100 mm  $\pm$  1 mm

Width = 15 mm  $\pm$  0.2 mm

Thickness = 2 mm  $\pm$  0.4 mm

For tests performed using a specimen with the standard dimensions, the span between supports (L) will be 80 mm  $\pm$  0.2 mm. When TRAPEZIUM software is used, the flexural stress can be automatically calculated and plotted in a graph from the test force and the specimen dimensions. The flexural strength and other characteristic values can also be obtained from a few simple operations.

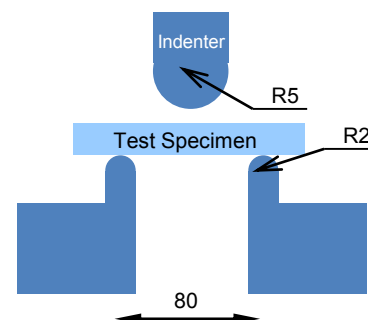


Fig. 1: Flexural Testing Schematic

#### Measurement Results



Fig. 2: Flexural Testing Status

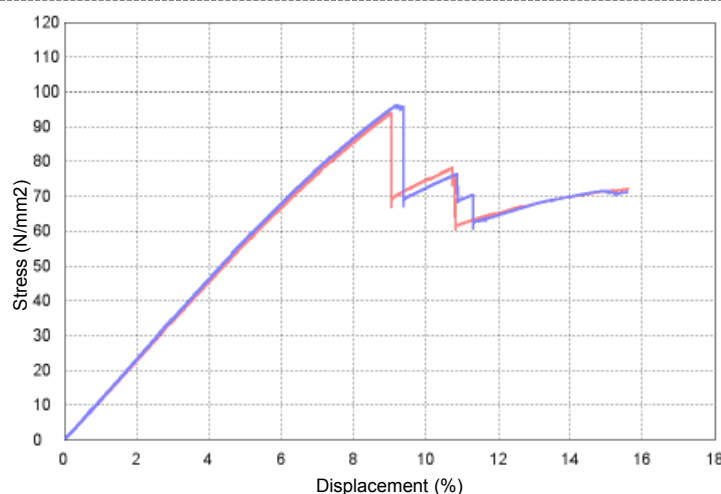


Fig. 3: Stress – Displacement Curve

Table 1: Test Conditions

Item	Set Value
Cell Capacity	5 kN
Load Speed	5 mm/min

Table 2: Test Results (Average)

Load at Fracture (N)	Bending Strength (%)
485	95

## CFRP Flexural Testing System

Tester: AG-Xplus  
Load Cell: 5 kN  
Test Jig: Three-point bending test jig for plastics  
Software: TRAPEZIUM X (Single)



AG-Xplus Table-Top Precision Universal Tester

## Features

- A high-precision load cell is adopted. (The high-precision type is class 0.5; the standard-precision type is class 1.) Accuracy is guaranteed over a wide range, from 1/1000 to 1/1 of the load cell capacity. This supports highly reliable test evaluations.
- Crosshead speed range  
Tests can be performed over a wide range from 0.0005 mm/min to 1,500 mm/min.
- High-speed sampling  
Ultrafast sampling, as fast as 0.2 msec. Sudden changes in test force, such as when brittle materials fracture, can be assessed.
- TRAPEZIUMX operational software  
Designed for intuitive operation, this software offers excellent convenience and user friendliness.
- Smart controller  
Real-time test force and position data is readily confirmed, and the manual dial can be used for fine adjustments to jig positioning.
- Optional Test Devices  
A variety of tests can be conducted by switching between an abundance of jigs in the lineup.

First Edition: February 2013



Shimadzu Corporation

[www.shimadzu.com/an/](http://www.shimadzu.com/an/)

For Research Use Only. Not for use in diagnostic procedures.  
The content of this publication shall not be reproduced, altered or sold for any commercial purpose without the written approval of Shimadzu. The information contained herein is provided to you "as is" without warranty of any kind including without limitation warranties as to its accuracy or completeness. Shimadzu does not assume any responsibility or liability for any damage, whether direct or indirect, relating to the use of this publication. This publication is based upon the information available to Shimadzu on or before the date of publication, and subject to change without notice.

© Shimadzu Corporation, 2013



# Application Data Sheet

No. 16

## Autograph Precision Universal Tester

Material Testing & Inspection

### Tensile Testing of Carbon Fiber

Standard No. ISO11566: 1996 (JIS R 7606: 2000)

#### Introduction

Carbon fiber is an important industrial material, being essential in carbon fiber reinforced plastics (CFRP), having a specific gravity one-fourth that of normal steels, and a specific strength of 7 times. In this Application Data Sheet, examples of tensile testing of single carbon fibers based on the ISO standard are introduced.

T. Murakami

#### Measurements and Jigs

In this test, the test sample is fixed to a test specimen mounting board made from a paper, metal, or resin sheet as shown in Fig. 1, installed in the grips, and the tensile test is performed. The standard describes in detail the shape of the mounting board, the type of adhesive used to fix the carbon fiber to the mounting board, and the procedure for installing the carbon fiber (for details refer to the standard). The tests were carried out using clip type grips whose grip force could be adjusted in accordance with the strength of the sample.

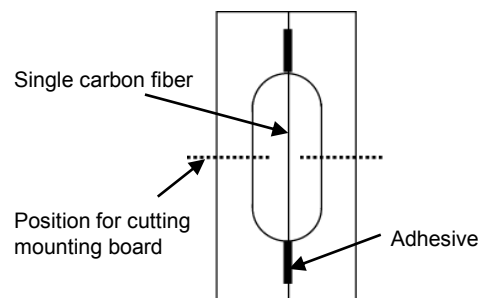


Fig. 1 Test Sample and Mounting Board (frame)

#### Measurement Results

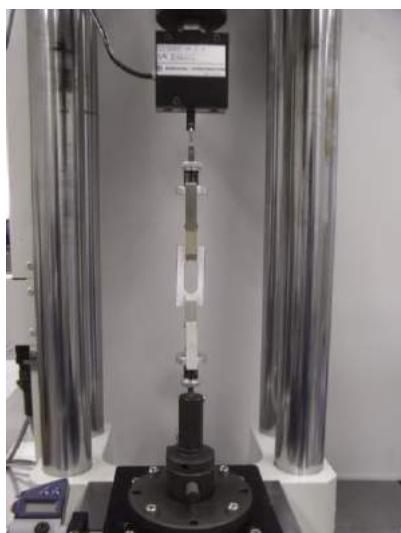


Fig. 2 Test Status

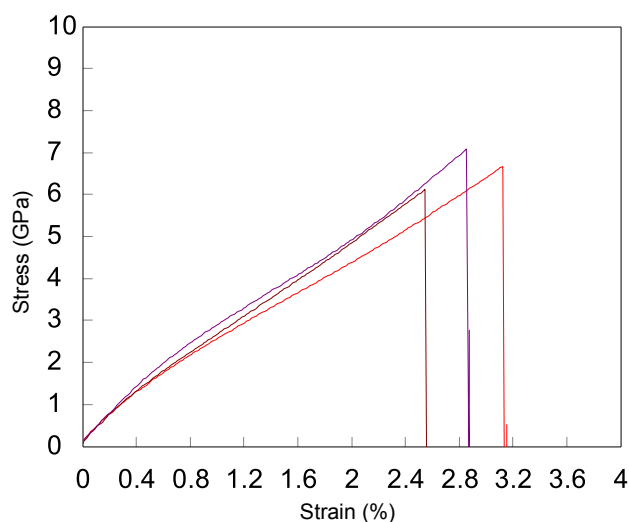


Fig. 3 Test Results

Table 1 Test Conditions

Item	Set Value
Test speed	1 mm/min
Distance between grips	25 mm

Table 2 Test Results (average)

Sample	Diameter	Tensile Strength	Elongation at Break
Carbon fiber	6 $\mu$ m	7.1 GPa	2.84 %

## Carbon Fiber Tensile Test System

Tester: MST-I Type HR  
Load Cell: 1 N  
Test Jig: 1 N clip type grips (rubber-coated teeth), X-Y stage  
Software: TRAPEZIUM X (Single)



Shimadzu Autograph MST-1 Micro Strength Evaluation Testing Machine

## Features

### ■ High Accuracy Displacement Measurement

A high accuracy ( $\pm 0.2 \mu\text{m}$ ) linear sensor has been adopted for measurement of displacement in the load direction. In addition, the backlash-free structure makes it possible to carry out testing with good accuracy. Displacement in the load direction of the test sample can be set accurately to a displacement display resolution of  $0.02 \mu\text{m}$  and a control resolution of  $0.005 \mu\text{m}$ .

### ■ Measurement of Micro Test Forces

A wide range of load cells from 0.5 N to 2 kN assures a precision of  $\pm 1 \%$  for measurements of testing forces of 2 mN at minimum.

### ■ Positioning Very Small Test Samples

Using an X-Y stage (optional), very small test samples can be easily positioned. The position of the test samples can be observed using a stereo microscope.

### ■ High Rigidity Frame

A high rigidity frame (45 kN/mm minimum) has been adopted to enable measurement of minute displacements.

### ■ Optional Test Devices

A variety of tests can be accommodated by switching between an abundance of jigs in the lineup.

First Edition: February 2013



Shimadzu Corporation

[www.shimadzu.com/an/](http://www.shimadzu.com/an/)

For Research Use Only. Not for use in diagnostic procedures.

The content of this publication shall not be reproduced, altered or sold for any commercial purpose without the written approval of Shimadzu. The information contained herein is provided to you "as is" without warranty of any kind including without limitation warranties as to its accuracy or completeness. Shimadzu does not assume any responsibility or liability for any damage, whether direct or indirect, relating to the use of this publication. This publication is based upon the information available to Shimadzu on or before the date of publication, and subject to change without notice.

© Shimadzu Corporation, 2013

# Application Data Sheet

No. 30

## Autograph Precision Universal Tester

Material Testing & Inspection

### Evaluating the Strength of Carbon Fiber Reinforced Plastics (CFRP)

#### ■ Introduction

Various types of plastic materials have been developed that are light weight and also perform better than previous materials in terms of environmental resistance and in terms of strength. Consequently, there is a growing demand for such materials in aircraft, automotive, and many other fields. These plastic materials, such as carbon fiber reinforced plastic (CFRP), glass fiber reinforced plastic (GFRP), and aramid fiber reinforced plastic, are characterized by using fibers with advanced functionality (low weight, high strength, deformation resistance, corrosion resistance, and also heat resistance). Carbon fiber reinforced plastic (CFRP) is particularly representative of such materials and is increasingly used in sports equipment and other everyday products. Therefore, evaluating its strength, its fundamental feature, is very important.

This article presents results from testing carbon fiber reinforced plastic (CFRP) using a Shimadzu Autograph precision universal testing machine. (Test specimens and loading conditions conformed to JIS K7073-1988 Testing Method for Tensile Properties of Carbon Fiber Reinforced Plastics.)

#### ■ Measurement and Jigs

Specimens were Type-IV specified by JIS K7073-1988 (rectangular strips with no tabs). Tensile tests were conducted with an extensometer attached to measure longitudinal strain and a width sensor attached to measure lateral strain, as shown in Fig. 1.



Fig. 1 Test Configuration

#### ■ Test Results

Test results indicate a tensile strength of  $8.31 \times 10^2$  MPa, an elastic modulus of  $5.76 \times 10^5$  MPa (determined from the slope between points at 100 MPa and 300 MPa), and a maximum tensile strain of 0.766 percent. Since these results were obtained using test specimens with fibers oriented perpendicular (lateral) to the direction of tensile load, the same test was performed with fibers oriented parallel (longitudinal) to the direction of tension. This resulted in an elastic modulus of about  $13.00 \times 10^5$  MPa, which indicates a significant difference depending on the fiber orientation.

Fig.3 shows the relationship between stress and displacement in the direction perpendicular to tension, for the same test as before. A calculation of Poisson's ratio between 100 MPa and 300 MPa, as before, resulted in a value of  $6.0 \times 10^{-2}$ .

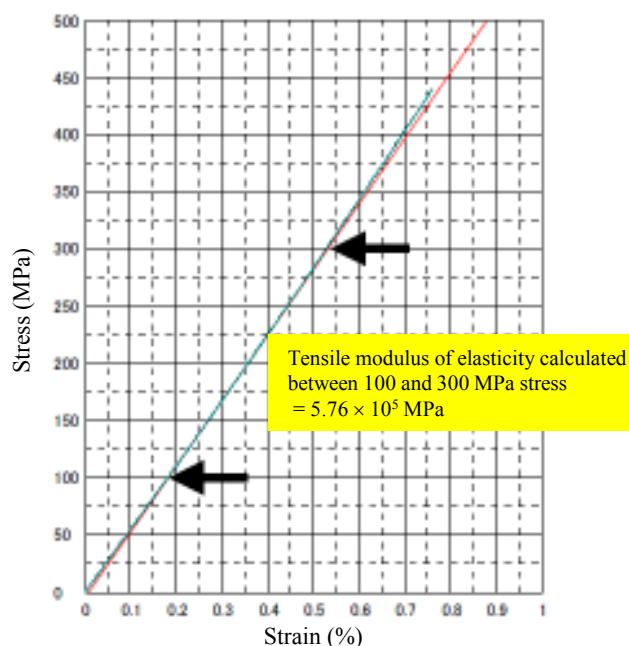


Fig.2 shows the results of testing to failure at a rate of 1 mm/min (stress vs. longitudinal strain curve).

Whereas the Poisson's ratio is about 0.3 for soft iron and about 0.46 to 0.49 for elastic rubber, the ratio for carbon fiber reinforced plastic (CFRP) is about one order of magnitude smaller, which means the deformation level of CFRP is extremely low.

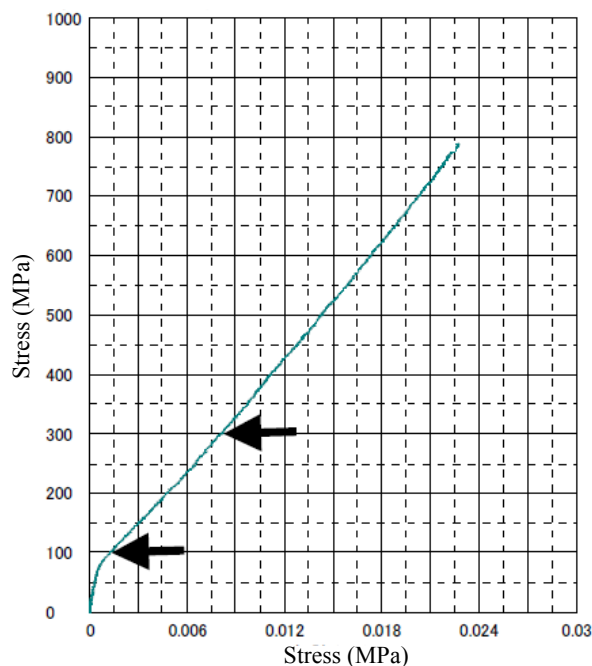


Fig. 3 Graph of Stress vs. Lateral Displacement

Poisson's ratio in left figure:  $6.0 \times 10^{-2}$   
(for range between 2 points, at 100 MPa and 300 MPa)

Method Used to Determine Poisson's Ratio

$$\nu_t = |\Delta \varepsilon_2 / \Delta \varepsilon_1|$$

$\nu_t$ : Poisson's ratio

$\Delta \varepsilon_1$ : Strain increase in tensile direction

$\Delta \varepsilon_2$ : Strain increase perpendicular to tension

## Test Conditions and Equipment Used

Tester: AG-Xplus  
Load Cell: 50 kN  
Test Jig: 50 kN non-shift wedge type grips  
Extensometer: SG50-10 for measuring strain in tensile direction  
SGW-5 for measuring strain perpendicular to tensile direction  
Software: TRAPEZIUM X (Single)



AG-Xplus Floor-Type Precision Universal Tester

- A high-precision load cell is adopted. (The high-precision type is class 0.5; the standard-precision type is class 1.)  
Accuracy is guaranteed over a wide range, from 1/1000 to 1/1 of the load cell capacity. This supports highly reliable test evaluations.
- Crosshead speed range  
Tests can be performed over a wide range from 0.0005 mm/min to 1,000 mm/min.
- High-speed sampling  
Ultrafast sampling, as fast as 0.2 msec, allows assessment of sudden changes in test force, such as when brittle materials fracture.
- TRAPEZIUMX X operational software  
Designed for intuitive operation, it offers a variety of convenient and user-friendly features.
- Smart controller  
Real-time test force and position data are readily confirmed, and the manual dial enables fine adjustments to jig positioning.
- Optional Test Devices  
A variety of tests can be performed by switching between an abundance of jigs in the lineup.

First Edition: July 2015



Shimadzu Corporation

[www.shimadzu.com/an/](http://www.shimadzu.com/an/)

For Research Use Only. Not for use in diagnostic procedures.  
The content of this publication shall not be reproduced, altered or sold for any commercial purpose without the written approval of Shimadzu.  
The information contained herein is provided to you "as is" without warranty of any kind including without limitation warranties as to its accuracy or completeness. Shimadzu does not assume any responsibility or liability for any damage, whether direct or indirect, relating to the use of this publication. This publication is based upon the information available to Shimadzu on or before the date of publication, and subject to change without notice.

© Shimadzu Corporation, 2015

# Application Data Sheet

No. 31

## Autograph Precision Universal Tester

Material Testing & Inspection

### Materials Testing Using Digital Image Correlation —3-Point Bending Test for Polypropylene and Open-Hole Tensile Test for Carbon Fiber Reinforced Thermo-Plastic—

#### ■ Introduction

In recent years, computer aided engineering (CAE), which has allowed significantly reducing the number of prototypes and costs required for product development by simulating product designs on a computer, has been widely used in scientific and industrial fields. This has resulted in an increased need to analyze the distribution of strain in test samples, where the areas prone to strain concentrations in such samples are evaluated by mechanical testing to determine the correlation between results from simulation and strain distribution obtained by mechanical testing.

Digital image correlation (DIC) analysis compares the random patterns on the surface of a test sample before and after deformation to determine the degree of deformation. A important feature of the method is that displacements can be measured and strain distributions analyzed from digital images, which means no sensors need to contact the test sample and no complicated optical systems are required. Consequently, DIC analysis is being used for a wide range of applications where strain is difficult to measure using conventional technology, such as analyzing the strain distribution in large structural members, materials at high temperatures, or micro-materials observed via a microscope.

This paper describes examples of using DIC analysis for 3-point bending tests of plastics and for open-hole tensile testing of thermoplastic carbon fiber reinforced plastics (CFRP) (fabric). The test data presented in this paper was obtained using a system comprising a Shimadzu AG-Xplus precision universal tester, a customized TRViewX non-contact video extensometer, and LaVision DaVis8 DIC analysis software. This system allows simultaneously acquiring JIS 0.5 class extensometer measurement results and video images for DIC analysis, as well as correlating DIC analysis results with test force data.

#### ■ Evaluation of Dependence on Distance Between Supports in 3-Point Bending Tests of Plastics

3-point bending tests are widely used throughout the world as a relatively easy way to evaluate the bending properties of materials. A photograph of the testing system is shown in Fig. 1. In 3-point bending tests, a punch applies a load to specimens supported at two points.

3-point bending test regulations for plastics (such as JIS K 7171 and ISO 178) specify that the  $L$ , the distance between supports, must be about 16 times greater than  $h$ , the specimen thickness ( $L/h \approx 16$ ), where this ratio,  $L/h$ , is an important factor for measuring the bending strength or bending elasticity correctly.<sup>1), 2)</sup> The following discusses  $L/h$  in more detail. Bending a specimen applies compressive stresses to the material above the center plane and tensile stresses below the center plane. The contribution of this compressive and tensile deformation to bending stresses is defined to be equal. Maximum bending stress occurs near the punch that applies the bending loads, where given a flat plate-shaped specimen, stress is defined as  $\sigma_f = 3FL/2bh^2$ . When a specimen bends, shear stresses also occur at the same time, where the shear stress is defined as  $\tau = 3F/4bh$ . Based on the above two equations, the relationship between specimen thickness and distance between supports is described by  $L/h = \sigma_f/2\tau$ . Given a uniformly formed specimen with a sufficiently large distance between the supports, relative to the specimen thickness, the definition of  $L/h$  indicates that the contribution of shear stresses in the specimen is small.<sup>3) to 5)</sup> To limit the effects of shear stresses during 3-point bending tests, the optimal  $L/h$  value must be specified for the specimen being tested.

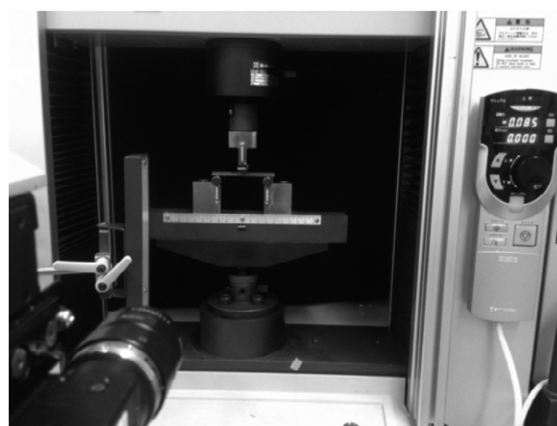


Fig. 1 3-Point Bending Testing System Using Non-Contact Video Extensometer

In the following example, a common plastic material, polypropylene, was tested by 3-point bending using three different distances between supports, and then DIC analysis was used to investigate how much the maximum shear stress distribution depends on the distance between supports. Test conditions are shown in Table 1.



Tests were performed at three L values (distance between supports), 64 mm for an L/h ratio of 16 specified in JIS K 7171, 48 mm for an L/h ratio of 12, where shear stress is predicted to have a large effect, and 32 mm for an L/h ratio of 8. Stress-strain curves obtained using different test conditions are shown in Fig. 2. Fig. 3 shows the maximum shear strain distribution near the elastic limit and near the maximum load point. Warmer colors indicate higher strain levels in the maximum shear strain distribution. This shows that at an L/h ratio of 16, strain is low even near the maximum load point and spreads out uniformly. However, L/h ratios of 8 and 12, where shear stress contribution is predicted to be large, generated large localized shear stresses near the maximum load point on the specimen surface under tension directly under the punch. Whereas localized shear stresses occurred from about the elastic limit for L/h ratio of 8, none were observed for the L/h ratio of 12.

This clearly shows that different deformation modes resulted from bending tests using different distances between supports and shows that DIC analysis provides an effective means of verifying the different modes. It also shows that L/h ratio of 16 recommended in the testing regulations is an appropriate value for 3-point bending tests.

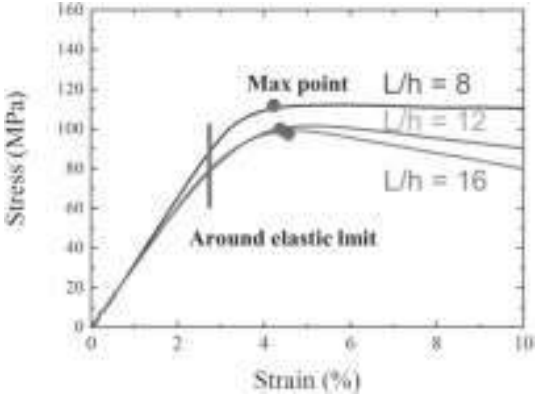


Fig. 2 Stress-Strain Curve

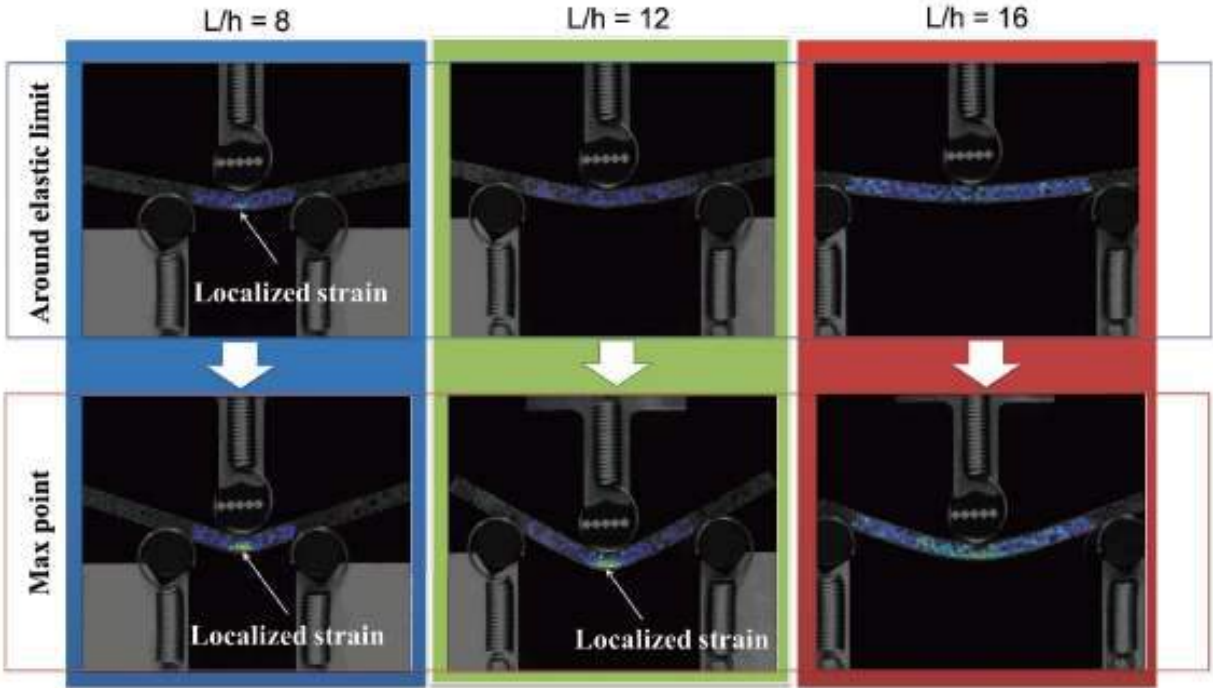


Fig. 3 Distribution of Maximum Shear Strain Around Elastic Limit and Maximum Load

Table 1 Test Conditions for 3-Point Bending Test of Plastic Material

1) Testing equipment	AG-Xplus precision universal tester
2) Load cell capacity	1 kN
3) Jig	Three-point bending test jig for plastic
4) Distance between supports	Three configurations: 32, 48, and 64 mm
5) Test speed	0.001 /s
6) Deflection measuring device	TRViewX120S non-contact video extensometer (customized)
7) Testing software	TRAPEZIUM X (Single)
8) DIC analysis software	DaVis8 (LaVision GMBH)
9) Specimen size	4 mm thick × 10 mm wide × 80 mm long

First Edition: July 2015



■Open-Hole Tensile Testing of Thermoplastic CFRP (Fabric)

Due to higher specific strength than steel materials, superior workability and formability than CFRP/epoxy, and short cycle times of only a few minutes possible for molding, thermoplastic CFRP materials are anticipated for use in production automobiles.<sup>6)</sup>

In general, CFRP materials start failing at the point where they are damaged. CFRP/epoxy used as structural materials in aircraft are mainly used for large components that are fastened with screws or rivets. Therefore, it is important to evaluate their open-hole tensile strength. The open-hole tensile test specified in ASTM D 5766, JIS K 7094, and other regulations is one of the essential evaluation criteria for understanding the properties of CFRP materials.<sup>7), 8)</sup>

In this case, we made a round hole in a thermoplastic CFRP specimen, applied a tensile load, and evaluated the resulting distribution of the maximum shear strain. Fig. 4 shows the testing system used for this test. Table 2 indicates testing conditions and information about the specimen. We chose to cut out type-I shaped specimens, as specified in JIS K 7094 (2012), from PA6 polymer-based thermoplastic CFRP material (with CF-3K flat woven [0]<sub>10</sub> fabric from Ichimura Sangyo), so that the fibers were oriented longitudinally.

The stress-strain curve obtained from testing is shown in Fig. 5 and the distribution of maximum shear strain that occurred on the observed specimen surface is shown in Fig. 6. Images (1) to (4) in Fig. 6 correspond to the numbers indicated on the stress-strain curve in Fig. 5.



Fig. 4 Open-Hole Tensile Testing System Using Non-Contact Video Extensometer

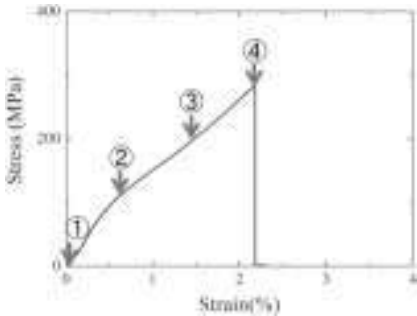


Fig. 5 Stress-Strain Curve

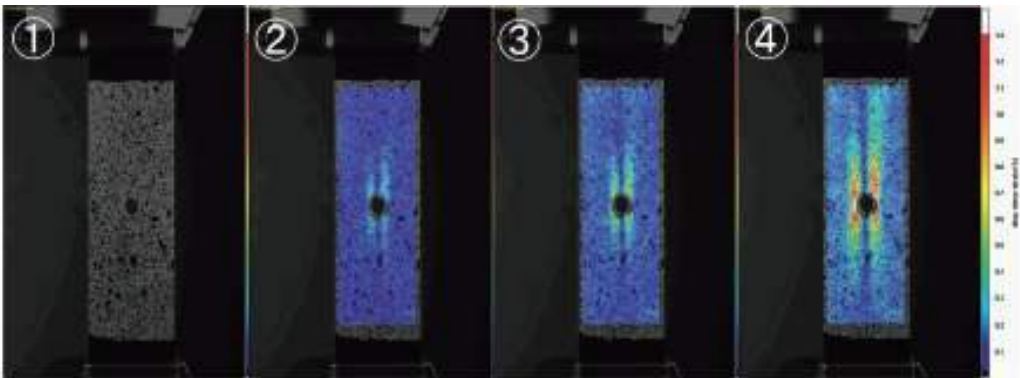


Fig. 6 Distribution of Maximum Shear Strain

Table 2 Test Conditions for Open-Hole Tensile Test of Carbon Fiber Reinforced Thermo-Plastic (Fabric)

1) Testing equipment	AG-Xplus precision universal tester
2) Load cell capacity	50 kN
3) Jig	50 kN non-shift wedge type grips (with trapezoidal file teeth on grip faces for flat specimens)
4) Distance between grips	100 mm
5) Test speed	0.5 mm/min
6) Deflection measuring device	TRViewX120S non-contact video extensometer (customized)
7) Testing software	TRAPEZIUM X (Single)
8) DIC analysis software	DaVis8 (LaVision GMBH)
9) Specimen size	2 mm thick × 36 mm wide × 150 mm long, with 6 mm diameter hole

First Edition: July 2015



The results showed that when the tensile load increased, the maximum shear strain distribution started near the tangent points on the left and right sides of the hole, and spread along the longitudinal direction of the specimen. Due to the orientation of the carbon fibers, the specimen has the greatest strength for bearing tensile loads in its longitudinal direction. The areas of strain concentration are the areas that contain continuous fibers, but they are presumably highly affected by the process of creating the hole. Fig. 7 is a photograph of the specimen after fracture. It shows that the specimen fractured in the direction perpendicular to the main tensile axis. The failure mode is typical of CFRP(fabric) specimens with an open hole, where cracking presumably progressed rapidly after the longitudinal carbon fibers near the hole fractured, resulting in specimen breaking.

Generally, open-hole tensile tests that involve creating a hole in specimens result in significantly lower stresses at the maximum load point, than for specimens without a hole, with some reports indicating a 1/3 to 1/2 drop in strength.<sup>9), 10)</sup> In addition to open-hole tensile testing, this research also involved tensile testing specimens without a hole for reference purposes. A resulting stress-strain curve and photograph of the specimen after fracture are shown in Figs. 8 and 9. The specimen fractured near the parallel area, at a value of about 700 MPa. In contrast, Fig. 5 indicates that the open-hole specimen failed at about 300 MPa, a result similar to CFRP/epoxy specimens.



Fig. 7 Picture of Fractured Specimen

## Conclusion

This paper describes using DIC analysis to evaluate the properties of polypropylene and thermoplastic CFRP (fabric), as examples of chemically engineered materials. However, there are many other types of chemically engineered materials available for which DIC analysis could be used for determining material properties, not only for bending or tensile tests, but also for various others tests, such as compression and shear tests. With high-speed video cameras developed in recent years that allow obtaining high-resolution video images with extremely high time resolution levels, technology has advanced to the point that DIC analysis can now be utilized to visualize strain distributions or obtain stress-strain curves for applications such as high-speed impact testing. Consequently, using DIC analysis for material testing in product design work provides an effective way of ensuring a higher level of safety and peace of mind by understanding the properties of the materials from various aspects.

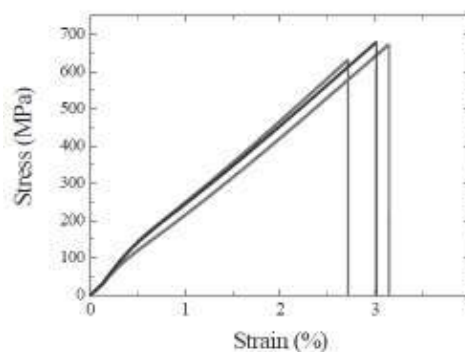


Fig. 8 Stress-Strain Curve

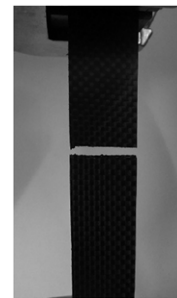


Fig. 9 Picture of Fractured Specimen

## References:

- 1) JIS K 7171: 2008 Plastics—Determination of flexural properties
- 2) ISO 178: 2001 Plastics—Determination of flexural properties
- 3) Masahiro Funabashi: Technology for Evaluating the Performance of Advanced Materials, Sangyo Gijutsu Service Center, pp. 286-287 (2014)
- 4) Leif A. Carlsson and R. Byron Pipes: Experimental Characterization of Advanced Composite Materials, Kokon Syoin, p. 75 (1990)
- 5) Ikuo Narisawa: Mechanical Properties of Plastics, Sigma Shuppan, pp. 105-108 (1994)
- 6) Takeshi Murakami and Tsuyoshi Matsuo: Summary of Presentations at the 39th Conference on Composite Materials, pp. 155-156 (2014)
- 7) ASTM D5766/D5766M -11 Standard Test Method for Open-Hole Tensile Strength of Polymer Matrix Composite Laminates
- 8) JIS K 7094: 2012 Test method for open-hole tensile strength of carbon fibre reinforced plastic
- 9) JAXA-ACDB Advanced Composites Database System <http://www.jaxa-acdb.com/> (as of December 17, 2014)
- 10) Wisnom, M. R., Hallett, S. R., and Soutis, C.: Scaling effects in notched composites, Journal of composite materials, 44, 195-210 (2010)

First Edition: July 2015



Shimadzu Corporation

[www.shimadzu.com/an/](http://www.shimadzu.com/an/)

For Research Use Only. Not for use in diagnostic procedures.  
The content of this publication shall not be reproduced, altered or sold for any commercial purpose without the written approval of Shimadzu. The information contained herein is provided to you "as is" without warranty of any kind including without limitation warranties as to its accuracy or completeness. Shimadzu does not assume any responsibility or liability for any damage, whether direct or indirect, relating to the use of this publication. This publication is based upon the information available to Shimadzu on or before the date of publication, and subject to change without notice.

© Shimadzu Corporation, 2015

# Application Data Sheet

No. 39

## Autograph Precision Universal Testing Machine

Material Testing & Inspection

### Evaluation of Open-Hole CFRP

— Static Tensile Testing, Fracture Observation,  
and Internal Structure Observation —

#### ■ Introduction

Recently, lightweight alternatives to conventional metal materials are being used as structural members where mechanical reliability is required. The main reason for this trend is that lighter products reduce transport weights, which reduces fuel consumption and carbon dioxide emissions during product transport. Fiber reinforced composite materials such as carbon fiber reinforced plastics (CFRP), which consist of a resin strengthened with carbon fibers, are extremely strong and light. Because of this, they are currently a material widely used in aircraft, and are expected to be used increasingly in various types of products, including automobiles, in order to make them lighter. For the development of fiber reinforced composite materials, not just a simple evaluation of their mechanical strength, but also the observation of failure events is important. In addition, from the perspective of quality management, the necessity for evaluation of internal structure of these materials, such as the oriented state of fibers and the presence of cracks, has increased.

In this article, we describe how we use a precision universal testing machine (Autograph AG-250kNXplus) and high-speed video camera (HyperVision HPV-X) (Fig. 1) to evaluate the static fracture behavior of a CFRP based on a test force attenuation graph and images of material failure. We also describe our subsequent examination of the state of the specimens internally using an X-ray CT system (inspeXio SMX-100CT) to investigate the state of fracture inside the specimen. Information on specimens is shown in Table 1. Specimens have a hole machined into their center that is 6 mm in diameter. Fracture is known to propagate easily through composite materials from the initial damage point, and when a crack or hole is present their strength is reduced markedly. Therefore, evaluation of the strength of open-hole specimens is extremely important from the perspective of the safe application of CFRP materials in aircraft, etc.

Table 1: Test Specimen Information

Laminate Structure	Dimensions
	L (mm) × W (mm) × T (mm), hole diameter (mm)
[+45/0/-45/+90] <sub>2s</sub>	150 × 36 × 2.9, Φ6

Note: The CFRP laminate board used in the actual test was created by laying up prepreg material with fibers oriented in a single direction. The [+45/0/-45/+90]<sub>2s</sub> shown as the laminate structure in Table 1 refers to the laying up of 16 layers of material with fibers oriented at +45°, 0°, -45°, and +90° in two layer sets.

#### ■ Static Tensile Testing (Ultra High Speed Sampling)

In this test, the change in load that occurs during specimen fracture was used as the signal for the HPV-X high-speed video camera to capture images. Specifically, the AG-Xplus precision universal testing machine was configured to create a signal when the test force on the specimen reaches half the maximum test force (referred to as Maximum test force in Fig. 3), with this signal being sent to the high-speed video camera. Static tensile testing and fracture observation were performed according to the conditions shown in Table 2. A test force-displacement plot for the open-hole quasi-isotropic CFRP (OH-CFRP) is shown in Fig. 2(a). A test force-time plot during the occurrence of material fracture is also shown in Fig. 2(b).

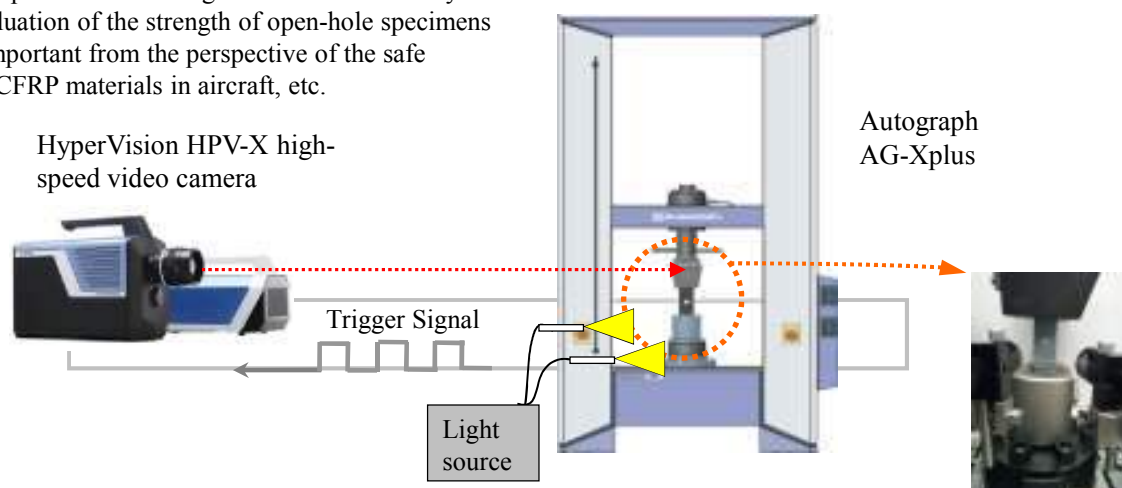


Fig.1: Testing Apparatus



Table 2: Test Conditions

Testing Machine	AG-Xplus
Load Cell Capacity	250 kN
Jig	Upper: 250 kN non-shift wedge type grips (with trapezoidal file teeth on grip faces for composite materials) Lower: 250 kN high-speed trigger-capable grips
Grip Space	100 mm
Loading Speed	1 mm/min
Test Temperature	Room temperature
Software	TRAPEZIUM X (Single)
Fracture Observation	HPV-X high-speed video camera (recording speed 600 kfps)
DIC Analysis	StrainMaster (LaVision GmbH.)

Note: fps stands for frames per second. This refers to the number of frames that can be captured in 1 second.

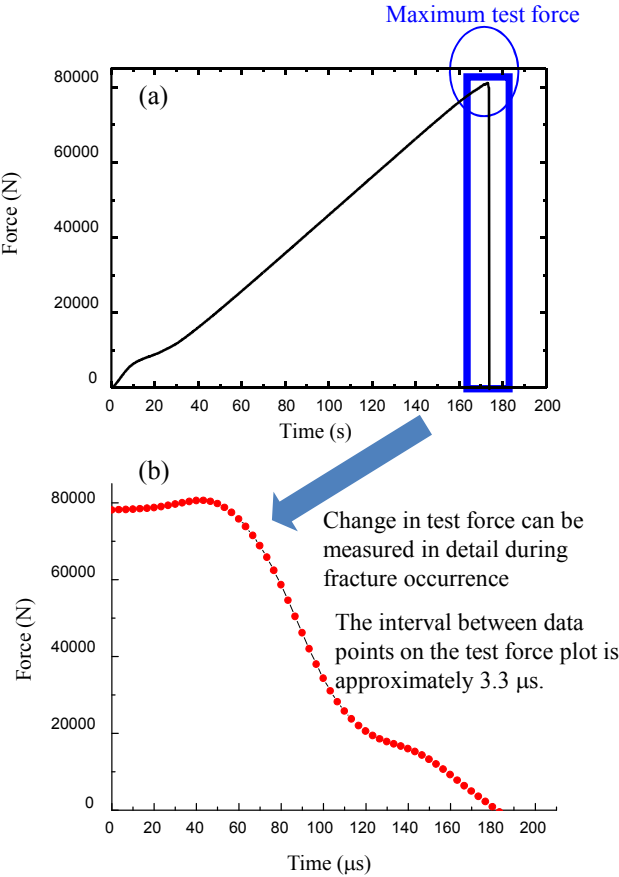


Fig. 2 (a) Test Force-Displacement Curve, and (b) Test Force-Time Curve (in Region of Maximum Test Force)

Fig. 2(a) can be interpreted to show the specimen fractured at the moment it reached the maximum test force, at which point the load on the specimen was suddenly released. This testing system can be used to perform high-speed sampling to measure in detail the change in test force in the region of maximum test force. The time interval between data points on the test force plot in Fig. 2(b) is 3.3 μs.

■ Fracture Observation (High Speed Imaging)

Images (1) through (8) in Fig. 3 capture the behavior of the specimen during fracture around the circular hole. Image (1) shows the moment cracks occur in a surface +45° layer. In this image, the tensile load being applied is deforming the circular hole, where hole diameter in the direction of the load is approximately 1.4 times that perpendicular to the load. In image (2), the cracks that occurred around the circular hole are propagating along the surface +45° layer. In images (3) through (6), a substantial change can be observed in the external appearance of the specimen near the end of the crack propagating to the bottom right from the circular hole. This suggests not only the surface layer, but internal layers are also fracturing. Based on the images of the same area and the state of the internal layers that can be slightly observed from the edges of the circular hole in images (7) and (8), the internal fracture has quickly propagated in the 18 μs period between images (3) and (8).

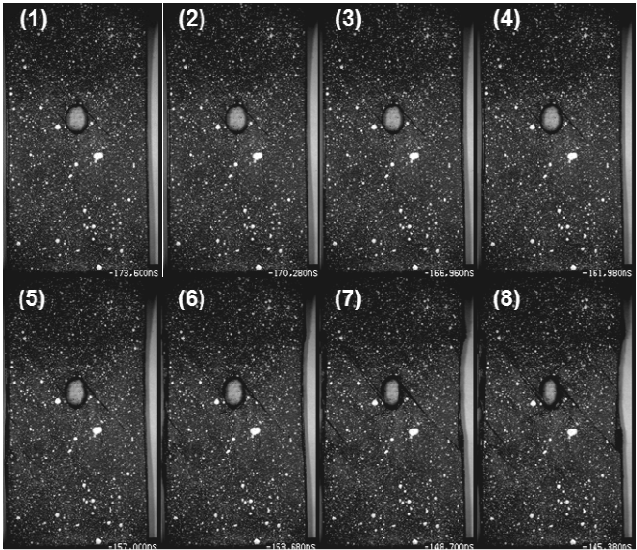


Fig. 3: Observations of OH-CFRP Fracture



Images (1) through (8) of Fig. 4 show the results of performing Digital image correlation (DIC) analysis on the fracture observation images of Fig. 3. Black signifies areas of the surface layer of the specimen under little strain, and red signifies areas under substantial strain. Looking at images (1) through (4), we can see that strain around the circular hole is focused diagonally toward the top-left ( $-45^\circ$ ) and toward the bottom-left ( $+45^\circ$ ) from the circular hole. Images (5) through (8) show the focusing of strain diagonally toward the bottom-right ( $-45^\circ$ ) and toward the top-right ( $+45^\circ$ ) from the circular hole in areas where it was not obvious in images (1) through (4). This shows an event is occurring in the surface layer of the specimen that is similar to the process of fracture often seen during tensile testing of ductile metal materials, which is crack propagation in the direction of maximum shearing stress.

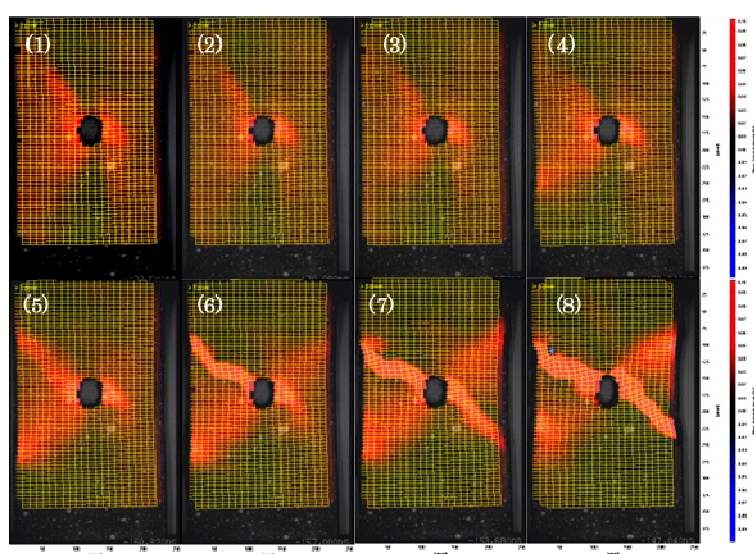


Fig. 4: Observation of OH-CFRP Fracture (DIC Analysis)

#### ■ Internal Structure Observation (CT)

Next, internal observations were performed around the circular hole using a micro focus X-ray CT system to check the state of internal damage to the specimen. The SMX-100CT micro focus X-ray CT system (Fig. 5) is capable of capturing CT images at high magnification. The system rotates a specimen between an X-ray generator and an X-ray detector, uses a computer to calculate fluoroscopic images obtained from all  $360^\circ$  of rotation, then reconstructs a tomographic view of the specimen (Fig. 6). This system was used to perform a CT scan of the fracture area of the OH-CFRP after the static tensile testing and fracture observation performed as described in the previous section, so that the cracks that occurred inside can be observed.



Fig. 5: Shimadzu inspeXio SMX-100CT Micro Focus X-Ray CT System

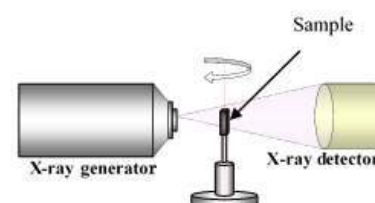


Fig. 6: Illustrated Example of X-Ray CT System Operation



Fig. 7: Specimen After Static Tensile Testing (Specimen Used for CT Scan)

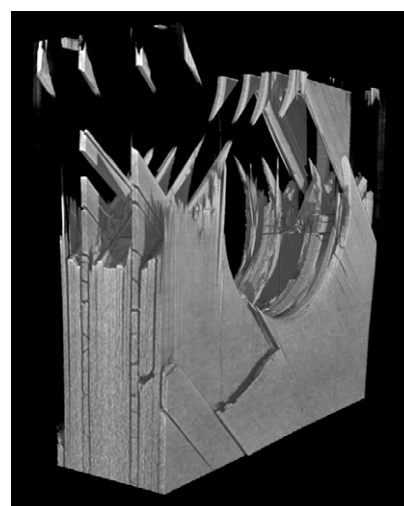


Fig. 8: Fracture Area 3D Image No. 1

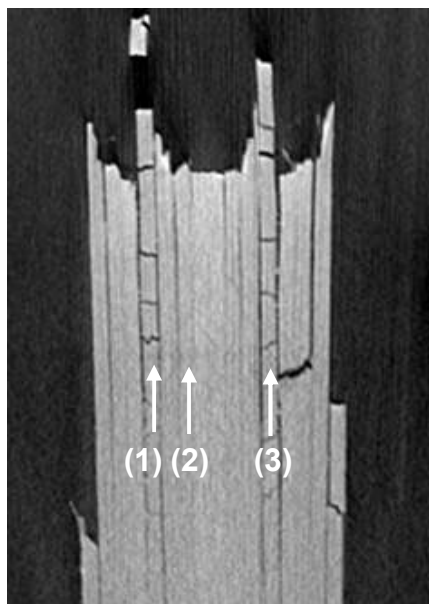


Fig. 9: CT Cross-Sectional Images of the Fracture Area

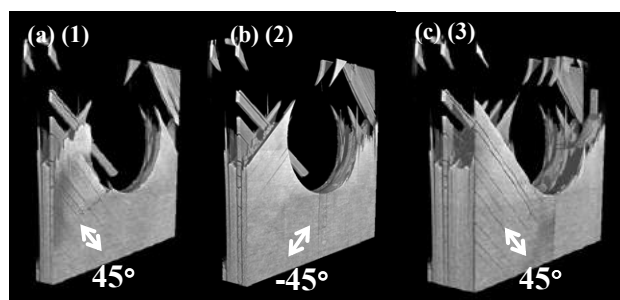


Fig. 10: Fracture Area 3D Image No. 2

#### ■ Acknowledgment

We would like to extend our sincere gratitude to the Japan Aerospace Exploration Agency (JAXA) for their cooperation in the execution of this experiment.

Note: The analytical and measuring instruments described may not be sold in your country or region.

Cross-sectional images of the specimen are shown as a 3D image in the 16 layers shown in Fig. 9, we can see that most cracks in the matrix occur in the  $+45^\circ$  layer inside the specimen, indicated by the number (1) and (3). (shown in Fig. 10 (a) and Fig. 10 (b), respectively). In this layer, the carbon fibers are all aligned together in a  $+45^\circ$  orientation, and the multiple matrix cracks occurring in this layer are probably due to the shearing force caused in this layer by tensile loading, together with deformation of adjacent layers in the direction of the loading. For comparison, a 3D image of the  $-45^\circ$  layer inside the specimen (Fig. 9 (2)) is shown in Fig. 10 (b). As is clear from the image, the matrix cracks that occurred in the  $+45^\circ$  layer have not occurred in the  $-45^\circ$  layer. This difference in fracture state has probably arisen due to different shearing forces and load directions occurring in each layer. Such detailed observation of fracture surfaces associated with multiple matrix cracks was difficult by conventional methods, since to observe fracture surfaces the specimen was processed such as by cutting and embedding in resin, which changed the characteristics of the specimen. However, by using the high-resolution X-ray CT system as described in this article, there is little X-ray absorption difference between air and specimen, and it is possible to observe the state of complex internal damage, even for OH-CFRP in which microscopic damage is normally difficult to observe by X-ray.

# Application Data Sheet

No. 1

## Autograph Precision Universal Tester

Material Testing & Inspection

## Tensile Test of Various Plastic Materials

Standard No. ISO527-1:2012 (JIS K 7161: 1994)

### Introduction

Tensile tests are widely used to evaluate plastic materials, and the results are used as indices for new materials development and for implementing quality control. Items evaluated as tensile characteristics of plastic materials include the tensile modulus, strength, and break strain. In this Data Sheet, the tensile modulus of polypropylene (PP), polyvinyl chloride (PVC), and polycarbonate (PC) specimens (dumbbell shaped and cut types) was calculated based on displacement data acquired using an extensometer. The strength and break strain for the respective plastic materials are then determined from the test force values and crosshead travel distances detected with the tester.

T. Murakami

### Measurements and Jigs

To find a sample's tensile modulus, it is necessary to use an extensometer capable of measuring tiny deformations of the sample with high accuracy. Measurements of crosshead travel distances include errors not only from sample deformation, but also from load cell and test jig deformation. When the deformation region is very small, the ratio of the error becomes significant, so this data is not suitable for tensile modulus calculations. In such cases, an extensometer that can measure changes in the gauge length with an accuracy of at least  $\pm 1\%$  must be used. When measuring the modulus of elasticity with a 50 mm gauge length, this corresponds to an accuracy of  $\pm 1\ \mu\text{m}$ . In this test, a strain gauge type one-touch extensometer that meets the above-mentioned conditions was used to measure elongation.

### Measurement Results



Fig. 1: Test Status

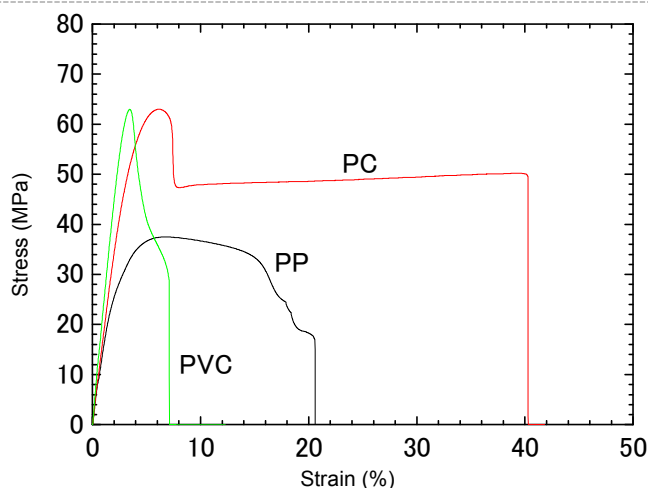


Fig. 2: Relationship Between Stress and Strain

Elongation was measured using the extensometer at a test speed of 1 mm/min within the elasticity region. After removing the extensometer, the test continued at a test speed of 50 mm/min until fracture of the specimen.

Table 1: Test Results

Sample	Tensile Modulus (MPa)	Strength (MPa)	Break Strain (%)
PP	1950	37.5	21.0
PVC	2390	62.4	7.2
PC	3060	63.0	42.2

## Plastic Material Tensile Test System

Tester: AGS-X  
Load Cell: 5 kN  
Test Jig: 5 kN pneumatic flat grips (single-side file teeth grip faces)  
Extensometer: Strain gauge type one-touch extensometer  
SSG50-10SH  
External Amplifier: ESA-CU200  
Software: TRAPEZIUM LITE X



AGS-X Table-Top Precision Universal Tester

## Features

- A high-precision load cell is adopted. (The high-precision type is class 0.5; the standard-precision type is class 1.) Accuracy is guaranteed over a wide range, from 1/500 to 1/1 of the load cell capacity. This supports highly reliable test evaluations.
- Crosshead speed range  
Tests can be performed over a wide range from 0.001 mm/min to 1,000 mm/min.
- High-speed sampling  
High-speed sampling, as fast as 1 msec.
- TRAPEZIUMX LITE X operational software  
This is simple, highly effective software.
- Jog controller (optional)  
This allows hand-held control of the crosshead position. Fine position adjustment is possible using the jog dial.
- Optional Test Devices  
A variety of tests can be conducted by switching between an abundance of jigs in the lineup.

First Edition: February 2013



Shimadzu Corporation

[www.shimadzu.com/an/](http://www.shimadzu.com/an/)

For Research Use Only. Not for use in diagnostic procedures.

The content of this publication shall not be reproduced, altered or sold for any commercial purpose without the written approval of Shimadzu. The information contained herein is provided to you "as is" without warranty of any kind including without limitation warranties as to its accuracy or completeness. Shimadzu does not assume any responsibility or liability for any damage, whether direct or indirect, relating to the use of this publication. This publication is based upon the information available to Shimadzu on or before the date of publication, and subject to change without notice.

© Shimadzu Corporation, 2013

# Application Data Sheet

## No. 2

## Autograph Precision Universal Tester

Material Testing & Inspection

## Flexural Testing of Plastics

Standard No. ISO178: 2010 (JIS K 7171: 1994)

### Introduction

In recent years, a large variety of synthetic resin (plastic) materials has become available for use in a diversity of products. They are used in applications that take advantage of their respective characteristics. For example, polyethylene (PE) is cheap and easy to mold, and thus used for containers, packaging film, and other everyday applications. In contrast, polycarbonate (PC) is transparent, has a high mechanical strength, and is heat-resistant; consequently, it is used for CDs and DVDs in the electrical and electronics fields, as well as in transportation equipment, optics, and medical fields.

In this Data Sheet, flexural testings are performed on four materials, including polyvinyl chloride (PVC) and polypropylene (PP).

T. Murakami

### Measurements and Jigs

In plastic flexural testings, the width of the two supports and central loading edge must be larger than the width of the specimen, and parallelism within  $\pm 0.2$  mm is required. The loading edge radius is  $5 \text{ mm} \pm 0.1$  mm, and the supports radius is specified as  $2 \text{ mm} \pm 0.2$  mm for specimens with a thickness of 3 mm or less, and  $5 \text{ mm} \pm 0.2$  mm for specimens with a thickness exceeding 3 mm. The span must be adjusted to a value of  $16 (\pm 1)$  times the specimen thickness. In this test, since a 4 mm-thick specimen is used, the span is set to 64 mm (specimen thickness of 4 mm  $\times$  16 = 64 mm).

### Measurement Results

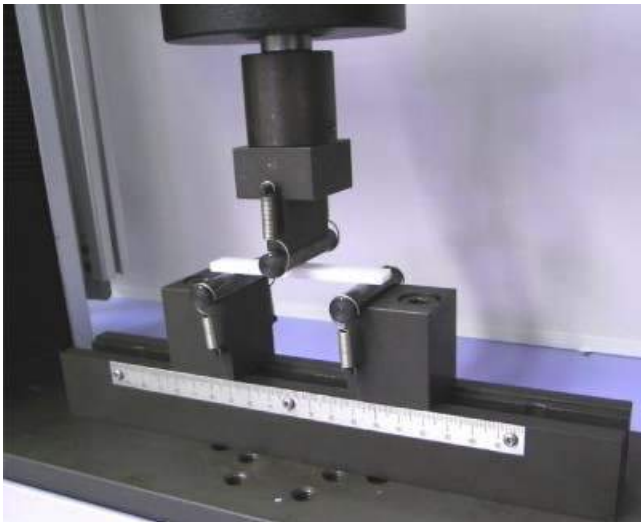


Fig. 1: Test Status

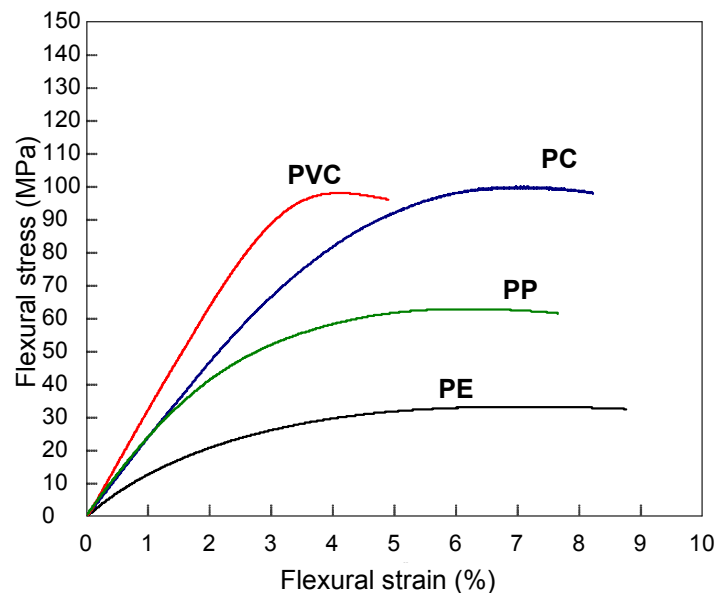


Fig. 2: Relationship Between Flexural Stress and Flexural Strain

Table 1: Test Conditions

Item	Set Value
Test Speed	2 mm/min
Span	64 mm

Table 2: Test Results

Sample	Flexural Modulus (MPa)	Flexural Strength (MPa)
PE (polyethylene)	1527	33.0
PC (polycarbonate)	2378	99.7
PVC (polyvinyl chloride)	3257	97.8
PP (polypropylene)	2559	62.6



## Plastic Flexural Testing System

Tester: AGS-X  
Load Cell: 1 kN  
Test Jig: Three-point bending test jig for plastics (loading edge radius.: 5 mm, supports radius.: 3 mm)  
Software: TRAPEZIUM LITE X



AGS-X Table-Top Precision Universal Tester

## Features

- A high-precision load cell is adopted. (The high-precision type is class 0.5; the standard-precision type is class 1.) Accuracy is guaranteed over a wide range, from 1/500 to 1/1 of the load cell capacity. This supports highly reliable test evaluations.
- Crosshead speed range  
Tests can be performed over a wide range from 0.001 mm/min to 1,000 mm/min.
- High-speed sampling  
High-speed sampling, as fast as 1 msec.
- TRAPEZIUMX LITE X operational software  
This is simple, highly effective software.
- Jog controller (optional)  
This allows hand-held control of the crosshead position. Fine position adjustment is possible using the jog dial.
- Optional Test Devices  
A variety of tests can be conducted by switching between an abundance of jigs in the lineup.

First Edition: February 2013



Shimadzu Corporation

[www.shimadzu.com/an/](http://www.shimadzu.com/an/)

For Research Use Only. Not for use in diagnostic procedures.  
The content of this publication shall not be reproduced, altered or sold for any commercial purpose without the written approval of Shimadzu. The information contained herein is provided to you "as is" without warranty of any kind including without limitation warranties as to its accuracy or completeness. Shimadzu does not assume any responsibility or liability for any damage, whether direct or indirect, relating to the use of this publication. This publication is based upon the information available to Shimadzu on or before the date of publication, and subject to change without notice.

© Shimadzu Corporation, 2013

# Application Data Sheet

No. 3

## Autograph Precision Universal Tester

Material Testing & Inspection

### Tensile Tests of Plastic Materials at Low Temperatures (-40 °C)

Standard No. ISO527-1: 2012 (JIS K 7161: 1994)

#### Introduction

Tensile tests are widely used to evaluate plastic materials, and the results are used as indices for new materials development and for implementing quality control. Items evaluated as tensile characteristics of plastic materials include the tensile modulus, strength, and break strain. In this Data Sheet, the tensile modulus of polypropylene (PP) and polyvinyl chloride (PVC) specimens (dumbbell shaped and cut types) was calculated based on displacement data acquired using an extensometer at a low temperature of -40 °C. In addition, the strength and break strain for the respective plastic materials were also evaluated.

T. Murakami

#### Measurements and Jigs

In finding a sample's tensile modulus, it is necessary to use an extensometer capable of measuring tiny deformations of the sample with high accuracy. Measurements of crosshead travel distances include errors not only from sample deformation, but also from load cell and test jig deformation. When the deformation region is very small, the ratio of the error becomes significant, so this data is not suitable for tensile modulus calculations. In such cases, an extensometer that can measure changes in the gauge length with an accuracy of at least  $\pm 1$  % must be used. When measuring the modulus of elasticity with a 50 mm gauge length, this corresponds to an accuracy of  $\pm 1 \mu\text{m}$ . In this test, a one-touch contact type extensometer, capable of operating even in a -40 °C environment, was used.

#### Measurement Results



Fig. 1: Test Status

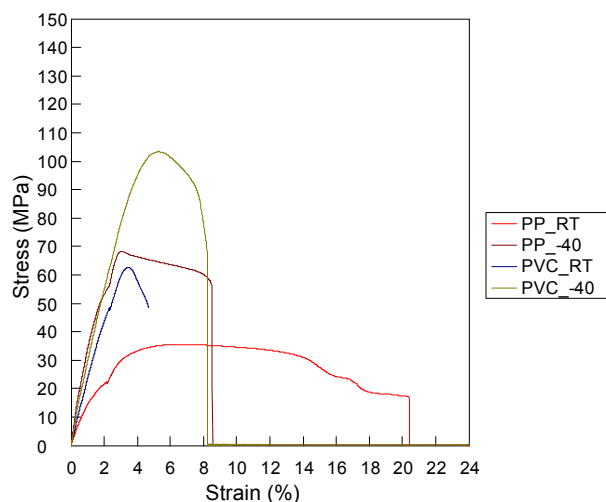


Fig. 2: Relationship Between Stress and Strain

In the results, samples with an "RT" suffix were measured in a room temperature environment, and those with a "-40" suffix were measured at -40 °C. In all cases, measurement was performed at a test speed of 1 mm/min up to 2 %, and then at a test speed of 50 mm/min. In the room temperature measurements, the extensometer measurement range was exceeded, so the extensometer was removed at the 2 % position.

Table 1: Test Results

Sample	Tensile Modulus (MPa)	Strength (MPa)	Break Strain (%)
PP_RT	1955	36	20.2
PP_-40	5333	68	7.8
PVC_RT	3150	63	4.3
PVC_-40	3942	103	7.1

## Plastic Material Thermostatic Tensile Test System

Tester: AGS-X  
Load Cell: 5 kN  
Test Jig: 5 kN pneumatic flat grips (Single-side file teeth grip faces)  
Extensometer: Strain gauge type one-touch extensometer  
EPC-50-10  
External Amplifier: ESA-CU200  
Thermostatic Chamber: TCR2W  
Software: TRAPEZIUM LITE X



AGS-X Table-Top Precision Universal Tester

## Features

- A high-precision load cell is adopted. (The high-precision type is class 0.5; the standard-precision type is class 1.) Accuracy is guaranteed over a wide range, from 1/500 to 1/1 of the load cell capacity. This supports highly reliable test evaluations.
- Crosshead speed range  
Tests can be performed over a wide range from 0.001 mm/min to 1,000 mm/min.
- High-speed sampling  
High-speed sampling, as fast as 1 msec.
- TRAPEZIUMX LITE X operational software  
This is simple, highly effective software.
- Jog controller (optional)  
This allows hand-held control of the crosshead position. Fine position adjustment is possible using the jog dial.
- Optional Test Devices  
A variety of tests can be conducted by switching between an abundance of jigs in the lineup.

First Edition: February 2013



Shimadzu Corporation

[www.shimadzu.com/an/](http://www.shimadzu.com/an/)

For Research Use Only. Not for use in diagnostic procedures.

The content of this publication shall not be reproduced, altered or sold for any commercial purpose without the written approval of Shimadzu. The information contained herein is provided to you "as is" without warranty of any kind including without limitation warranties as to its accuracy or completeness. Shimadzu does not assume any responsibility or liability for any damage, whether direct or indirect, relating to the use of this publication. This publication is based upon the information available to Shimadzu on or before the date of publication, and subject to change without notice.

© Shimadzu Corporation, 2013

# Application Data Sheet

No. 5

## Autograph Precision Universal Tester

Material Testing & Inspection

## Tear Tests of Crescent-shaped Rubber Specimens

Standard No. ISO34-1: 2004 (JIS K6252: 2007)

### Introduction

Rubber materials have characteristic mechanical properties including elasticity and flexibility, and are widely used for industrial parts, construction materials, and housewares. In particular, a diverse range of synthetic rubber materials with differing properties suited to match their application have been developed. Measuring these mechanical properties is extremely important to ensure quality control and for new materials development. This Data Sheet introduces an example of the evaluation of two synthetic rubber specimens (crescent-shaped specimens). Tear tests were performed, and the specimens were evaluated with respect to tear strength, one of their basic mechanical properties.

T. Murakami, J. Sakai

### Measurements and Jigs

Tear tests of crescent-shaped rubber specimens require grips that tighten automatically as the tear force increases. When tensile loads are applied to rubber materials, they elongate and their thickness decreases. For this reason, if there is no automatic tightening mechanism, the specimen will inadvertently break free of the grips before the maximum tear force is applied, making favorable measurements impossible. Accordingly, in rubber tear tests, it is necessary to use pneumatic parallel grippers, pantograph grips, eccentric roller type grips, Henry Scott type grips, or other grips equipped with this feature.

### Measurement Results



Fig. 1: Test Status

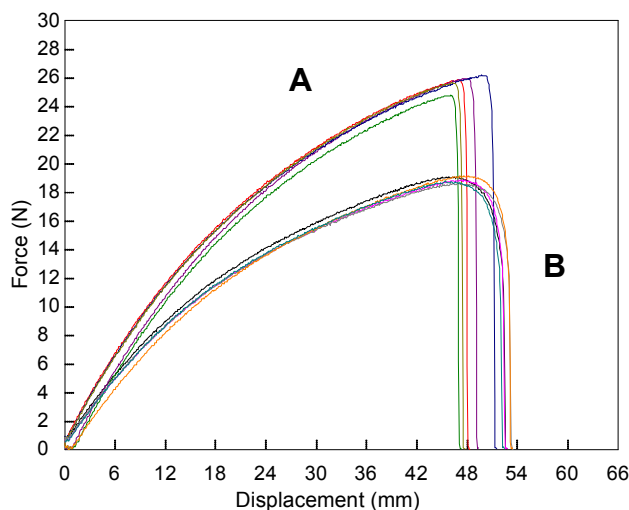


Fig. 2: Relationship Between Force and Displacement

Table 1: Test Conditions

Item	Set Value
Test Speed	500 mm/min
Initial Distance between Grips	60 mm

Table 2: Test Results (Average)

Sample	Main Component	Max. Force (N)	Tear Strength (kN/m)
A	CR rubber (black)	25.9	13.0
B	CR rubber (white)	18.9	9.5

The tear test results for the two samples are shown in Table 2. A graph showing the force-displacement relationship for each sample is shown in Fig. 2. Differences in tear strength between the samples are clearly apparent.

## Rubber Tear Test System

Tester: AGS-X  
Load Cell: 1 kN  
Test Jig: 1 kN pneumatic flat grips (Single-side file teeth grip faces)  
Software: TRAPEZIUM LITE X



AGS-X Table-Top Precision Universal Tester

## Features

- A high-precision load cell is adopted. (The high-precision type is class 0.5; the standard-precision type is class 1.)  
Accuracy is guaranteed over a wide range, from 1/500 to 1/1 of the load cell capacity. This supports highly reliable test evaluations.
- Crosshead speed range  
Tests can be performed over a wide range from 0.001 mm/min to 1,000 mm/min.
- High-speed sampling  
High-speed sampling, as fast as 1 msec.
- TRAPEZIUMX LITE X operational software  
This is simple, highly effective software.
- Jog controller (optional)  
This allows hand-held control of the crosshead position. Fine position adjustment is possible using the jog dial.
- Optional Test Devices  
A variety of tests can be conducted by switching between an abundance of jigs in the lineup.

First Edition: February 2013



Shimadzu Corporation

[www.shimadzu.com/an/](http://www.shimadzu.com/an/)

For Research Use Only. Not for use in diagnostic procedures.  
The content of this publication shall not be reproduced, altered or sold for any commercial purpose without the written approval of Shimadzu. The information contained herein is provided to you "as is" without warranty of any kind including without limitation warranties as to its accuracy or completeness. Shimadzu does not assume any responsibility or liability for any damage, whether direct or indirect, relating to the use of this publication. This publication is based upon the information available to Shimadzu on or before the date of publication, and subject to change without notice.

© Shimadzu Corporation, 2013



# Application Data Sheet

No. 6

## Autograph Precision Universal Tester

Material Testing & Inspection

### Tear Tests of Angle-Shaped Rubber Specimens

Standard No. ISO34-1: 2004 (JIS K6252: 2007)

#### Introduction

Rubber materials have characteristic mechanical properties including elasticity and flexibility, and are widely used for industrial parts, construction materials, and housewares. In particular, a diverse range of synthetic rubber materials with differing properties suited to match their application have been developed. Measuring these mechanical properties is extremely important to ensure quality control and for new materials development. This Data Sheet introduces an example of the evaluation of two synthetic rubber specimens (angle-shaped specimens). Tear tests were performed, and the specimens were evaluated with respect to tear strength, one of their basic mechanical properties.

T. Murakami, J. Sakai

#### Measurements and Jigs

Tear tests of angle-shaped rubber specimens require grips that tighten automatically as the tear force increases. When tensile loads are applied to rubber materials, they elongate and their thickness decreases. For this reason, if there is no automatic tightening mechanism, the specimen will inadvertently break free of the grips before the maximum tear force is applied, making favorable measurements impossible. Accordingly, in rubber tear tests, it is necessary to use pneumatic parallel grippers, pantograph grips, eccentric roller type grips, Henry Scott type grips, or other grips equipped with this feature.

#### Measurement Results



Fig. 1: Test Status

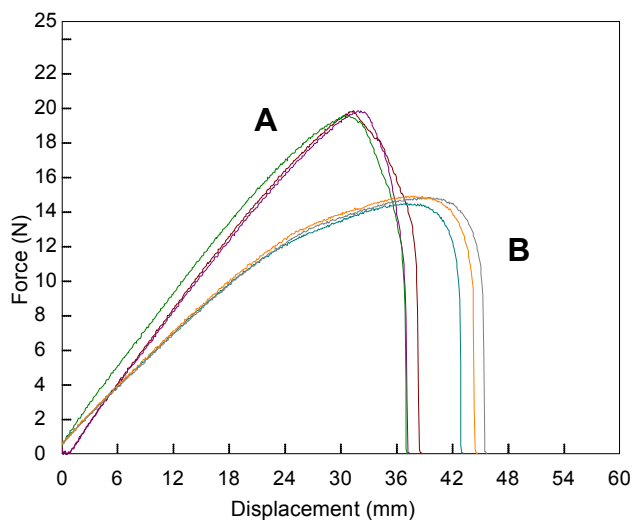


Fig. 2: Relationship Between Force and Displacement

Table 1: Test Conditions

Item	Set Value
Test Speed	500 mm/min
Initial Distance between Grips	60 mm

Table 2: Test Results (Average)

Sample	Main Component	Max. Force (N)	Tear Strength (kN/m)
A	CR rubber (black)	19.7	9.85
B	CR rubber (white)	14.7	7.35

The tear test results for the two samples are shown in Table 2. A graph showing the force-displacement relationship for each sample is shown in Fig. 2. Differences in tear strength between the samples are clearly apparent.

## Rubber Tear Test System

Tester: AGS-X  
Load Cell: 1 kN  
Test Jig: 1 kN pneumatic flat grips (Single-side file teeth grip faces)  
Software: TRAPEZIUM LITE X



AGS-X Table-Top Precision Universal Tester

## Features

- A high-precision load cell is adopted. (The high-precision type is class 0.5; the standard-precision type is class 1.) Accuracy is guaranteed over a wide range, from 1/500 to 1/1 of the load cell capacity. This supports highly reliable test evaluations.
- Crosshead speed range  
Tests can be performed over a wide range from 0.001 mm/min to 1,000 mm/min.
- High-speed sampling  
High-speed sampling, as fast as 1 msec.
- TRAPEZIUMX LITE X operational software  
This is simple, highly effective software.
- Jog controller (optional)  
This allows hand-held control of the crosshead position. Fine position adjustment is possible using the jog dial.
- Optional Test Devices  
A variety of tests can be conducted by switching between an abundance of jigs in the lineup.

First Edition: February 2013



Shimadzu Corporation

[www.shimadzu.com/an/](http://www.shimadzu.com/an/)

For Research Use Only. Not for use in diagnostic procedures.

The content of this publication shall not be reproduced, altered or sold for any commercial purpose without the written approval of Shimadzu. The information contained herein is provided to you "as is" without warranty of any kind including without limitation warranties as to its accuracy or completeness. Shimadzu does not assume any responsibility or liability for any damage, whether direct or indirect, relating to the use of this publication. This publication is based upon the information available to Shimadzu on or before the date of publication, and subject to change without notice.

© Shimadzu Corporation, 2013

# Application Data Sheet

No. 7

## Autograph Precision Universal Tester

Material Testing & Inspection

### Tensile Tests of Films

Standard No. ISO527-3: 2012 (JIS K 7127: 1999)

#### Introduction

Tensile tests are widely used to evaluate plastic materials, and the results are used as indices for new materials development and for implementing quality control. Items widely evaluated as tensile characteristics of plastic materials include the tensile modulus, strength, and break strain. In this Data Sheet, break strain was measured based on displacement data acquired using an extensometer. The strength was also evaluated.

T. Murakami

#### Measurements and Jigs

Non-contact type extensometers capable of displacement measurements without affecting the sample properties are effective for accurately measuring the break strain of a film. In measuring such physical properties, the sample must be gripped evenly, suppressing the occurrence of wrinkles, so it is important to choose the grips carefully. As in this test, the use of a non-contact type extensometer/width sensor and foil grips is recommended for film tensile tests.

#### Measurement Results



Fig. 1: Test Status

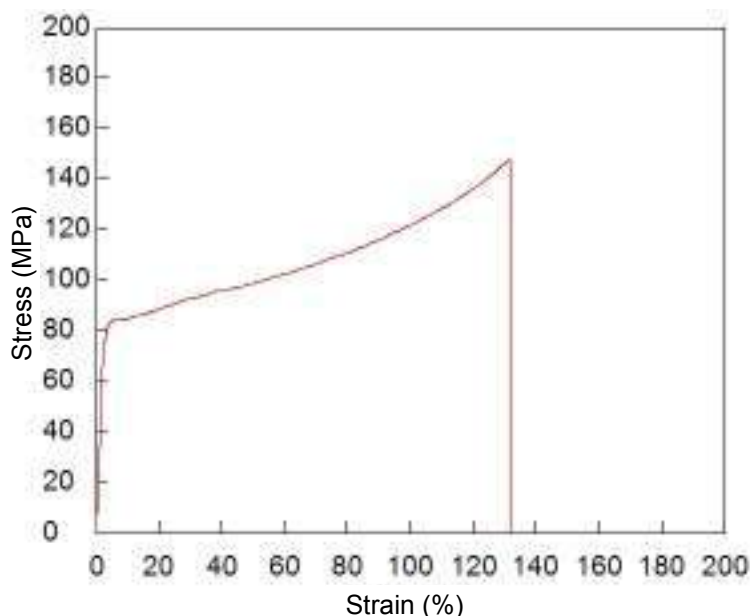


Fig. 2: Relationship Between Stress and Strain

Table 1: Test Conditions

Item	Set Value
Test Speed	50 mm/min
Initial Distance between Grips	100 mm

Table 2: Test Results

Sample	Thickness (μm)	Strength (MPa)	Break Strain (%)
PET Film	150	148	132

## Film Tensile Test System

Tester: AGS-X  
Load Cell: 1 kN  
Test Jig: 1 kN grips for foils  
Extensometer: TRViewX 240S non-contact extensometer/width sensor  
Software: TRAPEZIUM X



AGS-X Table-Top Precision Universal Tester

## Features

- A high-precision load cell is adopted. (The high-precision type is class 0.5; the standard-precision type is class 1.) Accuracy is guaranteed over a wide range, from 1/500 to 1/1 of the load cell capacity. This supports highly reliable test evaluations.
- Crosshead speed range  
Tests can be performed over a wide range from 0.001 mm/min to 1,000 mm/min.
- High-speed sampling  
High-speed sampling, as fast as 1 msec.
- TRAPEZIUMX operational software  
Designed for intuitive operation, this software offers excellent convenience and user friendliness.
- Jog controller (optional)  
This allows hand-held control of the crosshead position. Fine position adjustment is possible using the jog dial.
- Optional Test Devices  
A variety of tests can be conducted by switching between an abundance of jigs in the lineup.

First Edition: February 2013



Shimadzu Corporation

[www.shimadzu.com/an/](http://www.shimadzu.com/an/)

For Research Use Only. Not for use in diagnostic procedures.

The content of this publication shall not be reproduced, altered or sold for any commercial purpose without the written approval of Shimadzu. The information contained herein is provided to you "as is" without warranty of any kind including without limitation warranties as to its accuracy or completeness. Shimadzu does not assume any responsibility or liability for any damage, whether direct or indirect, relating to the use of this publication. This publication is based upon the information available to Shimadzu on or before the date of publication, and subject to change without notice.

© Shimadzu Corporation, 2013

# Application Data Sheet

No. 9

## Autograph Precision Universal Tester

Material Testing & Inspection

## Measurements of Modulus of Elasticity and Poisson's Ratio for Films

Standard Nos. ISO527-3: 2012 (JIS K 7127: 1999)  
ISO527-1: 2012 (JIS K 7161: 1994)

### Introduction

Tensile tests are widely used to evaluate plastic materials, and the results are used as indices for new materials development and for implementing quality control. Items evaluated as tensile characteristics of plastic materials include the tensile modulus, Poisson's ratio, strength, and break strain. With films, there are no standards specified with respect to test methods for the tensile elastic modulus and Poisson's ratio, yet there are demands for measurements of these values. In this Data Sheet, measurements of the tensile modulus and Poisson's ratio were performed for a PET film based on elongation and width data acquired using a non-contact type extensometer/width sensor.

T. Murakami

### Measurements and Jigs

Non-contact type extensometers/width sensors capable of fine displacement measurements without affecting the sample properties are required to accurately obtain the tensile modulus and Poisson's ratio for a film. In measuring such physical properties, the sample must be gripped evenly, suppressing the occurrence of wrinkles, so it is important to choose the grips carefully. The use of a non-contact type extensometer/width sensor and foil grips is recommended for film tensile tests.

### Measurement Results

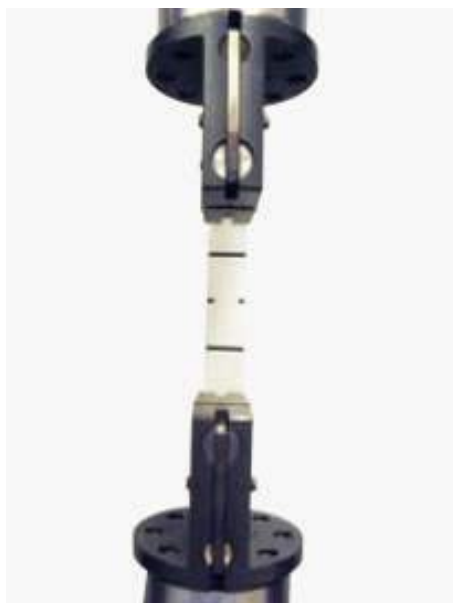


Fig. 1: Test Status

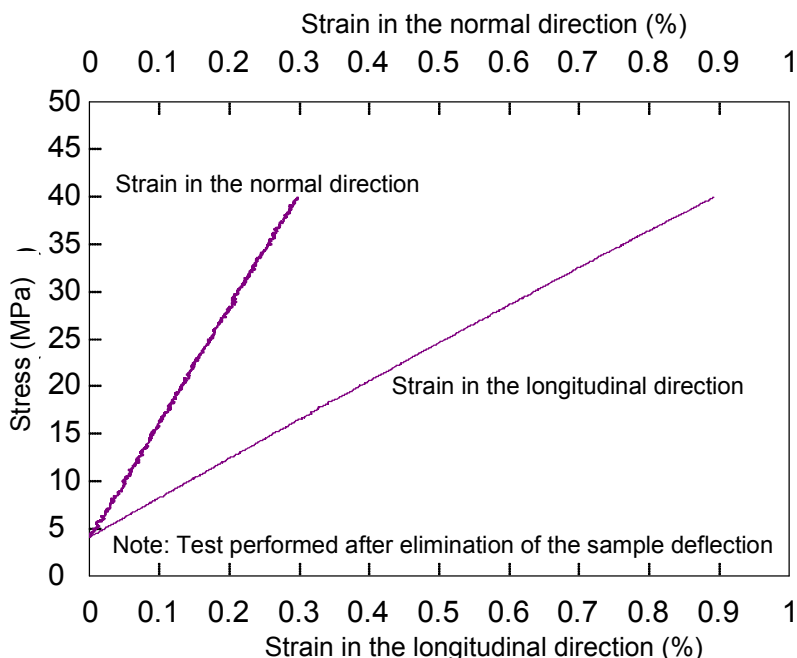


Fig. 2: Relationship Between Stress and Strain

Table 1: Test Conditions

Item	Set Value
Test Speed	1 mm/min
Initial distance Between Grip	100 mm
Gauge Length	40 mm

Table 2: Test Results

Sample	Thickness ( $\mu\text{m}$ )	Tensile Modulus (MPa)	Poisson's Ratio
PET Film	25	4139	0.37



## Young's Modulus Measurement System for Film

Tester: AG-Xplus  
Load Cell: 1 kN  
Test Jig: 1 kN grips for foils  
Extensometer: TRViewX 55S non-contact extensometer/width sensor  
Software: TRAPEZIUM X (Single)



AG-Xplus Table-Top Precision Universal Tester

## Features

- A high-precision load cell is adopted. (The high-precision type is class 0.5; the standard-precision type is class 1.) Accuracy is guaranteed over a wide range, from 1/1000 to 1/1 of the load cell capacity. This supports highly reliable test evaluations.
- Crosshead speed range  
Tests can be performed over a wide range from 0.0005 mm/min to 1,500 mm/min.
- High-speed sampling  
Ultrafast sampling, as fast as 0.2 msec. Sudden changes in test force, such as when brittle materials fracture, can be assessed.
- TRAPEZIUMX X operational software  
Designed for intuitive operation, this software offers excellent convenience and user friendliness.
- Smart controller  
Real-time test force and position data is readily confirmed, and the manual dial can be used for fine adjustments to jig positioning.
- Optional Test Devices  
A variety of tests can be conducted by switching between an abundance of jigs in the lineup.

First Edition: February 2013



Shimadzu Corporation

[www.shimadzu.com/an/](http://www.shimadzu.com/an/)

For Research Use Only. Not for use in diagnostic procedures.  
The content of this publication shall not be reproduced, altered or sold for any commercial purpose without the written approval of Shimadzu. The information contained herein is provided to you "as is" without warranty of any kind including without limitation warranties as to its accuracy or completeness. Shimadzu does not assume any responsibility or liability for any damage, whether direct or indirect, relating to the use of this publication. This publication is based upon the information available to Shimadzu on or before the date of publication, and subject to change without notice.

© Shimadzu Corporation, 2013

# Application Data Sheet

No. 17

## Autograph Precision Universal Tester

Material Testing & Inspection

### Measurement of Friction Coefficient of Film

Standard No. ISO 8295: 1995 (JIS K 7125: 1999)

#### Introduction

Plastic films are used for coating or wrapping of various materials. It is often necessary to measure sliding friction between two films or between a film and a different material. For example, the coefficient of friction of film for foods and that of protection film for smartphones are measured. In this Application Data Sheet, measurement examples of the static and dynamic coefficients of friction for polyethylene film in accordance with the ISO standard are introduced.

F. Yano

#### Measurement and Jigs

The standard specifies the method of measuring the coefficients of starting and sliding friction of plastic films and sheets. This method measures the coefficient of friction of plastic films and sheets that are not sticky up to 0.5 mm thickness. The test requires 2 test specimens of size about 80 mm × 200 mm, and the test apparatus generally includes a horizontal testing table, a sliding member, and a drive mechanism that produces relative motion between the test table and the sliding member. In these tests, the AGS-X Table-Top Precision Universal Tester and friction coefficient measuring apparatus were used to evaluate polyethylene film.

#### Measurement Results

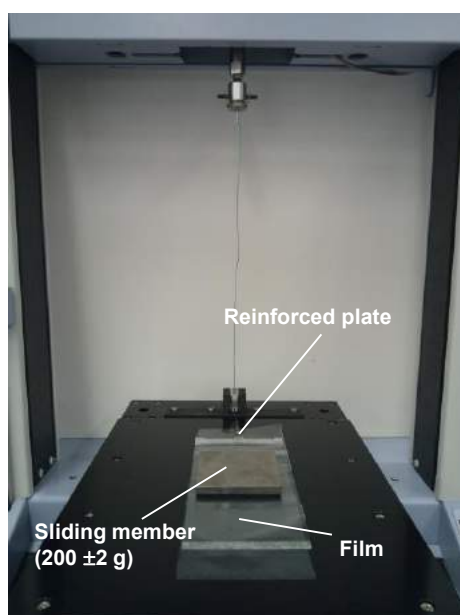


Fig. 1 Test Status

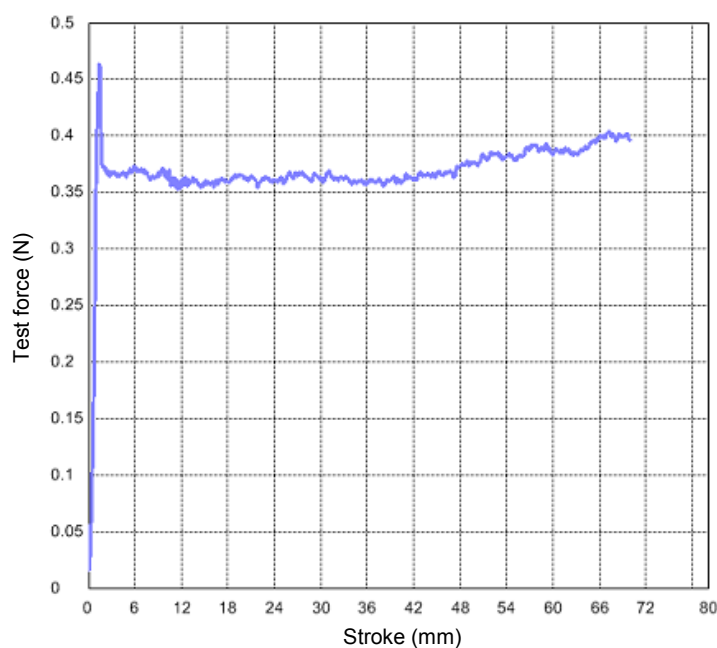


Fig.2 Test Results

Table 1 Test Conditions

Item	Set Value
Test speed	100 mm/min
Load cell capacity	5 N

Table 2 Test Results

Static Coefficient of Friction	Dynamic Coefficient of Friction
0.23	0.19

## Friction Coefficient Measurement System

Tester: AGS-X  
Load Cell: 5 N  
Test Jig: Friction coefficient measuring apparatus  
Software: TRAPEZIUM LITE X

TRAPEZIUM  
LITE X



AGS-X Table-Top Precision Universal Tester

## Features

- A high-precision load cell is adopted. (The high-precision type is class 0.5; the standard-precision type is class 1.) Accuracy is guaranteed over a wide range, from 1/500 to 1/1 of the load cell capacity. This supports highly reliable test evaluations.
- Cross head speed range  
Test can be performed over a wide range from 0.001 mm/min to 1,000 mm/min.
- High speed sampling  
High speed sampling, as fast as 1 msec.
- TRAPEZIUMX LITE X operational software  
This is simple, highly effective software.
- Jog controller (optional)  
This allows hand-held control of the crosshead position. Fine position adjustment is possible using the jog dial.
- Optional Test Devices  
A variety of tests can be accommodated by switching between an abundance of jigs in the lineup.

First Edition: February 2013



Shimadzu Corporation

[www.shimadzu.com/an/](http://www.shimadzu.com/an/)

For Research Use Only. Not for use in diagnostic procedures.

The content of this publication shall not be reproduced, altered or sold for any commercial purpose without the written approval of Shimadzu. The information contained herein is provided to you "as is" without warranty of any kind including without limitation warranties as to its accuracy or completeness. Shimadzu does not assume any responsibility or liability for any damage, whether direct or indirect, relating to the use of this publication. This publication is based upon the information available to Shimadzu on or before the date of publication, and subject to change without notice.

© Shimadzu Corporation, 2013

# Application Data Sheet

No. 18

## Autograph Precision Universal Tester

Material Testing & Inspection

## 90-Degree Peel Resistance Test of Adhesive Tape

Standard No. ISO29862: 2007 (JIS Z 0237 :2009)

### Introduction

Adhesives are widely used in many industrial fields such as electronics and electrical machinery. Starting from the use of materials such as glue to join solids together, adhesives that use synthetic polymers as the raw material have been commercialized with the progress of the chemical industry. In this Application Data Sheet, examples of the 90-degree peeling test for adhesive material used for adhesive tape are introduced.

T. Murakami

### Measurement and Jigs

General adhesive tape cut to a width of 24 mm and length of 300 mm was used as the test sample, and a SUS304 stainless steel plate was used as the test plate for setting the sample. An adhesive tape peel resistance test apparatus that was capable of peeling the sample at a constant 90 degree to the test plate was used.

### Measurement Results

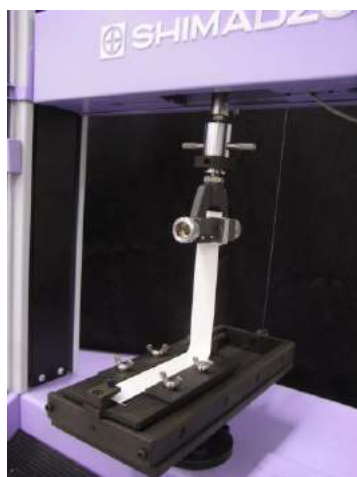


Fig. 1 Test Status

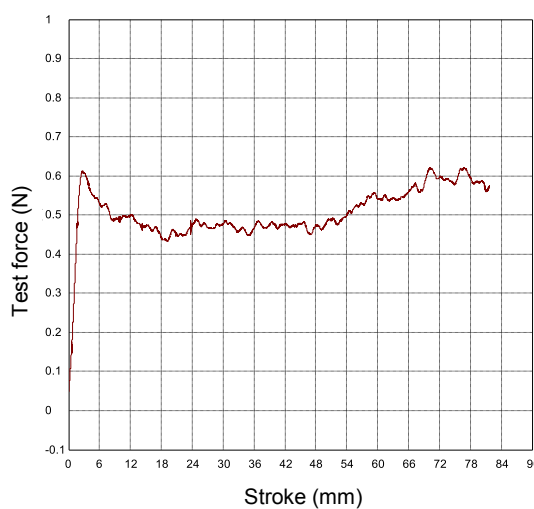


Fig. 2 Relationship Between Test Force and Stroke

The tests were carried out at a load rate of 300 mm/min. The measured values for the initial 25 mm length after start of testing were ignored, and the subsequent adhesion force measurement values for subsequent 50 mm length peeled from the test plate were averaged to obtain the peel adhesion force.

Table 1 Test Results

Peel Adhesion Force
0.238 N/10 mm

## Plastic Material Tensile Test System

Tester: AGS-X  
Load Cell: 50 N  
Test Jig: Adhesive tape peel resistance test apparatus  
Software: TRAPEZIUM LITE X



AGS-X Table-Top Precision Universal Tester

## Features

- A high-precision load cell is adopted. (The high-precision type is class 0.5; the standard-precision type is class 1.) Accuracy is guaranteed over a wide range, from 1/500 to 1/1 of the load cell capacity. This supports highly reliable test evaluations.
- Cross head speed range  
Test can be performed over a wide range from 0.001 mm/min to 1,000 mm/min.
- High speed sampling  
High speed sampling, as fast as 1 msec.
- TRAPEZIUMX LITE X operational software  
This is simple, highly effective software.
- Jog controller (optional)  
This allows hand-held control of the crosshead position. Fine position adjustment is possible using the jog dial.
- Optional Test Devices  
A variety of tests can be accommodated by switching between an abundance of jigs in the lineup.

First Edition: February 2013



Shimadzu Corporation

[www.shimadzu.com/an/](http://www.shimadzu.com/an/)

For Research Use Only. Not for use in diagnostic procedures.

The content of this publication shall not be reproduced, altered or sold for any commercial purpose without the written approval of Shimadzu. The information contained herein is provided to you "as is" without warranty of any kind including without limitation warranties as to its accuracy or completeness. Shimadzu does not assume any responsibility or liability for any damage, whether direct or indirect, relating to the use of this publication. This publication is based upon the information available to Shimadzu on or before the date of publication, and subject to change without notice.

© Shimadzu Corporation, 2013



# Application Data Sheet

No. 19

## Autograph Precision Universal Tester

Material Testing & Inspection

### 180-Degree Peel Resistance Test of Adhesive Tape

Standard No. ISO29862: 2007 (JIS Z 0237 :2009)

#### Introduction

Adhesives are widely used in many industrial fields such as electronics and electrical machinery. Starting from the use of materials such as glue to join solids together, adhesives that use synthetic polymers as the raw material have been commercialized with the progress of the chemical industry. In this Application Data Sheet, examples of the 180-degree peeling test for adhesive material used for adhesive tape are introduced.

T.Murakami

#### Measurement and Jigs

General adhesive tape cut to a width of 24 mm and length of 300 mm was used as the test sample, and a SUS304 stainless steel plate was used as the test plate for setting the sample. When the sample was peeled, the ends of the tape were held and folded through 180 degree so that the back of the tape was overlapped. After the sample was peeled 25 mm from the test plate, one end of the test plate from which the tape had been peeled was fixed in the lower jig set in the testing machine, and the adhesive tape was fixed in the upper jig.

#### Measurement Results



Fig. 1 Test Status

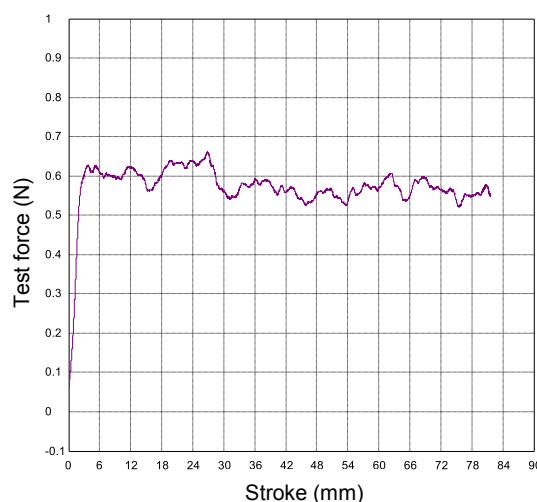


Fig. 2 Relationship Between Test Force and Stroke

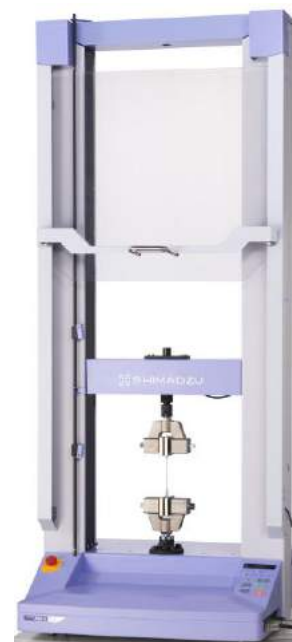
The tests were carried out at a load rate of 300 mm/min. The measured values for the initial 25 mm length after start of testing were ignored, and the subsequent adhesion force measurement values for subsequent 50 mm length peeled from the test plate were averaged to obtain the peel adhesion force.

Table 1 Test Results

Peel Adhesion Force
0.217 N/10 mm

## Plastic Material Tensile Test System

Tester: AGS-X  
Load Cell: 50 N  
Test Jig: 50 N pneumatic flat grips (plane teeth)  
Software: TRAPEZIUM LITE X



AGS-X Table-Top Precision Universal Tester

## Features

- A high-precision load cell is adopted. (The high-precision type is class 0.5; the standard-precision type is class 1.) Accuracy is guaranteed over a wide range, from 1/500 to 1/1 of the load cell capacity. This supports highly reliable test evaluations.
- Cross head speed range  
Test can be performed over a wide range from 0.001 mm/min to 1,000 mm/min.
- High speed sampling  
High speed sampling, as fast as 1 msec.
- TRAPEZIUMX LITE X operational software  
This is simple, highly effective software.
- Jog controller (optional)  
This allows hand-held control of the crosshead position. Fine position adjustment is possible using the jog dial.
- Optional Test Devices  
A variety of tests can be accommodated by switching between an abundance of jigs in the lineup.

First Edition: February 2013



Shimadzu Corporation

[www.shimadzu.com/an/](http://www.shimadzu.com/an/)

For Research Use Only. Not for use in diagnostic procedures.

The content of this publication shall not be reproduced, altered or sold for any commercial purpose without the written approval of Shimadzu. The information contained herein is provided to you "as is" without warranty of any kind including without limitation warranties as to its accuracy or completeness. Shimadzu does not assume any responsibility or liability for any damage, whether direct or indirect, relating to the use of this publication. This publication is based upon the information available to Shimadzu on or before the date of publication, and subject to change without notice.

© Shimadzu Corporation, 2013

# Application Data Sheet

No. 20

## Autograph Precision Universal Tester

Material Testing & Inspection

## Measurement of Friction Coefficient of Film

Standard No. ASTM D 1894 - 95 (JIS K 7312 - 1996)

### Introduction

Plastic films are used for coating or wrapping of various materials. It is often necessary to measure sliding friction between two films or between a film and a different material. For example, the coefficient of friction of film for foods and that of protection film for smartphones are measured. In this Application Data Sheet, measurement examples of the static and dynamic coefficients of friction for polyethylene film in accordance with the ASTM standard are introduced.

F. Yano

### Measurement and Jigs

The standard specifies the method of measuring the coefficients of starting and sliding friction of plastic films and sheets. These tests were carried out on polyethylene film using the AGS-X Table-Top Precision Universal Tester and friction coefficient measuring apparatus. Two test samples were prepared: a movable sample and a fixed sample. The measurements were carried out with the movable sample (a square test specimen of side 63.5 mm) fastened to a metal sled using double-sided tape, and the fixed sample (rectangular test specimen of width 130 mm and length 250 mm minimum) fastened to a platform using double-sided tape.

### Measurement Results

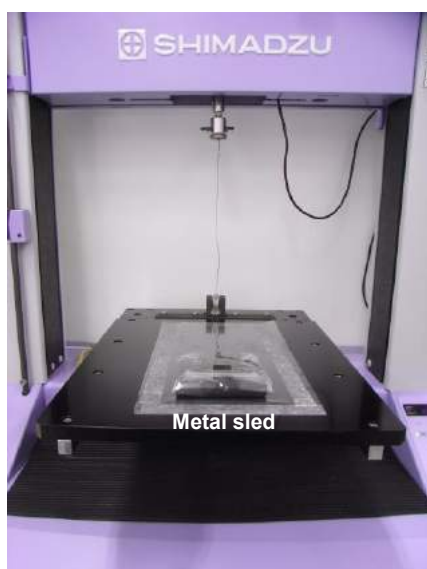


Fig. 1 Test Status

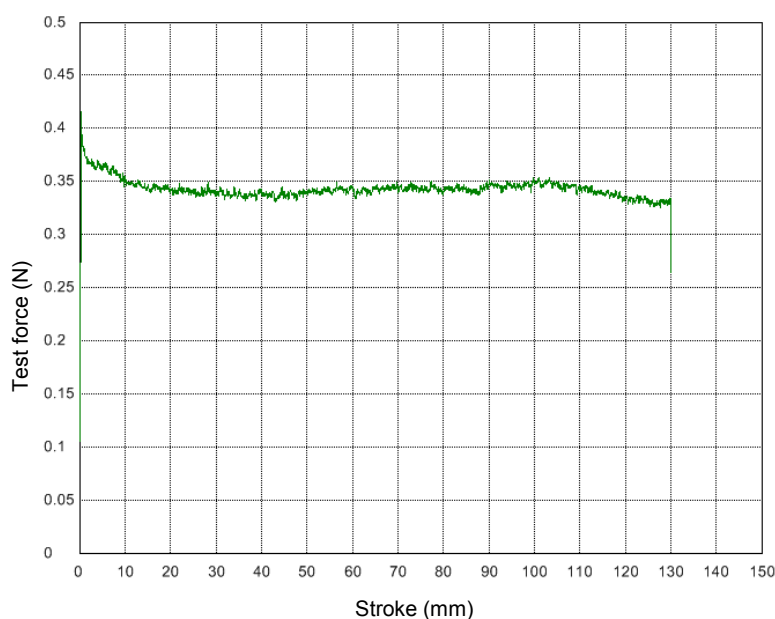


Fig.2 Test Results

Table 1 Test Conditions

Item	Set Value
Test speed	150 mm/min
Moving distance	130 mm
Load cell capacity	5 N

Table 2 Test Results

Static Coefficient of Friction	Dynamic Coefficient of Friction
0.21	0.17

## Friction Coefficient Measurement System

Tester: AGS-X  
Load Cell: 5 N  
Test Jig: Friction coefficient measuring apparatus  
Software: TRAPEZIUM LITE X

TRAPEZIUM  
LITE X



AGS-X Table-Top Precision Universal Tester

## Features

- A high-precision load cell is adopted. (The high-precision type is class 0.5; the standard-precision type is class 1.) Accuracy is guaranteed over a wide range, from 1/500 to 1/1 of the load cell capacity. This supports highly reliable test evaluations.
- Cross head speed range  
Test can be performed over a wide range from 0.001 mm/min to 1,000 mm/min.
- High speed sampling  
High speed sampling, as fast as 1 msec.
- TRAPEZIUMX LITE X operational software  
This is simple, highly effective software.
- Jog controller (optional)  
This allows hand-held control of the crosshead position. Fine position adjustment is possible using the jog dial.
- Optional Test Devices  
A variety of tests can be accommodated by switching between an abundance of jigs in the lineup.

First Edition: February 2013



Shimadzu Corporation

[www.shimadzu.com/an/](http://www.shimadzu.com/an/)

For Research Use Only. Not for use in diagnostic procedures.

The content of this publication shall not be reproduced, altered or sold for any commercial purpose without the written approval of Shimadzu. The information contained herein is provided to you "as is" without warranty of any kind including without limitation warranties as to its accuracy or completeness. Shimadzu does not assume any responsibility or liability for any damage, whether direct or indirect, relating to the use of this publication. This publication is based upon the information available to Shimadzu on or before the date of publication, and subject to change without notice.

© Shimadzu Corporation, 2013

# Application News

## No.i253

### Material Testing System

## Tensile Test of Plastic Materials

### ■ Introduction

The physical characteristics of plastic materials are an essential part of product design and quality control. Various materials tests are performed because of this, of which the most basic test is tensile testing that is cited in many product specifications. The tensile properties of plastic materials assessed by tensile testing include strength, elastic modulus, and breaking strain. Tensile testing of plastics was once performed according to the standard test methods described in ISO 527-1 (JIS K 7161), but ISO 527-1 was revised substantially in 2012 (and JIS K 7161 in 2014). This revision resulted in a number of important changes, of which the main changes are summarized below.

First, the preferred gauge length for type 1A geometry specimens was changed to 75 mm. The previous gauge length of 50 mm is still allowed, but since it became possible to set a longer gauge length, a gauge length of 75 mm is preferred since using this length makes it easier to produce a break within the gauge length. Also, a gauge length of 75 mm is recommended due to the relationship between gauge length and extensometer accuracy that is mentioned below. ISO 527-1 (JIS K 7161) noted that tests must be performed within a standard error of 1 % to calculate elastic modulus accurately. Fig. 1 shows absolute values for the extensometer accuracy required when using a 75 mm and 50 mm gauge length. It shows the absolute accuracy of a 75 mm gauge length is  $\pm 1.5 \mu\text{m}$ , while the absolute accuracy of a 50 mm gauge length is  $\pm 1.0 \mu\text{m}$ . In other words, performing the same test with a 75 mm gauge length increases the permissible range of absolute accuracy. This widens the choice of extensometers and allows the TRViewX non-contact digital video extensometer (absolute accuracy of  $\pm 1.5 \mu\text{m}$ ) to be used for standard testing.

The revision also added a method for calculating strain at yield point. The previous Method A calculated strain with equation (1). The newly added Method B calculates strain with equation (2).

$$\epsilon_t = \frac{L_t}{L} \quad (1)$$

$$\epsilon_t = \epsilon_y + \frac{\Delta L_t}{L} \quad (2)$$

$\epsilon_t$  : Nominal strain

$L$  : Initial distance between grips [mm]

$L_t$  : Increase in distance between grips [mm]

$\epsilon_y$  : Yield strain

$\Delta L_t$  : Increase in distance between grips beyond the yield point [mm]

Method B is preferred for materials that exhibit yielding and necking. Fig. 2 shows an illustrated image of a strain calculation performed using Method B. Shimadzu's TRAPEZIUM X software supports both Method A and Method B.

In this article, PP (polypropylene), PVC (polyvinyl chloride) and PC (polycarbonate) specimens are tested in accordance with current standards.

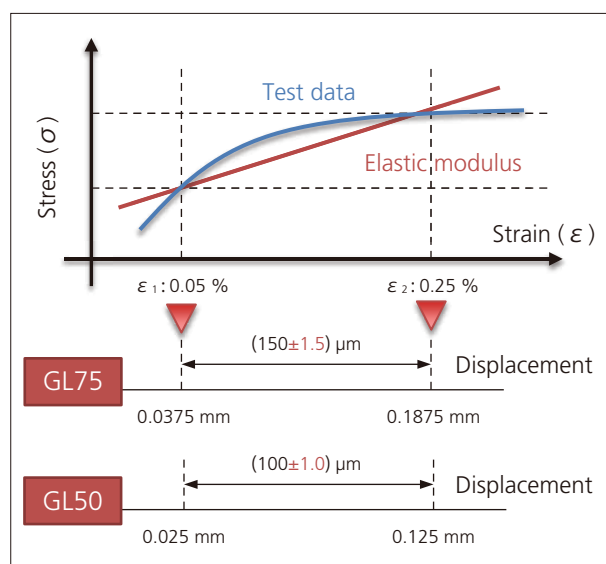


Fig. 1 Comparison of Absolute Accuracy between 75 mm and 50 mm Gauge Lengths

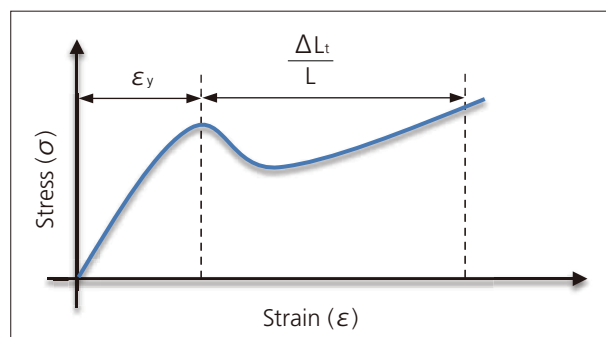


Fig. 2 Strain Calculated by Method B



Measurement System

Measurements were made using an AGS-X table-top precision universal testing instrument, a contact extensometer, and a non-contact digital video extensometer. A gauge length of 75 mm was used with both extensometers. Table 1 shows a list of the equipment used.

Table 1 Experimental Equipment

Testing Machine	: AGS-X
Load Cell	: 5 kN
Gripping Device	: Pneumatic parallel gripping device
Gripping Teeth	: Single-cut file teeth
Software	: TRAPEZIUM X (Single)
Displacement Gauge	: SG75-10, TRViewX 240S

Measured Results

An initial test speed of 1 mm/min was switched to 50 mm/min at 1 mm displacement. The contact extensometer was removed at 1 mm displacement. Fig. 3 shows testing with the SG75-10 and Fig. 4 shows testing with the TRViewX. The respective test results are shown in Table 2 and Table 3, and the stress-strain curve obtained using the SG75-10 is shown in Fig. 5. The results shown in Table 2 and Table 3 confirm that tests were performed successfully since there is almost no difference between them.

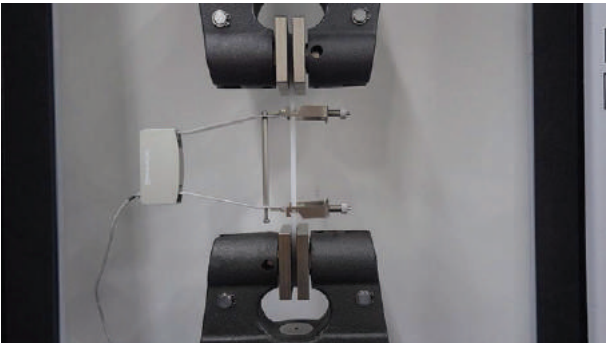


Fig. 3 Testing with SG75-10

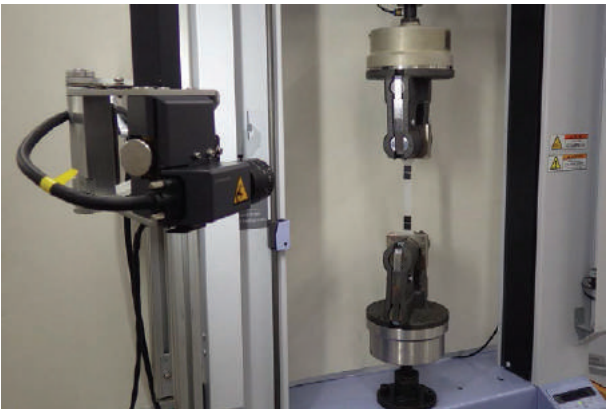


Fig. 4 Testing with TRViewX

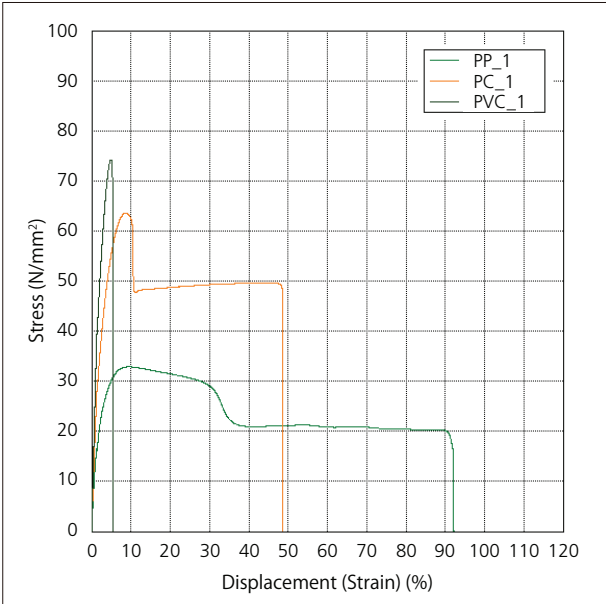


Fig. 5 Test Results Using SG75-10

Table 2 Test Results Using SG75-10

Specimen	Strength [MPa]	Elastic Modulus [GPa]
PP	32.5	1.66
PC	63.3	2.30
PVC	73.4	3.23

Table 3 Test Results Using TRViewX

Specimen	Strength [MPa]	Elastic Modulus [GPa]
PP	32.5	1.63
PC	63.7	2.26
PVC	73.4	3.12

Conclusion

The testing standard for tensile testing of plastic materials has undergone an important revision. Introduction of a 75 mm gauge length brings benefits that include an increased choice of extensometers for elastic modulus measurement and an easier break within the gauge length. Introducing Method B for calculating strain allows a more accurate determination of strain, in materials that exhibit yielding and necking in particular. Testing according to the current ISO 527-1: 2012 (JIS K 7161-1: 2014) standard can be performed successfully using the equipment described in this article.



Shimadzu Corporation  
www.shimadzu.com/an/

**For Research Use Only. Not for use in diagnostic procedure.**  
This publication may contain references to products that are not available in your country. Please contact us to check the availability of these products in your country.  
  
The content of this publication shall not be reproduced, altered or sold for any commercial purpose without the written approval of Shimadzu. Company names, product/service names and logos used in this publication are trademarks and trade names of Shimadzu Corporation or its affiliates, whether or not they are used with trademark symbol "TM" or "®". Third-party trademarks and trade names may be used in this publication to refer to either the entities or their products/services. Shimadzu disclaims any proprietary interest in trademarks and trade names other than its own.  
  
The information contained herein is provided to you "as is" without warranty of any kind including without limitation warranties as to its accuracy or completeness. Shimadzu does not assume any responsibility or liability for any damage, whether direct or indirect, relating to the use of this publication. This publication is based upon the information available to Shimadzu on or before the date of publication, and subject to change without notice.

Shimadzu Flowtester

# CFT-EX Series

Application Topic # 05

## Fluidity Evaluation of Unvulcanized Rubber

Rubber products are produced by forming rubber compounds (mixtures of rubber and additives that provide specific functional characteristics) in a mold and then applying heat to provide an elastic body. Therefore, the fluidity of rubber compounds can have a major effect on molding quality. Unformed rubber compounds change their characteristics after long storage periods, which can cause fluidity to deteriorate or the molding process to fail, depending on how they are stored.



Here, the example which evaluated the fluidity change by the storage method of the unvulcanized rubber is introduced.

## Fluidity Change by the Storage Method of Unvulcanized Rubber

In this case, a rubber compound was stored at ambient temperature and low temperature for 14 days and 28 days immediately after kneading and then the fluidity was evaluated.

The results showed that the given sample could be stored at low temperatures without a significant change in fluidity, even after one month.

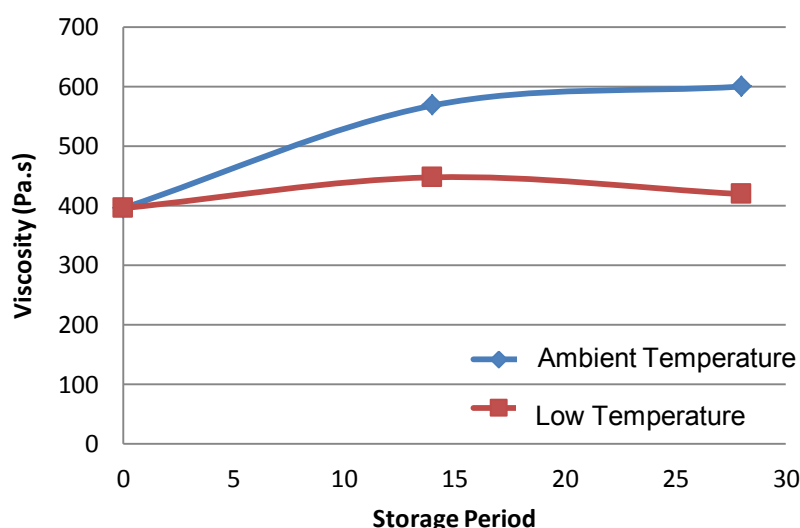
Using the CFT-EX series allows evaluating the rubber compounds storage temperatures and storage periods without actually having to mold any parts.

### Test condition

Test Method	Constant temperature test
Die Diameter	0.5 mm
Die Length	1 mm
Test Temperature	280 °C
Test Pressure	20.1 MPa
Preheating Time	0 sec
Sample Size	1.6 g

### Test result

Storage Temperature	Storage Period	Viscosity (Pa.s)
Ambient Temperature	0	395.7
	14	568.1
	28	600.0
Low Temperature	0	395.7
	14	447.5
	28	419.3



Changes in Viscosity Due to Storage Methods

## CFT-EX can use evaluation of unvulcanized rubber

CFT-EX which can evaluate thermosetting and thermoplastic resin in evaluation of unvulcanized rubber is recommended.

### The feature of CFT-EX

- Higher Level Evaluation Using a Variety of Analysis Methods
  - • • The evaluation of thermosetting resin and constant heating rate test is possible.
- Smooth, Easy Test Flow
  - • • New software compatible with Win7, 8.1
- Supported by More Than 50 Years of Technology and Know-How
  - • • Abundant applications cultivated for years

Shimadzu Flowtester

## **CFT-EX Series**



***Thermosetting resins***



***Thermoplastic resins***



***Rubbers***

***The fluidity of various materials  
&  
Evaluation of the heat characteristic***



***Ceramics***



***Toners***



***Composites***



Shimadzu Corporation

[www.shimadzu.com/an/](http://www.shimadzu.com/an/)

For Research Use Only. Not for use in diagnostic procedures.

The content of this publication shall not be reproduced, altered or sold for any commercial purpose without the written approval of Shimadzu. The information contained herein is provided to you "as is" without warranty of any kind including without limitation warranties as to its accuracy or completeness. Shimadzu does not assume any responsibility or liability for any damage, whether direct or indirect, relating to the use of this publication. This publication is based upon the information available to Shimadzu on or before the date of publication, and subject to change without notice.

# Shimadzu Flowtester CFT-EX Series

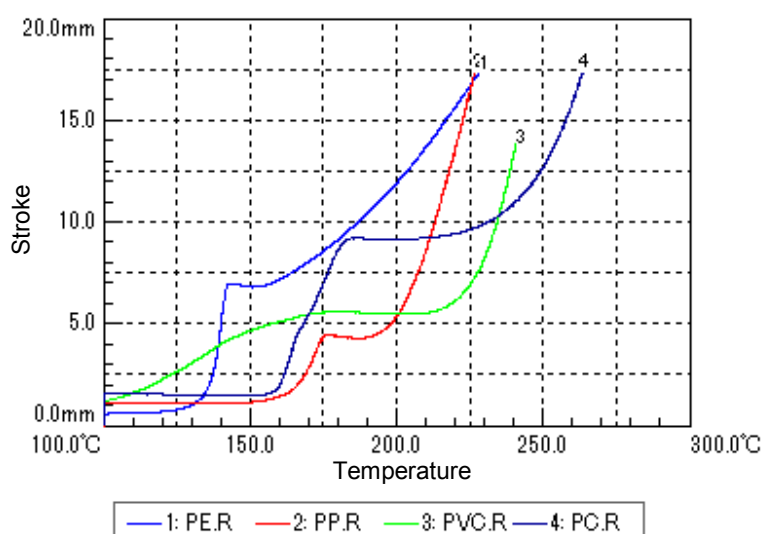
Application Topic # 06

## Evaluation of the Temperature Characteristics of General Plastics

The optimal measuring method is the constant heating rate method test that measuring the temperature where resins start softening and flowing, and their fluidity properties. Here, the example which tested with the constant heating rate method of typical general-purpose resin is shown.

The stroke-temperature graph shows that the sample starts flowing after it exceeds the flow beginning temperature and decreases in viscosity as the temperature increases (graph slope increases). The viscosity can be calculated for each temperature after initial flow.

To accurately determine the viscosity at each temperature, we recommend using the constant temperature method.



Stroke-Temperature Graph

### Test condition

Test Method	Constant heating rate test
Die Diameter	1 mm
Die Length	1 mm
Beginning Temperature	100 °C
Ending Temperature	300 °C
Heating Rate	5 °C/min
Test Pressure	0.98 MPa
Preheating Time	300 sec
Sample Size	1.2 g

### Test result

Sample Name	Softening Temperature (°C)	Flow Beginning Temperature (°C)	1/2 Method Temperature (°C)	1/2 Method Viscosity(Pa · s)
Polyethylene	142.4	153.6	203.6	16,370
Polypropylene	175.6	187.2	215.6	5,716
Polyvinyl chloride	175.3	208.2	234.4	6,138
Polycarbonate	183.1	205.1	253.9	10,590

## Cylinder Cooling Fan Improves Cycle Time for Constant Heating Rate Tests

Constant heating rate test measurements start at a low and finish at a high temperature. The cylinder cooling fan can be quickly attached to the bottom of the furnace to force-cool the cylinder, which can significantly shorten the cooling time.

A piston for force-cooling the cylinder with compressed air is also available.





## CFT-EX can use evaluation of general plastic.

CFT-EX is recommended for evaluation of a general-purpose plastic because it can simply evaluated about the flow characteristic for the temperature of resin by the constant heating rate method.

### The feature of CFT-EX

- Higher Level Evaluation Using a Variety of Analysis Methods
  - • • The evaluation of thermosetting resin and constant heating rate test is possible.
- Smooth, Easy Test Flow
  - • • New software compatible with Win7, 8.1
- Supported by More Than 50 Years of Technology and Know-How
  - • • Abundant applications cultivated for years

Shimadzu Flowtester

## **CFT-EX Series**



***Thermosetting resins***



***Thermoplastic resins***



***Rubbers***

***The fluidity of various materials  
&  
Evaluation of the heat characteristic***



***Ceramics***



***Toners***



***Composites***



Shimadzu Corporation  
[www.shimadzu.com/an/](http://www.shimadzu.com/an/)

For Research Use Only. Not for use in diagnostic procedures.  
The content of this publication shall not be reproduced, altered or sold for any commercial purpose without the written approval of Shimadzu.  
The information contained herein is provided to you "as is" without warranty of any kind including without limitation warranties as to its accuracy or completeness. Shimadzu does not assume any responsibility or liability for any damage, whether direct or indirect, relating to the use of this publication. This publication is based upon the information available to Shimadzu on or before the date of publication, and subject to change without notice.



# Application Data Sheet

## No. 4

## Autograph Precision Universal Tester

Material Testing & Inspection

## Tensile Tests of Rubber Dumb-bell Specimens

Standard No. ISO37: 2005 (JIS K6251: 2010)

### Introduction

Rubber materials have characteristic mechanical properties including elasticity and flexibility, and are widely used for industrial parts, construction materials, and housewares. In particular, a diverse range of synthetic rubber materials with differing properties suited to match their application have been developed. Measuring these mechanical properties is extremely important to ensure quality control and for new materials development. This Data Sheet introduces an example of the evaluation of three synthetic rubber (main components: chloroprene [1]; urethane [2]) specimens (dumb-bell test pieces). Static tensile tests were performed, and the specimens were evaluated with respect to tensile strength, stress at given elongation, and elongation at break, which are aspects of their basic mechanical properties.

T. Murakami

### Measurements and Jigs

In tensile tests of rubber dumb-bell specimens, the grips must tighten automatically. When tensile loads are applied to rubber materials, they elongate and their thickness decreases. For this reason, if there is no automatic tightening mechanism, the specimen will inadvertently break free of the grip before the maximum load is applied, making favorable measurements impossible. Accordingly, in rubber tensile tests, it is necessary to use pneumatic parallel grippers, pantograph grips, eccentric roller type grips, Henry Scott type grips, or other grips equipped with this feature.

### Measurement Results



Fig. 1: Test Status

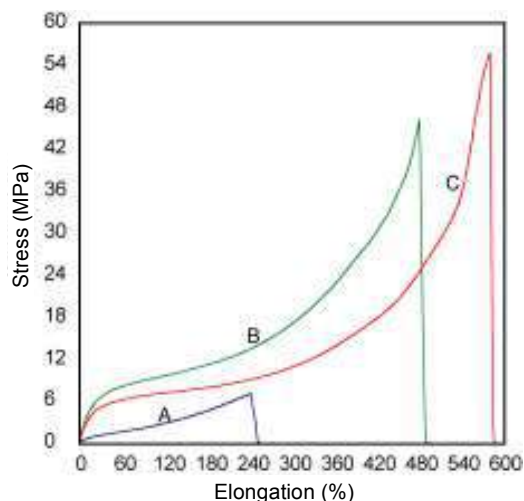


Fig. 2: Relationship Between Stress and Elongation

Table 1: Test Conditions

Item	Set Value
Test Speed	500 mm/min
Initial Distance between Grips	60 mm
Gauge Length	20 mm

Table 2: Test Results

Sample	Main Component	Tensile Strength (MPa)	Stress at 100 % Elongation (MPa)	Stress at 200 % Elongation (MPa)	Elongation at Break (%)
A	Chloroprene	7.1	2.4	5.4	242.3
B	Urethane	47.1	9.3	11.9	478.1
C	Urethane	55.5	7.0	8.4	572.6

The tensile test results for the three samples are shown in Table 2. A graph showing the stress-elongation relationship for the samples is shown in Fig. 2. Clear differences in mechanical properties such as tensile strength and elongation at break are apparent between the samples.

## Rubber (Dumb-bells test pieces) Tensile Test System

Tester: AGS-X  
Load Cell: 1 kN  
Test Jig: 1 kN pneumatic flat grips (Single-side file teeth grip faces)  
Extensometer: SES-1000 type extensometer for soft specimens  
Software: TRAPEZIUM LITE X



AGS-X Table-Top Precision Universal Tester

## Features

- A high-precision load cell is adopted. (The high-precision type is class 0.5; the standard-precision type is class 1.)  
Accuracy is guaranteed over a wide range, from 1/500 to 1/1 of the load cell capacity. This supports highly reliable test evaluations.
- Crosshead speed range  
Tests can be performed over a wide range from 0.001 mm/min to 1,000 mm/min.
- High-speed sampling  
High-speed sampling, as fast as 1 msec.
- TRAPEZIUMX LITE X operational software  
This is simple, highly effective software.
- Jog controller (optional)  
This allows hand-held control of the crosshead position. Fine position adjustment is possible using the jog dial.
- Optional Test Devices  
A variety of tests can be conducted by switching between an abundance of jigs in the lineup.

First Edition: February 2013



Shimadzu Corporation

[www.shimadzu.com/an/](http://www.shimadzu.com/an/)

For Research Use Only. Not for use in diagnostic procedures.

The content of this publication shall not be reproduced, altered or sold for any commercial purpose without the written approval of Shimadzu. The information contained herein is provided to you "as is" without warranty of any kind including without limitation warranties as to its accuracy or completeness. Shimadzu does not assume any responsibility or liability for any damage, whether direct or indirect, relating to the use of this publication. This publication is based upon the information available to Shimadzu on or before the date of publication, and subject to change without notice.

© Shimadzu Corporation, 2013

## Application News

Material Testing System AGS-X

No. SCA\_300\_038

### Tension - Compression Major Deformation Test of Rubber Vibration Isolator by Shimadzu Autograph Series

The Autograph Series features the ability to freely change test conditions while testing in addition to the reciprocating function (tension - compression).

Shown below is an example of a tension - compression major deformation test. This test is popular for evaluating the dynamic characteristics of rubber vibration isolators, executed by the Autograph.

Measurement was taken to record changes in energy loss (absorbed energy) on a hysteresis loop. Load and deformation were applied to an anti-vibration rubber developed for use in the architecture and civil engineering fields, load and deformation were then increased at return point per cycle...



#### ■ Test conditions

##### 1) Cycle test by means of load control

Test Mode	Cycle Tens/Comp. (Tens.)
Minimum Load	-50 kgf
Maximum Load	50 kgf
Test Speed	2 mm/min
Load Cell	10000 kgf
F/S Load	500 kgf

The above were load conditions at first cycle (+/- 50 kgf). +/- 100 kgf, +/- 200 kgf, +/- 300 kgf and +/- 400 kgf were applied successively thereafter

Test Mode	Cycle Tens/Comp. (Tens.)
Minimum Stroke	-1 mm
Maximum Stroke	1 mm
Test Speed	2 mm/min
Load Cell	10000 kgf
F/S Load	500 kgf

The above were displacement conditions at first cycle (+/- 1 mm). +/- 2 mm, +/- 3 mm, +/- 4 mm and +/- 5 mm were applied successively thereafter.

## ■ Test results

### 1) Cycle test by means of load control

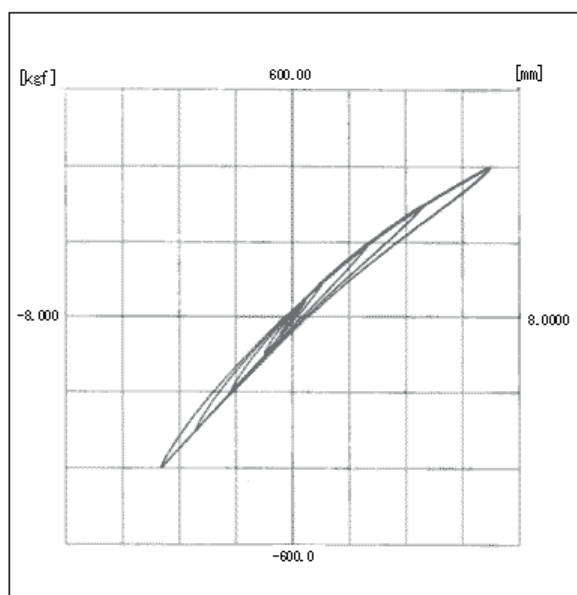


Fig. 1 Load versus Displacement Curve of Rubber Vibration Isolator (cycle test by load control)

### 2) Cycle test by means of displacement control

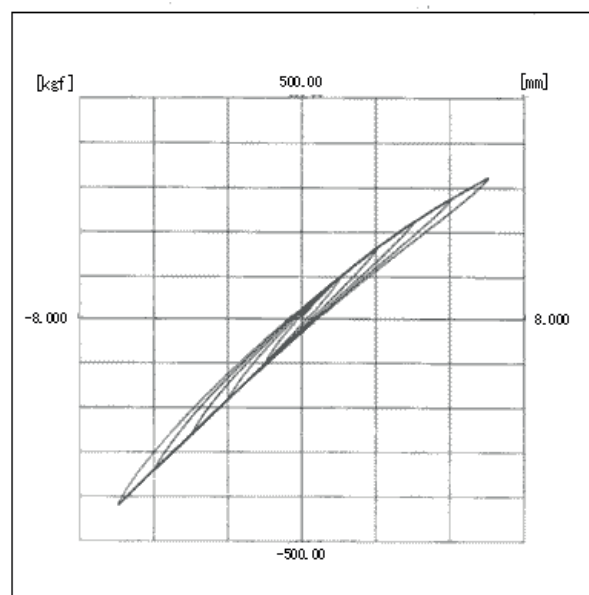


Fig. 2 Load versus Displacement Curve of Rubber Vibration Isolator (cycle test by stroke control)

\* Please be advised that data obtained before the implementation of the current Weights and Measures Law may be presented in terms of gravimetric unit.



## 6. Materials Testing & Inspection

---

### 6.2 Fatigue Testing

---

The standard series of Servopulser Fatigue/Endurance Testing Machines is typical of Shimadzu's lineup of electrohydraulic servotype fatigue testing machines. It boasts an extensive track record and consistent performance. It can cover static testing as well as fatigue tests.

<b>C225-E035</b>	High-speed material testing with 3D strain visualization!
<b>i247</b>	Material testing by strain distribution visualization – DIC analysis
<b>C225-E033</b>	Three-axis endurance evaluations of automobile steering mechanisms
<b>C225-E032</b>	Ultrasonic fatigue testing system with an average stress loading mechanism
<b>No. 36</b>	Evaluating the fatigue strength of GFRP materials
<b>C225-E034</b>	System to test fatigue and endurance of rubber in clean environment
<b>SCA_300_010</b>	Endurance testing and dynamic viscoelasticity measurement of EVA film by MMT-100N
<b>SCA_300_057</b>	Breaking strain measurement of ABS resin



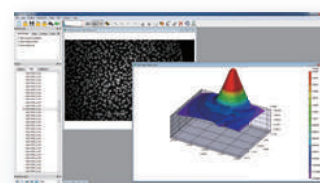
# High-Speed Material Testing with 3D Strain Visualization!



Test Speed:  
Max. 20 m/s /



Recording Speed:  
Max. 10 M fps /



by **correlated**  
**SOLUTIONS**

High-Speed Tensile Testing Machine  
**Hydrosot HIT-S-T10**

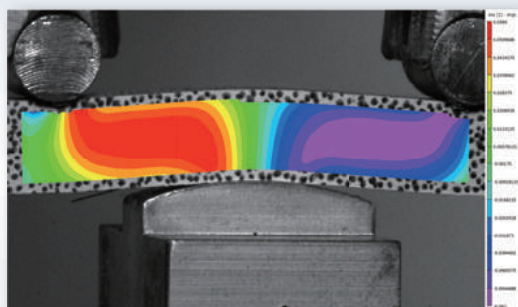
High-Speed Video Camera  
**Hyper Vision HPV-X2**

3D Deformations Analysis Software  
**VIC-3D**

- Visualize the strain distribution of rapidly occurring deformations in a specimen.
- Supports 3D strain distribution through synchronized recording with two HPV-X2 cameras.
- Directly control the HPV-X2 cameras using the strain distribution software (VIC-3D).

For evaluating the strength of CFRP, much attention has been placed on high-speed bending tests that are conducted under conditions that are as close as possible to the actual conditions of use. During the high-speed bending test of materials, deformations occur rapidly in a three-dimensional way. Since strain is distributed locally, conventional methods of measurement presented difficulties. With 3D-DIC, two HPV-X2 cameras are used, making it possible to dynamically measure strain distribution in a three-dimensional manner.

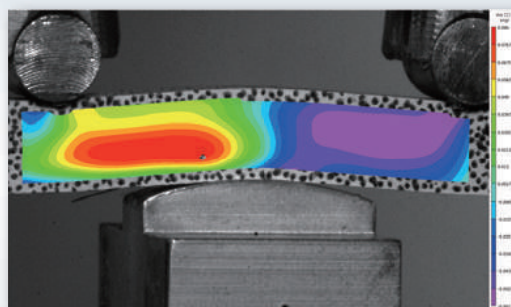
## Strain Distribution Presented by High-Speed, Three-Point Bending of CFRP



Before Interlaminar Peeling



After 1.5  $\mu$ s



After Interlaminar Peeling

## HPV-X2 Specifications

Lens Mount	Nikon F-mount	
Image Sensor	FTCMOS2 Image sensor	
Recording Speed (frames per second (fps))	HP mode	10 Mfps, 5 Mfps (fixed)
	FP mode	5 Mfps (fixed)
Resolution	Both modes	Variable recording speed between 60 fps and 2 Mfps
	HP mode	50,000 pixels (zigzag lattice pixel array)
	FP mode	100,000 pixels (400 × 250)
Color/ Gradations	Monochrome/, 10 bits	
Number of Frames Recorded	HP mode	256 frames
	FP mode	128 frames
Exposure Time	Approx. 50 ns at 10 Mfps, 110 ns at 5 Mfps	
	Variable in a 10 ns interval starting from 200 ns in a range from 60 fps to 2 Mfps	
External Trigger Input	Two channels (TRIGIN, STANDBY) TTL/contact	
External Monitor Output	NTSC	
Input/Output Ports	1000 Base-T / 100 Base-TX	
Trigger Mode	Internal trigger, external trigger, continuous trigger	
Dimensions (camera head)	W 160 × D 330 × H 260 mm	
Weight (camera head)	Approx. 6.4 kg	



Shimadzu Corporation

[www.shimadzu.com/an/](http://www.shimadzu.com/an/)

### For Research Use Only. Not for use in diagnostic procedures.

This publication may contain references to products that are not available in your country. Please contact us to check the availability of these products in your country.

Company names, products/service names and logos used in this publication are trademarks and trade names of Shimadzu Corporation, its subsidiaries or its affiliates, whether or not they are used with trademark symbol "TM" or "®".

Third-party trademarks and trade names may be used in this publication to refer to either the entities or their products/services, whether or not they are used with trademark symbol "TM" or "®".

Shimadzu disclaims any proprietary interest in trademarks and trade names other than its own.

The contents of this publication are provided to you "as is" without warranty of any kind, and are subject to change without notice. Shimadzu does not assume any responsibility or liability for any damage, whether direct or indirect, relating to the use of this publication.

© Shimadzu Corporation, 2016

# Application News

## No.i247

### Material Testing System

## Material Testing by Strain Distribution Visualization – DIC Analysis –

### ■ Introduction

Strain distribution in samples is an increasingly important component of material testing.

As background to this trend, CAE (Computer Aided Engineering) is an analytical technology that is becoming widely used in the fields of science and industry due to the cost savings achieved through the reduced use of costly prototyping which is now being replaced by computerized product design simulation. A typical requirement is to conduct mechanical testing analysis of the region of a product in which strain is likely to occur, and to elucidate the correlation between the simulated analysis results and the strain distribution obtained in actual mechanical testing.

DIC (Digital Image Correlation) analysis is a technique used to compare the random patterns on the surface of a test sample before and after deformation to determine the degree of deformation of the sample. The advantages of this technique include the ability to measure displacement and strain distribution from a digital image without having to bring a sensor into contact with a test sample, and without requiring a complicated optical system. For these reasons, application development for DIC analysis is expanding into a wide range of fields in which measurement using existing technologies<sup>\*1</sup> has been difficult.

Here we introduce examples of DIC analysis of CFRP (Carbon Fiber Reinforced Plastic) and ABS resin high-speed tensile impact testing.

<sup>\*1</sup>: Up to now, material strain distribution measurement has been conducted using various methods, including the direct attachment of large numbers of strain gauges to the test material. However, this method is not applicable for micro-sized samples to which strain gauges either cannot be attached, or attachment is difficult and complicated. These disadvantages also include the difficulty in measuring certain types of substances, such as films, that are easily affected by contact-type sensors.

### ■ Test Conditions

Fig. 1 shows the testing apparatus and software used in the high-speed tensile testing of CFRP. The test conditions are shown in Table 1, and information regarding the test specimens is shown in Table 2. For this experiment, special-shaped grips for composite materials were mounted to the HITS-T10 high-speed tensile testing machine, and the test specimen was affixed to the grips.

A high-speed HPV-2A video camera was mounted in front of the testing gap between the grips to collect video data of the specimen breaking, and the signal to start camera filming was a displacement signal from the high-speed tensile testing machine. The acquired video data was loaded into the StrainMaster (LaVision GmbH) DIC analysis software, and the strain distribution that occurred in the sample was analyzed.

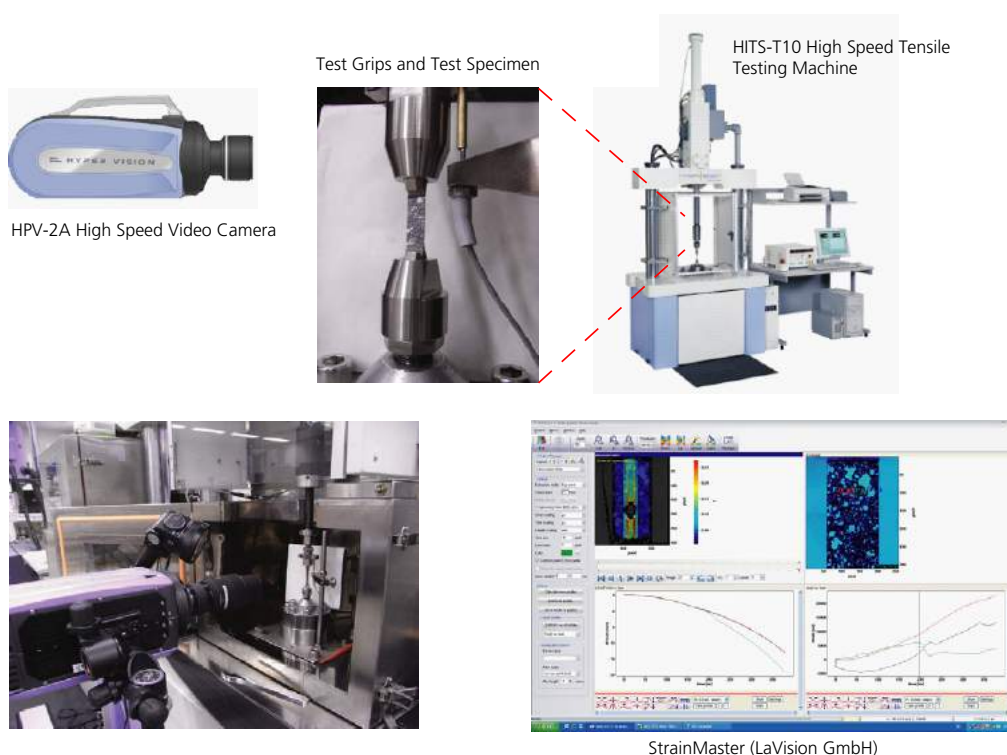


Fig. 1 Testing Apparatus

Table 1 Test Conditions

Instrumentation	HITS-T10 high-speed tensile testing machine
	HPV-2A high-speed video camera
Test Force Measurement	10 kN load cell
Test Speed	10 m/s
Grips	Special grips for composite materials
Sampling	250 kHz
Imaging Speed	500 kfps
Light Source	Strobe
DIC Analysis	StrainMaster (LaVision GmbH) With cooperation of MARUBUN CORPORATION

Table 2 Samples

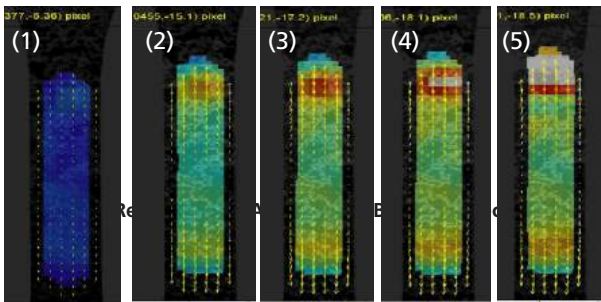
Samples (dimensions)	CFRP-OH <sup>*2</sup> Laminate method [0/90] <sub>2s</sub> <sup>*3</sup> (Hole diameter φ1 mm, W8 × t0.4 reed-shaped)
	ABS resin (ASTM L-shaped test specimen Total length 60 mm, Parallel part 3.2 (W) × 3.2 (T) mm)
Marking	CFRP-OH <sup>*2</sup> : White random pattern ABS resin : Black random pattern

\*2:OH: Abbreviation for Open Hole. Refers to a hole that is opened in a CFRP plate.

\*3:The CFRP laminate used in this experiment is prepared by laminating prepreg fibers oriented in one direction. The [0/90]<sub>2s</sub> specified for "Laminate method" in the table represents two sets of prepreg layers stacked in the 0° direction and 90° direction.

In this test, the HITS-T10 high speed tensile testing machine and HPV-2A high speed video camera were synchronized to take video at the instant the sample fractured. The sample was prepared prior to the test by spraying paint onto its surface in a random pattern, and the strain distribution on the surface of the test specimen was visualized by DIC analysis based on the amount of shift of the random pattern.

Fig. 2 and Fig. 3 show the DIC analysis results obtained in tensile testing of CFRP-OH and ABS resin test specimens, respectively. The images were extracted in the order of a typical time course analysis (image order corresponding to the numbers shown in images), from the start of the tensile test to the point that the specimen breaks. The appearance of coloring in the images corresponds to the strain distribution in the specimen. The amount of strain that occurs in the specimen corresponds to the degree of color warmth, with areas of darker color (such as blue-black) indicating low strain, and areas of brighter color (such as red-orange) indicating a greater degree of strain. It is clear that in Fig. 2, as the load is applied to the test specimen, the strain increases in the vicinity of the open hole. Because the test specimen is a [0/90]<sub>2s</sub> laminate material, it is believed that the fibers are aligned in the tensile direction in the test specimen surface layer which was subjected to random marking.



In Fig. 3, localized strain occurs from the edge of the parallel region of the test specimen, and as time progresses, localized strain is noticeable at the upper and lower edge of the parallel region. Thus, by combining a high-speed tensile testing machine with a high-speed video camera, in addition to DIC analysis software, it has become possible to visualize the distribution of strain generated in a test specimen.

Test Results

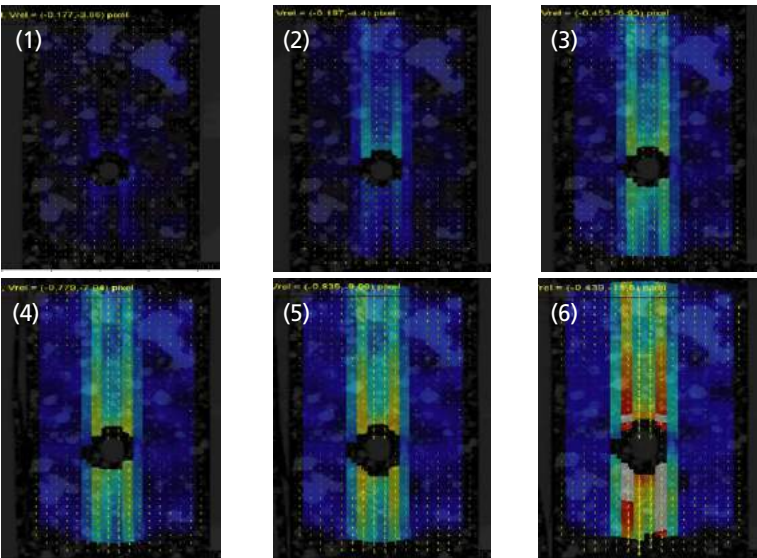


Fig. 2 Results of DIC Analysis of CFRP-OH Specimen



# Three-Axis Endurance Evaluations of Automobile Steering Mechanisms

## With Control via Actual Data, Endurance Evaluations Approximating Real Motion Can Easily Be Performed

Automobile steering units are important components that must be highly durable. There are also significant differences in driver arm strengths, so many cars are equipped with a power steering mechanism, which complicates the structure. In contrast, with luxury cars and sports cars, specifications are required that can achieve an operable feeling that heightens the sense of enhanced value. In regards to these new and diversified requirements, quantitation, not only evaluations by people, is increasingly needed. By combining three actuators with the 4830 controller, which is capable of high-accuracy control, this system can easily perform endurance tests under close to real conditions.

### System Appearance



### Evaluation Details

- Endurance tests in which the steering wheel is moved left and right more than one million times
- Endurance tests in which excessive force is applied to turn the steering wheel to the left or the right
- Quantitation of the sense of enhanced value (Rotational torque and angle of 1 and test force at 2 and 3 at each rotation point)

Endurance tests of the steering mechanism unit are performed by adding a rotational force via the steering wheel 1, and producing a reaction force originating from the tires in 2 and 3.

The reaction force from 2 and 3 corresponding to the rotational angle in 1 is obtained for use from an actual car.



## Main Specifications

### Left/Right Tire Units

- 1) Rated capacity:  $\pm 10$  kN stroke  $\pm 100$  mm  
(static maximum load capacity  $\pm 13$  kN)
- 2) With trunnion pin
- 3) Maximum speed: 500 mm/sec  
(20 L/min hydraulic source, when unloaded)

### Lifting Stand (For the left/right tire units)

- 1) Height: 300 mm to 800 mm  
(electric lift, manual bolt fastening)
- 2) Angle: top/bottom  $\pm 10^\circ$   
(can change fastened or mobile) and horizontal  $\pm 10^\circ$

### Steering Unit

- 1) Rated capacity:  $\pm 200$  Nm, Angle:  $\pm 1080$  deg
- 2) Maximum speed: 360 deg/sec
- 3) Excitation frequency: 0.01 Hz to 2 Hz ( $\pm 5$  deg or more)

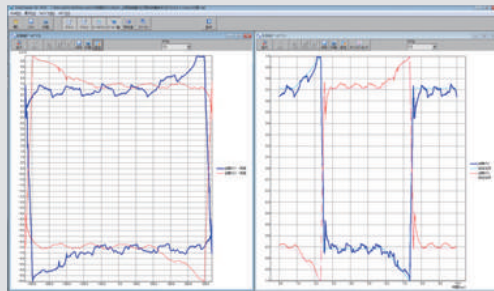
### Lifting Stand (For the steering unit)

- 1) Height: 800 mm to 1200 mm (electric lift, manual bolt fastening)
- 2) Angle: top/bottom  $0^\circ$  to  $60^\circ$  (can change fastened or mobile)



4830 Controller

## Data Processing Example (PC Screen)



The left window shows the data chart results when the steering unit is turned to the left and right from the center position, and then returns to the center.

The window on the left shows a chart of angle versus test force.

The window on the right shows a chart of time versus test force.

The blue line is the test force for the right tire unit.

The red line is the test force for the left tire unit.



Shimadzu Corporation

[www.shimadzu.com/an/](http://www.shimadzu.com/an/)

#### For Research Use Only. Not for use in diagnostic procedure.

This publication may contain references to products that are not available in your country. Please contact us to check the availability of these products in your country.

Company names, product/service names and logos used in this publication are trademarks and trade names of Shimadzu Corporation or its affiliates, whether or not they are used with trademark symbol "TM" or "®". Third-party trademarks and trade names may be used in this publication to refer to either the entities or their products/services. Shimadzu disclaims any proprietary interest in trademarks and trade names other than its own.

The contents of this publication are provided to you "as is" without warranty of any kind, and are subject to change without notice. Shimadzu does not assume any responsibility or liability for any damage, whether direct or indirect, relating to the use of this publication.

First Edition: August 2016

© Shimadzu Corporation, 2016

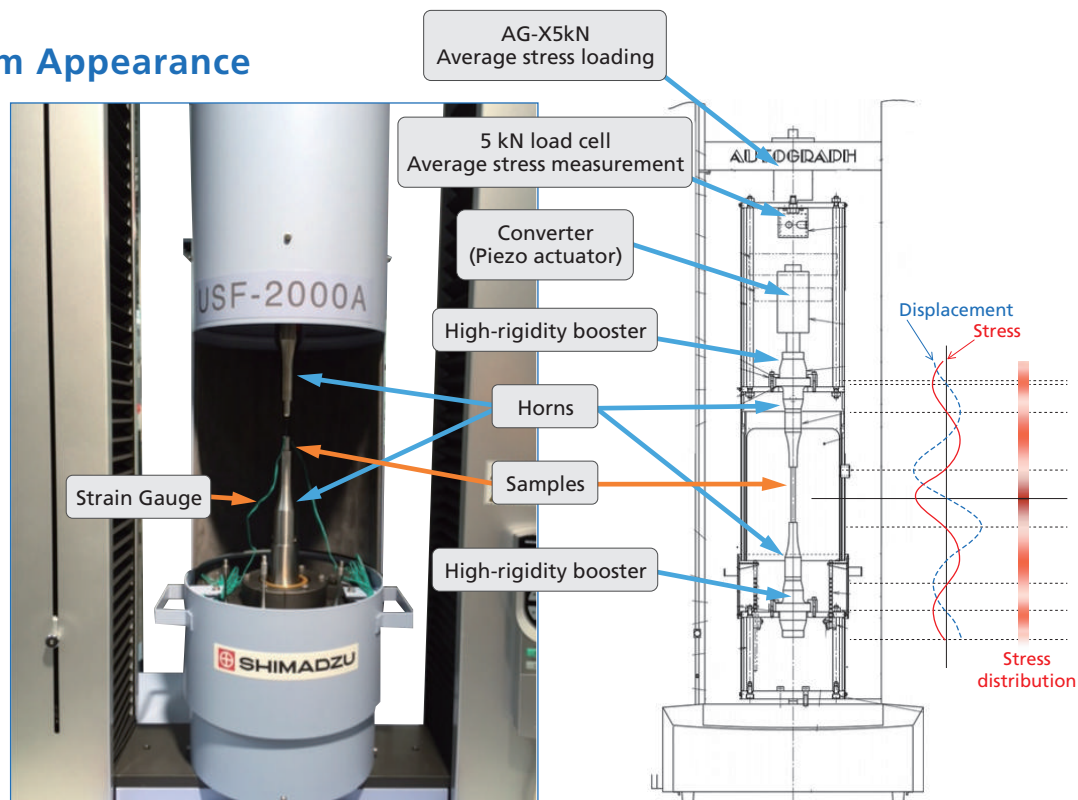
# Ultrasonic Fatigue Testing System with an Average Stress Loading Mechanism

## For Gigacycle Fatigue Tests with Average Stress Loaded

Actual components are rarely used under conditions in which the average stress is zero. Despite this, the USF-2000A, a standard ultrasonic fatigue testing system, can only perform testing under zero average stress conditions.

Using an ultrasonic fatigue testing system equipped with an average stress loading mechanism, gigacycle fatigue tests can be performed with average tensile stress loaded.

## System Appearance



## Ultrasonic Fatigue Testing System Effective for Gigacycle Fatigue Tests

With fatigue tests of high-strength steels, it is evident that internal fracture (fish-eye fracture), which is caused by inclusions and other micro defects, occurs at 10<sup>7</sup> cycles or more, a value considered the conventional fatigue limit.

An ultrasonic fatigue testing system is extremely effective when performing this sort of gigacycle fatigue test. (With a 100 Hz fatigue testing system, this would take 3 years, but if a 20 kHz ultrasonic fatigue testing system is used, testing can be completed in one week.)

# Main Specifications

## 1) Test Frequency: 20 kHz ± 500 Hz

- The recommended test range is 20 kHz ± 30 Hz.
- The test frequency is determined by the resonance frequency of the sample.

## 2) Horn End Face Amplitude

Min. approx. ±10 μm

Max. approx. ±50 μm

- The minimum and maximum amplitudes are the end face amplitude values at amplitude outputs of 20 % and 100 % respectively. Accordingly, the minimum and maximum amplitude values will change somewhat depending on the shape of the sample.

## 3) Test Stress

Standard circular tapered sample

Stress Min. 237 MPa

Max. 1186 MPa

- The test stress range can be changed by changing the sample shape.
- The minimum and maximum values are calculated with the end face amplitude values of 10 μm and 50 μm respectively.
- These are the values when the stress is within the elasticity range.

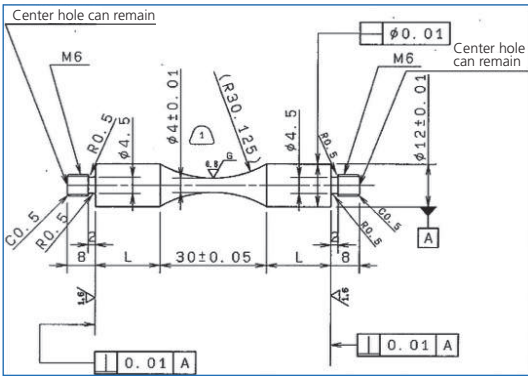
## 4) Average Stress

Max. 1.5 kN (tensile only)

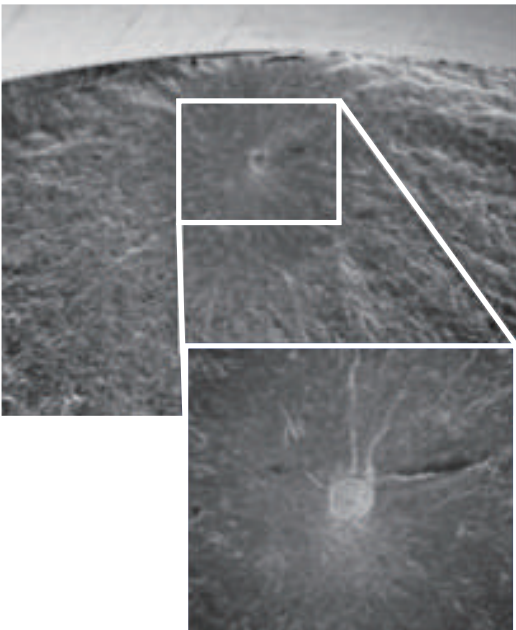
- Average stress loads exceeding 1.5 kN are possible, but will have an impact on the service life of the horn.

## Components

1	Ultrasonic resonance system Power supply, converter, booster (1 pair), horn (1 pair)
2	Personal computer (OS Windows 7) ADA/PIO interface board
3	Software Ultrasonic test control measurement software
4	Cooling system Air dryer, air piping <ul style="list-style-type: none"><li>• A separate 140 L/min air source is required.</li></ul>
5	Strain meter unit (option)
6	AG-X plus Autograph 5 kN + 250 extension
7	Average stress loading mechanism



Standard Circular Tapered Sample



Surface of the Fatigued Fracture Originating from the Inclusion



Shimadzu Corporation

[www.shimadzu.com/an/](http://www.shimadzu.com/an/)

**For Research Use Only. Not for use in diagnostic procedure.**

This publication may contain references to products that are not available in your country. Please contact us to check the availability of these products in your country.

Company names, product/service names and logos used in this publication are trademarks and trade names of Shimadzu Corporation or its affiliates, whether or not they are used with trademark symbol "TM" or "®". Third-party trademarks and trade names may be used in this publication to refer to either the entities or their products/services. Shimadzu disclaims any proprietary interest in trademarks and trade names other than its own.

The contents of this publication are provided to you "as is" without warranty of any kind, and are subject to change without notice. Shimadzu does not assume any responsibility or liability for any damage, whether direct or indirect, relating to the use of this publication.

First Edition: August 2016

© Shimadzu Corporation, 2016

# Application Data Sheet

No. 36

## Servo Dynamic Systems

Material Testing & Inspection

### Evaluating the Fatigue Strength of GFRP Materials

#### ■ Introduction

As an ultra-high-strength composite material with superior heat resistance and electrical insulation properties, the use of glass fiber reinforced plastics (GFRP) has been increasing rapidly in automobiles, office equipment, consumer electronics, and other fields. Due to the use of GFRP materials in the automotive industry in particular, the impact resistance and fatigue strength of the material is increasingly being scrutinized and there is increasing demand for the development of GFRP materials that offer higher functionality or performance.

Shimadzu Servopulser series servo-hydraulic fatigue and endurance testing machines are able to accurately measure the fatigue strength of resins, composites, metals, and components, making them ideal for evaluating the fatigue strength of GFRP materials.

This issue of Shimadzu Application News describes an example of testing the fatigue strength of a GFRP composite material containing 20 % glass fiber in a polyamide resin. It also shows the change in the interior status of test samples as the fatigue test progresses, observed using a Shimadzu X-ray fluoroscopy system.

#### ■ Testing Instruments and Samples

A Shimadzu EHF-LV20kN Servopulser series servo-hydraulic fatigue testing machine (a typical example is shown in Fig. 1) was used in conjunction with a Shimadzu SMX-225CT inspeXio X-ray fluoroscopy system used to observe the sample with X-ray fluoroscopy.

Sample details are as follows:

- (1) Polymer: Polyamide
- (2) Reinforcing material: 20 % glass fiber
- (3) Sample shape: Hard plastic flat plate with 20 mm neck width
- (4) Sample dimensions: 80(L) x 30(W) x 3(T) mm

#### ■ Test Conditions

Before fatigue testing, static testing was performed using the following conditions to determine fatigue loading conditions. Static testing results are shown below.

- (1) Tensile speed: 1 mm/min
- (2) Chuck clamping distance: 40 mm
- (3) Atmosphere: Room temperature of 25 °C
- (4) Tensile strength (measurement results): 96 MPa

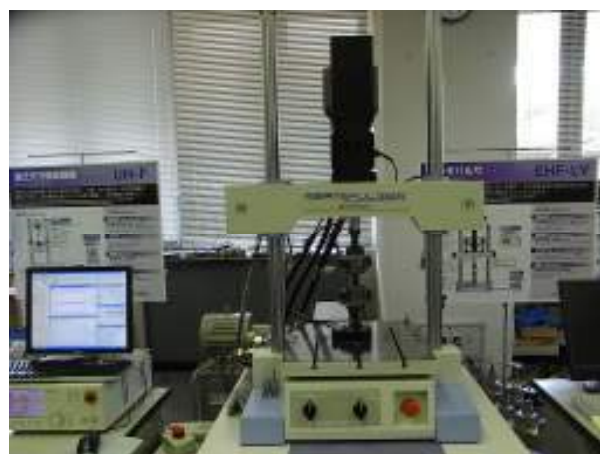


Fig.1 Shimadzu EHF-LV20kNX Servopulser Series Testing Machine

The following fatigue testing conditions (loading and data measurement/acquisition conditions) were determined based on the above static testing.

- (1) Testing frequency: 10 Hz
- (2) Maximum cyclic stress: Six levels, indicated below.
 

Level 1:	77 MPa (80 % of tensile strength)
Level 2:	67 MPa (70 % of tensile strength)
Level 3:	58 MPa (60 % of tensile strength)
Level 4:	48 MPa (50 % of tensile strength)
Level 5:	43 MPa (45 % of tensile strength)
Level 6:	38 MPa (40 % of tensile strength)
- (3) Stress ratio: 0 (given a minimum stress of 0 MPa)
- (4) Atmosphere: Room temperature of 25 °C
- (5) Testing machine: LV-20N Servopulser
- (6) Test force measurement: 20,000 N load cell
- (7) Chuck clamping distance: 40 mm
- (8) Data acquisition: 2 kHz

(The testing machine is capable of measuring at frequencies up to 40 kHz.)

Six cyclic stress levels were decided based on the tensile strength (96 MPa) determined by static tensile testing, with a cyclic load stress ratio (minimum stress divided by maximum stress) of zero. (For example, level 1 applies a maximum stress of 77 MPa, a minimum stress of 0 MPa, and stress amplitude of 38.5 MPa.)

Though the testing machine is capable of cyclic loading at cycle rates up to 100 Hz, in this case a 10 Hz sine wave was used in consideration of sample heat generation.

Fig. 2 shows a sample mounted in the testing machine grips.

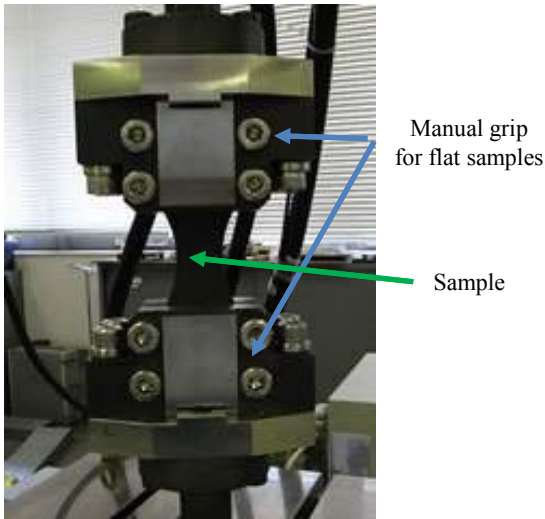


Fig. 2 Sample Mounted in Testing Machine

Test Results

Fig. 3 shows an example of peak stress (black) and displacement (blue) values (sine wave peak and valley values) measured from start of loading to sample fracture, given a stress level of 5.

The cyclic stress load applied to the sample causes it to gradually deform until a crack forms, after which the deformation increases rapidly and the sample fractures.

Fig. 4 is a stress versus cycle count plot for six stress levels (one sample for each level) that shows the relationship between the maximum stress load and the cycle count at sample fracture.

As shown in the results above, in addition to fatigue testing, the fatigue testing machine can also be used for a wide range of other strength testing, including static testing.

In addition, an industrial X-ray system was used to observe how the fiber orientation inside the GFRP material changes as the fatigue test progresses.

Fig. 5 shows the curious phenomenon of how the glass fibers inside the sample, which have no particular orientation before starting the fatigue test (left), begin to orient themselves a little in the longitudinal direction after a million load cycles (middle), and are all oriented in the longitudinal direction just before fracture (right).

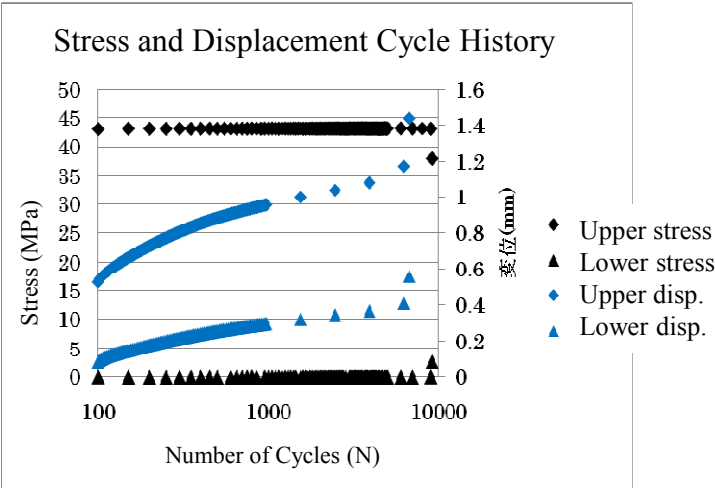


Fig. 3 Fatigue Test Results

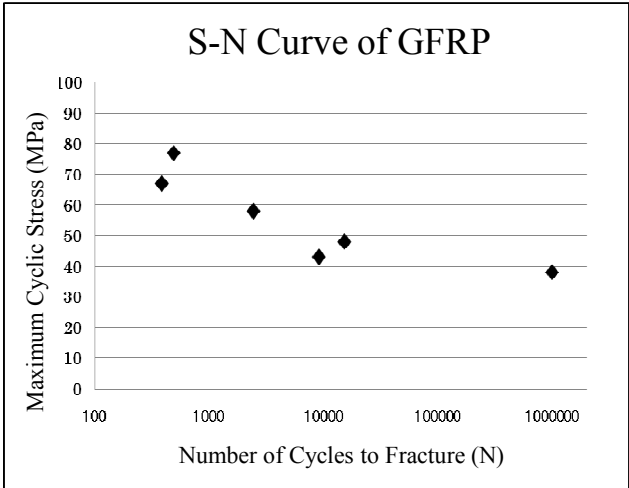
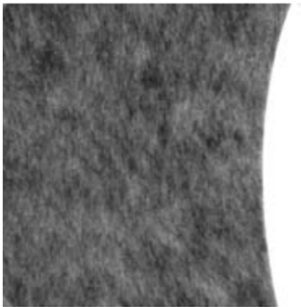


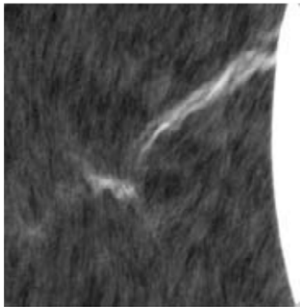
Fig. 4 Fatigue Test Results



Start of Fatigue Test



After 1 Million Load Cycles



Just Before Fracture

Fig.5 Fiber Orientation Inside GFRP

Note: The analytical and measuring instruments described may not be sold in your country or region.

First Edition: July, 2015





# System to Test Fatigue and Endurance of Rubber in a Clean Environment

## Oil-Less, Electrically-Driven, Long Stroke, High Speed, and High Precision

Rubber vibration isolators are important parts for quiet operation of cars and industrial systems. To design rubber, factors including spring constant, damping coefficient, and loss factor need to be measured in conditions from static to high cycle rates. Using the EMT testing system, these tests can be performed easily. Fatigue and endurance testing can be performed simply by connecting the system to a 200 V outlet. Highly-reliable data can be acquired by using the system with an extremely rigid four-frame structure that is resistant to resonance, electrically-driven actuator that reproduces input waveforms accurately, and 4830 controller that has been well-received for high-precision control.

### Product Lineup (EMT Series)

Model	EMT-1kNV-30	EMT-1kNV-50	EMT-5kNV-30	EMT-5kNV-50
Max. Test Force	$\pm 1$ kN (static/dynamic)		$\pm 5$ kN for dynamic, $\pm 3.5$ kN for static	
Stroke	$\pm 30$ mm	$\pm 50$ mm	$\pm 30$ mm	$\pm 50$ mm
Max. Speed	1m/s	2m/s	1m/s	1m/s
Max. Frequency	200Hz	200Hz	200Hz	100Hz
Accuracy	Test force: $\pm 0.5$ % of the indicated value, Stroke: $\pm 1$ % of the indicated value			

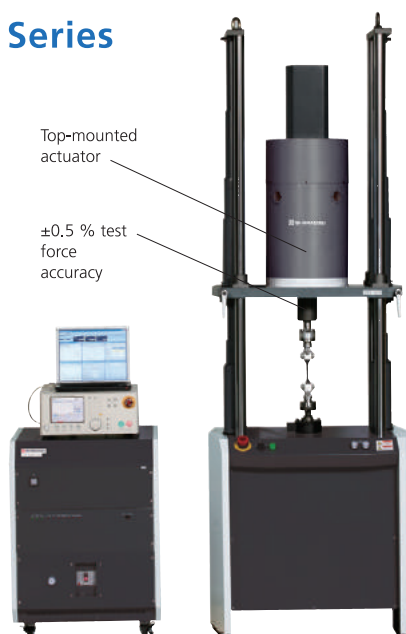
### 4830 Controller

- \*The auto-tuning function helps to input load waveforms accurately.
- \*The waveform strain correction function allows accurate control for the target waveform.



Standard Circular Tapered Sample

### EMT Series



Standard Circular Tapered Sample



Standard Circular Tapered Sample

## Application Example—Multi-Sample Measurement and Measurement in Various Testing Environments

Rubber is a raw material that requires a lot of testing, including evaluation of each production lot.

Since performance of rubber significantly varies according to the temperature, tests are performed under various temperature conditions.

In order to satisfy the demand for these tests, a multi-sample system (2-sample, 4-sample, 8-sample types) is available to provide high testing efficiency and save space for installing testing systems. By using the optional thermostatic chamber, tests can be performed at various temperatures from a low temperature of  $-35^{\circ}\text{C}$  to a high temperature of  $+150^{\circ}\text{C}$  which rubber is used at in products. A light resistance test and endurance test can be performed simultaneously using the latest system in combination with a light resistance testing machine.



System Type of a 4-Sample EMT  
+ Thermostatic Chamber ( $-30$  to  $150^{\circ}\text{C}$ )

Bottom-mounted actuator



System Type of a 2-Sample EMT  
+ Light Resistance Testing Machine

Xenon irradiation equipment



SHIMADZU Corporation

[www.shimadzu.com/an/](http://www.shimadzu.com/an/)

Company names, product/service names and logos used in this publication are trademarks and trade names of Shimadzu Corporation and its affiliates, whether or not they are used with trademark symbol "TM" or "®". Third-party trademarks and trade names may be used in this publication to refer to either the entities or their products/services. Shimadzu disclaims any proprietary interest in trademarks and trade names other than its own.

For Research Use Only. Not for use in diagnostic procedures.

The contents of this publication are provided to you "as is" without warranty of any kind, and are subject to change without notice. Shimadzu does not assume any responsibility or liability for any damage, whether direct or indirect, relating to the use of this publication.

© Shimadzu Corporation, August, 2016

## Endurance Testing and Dynamic Viscoelasticity Measurement of EVA Film by MMT-100N

### ■ Introduction

EVA (ethylene vinyl acetate) film, highly elastic, yet stress crack resistant, is widely used as a film for bonding of solar cells. Solar cells reach high temperatures in the daytime when exposed to sunlight, but cool down at night. This requires that the EVA film has sufficient durability to withstand the daily range of thermal expansion and thermal contraction.

### ■ Endurance Testing of EVA Film

Two types of EVA film samples were used for the endurance testing. One type consisted of original film samples ((1), (2), (3)) that had never been exposed to UV radiation, and the other consisted of samples ((4), (5), (6)) that had been exposed to UV radiation for 100 hours. The samples consisted of EVA film strips measuring 40 (L) × 20 (W) × 0.5 (T) mm. The testing machine and load jigs (grips) are shown in Fig. 1 and Fig. 3, respectively. The load stress in the endurance testing was set based on the static tensile strength (TS = 9 MPa) of the samples unexposed to UV radiation. These unirradiated samples showed an endurance of 100,000 cycles at a stress equal to 20 % (1.8 MPa) of static tensile strength. On the other hand, the samples that had been irradiated for 100 hours exhibited an endurance of 100,000 cycles at a stress equal to 10 % (0.9 MPa) of static tensile strength, but broke prior to reaching 100,000 cycles at a stress equal to 15 % (1.4 MPa) of static tensile strength. The results are summarized in Table 1.

EVA film is also gradually deteriorated with prolonged usage due to the constant exposure to ultraviolet rays during the daytime. Here, we introduce examples of tensile fatigue (endurance) testing and dynamic viscoelasticity measurement of EVA film before and after ultraviolet irradiation.



Fig. 1 Microservo MMT-100N

UV Irradiation Conditions	Not Irradiated			Irradiated for 100 Hours		
Sample No.	(1)	(2)	(3)	(4)	(5)	(6)
Maximum load stress (MPa)	1.8	1.4	0.9	1.8	1.4	0.9
Minimum load stress (MPa)	0,9	0,7	0,45	0,9	0,7	0,45
Repetitions before break	100,000*	100,000*	100,000*	139	4,883	100,000

Table 1 Results of Endurance Testing of EVA Film

The \* indicates that the sample did not break.

Using the endurance test data obtained for samples (1)-(6), an SN curve was plotted with stress amplitude on the Y-axis, and the number of cycle repetitions before breaking on the X-axis, as shown in Fig. 2. Based on the data, it can be concluded that ultraviolet irradiation of EVA film is a large factor that significantly contributes to diminished longevity with respect to loading frequency. Therefore, when evaluating the long-term reliability of solar cell products that will be used for long periods, this type of endurance testing is extremely important for assessing the parameters that include both stress due to the temperature effect (daily range of thermal expansion and contraction) and the amount of ultraviolet radiation received.

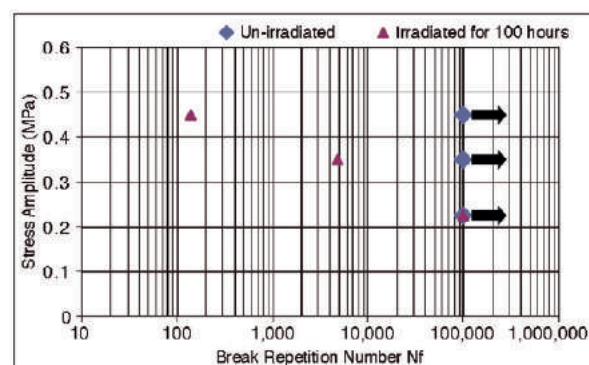


Fig.2 SN Curve for EVA Film

### ■ Dynamic Viscoelasticity Measurement of EVA Film

The dynamic viscoelasticity (as indicated by absolute spring constant, storage spring constant, loss spring constant, damping factor, and loss factor) of a sample can be measured using the Microservo endurance testing software. Here, focusing on the storage Young's modulus and loss Young's modulus obtained from the test force and testing machine's piston displacement measured using the number of cycles in the endurance test, we compared the changes in these constants while increasing the number of load cycle repetitions. Fig. 3 shows the history of the storage spring constant and loss spring constant for samples (2) and (5) from

the 100th load cycle onward. At the 100th cycle, the storage spring constant of the sample (5), irradiated for 100 hours, is 25 % smaller than that of the unirradiated sample (2), and as the number of cycles is increased, they both show a gradual decreasing trend. In addition, the loss spring constant at the early load stage is slightly less in sample (5) than in sample (2), and the degree of the gradual decrease in the loss spring constant is greater in sample (5). Furthermore, the storage spring constant and loss spring constant of sample (2) level off and exhibit a plateau region between 60,000 cycles and 100,000 cycles.



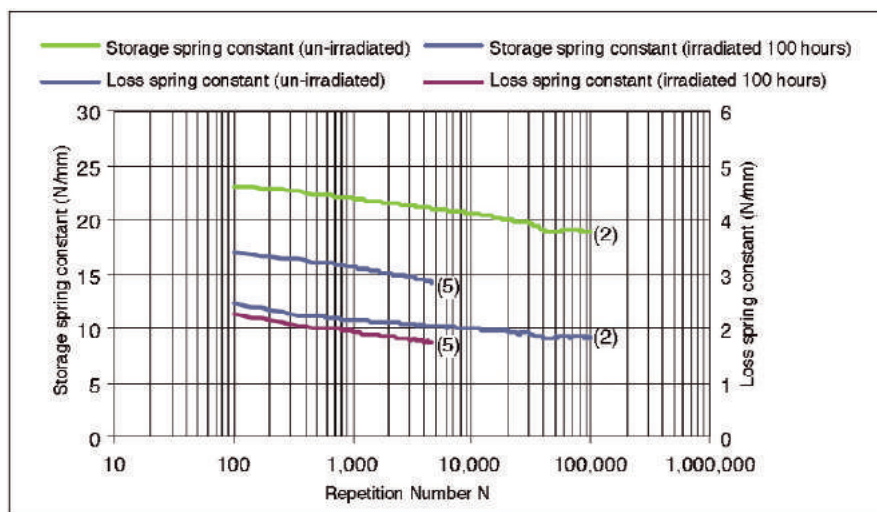


Fig. 3 Storage and Loss Spring Constants of EVA Film



Fig. 4 Grips and EVA Film

Thus, the Microservo is a material testing system that offers simultaneous endurance testing and dynamic viscoelasticity measurement of samples. Since this system adopts an electromagnetic actuator, not only is

testing conducted in a green environment, but a variety of evaluations become possible using a temperature atmospheric chamber and other optional attachments.

## ■ Reference Information

Absolute spring constant:

$$|K^*| = \frac{F_0}{x_0}$$

Storage spring constant:

$$K' = |K^*| \cdot \cos(\delta)$$

Loss spring constant:

$$K'' = |K^*| \cdot \sin(\delta)$$

Damping factor:

$$c = \frac{K''}{2\pi \cdot \text{Frequency}}$$

Loss factor:

$$Lt = \frac{K''}{K'}$$

The loss angle  $\delta$  is calculated below using FFT based on the test force and displacement waveform relative to time.

Loss angle  $\delta = 2\pi \cdot \Delta t \cdot \text{Frequency}$

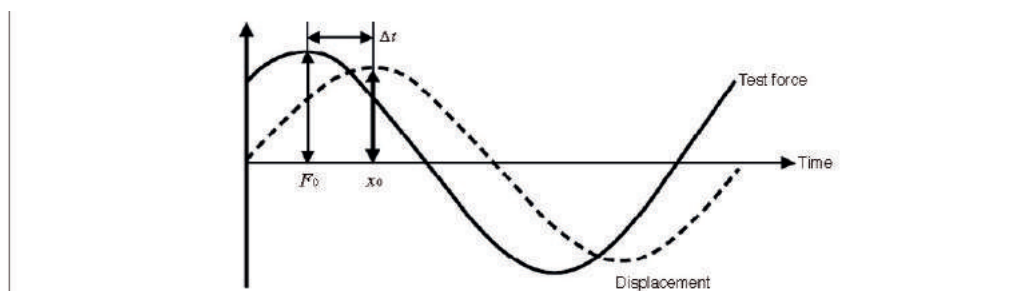


Fig. 5 Test Force and Displacement Waveform



Increasingly high performance engineering resins are being developed for use in a wide range of fields, such as the automotive industry, consumer electronics, office automation equipment, for their various functional characteristics. Some of the criteria that have become especially important for evaluating the performance of such materials is impact resistance and its associated material properties, such as strength and rigidity. In addition to evaluating materials in terms of conventional static tensile strength, high-rate tensile strength, longitudinal elasticity, and strain measurements up to the breakpoint are expected to become important new parameters for materials development. This example describes testing the high- rate tensile strength of a flat plate specimen of ABS resin and measuring strain up to the breakpoint.

Images of the high-rate tensile test were captured with a high-speed video camera and image analysis software was used to measure the strain between gauge length on the specimen.

### ■ Tensile test specimen

Fig. 1 shows the dumbbell-shaped flat ABS resin tensile test specimen mounted in the grips of the high- rate tensile testing machine. A chuck extensometer, capable of measuring the relative displacement of the fixed end and the upper grip, is attached to the top right of the specimen. A matrix of black dots is printed on the surface of the specimen. The strain between gauge length can be measured by using a high-speed video camera to record a moving image of the tensile test and automatically tracking the movement of the specified dots.

- (1) Specimen Material: ABS resin
- (2) Specimen Dimensions: 110 (L) × 10 (W) × 3 (T) mm and 19 mm wide grip tab
- (3) Dot Specifications: 0.5 mm diameter, spaced 2 mm apart

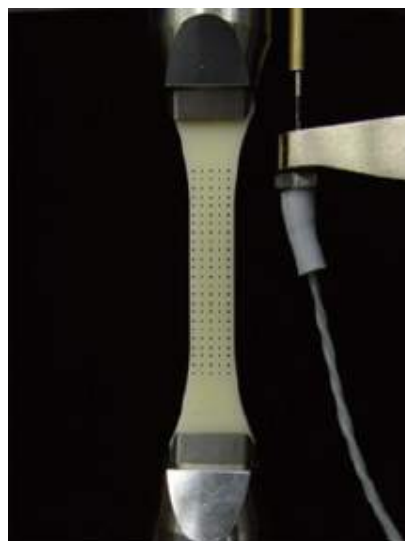


Figure 1: Tensile test specimen mounted in grips

### ■ Measuring High-Rate Tensile Strength and Recording Video Image

Tensile test was performed using the HITS-T10 hydroshoot hydraulic tensile machine. The HPV-2A high speed camera was mounted in front of the testing machine to capture 100 video frames of the specimen of the specimen behavior during tensile testing. Conditions for tensile testing and recording video in this example are indicated below:

- (1) Tensile rate: 3 m/s
- (2) Grip distance: 75 mm
- (3) Gauge length measuring strain: 30 mm
- (4) Test force measurement: 10 KN load cell
- (5) Data collection: 250 KHz
- (6) Recording speed: 32 kfps
- (7) Light source metal halide light

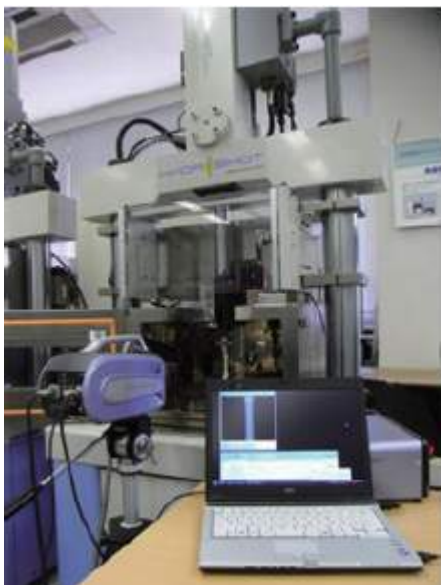


Figure 2: Setup of high rate test and video recording

### ■ Video high rate tensile test of ABS resin

Images of the ABS resin specimen (4 frames) before and after breakpoint during the high-rate tensile test are shown in Fig. 3. In this example, the recording speed was 32 kfps. The interval between frames was 32 microseconds.

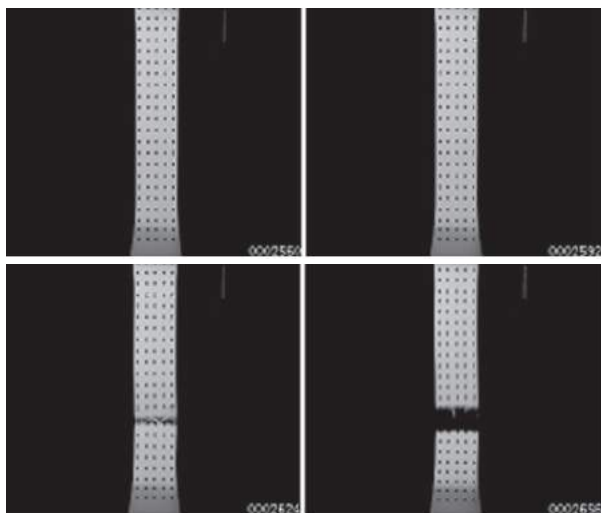


Figure 3: Four frames of specimen before and after breakpoint

### ■ Video high rate tensile test of ABS resin

A time history of strain between gauge length is determined by using image analysis software to analyze the images obtained. In this case, gauge length was specified longitudinally 30 mm apart on an image of the specimen not moving (16 consecutive dots apart at the center of the specimen), then that gauge length was automatically tracked as a function of time to measure the longitudinal strain. The resulting time history of strain obtained is shown in Fig. 4. In addition, a time history of stress measured by the high-rate tensile testing machine or external data logger can be displayed simultaneously as well. Furthermore, images are displayed synchronized with strain and stress in terms of time. This tensile test example resulted in a tensile strength and breaking strain of ABS resin that was 70 MPa and 30 %, respectively.

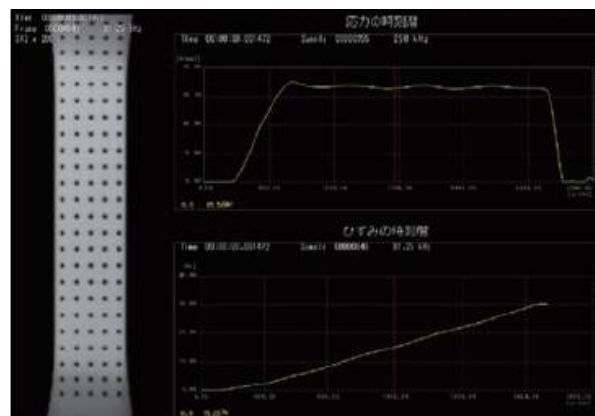


Figure 4: Video of tensile test and time history of strain and stress

## ■ Video high rate tensile test of ABS resin

Producing a stress-strain curve, which is easy for static tensile testing, is an extremely difficult technical challenge for high-rate tensile testing. Strain gauges can only measure a small range and contact type extensometers do not work for shock. In this example, a stress-strain curve was obtained for ABS resin by synchronizing the video image timing with the test force.

A stress-strain curve up to the specimen breakpoint is shown in Fig. 5.

In this way, combining a high-rate tensile testing machine, high-rate video camera, and image analysis software, enables simultaneously evaluating high-rate tensile properties, including breaking strain, and visualizing changes in the status of resins.

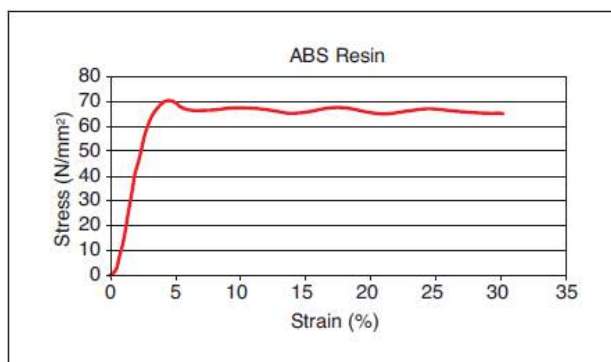


Figure 5: Stress-strain curve up to breakpoint



## 6. Materials Testing & Inspection

---

### 6.3 Hardness Testing

---

Hardness testers are widely used to measure hardness of quenched parts as well as welded parts. A hardness tester reads the distance across opposite corners of indents automatically.

- SCA\_300\_011** Evaluation of adhesive strength and hardness of protective surface layer of glass substrates
- SCA\_300\_012** Evaluation of hardness of painted surface with shimadzu dynamic ultra micro hardness tester model DUH
- SCA\_300\_019** Hardness evaluation of thin film with shimadzu dynamic ultra micro hardness tester (II)
- SCA\_300\_040** Evaluation of hardness of painted surface
- SCA\_300\_002** Compression test for structural materials of lithium-ion batteries by MCT
- SCA\_300\_023** Measurement of carburized case depth of steel with Shimadzu >>Micro Hardness Tester Model HMV
- SCA\_300\_024** Measurement of hardness of the machining deterioration layer of stainless steel with Shimadzu Dynamic Ultra Micro Hardness Tester, Model DUH
- SCA\_300\_034** A hardness measurement of steel surface treatment layer with Shimadzu Dynamic Ultra Micro Hardness Tester, Model DUH
- SCA\_300\_035** A hardness measurement of surface treatment layer on a steel sample using Shimadzu Dynamic Ultra Micro Hardness Tester, Model DUH
- SCA\_300\_036** A thickness measurement of a Ni-plating layer on a stainless-steel sample with Shimadzu Dynamic Ultra Micro Hardness
- SCA\_300\_047** Measurement of the surface treatment depth of steel with Shimadzu Micro Hardness Tester Model HMV
- SCA\_300\_050** Strength evaluation on metallic fine particles with Shimadzu Micro Compression Testing Machine Model MCT
- SCA\_300\_061** Compressive strength of metallic microspheres and dependence on heat treatment temperature. Shimadzu MCTM-500 Micro Compression Testing Machine
- SCA\_300\_037** Compression-rupture test of carbon fibers with different tensile characteristics Shimadzu Micro Compression Testing
- SCA\_300\_014** Evaluation of surface hardness of audiotapes with Shimadzu Dynamic Ultra Micro Hardness Tester Model DUH
- SCA\_300\_021** Hardness measurement of plastic tubes using the Shimadzu Dynamic Ultra Micro Hardness Tester DUH-W211S
- SCA\_300\_039** Evaluation of elastic recovery in hardness measurement of plastic materials with Shimadzu Dynamic Ultra Micro Hardness Tester

## Application News

No. SCA\_300\_011

Material Testing System DUH

### Evaluation of Adhesive Strength and Hardness of Protective Surface Layer of Glass Substrates



Rapid progress of thin film developing technology has accelerated expansion of film applications.

Thin film developing technologies based on vacuum evaporation, sputtering, or ion plating are featured not only in the improvement in quality of thin films, but also in adding new characteristics to a material, and are applied in various fields such as semiconductors, optical materials, and machine parts.

Adhesive strength and hardness are important factors for the evaluation of the mechanical strength of thin film that is produced by the aforementioned techniques.

Thin film that satisfies specifications of quality and properties may peel from its substrate board unless its adhesive strength is adequate. There may also be a problem of unimpeded wear and tear, if its hardness does not conform to specifications.

The following is an introduction to an evaluation of adhesive strength and hardness of a thin film on a glass substrate with Shimadzu Scanning Scratch Tester Model SST and Shimadzu Dynamic Ultra Micro Hardness Tester Model DUH.

#### ■ Test conditions

SST-101:

- (1) Stylus (needle): Diamond 100  $\mu\text{m}$
- (2) Swing amplitude: 60  $\mu\text{m}$
- (3) Scratch speed: 20  $\mu\text{m/s}$
- (4) Max load: 20 gf
- (5) Down speed of cartridge: 1  $\mu\text{m/s}$

DUH-211:

- (1) Testing mode: Indenter pressing test
- (2) Load: 2 gf
- (3) Loading rate constant: 1 (0.029 gf/s)
- (4) Indenter: 115° triangular pyramid

#### ■ Test piece

- 1) Name: Surface protective thin film of glass substrate
- 2) Type: 1 through 3
- 3) Thickness of films: approx. 1  $\mu\text{m}$  or all

Test piece	Peeling load (gf)			
	1	2	3	4
No. 1	1.3	1.4	1.3	1.33
No. 2	2.5	2.4	2.5	2.47
No. 3	7.4	7.4	7.1	7.30

Table 1: Test results of SST



## ■ Test results

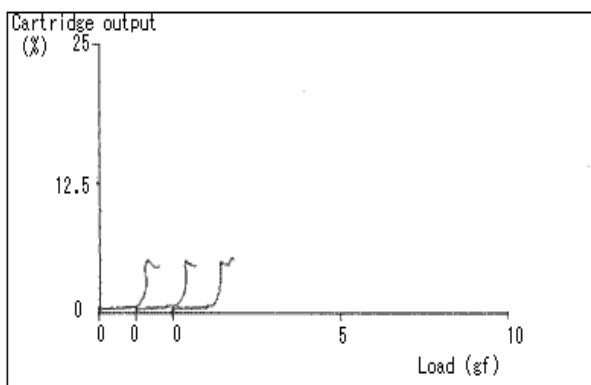


Figure 1: Load – cartridge output curves of test piece No.1 (with SST)

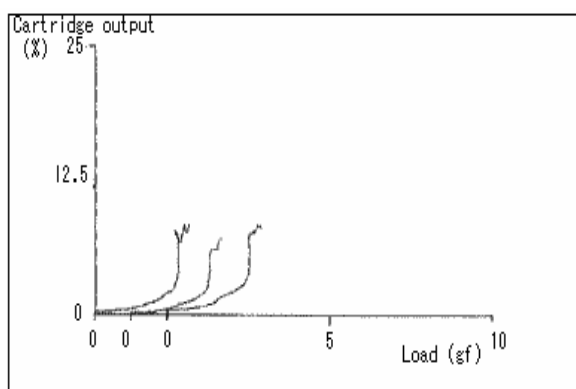


Figure 2: Load – cartridge output curves of test piece No.2 (with SST)

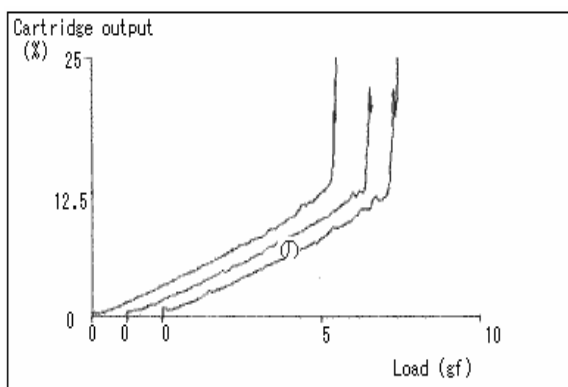


Figure 3: Load – cartridge output curves of test piece No.3 (with SST)

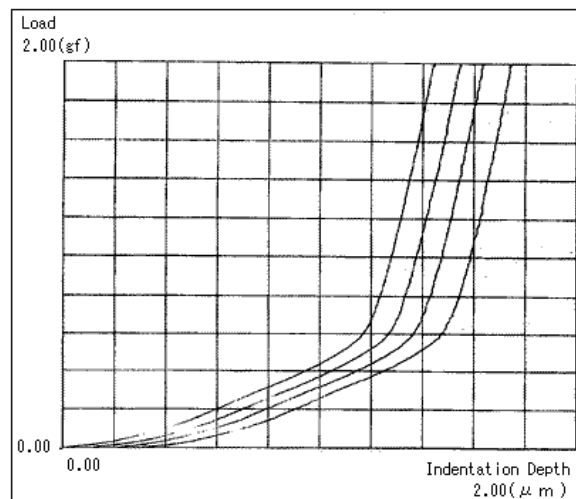


Figure 4: Load – indentation depth curves of test piece No.1 (with DUH)

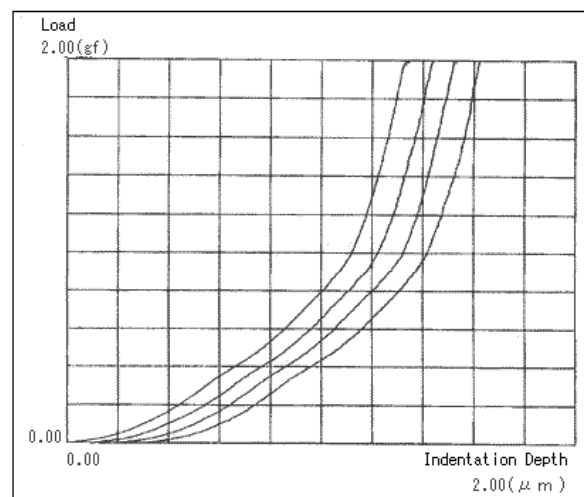


Figure 5: Load – indentation depth curves of test piece No.2 (with DUH)

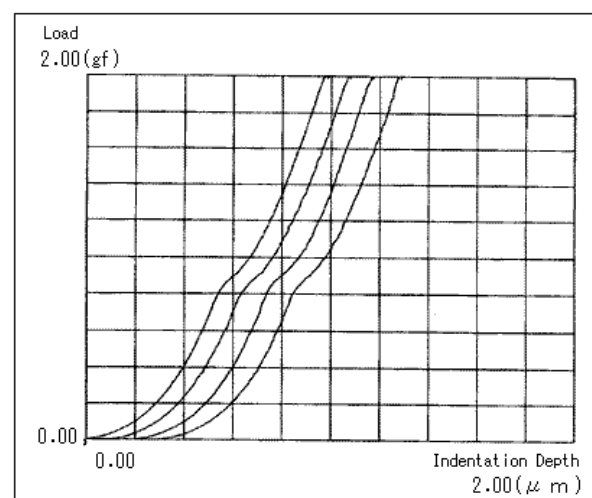


Figure 6: Load – indentation depth curves of test piece No.3 (with DUH)

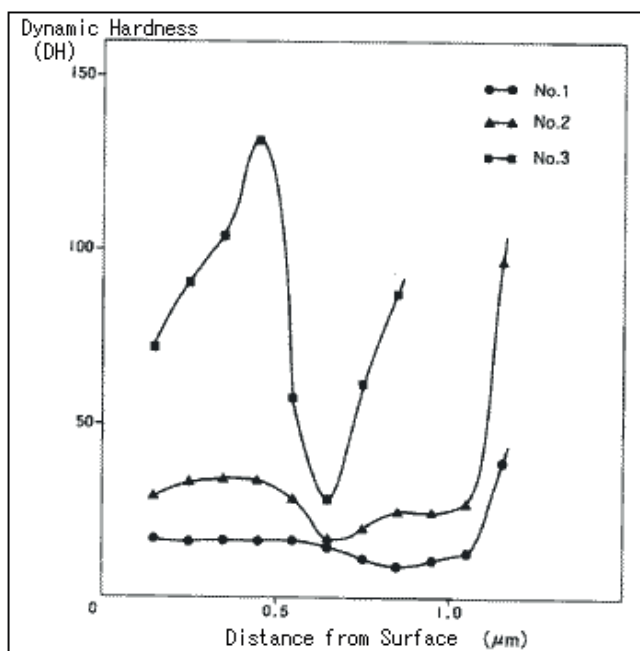


Figure 7: Hardness Distribution in Depth Direction

The result of peeling strength tests of surface protective films Nos.1-3 on glass substrates tested with Model SST-101 are shown in Table 1, from which it is known that adhesive strength estimated by the peeling load is greatest in the test piece No. 3 followed by No. 2 and No. 1, respectively. The hardness measurement's result is shown in Figs.4-6 in the form of load versus indentation depth curves. Hardness variation in depth direction is plotted in Fig.7 as well. According to this

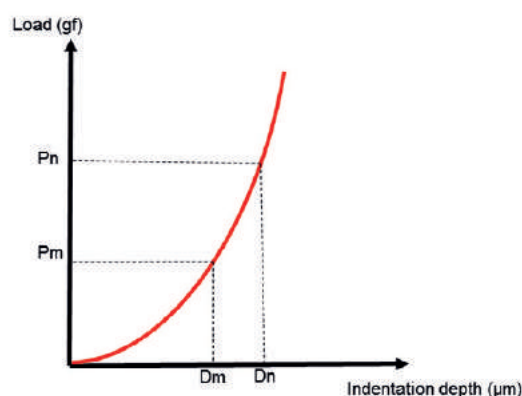
Hardness distribution was calculated by the following equation (Data analysis 2: Output data of load and indentation depth) as internal hardness distribution is not known from load-indentation depth curves.

$$DH_{m-n} = \frac{37,838 \cdot P_n \cdot \left(1 - \sqrt{\frac{P_m}{P_n}}\right)^2}{(D_n - D_m)^2}$$

Where  $DH_{m-n}$ : Hardness at indentation depth from  $D_m$  to  $D_n$ .

$P_m, P_n$ : Load (gf)

$D_m, D_n$ : Indentation depth (μm)



graph, it is known that the thin film hardness in the ultra-surface of specimen No. 3 is greatest among the three, and also that hardness of all the specimens gets lower at a depth below 0.5 μm, probably because cracks (ruptures) were produced during indentation. According to the hardness distribution curves from the surface down to 0.5 μm, hardness of test piece No. 3 (high adhesive strength) increases gradually, while the hardness of No. 1 (less adhesive strength) stays virtually unchanged.

## Application News

No. SCA\_300\_012

Material Testing System DUH

### **Evaluation of Hardness of Painted Surface with Shimadzu Dynamic Ultra Micro Hardness Tester Model DUH**



Painted surfaces are evaluated for properties such as weathering resistance, light resistance, adhesive strength, impact resistance and hardness by instrumental measurement, and for color, gloss, unevenness, rumples etc. by visual inspection. Of these, the hardness test of painted surfaces is most important in evaluating the quality of paint film. Wet paint is dried in order to transform wet paint into rigid paint film. Paint can be dried either by the natural drying method, in which the paint dries completely at room temperature, or by the forced drying method,

in which paint is dried under high temperatures of approx. 100 to 250 degrees Celsius. The surface hardness of paint films differs depending on the kind of paint and the drying method. Information for evaluating hardness near the surface of paint film can be obtained by the ultra micro area measuring technique of the Shimadzu Dynamic Ultra Micro Hardness Tester Model DUH. The following presents the results of hardness tests performed on paint films of paints for general use dried either by the natural or by the forced drying method.

## ■ Measurement of surface hardness of paint films

Testing machine

TEST MODE	2
CAL. MODE	1 ( 115° Triangular Pyramid Indenter )
AUTO or MANUAL	AUTO
F.S. DEPTH	2 & 5 $\mu\text{m}$
MAX LOAD	9,81mN & 49,03 mN
LOADING SPEED	1 (0,1,4632 [mN/sec]) 5 (13,3240 [mN/sec] )
TOUCH SPEED	50 ( 0,48 [mN/sec] ) 50 ( 0,048 [mN/sec] )
AFTER TIME	5 sec.
PRE TIME	5 sec.
LOT	5

Table 1 Test Conditions

(1) Paint film of meramin resin dried by forced drying

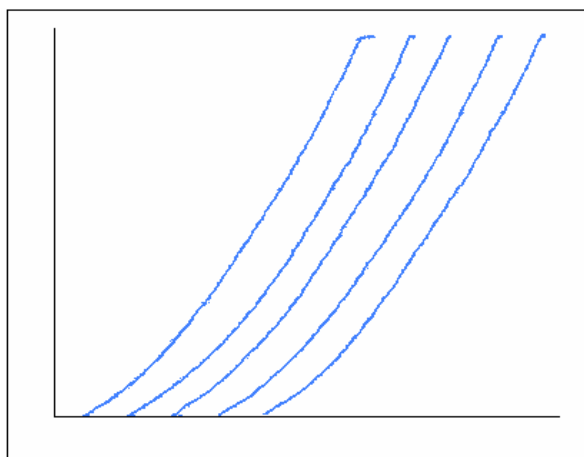


Fig.1 Indentation depth Load Curves of Painted Films of Meramin Resin

(2) Paint film of urethane resin dried by natural drying

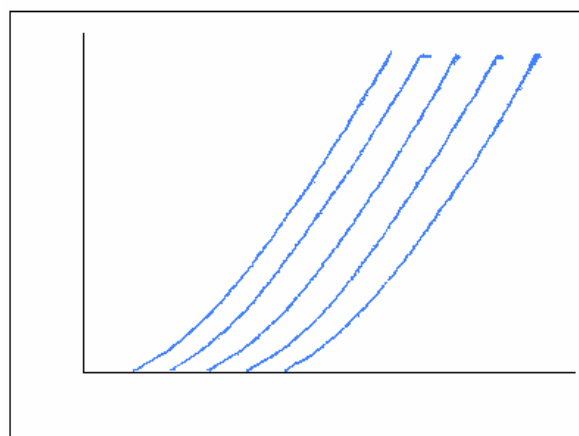


Fig.2 Indentation Depth Load Curves of Painted Films of Urethane Resin

(3) Paint film of acrylic resin dried by natural drying

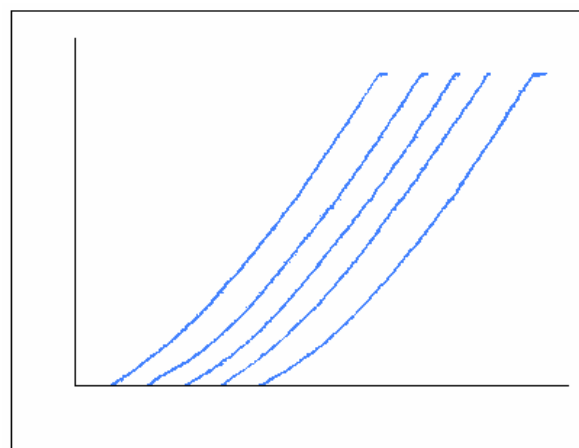


Fig.3 Indentation Depth Load Curves of Paint Films of Acrylic Resin

## ■ Result of Measurements

Sample Name	LOAD (mN)	DH (mean)
Meramin resin paint film thickness 38 µm - forced drying	9,81 mN	14,60
Overall thickness of paint film 177 µm	49,03 mN	12,00
Urethane resin paint film thickness 48 µm - forced drying	9,81 mN	13,00
Overall thickness of paint film 84 µm	49,03 mN	5,20
Acrylic resin paint film thickness 52 µm - forced drying	9,81 mN	10,50
Overall thickness of paint film 110 µm	49,03 mN	4,90

Table 2 Result of Measurements

Dynamic hardness is obtained based on the load value and indentation depth during the loading process. Since dynamic hardness is calculated from the indentation depth during the loading process, it includes both plastic deformation and elastic deformation.

DH: dynamic hardness

F: test load mN

h: dynamic indentation depth<sup>2</sup>

$$DH_{115} = 3.8584 \times F / h^2$$

DHT115: Dynamic hardness obtained with the triangular pyramid indenter with 115° tip angle

When LOAD is small, DEPTH is small, allowing the hardness of paint film at the outermost surface to be measured. When LOAD is large, DEPTH is also large, allowing the hardness at the deeper portion of paint film to be measured.

In tests on samples dried by natural drying and forced drying, a different trend was observed for the respective samples between the results of 9,81 mN and 49,03 mN LOADs. In other words, the difference between the data for 9,81 mN and 49,03 mN was large in case of natural drying, while significantly smaller in the case of forced drying. This indicates that forced drying creates hardness more evenly distributed throughout the depth of the paint film than natural drying.

\* Please be advised that data obtained before the implementation of the current Weights and Measures Law may be presented in terms of gravimetric unit.



## Hardness Evaluation of Thin Film with Shimadzu Dynamic Ultra Micro Hardness Tester (II)

### ■ Introduction

Thin film production technology has made a rapid progress and a great quantity of thin films are put to practical use in various applications. The evaluation of the hardness of thin films produced by CVD and PVD and surface coating layers plays an important role in production technology. In spite of such background, this method has not yet been definitively standardized, though some technical reports on hardness evaluation based on micro hardness method have been issued.

The Shimadzu Dynamic Micro Hardness Tester Model DUH, designed as a hardness evaluating machine, is also useful in the thin film market where a low electromagnetic load applying system is needed for information of material strength of a micro area on the basis of micro load measuring and controlling technique.

of hardness distribution in the depth direction. The following presents the results of two recent measurements.

### ■ Relation of load and indentation depth of a-Si thin film produced by CVD

DH hardness is calculated using the following equation, where  $D_1$  and  $D_2$  are depths at any two points on the chart and  $P_1$  and  $P_2$  are loads corresponding to  $D_1$  and  $D_2$  respectively.

$$DH = \alpha = \frac{P_2}{(D_2 - D_1)^2} \cdot \left( 1 - \sqrt{\frac{P_1}{P_2}} \right)^2$$

The distances between  $D_1$  and  $D_2$  can be set freely. If  $D$  points are set at regular intervals, hardness distribution in depth direction is calculated.

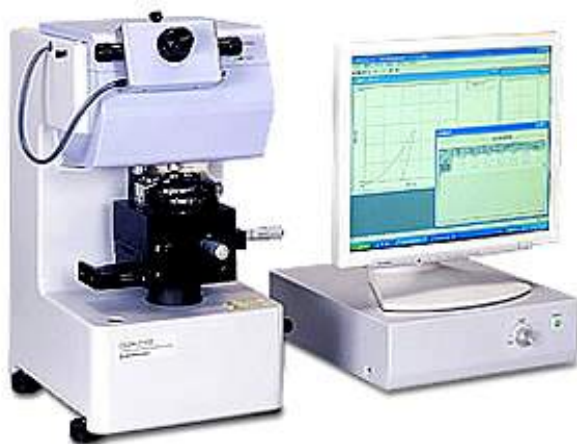


Fig. 1 External View of the DUH-211 series

In addition, a new method was developed for calculating dynamic hardness from the difference between two indentation depths at any two different loads, enabling calculation

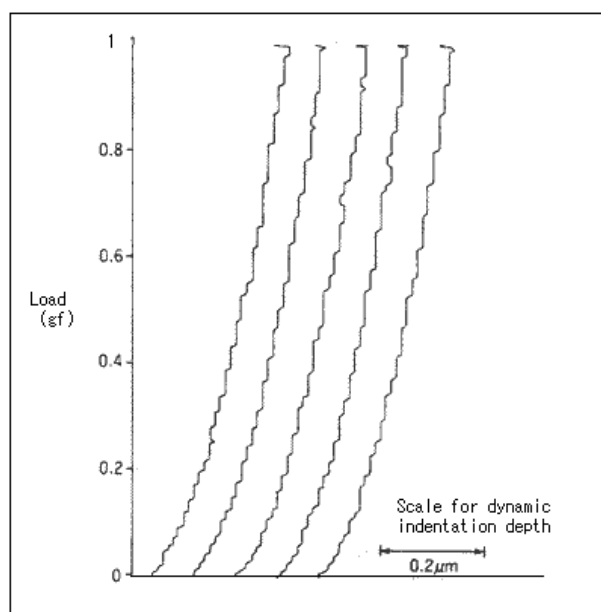


Fig. 2 Relation of Load versus Dynamic indentation depth of a-Si thin film

### ■ Evaluation of hardness distribution in depth direction for several kinds of thin films made by CVD

Hardness variation in the depth direction is shown for each thin film. These curves are useful to determine how hardness varies according to thin film processing conditions.

\* Please be advised that data obtained before the implementation of the current Weights and Measures Law may be presented in terms of gravimetric unit

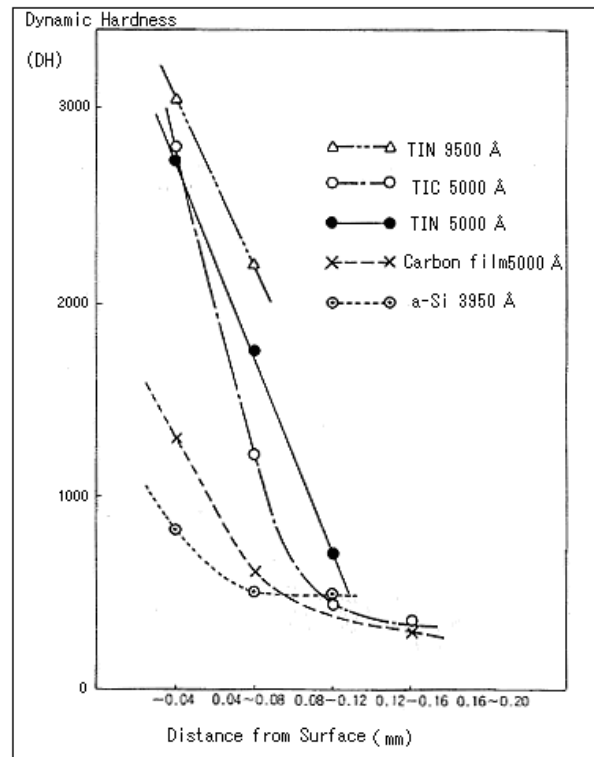


Fig. 3 Evaluation of Hardness distribution in depth direction for several kinds of thin films produced by CVD



Painted surfaces are evaluated for properties such as weathering resistance, light resistance, adhesive strength, impact resistance and hardness by instrumental measurement, and for color, gloss, unevenness, rumples etc. by visual inspection. Of these, the hardness test of painted surfaces is most important in evaluating the quality of paint film. Wet paint is dried in order to transform wet paint into rigid paint film. Paint can be dried either by the natural drying method, in which the paint dries completely at room temperature, or by the forced

drying method, in which paint is dried under high temperatures of approx. 100 to 250 degrees Celsius. The surface hardness of paint films differs depending on the kind of paint and the drying method. Information for evaluating hardness near the surface of paint film can be obtained by the ultra-micro area measuring technique of the Shimadzu Dynamic Ultra Micro Hardness Tester Model DUH. The following presents the results of hardness tests performed on paint films of paints for general use dried either by the natural or by the forced drying method.

**■ Measurement of surface hardness of paint films**

TEST MODE	2
CAL. MODE	1 ( 115° Triangular Pyramid Indenter )
AUTO or MANUAL	AUTO
F.S. DEPTH	2 & 5 $\mu\text{m}$
MAX LOAD	9,81 mN & 49,03 mN
LOADING SPEED	1 (0,1,4632 [mN/sec]) 5 (13,3240 [mN/sec] )
TOUCH SPEED	50 ( 0,48 [mN/sec] ) 50 ( 0,048 [mN/sec] )
AFTER TIME	5 sec.
PRE TIME	5 sec.
LOT	5

Table 1 Test Conditions

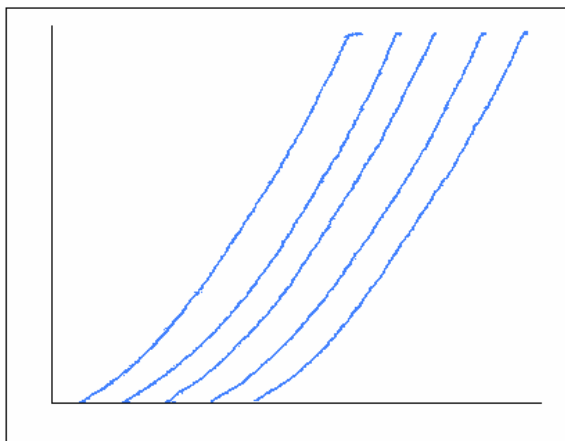
**■ Paint film of Meramin Resin dried by forced drying**

Fig. 1 Indentation depth Load Curves of Painted Films of Meramin Resin

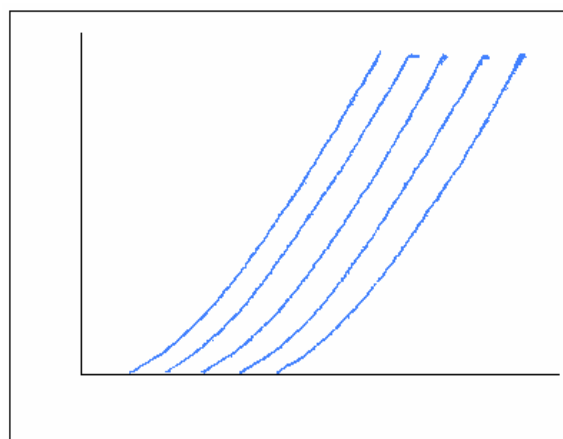
**■ Paint film of Urethane Resin dried by natural drying**

Fig. 2 Indentation Depth Load Curves of Painted Films of Urethane Resin

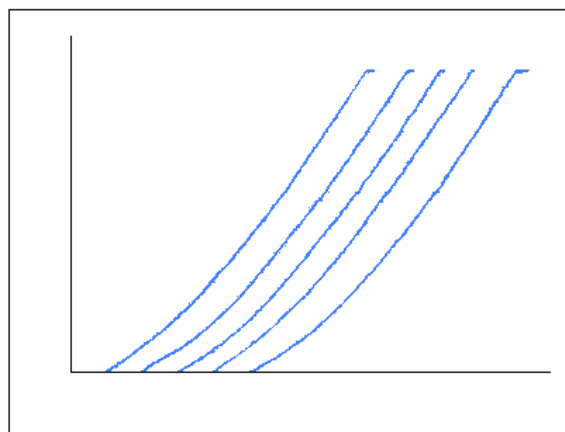
**■ Paint film of acrylic resin dried by natural drying**

Fig. 3 Indentation Depth Load Curves of Paint Films of Acrylic Resin

Sample Name	LOAD (mN)	DH (mean)
Meramin resin paint film thickness 38 µm - forced drying	9,81 mN	14,60
Overall thickness of paint film 177 µm	49,03 mN	12,00
Urethane resin paint film thickness 48 µm - forced drying	9,81 mN	13,00
Overall thickness of paint film 84 µm	49,03 mN	5,20
Acrylic resin paint film thickness 52 µm - forced drying	9,81 mN	10,50
Overall thickness of paint film 110 µm	49,03 mN	4,90

Table 2 Result of Measurements

Dynamic hardness is obtained based on the load value and indentation depth during the loading process. Since dynamic hardness is calculated from the indentation depth during the loading process, it includes both plastic deformation and elastic deformation.

DH: dynamic hardness

F: test load mN

h: dynamic indentation depth<sup>2</sup>

$$DH_{115} = 3.8584 \times F / h^2$$

DHT<sub>115</sub>: Dynamic hardness obtained with the triangular pyramid indenter with 115° tip angle

When LOAD is small, DEPTH is small, allowing the hardness of paint film at the outermost surface to be measured. When LOAD is large, DEPTH is also large, allowing the hardness at the deeper portion of paint film to be measured. In tests on samples dried by natural drying and forced drying, a different trend was observed for the respective samples between the results of 9,81 mN and 49,03 mN LOADs. In other words, the difference between the data for 9,81 mN and 49,03 mN was large in case of natural drying, while significantly smaller in the case of forced drying. This indicates that forced drying creates hardness more evenly distributed throughout the depth of the paint film than natural drying.

\* Please be advised that data obtained before the implementation of the current Weights and Measures Law may be presented in terms of gravimetric unit.



## Compression Test for Structural Materials of Lithium-Ion Batteries by MCT

No. SCA\_300\_002

### ■Introduction

Since lithium-ion batteries are light and small, they are used in a wide variety of products, from mobile electronic devices such as cellular phones and notebook PCs to electric cars and hybrid cars. Their inner structural materials are subjected to external force during production processes and to pressure during use. Therefore, evaluation of strength of each structural material is important to maintain consistent quality. A strength measurement was performed on thin or minute materials among various structural materials of lithium-ion batteries. Separators are

usually evaluated by a tensile test or penetration test. A compression test is also important to evaluate them because they are compressed in some processes. Active materials of approximately 10  $\mu\text{m}$  in size located near the electrode need to have a certain compression strength so they will not be destroyed during the coating process. Below are the results of compression tests performed on these materials using the MCT-211 Series Micro Compression Testing Machine.

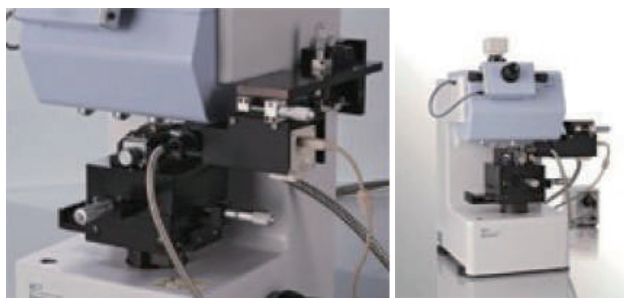


Fig. 1 External View of the MCT-211 Series (with the Side Observation Kit Mounted)

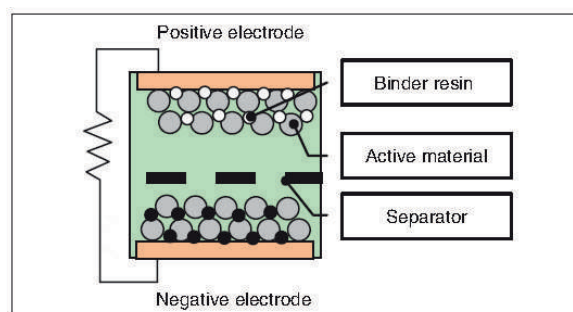


Fig. 2 Structure of Lithium-Ion Battery

## ■Compression Test on Separator of Lithium-Ion Battery

Table 1 shows the three types of specimens used for the measurement. Table 2 shows accessories used in the test and test conditions. Fig. 3 shows the conceptual diagram of the measurement. Table 3 shows the results of the compression tests on the three types of specimens. The specimens were evaluated by a compression rate where the same test

force was applied. The results clearly show the difference among the three types. Fig. 4 is a graph indicating the test force - displacement relationship of each specimen. The inflexion point of specimen 2 is at around 10 mN (pressure of approximately 5 MPa), indicating that applying too much compression pressure causes plastic deformation to the separator.

Table 1 Specimens

1) Specimen Name	Separator		
2) Specimen Number	1	2	3
3) Thickness	20 $\mu\text{m}$	20 $\mu\text{m}$	10 $\mu\text{m}$

Table 2 Test Conditions

1) Upper Indenter	Flat indenter (with a diamond tip), 50 $\mu\text{m}$ dia.
2) Test Mode	Load-unload test
3) Test Force (mN)	50
4) Loading Rate (mN/sec)	2.2
5) Holding Time (sec)	0
6) Test Method	A thin layer of liquid glue was applied to a glass plate, the separator was bonded to it, and a compression test was performed using the upper indenter. (See Fig. 2.)

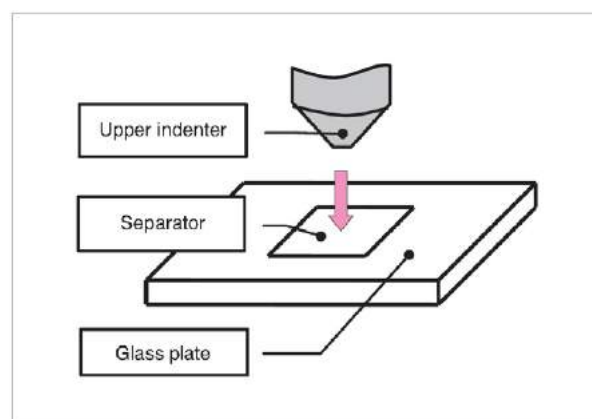


Fig. 3 Conceptual Diagram of Measurement

Table 3 Test Results

Specimen Name	Specimen Number	Maximum Force (mN)	Compression Variation ( $\mu\text{m}$ )	Compression Rate (%)
Separator	1	49.9	3.651	18.3
	2	49.9	3.371	16.9
	3	50.0	1.038	10.4

**Note:** The compression rate was calculated by the following calculation formula.

Compression rate (%) = (compression volume)/(thickness)  $\times$  100 (%)

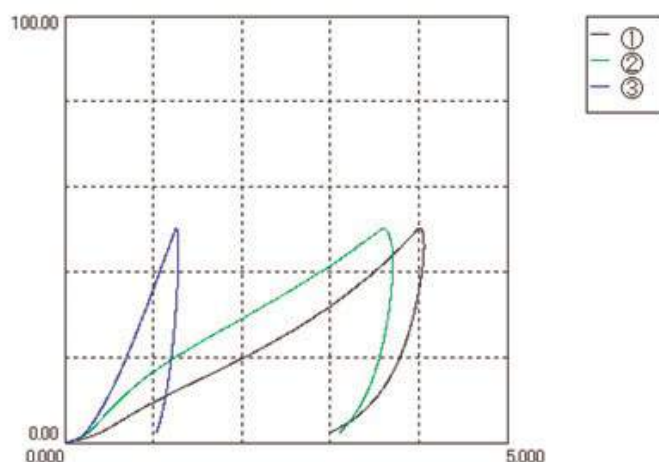


Fig. 4 Results of Compression Test

### ■Compression Test on Active Materials

A compression test was performed on two types of active material particles for positive electrode of lithium-ion battery. Table 4 shows test conditions and Fig. 5 shows an image of the test (compressed part). Measurement was performed ten times for each specimen. Then, average values were selected as a representative value for each specimen. (See Table 5 and Fig. 6.) The results clearly indicate the difference

in the strength between the two active materials and lithium cobalt oxide ( $\text{LiCoO}_2$ ) was confirmed to have the higher strength. As shown above, the MCT-211 Series Micro Compression Testing Machine enables accurate and efficient evaluation of compression characteristics of thin or minute materials used inside lithium-ion battery.

Table 4 Test Conditions

1) Upper Indenter	Flat indenter (with a diamond tip), 50 $\mu\text{m}$ dia.
2) Test Mode	Compression test
3) Test Force (mN)	50
4) Loading Rate (mN/sec)	2.2
5) Holding Time (sec)	0
6) Test Method	A very small amount of each specimen was spread on the lower compression plate and a compression test was performed on each single particle. (See Fig. 5.)

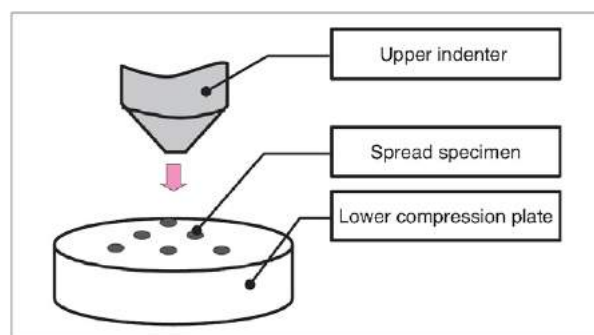


Fig. 5 Conceptual Diagram of the Compressed Part

Table 5 Test Results

Specimen Name	Fracture Force (mN)	Particle Diameter ( $\mu\text{m}$ )	Strength (MPa)
LiMn <sub>2</sub> O <sub>4</sub>	1.67	13.0	7.79
LiCoO <sub>2</sub>	16.23	13.3	72.75

**Note:** Fracture strength was calculated by the following calculation formula  
(Based on JIS R1639-5\*1).

$$Cs = 2.48 P / \pi d^2$$

Cs: Strength (MPa), P: Fracture force (N), d: Particle diameter (mm)

\*1: Test methods of properties of fine ceramic granules Part 5: Compressive strength of a single granule

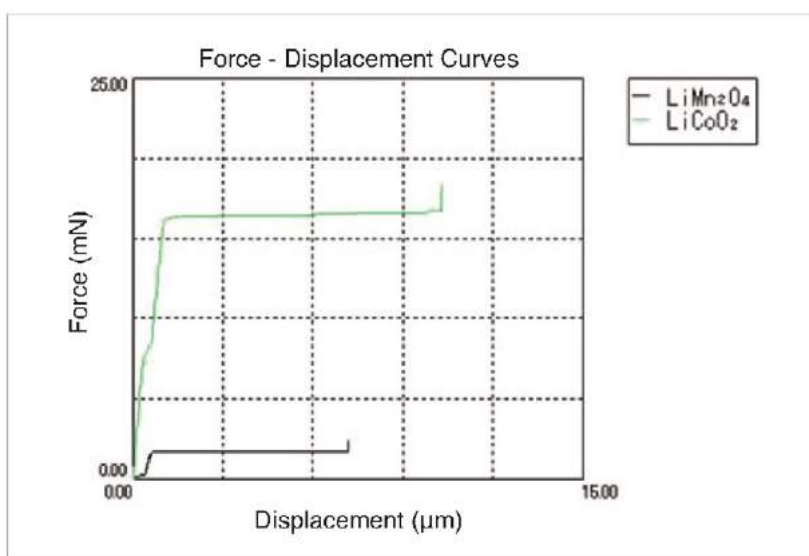


Fig. 6 Force - Displacement Curves

## Application News

No. SCA\_300\_023

Material Testing System HMV-G

### Measurement of Carburized Case Depth of Steel with Shimadzu Micro Hardness Tester Model HMV

G21 Series



#### ■ Introduction

Micro hardness testers are indispensable instruments for hardness evaluation, including surface composition, surface quenching layers, and machining transformation layers in research and development as well as quality control of parts of precision instruments, wires, metal foils, and electronic elements. The method for measuring the depth of layers hardened by carburizing or carburizing and quenching is specified in JIS-G-0557 "Method of measuring case depth hardened by carburizing treatment for steel." According to it, the effective depth or whole depth of hardened layer should be determined from the hardness distribution curve obtained on the cross section perpendicular to the hardened layer by use of a micro hardness tester.

The Shimadzu Micro Hardness Tester, which features very high reliability and excellent operability due to its built-in data processing functions, is best suitable for efficient measurement of the depth of carburized layers. The following is an example of such a measurement.

#### ■ Measurement of hardness distribution in a carburized layer of Ni-Cr-Mo steel

A specimen was prepared by molding a cross section of steel into resin and finished by buffing. Hardness was measured at every 0.1mm on the test surface. The printer output is shown in **Fig.1**. The hardness distribution plotted from the measured data is shown in **Fig.2**. JIS-G-0557 defines the effective depth of hardened layer as the distance between the surface and the point at which Vickers hardness matches 550. In this test, the effective depth is 0.6 mm. Shimadzu Micro Hardness Tester, featuring completely automatic load change, loading, and unloading, is used for quality control of low to high hardness's of small parts such as the gears and cams of watches, sewing machines, cameras and optical devices, and electronic elements like ICs and LSIs.



Date of test	Date 1987 2 14
Testing parameter file No	File No.
Specimen Number	Sample No.
Number of tests	Test 13
Number of lots	Lot 1
Testing mode	Vickers
Type of specimen surface	Flat
Repetitive number to read data	Read 2
Testing load	Load 200 GF
Load duration time	Loading Time 15 Sec
Correction coefficient	Correct 0,1273 $\mu\text{m}$
Number of lots and number of tests for a specimen	Lot = 1, Test = 1
Diagonal length of the indentation	D1 = 22,8
	D2 = 22,6
Vickers hardness	HV = 718
	Lot = 1, Test = 2
	D1 = 22,2
	D2 = 22,6
	HV = 735
	Lot = 1, Test = 3
	D1 = 22,3
	D2 = 22,6
	HV = 734
	Lot = 1, Test = 4
	D1 = 30,9
	D2 = 31,5
	HV = 380
Result of statistical calculation	--Statistics--
Measuring mode	HV
Number of lots	Lot = 1
Mean hardness	X = 572
Standard deviation	S = 143,7
Coefficient of variation	CV = 25,08 %
Minimum value in the lot	Min. = 380
Maximum value in the lot	Max. = 739

Fig. 1 Printer output of measured values

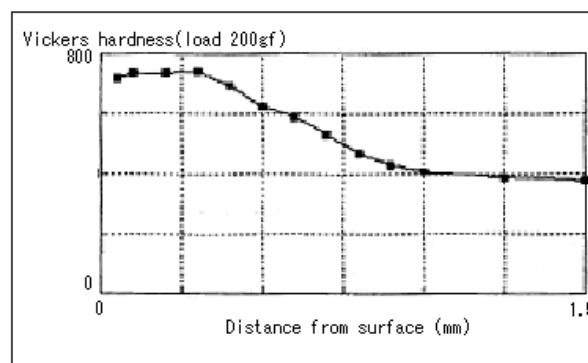


Fig. 2 Hardness Distribution in Carburized layer

\* Please be advised that data obtained before the implementation of the current Weights and Measures Law may be presented in terms of gravimetric unit.

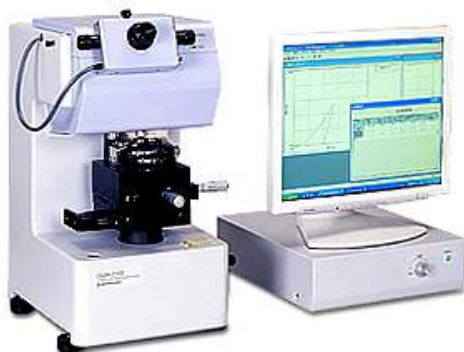
## Measurement of Hardness of the Machining Deterioration Layer of Stainless Steel with Shimadzu Dynamic Ultra Micro Hardness Tester DUH

### ■ Introduction

When a metallic material is processed with lathes, milling machines, or grinders, the upper portion of the material's surface is transformed into a so-called machining deterioration layer. This layer, which results from plastic transformation and increased temperature during the machining process, comprises an amorphous layer, a plastic deterioration layer, a fine particle layer, and micro structure deterioration layers. These have greater displacement than the inner part of the material, producing residual stress.

The following presents the results of dynamic indentation hardness testing on a thin surface layer (1-3  $\mu\text{m}$ ) of machine processed stainless steel (SUS304) performed with the Shimadzu Dynamic Ultra Micro Hardness Tester Model DUH.

This machine is widely applicable to a range of hard to soft materials as it measures hardness of thin films and thin layers in terms of the indentation depth of an indenter (dynamic indentation hardness) or the diagonal length of indentation (Vickers hardness).



### ■ Test conditions

1) Specimen : Stainless steel SUS304

Processing:

- A) Solution heat treatment only
- B) Polishing finish after solution heat treatment
- C) Turning and polishing by polishing paper after solution heat

### ■ Testing procedure

Dynamic indentation hardness (hereafter called hardness) was calculated from the relation of load versus depth at 0.2  $\mu\text{m}$  intervals from the surface with load being applied via indenter to each of three specimens finished in different ways. Load was continuously applied up to 100 gf.

### ■ Test results

Table 1 displays the values measured under the processing condition A (others under processing conditions B and C are omitted), Table 2 the variation of hardness (averaged) along the depth direction for each of the processing conditions, and Fig.1 the depth versus hardness curves. The tendency of curve B to approach A at a depth of around 2  $\mu\text{m}$  and to overlap A thereafter suggests that the machining deterioration layer remains influential until an indentation depth of around 2  $\mu\text{m}$ , but the hardness of the matrix material is predominant thereafter. Curve C suggests that the respective machining deterioration layer keeps its influence down to a significantly greater depth than curve B, as sample C has undergone a turning process just prior to the polishing paper finish.

No.	Load (gf)	Depth	Hardness
1	0.640	0.20	603.41
2	1.300	0.40	170.66
3	2.720	0.60	170.46
4	4.260	0.80	162.71
5	6.260	1.00	181.49
6	8.480	1.20	159.05
7	10.960	1.40	150.25
8	13.680	1.60	142.45
9	16.720	1.80	144.15
10	20.100	2.00	147.06
11	23.720	2.20	132.13
12	27.300	2.40	132.12
13	31.680	2.60	131.67
14	36.100	2.80	125.24
15	40.720	3.00	131.53
16	45.440	3.20	122.39
17	50.500	3.40	126.31
18	55.900	3.60	129.71
19	61.600	3.80	130.86
20	67.200	4.00	115.21
21	73.220	4.20	122.12
22	79.520	4.40	122.96
23	85.840	4.60	144.29
24	92.360	4.80	112.87
25	99.020	5.00	109.63

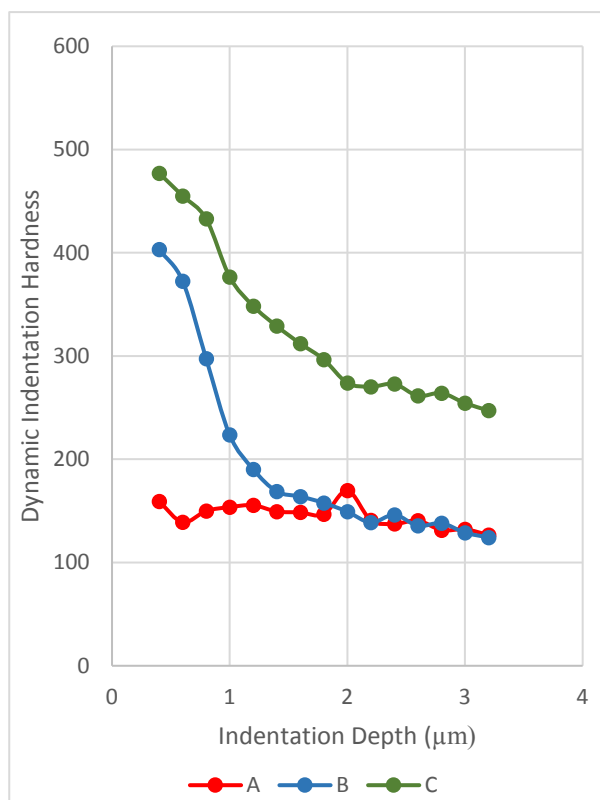
No.	Load (gf)	Depth	Hardness
1	0.640	0.20	603.41
2	1.360	0.40	126.85
3	2.380	0.60	134.12
4	3.560	0.80	111.99
5	5.100	1.00	130.57
6	7.000	1.20	141.99
7	9.300	1.40	154.27
8	11.940	1.60	155.80
9	14.920	1.80	156.86
10	18.220	2.00	155.81
11	21.820	2.20	153.40
12	23.720	2.40	151.38
13	25.720	2.60	146.06
14	34.200	2.80	139.23
15	38.640	3.00	128.13
16	43.420	3.20	131.80
17	48.640	3.40	140.11
18	54.080	3.60	136.36
19	59.720	3.80	132.29
20	65.420	4.00	122.86
21	71.940	4.20	146.46
22	78.320	4.40	128.18
23	84.660	4.60	116.69
24	91.720	4.80	133.71
25	98.860	5.00	120.38

No.	Load (gf)	Depth	Hardness
1	0.700	0.20	662.16
2	1.620	0.40	179.93
3	2.940	0.60	184.68
4	4.600	0.80	175.00
5	6.460	1.00	149.01
6	8.760	1.20	165.34
7	11.220	1.40	143.00
8	14.020	1.60	147.37
9	17.040	1.80	139.21
10	20.440	2.00	146.18
11	23.900	2.40	127.990
12	27.640	2.40	128.53
13	31.500	2.60	124.12
14	35.880	2.80	129.77
15	48.580	3.00	136.78
16	45.360	3.20	123.04
17	50.420	3.40	126.32
18	55.340	3.60	108.31
19	61.00	3.80	130.32
20	66.960	4.00	131.37
21	73.060	4.20	125.75
22	79.440	4.40	126.30
23	86.280	4.60	133.59
24	93.260	4.80	128.40
25	100.100	5.00	114.48

Table 1: Measured Values under Processing Condition A (measured in three trials

No.	Depth ( $\mu\text{m}$ )	Dynamic Indentation Hardness (DH)		
		A	B	C
1	0.20	-	-	-
2	0.40	159.15	403.21	477.13
3	0.60	139.09	372.56	155.11
4	0.80	149.90	297.51	432.84
5	1.00	153.69	223.65	376.67
6	1.20	155.46	190.37	348.49
7	1.40	149.44	168.84	328.97
8	1.60	148.54	164.00	312.09
9	1.80	146.74	157.75	296.65
10	2.00	169.68	149.26	273.96
11	2.20	141.00	138.73	270.36
12	2.40	137.41	146.23	272.86
13	2.60	140.62	135.57	261.47
14	2.80	131.41	138.12	264.10
15	3.00	132.15	128.96	254.45
16	3.20	126.68	124.28	247.20

Table 2: Variation of Dynamic Indentation Hardness along Depth Direction for Each of Three Different Processing Conditions



$$DH_n = 37,838 \cdot \frac{P_n}{(D_n - D_{n-1})^2} \cdot \left(1 - \sqrt{\frac{P_{n-1}}{P_n}}\right)^2$$

$DH_n$ : Dynamic Hardness in the sequence of n-th

$P_n$ : Load in sequence of n-th (gf)

$P_{n-1}$ : Load in sequence of n-1-th (gf)

$D_n$ : Indentation depth in the sequence of n-th ( $\mu\text{m}$ )

$D_{n-1}$ : Indentation depth in the sequence of n-1-th ( $\mu\text{m}$ )

\* Please be advised that data obtained before the implementation of the current Weights and Measures Law may be presented in terms of gravimetric unit.

## A hardness measurement of steel surface treatment layer with Shimadzu Dynamic Ultra Micro Hardness Tester, Model DUH

A variety of surface treatment is exercised to every part of industrial products, so that their functionality, corrosive resistivity, or decorating nature of the surficial layer should be made best fitted to their respective role. The following example is dedicated to represent an effective method for a dynamic hardness measurement by indenting onto the thin hardening layer (4 - 5 $\mu$ m deep) on the cut section, the surface of which is perpendicular to the longitudinal direction of a steel bar.

### ■ Testing parameters

- 1) Sample: steel (surficial hardening treatment), see Fig.1
- 2) Indenter: tip angle 136°, square pyramid indenter (Vickers indenter)
- 3) Measuring mode: load-load hold test (mode 1)
- 4) Test load: 1.0 gf
- 5) Loading speed: 0.0725 gf/sec.
- 6) Load hold-time: 10 sec.

### ■ Testing parameters

As the measuring area is limited to a very narrow range (4 - 5  $\mu$ m) of hardening treatment thin layer, the diagonal length of an indentation must be as small as about a fifth (0.8 - 1  $\mu$ m or less) of the width of the hardening layer so that the measurement would not undergo dimensional restriction. Accordingly, an optional X100 objective lens of was selected instead of standard X50, thus obtaining an overall magnifying power of X1000 with combined use of X10 eyepiece lens. This permits the measurement observing the indentation always near at the center of the surficial hardening layer through the optical monitor.

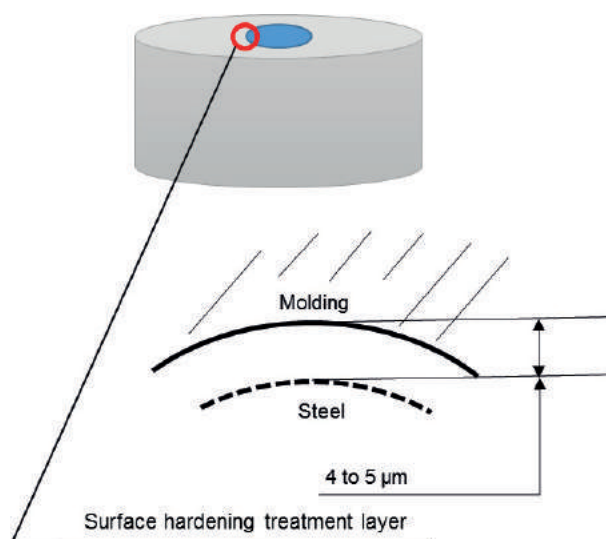


Fig. 1 Sample



## ■ Test Result

- 1) The average of three measurements are shown in Table 1, and the load - indentation depth curves are in Fig.2.

Load (gf)	Depth (μm)	Dynamic Hardness DHV
1,0015	0,126	2387

Dynamic Hardness was determined by the following formula:

$$DHV = \frac{37,838 \cdot P}{h^2}$$

Where:

DHV: Dynamic hardness by Vickers Indenter

P: Test Load (gf)

H: Indentation depth (μm)

- 2) Diagonal length of an indentation is known to be seven times of the indentation depth (using a Vickers indenter). Accordingly, the diagonal length is supposed to be about 0.9 μm in this case, which permits the measurement being not affected from the thickness of surficial hardening layer.

- 3) Fig.3 shows a photograph of the tested indentation (approx. X1000).

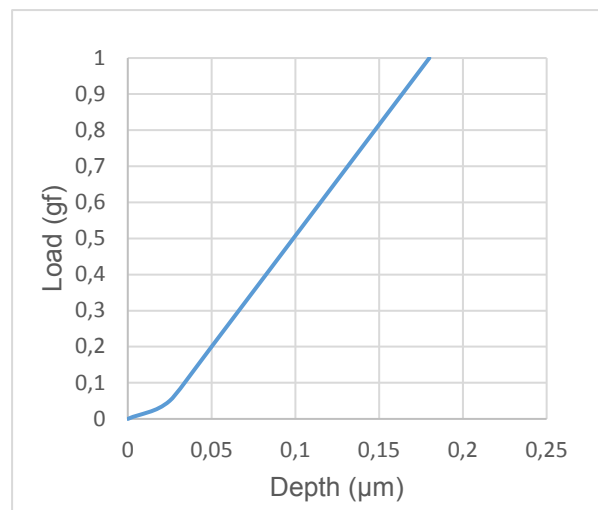


Fig. 2 Load- Indentation depth curve (in mode 1)

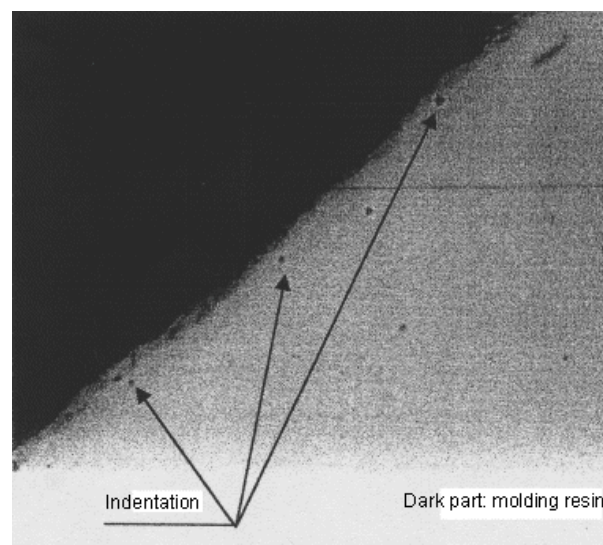


Fig. 3 Tested Indentation

## Application News

Material Testing System DUH

No. SCA\_300\_035

### **A hardness measurement of surface treatment layer on a steel sample using Shimadzu Dynamic Ultra Micro Hardness Tester, Model DUH**

Recent years have seen intensive requests for engineering materials with higher function ability and longer life, and as a result, surface treatment for such materials has become popular. Under this circumstance, hardness testers with micro load are enjoying an

increasing demand. In this regards, a test report is herein introduced on the hardness distribution measured from the sample surface toward depth direction with an interval of 2  $\mu\text{m}$ , using Shimadzu Dynamic Ultra Micro Hardness Tester Model DUH.

#### ■ Test Parameters

- 1) Sample: plating layer on a metal plate (See Fig. 1)
- 2) Indenter: tip angle  $136^\circ$ , square pyramid indenter (Vickers indenter)
- 3) Measuring mode: load-load-hold test (mode 1)
- 4) Test load: 2.0 gf
- 5) Loading speed: 0.029 gf/sec.
- 6) Load hold-time: 10 sec.

#### ■ Test Method

- 1) Vickers Hardness  
Testing procedures, the distance between the indentation center and the sample edge shall be 2.5 time the diagonal length or more (the diagonal length is 2.6  $\mu\text{m}$  or less). The test load was determined in accordance with this specification, and the tests were performed near the mid depth of the plating layer.
- 2) Hardness distribution measurements were performed at the location and with the depth intervals of 2  $\mu\text{m}$  starting from the sample surface as shown in Fig. 2

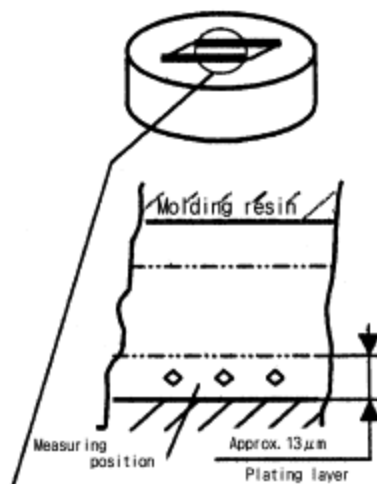


Fig. 1

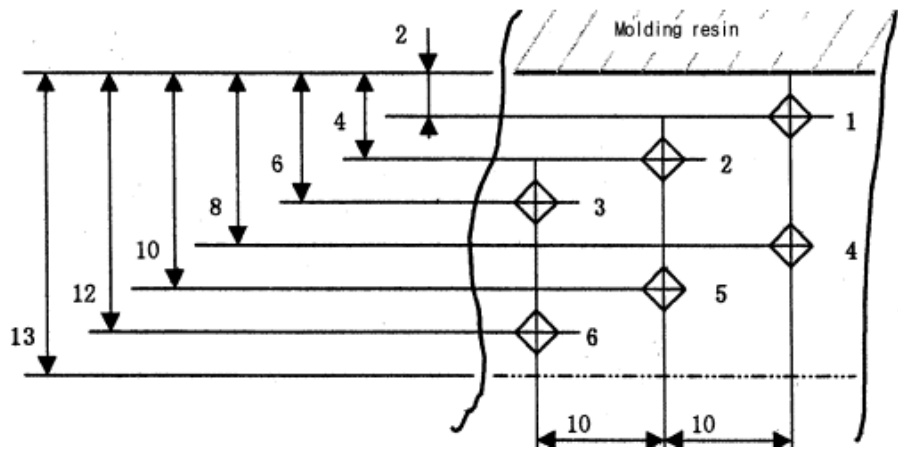


Fig. 2

■ Test Results

The average of five measurements is shown in Table 1, and the load-indentation depth curve is in Fig. 3

Test Load (gf)	Depth (μm)	Dynamic Hardness DHV
2,001	0,206	1065

Table 1 Hardness Test Result

Dynamic Hardness was determined by the following formula:

$$DHV = \frac{37,838 \cdot P}{h^2}$$

Where:

DHV: Dynamic hardness by Vickers Indenter

P: Test Load (gf)

H: Indentation depth (μm)

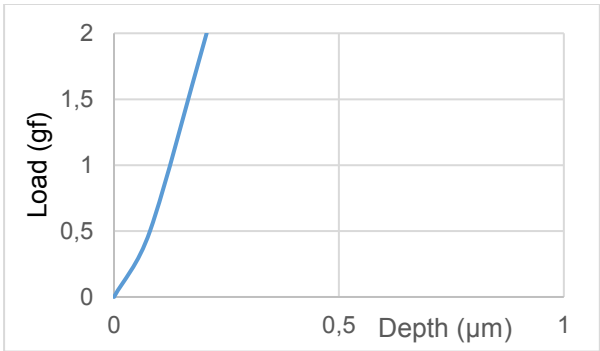


Fig. 3 Load-Indentation depth curve

■ Test Results

Result of five tests with a depth interval of 2 μm is listed in Table 2.

Test Load (gf)	DHV					
	1	2	3	4	5	6
2,0	847	1001	1070	1103	966	925

Table 2 Hardness Distribution

..

- Dynamic hardness was determined by the same formula as item 1) above.

The Relation of depth and hardness is shown in Fig. 4.

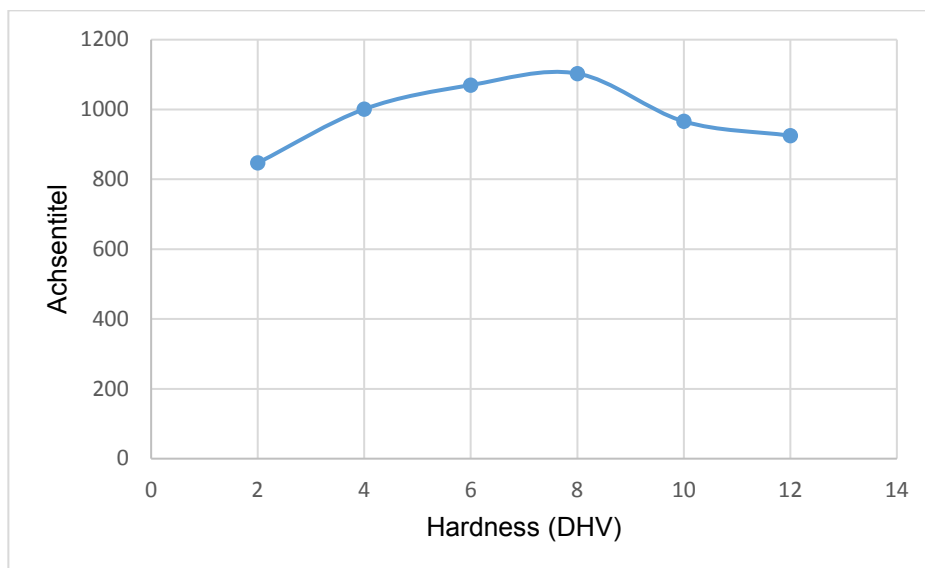


Fig. 4

Fig. 4 indicates a tendency that hardness increases as depth increases, reaches the max. at mid depth of the plating layer, and decreases thereafter.

## A thickness measurement of a Ni-plating layer on a stainless-steel sample with Shimadzu Dynamic Ultra Micro Hardness

### ■ Introduction

In general, Shimadzu Dynamic Ultra Micro Hardness Tester Model-DUH series (measuring depth 0 – 10  $\mu\text{m}$ ) are widely used for measuring hardness of thin films and surface treatment layer, and it can also be applied to the thickness measurement of thin layers (thickness below 10  $\mu\text{m}$ ). The followings is a test example in which thickness of Ni-plating on a stainless-steel sample was measured with Shimadzu Dynamic Ultra Micro Hardness Tester Model DUH-201S.

### ■ Test parameters

- 1) Sample: Ni-plating layer on stainless steel (See Fig.1)
- 2) Indenter: Triangle pyramid indenter, tip angle 115° (Berkovich Indenter)
- 3) Measuring mode: load-load hold test (mode 1)
- 4) Test load: 100 gf
- 5) Loading speed: 3.6 gf/sec.
- 6) Load hold-time: 10 sec.

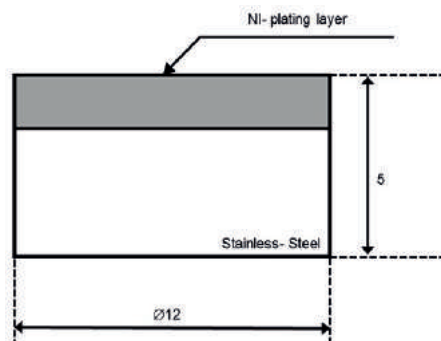


Fig. 1 Test Sample

### ■ Testing parameters

1) Measure each hardness while changing the test loads. Select 'Hardness-Indentation depth Curve between Two Points' in the data analysis menu and study how the state of curve changes, referring item 2) below.

2) At the earlier step when the test load is small and it makes an indentation of very shallow depth compared with the whole thickness of the plating layer, the indentation represents the hardness of the plating layer only, and its variation is moderately slow as the test load increases.

As the test load further increases, however, the indentation gradually undergoes the influence of the base-material, stainless-steel, and the indication of hardness changes steeply downward (or upward if the base-material is harder than the plating layer). The critical point (h1) will be observed, if the test load is further increased. There appears another critical point (h2), where the indentation is under significant influence from the hardness of base-material. The thickness of the plating layer can be estimated from these critical points.

3) In case of DUH series, the test load of the above item 2) need not be repeated many times but a few times only, just like 100 gf and 200 gf, the max. test load, for example.



## ■ Test Result

Fig. 2 shows the Load-Indentation depth Curve by the test using parameters in the above item 1. Fig. 3 is a 'Hardness-Depth Curve between Two Points' corresponding to the Fig.2.

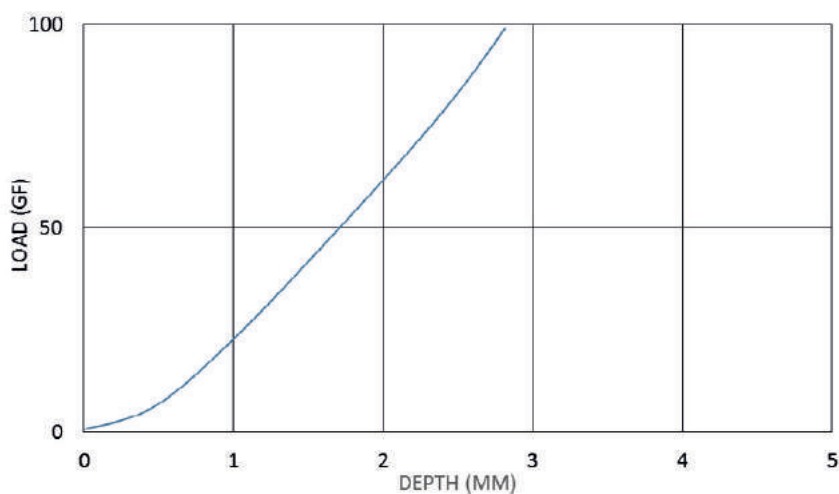


Fig. 2 Load- Indentation depth Curve (test mode 1)

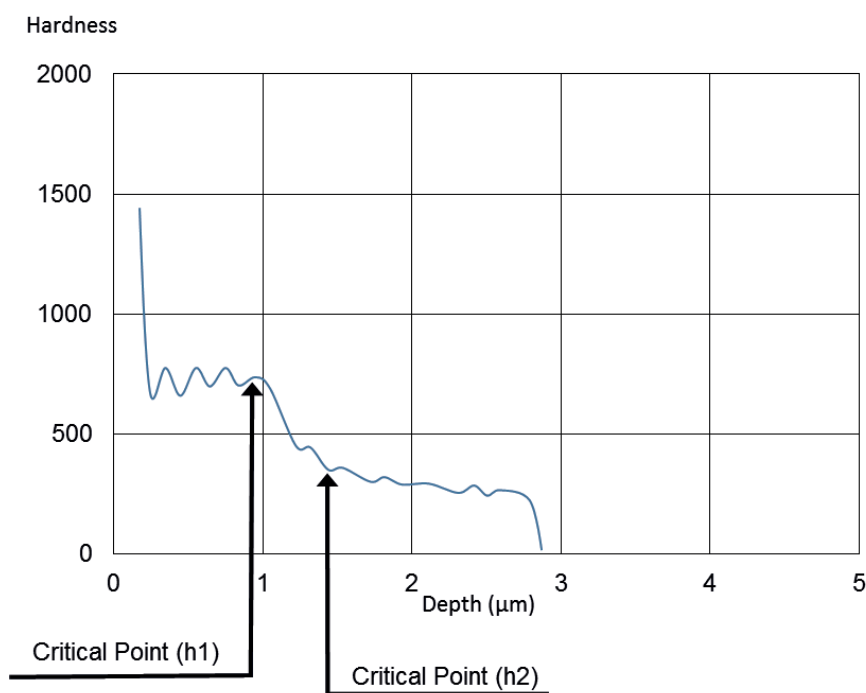


Fig. 3 Hardness- Depth Curve (test mode 1)

The thickness of the plating layer is estimated approx.1 μm from the critical point (h1) of Fig.3.

## Application News

Material Testing System HMV

No. SCA\_300\_047

### **Measurement of the surface treatment depth of steel with Shimadzu Micro Hardness Tester Model HMV**

The following is an example of output data obtained through a measurement of surface treatment depth of a steel sample with the Shimadzu Micro Vickers Hardness Tester, Model HMV. (Fig. 1)

#### ■ Testing parameters

- 1) Sample: steel (surface hardening)
- 2) Measuring indenter: Square pyramid diamond indenter tip angle of  $136^\circ$  (Vickers indenter)
- 3) Test load: 1000 gf
- 4) Load hold-time: 10 sec

#### ■ Testing method

- 1) A steel block is cut perpendicularly to the hardening surface. The surface of the cut section, after being polished, is applied to hardness measurement. Surface hardness shall be measured in the direction perpendicular to the cut section surface.
- 2) Hardness measurement shall be repeated starting from position 1 (surface) as shown in Fig. 2 until no substantial difference of hardness can be observed.



Fig. 1 Shimadzu Micro Vickers Hardness Tester, Model HMV

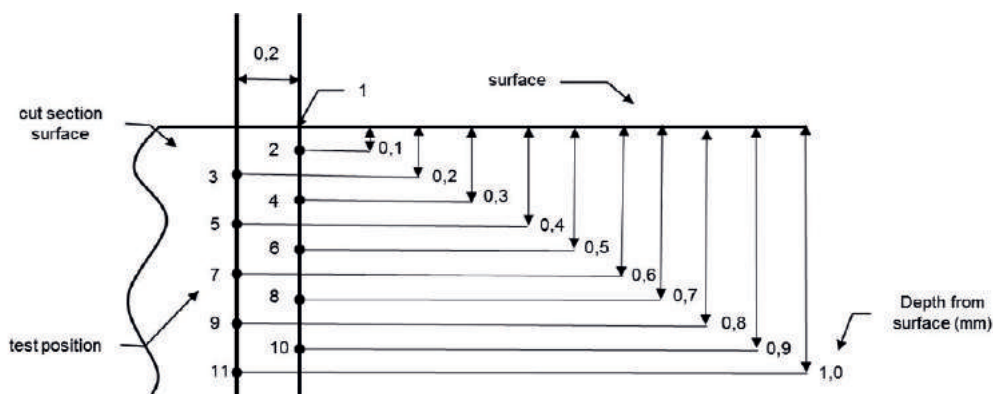


Fig. 2

### ■ Test results

1) Hardness at respective test positions is listed in Table 1, while the printer outputs of the test result and the plotted test result are shown in Table 1 and Fig. 3 respectively.

2) It is known from Table 1 and Fig. 3 that the depth of the hardening layer is 0.6 mm.

Depth (±0)	Test position No.	Hardness (HV)
Surface	1	1070
0.1	2	905
0.2	3	847
0.3	4	687
0.4	5	591
0.5	6	397
0.6	7	251
0.7	8	229
0.8	9	225
0.9	10	217
1.0	11	215

Table 1 Test Results of hardness

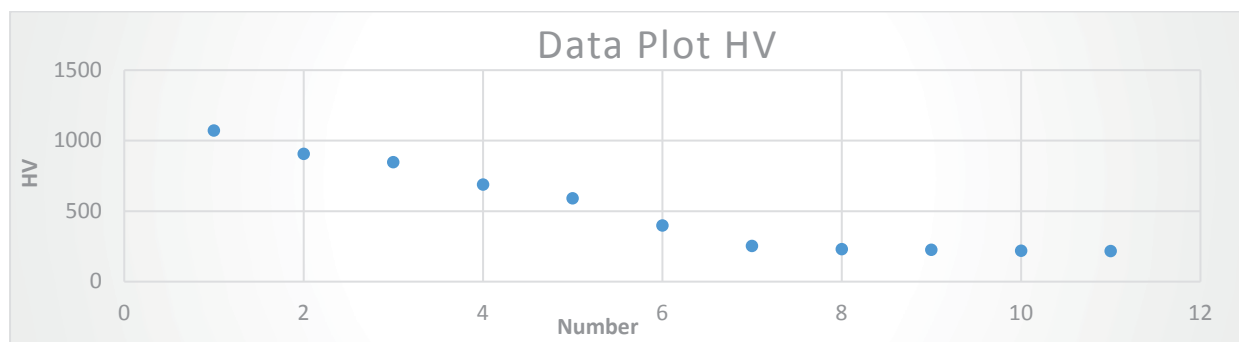


Fig. 3 Plot of Hardness

## Application News

No. SCA\_300\_050

Material Testing System MCT

### **Strength Evaluation on Metallic Fine Particles with Shimadzu Micro Compression Testing Machine Model MCT**

#### ■ Introduction

The role of fine particles and related technologies is becoming more and more important as one of the basic factors supporting the current high technology boom.

Powders and fine particles display characteristic behaviors which distinguish them from normal liquids and solids. They can be easily mixed, moved, split, scattered in liquid and gas, and they also have comparatively large surface area for their volume. As a particle body is an aggregation of fine solid particles, it has properties of an individual particle and of a mass of particles. For this reason, diametric compressive fracture load applied to individual particles is a critical factor in particle processing technology.

The following is an example of an examination of the physical behaviors of metallic fine particles of different hardness's under pressing loads performed with the Shimadzu Micro Compression Testing Machine Model MCTM.

The MCTM applies a pressing load of electromagnetic force at a constantly increasing rate onto a specimen placed between an upper pressing indenter and a lower anvil. It automatically measures the deforming behavior of a specimen and processes data for its relation to load. The MCTM is optimized for the evaluation of the physical strength of various micro parts, powders and fine particle bodies, micro fibers, etc.

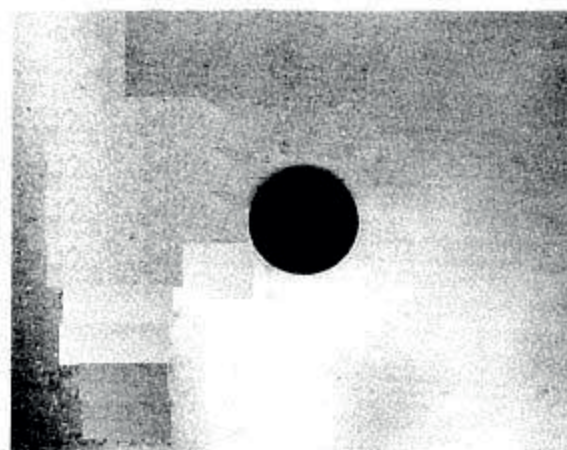


Fig. 1 Spherical particle      | 100 μm |

#### ■ Specimens

- 1) Name: metallic fine particles
- 2) Kinds: three different hardness's, A, B, and C
- 3) Shape: spherical (See Fig. 1)

## ■ Testing Method

1) Test mode : Compression

$$St = \frac{2,8 \cdot P}{\pi \cdot d^2}$$

2) Load: 500 gf

St: Tensile Strength /kg/mm<sup>2</sup>)

3) Loading rate constant: 1 (4,230 gf/sec)

P: Load (kgf)

4) Numbers of tests : 10 tests

d: Particle diameter (mm)

5) Calculation of strength: Strength was calculated by the following equation from the load and particle diameter when displacement reached 10% of diameter, since the three specimens did not reach compressive fracture. The calculated values in this method is shown as tentative strength with "-" before the figure, being distinguished from compressive fracture strength.

Specimen No.	Applied Loads (gf)	Strain (μm)	Diameter (μm)	Diameter (μm)	Mean Diameter (μm)	Tentative Strength
1	230,650	8,15	81,50	81,50	81,50	-30,965
2	225,800	8,27	83,00	82,50	82,75	-29,405
3	262,150	8,32	83,00	83,50	83,25	-33,729
4	223,100	8,50	85,00	85,00	85,00	-27,535
5	277,150	8,42	84,50	84,50	84,25	-34,843
6	221,750	8,10	81,00	81,00	81,00	-30,139
7	277,150	8,15	81,50	81,50	81,50	-37,207
8	228,600	8,15	81,50	81,50	81,50	-30,689
9	232,600	8,25	83,00	82,50	82,50	-30,474
10	215,450	8,21	82,00	82,50	82,00	-28,572
Mean Value	239,456	8,25	82,60	82,53	82,53	-31,356

Table 1 Test Result of Particle A



Specimen No.	Applied Loads (gf)	Strain ( $\mu\text{m}$ )	Diameter ( $\mu\text{m}$ )	Diameter ( $\mu\text{m}$ )	Mean Diameter ( $\mu\text{m}$ )	Tentative Strength
1	364,250	8,25	82,50	82,50	82,50	-47,722
2	405,450	8,30	83,00	83,00	83,00	-52,482
3	342,450	8,32	83,50	83,80	83,25	-44,061
4	393,650	8,30	83,00	83,00	83,00	-50,955
5	357,830	8,10	81,00	81,00	81,00	-48,629
6	412,350	8,45	84,50	84,50	84,50	-51,497
7	403,900	8,45	84,50	84,50	84,50	-50,442
8	381,850	8,10	81,00	81,00	81,00	-51,898
9	389,950	8,31	83,00	83,00	83,00	-50,359
10	365,300	8,30	83,00	83,00	83,00	-47,285
Mean Value	381,605	8,29	82,90	82,85	82,87	-49,533

Table 2 Test Result of Particle B

Specimen No.	Applied Loads (gf)	Strain ( $\mu\text{m}$ )	Diameter ( $\mu\text{m}$ )	Diameter ( $\mu\text{m}$ )	Mean Diameter ( $\mu\text{m}$ )	Tentative Strength
1	426,000	8,20	82,00	82,00	82,00	-56,495
2	402,300	8,28	82,00	82,00	82,00	-53,352
3	410,850	8,50	85,00	85,00	85,00	-50,708
4	444,450	8,40	84,00	84,00	84,00	-56,169
5	494,150	8,50	85,00	85,00	85,00	-60,989
6	413,900	8,12	81,50	81,50	81,25	-55,908
7	443,250	8,32	83,00	83,50	83,25	-57,031
8	431,900	8,15	81,50	81,50	81,50	-57,982
9	457,050	8,30	83,00	83,00	83,00	-59,161
10	455,100	8,22	82,50	82,00	82,25	-59,988
Mean Value	437,895	8,29	82,90	82,95	82,93	-56,778

Table 3 Test Result of Particle C

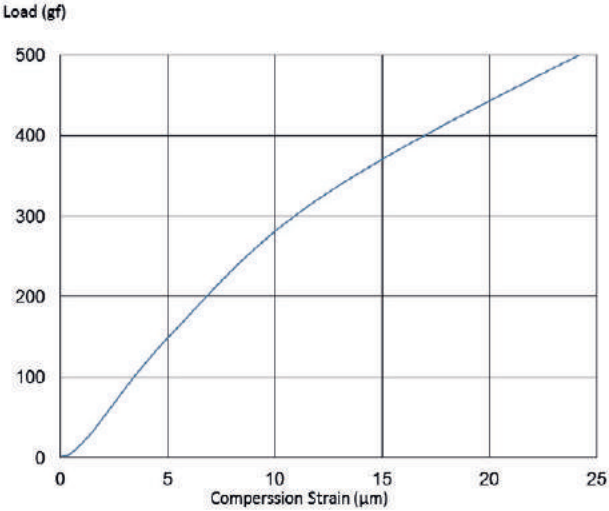


Fig. 2 Load- Strain Curve for Particle A

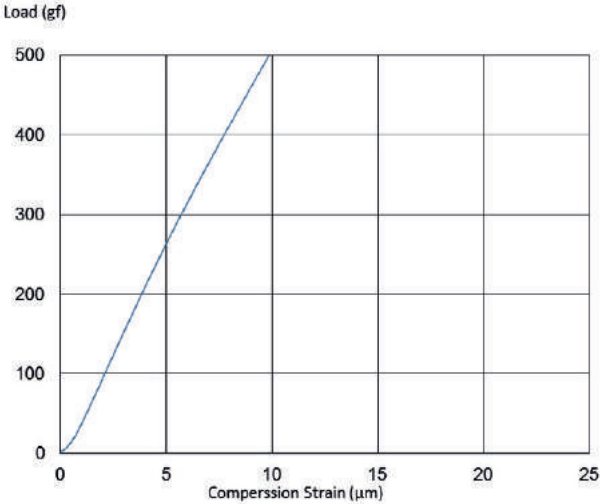


Fig. 3 Load- Strain Curve for Particle B

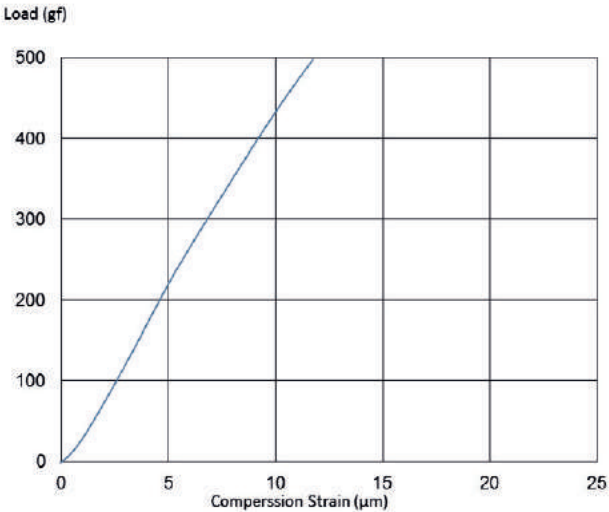


Fig. 4 Load- Strain Curve for Particle C

Kinds of Specimen	Compression Test		Hardness Test
	Tensile Strength (kgf/mm <sup>2</sup> )	Standard Deviation (kgf/mm <sup>2</sup> )	HRC <sup>2)</sup>
A	31.36	3.00	34
B	49.53	2.60	52
C	56.78	3.07	57

Table 4 summary of the test results

■ Test Conditions

Sample No	1
Test	5
Indenter	Vickers Flat
Read Time	2
Load	100 g
Loading Time	15 sec

	Kinds of Specimen		
	A	B	C
Test	1	1	1
D1	23,3	18,4	17,0
D2	23,4	18,1	16,8
HV	339	555	648
Test	2	2	2
D1	23,6	18,7	16,8
D2	23,3	18,3	17,2
HV	336	541	640
Test	3	3	3
D1	23,0	18,5	17,2
D2	23,2	18,2	17,0
HV	347	535	633
Test	4	4	4
D1	23,7	18,8	17,1
D2	23,6	18,4	16,7
HV	331	535	648
Test	5	5	5
D1	23,5	18,5	17,0
D2	23,8	18,7	17,2
HV	331	535	633
Average HV	337	543	640
Min HV	331	535	633
Max HV	347	555	648

Table 5 Result of Vickers Hardness

### ■ Comment on test results

Table 4 shows a summary of the test results, while Tables 1 through 3 and Figs. 2 through 4 present measured data. Figs. 2 through 4 show examples of load-strain curves for each kind of specimen having the same diameter. Vickers Hardness Indexes are shown in Table 5 for each respective particle specimen.

Table 4 indicates the correlation between tensile strength and Rockwell Hardness. Figs. 2 through 4 indicate that the order of strain size at a given load shows the same trend as that of hardness. According to these results, hardness decreases as strain increases, and increases as strain decreases.

## Compressive Strength of Metallic Microspheres and Dependence on Heat Treatment Temperature. Shimadzu MCTM-500 Micro Compression Testing Machine

### ■ Introduction

One advance in metallurgy is the recent development in forming technology for the production of metal powders composed of microspherical particles ranging in size from several  $\mu\text{m}$  to  $100\mu\text{m}$ . Evaluation of the mechanical properties of these particles as individual microspheres and as aggregates is required. The MCTM was applied to compression strength testing of Al-Ni alloy microspheres subjected to various heat treatments, and dependence of compression strength on the treatment temperature was observed.

The Model MCTM applies a pressing load of electromagnetic force at a constantly increasing rate onto a specimen placed between an upper pressing indenter and a lower anvil for automatic measurement of deforming behavior of the specimen and data processing for its relation to load. This testing machine is optimized for evaluating the physical strength of various micro-scale parts, powders and fine particle bodies, micro fibers, etc.

### ■ Specimens

1) Material name	Al-Ni type alloy
2) Kinds	Three different heat treatments <ul style="list-style-type: none"> <li>• no heat treatment,</li> <li>• 200 °C heat treatment,</li> <li>• 400 °C heat treatment</li> </ul>
3) Shape	micro sphere

### ■ Testing conditions

1) Testing mode	compression test
2) Upper pressing indenter	flat, diameter $50\mu\text{mD}$ (diamond)
3) Lower platen	SKS flat plate
4) Strength calculation	<p>A 10% strength was calculated from the load value and particle diameter when strain reached 10% of particle diameter with the following equation, as the three specimens did not reach the state of breakage or fracture.</p> <p>The values hereby obtained are shown on the data sheet as tentative strength with a minus sign (-) to discriminate from fracture strength.</p>

(Quoted from the equation by Hiramatsu, et al.)

$$St = \frac{2,8 \cdot P}{\pi \cdot d^2}$$

St: tensile strength (kgf/mm<sup>2</sup>)

P: Load (kgf)

d: Diameter of particle (mm)

Note: Mr. Hiramatsu, Mr. Oka, Mr. Kiyama, Mining Association Journals

If particle diameter is 6,7 µm, strength is calculated with a load of 1,085 gf (P1) at a compression displacement of 0,67 mm (D1)

S10=21,553 kgf/mm<sup>2</sup>)

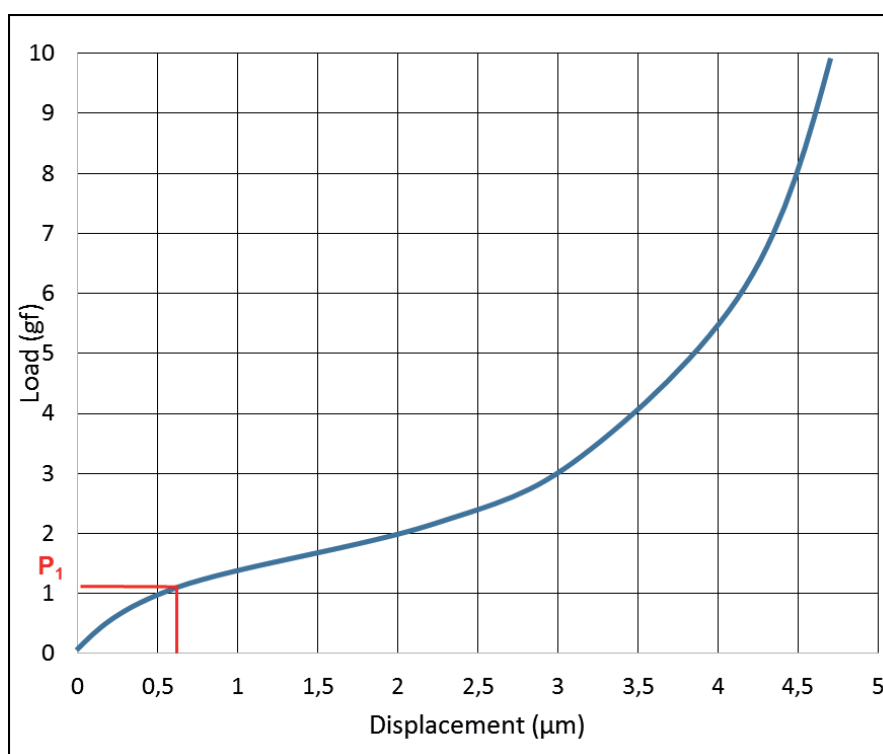


Fig. 1 Load-Displacement Curve



Table 1 Test results for untreated sample

Testing Conditions							
		File No.		AN408.D1			
Test mode	1	Indenter:		Flate plate 50			
Sample name	Aluminium-Nickel alloy						
Sample No.	4						
Testing load	100.00 (gf)			Loading rate constant: 1			
Displacement scale	10 ( $\mu\text{m}$ )						
No.	Load (gf)	Displacement ( $\mu\text{m}$ )	Diameter ( $\mu\text{m}$ )	Diameter ( $\mu\text{m}$ )	Average ( $\mu\text{m}$ )	Strength (kgf/mm <sup>2</sup> )	Tentative strength
1	1.085	0.67	6.70	6.70	6.70		-21.553
2	1.335	0.75	7.40	7.30	7.35		-22.036
3	6.480	1.49	15.00	14.90	14.95		-25.854
4	6.765	1.53	15.20	15.40	15.30		-25.770
5	11.860	1.88	18.90	18.70	18.80		-29.922
6	14.320	1.90	19.00	19.00	19.00		-35.372
7	13.430	1.92	19.20	19.20	19.20		-32.486
8	19.125	2.14	21.50	21.40	21.45		-37.066
9	20.860	2.18	21.90	21.80	21.85		-38.962
10	29.785	2.59	25.90	25.90	25.90		-39.594
11	27.975	2.71	27.10	27.10	27.10		-33.967
12	31.035	3.05	30.60	30.50	30.55		-29.652
13	36.040	3.35	33.50	33.50	33.50		-28.637
14	49.100	3.94	39.20	39.20	39.20		-28.493
15	61.400	4.46	44.60	44.70	44.65		-27.463
Average	-----	-----	23.05	23.02	23.03		
Average	22.040	2.30				-----	-30.455

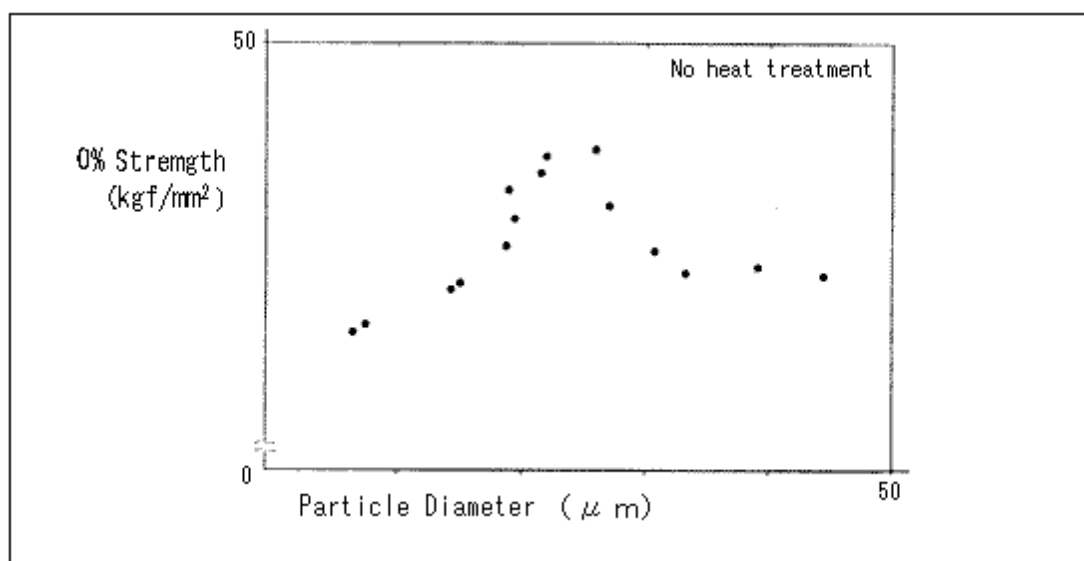


Fig. 2 10%Strength - Particle Diameter plot for untreated sample

Table 2 Test results for treated sample at 200 °C

Testing Conditions							
		File No.			4-200.D2		
Test mode	1	Indenter:			Flate plate 50		
Sample name	Aluminium-Nickel alloy						
Sample No.	4-200						
Testing load	100.00 (gf)				Loading rate constant: 1		
Displacement scale	10 (μm)						
No.	Load (gf)	Displacement (μm)	Diameter (μm)	Diameter (μm)	Average (μm)	Strength (kgf/mm <sup>2</sup> )	Tentative strength
1	1.580	0.65	6.30	6.30	6.45		-33.866
2	2.390	0.78	7.90	7.90	7.85		-34.585
3	4.705	1.12	11.20	11.20	11.20		-33.447
4	6.400	1.25	12.50	12.40	12.45		-36.819
5	12.515	1.67	16.70	16.70	16.70		-40.015
6	13.885	1.80	18.00	18.00	18.00		-38.215
7	15.235	1.83	18.20	18.40	18.30		-40.567
8	20.010	2.07	20.80	20.70	20.75		-41.442
9	23.460	2.26	22.60	22.70	22.65		-40.777
10	29.380	2.54	25.40	25.40	25.40		-40.608
11	34.765	2.85	28.80	28.30	28.55		-38.033
12	43.475	3.42	34.20	34.30	34.25		-33.048
13	43.970	3.81	38.20	38.00	38.10		-27.011
14	49.555	4.13	41.30	41.30	41.30		-25.907
15	46.455	4.16	41.60	41.70	41.65		-23.875
Average	-----	-----	22.91	22.90	22.91		
Average	23.185	2.29				-----	-35.214

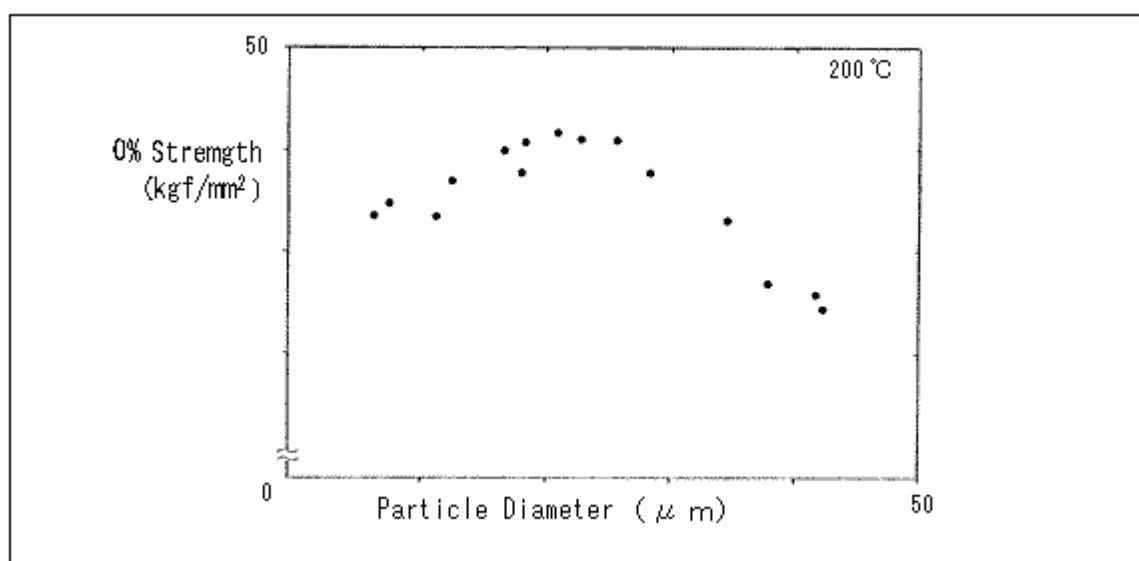


Fig. 3 10%Strength - Particle Diameter plot for sample treated at 200 °C

Table 3 Test results for treated sample at 400 °C

Testing Conditions							
		File No.	4-200.D3				
Test mode	1	Indenter:		Flate plate 50			
Sample name	Aluminium-Nickel alloy						
Sample No.	4-400						
Testing load	100.00 (gf)			Loading rate constant: 1			
Displacement scale	10 (μm)						
No.	Load (gf)	Displacement (μm)	Diameter (μm)	Diameter (μm)	Average (μm)	Strength (kgf/mm <sup>2</sup> )	Tentative strength
1	1.170	0.68	6.80	6.90	6.85		-22.235
2	1.655	0.83	8.20	8.20	8.20		-21.948
3	3.205	1.11	11.00	11.00	11.00		-23.620
4	5.145	1.35	13.60	13.40	13.50		-25.174
5	7.000	1.54	15.40	15.40	15.40		-26.320
6	9.880	1.91	19.20	19.00	19.10		-24.150
7	10.945	1.99	19.90	20.00	19.95		-24.522
8	12.190	2.10	21.00	21.00	21.00		-24.649
9	14.170	2.26	22.60	22.70	22.65		-24.630
10	18.190	2.73	27.40	27.20	27.30		-21.764
11	22.520	3.00	30.10	29.90	30.00		-22.313
12	24.550	3.11	31.10	31.20	31.15		-22.561
13	34.590	3.73	37.30	37.40	37.75		-22.110
14	44.200	4.06	40.60	40.60	40.60		-23.911
15	41.850	4.30	43.80	42.20	43.00		-20.183
42.20	-----	-----	23.20	23.07	23.14		
23.07	16.751	2.31				-----	-23.339

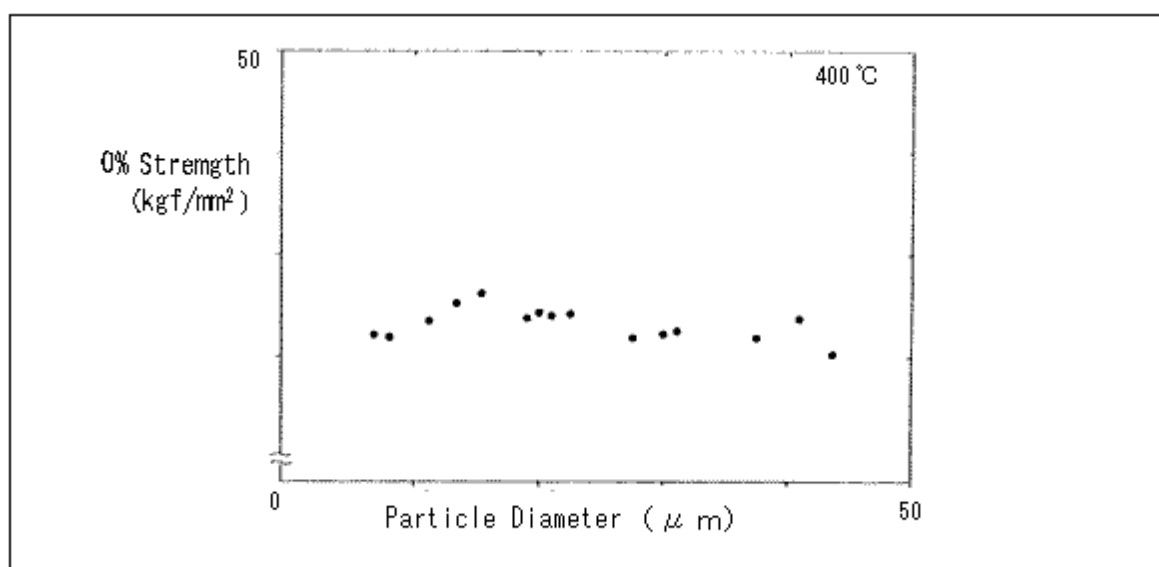


Fig. 4 10%Strength - Particle Diameter plot for sample treated at 400 °C

#### ■ Test results

Measured data are given in Tables 1 - 3 and Figs. 2 - 4.

Figs. 2 through 4 display 10% strength - particle diameter plots. The strength of the sample without heat treatment abruptly rises to approx. 40 kgf/mm<sup>2</sup> at a particle diameter of around 25 µm, as shown in Fig. 2. Compared with the specimen without heat treatment, the specimen with heat treatment at 200 °C has a

high level of strength at 35 to 40 kgf/mm<sup>2</sup> in the lower particle diameter range (below 20 µm). The strength of the sample with heat treatment at 400 °C remains at a low level of around 25 kgf/mm<sup>2</sup> without any significant variation across diameters. As shown above, this data provides much information about the difference of strength depending on diameter size or method of heat treatment.

\* Please be advised that data obtained before the implementation of the current Weights and Measures Law may be presented in terms of gravimetric unit.



## Compression-Rupture Test of Carbon Fibers with Different Tensile Characteristics Shimadzu Micro Compression Testing

### ■ Introduction

As the result of recent progress of research and development, carbon fiber materials have been put to practical use in a wide range of implements, including space aircraft parts, sporting goods like golf club shafts and tennis rackets, structure materials that must transmit X-rays, and acoustic materials.

A group of high-quality carbon fibers is further classified, according to its tensile strength, into several groups. One of these is a high-strength fiber group that features in excellent tensile strength; another is a high-elasticity fiber group characterized by high flexibility, but with a tensile strength of no more than around 2,000 MPa.

As described above, data on mechanical properties are indispensable information for classifying fibers.

The following is an example of tests for evaluation of physical behaviors under a compressive force applied to carbon fibers (single fibers) having different tensile strength levels with Shimadzu Micro Compression Testing Machine MCT.

### ■ Testing Conditions

- (1) Testing mode: compression test
- (2) Testing load: 200 gf
- (3) Loading rate constant: 1 (4,230 gf/sec.)
- (4) Calculation of strength: Compression strength is calculated by the following equation. \*1

$$ST = 2 \cdot P \cdot \pi \cdot d \cdot L$$

where:

ST: tensile strength (kg/mm<sup>2</sup>)  
P: compression strength (kgf)  
d: diameter of fiber (mm)  
L: length of fiber (mm)

**Note \*1:** from JIS A1113-1976 Method of tests for splitting tensile strength of concrete



## ■ Test Piece

- (1) Name: Carbon fibers (PAN type carbon fibers)
- (2) Types: 1 (high-ductility type)  
2 (high-strength type)  
3 (ultra-high elasticity type)
- (3) Shape: See Fig. 1

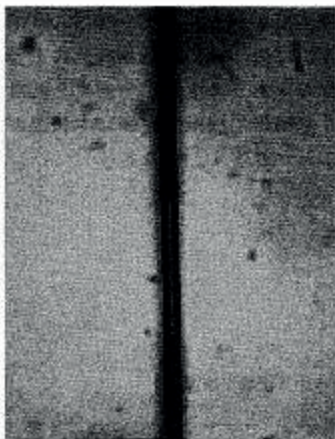


Fig. 1 A Microscopic photograph of Test Piece before Test



Fig. 2 A Microscopic photograph of Test Piece after Test

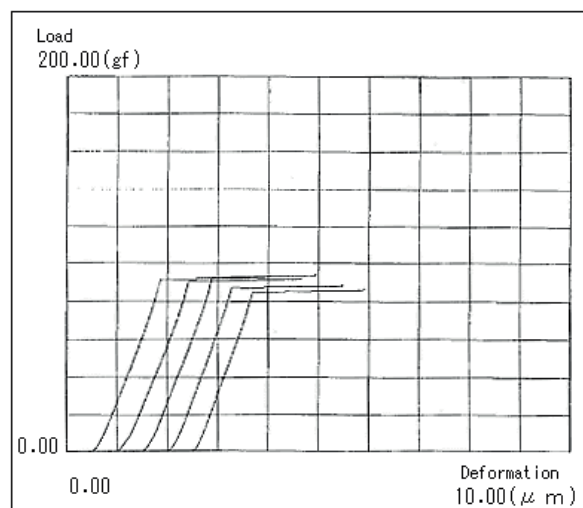


Fig. 3 Load- Deformation Curves of High Ductility Samples

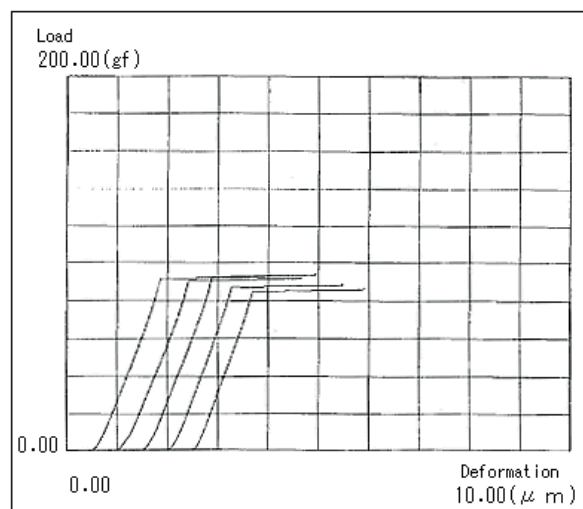


Fig.2 Load-Deformation Curves of High Ductility Samples

Fig. 4 Load- Deformation Curves of High Ductility Samples

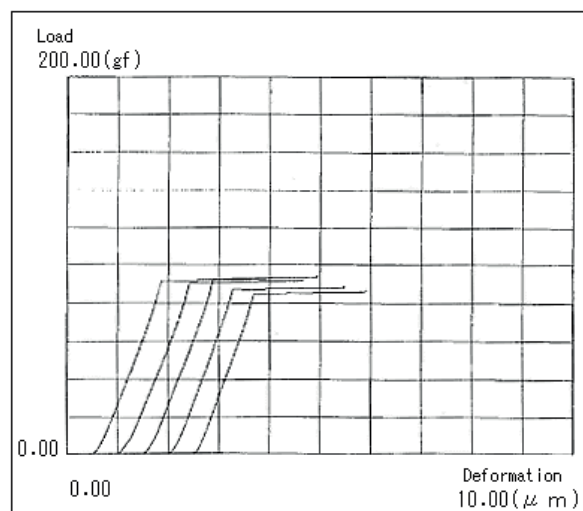


Fig. 5 Load- Deformation Curves of High Ductility Samples

Type of test piece	Compression-rupture strength(kgf/mm <sup>2</sup> )	Standard deviation (kgf/mm <sup>2</sup> )
High-ductility type	149.90	3.23
High-strength type	151.09	6.34
Ultra-high elasticity type	68.87	4.37

Table 1 Results of Compression-Rupture Test of Carbon Fibers

**Note:** The length of the indenter diameter (50 mm) was used for the length of fiber because the test piece was extraordinarily long.

## ■ Test Results

Table 1 shows a summary of test data, and Figs. 2-4 show the compression-rupture strength and the overlapping view of load-deformation curves for each test piece.

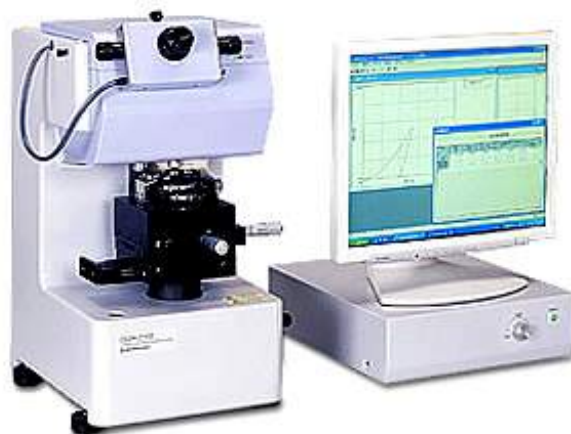
The difference of behavior between test pieces are observable in the load-deformation curves of Figs. 2-4.

The test pieces of the high-ductility type and the high-strength type have similar compression-rupture strength, while the ultra-high elasticity type has a remarkably low compression-rupture strength. (Refer to Table 1)

Admitting some deviation among the test data as a result of the surface conditions of the test pieces, the test results ensure that this testing machine is useful and effective for evaluation of mechanical properties of single fibers, provided that data are processed statistically.

\* Please be advised that data obtained before the implementation of the current Weights and Measures Law may be presented in terms of gravimetric unit.

## Evaluation of Surface Hardness of Audiotapes with Shimadzu Dynamic Ultra Micro Hardness Tester Model DUH



### ■ Introduction

Music cassette tapes are used by an enormous number of music lovers to enjoy beautiful sounds whenever and wherever they wish. High quality audiotapes with low noise levels are required to reproduce the full dynamic range of any music with a stable and balanced sound volume.

Ultra micro magnetic particles are scattered on the surface of the high polymer substrates of audiotapes. Audiotapes are classified into several types depending on the kinds of magnetic materials, each of which have respective frequency characteristics.

The following presents the result of surface hardness evaluation performed on audiotapes from several manufacturers using the Shimadzu Dynamic Ultra Micro Hardness Tester Model DUH. This unit works on the principle of a micro area measuring technique for providing information about the surface hardness of tape materials.

### Measurement of hardness of audiotapes

#### (1) Samples:

Brand A TYPE1 (NORMAL)  
Brand B TYPE1 (NORMAL)  
Brand C TYPE2 (CrO<sub>2</sub>)  
Brand D TYPE2 (CrO<sub>2</sub>)  
Brand E TYPE4 (METAL)  
Brand F TYPE4 (METAL)

#### (2) Testing machine

- 1) Shimadzu Dynamic Ultra Micro Hardness Tester Model DUH
- 2) Thin film attachment (type 2)

Test Mode	2
Cal. Mode	1 (115° triangular pyramid indenter)
Auto or Manual	Auto
F.S. Depth	2μm
Max. Load	0,5gf
Loading Speed	5 or 10
After Time	5sec
Pre Time	5sec
LOT	3

Table 1 Test Conditions

**Fig.1** shows dynamic hardness determined by the difference of displacement at two different loads.

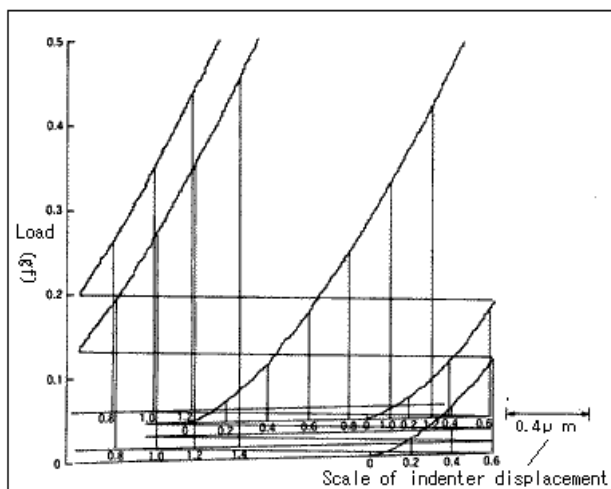


Fig. 1 Load – Indentation Depth Curves for Audiotape (Type 1)

Dynamic hardness was calculated by the following equation:

$$DH(115^\circ) = 37,838 \cdot \frac{P_2}{(D_2 - D_1)^2} \cdot \left(1 - \sqrt{\frac{P_1}{P_2}}\right)^2$$

DH(115°): Dynamic Hardness  
P1: Small testing load (gf)  
P2: Large testing Load (gf)  
D1: Indentation depth at P1 (μm)  
D2: Indentation depth at P2 (μm)

**Figs.2, 3 and 4** show hardness variations of respective tapes of types 1, 2, and 4 at various depths. The tape type 2 of brand C showed the highest surface hardness. The tape type 2 from brand D showed a hardness peak at 0.4 to 0.6 μm, suggesting a hard layer at that depth. The metallic tapes of type 4 from brands E and F show similar hardness properties. As seen above, useful information is attainable for evaluating micro hardness differences due to different processing or treatments of tape surfaces.

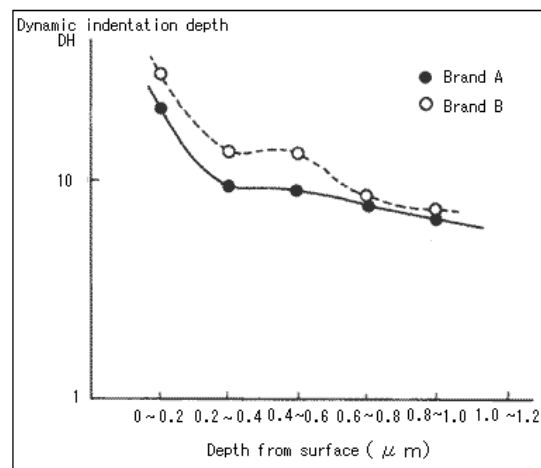


Fig. 2. Hardness from Surface towards Depth Direction on Audiotape Type 1

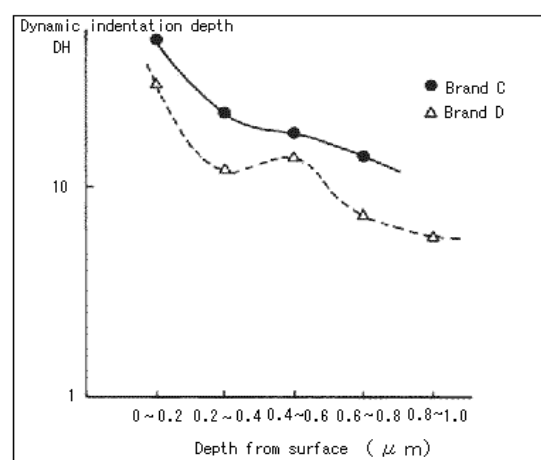


Fig. 3 Hardness from Surface towards Depth Direction on Audiotape Type 2

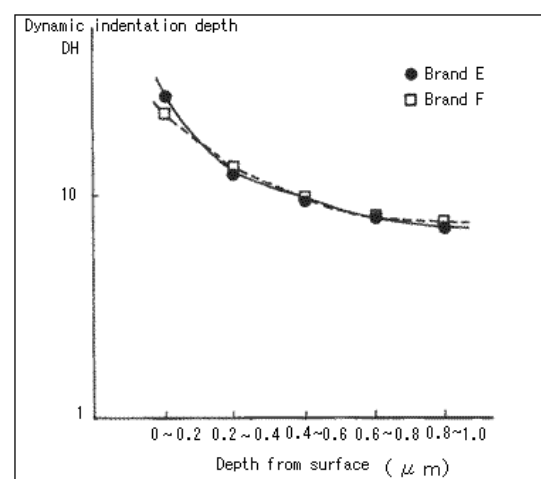


Fig. 4 Hardness from Surface towards Depth Direction on Audiotape Type 4

## Application News

No. SCA\_300\_021

Material Testing System DUH

### Hardness Measurement of Plastic Tubes using the Shimadzu Dynamic Ultra Micro Hardness Tester DUH-W211S



#### ■ Introduction

Light, strong and rust-free plastic tubes (pipes) are widely used for transporting liquids and gases, and for insulating and protecting electrical wiring. In these fields, the hardness of the tube material is an important factor that affects the usage conditions. If the tube is cut lengthways and held flat before measuring its hardness, the elasticity of the plastic causes minute bending (see Fig. 1) that impedes accurate measurement. Here, we present results from a test method that is ideal for such situations.

#### 1. Sample

(Plastic Tube)

- 1) Sample name: Plastic tube
- 2) Sample No.: No.1 to No.3
- 3) Sample size:  $\phi 2.2$  (Outer diameter) x  $\phi 1.2$  (Internal diameter) x 10 (Length) mm

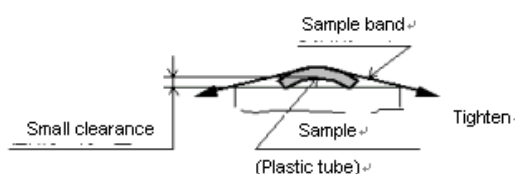


Fig.1

#### 2. Test conditions

- 1) Testing machine: Shimadzu Dynamic Ultra Micro Hardness Tester DUH-W201S
- 2) Indenter: Triangular pyramid indenter with tip angle 115° (Berkovitch type)
- 3) Test mode: Load - Load hold test
- 4) Test force: 9.8 mN
- 5) Loading rate: 0.284 mN/sec
- 6) Sample holding time: 1 sec
- 7) Temperature: 25 °C

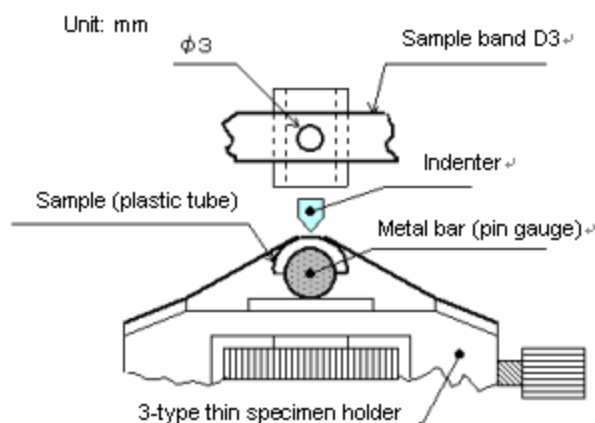


Fig.2



## 1. Test Method

The sample (plastic tube) was cut lengthways into two and set on a metal bar (pin gauge  $\varnothing$  1.2) as shown in Fig.2 to measure its hardness by indentation.

## 2. Test Results

1) Results of the hardness measurements are shown in Table 1, Fig.3 and Fig.4.

2) The DHT<sub>115</sub> values in Table 1 shows that the Sample No.1 is the hardest, followed by No.2 and No.3 in that order, when tested with the test force of 9.8 mN. Fig.4 (graph that presents the relation of test force and indentation depth) shows that the elasticity of the tube is correctly detected, validating the effectiveness of the data.

Table 1 Hardness measurement results (mean values)

Sample name	Sample No.	Dynamic hardness (DHT <sub>115</sub> )	Test force (mN)	Indentation depth (μm)
Tube A	No. 1	15.6	9.8	1.55
Tube B	No. 2	13.7	9.8	1.66
Tube C	No. 3	11.7	9.8	1.8

Ref.) Dynamic hardness was calculated as follows:

$DHT_{115} = 3,8584 P / D^2$

DHT<sub>115</sub>: Dynamic hardness (115° triangular indenter)

P: Test force (mN)

D: Indentation Depth (μm)

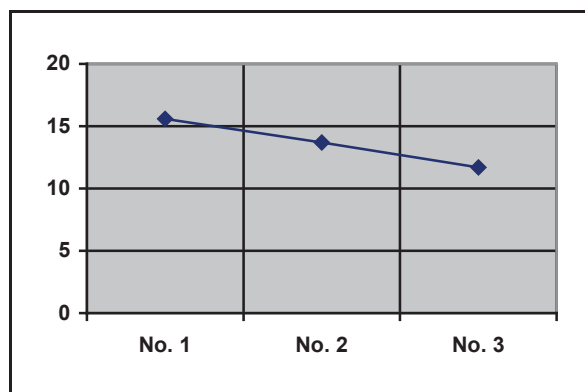


Fig. 3  
Sample number and dynamic hardness (DHT)

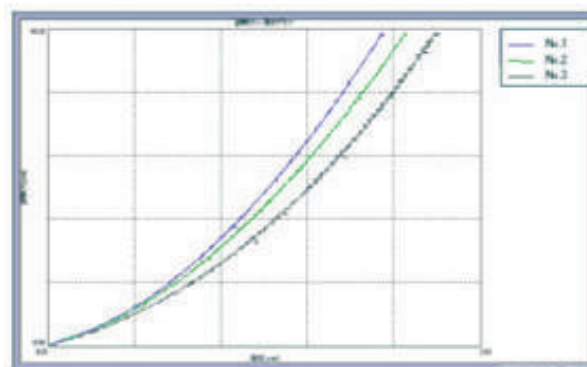


Fig. 4 Test force – indentation depth curve

\* Please be advised that data obtained before the implementation of the current Weights and Measures Law may be presented in terms of gravimetric unit.

## Application News

No. SCA\_300\_039

Material Testing System DUH

### **Evaluation of Elastic Recovery in Hardness Measurement of Plastic Materials with Shimadzu Dynamic Ultra Micro Hardness Tester**



Plastics often show viscoelasticity. They can be deformed by a relatively small external force, but return to their original state if the external force is removed. In addition, many plastics have a hardness dependent on their mechanical properties. Elastic recovery and temperature are the essential factors for the evaluation of the mechanical hardness of plastics.

The Shimadzu Dynamic Ultra Micro Hardness Tester allows you to measure the hardness of thin films and thin layers using the indentation depth of the indenter (dynamic indentation

hardness) or the diagonal length of indentation (micro Vickers hardness). This instrument can thus measure the hardness of various specimens from hard to soft materials, and has an extremely broad range of applications. Here, we will introduce an example of a hardness test in which this Ultra Micro Hardness Tester, installed in a room of constant temperature, was used to measure and compare the elastic recovery of two types of plastics, which have similar dynamic indentation hardness: nylon 66 and polyethylene.

#### **Test conditions**

Indenter:	Vickers
Maximum load:	50 gf
Retention time:	1 sec
Deformation scale:	10 $\mu$ m

## Test method

Load is applied up to 50 gf using the cyclic loading function of the Ultra Micro Hardness Tester. After the load is retained for one second, the load begins to decrease until it reaches zero. The depth of the indenter is measured at two points, when the load reaches

50 gf and when it returns to zero. The discrepancy in load between these two points is regarded as the amount of elastic recovery. The dynamic indentation hardness when the Vickers indenter is used is calculated by the following equation:

$$DH = 37,838 P/h^2$$

P : Test load (gf)

H : Indentation depth ( $\mu\text{m}$ )

Table 1 Test Results

	Nylon 66	Polyethylene
Load (gf)	50,00	50,00
Indentation depth when load reaches 50gf ( $\mu\text{m}$ )	18,20	19,13
Indentation depth when load returns to 0 ( $\mu\text{m}$ )	7,65	13,06
Amount of elastic recovery ( $\mu\text{m}$ )	10,55	6,07
Dynamic indentation hardness	5,71	5,17

## Test results

The test results are shown in Table 1, Figure 1 and 2.

As indicated by the table and figures, there is a major difference in the amount of elastic recovery between these two types of plastics despite their similar dynamic indentation hardness (that of nylon 66 is slightly greater

than that of the other). It is therefore presumed that in the method to measure the diagonal length of indentation, nylon 66 will exhibit a considerably higher hardness than that of polyethylene.

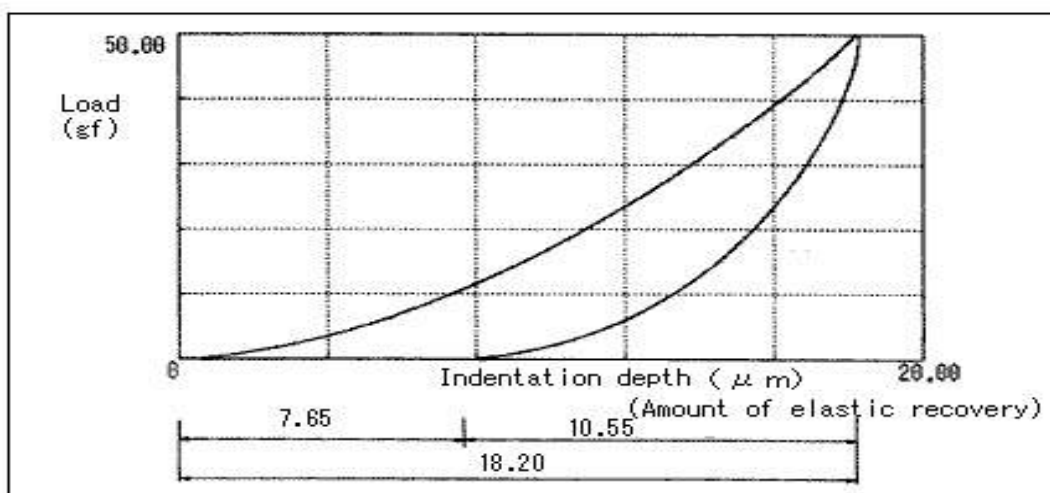


Fig. 1 Diagram of load Indentation Depth Relationship for Nylon 66

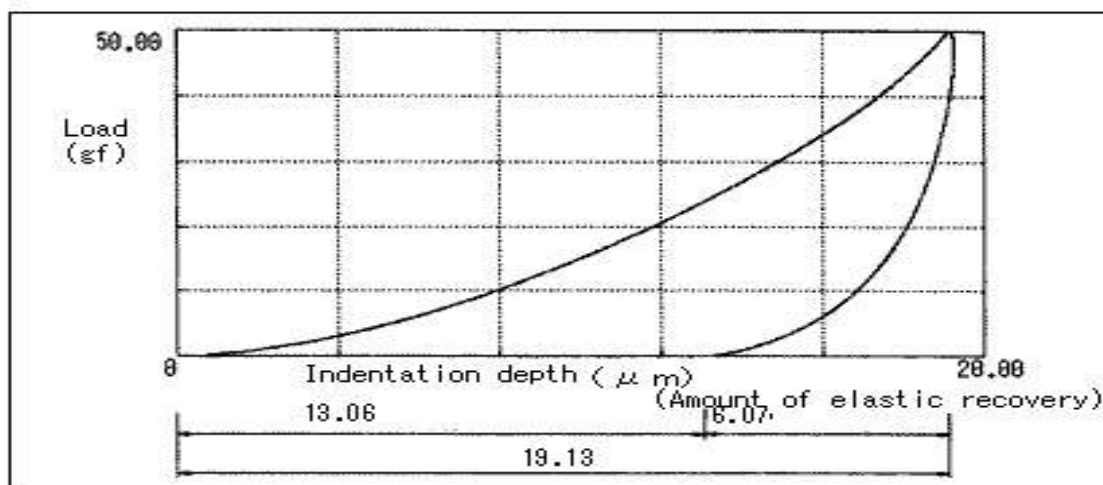


Fig. 2 Diagram of load Indentation depth for Polyethylene

\* Please be advised that data obtained before the implementation of the current Weights and Measures Law may be presented in terms of gravimetric unit.



## 6. Materials Testing & Inspection

---

### 6.4 High-Speed Video Camera

---

A combination of tensile testing machine and HPV-X2 high-speed video camera enables the measurement of distortion and test force under high-speed loads. The HPV-X2 can record the breaking of specimens at a high image capture speed of 10 million frames per second (fps), and the breaking of specimens can be expressed in sync with S-S curves by performing image analysis.

<b>V22</b>	High-speed imaging of fuel injection in automotive engines
<b>C225-E035</b>	High-speed material testing with 3D strain visualization!
<b>i247</b>	Material testing by strain distribution visualization – DIC analysis
<b>V21</b>	Observation of bending fatigue testing of metal plate at ultrasonic frequency
<b>V19</b>	Observing the failure of open-hole cfrp specimens in tensile tests
<b>No. 37</b>	Observing the failure of open-hole CFRP specimens in tensile testing
<b>No. 38</b>	Observing the fracture of unidirectional CFRP in static tensile testing
<b>No. 39</b>	Evaluation of open-hole CFRP
<b>V18</b>	Observing the fracture of unidirectional CFRP in static tensile testing
<b>SCA_300_059</b>	Observation of fracture in CFRP tensile test



# Application News

## No. V22

### High-Speed Video Camera

## High-Speed Imaging of Fuel Injection in Automotive Engines

### ■ Introduction

An important observational method. As an example, gasoline being injected from the injector and adhering to the cylinder walls is considered to be a cause of fine particles with a diameter of 2.5 micrometers or smaller (PM<sub>2.5</sub>), harmful particles contained in exhaust gas. In addition, ensuring that the gasoline is refined and homogenized during injection is important in regards to improving fuel efficiency.

This article introduces images of fuel injection by an injector, and the collision of the injected spray against a wall surface, obtained using the HPV-X2 high-speed video camera.

### ■ Measurement System

The HPV-X2 high-speed video camera was used in this experiment. Table 1 shows the instruments used. Instead of using a real engine, the experiment was performed with an injector placed on top and a flat plate below.

### ■ Results

Fig. 2 shows the test configuration. Figs. 3 to 6 show images obtained. Images were recorded in proximity to the nozzle outlet, as well as 1 mm, 2 mm, and 4 mm below the nozzle. It is evident that the fuel collected in proximity to the nozzle disperses as it travels downwards.

The fuel injected from the nozzle ultimately collides with the cylinder wall. Fig. 7 shows how the fuel collides with the cylinder wall. Image (2) in Fig. 7 clearly shows the collision of a droplet approximately 40 μm in diameter with the wall. Among the droplets produced after the collision, a droplet as small as 10 μm in diameter could be confirmed as indicated by the arrow in image (9).

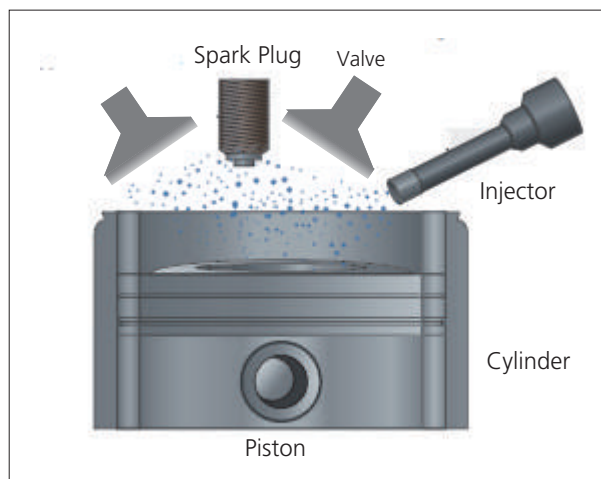


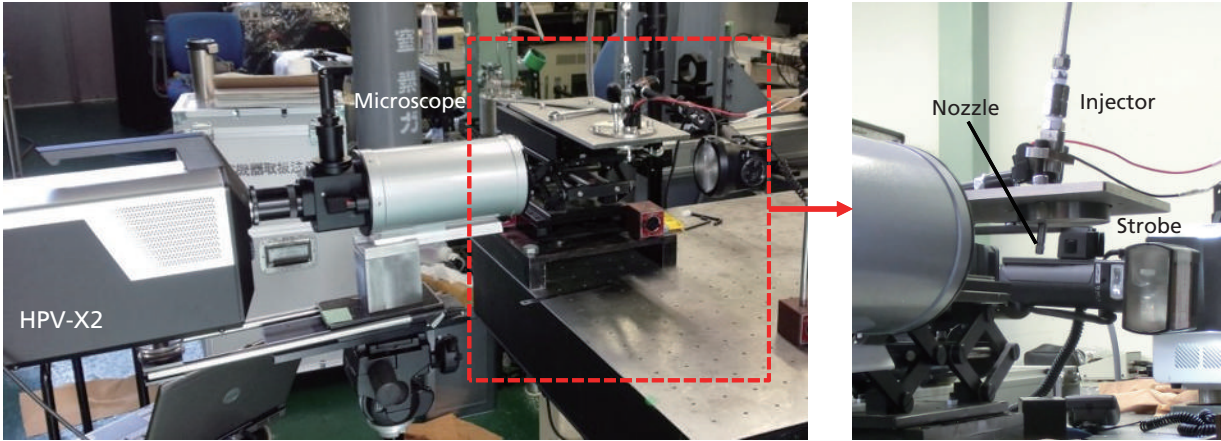
**Fig. 1 Structure of an Automotive Engine**

**Table 1 Experimental equipment**

High-Speed Video Camera	: HPV-X2
Microscope	: Long Range type
Light Source	: Strobe Light

**Table 2 Imaging Conditions**

Frame Rate: 10M frame/sec (Injection)
2M frame/sec (Collision)



Overall Setup (left); Around the Nozzle (right)  
Fig. 2 Test Configuration

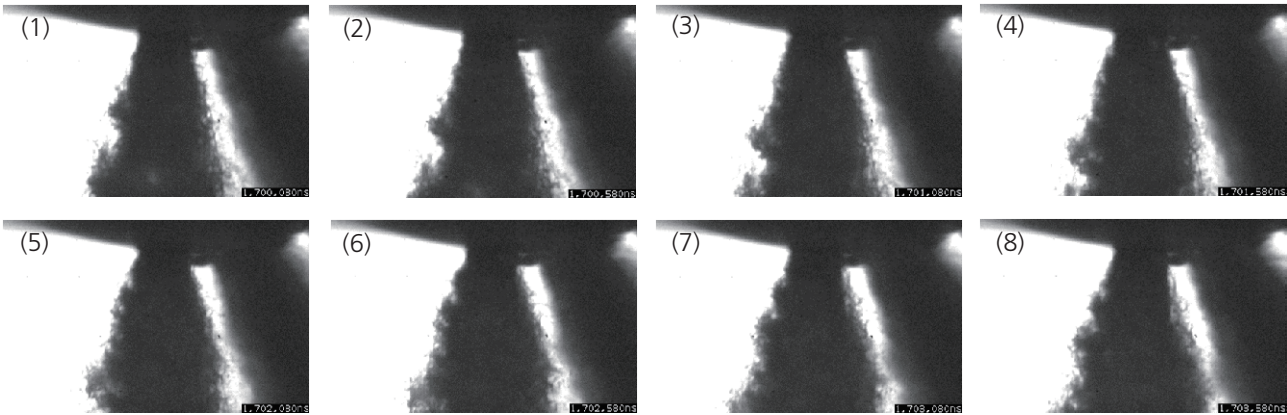


Fig. 3 Proximity to the Nozzle Outlet (500 nsec between images)

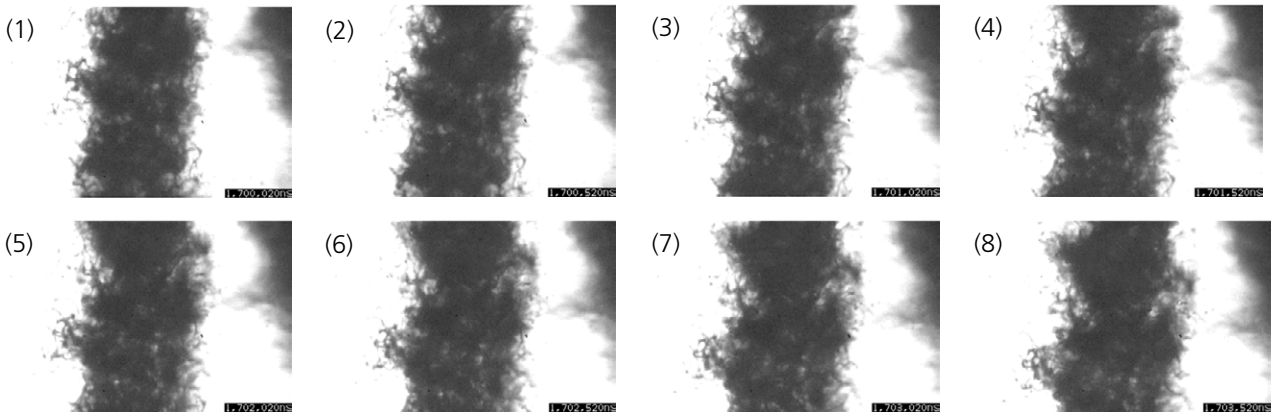


Fig. 4 1 mm Below the Nozzle (500 nsec between images)

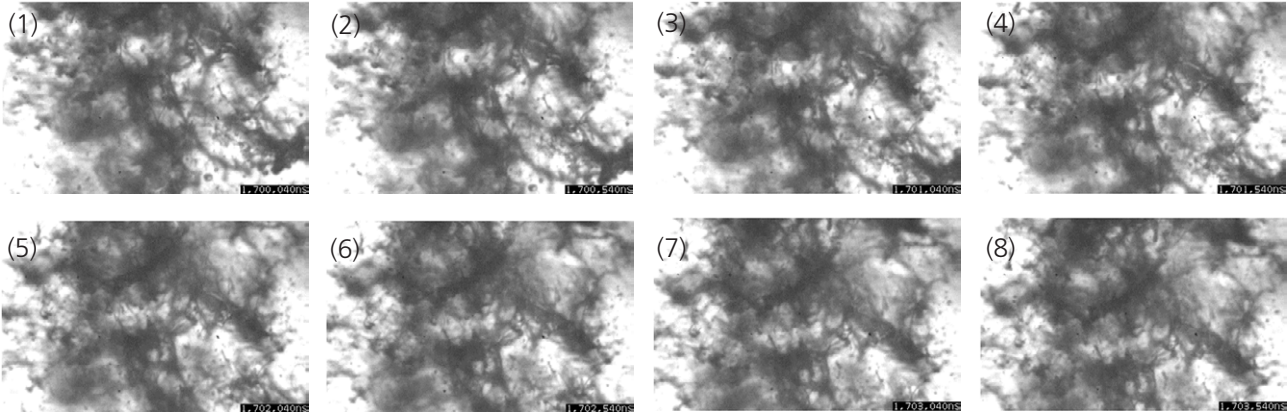


Fig. 5 2 mm Below the Nozzle (500 nsec between images)

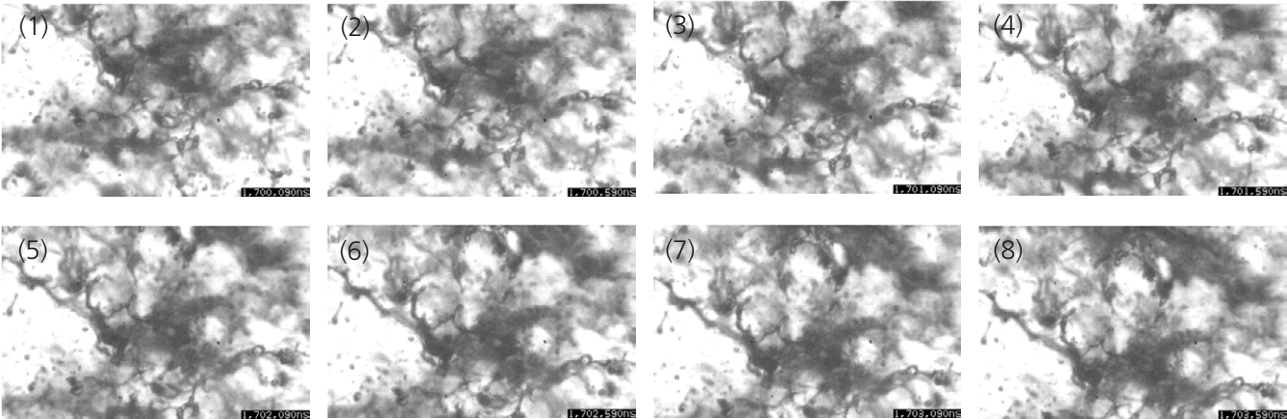
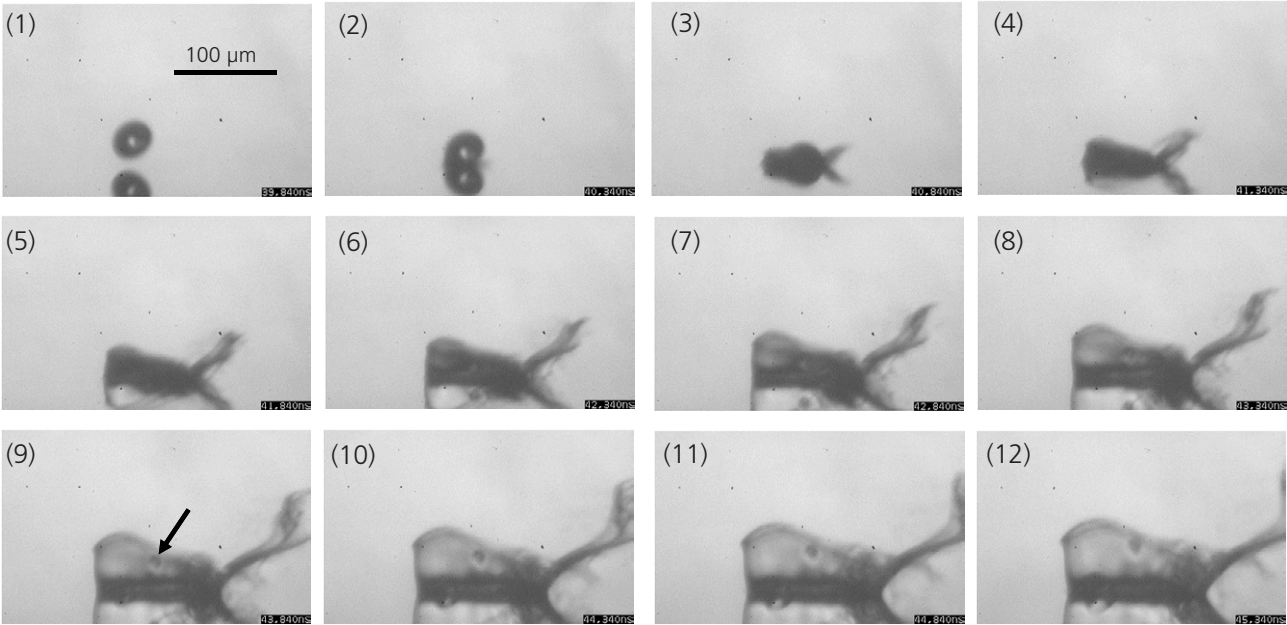


Fig. 6 4 mm Below the Nozzle (500 nsec between images)



Data provided by: Professor Kawahara, Okayama University

Fig. 7 Collision with the Wall (500 nsec between images)

## ■ Conclusion

Images of fuel injection by an injector, and the collision of the injection spray against a wall surface were taken using the HPV-X2 high-speed video camera. The speed of injection from the injector is very fast, and may reach 140 m/sec depending on the injection pressure. As a result, a recording speed of at least 10 Mfps is required to observe such a high speed phenomenon with a microscope. With the conventional model (HPV-X), clear images were not obtained due to insufficient sensitivity.

The HPV-X2 has at least six times the sensitivity of the HPV-X however, so the fine structure of the injection spray and the quality of the liquid are captured even through a microscope. The collision of the injection spray with the wall is also clearly recorded, and the size of the scattered particles can be measured using image processing software. The use of the HPV-X2 in this way can thus serve a role in the development of automobile engine injectors.

First Edition: Jul. 2015





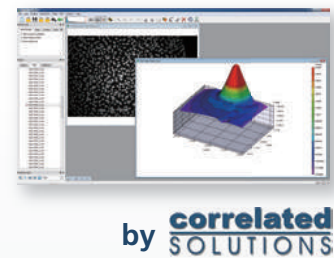
# High-Speed Material Testing with 3D Strain Visualization!



High-Speed Tensile Testing Machine  
**Hydrosot HITS-T10**



High-Speed Video Camera  
**Hyper Vision HPV-X2**

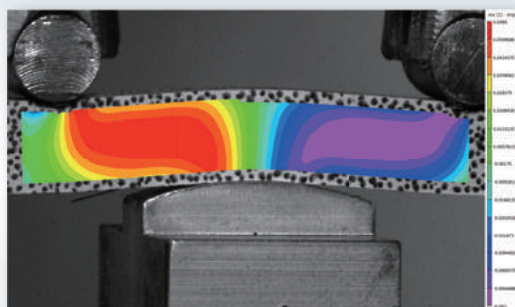


3D Deformations Analysis Software  
**VIC-3D**

- Visualize the strain distribution of rapidly occurring deformations in a specimen.
- Supports 3D strain distribution through synchronized recording with two HPV-X2 cameras.
- Directly control the HPV-X2 cameras using the strain distribution software (VIC-3D).

For evaluating the strength of CFRP, much attention has been placed on high-speed bending tests that are conducted under conditions that are as close as possible to the actual conditions of use. During the high-speed bending test of materials, deformations occur rapidly in a three-dimensional way. Since strain is distributed locally, conventional methods of measurement presented difficulties. With 3D-DIC, two HPV-X2 cameras are used, making it possible to dynamically measure strain distribution in a three-dimensional manner.

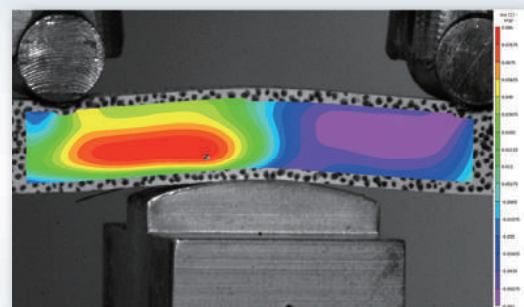
## Strain Distribution Presented by High-Speed, Three-Point Bending of CFRP



Before Interlaminar Peeling



After 1.5  $\mu$ s



After Interlaminar Peeling



## HPV-X2 Specifications

Lens Mount	Nikon F-mount	
Image Sensor	FTCMOS2 Image sensor	
Recording Speed (frames per second (fps))	HP mode	10 Mfps, 5 Mfps (fixed)
	FP mode	5 Mfps (fixed)
Resolution	Both modes	Variable recording speed between 60 fps and 2 Mfps
	HP mode	50,000 pixels (zigzag lattice pixel array)
	FP mode	100,000 pixels (400 × 250)
Color/ Gradations	Monochrome/, 10 bits	
Number of Frames Recorded	HP mode	256 frames
	FP mode	128 frames
Exposure Time	Approx. 50 ns at 10 Mfps, 110 ns at 5 Mfps	
	Variable in a 10 ns interval starting from 200 ns in a range from 60 fps to 2 Mfps	
External Trigger Input	Two channels (TRIGIN, STANDBY) TTL/contact	
External Monitor Output	NTSC	
Input/Output Ports	1000 Base-T / 100 Base-TX	
Trigger Mode	Internal trigger, external trigger, continuous trigger	
Dimensions (camera head)	W 160 × D 330 × H 260 mm	
Weight (camera head)	Approx. 6.4 kg	



Shimadzu Corporation

[www.shimadzu.com/an/](http://www.shimadzu.com/an/)

### For Research Use Only. Not for use in diagnostic procedures.

This publication may contain references to products that are not available in your country. Please contact us to check the availability of these products in your country.

Company names, products/service names and logos used in this publication are trademarks and trade names of Shimadzu Corporation, its subsidiaries or its affiliates, whether or not they are used with trademark symbol "TM" or "®".

Third-party trademarks and trade names may be used in this publication to refer to either the entities or their products/services, whether or not they are used with trademark symbol "TM" or "®".

Shimadzu disclaims any proprietary interest in trademarks and trade names other than its own.

The contents of this publication are provided to you "as is" without warranty of any kind, and are subject to change without notice. Shimadzu does not assume any responsibility or liability for any damage, whether direct or indirect, relating to the use of this publication.

© Shimadzu Corporation, 2016

# Application News

## No.i247

### Material Testing System

## Material Testing by Strain Distribution Visualization – DIC Analysis –

### ■ Introduction

Strain distribution in samples is an increasingly important component of material testing.

As background to this trend, CAE (Computer Aided Engineering) is an analytical technology that is becoming widely used in the fields of science and industry due to the cost savings achieved through the reduced use of costly prototyping which is now being replaced by computerized product design simulation. A typical requirement is to conduct mechanical testing analysis of the region of a product in which strain is likely to occur, and to elucidate the correlation between the simulated analysis results and the strain distribution obtained in actual mechanical testing.

DIC (Digital Image Correlation) analysis is a technique used to compare the random patterns on the surface of a test sample before and after deformation to determine the degree of deformation of the sample. The advantages of this technique include the ability to measure displacement and strain distribution from a digital image without having to bring a sensor into contact with a test sample, and without requiring a complicated optical system. For these reasons, application development for DIC analysis is expanding into a wide range of fields in which measurement using existing technologies<sup>\*1</sup> has been difficult.

Here we introduce examples of DIC analysis of CFRP (Carbon Fiber Reinforced Plastic) and ABS resin high-speed tensile impact testing.

<sup>\*1</sup>: Up to now, material strain distribution measurement has been conducted using various methods, including the direct attachment of large numbers of strain gauges to the test material. However, this method is not applicable for micro-sized samples to which strain gauges either cannot be attached, or attachment is difficult and complicated. These disadvantages also include the difficulty in measuring certain types of substances, such as films, that are easily affected by contact-type sensors.

### ■ Test Conditions

Fig. 1 shows the testing apparatus and software used in the high-speed tensile testing of CFRP. The test conditions are shown in Table 1, and information regarding the test specimens is shown in Table 2. For this experiment, special-shaped grips for composite materials were mounted to the HITS-T10 high-speed tensile testing machine, and the test specimen was affixed to the grips.

A high-speed HPV-2A video camera was mounted in front of the testing gap between the grips to collect video data of the specimen breaking, and the signal to start camera filming was a displacement signal from the high-speed tensile testing machine. The acquired video data was loaded into the StrainMaster (LaVision GmbH) DIC analysis software, and the strain distribution that occurred in the sample was analyzed.

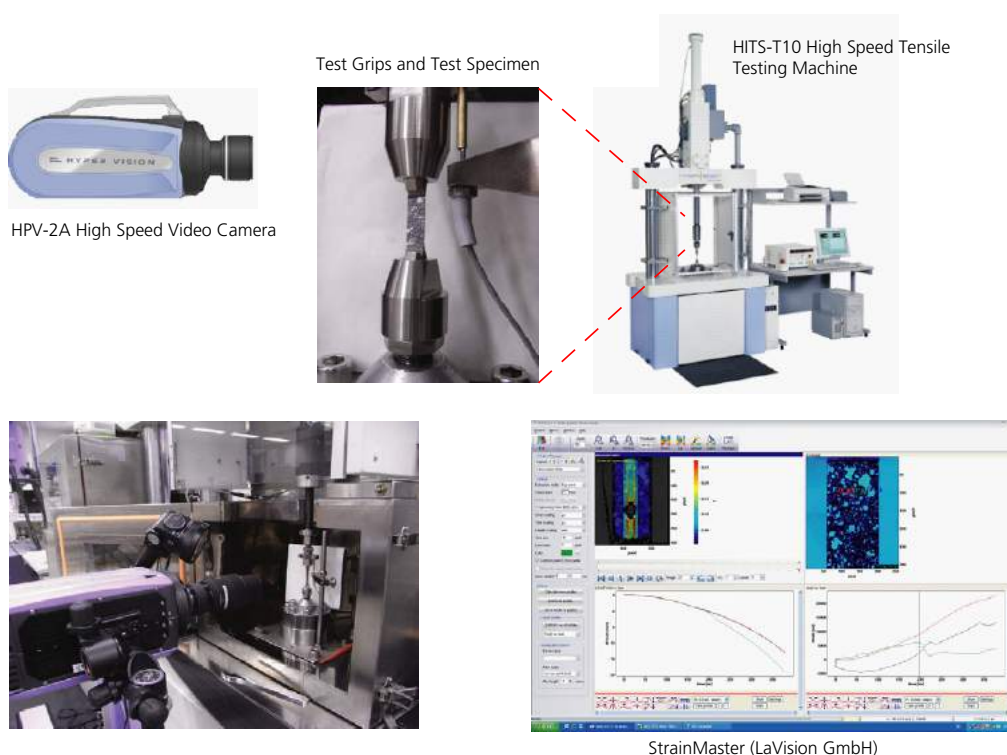


Fig. 1 Testing Apparatus

Table 1 Test Conditions

Instrumentation	HITS-T10 high-speed tensile testing machine
	HPV-2A high-speed video camera
Test Force Measurement	10 kN load cell
Test Speed	10 m/s
Grips	Special grips for composite materials
Sampling	250 kHz
Imaging Speed	500 kfps
Light Source	Strobe
DIC Analysis	StrainMaster (LaVision GmbH) With cooperation of MARUBUN CORPORATION

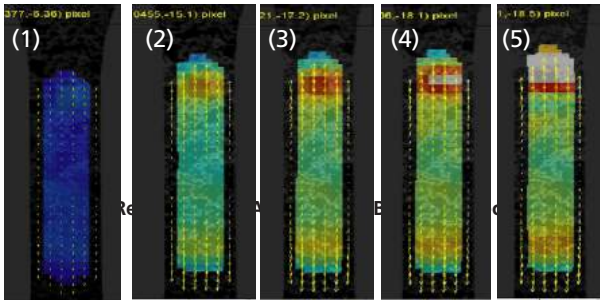
Table 2 Samples

Samples (dimensions)	CFRP-OH <sup>*2</sup> Laminate method [0/90] <sub>2s</sub> <sup>*3</sup> (Hole diameter φ1 mm, W8 × t0.4 reed-shaped)
	ABS resin (ASTM L-shaped test specimen Total length 60 mm, Parallel part 3.2 (W) × 3.2 (T) mm)
Marking	CFRP-OH <sup>*2</sup> : White random pattern ABS resin : Black random pattern

\*2: OH: Abbreviation for Open Hole. Refers to a hole that is opened in a CFRP plate.  
\*3: The CFRP laminate used in this experiment is prepared by laminating prepreg fibers oriented in one direction. The [0/90]<sub>2s</sub> specified for "Laminate method" in the table represents two sets of prepreg layers stacked in the 0° direction and 90° direction.

In this test, the HITS-T10 high speed tensile testing machine and HPV-2A high speed video camera were synchronized to take video at the instant the sample fractured. The sample was prepared prior to the test by spraying paint onto its surface in a random pattern, and the strain distribution on the surface of the test specimen was visualized by DIC analysis based on the amount of shift of the random pattern.

Fig. 2 and Fig. 3 show the DIC analysis results obtained in tensile testing of CFRP-OH and ABS resin test specimens, respectively. The images were extracted in the order of a typical time course analysis (image order corresponding to the numbers shown in images), from the start of the tensile test to the point that the specimen breaks. The appearance of coloring in the images corresponds to the strain distribution in the specimen. The amount of strain that occurs in the specimen corresponds to the degree of color warmth, with areas of darker color (such as blue-black) indicating low strain, and areas of brighter color (such as red-orange) indicating a greater degree of strain. It is clear that in Fig. 2, as the load is applied to the test specimen, the strain increases in the vicinity of the open hole. Because the test specimen is a [0/90]<sub>2s</sub> laminate material, it is believed that the fibers are aligned in the tensile direction in the test specimen surface layer which was subjected to random marking.



In Fig. 3, localized strain occurs from the edge of the parallel region of the test specimen, and as time progresses, localized strain is noticeable at the upper and lower edge of the parallel region. Thus, by combining a high-speed tensile testing machine with a high-speed video camera, in addition to DIC analysis software, it has become possible to visualize the distribution of strain generated in a test specimen.

Test Results

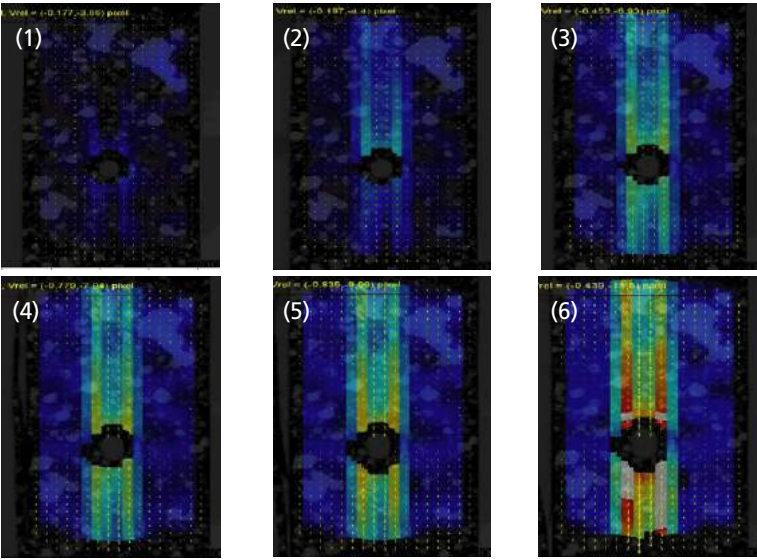


Fig. 2 Results of DIC Analysis of CFRP-OH Specimen

# Application News

No. **V21**

## High-Speed Video Camera

### Observation of Bending Fatigue Testing of Metal Plate at Ultrasonic Frequency

#### ■ Introduction

Fatigue failure refers to the fracture of a component due to repeated load cycles, which can occur using a force much smaller than the static fracture strength. Also, because fatigue-related failure occurs suddenly, there are cases where this has led to serious accidents involving ships and aircraft. Therefore, knowledge of the fatigue properties of materials used in products is very important. However, determination of fatigue characteristics typically requires time-consuming testing using  $10^7$  repetitions (as per JIS Z2273, General Rules for Fatigue Testing of Metals), which at 10 Hz, takes about 12 days to complete. Also, due to enhancements in equipment efficiency and speed, there are now requests for fatigue evaluation with more than  $10^7$  repetitions. In response to this, an ultrasonic testing machine capable of 20 kHz ultrasonic fatigue testing is now in use. However, due to the very rapid vibration that is generated during measurement with this instrument, visual confirmation of the movement and deformation of the specimen is not possible. Therefore, a high-speed video camera was used to observe the movement of a metal plate vibrating while conducting a 20 kHz bending fatigue test. Previously, gaining an understanding of the overall movement of the test specimen required incremental repositioning of a displacement gauge, but with the high-speed video camera, it is possible to evaluate the movement of the specimen in a single observation process. Further, the possibility of determining the amount of movement of the specimen from captured images was also demonstrated.

#### ■ Measurement System

The USF-2000 Ultrasonic Fatigue Testing System and the HPV-X2 high-speed video camera were used for this experiment. Table 1 lists all the instrumentation that was used. Shooting during the test can be conducted at any desired timing. Fig. 1 shows a photograph of the test specimen. For the bending vibration, the vibration modes shown in Fig. 2 are available, with a test specimen dimensioned to resonate for each vibration mode. Here, a test specimen was prepared to provide a second-order bending mode.

**Table 1 Imaging Equipment**

High-speed video camera	: HPV-X2
Microscope	: Z16 APO
Lighting	: Strobe
Testing apparatus	: USF-2000

**Table 2 Measurement Conditions**

Measurement speed	: 2 million frames/sec
Test frequency	: 20 kHz
Test specimen size	: 10.0 × 3.020 × 0.406 mm

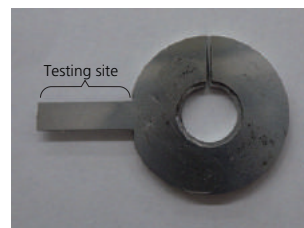


**Fig. 1 Specimen**

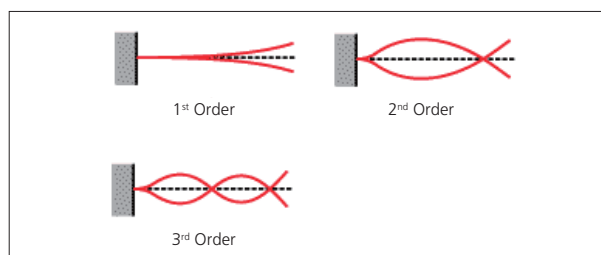


**Fig. 2 Bending Mode Examples**

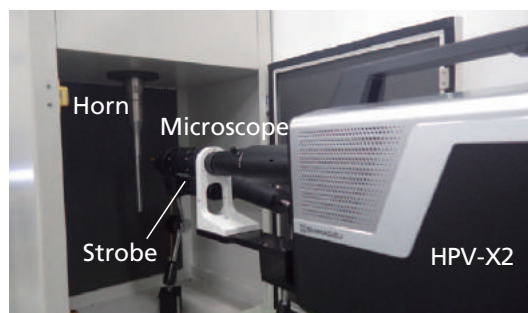


**Fig. 3 Overview of Test**

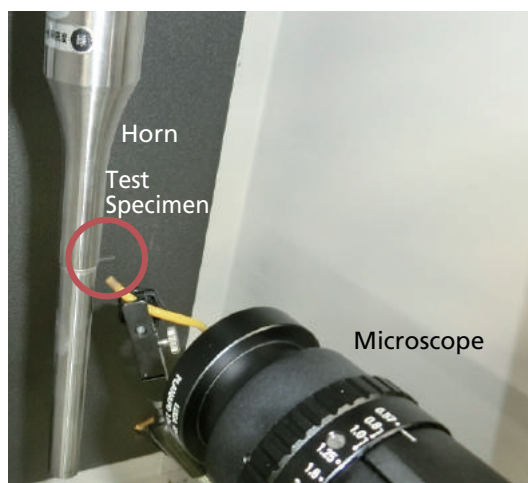


**Fig. 4 Periphery of Specimen**



### ■ Measurement Results

Fig. 3 shows an overview of the test setup, and Fig. 4 shows a close-up view of the vicinity of the specimen. The vibration generated by the actuator is amplified by the horn, causing the specimen to vibrate. Table 2 shows the measurement conditions. To obtain image data at more than 100 frames per cycle, the shooting speed must be set to two million frames/sec. Fig. 5 shows a series of captured images. The blue line traversing the images in Fig. 5 is situated at the center of the specimen in image (1). The central portion of the specimen is shifted in the downward direction as the images proceed from (1) to (3). Then, the center portion of the specimen shifts in the upward direction, reaching a maximum at image (9). From image (9), the specimen center descends once again, returning at image (11) to the same position as in image (1). From the above, the vibration cycle of the specimen was determined to be 20 kHz. Also, from Fig. 5, the specimen tip does not move very much, although it can be seen that the specimen is in a second-order bending mode due to movement of the test specimen center. Applying image processing software to the captured images permits determination of the range of movement of the test specimen. Here, we determined the amount of movement of the central part of the specimen. Fig. 6 shows the relationship between time and the amount of movement of the specimen center. Also, from Fig. 6, the amplitude in the bending test is determined to be about 80  $\mu\text{m}$ , and the vibration frequency is determined to be 20 kHz.

### ■ Conclusion

Fatigue testing of a target component conducted using the ultrasonic frequency was documented using the HPV-X2, and the movement characteristics of the test specimens were confirmed. The HPV-X2 proved to be effective in capturing the high-speed movement generated during the test, and installation of a microscope permitted visual documentation of these minute movements. Aside from this confirmation of movement in the specimen during the test, the actual degree of movement in the test specimen can be determined from the captured images. The USF-2000 calculates the stress amplitude from the amplitude of vibration, thereby permitting the determination of the stress load on the test specimen from the images. Thus, the HPV-X2 can effectively serve in the very important fatigue testing process during product development.

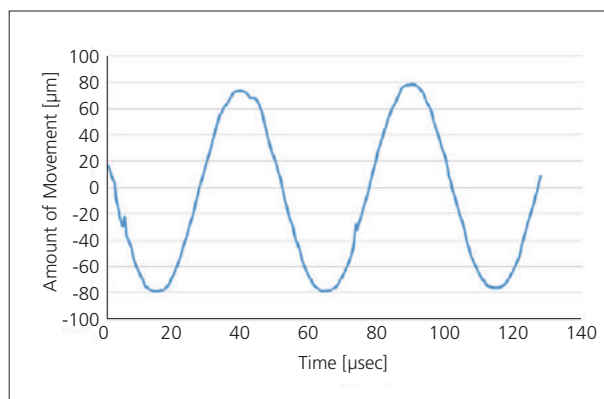


Fig. 6 Amount of Movement of Specimen

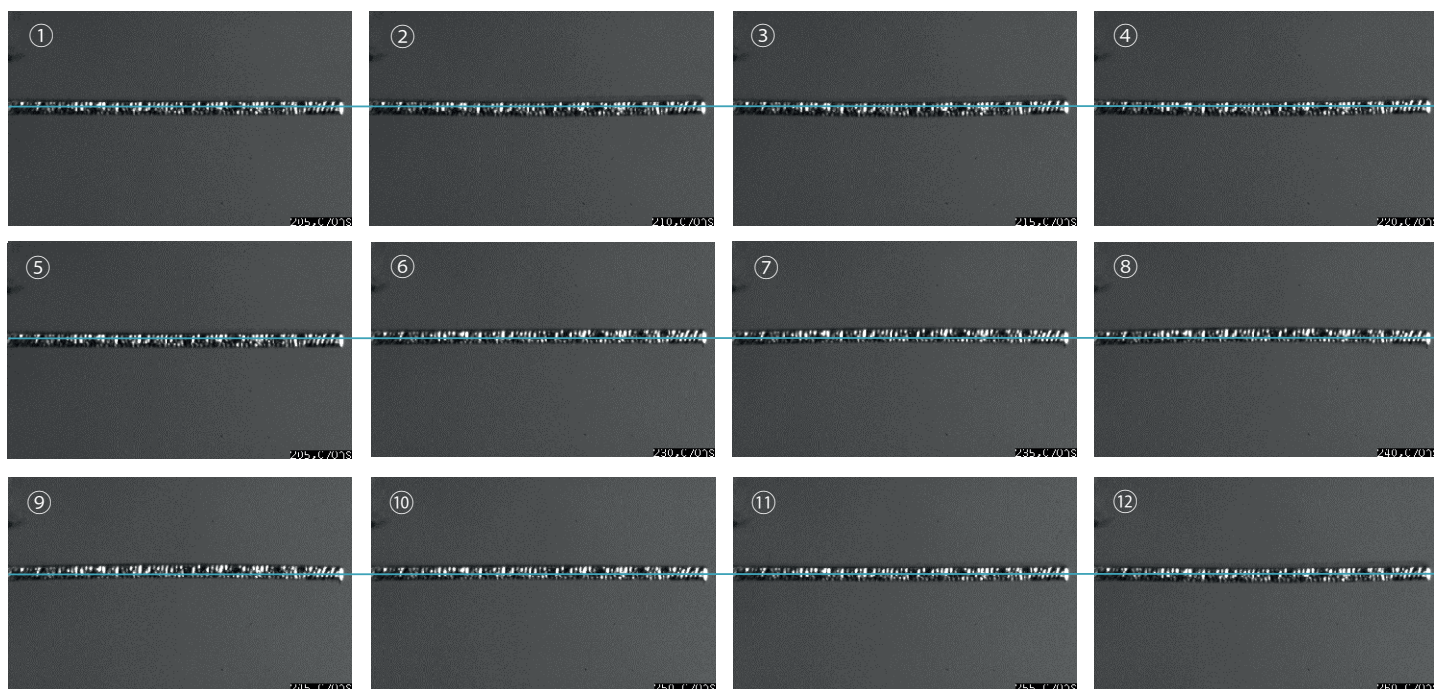


Fig. 5 High-Speed Images (Imaging interval: 5  $\mu\text{sec}$ )

First Edition: Sep. 2015



Shimadzu Corporation

[www.shimadzu.com/an/](http://www.shimadzu.com/an/)

For Research Use Only. Not for use in diagnostic procedures.

The content of this publication shall not be reproduced, altered or sold for any commercial purpose without the written approval of Shimadzu. The information contained herein is provided to you "as is" without warranty of any kind including without limitation warranties as to its accuracy or completeness. Shimadzu does not assume any responsibility or liability for any damage, whether direct or indirect, relating to the use of this publication. This publication is based upon the information available to Shimadzu on or before the date of publication, and subject to change without notice.

© Shimadzu Corporation, 2015



# Application News

## No. V19

### High-Speed Video Camera

## Observing the Failure of Open-Hole CFRP specimens in Tensile Tests

-Synchronized Imaging Using Two High-Speed Video Cameras-

### ■ Introduction

Offering superior specific strength, even compared to other composite materials, carbon fiber reinforced plastic (CFRP) is used in aircraft and some transport vehicles for the purpose of saving fuel through weight reduction. Composite materials have excellent mechanical properties. However, a general feature of composite materials is that their strength decreases markedly when they are notched. CFRP is no exception, so tests of notched specimens are important. In this case, testing is performed using specimens notched with a circular hole at the center. In this experiment, tensile tests were performed using CFRP specimens (laminate method [45/0/-45/90]<sub>2s</sub>) with a total length of 150 mm, a width of 36 mm, and a thickness of 2.5 mm, prepared with a 6 mm circular hole at the center. The failure process of the CFRP specimens was observed during the tensile tests. In particular, it is important to confirm the failure process of weak regions, such as the periphery of circular holes, for CFRP development and to confirm the validity of CAE analysis. However, since the failure of CFRP is a brittle phenomenon, where failure occurs instantaneously, it cannot be confirmed with the naked eye. For this reason, high-speed video cameras are used to observe the failure. In this experiment, synchronized images were obtained at the front and the side of the specimens using two HPV-X2 high-speed video cameras.

### ■ Measurement System

In this experiment, the AG-Xplus precision universal testing machine and two HPV-X2 high-speed video cameras were used. Table 1 shows the instruments used. To observe the specimen failure in a tensile test, a trigger signal synchronized to the failure must be transmitted to the high-speed video cameras. The failure starts on the periphery of the circular hole. Accordingly, aluminum foil was affixed to the periphery of the circular hole using adhesive, as shown in Fig. 1, so that conduction would be lost when the specimen fails. The failure was observed using this timing to trigger the cameras.

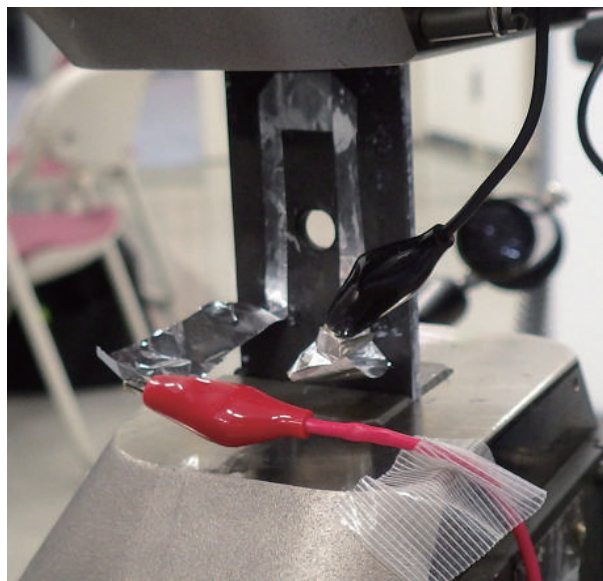


Fig. 1 Aluminum foil Trigger

### ■ Measurement Results

Table 2 shows the measurement conditions, and Fig. 2 shows the test configuration. As shown in Fig. 2, the failure of the specimen was recorded from the front by camera (1) and from the side by camera (2). Fig. 3 shows the test results from the AG-Xplus. Failure begins where the test force suddenly drops in Fig. 3. Fig. 4 shows the specimen failure observed from the front, and Fig. 5 from the side. Image (2) in Fig. 4 shows that the failure starts on the left side of the circular hole. In image (3), a crack also appears on the right side of the circular hole. Subsequently, cracks progressed in an orientation of 45 degrees, the orientation of the fibers in the outer layer. Further, as the test progressed, multiple cracks were confirmed, as in images (7) and (8). In the observations from the side, no failure was confirmed at the time the failure started, and was only initially confirmed in image (5). This is likely because the cracks started at the periphery of the circular hole reached the side of the specimen in image (5). Subsequently, failure was confirmed in multiple layers, except for the 0-degree layer, in image (6). Further, in image (7), failure was confirmed in the 0-degree layer, after which the failure progressed toward the outersurface. The final condition of the specimen is shown in Figs. 6 and 7.

Table 1 Testing Equipment

High-Speed Camera	: HPV-X2 x2
Lens	: 105 mm Micro lens x2
Illumination	: Metal halide lamp x2
Testing Machine	: AG-Xplus
Load Cell	: 100 kN
Grips	: 100 kN Non-shift wedge-type grips
Grip Teeth	: Trapezoidal file teeth for composite mater
Software	: TRAPEZIUM X (Single)



Table 2 Measurement Conditions

Test Speed : 5 mm/min  
Frame Rate : 1M frames/sec  
2M frames/sec

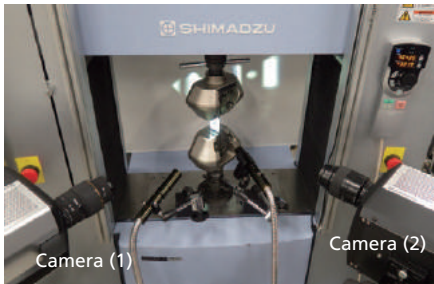


Fig. 2 Test Configuration

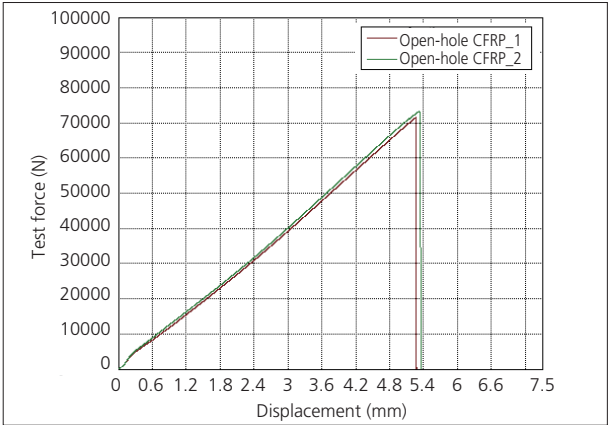


Fig. 3 Test Results

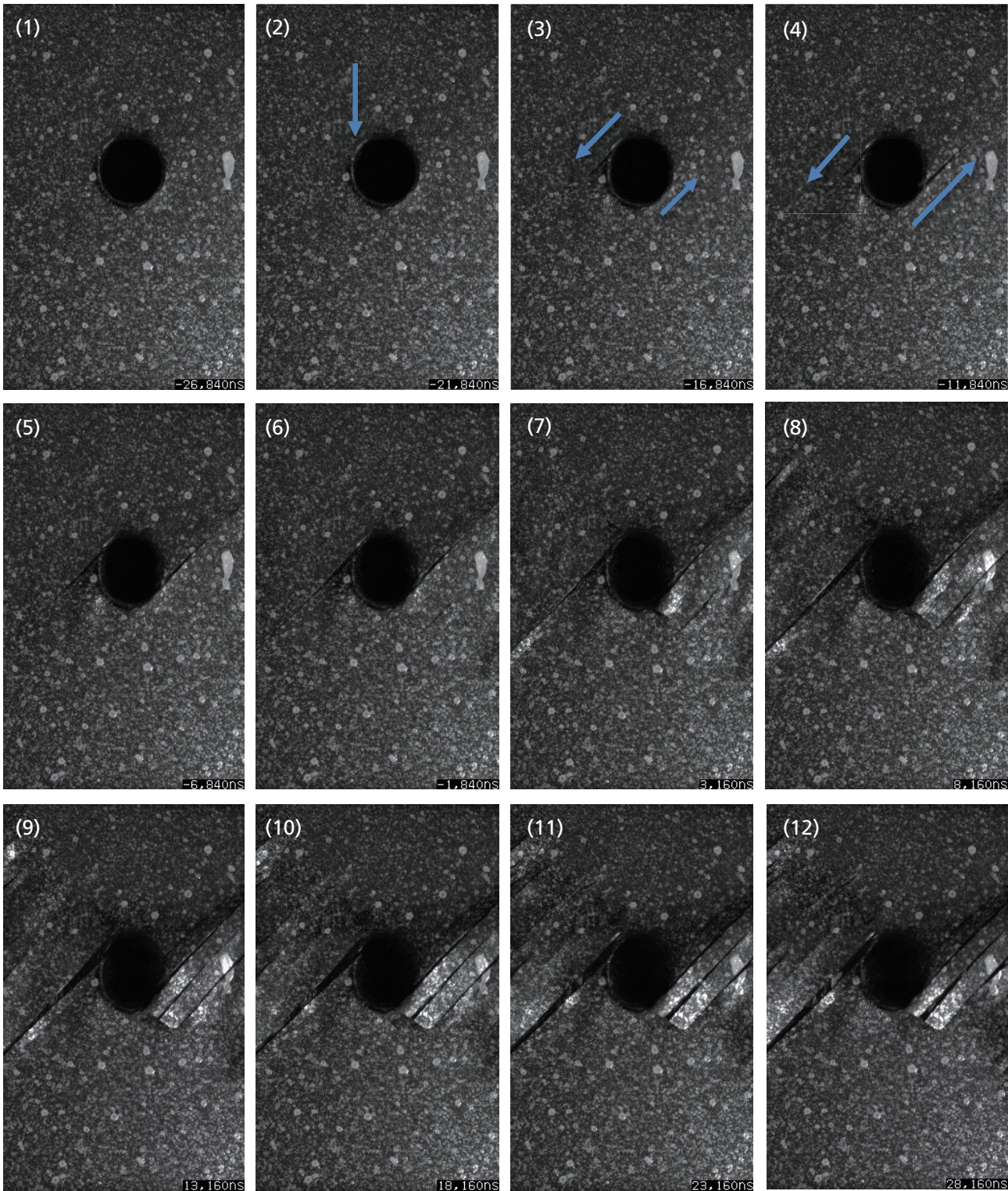


Fig. 4 Images from Camera (1) (5  $\mu$ s between images)



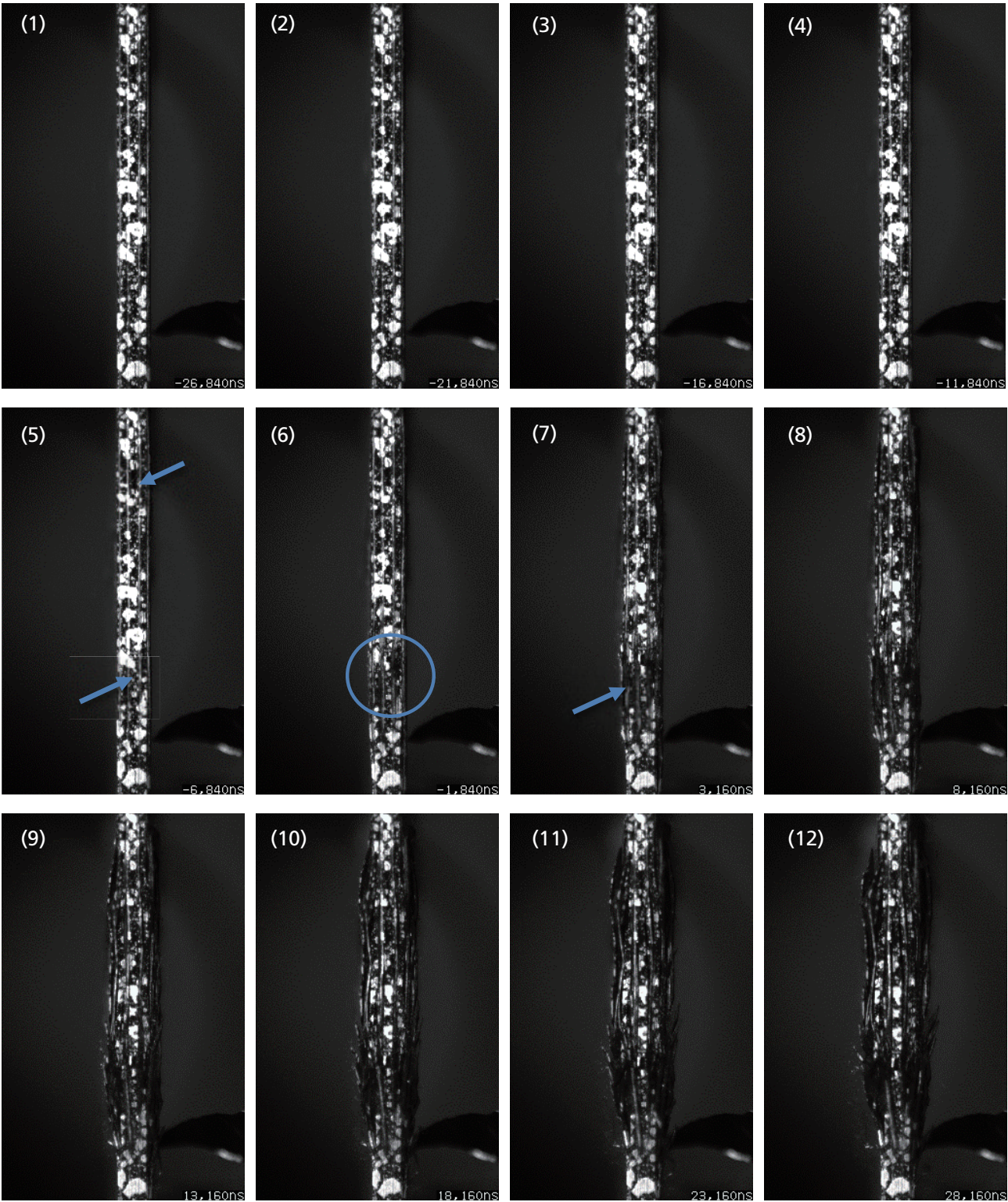


Fig. 5 Images from Camera (2) (5  $\mu$ s between images)



Fig. 6 Specimen After Failure (front)

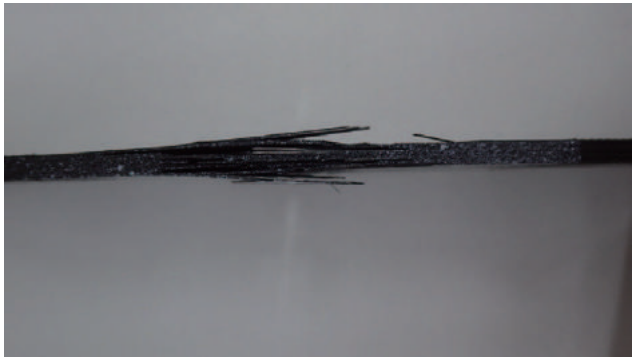


Fig. 7 Specimen After Failure (side)

## ■ Conclusion

The conventional HPV-X does not have a synchronization function, and so is incapable of recording from two directions. Also, the sensitivity of the HPV-X is insufficient, so it cannot record at imaging speeds of 500,000 fps or faster. The HPV-X2 is equipped with a synchronization function, and features improved sensitivity, so this instrument is capable of synchronized recordings at 2 Mfps, as in this case. As a result, failures can be observed in tensile tests of materials like CFRP that fails at high speeds.

Generally, failure observations are often recorded from the front of the specimen. However, adding recording from the side enables confirming the failure process that cannot be observed just from the front. In particular, with CFRP materials with different fiber orientations for each lamination layer, where failure progresses in different manner for each layer, as shown in this article, the failure process can be observed in more detail by recording from two directions.

First Edition: Jul. 2015





## Application Data Sheet

No. 37

### High-speed Video Camera HPV-X2

## Observing the Failure of Open-Hole CFRP Specimens in Tensile Testing

### Synchronized Imaging Using Two High-Speed Video Cameras

#### ■ Introduction

Offering superior specific strength, even compared to other composite materials, carbon fiber reinforced plastic (CFRP) is used in aircraft and some transport vehicles for the purpose of saving fuel through weight reduction. Composite materials have excellent mechanical properties. However, a general feature of composite materials is that their strength decreases markedly when they are notched. CFRP is no exception, so tests of notched specimens are important. In this case, testing is performed using specimens notched with a circular hole at the center. In this experiment, tensile tests were performed using CFRP (laminated method  $[45/0/-45/90]_{2s}$ ) with a total length of 150 mm, a width of 36 mm, and a thickness of 2.5 mm, prepared with a 6 mm circular hole at the center. The failure process of CFRP was observed during the tensile test. In particular, it is important to confirm the failure process of weak regions, such as the periphery of circular holes, for CFRP development and to confirm the validity of CAE analysis. However, since the failure of CFRP is a brittle phenomenon, where failure occurs instantaneously, it cannot be confirmed with the naked eye. For this reason, high-speed video cameras are used to observe the failure. In this experiment, synchronized images were obtained at the front and the side of the specimens using two HPV-X2 high-speed video cameras.

#### ■ Measurement system

In this experiment, the AG-X precision universal testing machine and two HPV-X2 high-speed video cameras were used. Table 1 shows the instruments used. To observe the specimen failure in a tensile test, a trigger signal synchronized to the failure must be transmitted to the high-speed video cameras. The failure starts on the periphery of the circular hole. Accordingly, aluminum foil was affixed to the periphery of the circular hole using adhesive, as shown in Fig. 1, so that conduction would be lost when the sample fails. The failure was observed using this timing to trigger the cameras.

Table 1 Testing Equipment

High-speed Camera	HPV-X2 ×2
Lens	105 mm Macro lens ×2
Illumination	Metal halide lamp ×2
Testing Machine	AG-X plus
Load cell	100 kN
Grips	100 kN Non-shift wedge-type grips
Grip teeth	Trapezoidal file teeth for composite mater
Software	TRAPEZIUM X(Single)

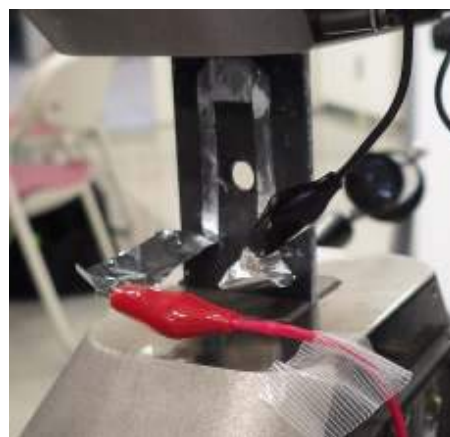


Fig.1 Aluminum foil Trigger

#### ■ Measurement Results

Table 2 shows the measurement conditions, and Fig. 2 shows the test configuration. As shown in Fig. 2, the failure of the specimen was recorded from the front by camera (1) and from the side by camera (2). Fig. 3 shows the test results from the AG-Xplus. Failure begins where the test force suddenly drops in Fig. 3. Fig. 4 shows the specimen failure observed from the front, and Fig. 5 from the side. Image (2) in Fig. 4 shows that the failure starts on the left side of the circular hole. In image (3), a crack also appears on the right side of the circular hole. Subsequently, cracks progressed in an orientation of 45 degrees, the orientation of the fibers in the outer layer. Further, as the test progressed, multiple cracks were confirmed, as in images (7) and (8). In the observation from the side, no failure was confirmed at the time the failure started, and was only initially confirmed in image (5). This is likely because the cracks started at the periphery of the circular hole reached the side of the specimen in image (5). Subsequently, failure was confirmed in multiple layers, except for the 0-degree layer, in image (6). Further, in image (7), failure was confirmed in the 0-degree layer, after which the failure progressed toward the outersurface. The final condition of the specimen is shown in Figs. 6 and 7.



Table 2 Measurement Conditions

Test speed	5 mm/min
Frame rate	1M frames/sec
	2M frames/sec

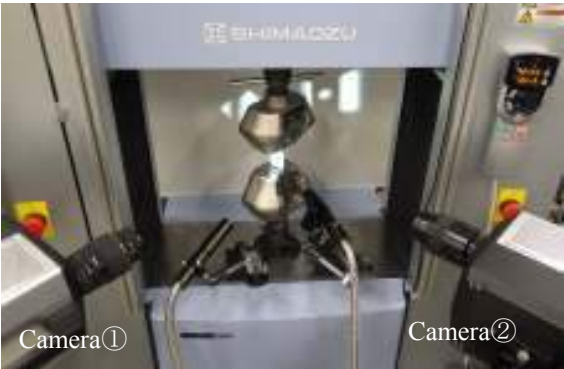


Fig.2 Test Configuration

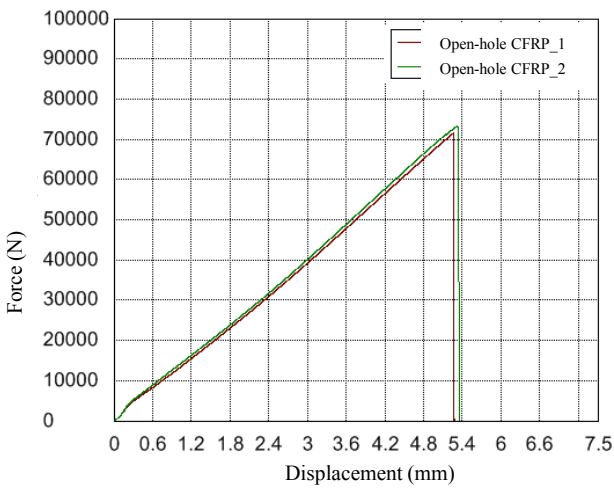


Fig.3 Test Results

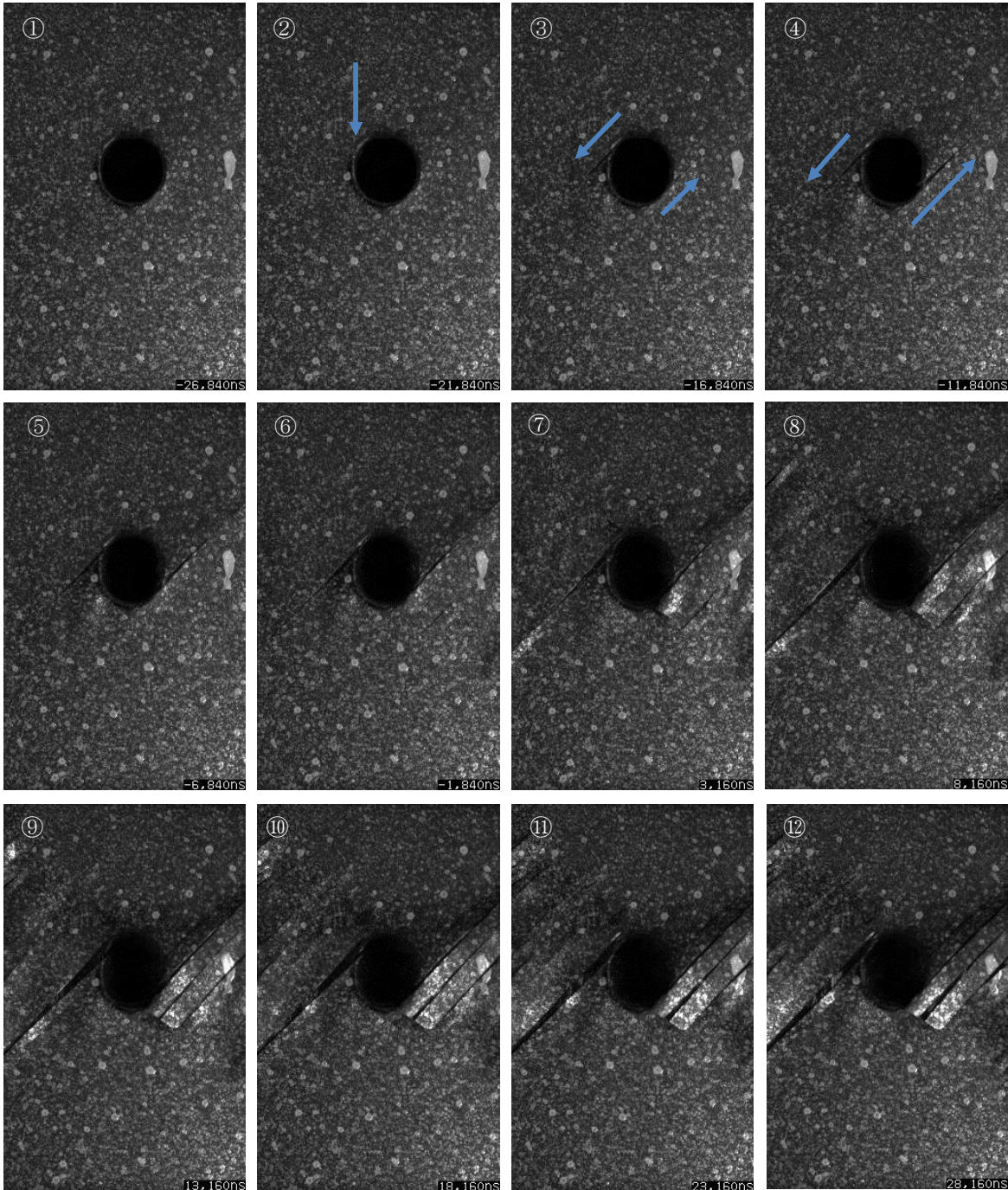


Fig.4 Images from Camera (1) (5  $\mu$ s between images)

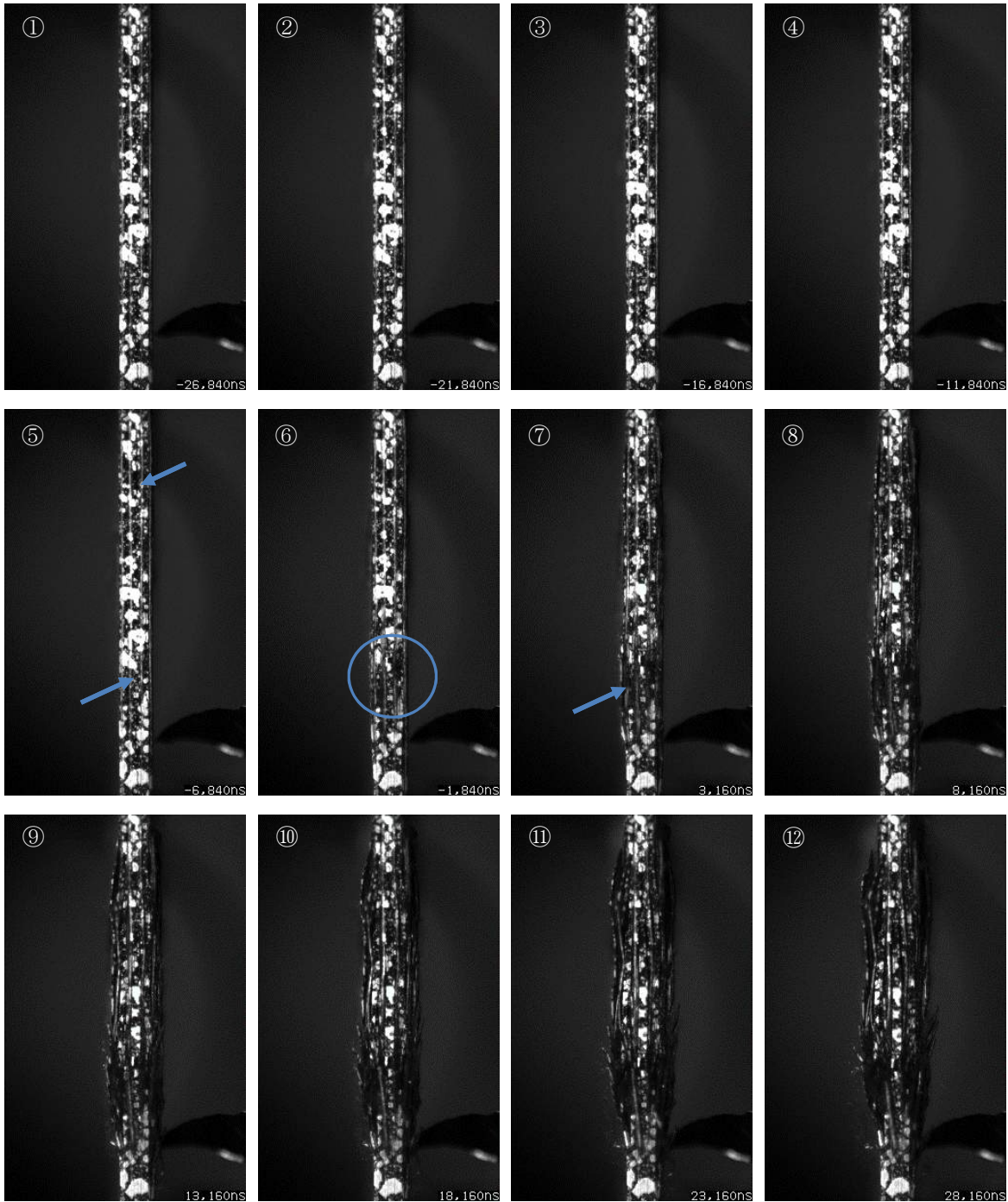


Fig.5 Images from Camera (2) (5  $\mu$ s between images)



Fig.6 Specimen After Failure (front)



Fig.7 Specimen After Failure (side)

## ■ Conclusion

The conventional HPV-X does not have a synchronization function, and so is incapable of recording from two directions. Also, the sensitivity of the HPV-X is insufficient, so it cannot record at imaging speeds of 500 kfps or faster. The HPV-X2 is equipped with a synchronization function, and features improved sensitivity, so this instrument is capable of synchronized recordings at 2 Mfps, as in this case. As a result, failures can be observed in tensile tests of materials like CFRP that fail at high speeds.

Generally, failure observations are often recorded from the front of the specimen. However, adding recording from the side enables confirming the failure process that cannot be observed just from the front. In particular, with CFRP materials with different fiber orientations for each lamination layer, where failure progresses in different manner for each layer, as shown in this article, the failure process can be observed in more detail by recording from two directions.

First Edition: July, 2015



Shimadzu Corporation

[www.shimadzu.com/an/](http://www.shimadzu.com/an/)

For Research Use Only. Not for use in diagnostic procedures.  
The content of this publication shall not be reproduced, altered or sold for any commercial purpose without the written approval of Shimadzu. The information contained herein is provided to you "as is" without warranty of any kind including without limitation warranties as to its accuracy or completeness. Shimadzu does not assume any responsibility or liability for any damage, whether direct or indirect, relating to the use of this publication. This publication is based upon the information available to Shimadzu on or before the date of publication, and subject to change without notice.

© Shimadzu Corporation, 2015



# Application Data Sheet

No. 38

## HPV-X2 High-Speed Video Camera

High-Speed Video Camera

### Observing the Fracture of Unidirectional CFRP in Static Tensile Testing

#### ■ Introduction

Carbon fiber reinforced plastic (CFRP) is a composite material with a particularly high specific strength. It is used in aircraft and in some transport equipment to reduce fuel costs by reducing weight. While it has some excellent mechanical characteristics as a composite material, when in-plane damage occurs it displays brittle failure behavior, with fracture propagating instantly from the point of damage. Consequently, CFRP development involves not only material testing, but also observation of material failure to check for fracture locations at weak points. Furthermore, material failure is observed to evaluate the validity of computer aided engineering (CAE) recently. As mentioned above, a CFRP fracture event occurs extremely quickly and cannot be observed by the naked eye, so a high-speed video camera is used. Shimadzu has published an Application News on this topic in the past (No. V017 Observing the Failure of CFRP Materials in High-Speed Tensile Tests). High-speed tensile testing involves an instantaneous testing time. To accommodate this, a strobe capable of emitting very intense light instantaneously is used to achieve an image capture speed of over 1 million frames/second. Meanwhile, static testing involves longer testing times with a metal halide lamp used as a light source for continuous lighting (a relatively weak light source compared to a strobe), which cannot produce enough light to capture images at more than 500 thousand frames/second.

The newly developed HPV-X2 camera is 6 times more sensitive than the previous HPV-X camera, which allows it to capture over 1 million frames/second using even a metal halide lamp as a light source. In this article, we demonstrate the observation of unidirectional CFRP failure in static testing.

#### ■ Measurement

The AG-X precision universal testing machine and HPV-X2 high-speed video camera were used in experiments. The equipment used is shown in Table 1. Observing material failure during tensile testing requires a signal to trigger the high-speed video camera in time with material failure. Since cracks propagate in the direction of the unidirectional fibers when failure occurs in unidirectional CFRP, we attached aluminum foil perpendicular to the direction of the fibers with adhesive. A specimen with the aluminum foil attached is shown in Fig. 1. A break in conduction through the aluminum foil caused by a break in the specimen triggers observation of the failure event.

#### ■ Results

A view of the test is shown in Fig. 2 and Fig. 3. As shown in Fig. 3, aluminum foil is also attached to the jigs around the specimen in order to focus light onto the specimen. Test conditions are shown in Table 2.

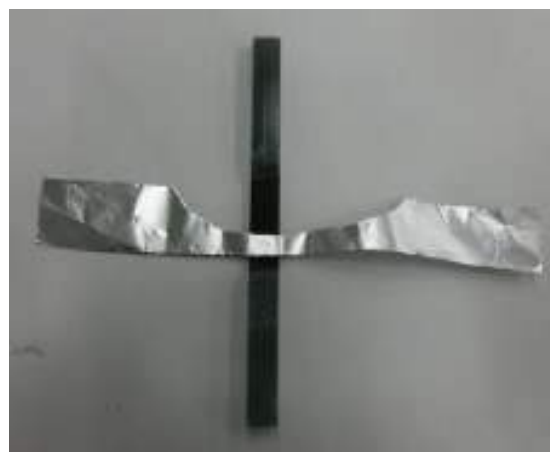


Fig. 1 Test Specimen

Table 1 Testing System

High-Speed Video Camera	HPV-X2
Lens	105 mm, F1.8
Lighting	Two metal halide lamps
Testing Machine	AG-Xplus
Load Cell	50 kN
Grip	50 kN non-shift wedge-type grips
Grip Face	Trapezoidal file teeth for composite materials
Software	TRAPEZIUM X (Single)

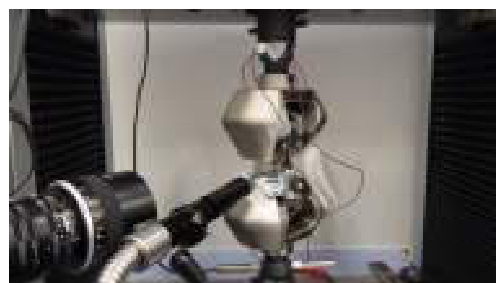


Fig. 2 View of the Test

Table 2 Test Conditions

Test speed	5 mm/min
Recording Speed	5 million frames/sec
Specimen Size	Width: 6 mm, thickness: 0.4 mm
Lamination Method	[0] <sub>2</sub>

The failure of unidirectional CFRP is shown in Fig. 4. Longitudinal cracks can be seen on the left side of the specimen in image (2) of Fig. 4. In image (3), these cracks have propagated as far as the upper tab. Longitudinal cracks can also be seen on the right side of the specimen in image (3). Image (6) is a later view of the specimen as it is breaking apart. Using the HPV-X2 allows for the observation of CFRP failure during the static tensile test, which is useful for future CFRP development.

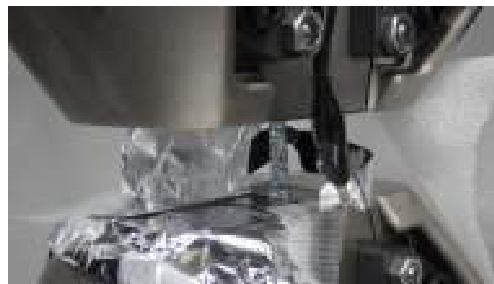


Fig. 3 View of the Test (Magnified View)

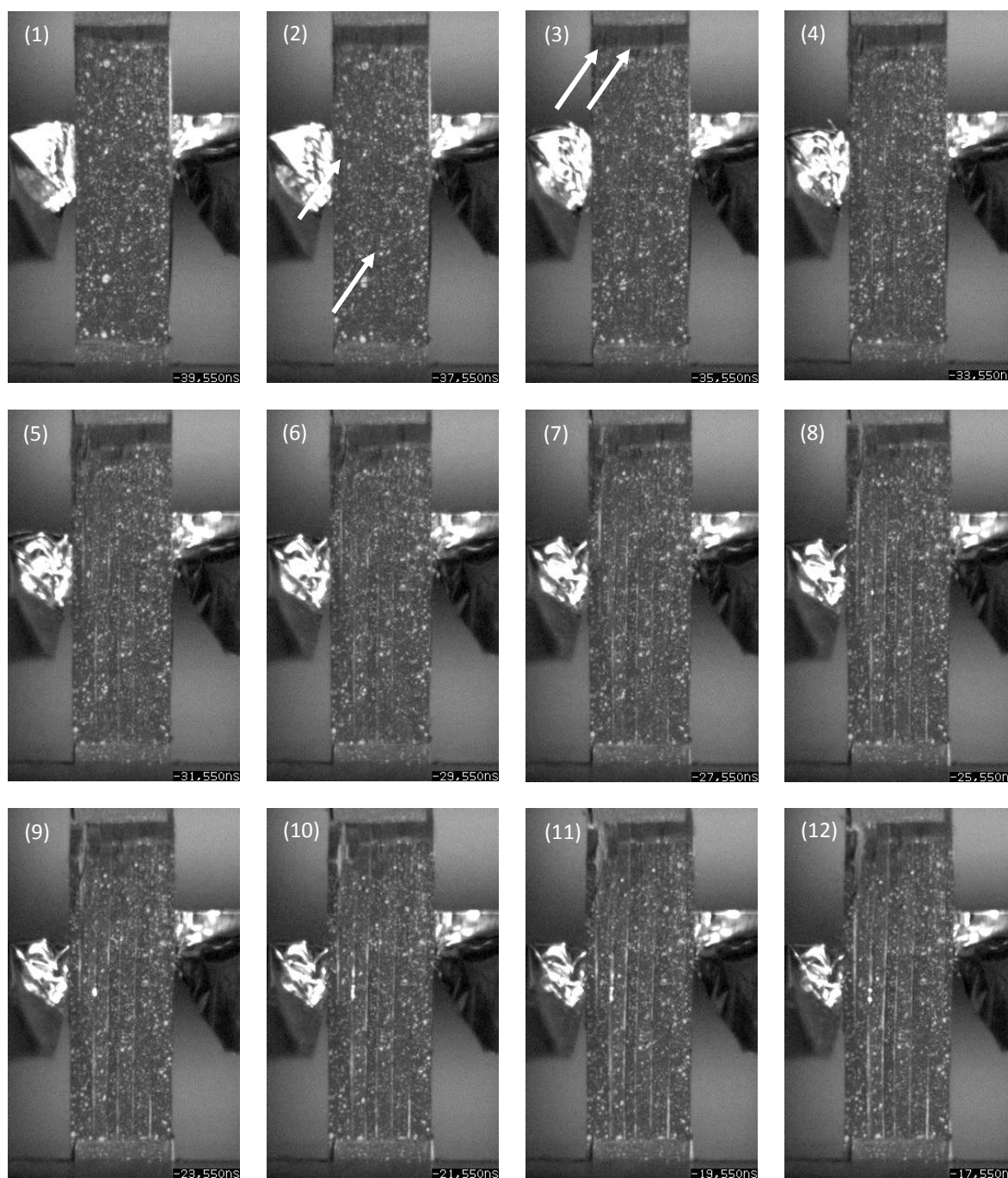


Fig. 4 Captured Images (Interval between captured images is 2 μs.)

First Edition: July, 2015



Shimadzu Corporation

[www.shimadzu.com/an/](http://www.shimadzu.com/an/)

For Research Use Only. Not for use in diagnostic procedures.  
The content of this publication shall not be reproduced, altered or sold for any commercial purpose without the written approval of Shimadzu. The information contained herein is provided to you "as is" without warranty of any kind including without limitation warranties as to its accuracy or completeness. Shimadzu does not assume any responsibility or liability for any damage, whether direct or indirect, relating to the use of this publication. This publication is based upon the information available to Shimadzu on or before the date of publication, and subject to change without notice.

© Shimadzu Corporation, 2015



# Application Data Sheet

No. 39

## Autograph Precision Universal Testing Machine

Material Testing & Inspection

### Evaluation of Open-Hole CFRP

— Static Tensile Testing, Fracture Observation, and Internal Structure Observation —

#### ■ Introduction

Recently, lightweight alternatives to conventional metal materials are being used as structural members where mechanical reliability is required. The main reason for this trend is that lighter products reduce transport weights, which reduces fuel consumption and carbon dioxide emissions during product transport. Fiber reinforced composite materials such as carbon fiber reinforced plastics (CFRP), which consist of a resin strengthened with carbon fibers, are extremely strong and light. Because of this, they are currently a material widely used in aircraft, and are expected to be used increasingly in various types of products, including automobiles, in order to make them lighter. For the development of fiber reinforced composite materials, not just a simple evaluation of their mechanical strength, but also the observation of failure events is important. In addition, from the perspective of quality management, the necessity for evaluation of internal structure of these materials, such as the oriented state of fibers and the presence of cracks, has increased.

In this article, we describe how we use a precision universal testing machine (Autograph AG-250kNXplus) and high-speed video camera (HyperVision HPV-X) (Fig. 1) to evaluate the static fracture behavior of a CFRP based on a test force attenuation graph and images of material failure. We also describe our subsequent examination of the state of the specimens internally using an X-ray CT system (inspeXio SMX-100CT) to investigate the state of fracture inside the specimen. Information on specimens is shown in Table 1. Specimens have a hole machined into their center that is 6 mm in diameter. Fracture is known to propagate easily through composite materials from the initial damage point, and when a crack or hole is present their strength is reduced markedly. Therefore, evaluation of the strength of open-hole specimens is extremely important from the perspective of the safe application of CFRP materials in aircraft, etc.

Table 1: Test Specimen Information

Laminate Structure	Dimensions
	L (mm) × W (mm) × T (mm), hole diameter (mm)
[+45/0/-45/+90] <sub>2s</sub>	150 × 36 × 2.9, Φ6

Note: The CFRP laminate board used in the actual test was created by laying up prepreg material with fibers oriented in a single direction. The [+45/0/-45/+90]<sub>2s</sub> shown as the laminate structure in Table 1 refers to the laying up of 16 layers of material with fibers oriented at +45°, 0°, -45°, and +90° in two layer sets.

#### ■ Static Tensile Testing (Ultra High Speed Sampling)

In this test, the change in load that occurs during specimen fracture was used as the signal for the HPV-X high-speed video camera to capture images. Specifically, the AG-Xplus precision universal testing machine was configured to create a signal when the test force on the specimen reaches half the maximum test force (referred to as Maximum test force in Fig. 3), with this signal being sent to the high-speed video camera. Static tensile testing and fracture observation were performed according to the conditions shown in Table 2. A test force-displacement plot for the open-hole quasi-isotropic CFRP (OH-CFRP) is shown in Fig. 2(a). A test force-time plot during the occurrence of material fracture is also shown in Fig. 2(b).

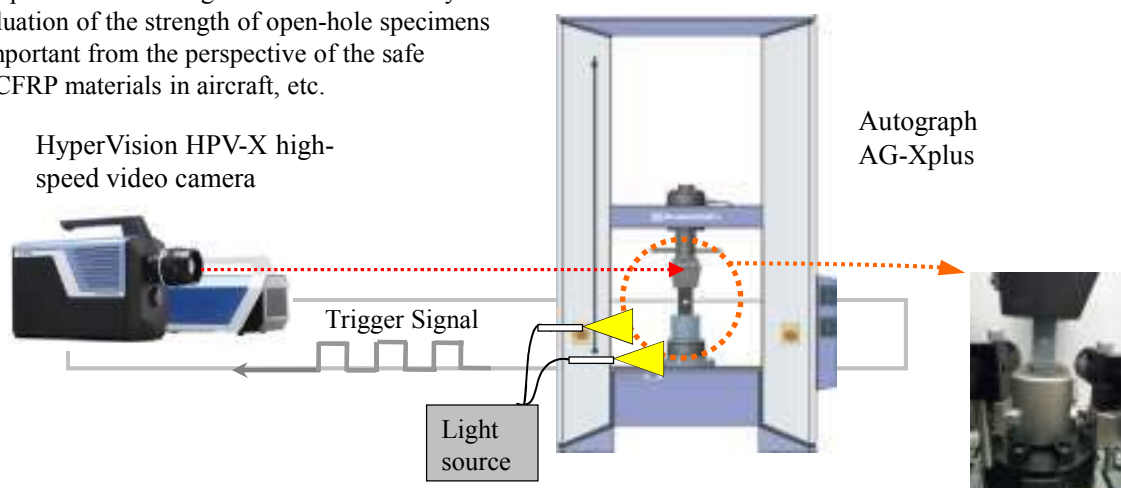


Fig.1: Testing Apparatus

Table 2: Test Conditions

Testing Machine	AG-Xplus
Load Cell Capacity	250 kN
Jig	Upper: 250 kN non-shift wedge type grips (with trapezoidal file teeth on grip faces for composite materials) Lower: 250 kN high-speed trigger-capable grips
Grip Space	100 mm
Loading Speed	1 mm/min
Test Temperature	Room temperature
Software	TRAPEZIUM X (Single)
Fracture Observation	HPV-X high-speed video camera (recording speed 600 kfps)
DIC Analysis	StrainMaster (LaVision GmbH.)

Note: fps stands for frames per second. This refers to the number of frames that can be captured in 1 second.

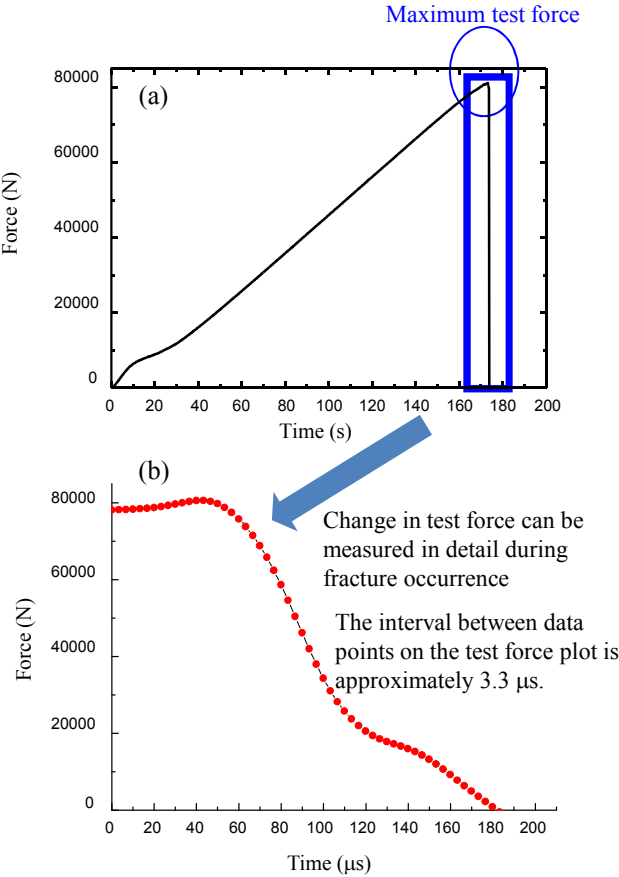


Fig. 2 (a) Test Force-Displacement Curve, and (b) Test Force-Time Curve (in Region of Maximum Test Force)

Fig. 2(a) can be interpreted to show the specimen fractured at the moment it reached the maximum test force, at which point the load on the specimen was suddenly released. This testing system can be used to perform high-speed sampling to measure in detail the change in test force in the region of maximum test force. The time interval between data points on the test force plot in Fig. 2(b) is 3.3 μs.

■ Fracture Observation (High Speed Imaging)

Images (1) through (8) in Fig. 3 capture the behavior of the specimen during fracture around the circular hole. Image (1) shows the moment cracks occur in a surface +45° layer. In this image, the tensile load being applied is deforming the circular hole, where hole diameter in the direction of the load is approximately 1.4 times that perpendicular to the load. In image (2), the cracks that occurred around the circular hole are propagating along the surface +45° layer. In images (3) through (6), a substantial change can be observed in the external appearance of the specimen near the end of the crack propagating to the bottom right from the circular hole. This suggests not only the surface layer, but internal layers are also fracturing. Based on the images of the same area and the state of the internal layers that can be slightly observed from the edges of the circular hole in images (7) and (8), the internal fracture has quickly propagated in the 18 μs period between images (3) and (8).

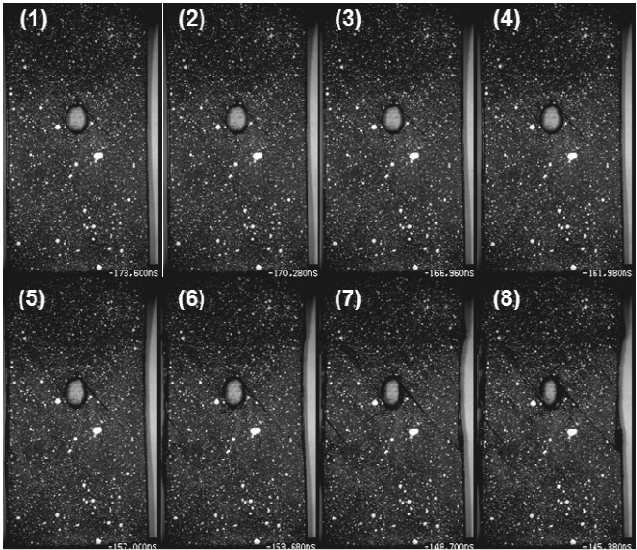


Fig. 3: Observations of OH-CFRP Fracture

Images (1) through (8) of Fig. 4 show the results of performing Digital image correlation (DIC) analysis on the fracture observation images of Fig. 3. Black signifies areas of the surface layer of the specimen under little strain, and red signifies areas under substantial strain. Looking at images (1) through (4), we can see that strain around the circular hole is focused diagonally toward the top-left ( $-45^\circ$ ) and toward the bottom-left ( $+45^\circ$ ) from the circular hole. Images (5) through (8) show the focusing of strain diagonally toward the bottom-right ( $-45^\circ$ ) and toward the top-right ( $+45^\circ$ ) from the circular hole in areas where it was not obvious in images (1) through (4). This shows an event is occurring in the surface layer of the specimen that is similar to the process of fracture often seen during tensile testing of ductile metal materials, which is crack propagation in the direction of maximum shearing stress.

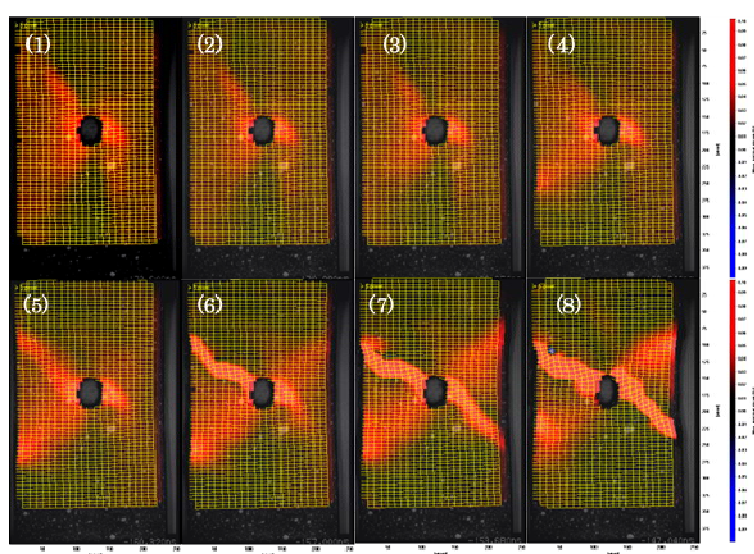


Fig. 4: Observation of OH-CFRP Fracture (DIC Analysis)

#### ■ Internal Structure Observation (CT)

Next, internal observations were performed around the circular hole using a micro focus X-ray CT system to check the state of internal damage to the specimen. The SMX-100CT micro focus X-ray CT system (Fig. 5) is capable of capturing CT images at high magnification. The system rotates a specimen between an X-ray generator and an X-ray detector, uses a computer to calculate fluoroscopic images obtained from all  $360^\circ$  of rotation, then reconstructs a tomographic view of the specimen (Fig. 6). This system was used to perform a CT scan of the fracture area of the OH-CFRP after the static tensile testing and fracture observation performed as described in the previous section, so that the cracks that occurred inside can be observed.



Fig. 5: Shimadzu inspeXio SMX-100CT Micro Focus X-Ray CT System

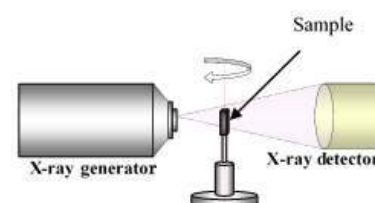


Fig. 6: Illustrated Example of X-Ray CT System Operation



Fig. 7: Specimen After Static Tensile Testing (Specimen Used for CT Scan)

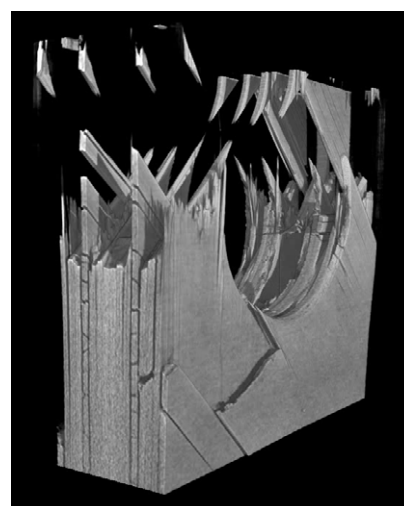


Fig. 8: Fracture Area 3D Image No. 1



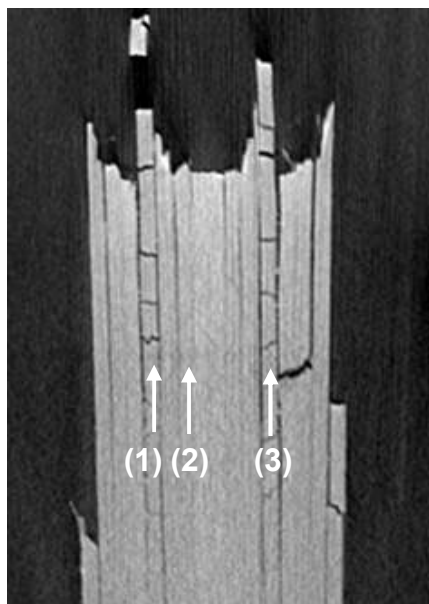


Fig. 9: CT Cross-Sectional Images of the Fracture Area

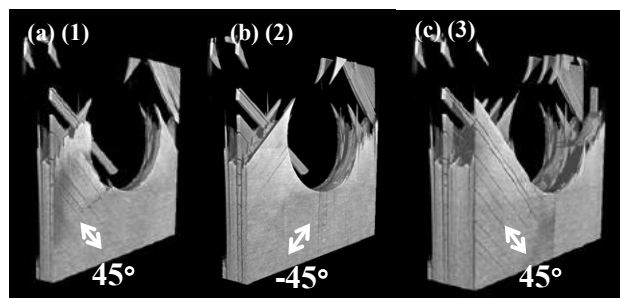


Fig. 10: Fracture Area 3D Image No. 2

#### ■ Acknowledgment

We would like to extend our sincere gratitude to the Japan Aerospace Exploration Agency (JAXA) for their cooperation in the execution of this experiment.

Note: The analytical and measuring instruments described may not be sold in your country or region.

Cross-sectional images of the specimen are shown as a 3D image in the 16 layers shown in Fig. 9, we can see that most cracks in the matrix occur in the  $+45^\circ$  layer inside the specimen, indicated by the number (1) and (3). (shown in Fig. 10 (a) and Fig. 10 (b), respectively). In this layer, the carbon fibers are all aligned together in a  $+45^\circ$  orientation, and the multiple matrix cracks occurring in this layer are probably due to the shearing force caused in this layer by tensile loading, together with deformation of adjacent layers in the direction of the loading. For comparison, a 3D image of the  $-45^\circ$  layer inside the specimen (Fig. 9 (2)) is shown in Fig. 10 (b). As is clear from the image, the matrix cracks that occurred in the  $+45^\circ$  layer have not occurred in the  $-45^\circ$  layer. This difference in fracture state has probably arisen due to different shearing forces and load directions occurring in each layer. Such detailed observation of fracture surfaces associated with multiple matrix cracks was difficult by conventional methods, since to observe fracture surfaces the specimen was processed such as by cutting and embedding in resin, which changed the characteristics of the specimen. However, by using the high-resolution X-ray CT system as described in this article, there is little X-ray absorption difference between air and specimen, and it is possible to observe the state of complex internal damage, even for OH-CFRP in which microscopic damage is normally difficult to observe by X-ray.

# Application News

No. **V18**

## High-Speed Video Camera

### Observing the Fracture of Unidirectional CFRP in Static Tensile Testing

#### ■ Introduction

Carbon fiber reinforced plastic (CFRP) is a composite material with a particularly high specific strength. It is used in aircraft and in some transport equipment to reduce fuel costs by reducing weight. While it has some excellent mechanical characteristics as a composite material, when in-plane damage occurs it displays brittle failure behavior, with fracture propagating instantly from the point of damage. Consequently, CFRP development involves not only material testing, but also observation of material failure to check for fracture locations at weak points. Furthermore, material failure is observed to evaluate the validity of computer aided engineering (CAE) recently. As mentioned above, a CFRP fracture event occurs extremely quickly and cannot be observed by the naked eye, so a high-speed video camera is used. Shimadzu has published an Application News on this topic in the past (No. V017 Observing the Failure of CFRP Materials in High-Speed Tensile Tests). High-speed tensile testing involves an instantaneous testing time. To accommodate this, a strobe capable of emitting very intense light instantaneously is used to achieve an image capture speed of over 1 million frames/second. Meanwhile, static testing involves longer testing times with a metal halide lamp used as a light source for continuous lighting (a relatively weak light source compared to a strobe), which cannot produce enough light to capture images at more than 500 thousand frames/second.

The newly developed HPV-X2 camera is 6 times more sensitive than the previous HPV-X camera, which allows it to capture over 1 million frames/second using even a metal halide lamp as a light source. In this article, we demonstrate the observation of unidirectional CFRP failure in static testing.

#### ■ Measurement

The AG-Xplus precision universal testing machine and HPV-X2 high-speed video camera were used in experiments. The equipment used is shown in Table 1. Observing material failure during tensile testing requires a signal to trigger the high-speed video camera in time with material failure. Since cracks propagate in the direction of the unidirectional fibers when failure occurs in unidirectional CFRP, we attached aluminum foil perpendicular to the direction of the fibers with adhesive. A specimen with the aluminum foil attached is shown in Fig. 1. A break in conduction through the aluminum foil caused by a break in the specimen triggers observation of the failure event.

#### ■ Results

A view of the test is shown in Fig. 2 and Fig. 3. As shown in Fig. 3, aluminum foil is also attached to the jigs around the specimen in order to focus light onto the specimen. Test conditions are shown in Table 2.

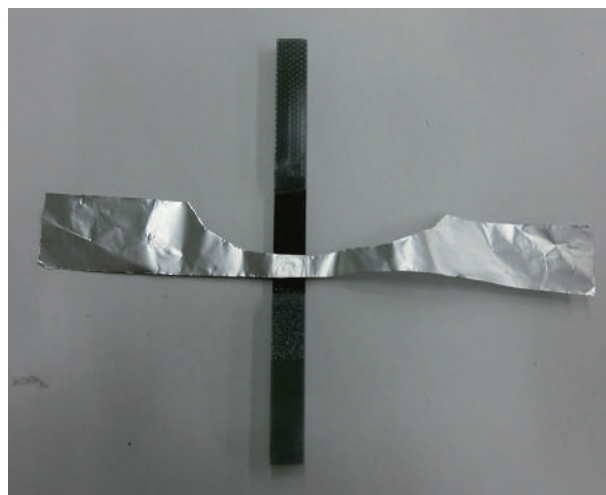


**Fig. 1 Test Specimen**

**Table 1 Testing System**

High-Speed Video Camera	: HPV-X2
Lens	: 105 mm, F1.8
Lighting	: Two metal halide lamps
Testing Machine	: AG-Xplus
Load Cell	: 50 kN
Grip	: 50 kN non-shift wedge-type grips
Grip Face	: Trapezoidal file teeth for composite materials
Software	: TRAPEZIUM X (Single)

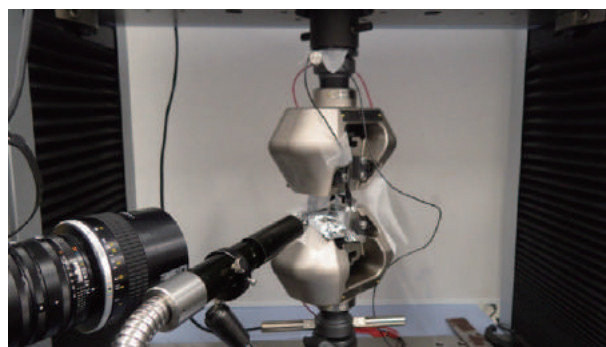


**Fig. 2 View of the Test**

**Table 2 Test Conditions**

Test Speed	: 5 mm/min
Recording Speed	: 5 million frames/sec
Specimen Size	: Width: 6 mm, thickness: 0.4 mm
Lamination Method	: [0] <sub>2</sub>



The failure of unidirectional CFRP is shown in Fig. 4. Longitudinal cracks can be seen on the left side of the specimen in image (2) of Fig. 4. In image (3), these cracks have propagated as far as the upper tab. Longitudinal cracks can also be seen on the right side of the sample in image (3). Image (6) is a later view of the sample as it is breaking apart. Using the HPV-X2 allows for the observation of CFRP failure during static tensile tests, which is useful for future CFRP development.



Fig. 3 View of the Test (Magnified View)

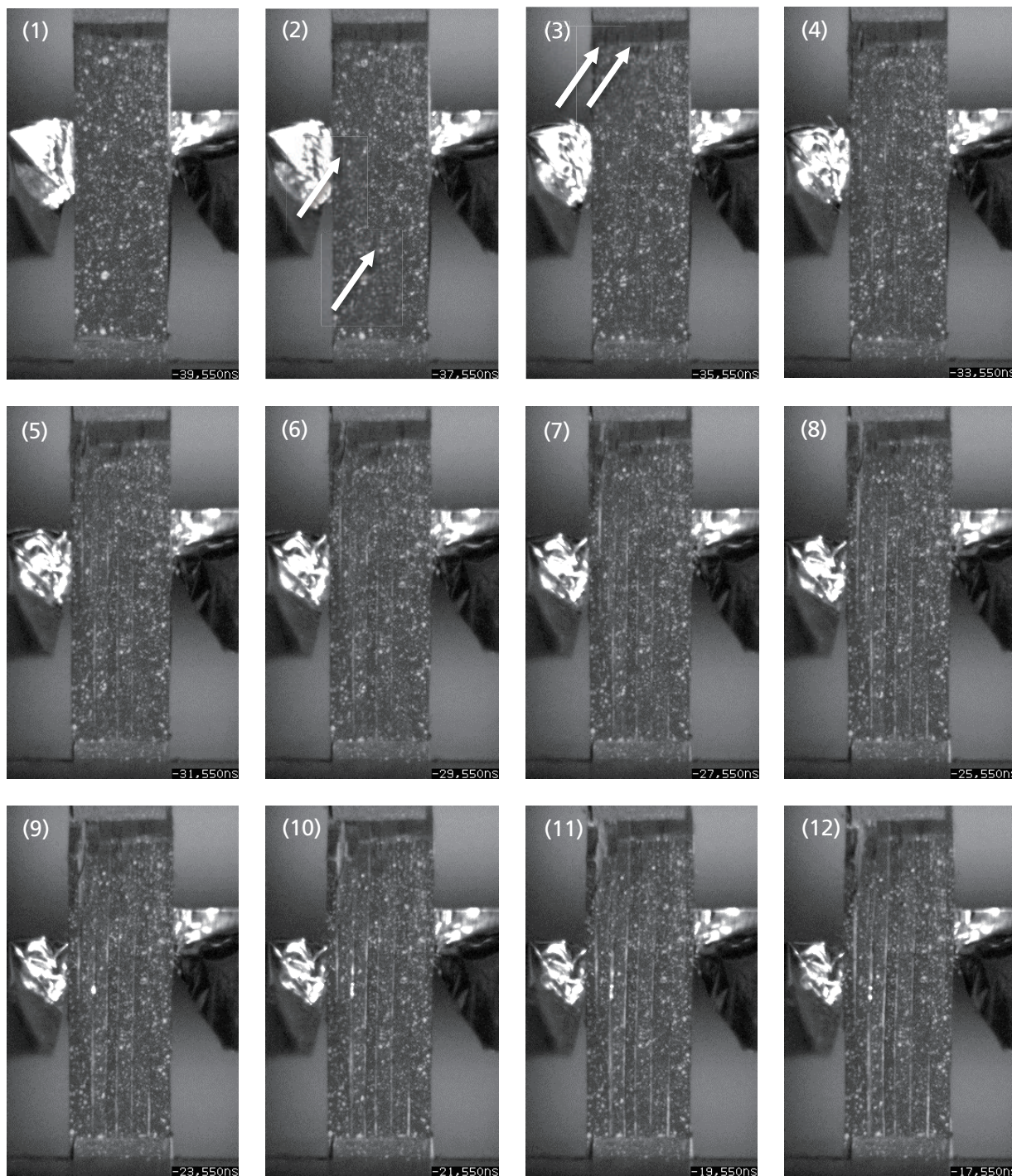


Fig. 4 Captured Images (Interval between captured images is 2 μs.)

First Edition: Jul. 2015



Shimadzu Corporation  
[www.shimadzu.com/an/](http://www.shimadzu.com/an/)

For Research Use Only. Not for use in diagnostic procedures.  
The content of this publication shall not be reproduced, altered or sold for any commercial purpose without the written approval of Shimadzu. The information contained herein is provided to you "as is" without warranty of any kind including without limitation warranties as to its accuracy or completeness. Shimadzu does not assume any responsibility or liability for any damage, whether direct or indirect, relating to the use of this publication. This publication is based upon the information available to Shimadzu on or before the date of publication, and subject to change without notice.

© Shimadzu Corporation, 2015

## Observation of fracture in CFRP tensile test

CFRP (carbon fiber reinforced plastic) has attracted attention as a high-performance composite material with high strength and rigidity, yet low in weight, and is being applied in various fields, such as for aircraft, railroad vehicles, automobiles and civil engineering. This example describes evaluating the characteristics of a flat plate specimen of CFRP material when a tensile load is applied (tensile test) and observing the fracture status. Tensile testing consisted of static testing of material strength and measuring the modulus of elasticity using a precision universal testing machine. In addition, high-rate tensile impact test was also performed. In the latter case, a high-speed video camera was used to record specimen fracture, which allowed capturing image data of the instant the CFRP material fractured.

### ■ Test specimen

The tensile test specimen tested in this example is shown in figure 1. Included 50 mm long CFRP tabs attached to both ends of the CFRP strip with thermosetting resin adhesive. Reinforcing the grip area with tabs ensures a stable tensile test with good reproducibility.



Figure 1: CFRP test specimen

Specimen details are as follows:

- 1) Material: unidirectional CFRP
- 2) Shape: strip (with tabs on both ends)
- 3) Specimen dimensions: for static tensile testing 200(L) x 12.5(W) x 1(T) mm. For recording image of impact fracture 70(L) x 6.25(W) x 0.3(T) mm

### ■ Static tensile test

A strain gauge type extensometer was attached to the specimen and a tensile test was performed using a precision testing machine. The extensometer was removed when strain exceeded the elasticity measurement range. It is also possible to measure strain by affixing a strain gauge instead of an extensometer. Tensile test parameters are indicated below.

- (1) Tensile rate: 10 mm/min
- (2) Grip distance: 100 mm
- (3) Test force detection: 50 kN load cell
- (4) Extensometer gauge length: 50 mm
- (5) Elasticity calculation range: 5/10,000 to 25/10,000 strain

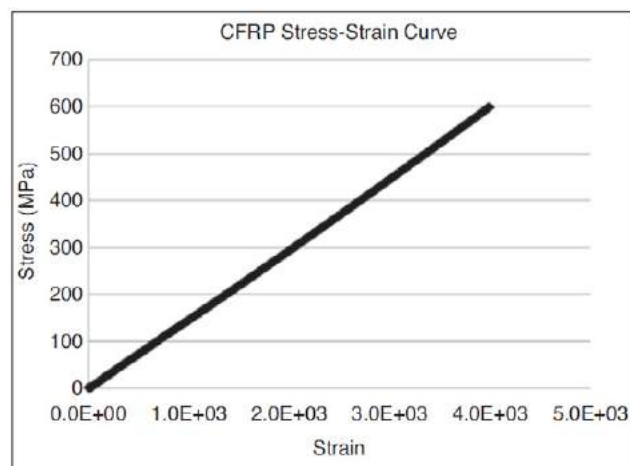


Figure 2: Static test results



The elasticity of CFRP specimen can be determined by calculating the slope of the given strain region (elasticity calculation range) in the stress-strain curve (figure 2) obtained from test results. Tensile strength can be determined from the maximum stress in the stress-displacement curve (figure 3) before the specimen breaks.

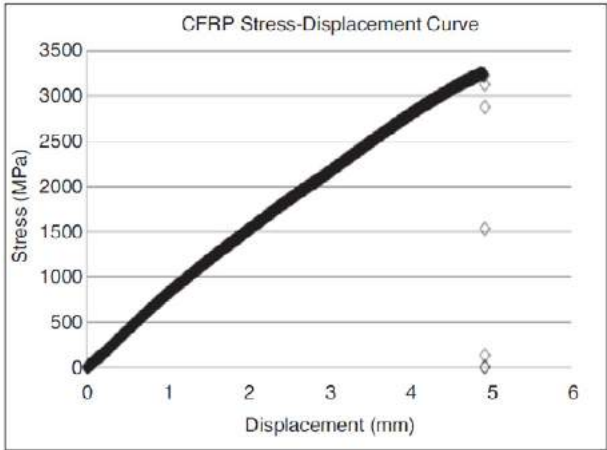


Figure 3: Static test results

The following values were obtained from the measurement data.

- (1) Tensile strength: 346 GPa
- (2) Elasticity: 148 GPa

The post-test status of the specimen is shown in figure 4. Compared to the starting status in figure 1, it clearly shows how the fibers within the resin have failed.



Figure 4: Specimen status after static test

■ Static tensile test

To verify functionality, development of composite materials involves not only static Static strength testing, but also involves the objective of ensuring active safety. Consequently, it is important to determine the shock strength and understand the process of fracture propagation. Therefore, the fracture process during tensile chock testing of a CFRP specimen was observed by combining a high-speed video camera with high-rate tensile shock test machine. Observation conditions are indicated below.

Specimen tensile rate:	6 m/s
Grip distance:	30 mm
Camera lens:	105 mm macro, with 2 x teleconverter
Camera lighting:	strobe
Camera trigger:	signal synchronized with tensile displacement is sent from testing machine to camera.

The setup used to record video of the test is shown in figure 5, with a high-speed video camera mounted about 450 mm in front of the specimen. Recording was activated by an external start trigger signal sent from the testing machine to the camera, which was synchronized to the tensile displacement. A strobe light synchronized to the video timing was used as lighting.

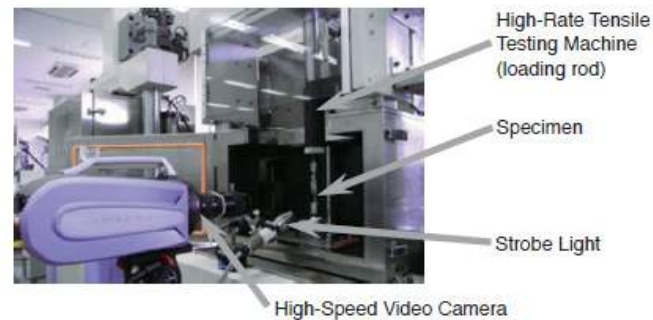


Figure 5: Setup of high-rate shock test

Using this test configuration, a load was applied to the CFRP specimen according to the parameters indicated above and a high-speed camera captured the instant of fracture, at 250.000 frames per second. This image data shown in figure 6.

This shows 8 consecutive frames, from (1) TO (8), with an interval of 4 microseconds between each frame. This camera features highly detailed image resolution of 312

horizontal by 260 vertical pixels that is constant, regardless of the frame rate.

This example shows, combining a high-speed video camera and material testing machine makes it possible to evaluate material properties and observe fracture behavior at the same time. This enables supporting a wide range of material development applications, from developing individual functionally enhanced resins to developing composite materials.

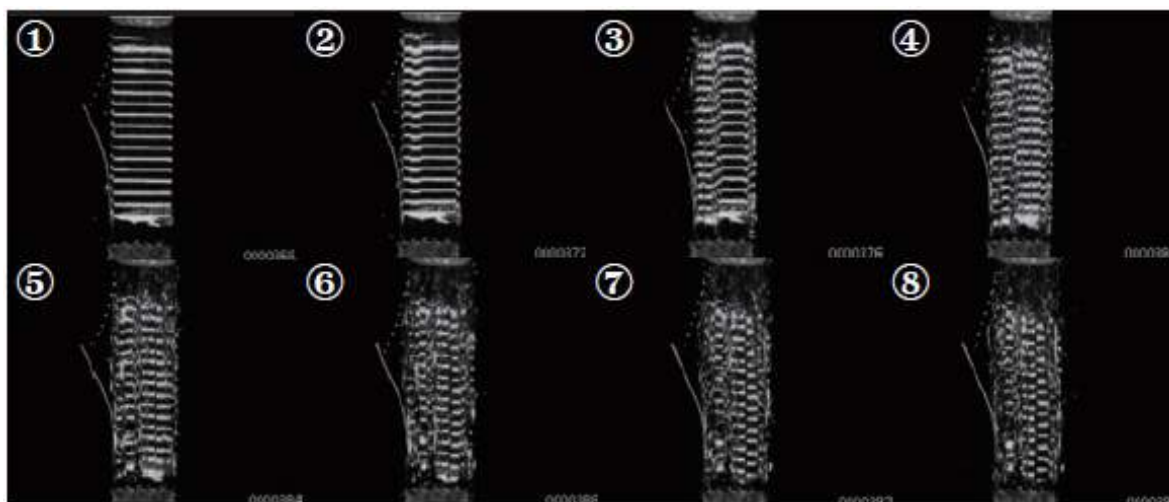


Figure 6: Images of specimen during fracture



## 6. Materials Testing & Inspection

---

### 6.5 Rheometer

---

The CFT-EX series is ideal for research and development, production process and quality control of thermoplastic resins, thermosetting resins, toners, composites, rubbers, and other flowable materials.

- SCA\_300\_055** Viscosity evaluation of thermoplastic resins (GFRP)
- SCA\_300\_056** Viscosity evaluation of thermoplastic resins (GFRP)
- No. 7** CFT EX useful to evaluation of LED package
- No. 8** Why Is CFT used to evaluate thermosetting resins
- No. 9** Fluidity evaluation of epoxy resin
- No. 10** Fluidity evaluation of IC sealant
- SCA\_300\_017** Flowtester flow tests of various kinds of plastics with Shimadzu Flowtester Model CFT
- SCA\_300\_026** Measurement of surface hardness of erasers with Shimadzu Dynamic Ultra Micro Hardness Tester
- SCA\_300\_031** Test on thermosetting resin with Shimadzu Flow Tester Model CFT
- SCA\_300\_043** Fluidity evaluation of unvulcanized rubber
- SCA\_300\_054** Viscosity evaluation of thermoplastic resins (epoxies)



## Application News

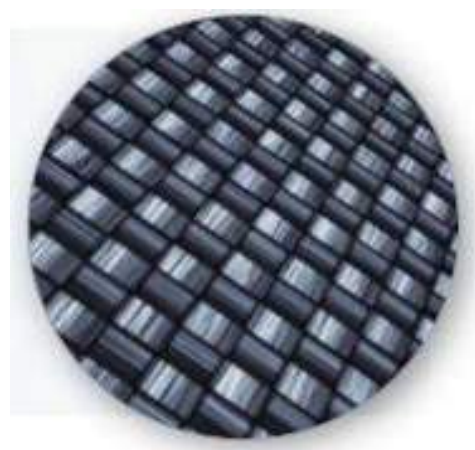
Material Testing System CFT

No. SCA\_300\_055

### Viscosity Evaluation of Thermoplastic Resins (GFRP)

#### ■ Introduction

Most mass produced molded plastic products are injection-molded. The appropriate temperature and pressure for injection molding differs depending on the type of resin and shape of the die, over-filling, under-filling, sink marks, voids, or other molding defects. Even if appropriate molding parameters are used, any changes in the status of the resin raw materials used could cause molding defects as well. Therefore, it control the quality of resin raw materials on a daily basis. Furthermore, it is important to perform the daily resin high pressure conditions that approximate molding conditions, which is not possible using the melt flowrate measurement method.

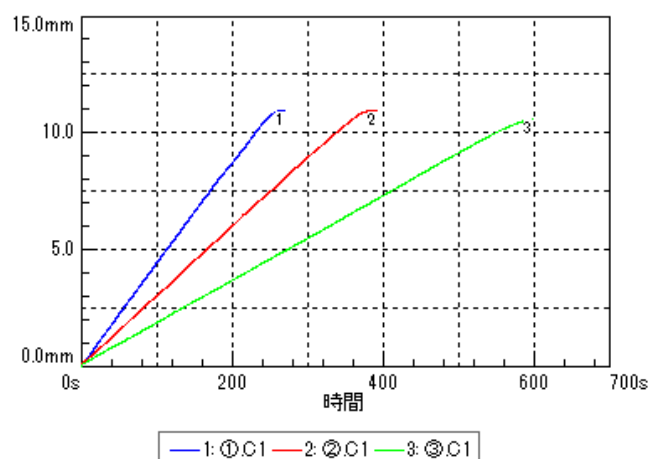


#### ■ Viscosity Evaluation Using Constant Temperature Method

Polycarbonate (PC) samples of various molecular weights containing 33 % glass fiber (GF) were measured using constant temperature method. The flow curves clearly show that the higher the molecular weight, the higher the sample's viscosity.

Test Method	Constant temperature test
Die Diameter	1 mm
Die Length	10 mm
Test Temperature	280 °C
Test Pressure	1.96 MPa
Preheating Time	300 sec
Sample Size	1.5 g

Test Conditions



Test result

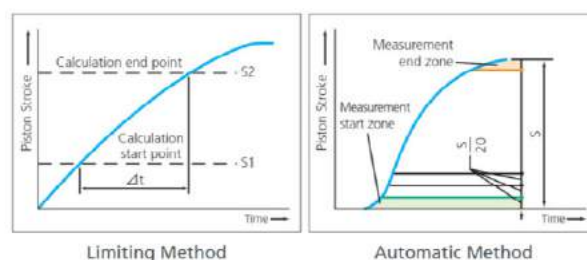
Sample No.	Component	Molecular Weight	GF Ratio (%)	Shear Rate (S <sup>-1</sup> )	Viscosity (Pa•s)
1	PC/SGF	17000	33	44,7	1,098
2	PC/SGF	22000	33	30,6	1,604
3	PC/SGF	26000	33	18,5	2,657

Test Results

## ■ Selection of Measurement Method According to Material

### Constant Temperature Method

In the testing method based on the use of a constant temperature, two calculation points on the piston's descent are set beforehand. The calculation is conducted using either the limiting method or the automatic method. In the limiting method, the flowrate is determined from the stroke-time curve of the piston between the above two points. In the automatic method, the stroke-time curve is divided into 20 segments, and the flowrate is determined from the gradients of the curves of those segments except for the first and last segment, with the maximum value taken automatically as the flowrate.



Thermosetting resins



Thermoplastic resins



Rubbers

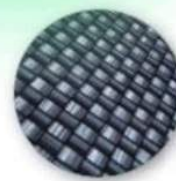
*The fluidity of various  
materials  
&  
Evaluation of the heat  
characteristic*



Ceramics



Toners



Composites



## Application News

Material Testing System CFT

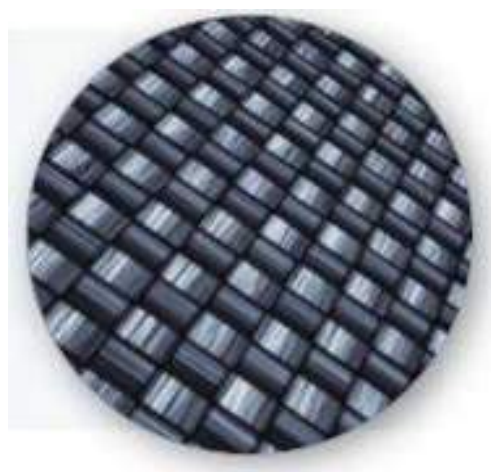
No. SCA\_300\_056

### Viscosity Evaluation of Thermoplastic Resins (GFRP)

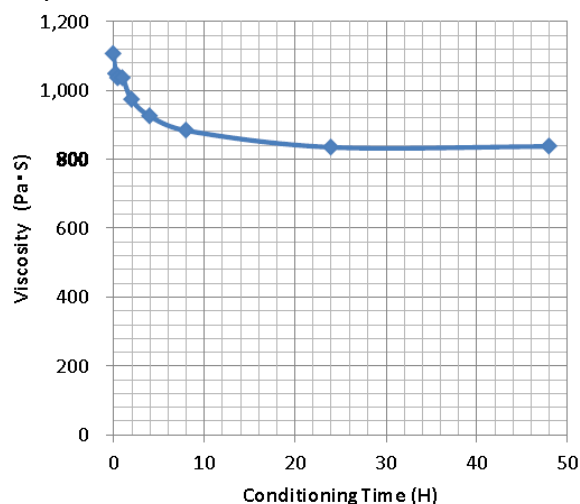
Most mass produced molded plastic products are injection-molded. The appropriate temperature and pressure for injection molding differs depending on the type of resin and shape of the die, over-filling, under-filling, sink marks, voids, or other molding defects. Even if appropriate molding parameters are used, any changes in the status of the resin raw materials used could cause molding defects as well. Therefore, it control the quality of resin raw materials on a daily basis. Furthermore, it is important to perform the daily resin high pressure conditions that approximate molding conditions, which is not possible using the melt flowrate measurement method.

#### ■ Changes in Viscosity Due to Moisture Absorption Time

The change in resin viscosity due to moisture absorption was measured using sample (1), with a molecular weight of 17,000. After drying for 13 hours in a vacuum environment at 100 °C, the sample was left in a room with a temperature of about 23 °C and about 50 % relative humidity for constant temperature testing. The graph shows that the fluidity increases and viscosity decreases as more moisture is absorbed. The results show that about 4 hours after leaving the sample there, viscosity drops sharply and then almost stops decreasing after about 24 hours. Due to the large changes in resin viscosity that result from moisture absorption, using resin materials that have not been controlled for moisture can result in injection molding failures.



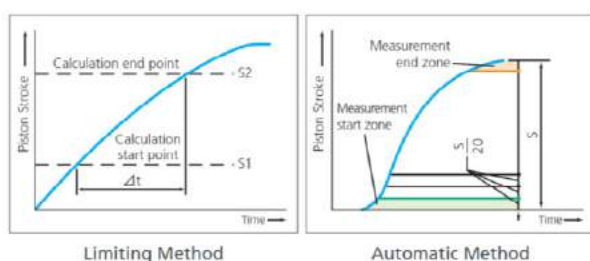
Therefore, such injection molding problems can be avoided by using a CFT-EX series flowtester to measure the viscosity to ensure that it is within given standards before molding the parts.



Test Results

Conditioning Time(H)	Share Rate (s <sup>-1</sup> )	Viscosity (Pa · s)
0	44,38	1,105
0,25	46,84	1,047
0,5	47,35	1,036
1	47,38	1,035
2	50,41	973
4	53,03	925
8	55,54	883
24	58,77	834
48	58,61	837

Test Results



## ■ Selection of Measurement Method According to Material

### Constant Temperature Method

In the testing method based on the use of a constant temperature, two calculation points on the piston's descent are set beforehand. The calculation is conducted using either the limiting method or the automatic method. In the limiting method, the flowrate is determined from the stroke-time curve of the piston between the above two points. In the automatic method, the stroke-time curve is divided into 20 segments, and the flowrate is determined from the gradients of the curves of those segments except for the first and last segment, with the maximum value taken automatically as the flowrate.

## ■ CFT-EX Series



**Thermosetting resins**

**Thermoplastic resins**



**Rubbers**

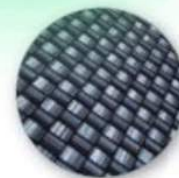
*The fluidity of various materials  
&  
Evaluation of the heat characteristic*



**Ceramics**



**Toners**



**Composites**



Shimadzu Flowtester

# CFT-EX Series

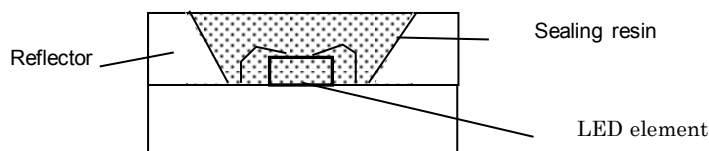
Application Topic # 07

## CFT-EX Useful to Evaluation of LED Package

LEDs are used in various fields for their beneficial features such as long lifetime, low energy consumption, and small size. We often see LEDs in our everyday life since they are used in illuminations, traffic signals, lighting, backlights for LCD televisions, cellular phones, and car lights. To manufacture LEDs, electrode or other parts are attached on elements, wires are connected, and then the parts are sealed with resin for protection. This process is called packaging. In addition to more efficient elements, optimized packaging technology helps to draw light from LED elements efficiently and enhance light directionality.



Round LED Package



Mounted LED Package

Resins used in LED packages have a lens-like function to focus light or a reflector-like function and also disperse phosphors for white LEDs. For the lens, thermoplastic resins such as transparent acrylic resin and polycarbonate resins are used. For resin material to mold LED elements, thermosetting resins such as epoxy resin and silicon resin are used. The optimum resin selection, higher functions, and more consistent quality are demanded for easier molding and higher adhesiveness with elements and other parts.

Recently, there has been a growing awareness about white LEDs which are expected to be applied to a wide range of products, from backlights for televisions to general lighting fixtures. (The global market of sealing materials for LEDs is estimated to grow to 22.7 billion yen in year 2013 which is approximately three times larger than the market size in 2008.) Mainstream white LEDs are currently created by combining blue diode and phosphor. White LEDs have a problem of shorter lifetime due to deterioration of packaging resins caused by heat along with higher luminance and deterioration caused by UV ray generated by luminance of phosphor. In order to solve these problems, there is a growing demand for higher heat resistance and UV-proof functions on packaging resins.

Shimadzu flowtester is an optimum system to evaluate these resins for packaging LEDs because fluidity properties and hardening properties (by heating test) can be measured easily and accurately.

## For LED lighting

The replacement from a filament lamp to white LED lighting is progressing because of the energy-saving, and the new product has come out one after another. One of the big features of LED lighting is a longer operating life (20,000 hours: filament lamp is 1,500 hours), and the major factor which influences the life is "heat." For this reason, the heat-resistant design and the heat dissipation design are important.

Therefore, the filler of a carbon system or a ceramic system is used for resin, or the material which made insulation and heat dissipation compatible by unification with a printed circuit board is developed, and the manufacturing cost reduction which includes a moldability as a metaled substitute article is proposed.

The moldability (fluidity) is an important item for evaluation of plastic new materials. CFT-EX is the optimal equipment at this evaluation.



## CFT-EX can use evaluation of LED

CFT-EX which can evaluate thermosetting and thermoplastic resin in evaluation of the LED package for which various resin is used is recommended.

### The feature of CFT-EX

- Higher Level Evaluation Using a Variety of Analysis Methods
  - • • The evaluation of thermosetting resin and constant heating rate test is possible.
- Smooth, Easy Test Flow
  - • • New software compatible with Win7, 8.1
- Supported by More Than 50 Years of Technology and Know-How
  - • • Abundant applications cultivated for years

Shimadzu Flowtester

## ***CFT-EX Series***



***Thermosetting resins***



***Thermoplastic resins***



***Rubbers***

***The fluidity of various materials  
&  
Evaluation of the heat characteristic***



***Ceramics***



***Toners***



***Composites***



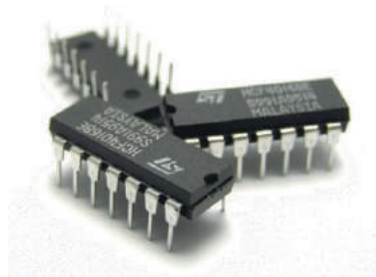
Shimadzu Corporation  
[www.shimadzu.com/an/](http://www.shimadzu.com/an/)

For Research Use Only. Not for use in diagnostic procedures.  
The content of this publication shall not be reproduced, altered or sold for any commercial purpose without the written approval of Shimadzu.  
The information contained herein is provided to you "as is" without warranty of any kind including without limitation warranties as to its accuracy or completeness. Shimadzu does not assume any responsibility or liability for any damage, whether direct or indirect, relating to the use of this publication. This publication is based upon the information available to Shimadzu on or before the date of publication, and subject to change without notice.

## Why Is CFT Used to Evaluate Thermosetting Resins?

### What is thermosetting resins?

Resins are generally classified into thermoplastic resins and thermosetting resins. Similar to chocolate, thermoplastic resins soften and become deformed when heated. They can be processed when they are soft and harden when cooled. They soften if heated again and can be used repeatedly. Major examples are polyethylene terephthalate (PET) used in PET bottles and polypropylene (PP) used in kitchen goods.



By contrast, though thermosetting resins also soften and become fluidized at the early stage of heating, they gradually harden due to chemical reaction and do not soften again, no matter how long they are heated. (They are often compared to biscuits.) Major examples are phenol resin (PF) used in engine parts; epoxy resin (EP) used in packaging of electronic parts such as ICs, semiconductors; and unsaturated polyester resin (UP) used in bathtubs.

### Why Is CFT Suitable to Evaluate Thermosetting Resins?

Although thermosetting resins get fluidized at the early stage of heating, they gradually harden when heated more. The relationship between the temperature and viscosity is an important parameter for molding.

In CFT-EX, viscosity is calculated by measuring the piston's travel distance (travel rate) in the constant test force extrusion method. In this method, even if a thermosetting resin hardens due to heating, only the displacement of the piston stops. Therefore, measurement is very easy and data with a high rate of reproducibility can be obtained.

## Applications of Thermosetting Resins

- Phenol resin (PF)
  - Automobile field: Engine-related parts, electric parts, disk pads, clutch facing, or other bonding materials
  - Electric fields: Parts such as switches and breakers, power supply transformer bobbins
  - Bonding material for grind stones
- Epoxy resin (EP)
  - Cast products: Circuit units of AC transformers and open/close equipments
  - Laminated products: Printed circuit boards, insulating boards
  - Molded products: Packaging and connectors of electronic parts such as ICs, semiconductors, and LEDs
- Urea resin (UF)
  - Molding materials: Wiring instrument parts, lighting apparatus parts, lacquerware
- Melamine resin (MF)
  - Adhesives and paints
  - Molding: Dishes, kitchen utensils, electric parts
- Unsaturated polyester resin (UP)
  - Unsaturated polyester resin (UP) is mostly used for fiber reinforced plastics (FRP).
  - Building material field: Water tanks, bathtubs, bathroom vanities, kitchen counters, septic tanks
  - Industrial equipment field: Chemical tanks, pipes, ducts, helmets
  - Transportation field: Fishing vessels, boats, yachts, car bodies, aero parts
  - Other than FRP: Cast molding (cultured marble, resin concrete, floor materials), paints, decorative boards
- Diallyl phthalate resin (PDAP or DAP)
  - Often used in the electric and electronic fields.: Sealing of connectors, switches, relay parts, coils/elements
- Other: Binder for decorative boards or grind stones

## CFT-EX can use evaluation of epoxy resin (thermosetting resin).

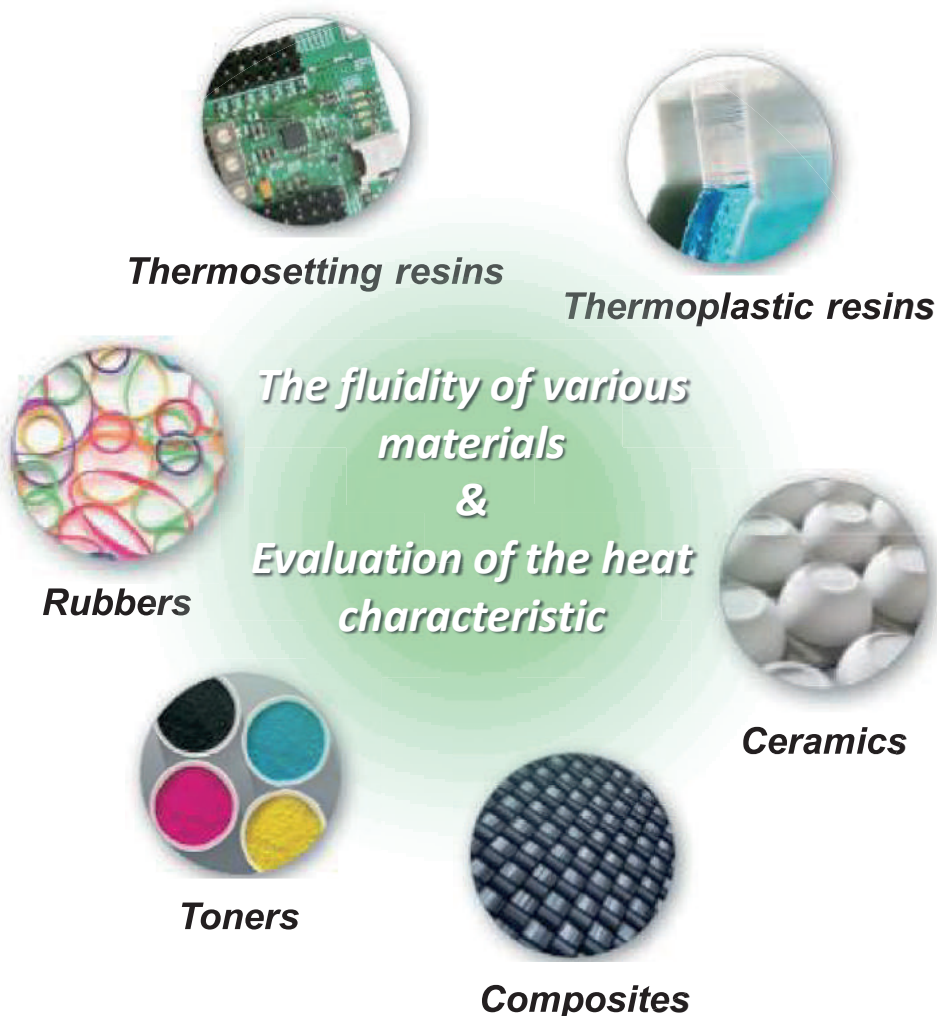
Thermosetting resin can also be evaluated very easily with CFT-EX which has adopted the constant test force extrusion type.

### The feature of CFT-EX

- Higher Level Evaluation Using a Variety of Analysis Methods
  - • • The evaluation of thermosetting resin and constant heating rate test is possible.
- Smooth, Easy Test Flow
  - • • New software compatible with Win7, 8.1
- Supported by More Than 50 Years of Technology and Know-How
  - • • Abundant applications cultivated for years

Shimadzu Flowtester

## **CFT-EX Series**



Shimadzu Corporation  
[www.shimadzu.com/an/](http://www.shimadzu.com/an/)

For Research Use Only. Not for use in diagnostic procedures.  
The content of this publication shall not be reproduced, altered or sold for any commercial purpose without the written approval of Shimadzu.  
The information contained herein is provided to you "as is" without warranty of any kind including without limitation warranties as to its accuracy or completeness. Shimadzu does not assume any responsibility or liability for any damage, whether direct or indirect, relating to the use of this publication. This publication is based upon the information available to Shimadzu on or before the date of publication, and subject to change without notice.

## Shimadzu Flowtester

# CFT-EX Series

Application Topic # 09

### Fluidity Evaluation of Epoxy Resin

Epoxy resin or epoxy resin with filler are used for Printed Circuit Board. To make the throughput high and keep the quality constant you need more fast extrusion and fast hardening conditions and materials. To obtain such conditions or materials the viscosity, hardening time and hardening temperature of material are very important.

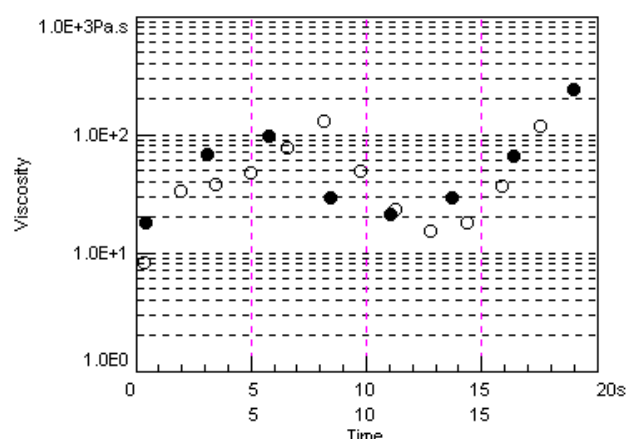
Epoxy resins are also used for the package of LSI. The main focus of LSI manufacturer is also how to make the throughput high. It means how to make the extrusion speed higher and how to make the hardening time shorter. Many researchers try to find more excellent combination of compounds. And to find such conditions CFT is the most suitable equipment.

With using CFT you can obtain the viscosity vs. time properties and the time up to hardening. Because these results are changed with the compounds, temperature and pressure, it is also very important to check the properties of compound to control the product line.

The right graph shows the Viscosity vs. Time curve of Epoxy resin under constant temperature test. Samples are same for both data but the temperature under extrusion test is different. Extrusion pressure is 0.98Mpa.

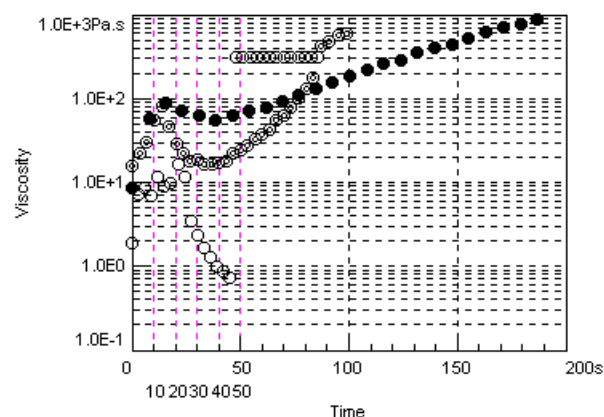
You can see the difference on Viscosity and the time of lowest viscosity. CFT-EX is the most suitable equipment in order to find such conditions.

Filename	Viscositu1	Viscositu2	Viscositu3
SMTC1.c1	4.624E+1	4.316E+1	2.298E+1
SMTC2.c1	8.514E+1	2.357E+1	4.184E+1



### The Example Measured by Three Kinds of Epoxy Resins

The right graph shows the differences of 3 kinds of Epoxy. Temperature condition of these results was at 150 degree C. And the below table shows the calculated viscosity number at 10, 20, 30, 40 and 50 sec from the beginning of extrusion. You can see the big difference between samples.



Filename	Viscositu1	Viscositu2	Viscositu3	Viscositu4	Viscositu5
SMTC11.c1	7.498E+0	1.241E+1	2.417E+0	9.470E-1	3.016E+2
SMTC12.c1	6.284E+1	7.762E+1	6.313E+1	5.534E+1	6.499E+1
SMTC13.c1	4.727E+1	3.133E+1	1.789E+1	1.684E+1	2.337E+1



## CFT-EX can use evaluation of epoxy resin (thermosetting resin).

Thermosetting resin can also be evaluated very easily with CFT-EX which has adopted the constant test force extrusion type.

### The feature of CFT-EX

- Higher Level Evaluation Using a Variety of Analysis Methods
  - • • The evaluation of thermosetting resin and constant heating rate test is possible.
- Smooth, Easy Test Flow
  - • • New software compatible with Win7, 8.1
- Supported by More Than 50 Years of Technology and Know-How
  - • • Abundant applications cultivated for years

Shimadzu Flowtester

## **CFT-EX Series**



**Thermosetting resins**



**Thermoplastic resins**



**Rubbers**

*The fluidity of various materials  
&  
Evaluation of the heat characteristic*



**Ceramics**



**Toners**



**Composites**



Shimadzu Corporation

[www.shimadzu.com/an/](http://www.shimadzu.com/an/)

For Research Use Only. Not for use in diagnostic procedures.

The content of this publication shall not be reproduced, altered or sold for any commercial purpose without the written approval of Shimadzu. The information contained herein is provided to you "as is" without warranty of any kind including without limitation warranties as to its accuracy or completeness. Shimadzu does not assume any responsibility or liability for any damage, whether direct or indirect, relating to the use of this publication. This publication is based upon the information available to Shimadzu on or before the date of publication, and subject to change without notice.



## Fluidity Evaluation of IC Sealant

Epoxy resin or epoxy resin with filler are used for Printed Circuit Board. To make the throughput high and keep the quality constant you need more fast extrusion and fast hardening conditions and materials. To obtain such conditions or materials the viscosity, hardening time and hardening temperature of material are very important.

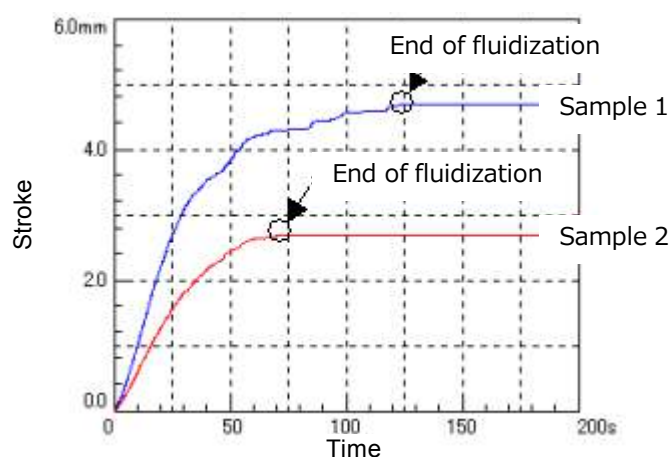
Epoxy resins are also used for the package of LSI. The main focus of LSI manufacturer is also how to make the throughput high. It means how to make the extrusion speed higher and how to make the hardening time shorter. Many researchers try to find more excellent combination of compounds. And to find such conditions CFT is the most suitable equipment.

With using CFT you can obtain the viscosity vs. time properties and the time up to hardening. Because these results are changed with the compounds, temperature and pressure, it is also very important to check the properties of compound to control the product line.

The right graph shows the stroke-time curve of IC sealant (epoxy resin + filler) measured by the constant temperature test. The sample is comparing by an unsettled and an dried resin.

The result that the sample 1 is an unsettled resin, its hardening time is long, and viscosity is low. On the other hand, the sample 2 which dries the sample 1, its hardening time is short, and viscosity is high.

Thus, the check of the viscosity difference of two kinds of samples, i.e., the ease of fabrication and a storage state (moisture absorption etc.) can be evaluated easily.



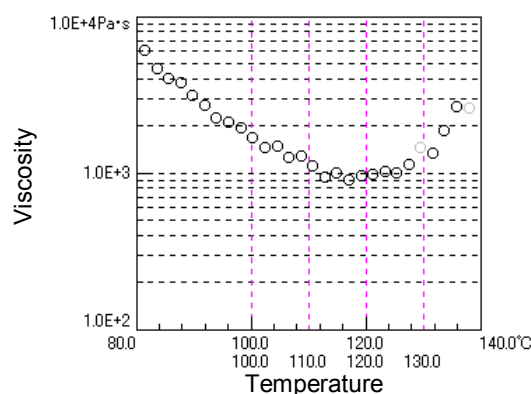
## Evaluation by Constant Heating Rate Method

In addition to the constant temperature method which maintaining test temperature at constant temperature, the constant heating rate methods which measure the dependence of the viscosity to temperature as heating sample temperature at a fixed rate can be used.

Especially, the constant heating rate method is a original method of flowtester and its feature is that rheology character of a wide temperature span to reach a flow region through a rubber domain from the solid region of a sample can be measured at one time. And there is not in other capillary rheometers.

A right graph is a viscosity-time graph at the time of testing IC sealant by the constant heating rate method as minimum viscosity (viscosity change) evaluation. It has the minimum viscosity near 117 degree C as the graph shown.

Thus, the change of physical properties to temperature or temperature can be evaluated easily, namely, the moldability at molding temperature can be evaluated.



## CFT-EX can use evaluation of IC sealant (thermosetting resin)

Thermosetting resin can also be evaluated very easily with CFT-EX which has adopted the constant test force extrusion type.

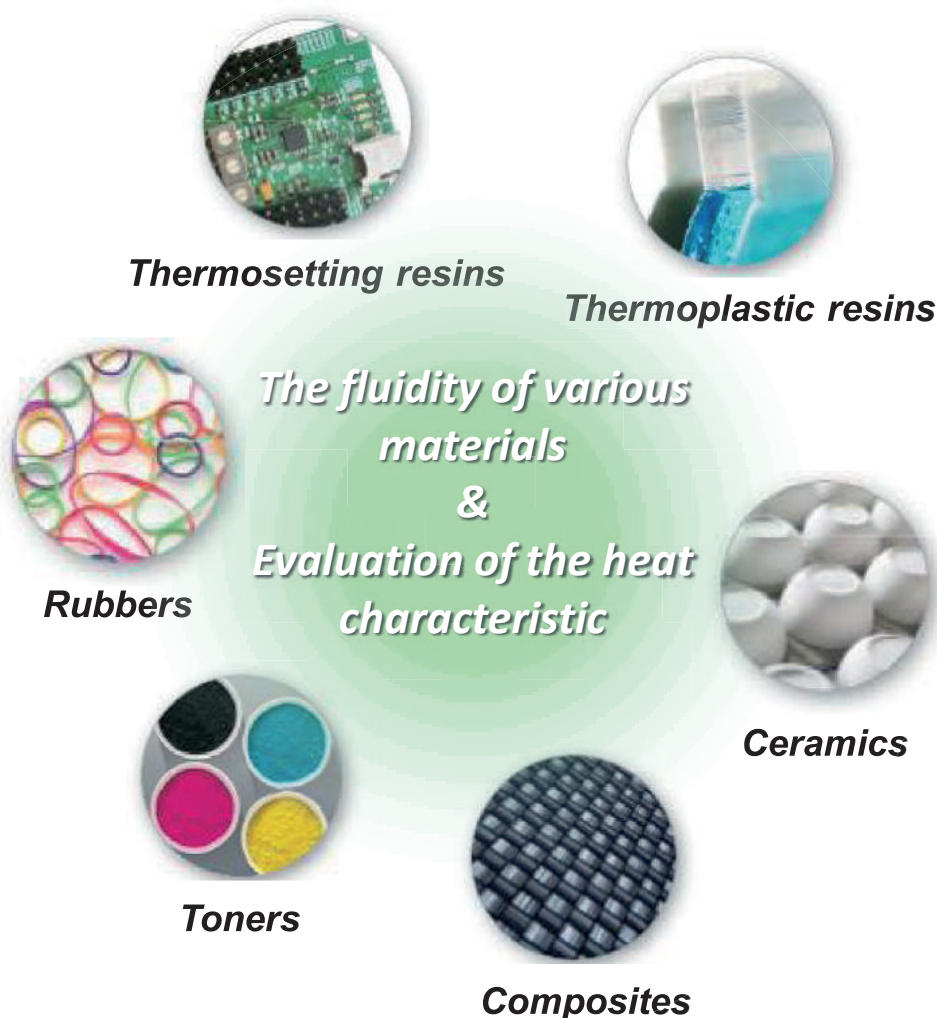
Furthermore, since the constant heating rate method is also possible in addition to the constant temperature method, efficient evaluation is possible.

### The feature of CFT-EX

- Higher Level Evaluation Using a Variety of Analysis Methods
  - • • The evaluation of thermosetting resin and constant heating rate test is possible.
- Smooth, Easy Test Flow
  - • • New software compatible with Win7, 8.1
- Supported by More Than 50 Years of Technology and Know-How
  - • • Abundant applications cultivated for years

Shimadzu Flowtester

## CFT-EX Series



Shimadzu Corporation

[www.shimadzu.com/an/](http://www.shimadzu.com/an/)

For Research Use Only. Not for use in diagnostic procedures.

The content of this publication shall not be reproduced, altered or sold for any commercial purpose without the written approval of Shimadzu. The information contained herein is provided to you "as is" without warranty of any kind including without limitation warranties as to its accuracy or completeness. Shimadzu does not assume any responsibility or liability for any damage, whether direct or indirect, relating to the use of this publication. This publication is based upon the information available to Shimadzu on or before the date of publication, and subject to change without notice.

## Flowtester Flow Tests of Various Kinds of Plastics with Shimadzu Flowtester Model CFT



The Shimadzu Flowtester Model CFT is used for measurement of melting viscosity and rheological properties of raw materials such as thermo plastics, thermosetting resins, and ceramics, or for determination of temperature and pressure of pressing or injection molding.

Two testing modes are available, the constant temperature mode and constant heating rate mode. The former is a method of pressing specimens in a condition of constant temperature, and is suitable for general quality control. The latter is a method pressing specimens in a constant rate heating mode and is often used in measurements of softening and hardening temperatures for flowability evaluation.

The following presents the results of flow tests performed in the constant heating rate mode on four kinds of plastics.

### ■ Softening - flowability curve of polycarbonate resin in constant heating rate mode (Fig.1)

#### ■ Test conditions:

Test temperature:	preset temperature 250 °C to max. 300 °C
Constant heating rate:	6 °C / min
Pressing condition:	Pressure: 10 kgf/cm <sup>2</sup> Die: 1 mm D x 10mm (diam. x length)

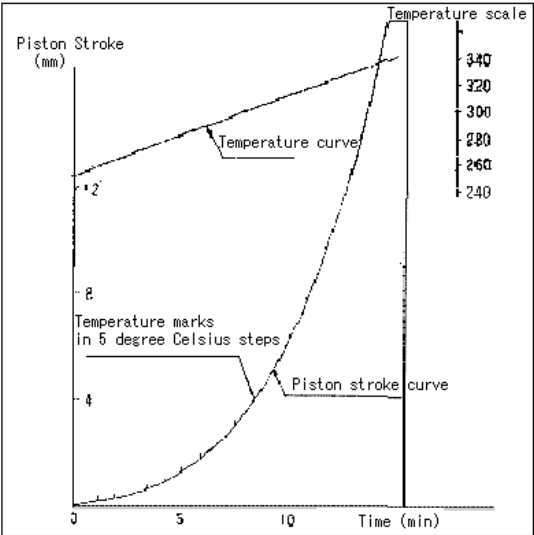


Fig. 1  
Softening – Flowability Curve of Polycarbonate Resin in Constant Heating Rate Mode

■ Softening - flowability curve of polyurethane resin in constant heating rate mode (Fig. 2)

Test temperature:	Preset temperature 100 °C to max. 200 °C
Constant heating rate:	5 °C/min
Pressing conditions:	Pressure: 10 kgf/cm <sup>2</sup> Die: D1 x 1 mm (diam. x length)

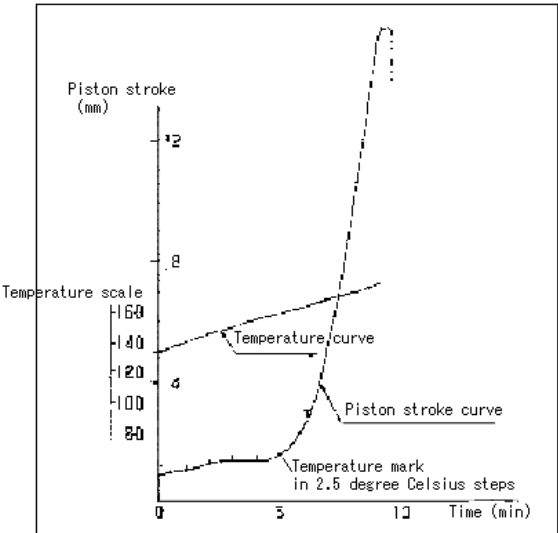


Fig. 2  
Softening- Flowability of Polyurethane Resin in Constant Heating Rate Mode

■ Softening - flowability curve of polyester resin in constant heating rate mode (Fig. 3)

Test temperature:	preset temperature 220 °C to max. 350 °C
Constant heating rate:	3 °C/min
Pressing conditions:	Pressure: 50 kgf/cm <sup>2</sup> Die: D 0.5 x 1 mm (diam. x length)

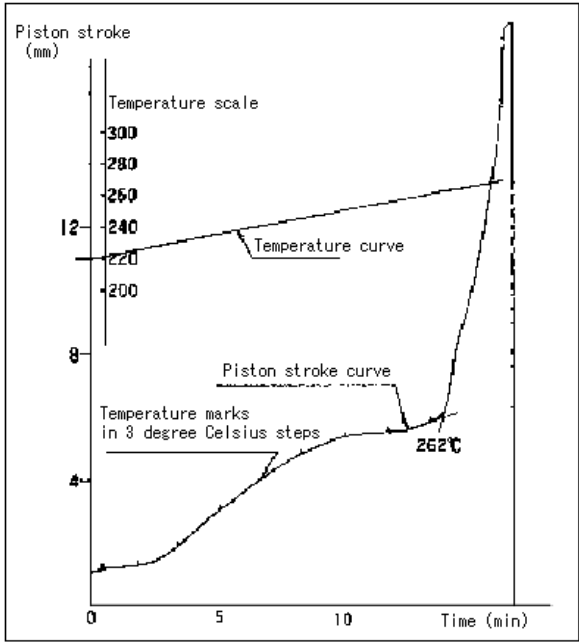


Fig. 3  
Softening- Flowability of Polyester Resin in Constant Heating Rate Mode

■ Softening - flowability curve of polychlorinated resin in constant heating rate mode (Fig.4)

Test temperature:	Preset temperature 150 °C to max. 300 °C
Constant heating rate:	6 °C/min
Pressing conditions:	200 kgf/cm <sup>2</sup> Die: D1 x 10 mm (diam. x length)

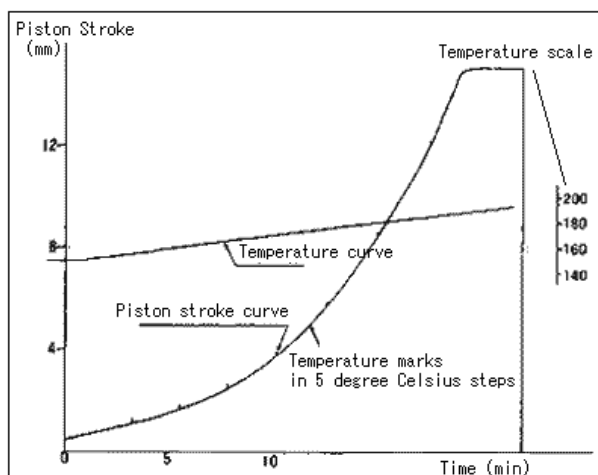


Fig. 4  
Softening- Flowability of Polychlorinated Vinyl in  
Constant Heating Rate Mode

#### ■ Softening - flowability characteristic curves

As temperature is elevated at a given constant rate, the flow rate, apparent viscosity, shear rate, or shearing stress of respective resin specimens can be recorded at any test temperature.

\* Please be advised that data obtained before the implementation of the current Weights and Measures Law may be presented in terms of gravimetric unit.



## Application News

No. SCA\_300\_026

Material Testing System DUH

### Measurement of Surface Hardness of Erasers with Shimadzu Dynamic Ultra Micro Hardness Tester

-Surface hardness evaluation of soft materials-



#### ■ Introduction

JIS S6004 stipulates a fixed set of conditions for product tests on erasers, while hardness tests should be conducted according to JIS K6301 (Physical testing methods for vulcanized rubber). Since the erasing ability (erasing rate) is affected by the mechanical properties of the eraser surface which comes in contact with paper, the hardness near its surface is a particularly important factor for evaluation.

The Shimadzu Dynamic Ultra Micro Hardness Tester allows you to measure the hardness of thin films and thin layers, using the indentation depth of the indenter (dynamic indentation hardness) or the diagonal length of indentation (micro Vickers hardness). This instrument can thus measure the hardness of various specimens from hard to soft materials, and has an extremely broad range of applications. Here, we will introduce an example of a test in which this Hardness Tester was used to measure the hardness of three types of pencil erasers and two types of soft rubbers in terms of the relationship between the load and the indentation depth.

## Test results

Eraser (A)							
No.	Load (gf)	Depth ( $\mu\text{m}$ )	Hardness	No.	Load (gf)	Depth ( $\mu\text{m}$ )	Hardness
1	0.114	21.85	0.0090	2	0.114	21.53	0.0093
3	0.098	19.94	0.0094				
Average	0.109	21.11	0.0092				

Eraser (B)							
No.	Load (gf)	Depth ( $\mu\text{m}$ )	Hardness	No.	Load (gf)	Depth ( $\mu\text{m}$ )	Hardness
1	0.127	15.17	0.0209	2	0.115	14.50	0.0207
3	0.114	13.44	0.0238				
Average	0.118	14.37	0.0218				

Eraser (C)							
No.	Load (gf)	Depth ( $\mu\text{m}$ )	Hardness	No.	Load (gf)	Depth ( $\mu\text{m}$ )	Hardness
1	0.179	13.28	0.0384	2	0.147	12.33	0.0366
3	0.159	13.71	0.0320				
Average	0.162	13.11	0.0357				

Soft rubber (A)							
No.	Load (gf)	Depth ( $\mu\text{m}$ )	Hardness	No.	Load (gf)	Depth ( $\mu\text{m}$ )	Hardness
1	0.029	17.71	0.0035	2	0.033	19.21	0.0034
3	0.028	17.27	0.0036				
Average	0.030	18.06	0.0035				

Soft rubber (B)							
No.	Load (gf)	Depth ( $\mu\text{m}$ )	Hardness	No.	Load (gf)	Depth ( $\mu\text{m}$ )	Hardness
1	0.312	17.82	0.0372	2	0.342	18.86	0.0364
3	0.370	19.47	0.0369				
Average	0.342	18.72	0.0369				

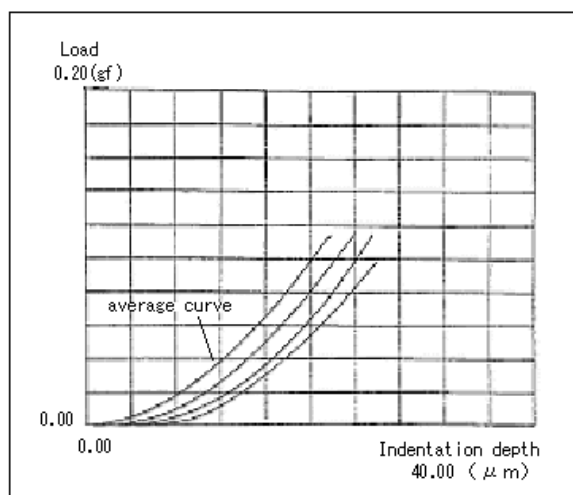


Fig. 1 Eraser (A)

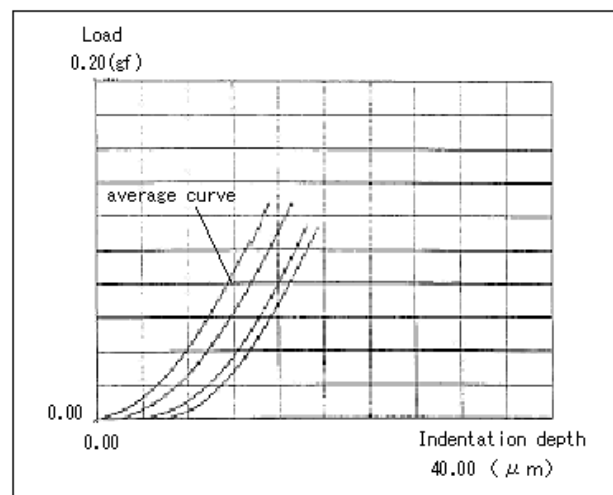


Fig. 2 Eraser (B)

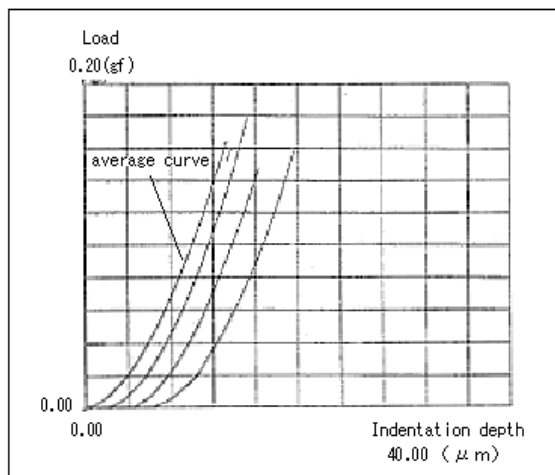


Fig. 3 Eraser (C)

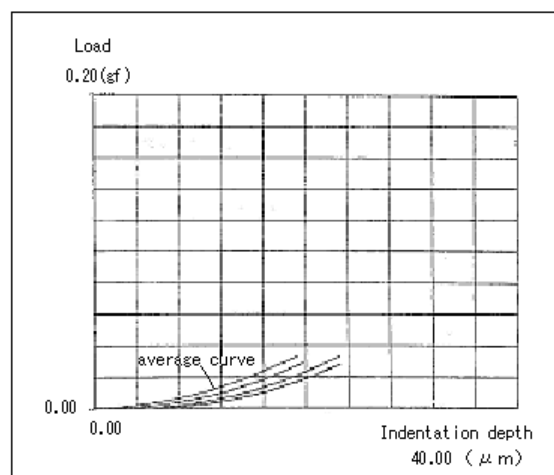


Fig. 4 Soft Rubber (A)

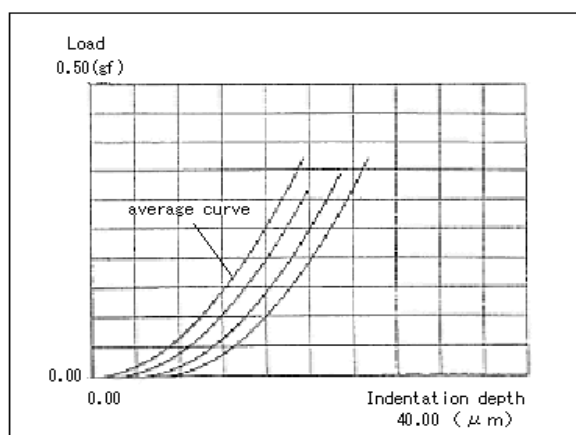


Fig. 5 Soft Rubber (B)

**Figs. 1, 2 and 3** are diagrams of the test results that indicate the load-indentation depth relationships for pencil erasers (A), (B), and (C) respectively. **Figs. 4 and 5** display those for soft rubbers (A) and (B).

In each respective diagram, the data obtained from three tests and their average values are indicated as four curves. The average value is shown in the first curve in each diagram. For the hardness (DH) measurement, a triangular pyramid indenter with a tip angle of 115 degrees was used, and the calculation was performed using the following equation:

$$DH = 37,838 P/h^2$$

P: Test Load (gf)

h: Indentation depth (μm)

## Test on Thermosetting Resin with Shimadzu Flow Tester Model CFT



Epoxy resin, characterized by its excellent electrical, mechanical and adhesive properties as well as its chemical proof properties, is utilized in a wide range of materials including electric insulators, paints, structural assemblies, adhesive agents, etc.

The thermosetting nature of epoxy resin materials, processed in combination with curing agent, has to be evaluated in terms of curing speed by the extruding type flow test method, and not by usual physical strength methods. The Shimadzu Flow Tester Model CFT, with the ability to test flow rates under pressures and shear rates similar to those of the usual forming process, can be used not only for testing thermoplastic resin, but also thermosetting resin, adhesive agents, copying toner, rubber materials, ceramic materials, foods, cosmetics, medicines, etc. The following presents the results of measurement in curing time of epoxy resin performed with the Shimadzu Flow tester Model CFT.

### ■ Outline of Shimadzu flow tester CFT

- 1) Method of pressure application: Constant load extruding
- 2) Extruding pressure: Max. 500 kgf/cm<sup>2</sup>
- 3) Testing mode: Constant temperature or constant heating rate
- 4) Test temperature: Max. 400 °C
- 5) Cylinder diameter: 11.329 mm (1 cm<sup>2</sup> cross sectional area)

### ■ Testing conditions

Specimen: Epoxy resins

Curing agent: Anhydrous phthalic acid + acid absorption amine

Temperature conditions: Constant temperature mode, 150 °C.

Extruding condition: Pressure kgf/cm<sup>2</sup>

Die orifice: Diam 1.0 x Length 1.0 mm

### ■ Test results

**Figs.1, 2 and 3** show flow curves of three different epoxy resins with different concentrations of curing agent. Flow starting times, curing times etc. for respective specimens can be discerned immediately from these curves. Test conditions and data such as shear stress, flow rate, shear rate, viscosity, etc. are simultaneously printed automatically at the portion above the graph, presenting all necessary information on a sheet.

The three curves of Figs.1, 2 and 3 are shown in Fig. 4 in overlap mode for at-a-glance comparison with each other. Overlap mode helps present mean values and deviation of test data for a single specimen as well.

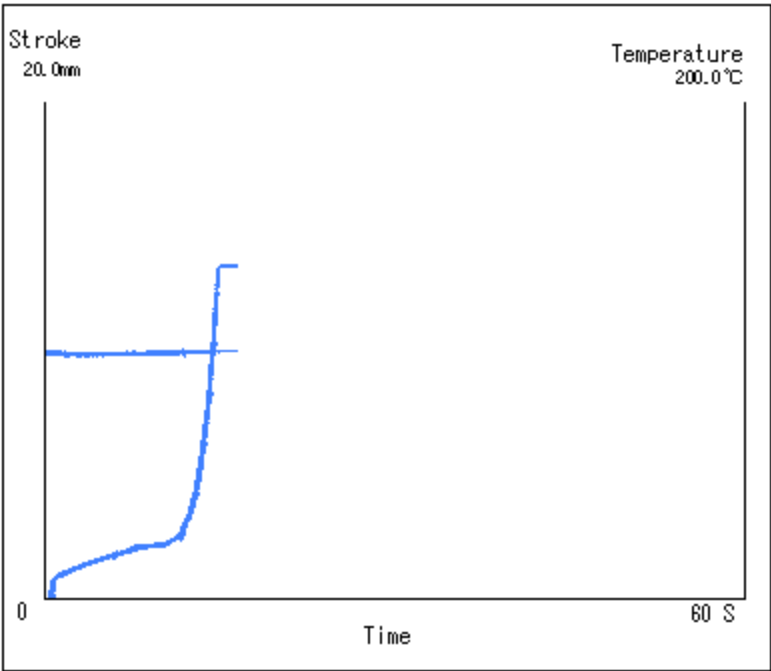


Figure 1: Flow curve of epoxy resin (A)

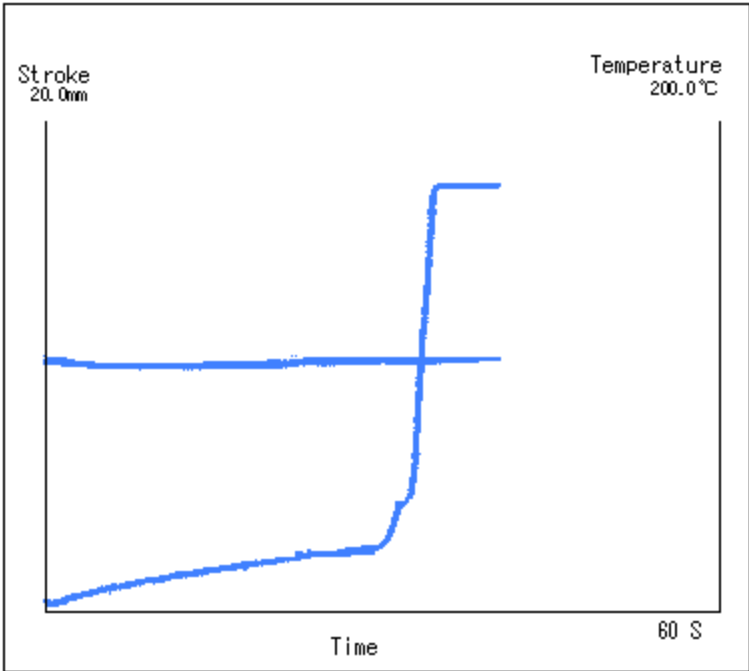


Figure 2: Flow curve of epoxy resin (B)



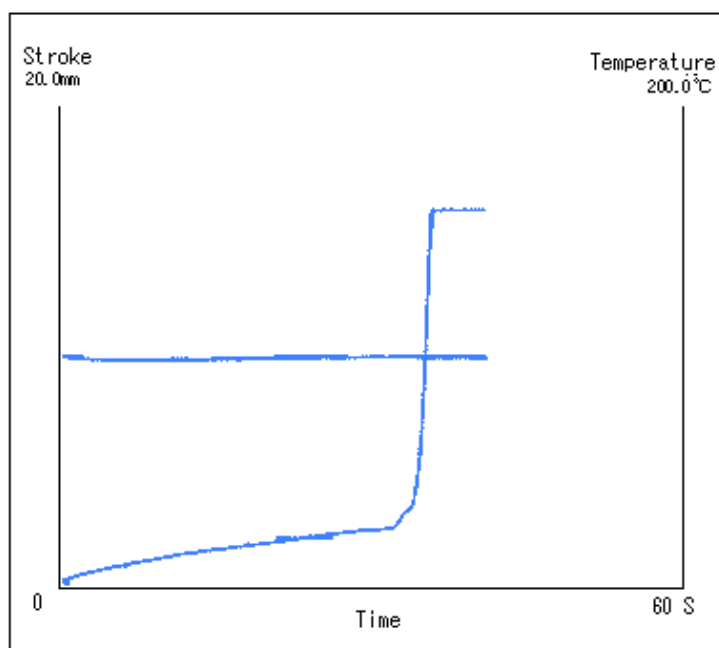


Figure 3: Flow curve of epoxy resin (C)

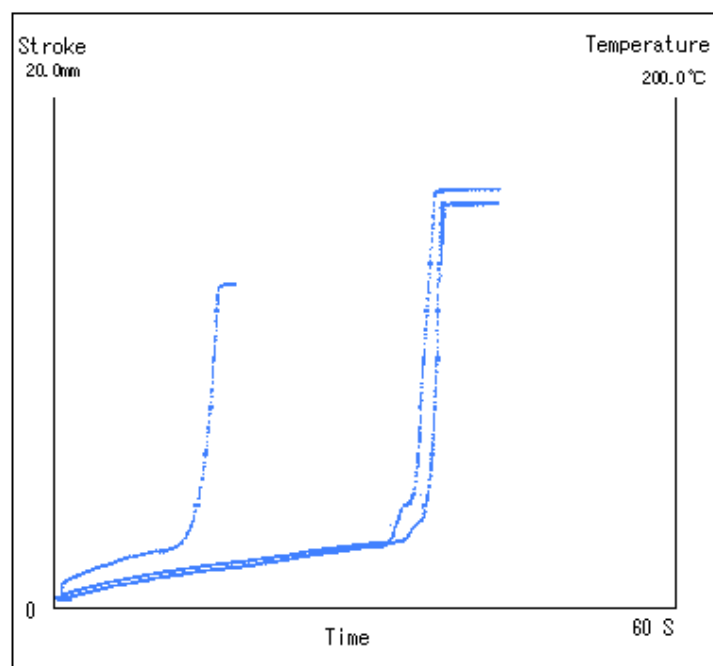


Figure 4: Overlapping flow curves of epoxy resins (A, B and C)

\* Please be advised that data obtained before the implementation of the current Weights and Measures Law may be presented in terms of gravimetric unit.

### ■ Introduction

Rubber products are produced by forming rubber compounds (mixtures of rubber and additives that provide specific functional characteristics) in a mold and then applying heat to provide an elastic body. Therefore, the fluidity of rubber compounds can have a major effect on molding quality. Unformed rubber compounds change their characteristics after long storage periods, which can cause fluidity to deteriorate or the molding process to fail, depending on how they are stored. Here, the example, which evaluated the fluidity change by the storage method of the unvulcanized rubber, is introduced.



### ■ Fluidity Change by the Storage Method of Unvulcanized Rubber

In this case, a rubber compound was stored at ambient temperature and low temperature for 14 days and 28 days immediately after kneading and then the fluidity was evaluated. The results showed that the given sample could be stored at low temperatures without a significant change in fluidity, even after one month. Using the CFT-EX series allows evaluating the rubber compounds storage temperatures and storage periods without actually having to mold any parts.

Test Method	Constant temperature test
Die Diameter	0,5 mm
Die Length	1 mm
Test Temperature	280 °C
Test Pressure	20,1 MPa
Preheating Time	0 sec
Sample Size	1.6 g

Test Conditions

Storage Temperature	Storage Temperature	Viscosity(Pa·s)
Ambient Temperature	0	395,7
	14	568,1
	28	600,0
Low Temperature	0	395,7
	14	447,5
	28	419,3

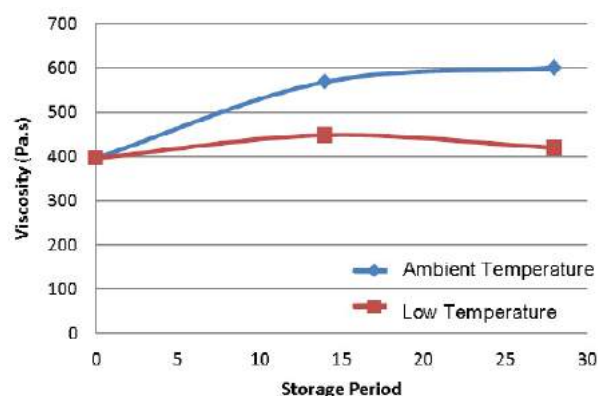
Test Result

### ■ CFT-EX can use evaluation of unvulcanized rubber

CFT-EX, which can evaluate thermosetting and thermoplastic resin in evaluation of unvulcanized rubber, is recommended.

The feature of CFT-EX

- Higher Level Evaluation Using a Variety of Analysis Methods  
The evaluation of thermosetting resin and constant heating rate test is possible.
- Smooth, Easy Test Flow  
New software compatible with Win7, 8.1
- Supported by More Than 50 Years of Technology and Know-How  
Abundant applications cultivated for years



Changes in Viscosity Due to Storage Methods



**Thermosetting resins**



**Thermoplastic resins**



**Rubbers**

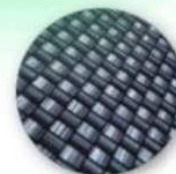
*The fluidity of various materials  
&  
Evaluation of the heat characteristic*



**Ceramics**



**Toners**



**Composites**

## Application News

Material Testing System CFT

No. SCA\_300\_054

### Viscosity Evaluation of Thermoplastic Resins (Epoxies)

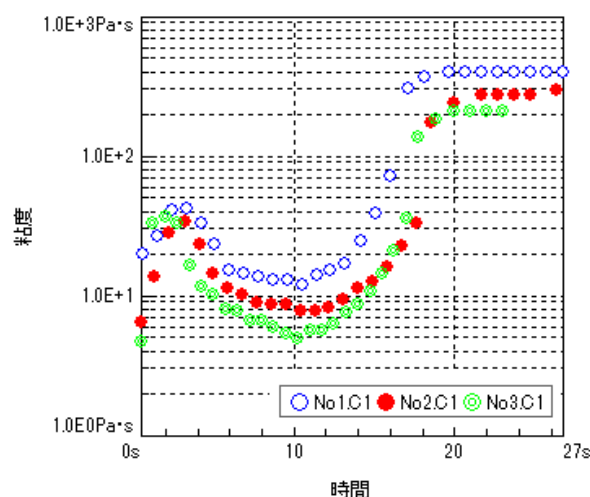
When thermosetting resins are heated, they melt and are able to flow, but further increases causes curing. The minimum viscosity value, the time it takes to reach that minimum, curing depend on the temperature used to melt the resin. Unless these viscosity and time molding process, they can result in molding defects. For resins, characteristic values due to other factors. Therefore, controlling the resin viscosity is very important to ensure vary and good products are produced.



#### ■ Measurement of the Minimum Melt Viscosity Value

The fluidity properties of thermosetting resins are often measured using constant temperature testing. Unlike thermoplastic resins, the thermoset viscosity is constantly changing. Therefore, the minimum melt viscosity value can be determined automatically by using automatic constant temperature testing. In this case, three types of thermosetting resins were tested using the constant temperature method. The testing pressure was selected so that the sample would melt and flow and then stop flowing due to curing. Test condition Viscosity-Temperature Graph The viscosity-time graph, which shows the change in viscosity over time, indicates that the sample melts and starts to flow after about 3 seconds, reaches its minimum viscosity after about 10 seconds, and then stops flowing after about 18 seconds. The CFT calculates viscosity by measuring the amount of piston movement (movement speed) during constant test force extrusion.

Therefore, even when the sample cures due to heating, the piston displacement merely stops, which has no effect on controlling test force. Consequently, it provides extremely stable and highly reproducible test.



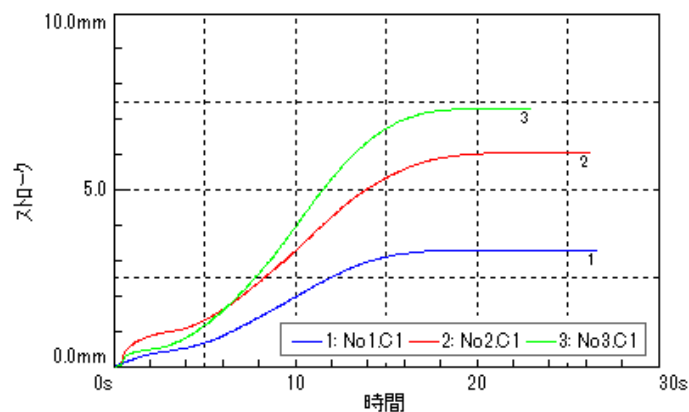
Viscosity-Temperature Graph

Test Method	Constant Temperature Test
DIE Diameter	0,5 mm
DIE Length	10 mm
Test Temperature	185 °C
Test Pressure	245 Mpa
Preheating Time	15 sec
Sample Size	2,5 g (Pellets)

## Test Conditions

Sample Number	Shear Rate ( $S^{-1}$ )	Viscosity ( $Pa \cdot s$ )
1	2,471	12,4
2	4,073	7,5
3	5,810	5,3

## Test Result



Stroke-Temperature Graph

### ■ A Split Nozzle Makes Cleaning Easy

Due to the relatively low minimum melt viscosity and high fluidity of thermosetting resins, long nozzles with small hole diameters are often used. Therefore, it can be difficult to remove the residual resin inside the nozzle once the resin has cured after measurements. However, using a split nozzle, which splits into two halves down its center, allows the resin to be removed easily, thereby cleaning and measuring more efficiently.



### ■ CFT-EX Series







## 6. Materials Testing & Inspection

---

### 6.6 Non-Destructive Inspection (NDI)

---

Non-destructive inspection instruments utilize X-rays to penetrate materials. They include both fluoroscopy instruments and CT instruments which are capable of creating tomographical images and performing 3-D observation. The images obtainable within minutes of X-rays focus on delivery with high magnification. These instruments are essentially microscopes, enabling viewing of materials without destroying them.

**Application Note** Taking innovation to new heights with Shimadzu X-Ray inspection system

# SMX-1000 Plus

## Microfocus X-Ray Inspection System

### Taking Innovation to New Heights with Shimadzu X-Ray Inspection System

Shimadzu's SMX-1000Plus produce extremely clear, distortion-free images thanks to a flat-panel detector and sealed microfocus X-ray tube.

The enlarged fluoroscopic exterior image view provides a new level of visibility.

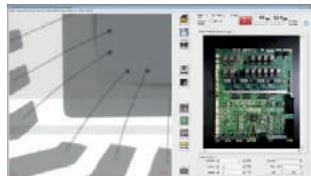
New functions such as enhanced region-of-interest display have been incorporated, complementing a wealth of conventional functions including navigation via exterior images, step feed, teaching, and image browsing.

The measurement functions are so much easier to use that results can now be obtained with just a click, and require no complicated parameter settings.



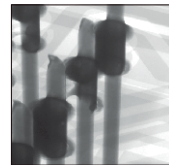
#### Further Improved Operability

Remodeled windows and an enlarged display with a simple, user-friendly layout ensure the intended operation is performed without guesswork.



#### Inclined Fluoroscopy

The flat panel detector with a tilt angle of up to 60° enables fluoroscopy over an extensive range while maintaining constant magnification, so defects that are undetectable with vertical fluoroscopy can be detected.



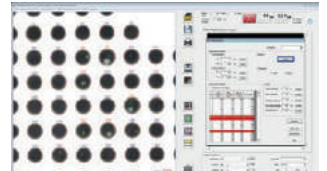
#### Clear Images

As with earlier models, the combination of flat panel detector with Shimadzu image processing technology leads to clear, distortion-free images.



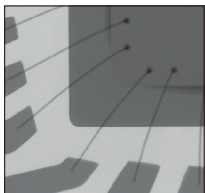
#### Easy Measurements

Troublesome measurement parameter settings are automatically optimized, and thanks to our proprietary image-processing technology, measurement results are now obtained with simple mouse operations.



### Applications

#### IC Bonding Wire



#### Batteries and Capacitors

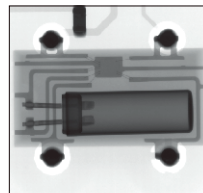


Li-ion battery



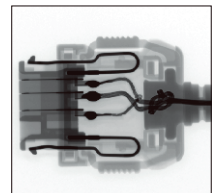
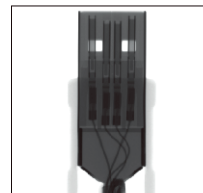
Electrolytic capacitor

#### Electronic Components

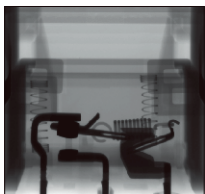


Crystal oscillator

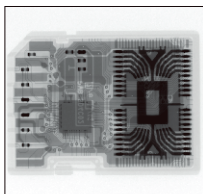
#### Connectors



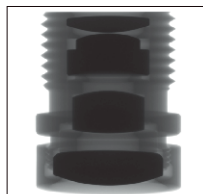
#### Components



Switch



SD card



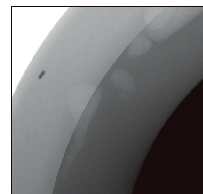
Camera lens

#### Bottles

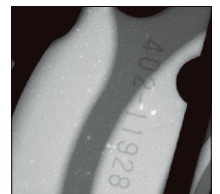


Spray mechanism

#### Resin Molded Products and Aluminum Die Casting

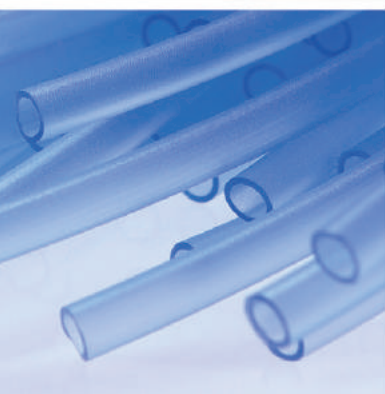


Resin (void)



Aluminum die casting (void)

# 7. Particle Size





## 7. Particle Size

---

### 7.1 Laser Diffraction Particle Size Measurement

---

A wide variety of principles are available for measuring particle size distribution, e.g. particle size analyzers adopting the “laser diffraction/scattering method”. This measurement principle evolved rapidly from the early 1990’s onwards based on advances made in computer and sensor technology and ingenious devices incorporated into these systems.

**EG-04**

Measuring of coating additives

**EG-13**

Measuring of steel balls

**EG-15**

Measuring of carbon black



## Application News

No. EG-04

Particle Size Measurements

## Measuring of Coating Additives

SALD-7101 and BC -71

### Alternative instruments and accessories leading to similar results:

- SALD -2300 with BC-23



### Measurement

For the measurement two sample solutions were measured 5 times. Each measurement was done with a fresh solution. Before measuring the samples with Shimadzu's batch cell BC-71 they were diluted using isopropanol.

### Discussion

(Please find measurement results on the next page)

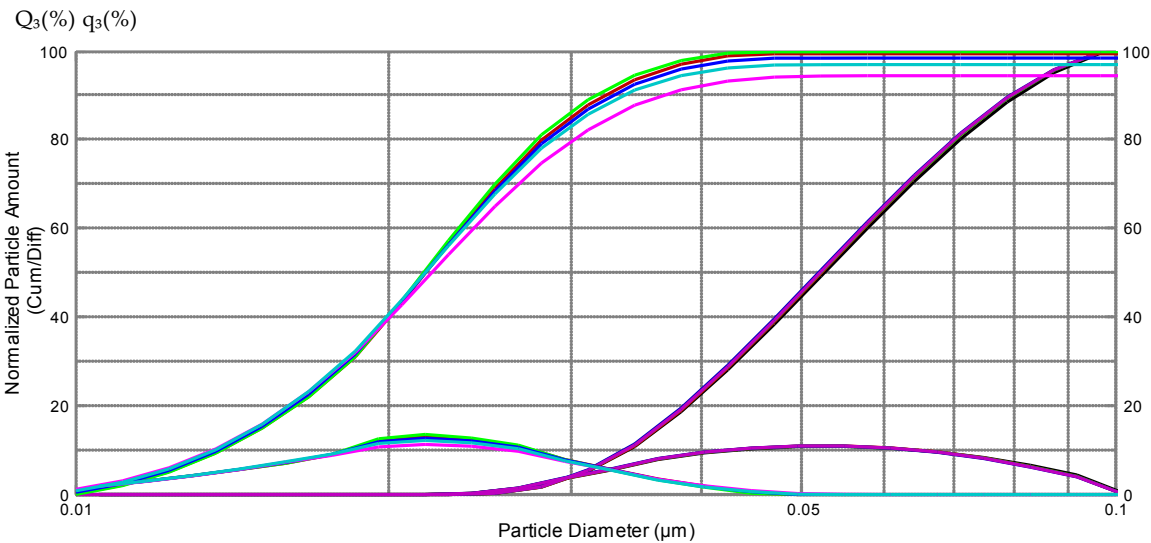
The SALD-7101 in combination with BC-71 can successfully be used to measure nanoparticles respectively additives for coatings.

### Background

Coatings are an ideal protection for different kind of materials. They protect against moisture, UV radiation, rust and other influences. Additives can enhance the properties of the coating, e.g. the scratch resistance. Like in this application note these additives can be made out of non-polar surface modified silicon dioxide nanoparticles.



Results



	Median D ( $\mu\text{m}$ )	Modal D ( $\mu\text{m}$ )	Mean V ( $\mu\text{m}$ )	Std Dev	25%D ( $\mu\text{m}$ )	50%D ( $\mu\text{m}$ )	75%D ( $\mu\text{m}$ )	0%D ( $\mu\text{m}$ )	0%D ( $\mu\text{m}$ )	0%D ( $\mu\text{m}$ )	0%D ( $\mu\text{m}$ )	0%D ( $\mu\text{m}$ )	0%D ( $\mu\text{m}$ )
1	0.015	0.014	0.016	0.130	0.012	0.015	0.020	0.000	0.000	0.000	0.000	0.000	0.000
2	0.015	0.014	0.016	0.127	0.012	0.015	0.020	0.000	0.000	0.000	0.000	0.000	0.000
3	0.015	0.014	0.016	0.134	0.012	0.015	0.019	0.000	0.000	0.000	0.000	0.000	0.000
4	0.015	0.014	0.015	0.141	0.012	0.015	0.019	0.000	0.000	0.000	0.000	0.000	0.000
5	0.015	0.014	0.015	0.137	0.012	0.015	0.019	0.000	0.000	0.000	0.000	0.000	0.000
6	0.038	0.035	0.039	0.124	0.032	0.038	0.047	0.000	0.000	0.000	0.000	0.000	0.000
7	0.038	0.035	0.039	0.123	0.031	0.038	0.047	0.000	0.000	0.000	0.000	0.000	0.000
8	0.037	0.035	0.039	0.123	0.031	0.037	0.047	0.000	0.000	0.000	0.000	0.000	0.000
9	0.037	0.035	0.039	0.123	0.031	0.037	0.047	0.000	0.000	0.000	0.000	0.000	0.000
10	0.037	0.035	0.039	0.123	0.031	0.037	0.047	0.000	0.000	0.000	0.000	0.000	0.000

Above graph shows a volume based particle size distribution of two different samples. The table contains the corresponding measurement results. Sample 1-5 and sample 6-10 are two independent samples. The mean diameter of the first sample is 22nm the mean diameter of the second 52nm.



## Application News

No. EG-13

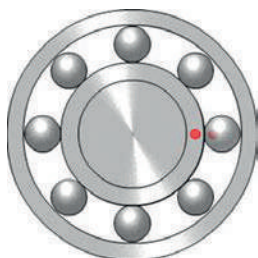
Particle Size Measurements

### Measuring of Steel Balls

SALD-2300 and MS-23

#### Alternative instruments and accessories leading to similar results:

- SALD -3101 with MS-30



#### Background

A ball bearing is a type of rolling-element bearing that uses balls to maintain the separation between the bearing races.

The purpose of a ball bearing is to reduce rotational friction and support radial and axial loads.

It achieves this by using at least two races to contain the balls and transmit the loads through the balls. In most applications, one race is stationary and the other is attached to the rotating assembly (e.g., a hub or shaft). As one of the bearing races rotates it causes the balls to rotate as well. Because the balls are rolling they have a much lower coefficient of friction than if two flat surfaces were sliding

against each other.

#### Measurement

For this application the sampler MS-23 in combination with SALD-2300 is needed. The 2mm steel balls with an density of 7,8 g/cm<sup>3</sup> were dispersed in water. No additional detergents were needed. A high pump speed is needed to ensure that the balls are circulated properly.

It's obvious that a micrometer screw is probably better suited to measure the particle diameter of 2mm stainless steel balls but this application shows impressively the strength of the MS-23 sampler.

#### Discussion

The technical requirements for pumping stainless steel balls are surprisingly close to requirements needed to measure quite common samples for particle size instruments.

Attached table shows that already ceramics need a powerful pumping unit.

Density of soil samples:	~3g/cm <sup>3</sup>
Density of ceramics:	~4g/cm <sup>3</sup>
Density of steel:	7,8g/cm <sup>3</sup>

## Measuring of Carbon Black

SALD-7101H and MS -71

### Alternative instruments and accessories leading to similar results:

- SALD -2300 with BC-23



### Background

Carbon blacks color and small size make it basically difficult to measure it by Laser Diffraction Methods. Due to the strong light absorption of the particles, the sensor of the instrument detects only very weak intensities of diffracted light. SALD-7101H has a high sensitive optical system and therefore it's possible to measure such kind of samples.

### Measurement

A small spoon of sample from the sample was carefully suspended with 3 drops of neutral detergent. Afterwards 40-50ml of pure water was added and the suspension was set 60s into an ultrasonic bath.

The pump of the sampler MS-71 was started and a few droplets from the suspension were added to the water filled beaker of the sampler until an optimum light intensity of 40-50% is obtained. Now the measurements were started.

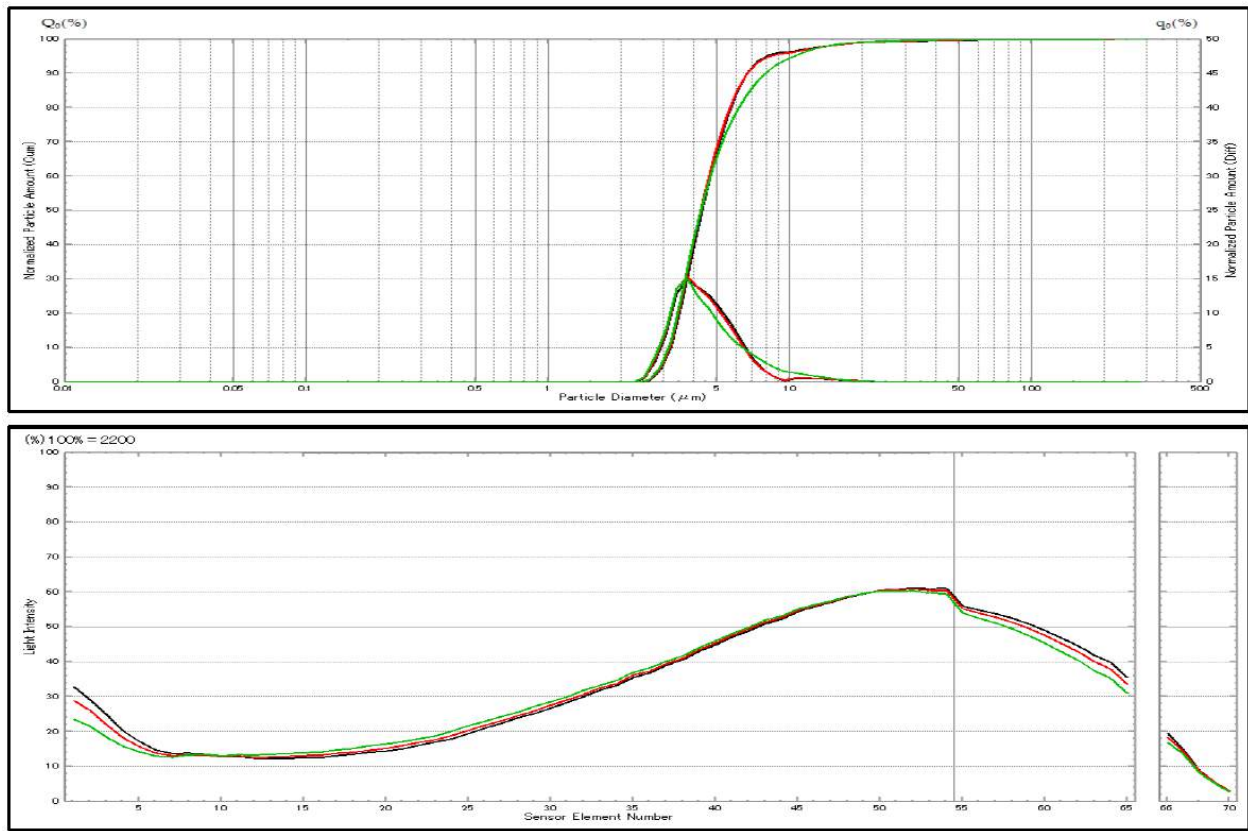
### Discussion

(Please find measurement results on the next page)

Small and dark colored particles are a challenge for particle size instruments using laser diffraction methods in general. Nevertheless with our SALD-7101H and our SALD-2300 such measurements are easy to realize due to their high sensitive optical setup.

Another advantage of this optical setup is that rather low concentrated samples can be measured as well

Results



	Median D (μm)	Modal D (μm)	Mean V (μm)	Std Dev	25%D (μm)	50%D (μm)	75%D (μm)	0%D (μm)	0%D (μm)	0%D (μm)	0%D (μm)	0%D (μm)	0%D (μm)
1	4.332	3.548	4.586	0.165	3.576	4.332	5.422	0.000	0.000	0.000	0.000	0.000	0.000
2	4.268	3.548	4.546	0.167	3.537	4.268	5.355	0.000	0.000	0.000	0.000	0.000	0.000
3	4.288	3.548	4.685	0.179	3.520	4.288	5.690	0.000	0.000	0.000	0.000	0.000	0.000

The upper graph shows a volume based particle size distribution with a peak around 5μm. The lower graph shows the corresponding light distribution. Despite the high absorption of the particles the lower graph shows a reasonable high light intensity.



Founded in 1875, Shimadzu Corporation, a leader in the development of advanced technologies, has a distinguished history of innovation built on the foundation of contributing to society through science and technology. We maintain a global network of sales, service, technical support and applications centers on six continents, and have established long-term relationships with a host of highly trained distributors located in over 100 countries.

For information about Shimadzu, and to contact your local office, please visit our website at [www.shimadzu.eu](http://www.shimadzu.eu)



**Shimadzu Europa GmbH**  
Albert-Hahn-Str. 6-10 · D-47269 Duisburg  
Tel.: +49 - (0)203 - 76 87-0  
Fax: +49 - (0)203 - 76 66 25  
[shimadzu@shimadzu.eu](mailto:shimadzu@shimadzu.eu)  
[www.shimadzu.eu](http://www.shimadzu.eu)